Development, Validation, and Assessment of a Multiple Model Structural Identification Method

Volume 1

A Thesis

Submitted to the Faculty

of

Drexel University

by

Nathaniel Charles Dubbs

in partial fulfillment of the

requirements for the degree

of

Doctor of Philosophy

February 2012

Acknowledgments

I would like to express my sincere gratitude to my advisor, Dr. Franklin Moon, for his support, insight, and guidance throughout my studies at Drexel University. He has not only been a remarkable advisor and mentor, but also a true friend to whom I am indebted for the time and effort he devoted to assisting me in my work.

I would also like to thank Dr. Emin Aktan for his advice and recommendations throughout my research. He brought a wealth of experience and expertise within the field of Structural Identification, for which I am grateful.

I am also indebted to my thesis committee, led by Dr. Moon, who not only guided me throughout my research but took the time to review the 800 plus pages within this thesis and offer exceptional reviews and insight from various fields. Thank you Dr. Emin Aktan, Dr. Patrick Gurian, Dr. Tein-Min Tan, Dr. Ivan Bartoli, and Dr. Anu Pradhan.

I would also like to thank my good friends and colleagues Jeffrey Weidner, John Prader, and Matt Yarnold as well as the rest of our research team for their assistance with field work as well as review of my research.

I am grateful for the assistance provided by engineers and staff from Pennoni Associates, Inc., specifically Jack DiGiovanna, Larry Egan, and David Lowdermilk, as well as the staff at the Burlington County Bridge Commission, for their insight and assistance during the field work on the Burlington Bristol Bridge. Even during extreme cold and inclement weather, they did not waver in assisting me with installing sensors critical to this research.

The research presented within this thesis would not have been possible without the support and funding by The National Science Foundation, and the Burlington County Bridge Commission. The findings and conclusions reported herein are those of my own and do not necessarily represent the opinions, conclusions, or recommendations of the National Science Foundation or the Burlington County Bridge Commission.

I would like to thank my parents, Cary and Mary Dubbs, my sisters Emily and Rachel, and the rest of my family for their never-ending support and love not only during my college education but in every goal I ever sought to achieve.

Finally, to my fiancée Kimberly Suessegger, whose love, patience, and support provided me with the strength to accomplish this amazing achievement. She picked me up as I went through the struggles and challenges of research and celebrated every achievement or hurdle passed as I finished my work. For having you in my life, I am forever grateful.

Table of Contents

List of Tables

List of Figures

Abstract

Development, Validation, and Assessment of a Multiple Model Structural Identification Method
Nathaniel Dubbs

The overarching aim of this thesis is to develop, validate and assess the value of a novel multiple model (MM) Structural Identification (St-Id) approach to inform decisions related to the preservation of critical infrastructures, such as long-span bridges. The approach developed employs: (a) heuristic knowledge along with various search and sampling techniques to generate populations of candidate models (composed of distinct parameter values, parameterization approaches and/or model forms), (b) various deterministic and probabilistic weighing approaches driven by a set of observed responses, and (c) simulations to estimate un-measureable attributes and their respective variability. To examine the value of this approach compared to conventional single-model methods, a multi-phase research program was carried out that included numerical applications, laboratory studies (using a physical grid model), and ultimately an application to an operating long-span bridge. In addition to numerous conclusions regarding the specific formulation and application of the approach, three principal conclusions were drawn. First, the proposed approach is capable of estimating the degree of non-uniqueness associated with the model-experiment correlation process, and thus provides important insight into the nature and reliability of the desired predictions. Second, the predictions produced by the method implicitly reflected the strength of the correlation between the observations and the desired responses. In addition, it was shown that the strength of this correlation could be amplified if proper mechanistic or heuristic-

based weighing schemes were employed. Third, the method was capable of identifying member “elastic” redundancy within a complex structural system through the estimation of the variability of member forces (which is a direct measure of the presence of multiple load paths). Using this approach, it was shown that the level of redundancy not only varies significantly from member to member within a large constructed system, but that redundancy can vary for a single member depending on the direction of the forcing function.

CHAPTER 1: INTRODUCTION

1.1. Background

This thesis is primarily motivated by the challenges associated with the analysis and assessment of aged long span bridges. Owners of such structures are currently forced into the management goal of indefinite preservation for many reasons including: political influence, alignment issues, historical relevance and potential loss of toll revenue during construction, which preclude out-right replacement. For example, the NYC DOT recently opted to spend $1.2 billion to rehabilitate the Williamsburg Bridge while it was in service as opposed to spending $700 million for a complete replacement (Diemer 2007). Given the complexity of these structures and the challenges associated with indefinite preservation, the typical design approach of leveraging conservatism to address the significant uncertainties is insufficient. Rather, owners and engineers tasked with maintaining the safety of such systems require a reliable and comprehensive understanding of the current performance and vulnerability of the system to make sound judgments regarding appropriate interventions.

Although the significant advances in simulation modeling, especially related to the finite element (FE) method, provide engineers with far better tools than the original designers of most long-span bridges had, the use of such models inevitably requires numerous assumptions and simplifications based on heuristics and intuition. Such assumptions include the selection of appropriate model resolution and model extent, dead load distribution (related to construction staging, past temperature events, etc.), numerous

continuity and boundary conditions, member geometric constants, material constants, among others. Given the level of uncertainty associated with these attributes, and their influence over the performance of the structure, simply aiming for a conservative estimate is not appropriate, as this typically leads to extremely expensive interventions that over the long-term would prove cost-prohibitive. Rather, in the case of existing long-span bridges, owners have begun to recognize the value of reliable performance information and are willing to pay a premium to obtain it if there is potential to reduce the cost of rehabilitation and preservation. That is, owners are increasingly opting to spend more on engineering services with the goal of eliminating, reducing or (at a minimum) better justifying the much large sums of money required for any intervention.

To obtain such information, the paradigm of Structural Identification (St-Id), which aims to estimate structural performance and vulnerability through the correlation of simulation models and experimental observations, has received increasing attention over the last decade. The St-Id process (Figure 1-1), which was first introduced by Liu and Yao (1978), begins with a conceptualization of the structure to inform the development of an a priori model and to identify influential sources of uncertainty. The model is then used to design various experiments, and ultimately correlated with the experimental data to reduce the identified uncertainties associated model (Mottershead and Friswell 1993; Aktan, Farhey et al. 1997; Moller and Friberg 1998). One common approach to performing the correlation between the model and the experiment is termed parameter estimation. In this approach, a subset of the unknown or uncertain parameters within the model are updated using optimization algorithms to minimize an objective (or error)

function (Mottershead and Friswell 1993). Once the parameters have been estimated to correlate the model with the experiment, the model is then generally considered calibrated and is used to estimate the desired performance or vulnerability needed to inform decisions.

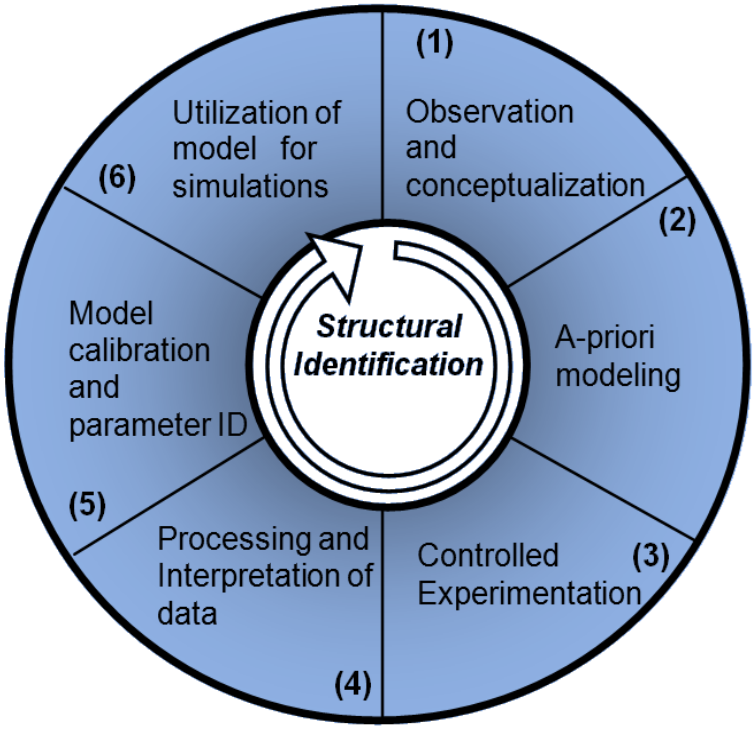

Figure 1-1: Structural Identification Process

1.2. Motivation

Given the definition of St-Id adopted above, it is illustrative to view St-Id as a tool to translate observable structural responses (e.g. strains, displacements, modal parameters)

into unobservable responses or attributes of a structure (e.g. location of critical regions, load carrying capacity, seismic vulnerability, etc.). This viewpoint is important as in many circles St-Id has been cast as a means to "calibrate" or "update" FE models without an explicit consideration of what the model will be expected to predict. Given the complexity of constructed systems together with the relatively low spatial resolution in which data is acquired, it is difficult to accept that a generic calibrated model capable of accurately predicting responses/attributes associated with a diverse set of performance limit states is possible.

This line of argument is supported by perhaps the most widely recognized challenge associated with St-Id: the inherent non-uniqueness of the process. In other words, many different models can be tuned to equally (or nearly equally) match experimental results/observations. Fundamentally, this arises for three reasons: (1) the number of uncertain aspects of the model is greater than the number of responses available (i.e. the problem is under-determined), (2) some of the uncertain aspects of the model have very little influence on the responses which are available from the experiment (i.e. a wide range of certain parameter values may equally or nearly equally match the experimental results, given the presence of noise or small error), and (3) several uncertain aspects of the model influence the available responses in a similar manner (i.e. they may compensate for one another).

While some have correctly pointed out that these limitations imply that one should avoid overly complex models that cannot be justified by the available data (as Beck and Yeun (2004) have shown through a Bayesian model selection framework), in practice this is difficult to do. For example, in most cases the goal of the application is to estimate

unobservable attributes (such as those listed above) that required much higher resolution models than may be uniquely identified due to (1) to (3). While various approaches to parameter selection/grouping and regularization may provide stability to the model updating problem, they do not mitigate the inherent challenges associated with non-uniqueness.

It is important to recognize that if one adopts the view of St-Id as a means of translation, then the inherent problem of non-uniqueness is not associated with the model, but rather with the predictions of the unobservable attributes/responses. That is, it would be unimportant if more than one model matches the experimental data/observations as long as they provided similar predictions of the desired unobservable response/attribute. For example, if both E and I of a beam were uncertain, but their product influenced both the observable responses and the unobservable attributes/responses in an equal manner, the inability to identify specific values for each parameter would be unimportant. This would occur if one measured displacement (e.g. $PL^3/48EI$) and desired to predict flexural strain (e.g. My/EI). This, of course, would not be the case if one measured displacement and desired to predict flexural stress (My/I). Unfortunately, in practice, cases where the former, "direct" translation is possible are rare. Typically the desired attributes/responses have complex relationships with the observable responses, and such relationships are often not intuitively obvious.

For example, it is somewhat common to use operational responses (e.g. ambient vibration) to help inform estimates of nonlinear responses (e.g. due to an earthquake). In this case many different models may match the observed 'elastic' modal parameters, but they may have very different force distribution patterns, and thus may result in very

different nonlinear predictions. There are many other such examples, but the important point is that in these instances talk of unique estimates is naïve; the critical question is related to the degree of non-uniqueness, i.e., what are the likely bounds of the desired attribute?

Given the non-uniqueness of the model updating problem, such a question can obviously not be answered by examining (or selecting) a single point within the model space, even if the point selected represents the "optimum" model (meaning the model that most accurately simulates the observed responses [whether in a deterministic or probabilistic manner]). Rather, to answer this question, a more comprehensive understanding of the model space is needed.

1.3. Objective and Scope

The aim of this thesis is to develop, implement, and assess the ability and value of a multiple model (MM) St-Id approach to quantify the degree of non-uniqueness within the model-experiment correlation process. This multiple model St-Id approach will aim to generate a large population of models to map out the model space and will examine to what extent such information is useful and distinct from conventional single model approaches for the estimation of desired attributes. Within the overall scope of St-Id, the term "model" can be assumed to represent a varied collection of information which is representative of some uncertainties within the structure. For example, a model could consist of many specific model forms, a set of uncertain parameters, varied spatial resolution of parameters, varied analysis approaches and varied model resolution. While all of these model types are possible for a given MM St-Id application, the scope of this

research will focus on models consisting of parameter values and varied approaches to spatial resolution of parameters.

To achieve this overarching goal, three primary objectives were adopted:

1. Investigate and validate shortcomings in model correlation to experiment including identifying primary challenges and their relevance to common applications
2. Establish and validate approach for quantifying non-uniqueness and quantifying vulnerabilities within Structural Identification using multiple models
3. Demonstrate with a case study, the application of the developed method to an actual constructed system, and compare with conventional single model approaches.

The objectives listed above were designed to assess the value of an advanced St-Id tool to incorporate modeling uncertainties, to develop and validate in a laboratory environment the framework of the tool and then finally implement the tool on an actual constructed system. Given the broad range of topics required for the development and implementation of the envisioned MM St-Id approach and the broad range of hazards and vulnerabilities relevant to the assessment of an actual constructed system, the research was organized into two interdependent phases, as described in the following subsections.

1.3.1. Development Phase Scope (Phase I)

i. Define the MM St-Id framework and demonstrate its capability with an example.

ii. Investigate the different manners in which the model space can be sampled and identify a strategy which best fits within the goals of the MM St-Id framework.

iii. Investigate the different manners in which the sampled models can be weighed with respect to how well they correlate with experimental observations.

iv. Investigate the ways in which the desired response predictions are generated for each of the sampling and weighing techniques used

v. Develop and implement each of the identified sampling and weighing schemes on a laboratory structure with well-known physical properties.

vi. Identify a single sampling and weighing best suited to an application within structural engineering and assessment of complex constructed systems.

1.3.2. Implementation Phase Scope (Phase II)

i. Identify and conceptualize a complex constructed system for use within the MM St-Id framework developed in the first phase.

ii. Construct an a priori FE model following best practice methods and identify a subset of hazards for preliminary analysis.

iii. Design and implement an appropriate experimental program aimed at mitigating a specific set of hazards

iv. Apply the developed MM St-Id framework from Phase I to the structure

v. Provide a set of recommendations on the use of MM St-Id on complex structural systems based on the results of this phase

1.4. Thesis Structure

The thesis is structured as follows:

Chapter 1 provides a brief background on St-Id and some of its limitations and shortcomings. A need for an advanced tool within a St-Id framework is demonstrated. The objectives of this thesis and the scope required to accomplish those objectives are presented.

Chapter 2 provides a comprehensive literature review of St-Id methods. The review documents research carried out in applications of St-Id to long span structures as well as laboratory structures. Additionally, advances in St-Id tools such as parameter estimation are documented. Finally, research similar in nature to that in this thesis is documented to establish the current level of work carried out using multiple models.

Chapter 3 defines and explains the generalized framework for the MM St-Id approach. The main shortcomings of traditional St-Id applications are discussed. The method is explained with the aid of a flowchart and a description of each step. The main areas of research carried out in subsequent chapters are discussed, such as the various ways of generating and weighing models.

Chapter 4 will discuss the identification and conceptualization of the structure used for verification and validation of the MM St-Id method. In order to develop and validate the MM St-Id method, the structure to be studied had to be simple enough to ensure that the fundamental principles behind the proposed method were sound, yet also needed to have the ability for increased complexity to ensure a seamless transition to more complicated

constructed systems. Additionally, the specimen needed to have significant uncertainties so that sufficient building blocks could be generated.

Chapter 5 will discuss the construction of a priori finite element models. An effective a priori finite element model is critical for multiple applications during the MM St-Id method. First, as with traditional St-Id applications, the finite element model is used for experimental design by investigating sensor locations and designing instrumentation layouts. Secondly, and unique to MM St-Id, a series of base models must be generated that will serve as the basis of the model population.

Chapter 6 discusses the design of instrumentation for the grid structure as well as presents results from those experiments carried out. In order to provide detailed and high quality information for the purpose of developing and validating the proposed MM St-Id method previously outlined, two main types of experimental measurements were designed for the grid structure. The first experimental program carried out was an in-depth dynamic impact test while the second experimental program consisted of an in-depth static load test of the grid.

Chapter 7 focuses primarily on the exploration of sampling and weighing strategies in addition to selection of measurement type, and provides a set of recommendations based on the comparison of these different methods. The chapter discusses deterministic, threshold and probabilistic approach methods to the MM St-Id framework. The chapter also explores the effects of increased structural complexity on the recommended method and discusses an investigation into the effects of measurement quantity. The chapter

concludes with a discussion on how well different types of experimental observations can predict other response indices and finally an overall conclusions and recommendations.

The focus of Chapter 8 is to investigate identified questions from Chapter 7 and to further validate the approach identified in Chapter 7 to a wider variety of complexity, limitations in measurements, types of measurements, and how to most effectively leverage the method to provide relevant predictions with respect to the observations used. This chapter is organized into four main sections: (1) Investigation into Increased Structural Complexity, (2) Investigation into Measurement Quantity, (3) Investigation into Selection of Observations, and (4) Investigation into Weighing Observations Based on the Desired Prediction

Chapter 9 introduces an advanced sampling methodology called Reversible Jump Markov Chain Monte Carlo (RJMCMC) which is able to not only generate models within a single a priori model framework, but any dimension a priori model. For example, one a priori model could have five model building blocks while another has twenty building blocks. The algorithm utilizes multi-dimensional calculus techniques to explore the variable dimension a priori model spaces. In addition to varying number of building blocks, the method also allows for the exploration of models with varying element types.

Chapter 10 discusses the history of the Burlington Bristol Bridge, how the relationship between Drexel University and the Burlington County Bridge Commission was developed, and why the bridge was selected for thorough health monitoring.

Chapter 11 discusses the conceptualization of the Burlington Bristol Bridge. The chapter discusses the various site visits required in the conceptualization process, collection of

structural documentation, development of geometric models, and identification of hazards and vulnerabilities.

Chapter 12 describes two a priori finite element models which were constructed for differing purposes. An initial a priori model was built in SAP2000 for the purpose of an initial load rating as well as for instrumentation design. The second a priori model was built in Strand7 and was the base model used for the MM St-Id application to the BBB. The section also discusses the selection of model building blocks and the sensitivity studies carried out on those building blocks.

Chapter 13 discusses the overall experimental program designed and implemented on the BBB for the purpose of structural health monitoring and for the purpose of informing models within the MM St-Id framework. The chapter includes discussions on a preliminary ambient vibration monitoring survey, the design, verification and implementation of load cell bearings, the design and implementation of a live load strain monitoring system, the design, verification and implementation of a laser-based height monitoring system for the movable lift span and finally the design and implementation of the full ambient vibration monitoring of the major spans of BBB.

Chapter 14 discusses the implementation of the MM St-Id on the BBB finite element model. The section discusses the sampling of model building blocks to generate the candidate model set and what the resulting predictions for a set of identified hazards were as well as what the predictions were for member strains due to a known load for direct comparison with the measurements from the top chord live load strain monitoring system.

Chapter 15 discusses the overall conclusions drawn from the research. Conclusions are presented based on the work discussed in Chapters 4 through 9 on the development and validation of the MM St-Id method in general, as well as conclusions drawn from the implementation of the approach to an actual constructed system, the BBB.

CHAPTER 2: LITERATURE REVIEW OF ST-ID

2.1. Introduction

The process of St-Id came to civil engineering from electrical engineering in the late 1970's, and has since been an active research area (Liu and Yao 1978; Aktan, Farhey et al. 1997; Yun, Lee et al. 1997; Moon and Aktan 2006; Catbas, Ciloglu et al. 2007; Catbas, Moon et al. 2008; Gul and Catbas 2008). St-Id is often described in six fundamental steps (Aktan, Farhey et al. 1997):

1.) Observation and Conceptualization – Identify the structure's structural system, critical load paths and force resisting mechanisms, likely vulnerabilities and hazards, history, available documentation, current usage, and owner objectives/scope.
2.) A-priori Modeling – Development of a first generation FE model for parametric studies to bound critical responses and identify key sensitivities.
3.) Controlled Experimentation – Design and implementation of an appropriate experimental approach, instrumentation plan, sensing systems, etc. through a cost-benefit assessment associated with the type and resolution of data needed for the model calibration
4.) Processing and Interpretation of Data – Error screening, filtering, averaging, signal modeling, etc. to extract key responses and response indices that may be interpreted using heuristics and the results of the initial parametric studies.
5.) Model Correlation – The correlation of an FE model (typically the one developed in Step 2) with the processed experimental data through either

heuristics-based approaches such as trial and error, or more formal approaches such as parameter estimation.

6.) Utilization of Model for Simulations – The estimation of vulnerability and/or performance through the use of the correlated model. In many cases this is done through the use of parametric studies to identify the influence of remaining sources of uncertainty.

One of the most challenging components of St-Id is the task of model correlation. The general process of model correlation, typically done via parameter estimation, is an iterative one that incorporates the following fundamental steps:

1.) Experimental Data Preparation – As necessary, prepare the extracted data in a way to best formulate the residue vectors in the objective function
2.) Parameter Selection – Define appropriate parameters or groups of parameters which represent uncertainties within the model and which can be updated, and assess whether such parameters are identifiable.
3.) Objective Function Selection – Define an objective function which expresses the difference between calculated values and experimentally determined responses in a relevant manner
4.) Optimization Algorithm Selection – Choose an optimization algorithm or algorithms to best minimize the objective function
5.) Analysis – Carry out the updating process

6.) Quality Assurance / Corrective Measures – Justify the results of the updating process. Test for ill-conditioning in the updating process. Apply corrective measures as necessary and repeat process.

Given the discussion in Chapter 1, it is clear that some fundamental challenges related to a priori modeling and St-Id continue to plague applications. Although in many ways the literature related to parameter estimation is less than satisfying as it does not directly mitigate these challenges, it has proven useful and is currently enjoying increasing attention by the practicing population, especially for long-span signature structures.

The general process of parameter estimation outlined above has attracted the attention of numerous researchers for decades (Mottershead and Foster 1991; Mottershead and Friswell 1993; Friswell, Mottershead et al. 2000; Teughels 2003; Jaishi and Ren 2005; Pan 2007; Živanović, Pavic et al. 2007). The most significant advances made in the past twenty years in Civil Engineering have come from new and improved methods of preparing/processing experimental data for inclusion in the parameter estimation process, new formulations of error/objective functions and new optimization algorithms. Also, the emergence of powerful software tools such as FEMTools and Matlab's Optimization Toolbox (Mathworks 2008; Dynamic-Design-Solutions 2009) provided researchers with unprecedented capabilities in updating complicated models. This chapter intends to review the most recent advances and current state of the art in parameter estimation and multiple model analysis, and the format will be such that the process is described in the order which the various approaches/decisions must be implemented/made by an engineer during an application. Since parameter estimation falls within the fifth step in the overall

St-Id procedure described by Aktan (1997), it is assumed that a “reasonably-correct” a-priori model is constructed and that field experiments have been executed to best capture the fundamental properties of the structure to be identified.

2.2. Model Experiment Correlation

2.2.1. Available Experimental Data

Long span bridges are not only challenging in how they are inspected and modeled, but they also pose a great challenge in experimentally capturing global structural characteristics. Perhaps the most common experimental approach to characterize bridges is static testing, which include measuring strain, displacement and rotation due to a known applied load. For short span structures, this type of testing is adequate in capturing global response indices, however for long span bridges this type of testing is not reasonable (Catbas, Ciloglu et al. 2007). Primarily, long span structures lack a reference frame for accurate displacement measurements and experience rather large ambient vibrations due to their flexibility which cannot typically be overcome by static loading. This poses a serious problem because it essentially limits any displacement type measurement to using GPS sensors, which are still a developing technology in terms of their application to high resolution displacement measurement. Without displacement measurements, static testing would be forced to rely heavily on strain measurements, which tend to capture more local effects than overall global characteristics. Given the resolution of models that are feasible for such massive structures, such localized information is of little value within the parameter estimation process.

As a result, most St-Id of long-span structures focus on dynamic experimental techniques, which are typically separated into forced vibration testing and ambient vibration monitoring. The main difference between the two methods is that in forced vibration testing the input is supplied by the experimentalist and known spatially and quantitatively, thereby allowing the full transfer functions to be obtained. Unfortunately, in the case of long-span bridges, the amount of input energy needed to sufficiently excite the structure to overcome the large ambient vibrations has proven too expensive and difficult to implement in practice. When such tests are used, they are typically relegated to examine a small portion (or substructure) of the overall system, such as floor systems, member dynamic response, etc. Although such tests may be useful in certain circumstances, they are unable to provide analysts with global response measurements, which are most useful for the resolution of models used for long-span bridges.

As a result of the shortcomings of static testing and forced vibration testing, the most common technique to capture global response indices of long-span structures is ambient vibration monitoring. The main drawback of this approach is that the source of excitation is not measured so the full transfer function cannot be formed. The type of loading typically applied to the structure includes traffic, wind, and seismic events, which provide excellent global excitation, but both their frequency content and spatial distribution are essentially impossible to reliably capture. Through proper experimental design and instrumentation, a sufficient set of global parameters can be calculated for the use of model updating. The most common type of structural indices used for model updating of

long span structures are the eigenfrequencies, λ, and respective mode shapes, Φ (Mottershead and Foster 1991; Mottershead and Friswell 1993; Moller and Friberg 1998; Catbas and Aktan 2000; Brownjohn, Xia et al. 2001; Catbas and Aktan 2002; Brownjohn, Moyo et al. 2003; Jaishi and Ren 2005; Gul and Catbas 2008). There are fundamental assumptions made through the process of vibration monitoring and data processing that must be understood and tested for validity, if possible, before utilizing these global parameters. Some of the key assumptions in modal analysis are listed in Table 2-1.

Table 2-1: Assumptions required for modal analysis

Linear structural system
Time-invariant
Broadband input
Observable system

A linear structural system is a key assumption in most structural analysis and dynamics applications, however it is also listed as a key uncertainty as previously described. Regardless, it is still anticipated that the assumption of a linear structural system most closely approximates the actual conditions. As also seen previously in the list of uncertainties, the second assumption is that the structure is time-invariant. This is more important to consider over the duration of experimentation, and must be accounted for in the experimental design. For instance, it would not be wise to monitor vibration characteristics during a season when the temperature is drastically changing from one day to the next because the structure might respond differently. It is also assumed that the structure is observable, or that enough measurements are made to appropriately and

accurately calculate the modal properties. The assumption of broadband, or random, input is also important in analyzing the data because it is assumed that all of the structural modes are equally excited.

2.2.2. Updating Parameter Selection

After the ambient vibration test and subsequent extraction of response indices (such as modal parameters (φ_{ij} and ω)), the uncertain parameters to be updated in the model must be chosen. The two main types of parameter updating are direct matrix updating and sensitivity-based updating. These two methods differ greatly in their application and eventual output.

Direct matrix updating includes those methods which calculate mass and stiffness matrices directly from the equations of motion and experimental data (Friswell, Inman et al. 1998; Teughels 2003; Pan 2007; Yang and Chen 2009). The main drawback with the direct method of updating models is the lack of physical understanding at the end of the updating process. Also, any errors in the measurement data are directly transferred into the updated model since variability in the experimental data is neglected. Methods were explored to update the stiffness and damping matrix directly, however positive definiteness and connectivity could not be guaranteed (Friswell, Inman et al. 1998). Even in constraining the bandwidth of the updated mass and stiffness matrices, researchers could not justifiably produce physically meaningful results from direct updating (Yang and Chen 2009).

Sensitivity-based updating is a much more common approach in civil engineering applications due to the reasons mentioned above as well as for consideration of FE model size. In the sensitivity-based method, there are many different types of analytical approaches outlined in great detail (Mottershead and Friswell 1993; Teughels 2003). Essentially, the process involves iteratively updating a group of parameters until the discrepancy of the experimental and calculated properties is minimized. These parameters are typically geometric or material properties of the model. The shortcoming of the sensitivity-based method is that an exact solution is not always reached, and that ill-conditioning can lead to major uncertainty in the updated parameters. Ill-conditioning refers to a poorly defined optimization problem due to many factors such as the inclusion of too many parameters or low signal-to-noise in experimental data, and will be discussed in further detail in Section 5.

The first step to take in beginning the iterative model updating process is to choose which types of parameters are to be updated. The elastic modulus, Poisson's ratio, material density and member thickness are all typical material and member parameters to update (Mottershead and Friswell 1993). There has also been much research into updating damage as a parameter (Doebling, Farrar et al. 1996; Sohn and Law 1997; Zhao and DeWolf 1999; Catbas and Aktan 2002; Teughels, Maeck et al. 2002). Damage is typically modeled as a multiplication factor of the bending stiffness, EI, and incorporated as an updateable parameter. Researchers also use spring constants at various boundary conditions or connections in attempts to account for stiff rollers or partially rigid

connections (Sanayei, McClain et al. 1999; Brownjohn, Moyo et al. 2003; Sanayei, Bell et al. 2006; Pan 2007; Živanović, Pavic et al. 2007).

Not all material or geometric properties are ideal for model updating. There are two major rules that must be enforced in selecting updateable parameters (Mottershead and Foster 1991; Teughels 2003; Pan 2007):

1.) All parameters must have uncertainty

2.) Parameter must influence the model

For instance, choosing the elastic modulus of steel as the parameter to be updated is highly questionable. Although it may greatly influence the model, it is essentially a deterministic quantity and thus it is difficult to justify anything but extremely small modifications (Pan 2007). Conversely, if a concrete girder is being modeled and it is decided that its elastic modulus is going to be updated, it will be justified due to the variability in concrete properties. Although some parameters that are deterministic do not serve as ideal updating candidates, they may serve as good indicators of a poorly constructed FE model (Moon 2009). For instance, if the mass distribution factor $\bar{m}$ is being updated, and the results tend to distort the known mass distribution then it may be concluded that the model has significant errors, which may be diagnosed using the type of distortion observed. . Similarly, if E is updated for a steel beam and it increases 50% then there could be an underestimation of stiffness in the member.

The second requirement of an ideal candidate for an updateable parameter is that it must influence the response which is being compared to the experiment (Figure 2-1). This

usually requires sensitivity analysis to be carried out on a set of predetermined parameter candidates. This will not only select the most sensitive group of parameters, it will subsequently reduce the chance for ill-conditioning within the model by reducing the number of total parameters.

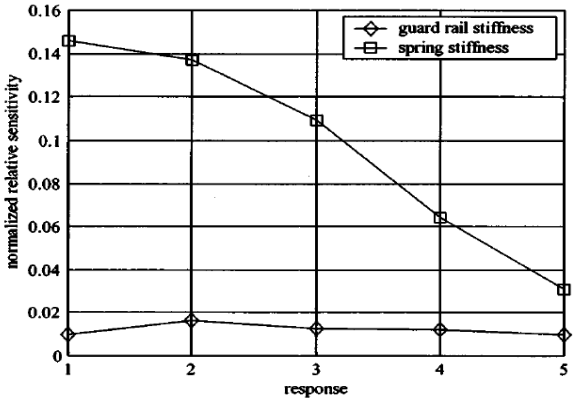

Figure 2-1: Sensitivity Diagram for Two Parameters showing one with Significant Influence while the other is Relatively Ineffective (Brownjohn 2003)

2.2.2.1. Sensitivity Analysis of Parameters and Parameter Identifiability

When performing the sensitivity analysis on candidate parameters, there are generally three major types of analyses to carry out (Teughels 2003, Pan 2007, and Brownjohn 2001). The first is a "one-at-a-time" approach (Catbas et al 2007), which is implemented exactly as its name suggests. The parameters are all held constant except for one candidate, which is varied over the range of its acceptable bounds. The model output (which will be compared to the experimental results, e.g., frequencies and/or mode shapes) is then plotted versus the percent change in the parameter so that all units are

consistent for comparative purposes. This process is repeated for all proposed parameter candidates, and then the total parameter sensitivity plot is prepared for analysis.

The second type of analysis used to identify which of the candidate parameters is most suitable for model updating is the Two-level Factorial Orthogonal Design of Experiment process described by Pan (2007). The described method is very effective in examining not only one parameter's influence on the model, but multiple parameters and their coupling/collective influence on the model. The effect of multiple parameters acting together can sometimes be more substantial than the effect of each parameter changing solely (Pan 2007). The method is based off of Design of Experiments, and is not frequently referenced in any other structural model updating applications, as most use proprietary software for this purpose (Brownjohn 2000).

A further refined approach to selecting the updateable parameters is to apply the criterion of identifiability. In order for a set of parameters to be classified as identifiable, it must satisfy two conditions. The first is that the model is sensitive to the parameters, determined by the above methods. The second condition for identifiability is that effect of a subset of the parameters cannot cancel out the effect of the remaining parameters in the total set (Brun and Reichert 2001; Brun, Kuhni et al. 2002). Parameter identifiability is typically seen in probabilistic updating approaches in structural engineering applications (Katafygiotis and Beck 1998; Vanik, Beck et al. 2000; Beck and Au 2002; Cheung and Beck 2009). For example, if one were to update both elastic modulus and moment of inertia simultaneously, then there would be an infinite number of combinations that

would provide the same response estimates because in deriving the stiffness matrices, E and I are multiplied together.

2.2.2.2. Parameter Grouping

Once a set of identifiable parameters is defined, then parameter grouping may be explored to reduce the quantity of parameters to update in the optimization process. This is done by assuming a group of parameters vary according to a defined relationship. Typically EI for a structure is updated for damage detection by using damage functions, which are a form of parameter grouping (Doebling, Farrar et al. 1996; Brownjohn, Xia et al. 2001; Teughels, Maeck et al. 2002; Teughels 2003; Teughels and Roeck 2004; Teughels and Roeck 2005; Sanayei, Bell et al. 2006; Pan 2007). These functions assume some variation of EI over the structure. It is the magnitude of variation in the function that is updated, not every element's EI term. For an example, see Figure 2-2. In this case 28 elements are reduced to 7 damage elements. It is assumed that the stiffness varies in a linear piecewise manner, and the coefficients of each function are updated. Then the reduction of each original element is calculated through interpolation of the damage elements.

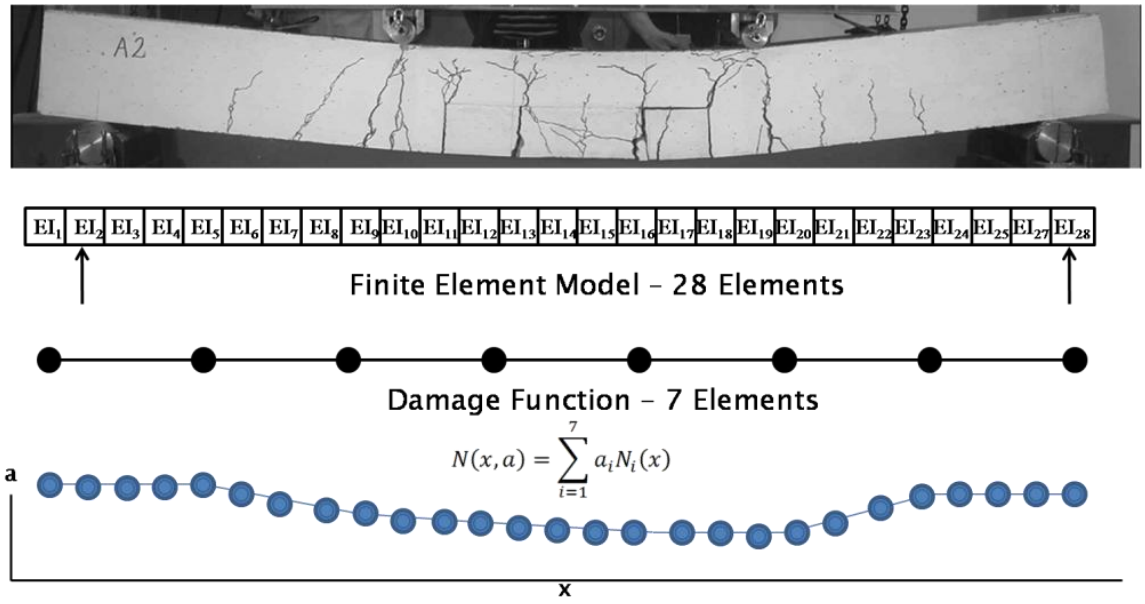

Figure 2-2: Damage functions used to group different values of EI.

Parameter grouping does not always have to include damage functions, and can be viewed in much more simplistic terms. For example, the properties of a certain material used in the model may be updated similarly for all instances of that material. In a similar manner, the weight of a uniformly distributed but uncertain system component such as paint could be updated assuming a constant applied thickness over the entire structure.

2.2.3. Objective Function

There are two general approaches to formulating objective functions, which define the goal for the optimization process: deterministic and probabilistic. The former uses discrepancies between experimental data and calculated response to create a function to

be minimized by the updating of a select group of parameters. Probabilistic updating also uses discrepancies between experimental and calculated data; however it uses laws of probability to maximize the likelihood that a model is correct. For deterministic approaches, it is assumed that the experimental data is perfect and free of uncertainty or that it has a fixed error (e.g. 4%). Along with the data, the model can either be assumed to be free of error, or account for modeling uncertainties described by Moon and Aktan (2006) as aleatory and/or epistemic. Aleatory uncertainty includes those introduced by the inherent randomness of the model and its parameters while epistemic uncertainty is influenced by a lack of knowledge of the structure or mistakes in the structural model.

2.2.3.1. Multi-objective Functions

Multi-objective functions are typically seen in design applications (Lounis and Cohn 1993; Cheng and Li 1997; Wei and Yuying 2008), however, they also have applications in St-ID (Christodoulou, Ntotsios et al. 2008). The goal of multi-objective functions is to find a compromise, defined as a Pareto subset of models, which satisfies each of the objective functions optimally (Barroso, Takahashi et al. 2007). Then each model is assigned a set of Pareto estimators, which are used in a second optimization run which minimizes the Pareto subset to find the model which best fits the data and constraints. This is a very effective method when there are two distinct objectives, such as optimizing strength and serviceability while minimizing cost. Pareto optimization techniques have been used with global optimization methods (Cheng and Li 1997), explained later, allowing for a robust calculation of the optimal solution.

2.2.3.2. Deterministic Approach

The deterministic approach is a commonly used formulation for the objective function. It is a fairly straightforward concept, however does not account for variability in experimental data and uncertainty in the FE model. Nonetheless, it is still powerful in updating large models. In St-Id of long span bridges, the common parameters measured through experimentation are natural frequencies and modeshapes, as described previously. Therefore, only objective functions which use these quantities will be studied. The first objective function shown is the most commonly used in St-Id (Eq. 2-1).

$$r_f(\theta) = \frac{\lambda_{ANA} - \lambda_{EXP}}{\lambda_{EXP}} \qquad \textbf{Eq. 2-1}$$

The next four objective functions all are relationships of the experimental mode shapes to analytical mode shapes (Eq. 2-2 through Eq. 2-5). They utilize mode shape coefficients, the Modal Assurance Criterion (MAC) values (Allemang 2003) or Normalized Modal Difference (NMD) values (Teughels 2003).

$$r_f(\theta) = \frac{\varphi_{ANA}}{\varphi^r_{ANA}} - \frac{\varphi_{EXP}}{\varphi^r_{EXP}} \qquad \textbf{Eq. 2-2}$$

$$r_f(\theta) = 1 - MAC(\varphi_{EXP}\varphi_{ANA}) \qquad \textbf{Eq. 2-3}$$

$$r_f(\theta) = \frac{\left(1 - \sqrt{MAC(\varphi_{EXP}\varphi_{ANA})}\right)^2}{MAC(\varphi_{EXP}\varphi_{ANA})} \quad \textbf{Eq. 2-4}$$

$$r_f(\theta) = NMD(\varphi_{ANA}, \varphi_{EXP}) \quad \textbf{Eq. 2-5}$$

Weighting coefficients may also be assigned to the various residue vectors. Typically, weighting coefficients are incorporated to place emphasis on the most reliable components of the residue vector. Due to the difficulty in generating clean experimental mode shapes because of their influence by noisy data, they are typically weighted lower than the much more reliable eigenfrequencies. Aside from influencing which modal parameter is to be updated, weighting factors are also used to enforce the modal order of a model output as compared to the experimentally determined order. By enforcing modal order, the updating process will converge on a solution which captures the correct relative order of longitudinal, lateral, bending and torsional stiffness.

One challenge in formulating the objective function, especially in the case where modal order is enforced, occurs when a mode shape and frequency are not captured experimentally. This could greatly influence the updating process since the objective function would either attempt to enforce a natural frequency and mode shape that is absent in the collected data (leading to an infinite penalty and an ill-conditioned problem), or alternatively ignore the missed mode by omitting it from the error function formulation.

2.2.3.3. Probabilistic Approach

A separate approach to optimizing an FE model to fit experimental data is to maximize the probability that the model is correct. The most common probabilistic approach uses a Bayesian statistical framework (Sohn and Law 1997; Beck and Katafygiotis 1998; Vanik, Beck et al. 2000; Zhang and Mahadevan 2000; Gurian, Castro et al. 2004). This method utilizes Bayes Theorem in calculating the posterior probability, $P(\theta|\tilde{z})$, of the updated model. A distribution is assigned to each parameter, known as the prior distribution ($P(\theta)$), which may or may not be informed (for uninformed priors, all models are considered equally likely). Then the likelihood function $P(\tilde{z}|\theta)$ is calculated for the given set of parameters and incorporated in the objective function below (Eq. 2-6).

$$P(\theta|\tilde{z}) = \frac{P(\tilde{z}|\theta)P(\theta)),}{\sum P(\tilde{z}|\theta)P(\theta))} \qquad \textbf{Eq. 2-6}$$

The probability of the parameters is multiplied by the likelihood function (probability of the data given the model estimate using the set of parameters θ), which forces the optimization process to select only parameters which have a high probability. This feature of the probabilistic objective function takes into account parameter variability and penalizes the optimization process for selecting parameters which may have unrealistic values (e.g. a lack of physical meaning or consistency), such as updating the elastic modulus of steel to a value that is half of the well-established property. The product of the likelihood function and the parameter probability is then divided over the entire parameter space and their respective likelihood functions to generate the a posterior

probability ($P(\theta|\tilde{z})$), which is the probability of the parameters given the experimental data. This is the value which is then maximized through the optimization process (Beck and Au 2002; Beck and Yuen 2004; Ching and Beck 2004; Cheung and Beck 2009).

2.2.4. Updating Algorithm Selection

In order to minimize the defined objective functions, an optimization algorithm is needed. There are countless optimization algorithms available for researchers to use. Teughels (2003) and Pan (2007) both provide exhaustive reviews of the analytical methods available as well as their benefits and shortcomings. The updating algorithms most commonly used for civil structures fall into one of two main categories: Gradient Based and Non-Gradient Based. Gradient based algorithms utilize the slope of the objective function to estimate parameters which minimize the objective function in the quickest fashion. Therefore, the various gradient based methods typically travel "downhill" as they search the objective function surface for a minimum. Non-Gradient Based methods attack the minimization problem in a probabilistic manner. They seek the minimum over a large surface usually by leveraging multiple search points and correlating their output at each time step. The two methods each have their unique contributions and downfalls in the model updating process (discussed below)

2.2.4.1. Gradient Based Minimization Algorithms

The most commonly used gradient based, or local, optimization algorithms used in St-Id can be classified under the Inverse Eigensensitivity method (Sanayei, McClain et al.

1999; Friswell, Mottershead et al. 2000; Modak, Kundra et al. 2002; Teughels 2003; Teughels and Roeck 2005; Pan 2007). This method encompasses nonlinear least squares (Gauss-Newton Method), the most common overall updating algorithm, as well as the Newton-Raphson method, a root-finding technique. The nonlinear least square methods minimize an objective function by calculating the gradient of the objective function surface in iterative steps. The solution is sought by following the path of steepest descent until convergence is reached. The Newton-Raphson method seeks a minimum by iteratively updating an initial guess of the abscissa and optimizing for the root of the equation.

2.2.4.2. Non-Gradient Based Updating Algorithms

One of the major shortcomings of local optimization algorithms is that the solution may get "trapped" or appear to converge at a local minimum. This could lead to the identification of unrealistic parameters, and therefore an unreliable updated model. In an effort to prevent this from happening during the model updating process, non-gradient based, or global, algorithms were developed to search the entire objective function surface for global minimums. This could be a computationally expensive task; however three main algorithm types have emerged, which establish means of locating global minimums in an efficient manner:

1.) Genetic Algorithm (GA) (Holland 1975)
2.) Simulated Annealing (SA) (Kirkpatrick, Gelatt et al. 1983)
3.) Coupled Local Minimizers (CLM) (Suykens, Vandewalle et al. 2001; Teughels 2003; Teughels and Roeck 2005)

These methods are becoming more popular in updating civil structures, and are evolving with improved computing power and sampling methods (Levin and Lieven 1998; Koh, Hong et al. 2000; Modak, Kundra et al. 2002; Franco, Betti et al. 2004; Teughels and Roeck 2005; Gul and Catbas 2008). GA and SA each simulate a natural process in an effort to make more informed parameter choices at successive iterations. CLM utilizes synchronization constraints to allow for communication between multiple start points. The method constrains the problem so that each start point has to converge to the same minimum, thereby minimizing the chance of becoming trapped in local minima.

2.2.4.3. Local vs. Global Optimization

In choosing an optimization method, one must investigate the pros and cons of global and local methods. Local optimization methods allow for a fast convergence rate and accurate calculation of the minimum; however they can easily get trapped in local minima. Global optimization is a much more robust method and always finds the global minimum regardless of the starting position. However, the cost comes in high iterations of the objective function and inaccuracies in the local regions. This may be avoided with the combination of global - in finding the area of the minimum - and local - in converging on the accurate solution. In this hybrid optimization scheme, both methods find very accurate solutions of the global minimum.

2.2.5. Parameter Identification Challenges and Mitigation Strategies

One of the main sources of error which can arise in model updating is ill-conditioning of the problem in various steps. This can arise from noise in the data carried through into the solution, as well as ill-posed weighting vectors, inappropriate selection of algorithms and ill-conceived constraints (Sanayei, McClain et al. 1999; Friswell, Mottershead et al. 2000; Brownjohn, Xia et al. 2001; Teughels 2003; Živanović, Pavic et al. 2007). It can be difficult to locate the source of ill-conditioning; however there are accepted means of localizing the errors or eliminating the source of ill-posedness. The first potential error is having too many parameters, in which case the solution would be to incorporate damage functions or other grouping strategies to reduce the total quantity. Typically, similar material properties or connections are grouped together to eliminate competing terms, described in the next section.

Another potential error is that the optimization algorithm itself may be inappropriate for the type of problem being solved. Local and global methods must be explored for potential respective contributions. For instance, global optimization techniques may be used first to identify regions of global minima, while local optimization methods would then be used to find an accurate location of this minimum. This would eliminate one of the main drawbacks of local optimization algorithms, which is becoming trapped in local minima.

Also, the optimization may be diverging based on the nature of the objective function and the selected algorithm. Poorly defined constraints or penalty functions may be limiting

the problem to a region where there are no minima, in which case it may be beneficial to impose less restrictive constraints or penalty functions on the problem. Last, regularization may be incorporated to control the rate the solver is searching the minimum at and to prevent ‘over-fitting’, or converging on a solution heavily influenced by noise (Friswell, Mottershead et al. 2000). Regularization penalizes for over-complexity, and enforces a smooth, or regular, solution surface.

2.2.5.1. Quality of updated parameters

At the end of the optimization process, careful attention has to be paid to the updated parameters and what information they are conveying. In some of the few cases where model updating has been carried out on long span structures the updated parameters do not always make sense. In some cases, the selection of parameters seems it would lead to an ill-conditioned problem by updating competing parameters (such as updating the elastic modulus and moment of inertia simultaneously). This is unreasonable because the stiffness of the structure is based off of the quantity EI. E and I can then update to an infinite number of solutions, but still have the same product. This is not only computationally expensive, but will result in a physically meaningless model and serves as an example of the definition of an unidentifiable problem (Katafygiotis and Beck 1998; Brun and Reichert 2001; Brun, Kuhni et al. 2002).

The basis for characterizing the quality of the updated parameters relies heavily on the heuristics of the engineer optimizing the model. Additionally, probabilistic updating methods can be used to generate the updated probabilities of the parameters which are

direct indications of the variability. Also, engineers need to impose realistic constraints or bounds on parameters to prevent unrealistic parameter updating.

As seen throughout the paper, there are many challenges and sources of error within the process of parameter estimation. However, some of the greatest challenges arise when the model is updated with a set of "identified" parameters and the engineer needs to make decisions based on the output of the model. In structural engineering, models are typically used to estimate capacity and load ratings, as in the Burlington Bristol Bridge research study. However, by calibrating the model to dynamic data, what is the measure of uncertainty with estimating static response indices? This is one of the shortcomings of the current model updating approaches. For long span structures, experimental data is limited to ambient vibration monitoring for global response assessment. One of the driving questions of current research asks, "Is this enough information to update a single model with a unique set of parameters?" Currently, the answer is, "No".

2.2.5.2. Non-uniqueness

One of the major challenges within parameter estimation is deterministically obtaining a unique set of parameters which provides a single optimal solution. This is no simple task, as it is common to find many combinations of parameters which yield similar levels of success in minimizing the objective function. Currently, most research is focused on obtaining a single, 'correct', model to be used for various load rating and analysis problems; however this can lead to poor management decisions. For instance, the Burlington-Bristol Bridge case study illustrated two unique models and corresponding

sets of parameters which similarly matched the experimental data. However, these models told drastically different stories of how the bridge was performing according to current load rating techniques.

Probabilistic methods hold the greatest potential for addressing the issue of non-uniqueness; however some researchers recognize that there has been no application to real structures. St-ID is a necessary process in evaluating the performance and health of our infrastructure, yet the process is still not providing engineers with sound decision making tools. With the addition of multiple model methods and advanced probabilistic approaches, St-ID may be able to be transformed into a viable tool for decision making and risk management for owners of long span structures.

2.2.5.3. Inferring Unobservable Responses from Observable Responses

As previously discussed, there is a major lack of understanding in estimating unobservable properties or responses (e.g. load ratings, capacities, remaining life, etc.) of a structure from observable responses, which are limited to ambient vibration measurements in the case of long span bridges. There currently is no way to assess the quality of inferred properties of a structure from a model updated with a certain level of success to observed measurements. This disconnect is critical in evaluating the structural performance of aged long span bridges, since static measurements are often unobtainable and must be assumed to be correct based on the level of success of the calibration. A method of evaluating the feasibility of unobservable responses is clearly needed.

2.3. Multiple Model Structural Identification

Although the challenges associated with parameter estimation have received significant attention over the last few decades, the equally important challenge associated with model selection has been largely ignored. This lack of attention was pointed out by Beck and Yeun (2004) who developed a Bayesian model selection framework that implicitly penalizes overly complex models that cannot be justified with the available data. More recently, Smith and his colleagues have begun examining the use of multiple models within the St-Id process to alleviate some of the arbitrary decisions associated with model selection. In general, this novel approach generates hundreds of FE models in an automated manner and then down-selects a set of 'candidate' models based on an error threshold (Robert-Nicoud et al. 2005, Smith and Saitta 2008, Kripakaran and Smith 2008, Goulet et al. 2010). There are many implications of this approach related to all aspects of St-Id including experimental design (including iterative designs), model selection, experiment-model correlation and decision support.

While the approach presented in this paper is founded on the work of Smith and his colleagues, it has a significant distinction in that it is not concerned with selecting the best model or in fact selecting any particular model. Rather the proposed approach focuses exclusively on trying to estimate structural attributes or responses that are not directly observable, and particularly, to estimate the degree of non-uniqueness associated with such estimates. That is, the proposed approach aims to assess to what degree certain response observations can inform the estimation of different responses or structural attributes. The specifics of the approach are presented in the following section.

2.4. Discussion on St-Id

St-Id can be viewed as a tool to translate observable responses, such as accelerations, strains and displacements, into estimates of unobservable attributes, such as safety factors, seismic vulnerability, etc. In different applications of St-Id since its inception in structural engineering, the goal of obtaining a calibrated model has been done with little regard to the effect that the process has on predictions, only with how well the analytical model matches the experimental measurements. However, given the complexity of constructed systems and the generally sparse data acquired, it is difficult to accept that a single model calibrated with limited data is capable of reliably predicting responses or attributes associated with a wide variety of performance limit states. This arises from the widely recognized challenge associated with St-Id: the inherent non-uniqueness of the process. There can be many different models calibrated with similar levels of accuracy to experimental data; however the variation in prediction of un-measureable responses is not very well understood. Non-uniqueness can occur for several different reasons: (1) the problem is underdetermined, meaning that there are more model uncertainties than measured responses, (2) the problem suffers from ill-conditioning, meaning that the uncertainties associated with the model are not sensitive to the measured responses and (3) several model uncertainties are inter-related and influence available responses in a similar manner by compensating one another. While different parameter estimation approaches have been incorporated in the St-Id process to stabilize the first two challenges (regularization, parameter grouping, model reduction etc.), they have either not been able to mitigate them altogether or end up creating a model which is unable to generate the desired predictions (through oversimplification).

CHAPTER 3: INTRODUCTION OF MULTIPLE MODEL METHOD

Structural Identification (St-Id), as described in Chapter 2, can be defined conventionally as developing reliable estimates of structural vulnerability and performance by tuning an analytical model to match experimental observations. In this thesis, St-Id is viewed as a tool to translate measurable responses into desired unobservable responses or attributes. In light of this viewpoint, non-uniqueness is not necessarily associated with the model but with its corresponding prediction. If many models are similarly calibrated to experimental data, it is unimportant what the values of the uncertainty are if they each provide similar predictions of the desired responses. For example, if both E and I of a structure were uncertain, but their product influenced the observable and unobservable responses similarly, then it would be unnecessary to determine the specific values of E and I. This would occur if one were to measure displacements and predict strains, both of which are functions of the product EI. However if stress, a function of I alone, was predicted then many different values of predicted stress would be equally as likely since a specific value of I is now required. Instead of attempting to determine a unique value of the uncertain model parameter, the critical question is related to the degree of non-uniqueness, or what bounds, exist on the desired responses.

To address the challenges and questions associated with single model St-Id, a novel multiple model method is introduced to provide insight into the degree of non-uniqueness associated with desired estimates of vulnerabilities or response indices. The approach aims to address these issues by generating large populations of a priori models, and quantifying the effects of model uncertainties on structural vulnerabilities through

correlation to available experimental measurements. The methodology associated with the multiple model approach will be described in this chapter in addition to a discussion on the benefits associated with the method.

3.1. Introduction to the Multiple Model Method

The multiple model method utilizes a seven step process (Figure 3-1), which has similarities to the classic St-Id method described in Chapter 2 but differs greatly in its specific approach and results. The method will briefly be described here, but the remainder of this chapter will focus on a more thorough explanation and then a discussion on how the method will be developed and validated.

The method begins by identifying the structural vulnerabilities of interest (settlement, corrosion, member failure, etc.) as well as the modeling uncertainties, defined as model building blocks, to be incorporated into the study (boundary condition effects, material properties, model resolution, etc.). The structure also has to be conceptualized in terms of its geometry and key mechanisms.

A priori models are then generated to assist in experimental design, after which models are then regenerated and subsequently weighed based upon the experimental observations. Once a set of weighed candidate models is generated, response prediction distributions corresponding to the desired estimates of vulnerability are produced and used in calculating the risks associated with the specific vulnerability identified at the

beginning of the process. This thesis will specifically focus on Steps 1, 2, 5 and 6 in the development stage.

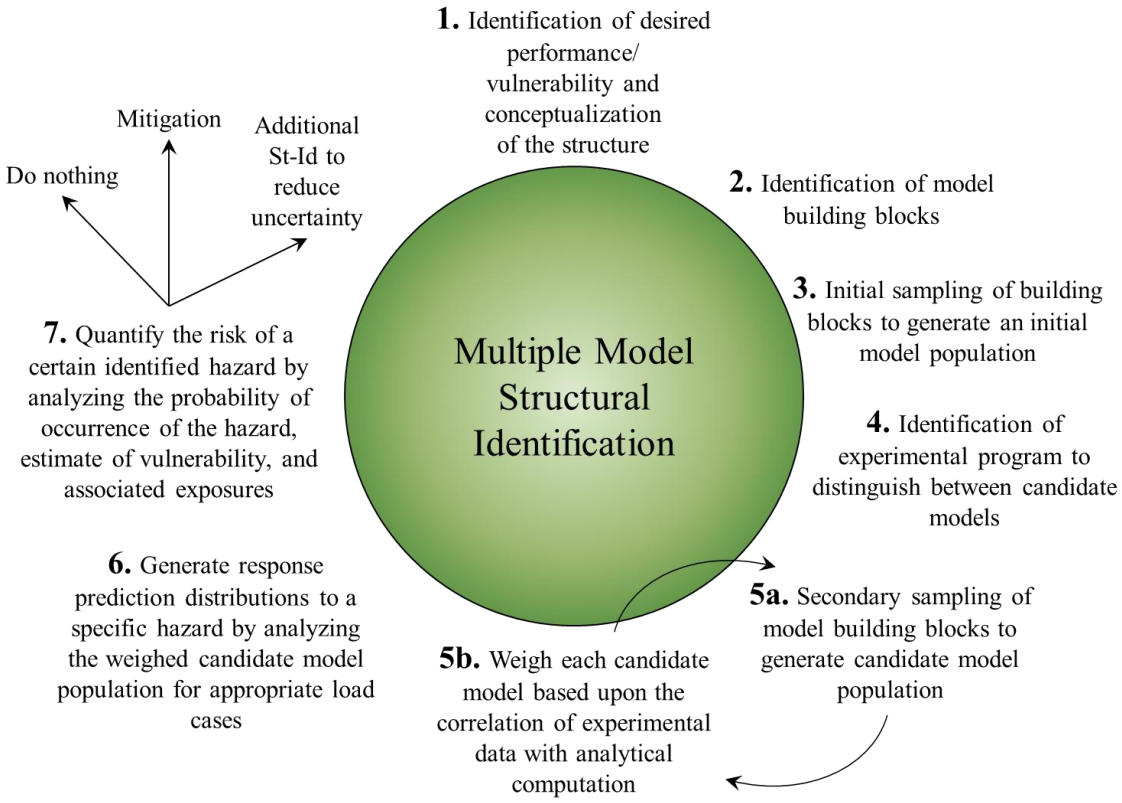

Figure 3-1: Proposed multiple model method (Moon 2008)

3.1.1. Demonstration of the Method with an Example

To better illustrate the steps of the method outlined above, a simple example is shown in this section and the corresponding results of each step are shown for a more clear understanding of the overall framework. This guiding example consists of a cantilevered

beam structure and was selected for its inherent transparency in terms of structural properties and predicted responses.

3.1.2. Conceptualization and Hazard/Vulnerability Identification

As described above, the process begins with the selection of desired performance or vulnerabilities to be studied as well as the conceptualization of the structure. It is important to have a detailed understanding of the structure, so that relevant and meaningful hazards and vulnerabilities can be identified. The conceptualization of a structure includes gathering as much existing information as possible regarding the performance, operation, construction, and maintenance activities. It is critical to the success of the entire method that the structure is conceptualized appropriately so that key mechanisms that have uncertainty associated with them are not underestimated. For large constructed systems, this step requires a great deal of cooperation with the infrastructure owners, as all information must be provided upfront.

Examples of necessary information to obtain include: original design and as-built drawings, any design and as-built drawings for subsequent rehabilitation efforts, maintenance logs, inspection reports and load rating analyses. In addition to collecting the above information, it is also important to verify key structural attributes such as geometry and to identify the characteristics of the structure in its current state. For the simple cantilever structure example, the conceptualization consists of a geometric representation of the structure is shown in Figure 3-2.

Obviously, this step for a large constructed system is quite vast in nature; however the simplicity of the example is solely to demonstrate the method. The conceptualization of this cantilever structure includes the determination of such characteristics which are necessary for physics-based modeling, including the elastic modulus of the material (E), the moment of inertia of the cross-sectional shape (I), and the mass density of the material (ρ).

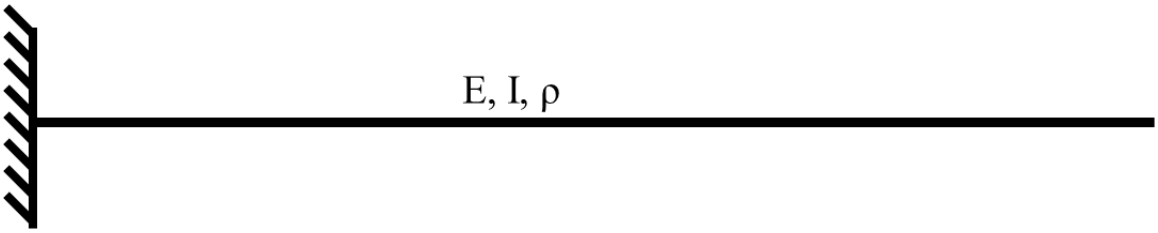

Figure 3-2: Conceptualization of the Cantilever Structure

After the structure has been appropriately conceptualized, a list of key hazards and vulnerabilities must be generated. A hazard for a transportation infrastructure could vary from a ship impact of a critical element to the routine application of salt during winter months to prevent roadway icing. Once a set of hazards is identified, then corresponding vulnerabilities must also be identified. For a ship impact, a corresponding vulnerability could consist of the loss of a critical member. For the hazard of application of deicing salts during winter months, the associated vulnerability could consist of the corrosion of structural members of a floor system. Finally, the exposures corresponding to the

combination of the vulnerability and hazard are to be identified so that a quantification of risk can be obtained, defined as the product of the probability of the hazard, probability of the vulnerability given the hazard and the resulting exposure. If a ship were to impact a given span and cause the loss of critical members such that structural collapse was imminent, then corresponding exposures could include the cost of replacing the structure and the human lives lost or injured during the collapse. It is also important to note that it is fairly common practice to elicit expert opinion in identifying the hazards, vulnerabilities and exposures.

There are clearly many more hazards, vulnerabilities and exposures (the development of such a list for a constructed system is shown in Chapter 11), however for the sake of this example the hazard will consist of a 100 pound vertical point load at the tip of the cantilever, and the associated vulnerabilities of interest are defined as the tip displacement and the stress and strain within the member at the base of the cantilever.

3.1.3. Identification of Model Building Blocks

The second step described in Figure 3-1 is to identify the multiple model building blocks. The success of the method depends on appropriate selection of model building blocks, defined as any uncertain choice a user makes in the construction of an a priori FE model. A set of five model building block classifications was developed to assist users with ensuring that all appropriate sources of uncertainty are incorporated within the process. The first model building block classification aims to identify uncertainties at the material property level. Uncertainties such as elastic modulus and mass density would fall within

this category. The second classification aims to identify uncertainties associated with continuity conditions within the model. Uncertainties such as degree of composite action between stringers and roadway deck elements would fall within this classification.

The third classification of model building blocks aims to identify uncertainties associated with boundary conditions. Degree of support fixity, soil stiffness properties and the decision of pin/roller or somewhere in between all would fall within this classification. A fourth classification aims to identify uncertainty in the spatial resolution of model building blocks. If a gusset plate connection stiffness is identified as a source of uncertainty within a model and is identified as a model building block, is it most appropriate to smear all typical gusset plate connections within the model to a single building block, or do multiple patterns of spatially representing the building block exist? This lack of knowledge in an a priori sense would fall within this classification of model building blocks and can be explicitly included within the method. The fifth model building block classification proposed within this section represents the uncertainty associated with element selection and overall model form. When constructing a model for a given structure, is it more appropriate to represent a certain element with frame elements, shell elements or solid elements? This uncertain decision can explicitly be incorporated within the MM St-Id process.

For the guiding example, a finite element model consisting of beam elements was created using manually developed software within MATLAB , a computational software framework. In order to represent the physical structure, beam elements must have properties assigned to them such as unit density per length, moment of inertia and elastic

modulus. A set of three model building blocks was identified to represent key uncertainties in analyzing the cantilever structure finite element model. Two model building blocks were identified at the material level and consist of the elastic modulus of steel, and the moment of inertia of the member cross section. For this example, an HSS tube was assumed to be the member cross section, and due to fairly high allowable tolerances in fabrication of the wall thicknesses, it was deemed appropriate to account for the uncertainty associated with the moment of inertia. Finally, a third model building block was selected at the boundary condition level as the rotational stiffness of the support.

3.1.4. Initial Sampling of Model Building Blocks

After defining the model building blocks and vulnerabilities of interest, the building blocks are sampled to create an initial model population. The models are generated using heuristics and design of experiments. For example, the value of a model building block must have bounds assigned, using heuristics, and an initial sampling of the building block might consists of a full factorial design of experiments approach where all possible combinations of building block values are realized. Considering this is an initial sampling of the population, it is thought that a small, evenly spaced, number of samples per parameter is used.

For the cantilever structure example, the model building blocks needed to be conceptualized within the model and defined analytically. To represent the elastic modulus of steel, a normalized model building block was generated. This normalized

value, with bounds defined from zero to two, represented the deviation from the well-defined elastic modulus of steel of 29,000ksi. Similarly, the moment of inertia of the cantilever was represented by a building block which normalized the value of the inertia by its nominal value according to manufacturer specifications. This model building block was also defined over the bounds of zero to two, meaning that the moment of inertia could feasibly be twice as high as its nominal value or almost fully reduced (while these bounds may seemingly be unrealistic, once again this example is for demonstrative purposes). Finally, the model building block representing the degree of rotational stiffness of the support was represented as a rotational spring within the finite element model and was allowed to vary between 0% and 100% rigidity.

Once the initial sampling is generated, the population will be analyzed and used to design an appropriate experimental program so that candidate models can be sufficiently distinguished. Methods that have been proposed to accomplish this step in the MM St-Id process include K-Means and Principle Component Analysis (PCA) (Moon 2008). It is envisioned that any data exploration tool used to produce the most efficient experimental program is also acceptable.

3.1.5. Experimental Program

Using the developed experimental program, the user must then acquire the desired structural response data. This step must also involve heuristics and informed users, since deploying unnecessary instrumentation and labor can be expensive and incapable of contributing to the success of the method. It is essential that an appropriate data

acquisition scheme is carried out and that all methods are consistent with current best practice standards available. For the example cantilever structure, it was decided (without any a priori model analysis due to the nature of the example) that a forced impact test would provide sufficient characteristics about the cantilever structure in order to appropriately inform the desired estimates of vulnerability. The impact test would consist of four accelerometers spaced evenly along the length of the cantilever, providing sparse estimates of modeshapes. The results from the hypothetical forced impact dynamic test on a cantilever beam are shown in Table 3-1 and Figure 3-3 below for demonstrative purposes.

Table 3-1: Observations of Natural Frequencies for the Example Cantilever Structure

Mode 1	2.8 Hz
Mode 2	17.4 Hz
Mode 3	48.6 Hz

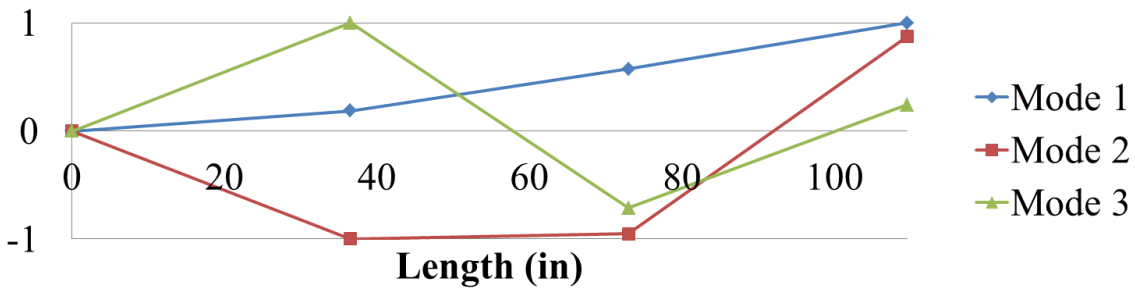

Figure 3-3: Observed Modeshapes of the Example Cantilever Structure

3.1.6. Model Building Block Sampling and Weighing

The model building blocks, previously identified, are then resampled and weighed based on their ability to correlate with experimental data. It is feasible that many types of model space sampling schemes are possible for application to the MM St-Id technique. In this thesis, three major sampling schemes are explored for application to the method and are discussed in detail in Chapter 7. The techniques include a deterministic sampling approach, where all model building block samples are defined by the user, a threshold sampling approach where probabilistic sampling techniques taking into account user defined uncertainties are applied, and fully probabilistic sampling where Bayesian probability theory is applied. The various techniques explored in Chapter 7 are defined at the end of this chapter.

The models must also be weighed with respect to their correlation with experimental data. In some sampling schemes, weighing of models occurs simultaneous with the sampling, as seen when using Monte Carlo Markov Chain probabilistic methods. When the models are weighed, a measure of how well a given model matches the experimental data is made, whether it is a deterministic or probabilistic function by nature. After all models within the candidate population are analyzed and weighed, the predictions for each model are also weighed by its respective weighing factor and a response distribution is generated. The practice of sampling and weighing the models, given the various approaches introduced, is discussed and explored in detail in Chapter 7 and constitutes a major contribution of this thesis to the development of the MM St-Id approach.

To continue the guiding example, probabilistic methods for sampling and weighing the models within the candidate model space were utilized. A program was developed to automatically generate new samples from each of the building blocks, analyze the finite element model for the observed responses and weigh the model according to the correlation between the finite element analysis prediction and observed quantities. Finally, the models were analyzed for the desired estimate of vulnerabilities and response prediction distributions were generated. Given the experimental data observed and the model building blocks incorporated into the process, the ability of the candidate model population to represent the physical observations made (natural frequencies and modeshapes) was explored to determine the success of the method in characterizing the model space. The weighed response predictions were organized into histograms for visualization purposes of this example, and are seen in Figure 3-4 and Figure 3-5.

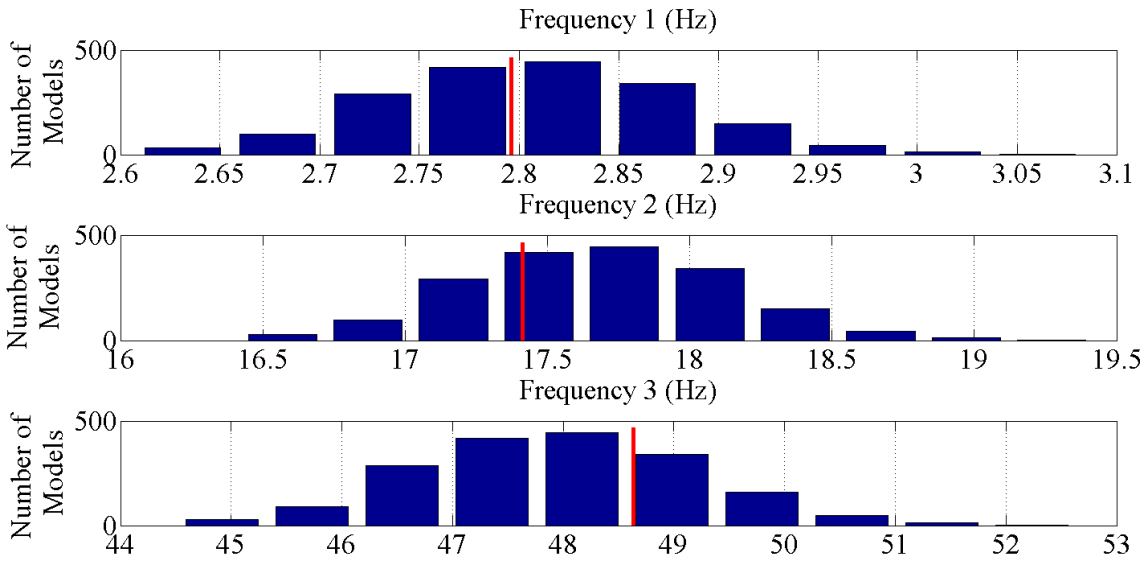

Figure 3-4: Histograms Representing Weighed Model Predictions of Observed Data

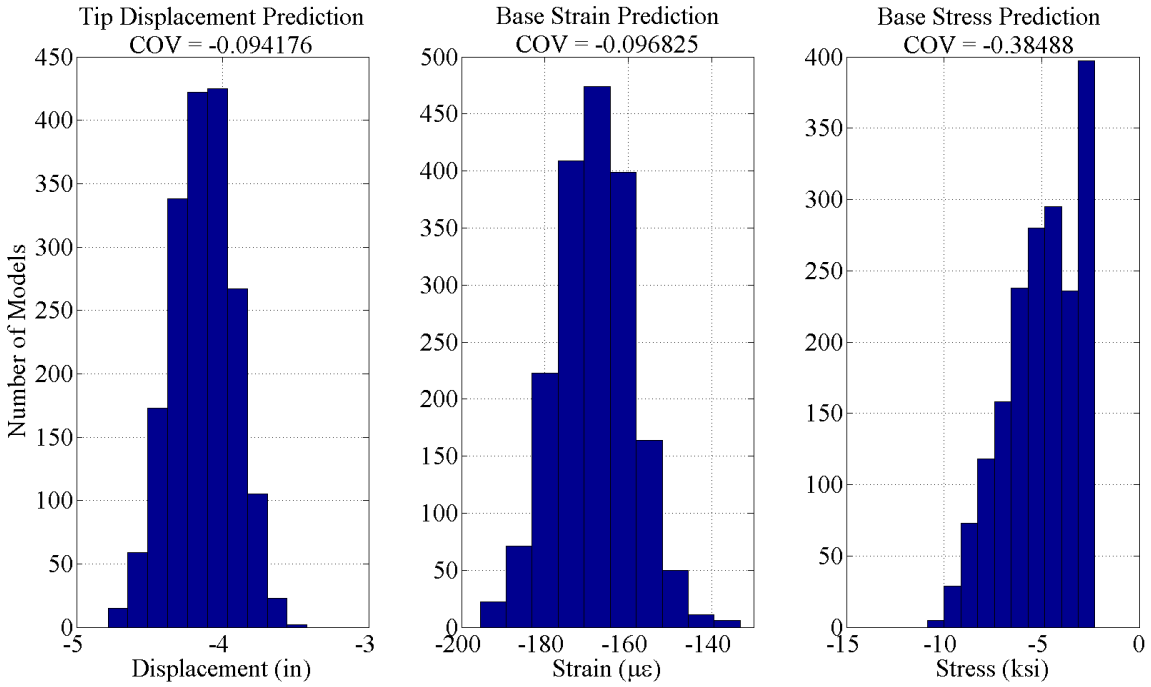

Figure 3-5: Histograms Representing Weighed Model Predictions of Displacement (l), Strain (m) and Stress (r)

While the analytical methods used to generate the results are discussed in detail in Chapter 7, 8 and 9, care will be taken to explain and discuss the results presented above so that the reader can appreciate the insight provided by the MM St-Id approach. First, the ability of the method to produce a candidate model population which is representative of the structure at hand is critical. To do this, the distributions of frequency predictions for the first three modes of the cantilever were plotted against the observed value (shown as the vertical line). In the case of all three frequencies, the sampling scheme was able to produce a candidate model population which was representative of the physical structure, due to the observed value being near the mean of all three distributions.

The value of the MM St-Id method does not lie in the identification of the uncertain parameters, but in the quantification of the uncertainty of unknown structural responses. In the example, the tip displacement and base strain and stress were identified as the unobservable response indices of interest to be estimated by the MM St-Id approach. In Figure 3-5, the coefficient of variation for each of the histograms, defined as the standard deviation of the candidate model population response prediction divided by its mean, is shown. While the quantities of the histograms are not relevant since this is a fictitious scenario, the characteristic of the response predictions is still very relevant and highlighted by comparing the coefficient of variations (COV) for the three distributions.

The displacement and strain prediction distributions have similar levels of COV and directly reflect the uncertainty explicitly incorporated within the process. However, the COV of the stress prediction roughly four times that of the other response predictions, essentially rendering the analysis useless as little information was learned. While seemingly obvious, a clear benefit of the MM St-Id method was demonstrated with this example. In this case, both the elastic modulus of steel and moment of inertia of the member were selected as model building blocks. The natural frequencies, tip displacement and strain are all functions of the stiffness of the cantilever, or in other words of the product *EI*. However, stress is only a function of *I*. The prediction of stress was compromised because the model building blocks utilized did not inform the desired responses as it did the observed data. While it is generally not good practice to include both *E* and *I* for a given structure within a model updating routine, it was in this case to demonstrate the ability of the method to clearly show the inability of the observed data to

reliably predict stresses due to a static load, given the included model building blocks. For more complex structures, these types of model building block interactions may not always be so intuitively obvious, as in the case of those chosen in this example, so the ability to directly incorporate that uncertainty within the response predictions provides a vast amount of information to the analyst. If such predictions were acquired in a real world application, it would be apparent that the model building blocks were not chosen appropriately, or that more information is required to reduce the uncertainty with that specific prediction. In traditional St-Id this contribution is not currently available.

3.2. Discussion

When the concept for an analytical approach is being conceptualized, it is always important to compare the new method to existing methods to determine whether the time and effort spent in development and validation will be worthwhile. To that end, two sections will address the MM St-Id method outlined above in comparison to traditional St-Id methods reviewed in Chapter 2.

3.2.1. Why is MM St-Id Different than Traditional St-Id?

The main goal of both traditional St-Id and MM St-Id is to develop a prediction of vulnerabilities and/or structural performance capabilities by leveraging model-experiment correlation. The main difference between the two methods is that where traditional St-Id aims to produce a single, optimal model capable of both matching experimental data and predicting desired response indices, MM St-Id addresses an acknowledged shortcoming

in traditional St-Id, non-uniqueness, and aims to develop not only estimates of desired response indices based on how well modes are correlated with experimental data but also what degree of non-uniqueness is associated with the translation from observed response to unobservable structural attribute. In the case of traditional St-Id, it is rarely seen that the model most likely in terms of observed data is able to produce the most likely unobservable response prediction. This inability was experienced by the author over the course of various St-Id implementations and shown in this thesis. Additionally, due to advanced techniques discussed with the thesis, MM St-Id approaches allow the analyst to not have to decide on the spatial resolution of building blocks or even model form. While the two methods are founded on the same principles of structural conceptualization, model construction, experimental techniques and parameterization, MM St-Id is able to specifically address a key shortcoming with the St-Id process. The two approaches are different not only in their approach to model-experiment correlation but also in their applicability at the end of the process. While traditional St-Id produces a single model for prediction purposes, the population of models generated with the MM St-Id method lends itself to further analysis within a risk assessment framework.

3.2.2. Benefits and Drawbacks of the MM St-Id and Traditional St-Id Methods

While MM St-Id addresses a main shortcoming in the traditional St-Id method, there are still anticipated downfalls to the MM approach. The main detractor to the method is the need to analyze a population of models and the potential for exceptionally long analysis times. While the method development will explore the most efficient sampling methods applicable to the method, it is still envisioned that thousands of models will need to be

generated. However, technology advancements will only improve the method, and not out-date it, with improved computing power and increased abilities to solve analyses on clusters of machines.

An area where traditional St-Id is more appropriate than MM St-Id is in the need for complicated analytical solvers such as time history, nonlinear and other solvers where many iterative steps are taken for each solution. However, while it might be unrealistic for the MM St-Id approach to include time history analyses at each model execution, the method can be used to develop likely ranges of uncertain building blocks. For example, these ranges can then be used to formulate two models to run with the long analysis corresponding to the model with the likely prediction of a low response and one model with the likely prediction of a large response, so that an expected range of results can still be achieved.

3.2.3. Influence of Missing Mechanisms

In light of the example of the MM St-Id method above and the comparison to traditional St-Id approaches where parameters are manually perturbed, it is critical to note that MM St-Id does not replace the need for qualified structural engineers to use the analysis tool. In fact, the method can distort the results, often unbeknownst to the analyst, if care is not taken in identifying the mechanisms within the model being analyzed as well as the structure being represented. The best way to be able to identify the most critical and influential mechanisms within a structure and model representation is through experienced engineers running the process.

To highlight this point, an example was developed to compare what happens to response predictions when a critical model mechanism is intentionally left out in comparison to when it is included. The same cantilever model discussed above was once again utilized for this demonstration, however in this case the "experimental" configuration consisted of a finite rotational stiffness at the base of the cantilever, equal to EI/L. Two cases were then analyzed: (1) one building block representing the elastic modulus of steel, and (2) two building blocks representing the elastic modulus of steel and the rotational stiffness at the base.

The MM St-Id process was applied to each case as was done in Section 3.1. In the first case, with the missing model mechanism, the response predictions for the tip displacement and strain at the base are shown in comparison to the experimental values in Figure 3-6. It is seen that while the tip displacements were still able to be characterized in the presence of the missing mechanism, the strains were incredibly inaccurate from the experimental value. This is because the analysis became biased in the presence of the missing mechanism and distorted the value of the elastic modulus, thus resulting in a distorted prediction of the base strain. In the analysis, the updated elastic modulus of steel was decreased by almost 10%, which is very unrealistic given our knowledge of its value.

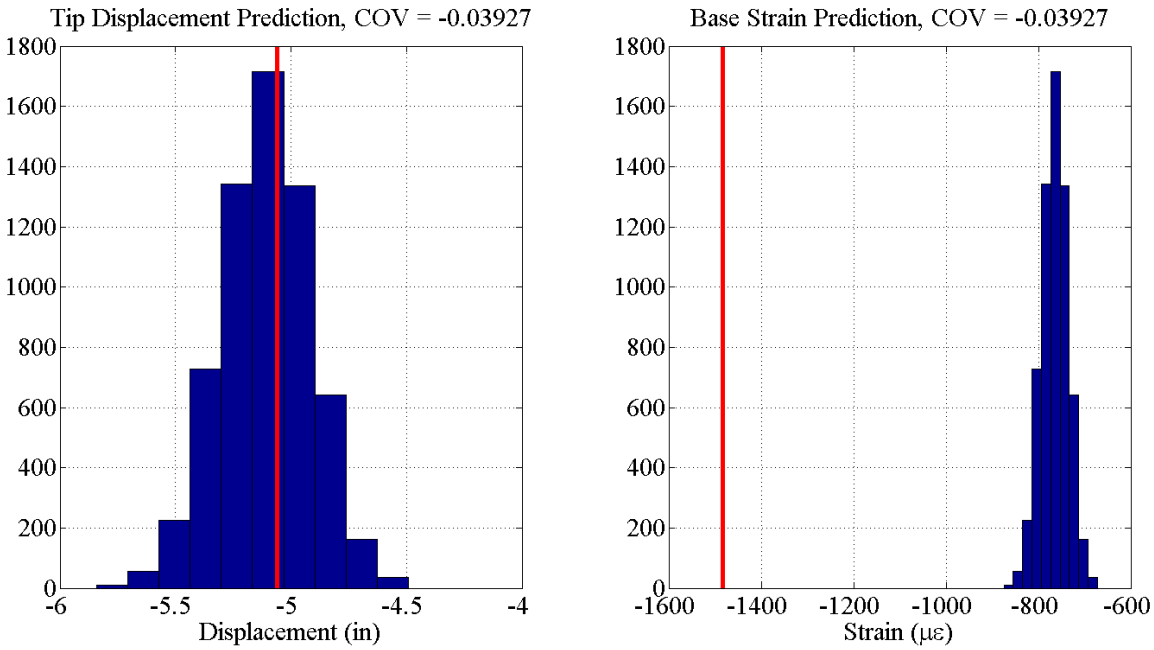

Figure 3-6: MM St-Id Analysis with Missing Mechanism

When the same analysis is run, however the rotational spring is included within the process, the results are much different. When including the main mechanisms of the model and the structure, the response predictions now become much more accurate for both the displacements and the strains and the updated value of the elastic modulus of steel was centered on its well-known value of 29,000ksi. The response predictions, shown in Figure 3-7, indicate the increased accuracy by acknowledging the presence of the rotational spring as a critical mechanism.

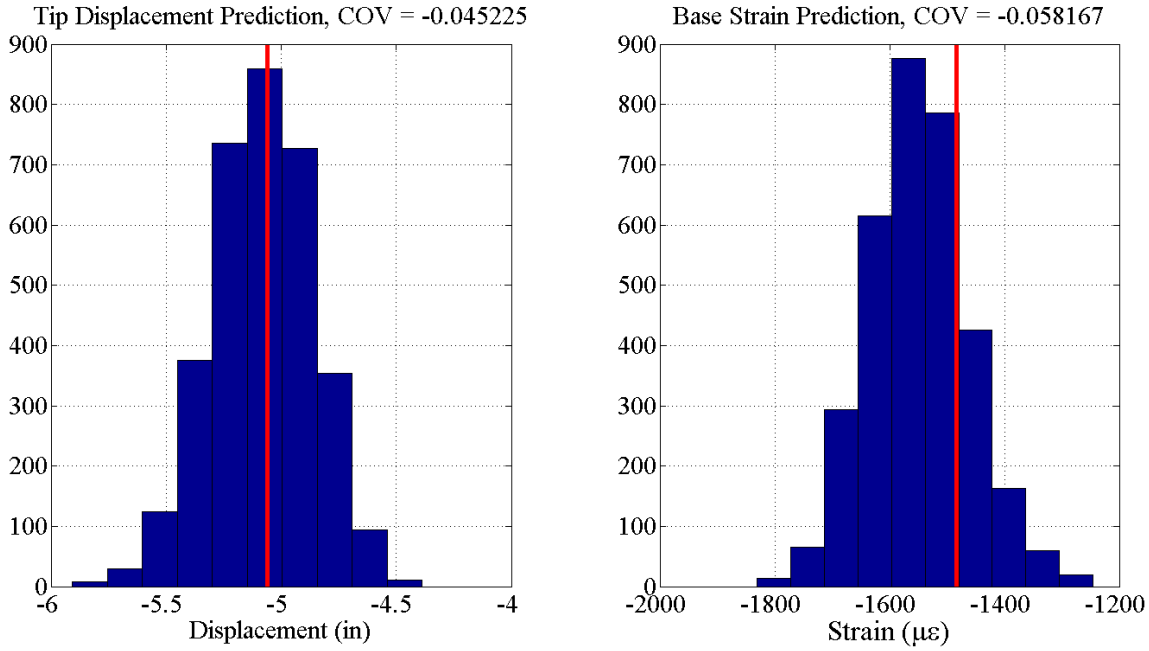

Figure 3-7: MM St-Id Analysis with Mechanism

It is critically important that an experienced structural engineer is always utilizing the MM St-Id tool, as with any St-Id application. The example shown within this section clearly demonstrates the danger in not including fundamental mechanisms within the process, and although seemingly obvious in this case it is not expected to be so obvious when analyzing more complex models and structures.

3.2.4. A Discussion on Building Block Covariance within the MM St-Id Method

In the MM St-Id process, it is conceivable that multiple model building blocks exhibit a strong correlation or covariance, meaning that as long as they either are sampled most often in the same manner (strong positive correlation), or in the opposite manner (strong negative correlation). This phenomenon could be demonstrated by selecting both the

elastic modulus and the moment of inertia as model building blocks. Since natural frequencies and displacements depend on the product of EI, as long as the building blocks are sampled in a negatively correlated fashion, the product EI will not change significantly. In traditional parameter estimation approaches, this would present a challenge and would be detrimental to the approach because it is of the interest of those researchers to identify the updated values of the parameters. However, a clear distinction to be made is that it is the interest of the MM St-Id method to identify predictions of desired responses.

With that in mind, it is not important if strong correlations exist between parameters, as long as their net outcome affects the desired prediction in the same manner. However, when this is not the case, then the building block correlation will cause the response prediction distribution of the stress to be broad in nature. This would occur when trying to predict stresses, a function of I alone, when sampling E and I of a structure. In traditional St-Id approaches, this building block covariance or correlation is not readily identifiable. The analyst is provided with a single prediction for stress, when in reality the St-Id approach could not reliably identify an accurate prediction for that response, unbeknownst to the user. The strength of the MM St-Id approach is in explicitly incorporating these challenges identified within St-Id, not only to provide more accurate predictions but to provide more honest predictions representative of the uncertainty in the process.

3.3. Plan for Developing and Validating the MM St-Id Approach

This chapter has focused primarily on defining the framework of the MM St-Id method. The main research contribution of this thesis is the development and validation of the method, so this chapter will conclude with a discussion on the steps taken in exploring options within the method and what steps serve as the focus of this thesis.

3.3.1. Development of Test Bed (Design of Experiments)

The objective of this task was to generate reliable structural response measurements to be used for weighing and validation purposes. The success of any St-Id exercise is completely dependent on the accuracy and representativeness of the acquired data. This is even more critical in light of the use of the acquired data in this phase. Since it is necessary that the MM St-Id approach is to be validated using this data, best practice methods must be enforced in the design and execution of the experiments. The main forms of structural response measurements obtained include static and dynamic testing to capture flexibility response indices (displacement, strains) as well as frequency and respective mode shape content. A specimen was selected that reflects some of the challenges associated with constructed systems however remain reliably identifiable so that the validity of the proposed approach can be fairly assessed. The specimen chosen for this purpose is the Drexel Institute of Intelligent Infrastructure's grid structure. The grid will be discussed in much greater detail in Chapter 4.

3.3.2. Investigation into Model Building Blocks

The most fundamental step in the MM St-Id is the selection of building blocks. It is in this step that the model space is populated by defining ways in which the model can change. In its most simplistic form, a model building block can simply be a parameter of the model, such as elastic modulus. This is considered a *low level* building block, since it does not require any change in the physical construction of the FE model. *High level* building blocks are more complicated and aim to cover the region of the model space where user input or preference plays a role. For example, the FE model of a truss could be assumed to be sufficiently characterized with a 2D plane frame analysis. In other aspects, a solid-element, fully three-dimensional model may be considered as the most appropriate. The benefit of the MM St-Id approach is that this bias uncertainty is directly incorporated by including analysis of all major model forms as well as spatial resolution of model building block techniques.

The objective of this step is to identify only the most critical building block forms necessary to carry out an appropriate analysis. It is unreasonable to assume that the set of building blocks that is most appropriate for one structure is the best set of building blocks for all structures. An informed and aware user is going to have to select the set of building blocks that best represents the desired vulnerability being estimated.

Another challenge associated with model building block selection is the ability to know when a critical building block is not included. The inability to appropriately cover the model space could have far reaching effects on the desired prediction of vulnerability. A set of recommendations to screen the MM St-Id analysis for sufficient building block

inclusion is going to be necessary. A preliminary idea to address this challenge, and to be later addressed in further detail, includes utilizing deterministic parameters, such as the elastic modulus of steel. Since this parameter has a well-known mean and variance, it can be used for truth checking the updated results. If the updated distribution of the elastic modulus indicates a different mean or increased variability, then a flag will be raised and the user will need to study the model for specific building blocks that may not be represented sufficiently. While other methods may exist, such as using training and validation datasets, the focus of this thesis concentrates on the fundamentals and development of the method. This among other topics identified as being improvements upon the work presented in this thesis will be discussed in Chapter 11.

3.3.3. Sampling Methods

The next step following building block selection is to generate a suite of candidate models by sampling the building blocks. The selection of an appropriate sampling scheme has direct implications to the success of the overall method. If the sampling technique cannot efficiently and effectively sample the building blocks, the results will be meaningless or wasteful. For example, in the Bayesian expression for posterior probability (Eq. 3), the denominator requires the integration of the product of the likelihood estimator and the prior probability of *each* model in the population. As structures become more complicated and the number of building blocks grows, the efficiency of the sampling technique is paramount. A set of common sampling schemes has been selected for investigation into their ability to efficiently sample within this application:

3.3.3.1. Deterministic Sampling

This sampling technique is the most basic and computationally expensive. A set of samples is manually selected (often by selecting bounds and evenly- spaced samples within the bounds) through a Design of Experiments Full Factorial approach, each possible combination of building blocks is evaluated. The major disadvantage associated with this technique is the computation required for large numbers of parameters. As additional building blocks are added, the total number of iterations grows exponentially. For a model that takes 5-10 minutes to analyze, this could mean months if not years of analysis time. The benefit to this approach is the direct control over how the building blocks are sampled, and the one benefit seen from this sampling technique is the ability to investigate, in the validation stage, how well other sampling techniques sample the building blocks as compared to the deterministic case. This is in fact the intended approach for validation of the MM St-Id method. The first analysis will be run with a thorough deterministic sampling scheme, and more refined sampling approaches will be utilized from there and compared with the deterministic sampling results.

3.3.3.2. Monte Carlo (MC) Sampling

Monte Carlo sampling (Anderson 1986; Metropolis 1987; Mosegaard 1995) was developed within the Manhattan Project by scientists looking for ways of computing average distances neutrons travelled into various substances. The approach required the generation of large amounts of random numbers, and with the development of computers in the 40’s and 50’s pseudo-random number generators became more widely used in the fields of physics and mathematics. Through the years, many physical events have been

simulated using Monte Carlo methods; some as simple as simulating a coin flip or roll of the die to integration of complex multi-dimensional surfaces. By evaluating random points for their contribution to the integral, the estimation of the entire integral can be achieved by dividing the sum of these function evaluations by the number of samples. In the long run, this estimate of the expected value of the integral will converge on the actual solution.

Also, MC methods can take advantage of assumed prior distributions and draw samples directly from them. There has been a great deal of published research on random number generators and how to select randomly from a defined distribution (Gelman, Carlin et al. 1995; Chen, Shao et al. 2000), and modern advances in computer technology has allowed researchers to easily generate large quantities of random numbers with the push of a button.

It is envisioned that MC methods can be used to follow up deterministic sampling approaches to see how many MC samples it takes to converge on the results obtained by the deterministic method. One shortcoming of this approach is that the success of any given sample is not taken into account to produce the subsequent sample, and that samples which produce poor correlation with experimental data always have equal probability of being selected as those who produce superior correlation.

3.3.3.3. Markov Chain Monte Carlo Sampling

The third method of sampling to be investigated is the Markov Chain Monte Carlo (MCMC) family of sampling techniques, which draws samples directly from the target distribution. By sampling directly from the target distribution, there are fewer wasted samples, as seen in both the Deterministic and MC approaches, and more samples are clustered around areas of interest. This method utilizes Markov Chains, which have the stochastic property that the probability of moving to the next position is only dependent on the current position.

Within the family of MCMC algorithms, a few were originally slated for investigation for their usefulness: the Metropolis-Hastings Sampler (M-H) (Anderson 1986; Richardson and Spiegelhalter 1996; Wasserman 2000; Beck and Au 2002)and the Gibbs Sampler (Richardson and Spiegelhalter 1996). However, it was later discovered that the Gibbs Sampler performs poorly when the probability density it is sampling from has multiple islands of high probability regions with no clear path between them. The Gibbs Sampler tends to become trapped in one of these regions. However, considering the Metropolis-Hastings is a random-walk algorithm, this problem does not threaten this approach. One limitation of the M-H sampling technique is that it tends to take a long time to converge (to be discussed in greater detail in Chapter 5). An established method of improving the efficiency of the M-H sampling technique is a method called Delayed-Rejection Adaptive-Metropolis (DRAM) Sampling. This technique will also be explored and explained in Chapter 7 (Haario, Laine et al. 2006).

Another benefit of this approach is that only a function proportional to the posterior distribution is necessary, which negates the need for computing the normalizing constant in Eq. 3 altogether. This task required an in depth investigation into theory so that the techniques were being applied in an appropriate manner, consistent with developed practices in other fields, and the results can be trusted.

3.3.4. Investigation into Weighing Approaches

The objective of this task is to investigate the effectiveness of different weighing schemes. Weighing schemes are used to incorporate the results of all models only that are most likely to fit the experimental data. Models that best represent the measured responses are given high weights, and correspondingly low correlated models given low weights. These weights are then used to compute the estimated outcome of each parameter and desired estimates of vulnerability. In the framework described in the beginning of this chapter, the posterior probability of each model is directly used to weigh that model's contribution to the predicted response. However, other weighing schemes were analyzed:

3.3.4.1. Deterministic

In deterministic weighing, the model is ranked based on the value of its respective cumulative error function evaluation for all observations. This methodology is utilized in deterministic optimization approaches, which usually seeks to minimize the error function. In this case, the optimum model is not being sought but the models would be

weighed in a way that those with the smallest error function values would contribute the most toward the predicted response.

3.3.4.2. Probabilistic

As previously described, probabilistic approaches seek to maximize the likelihood of each model. Once again, optimization approaches are traditionally incorporated to maximize the likelihood function to obtain a single model; however it is not the intention of this research to find a single optimum model. Instead, each model will be weighed by its posterior probability coefficient.

3.3.4.3. Error Threshold

This form of weighing looks at the discrepancy between any measurement and its analytical counterpart and rejects those above some predefined threshold, based on recognition of uncertainties associated with the process. This form of weighing is different than deterministic in that it looks at the percent error between any observation/model correlation and not the cumulative representation of all observations. Additionally, threshold weighing has defined bounds for model acceptance / rejection as opposed to a continuous weighing function. The method has been developed and published by others (Smith and Saitta 2006; Smith and Saitta 2008; Goulet, Kripakaran et al. 2010; Smith 2010), and their work will be investigated for applicability to the MM St-Id framework.

3.3.4.4. Consistent Approach

Instead of looking at various combinations of deterministic and probabilistic methods, it was decided to follow a more consistent approach, and examine three main MM methods: Deterministic, Threshold and Probabilistic. Thus, probabilistic tools are not being used to weigh populations of models generated with deterministic sampling, since there are more appropriate and consistent methods developed under probabilistic sampling. A final comparison will be made among the three approaches and what the difference might be given different weighing combinations though as a means of showing how superior sampling techniques can drastically affect the success of any method. The three approaches will be discussed and investigated in Chapter 7, followed by the development of advanced applications of the MM St-Id approach in Chapters 8 and 9.

3.3.4.5. Quantification of Non-uniqueness

A fundamental principle to the MM St-Id approach argued above is that the approach will provide a means for translating, and more specifically quantifying the non-uniqueness associated with the translation, unobservable structural attributes from observed structural responses. The ability of the method to produce such quantification is then necessary and was accomplished by investigating the success of using different experimental modalities and by providing a set of recommendations for reasonable vulnerability estimates given the experimental data used.

The goal of this specific task is to determine to what extent certain experimental modalities can estimate independent experimental modalities. For example, if a model is

correlated with modal response data, how well can it predict displacements and strains? Conversely, how well can a model correlated with displacements predict vibration responses or strains? This step will fully utilize the thorough experimental program designed for the validation structure. It will also require all responses to be extracted from the models simultaneously so that this backward and forward comparison can be made.

3.3.5. Implementation of Method on Constructed System – The Burlington Bristol Bridge

As a case study of the validated approach, the Burlington Bristol Bridge (BBB) (Figure 3-8) was analyzed for a select set of key vulnerabilities. This case study was structured into five main tasks, the first of which being the development of models (building blocks). The second step required the acquisition of necessary data, followed by the selection of the specific scenarios to be investigated. Chapters 10 through 13 discuss the history and background of the bridge, conventional St-Id approaches taken and all experimental work. Finally, the method is implemented on the structure and discussed in Chapter 14. A thorough comparison of the MM approach and conventional St-Id approaches will be discussed in Chapter 10, followed by a set of recommendations and concluding remarks in Chapter 15.

Figure 3-8: The Burlington Bristol Bridge

CHAPTER 4: CONCEPTUALIZATION OF THE GRID STRUCTURE

In order to develop and validate the effectiveness of the proposed multiple model methodology, a thorough laboratory experimental program was developed. In order to truly test the proposed method, the structure to be studied had to be simple enough to ensure that the fundamental principles behind the proposed method were sound, yet also needed to have the ability for increased complexity to ensure a seamless transition to more complicated constructed systems. Additionally, the specimen needed to have significant uncertainties so that sufficient building blocks could be generated. This chapter will discuss the identification and conceptualization of the structure used for verification and validation of the MM St-Id method.

4.1. Overall Structure Geometry

The structure used for the laboratory verification is a scale model of a typical highway overpass that is constructed in a Drexel University laboratory and has overall dimensions of twenty feet long and nine feet wide (Figure 4-1 - Figure 4-4). The structure consists of three continuous longitudinal members supported by six pedestals. The longitudinal members are connected with fourteen equally spaced transverse members by bolted gusset plate joints. All of the members in the grid structure consist of HSS 3x2x3/16 sections and were acquired in the 1990's, requiring the use of relevant AISC Manual of Steel Construction specifications for member section properties. The grid consists of twenty-one nodes, which are labeled for all future reference in Figure 4-2.

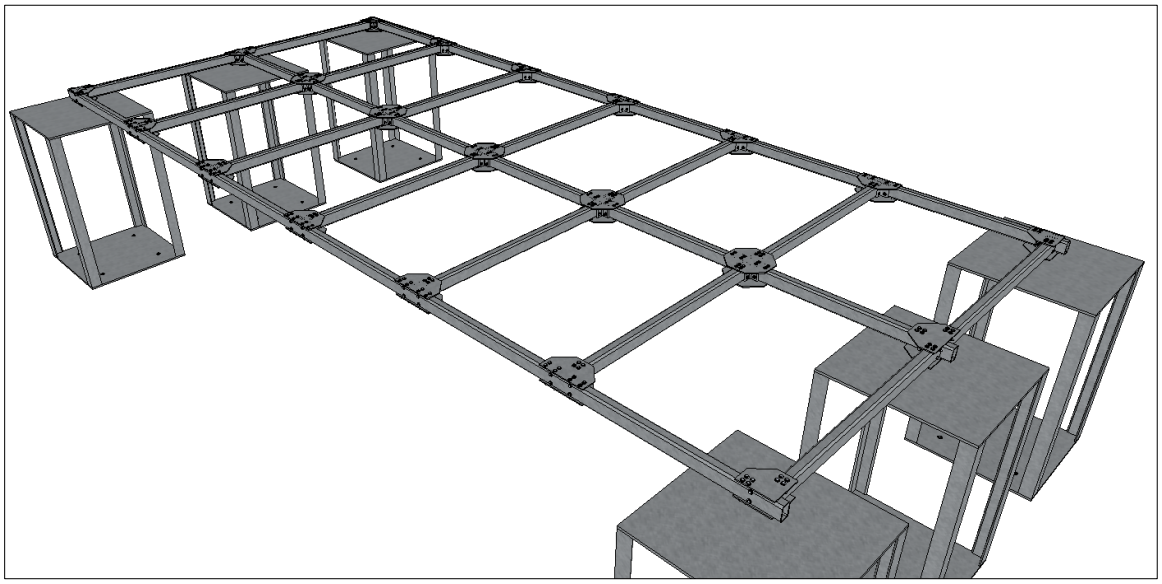

Figure 4-1: 3D CAD of Grid Structure with Pedestal Supports

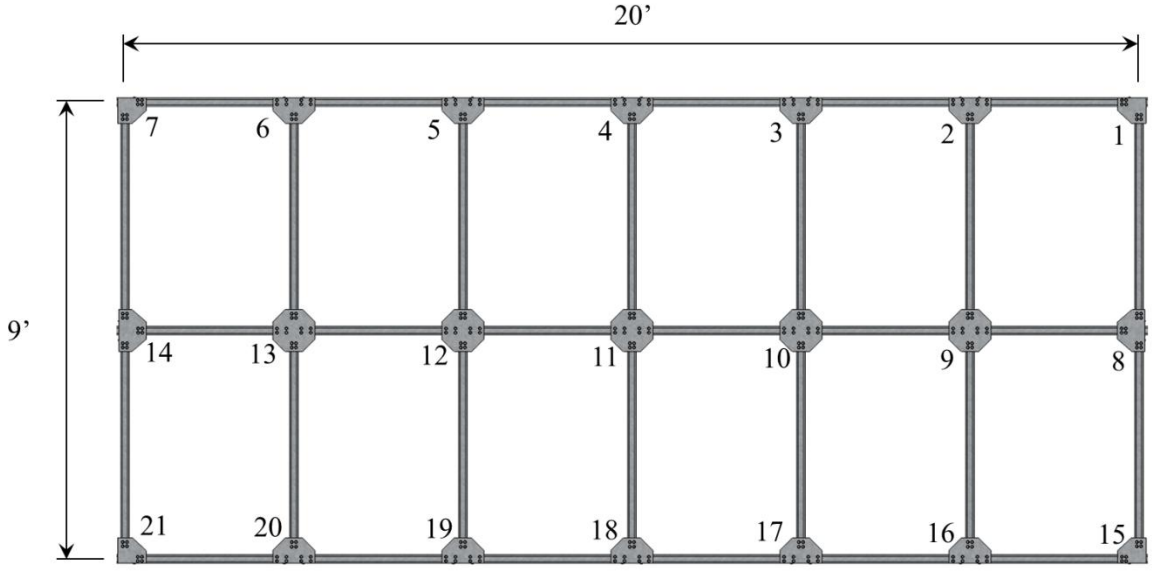

Figure 4-2: Plan View of Grid Structure with Nodes Labeled

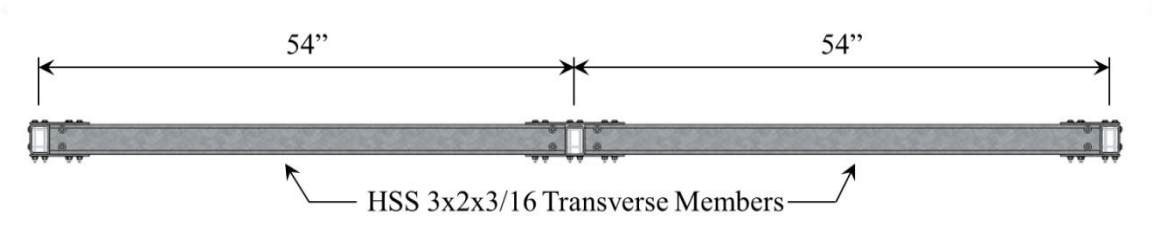

Figure 4-3: Cross Section View of Grid Structure

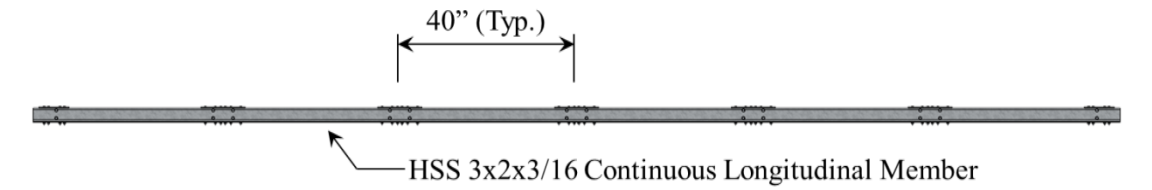

Figure 4-4: Elevation View of Grid Structure

4.2. Connection Details

There are three main types of connections used to join the longitudinal members and transverse members (Figure 4-5). Connection Type I exists in the interior of the grid structure, joining the center longitudinal member to the five interior transverse members. This connection consists of two octagonal plates, four clip angles and twenty-four bolts. Connection Type II exists at all connections along the exterior of the grid except for those at the corners. This connection consists of two hexagonal plates, two clip angles and

eighteen bolts. Connection Type III exists at each of the four corners and consists of two pentagonal plates, one clip angle and twelve bolts. All gusset plates are constructed from 0.2” thick A36 steel and all clip angles are L 2x2x1/4 sections with a length of three inches. The grid structure was designed with bolted connections in lieu of welded connections to allow for variable stiffness at the connections as well as to apply damage scenarios to the grid for potential identification strategies. All steel materials within the connections used in the grid are also of A36 grade steel.

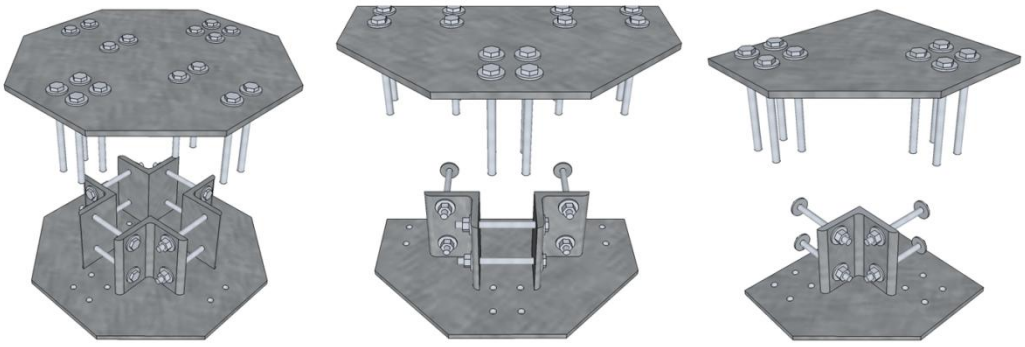

Figure 4-5: Grid Structure Connections (L to R): Connection I, Connection II, and Connection III

4.3. Steel Pedestal Supports

The grid is supported by six pedestals constructed from steel angles and plates (Figure 4-6 - Figure 4-7). The pedestals are anchored into a 12” thick concrete slab on grade with four anchor bolts. The pedestals have an overall height of 4’-1” and provide a total support area of 30” in width x 30” in length (Figure 4-7). The steel plates at the bottom and the top of the pedestal are ½” thick A36 steel and are supported by four 3x3x3/8 steel angles, one at each corner. The vertical angles are welded along the entire length of their edges to the steel plates.

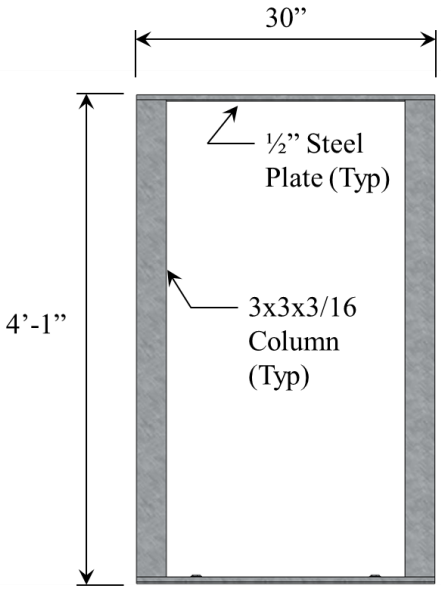

Figure 4-6: Elevation View of Pedestal Supports

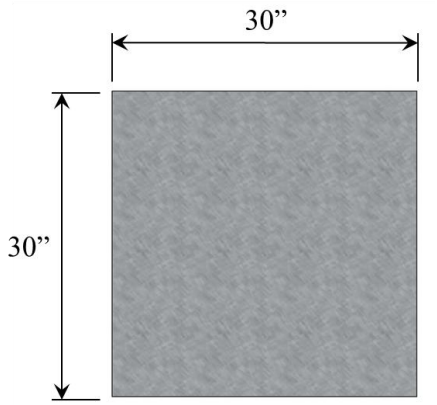

Figure 4-7: Plan View of Pedestal Support Area

4.4. Bearing Details

The bearings which support the grid structure were originally designed to function as rollers, by providing vertical restraint but not rotational or longitudinal restraint. Due to the nature of the bearings, they do provide a limited longitudinal restraint however this is only to prohibit the grid structure from slipping off the bearing entirely. The bearing consists of three components: (1) a top bearing plate, (2) a pin, and (3) a bottom bearing plate (Figure 4-8).

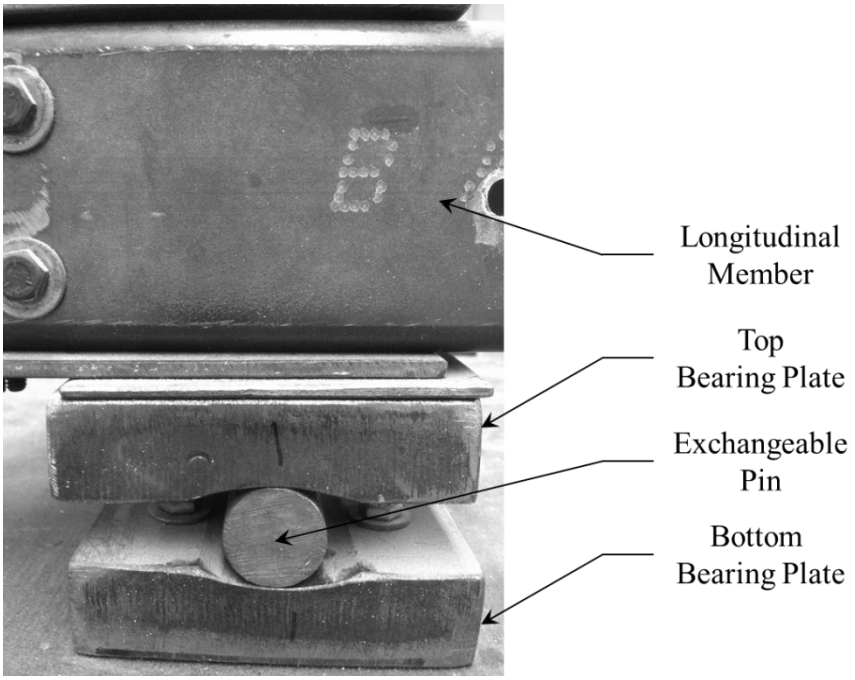

Figure 4-8: Grid Structure Bearing Detail

The top bearing plate is bolted to the longitudinal members through the gusset plates at the connection. The inside face of both the bottom bearing plate and the top bearing plate is machined to form a circular depression where the bearing pin rests. This depression is of a larger radius than the pin, allowing the pin to physically roll along the length of the grid structure. There is no mechanical bearing restraint in the lateral direction (along the transverse members), however the friction provided at the bearings are sufficient enough to prevent any lateral movement at the bearing during vibration testing or vertical static loading.

4.5. Structural Modifications

The grid structure lends itself to variable degrees of complexity by having the ability to modify support conditions and member connection stiffness in a controlled manner. To fully utilize this capability of the structure and to provide a range of complexity in structural forms in developing and validating the MM St-Id approach, a set of various structural configurations was designed.

4.5.1. Support Modifications

The bearings can be modified by installing steel pins or neoprene pins between the top and bottom bearing plates (Figure 4-9 - Figure 4-10). This modification allows for a very stiff bearing in the steel pin and a more flexible bearing in the neoprene pin. Additionally, the top plate of the steel pedestal will provide some flexibility in the vertical support of the grid due to out of plane deformation of the plate while subjected to the dead load reaction of the grid.

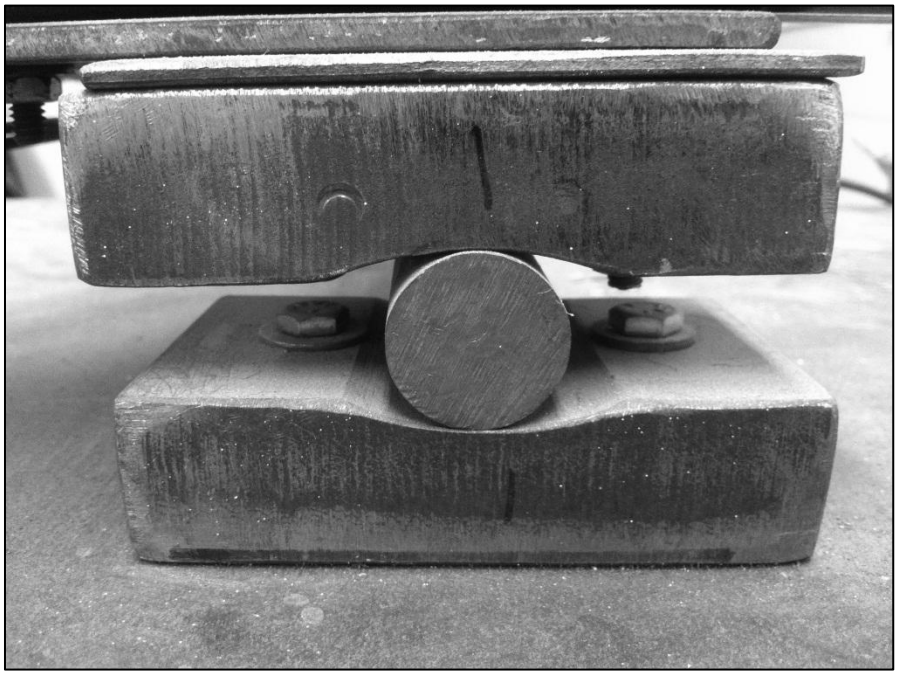

Figure 4-9: Steel Pin Support Configuration

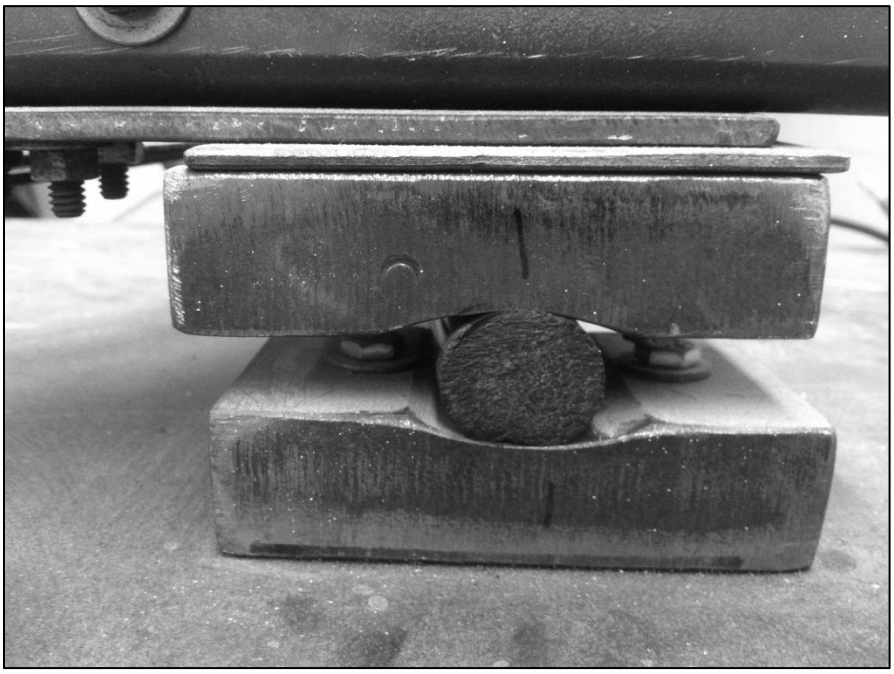

Figure 4-10: Neoprene Pin Support Configuration

4.5.2. Connection Stiffness Modifications

As mentioned previously, the connections between transverse and longitudinal members are bolted with various clip angles and gusset plates. This bolted connection allows for manipulation to achieve various levels of connection rigidity. To introduce uncertainties associated with a single connection weakening, the connection at Node 19 was selected to introduce various rigidity levels by altering its connection. The first level of connection rigidity was fully fixed, meaning that all bolts were firmly tightened and all plates and angles were present (Figure 4-11). The second connection type was generated by removing the gusset plates completely, but leaving all remaining bolts and clip angles in place and fully tightened (Figure 4-12). The final connection type was generated by loosening the bolts which fastened the clip angles to the longitudinal and transverse members, but leaving them in place (Figure 4-13). Also, the gusset plates and respective bolts were removed, as with the second connection type.

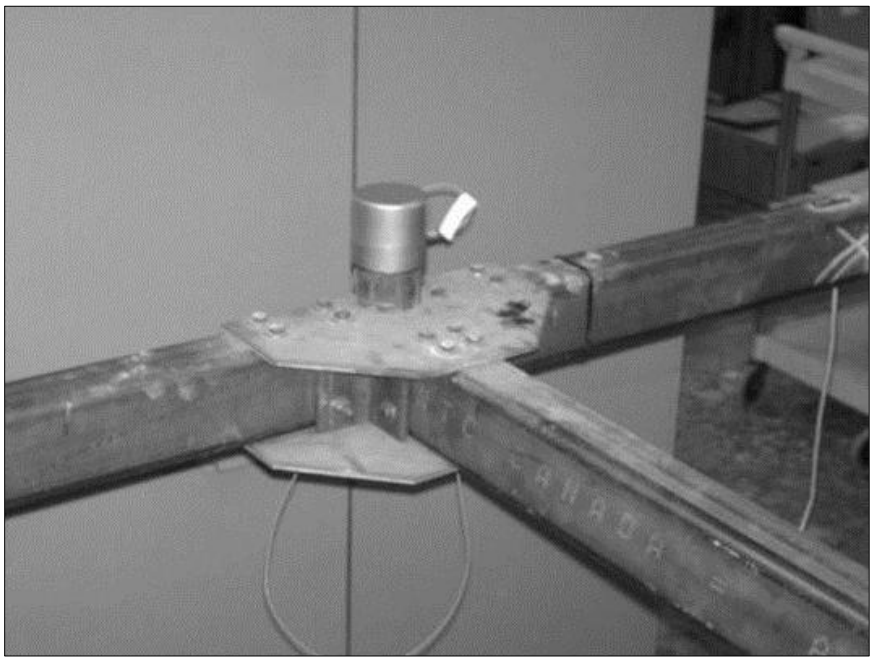

Figure 4-11: Connection Type I: Fully Tightened

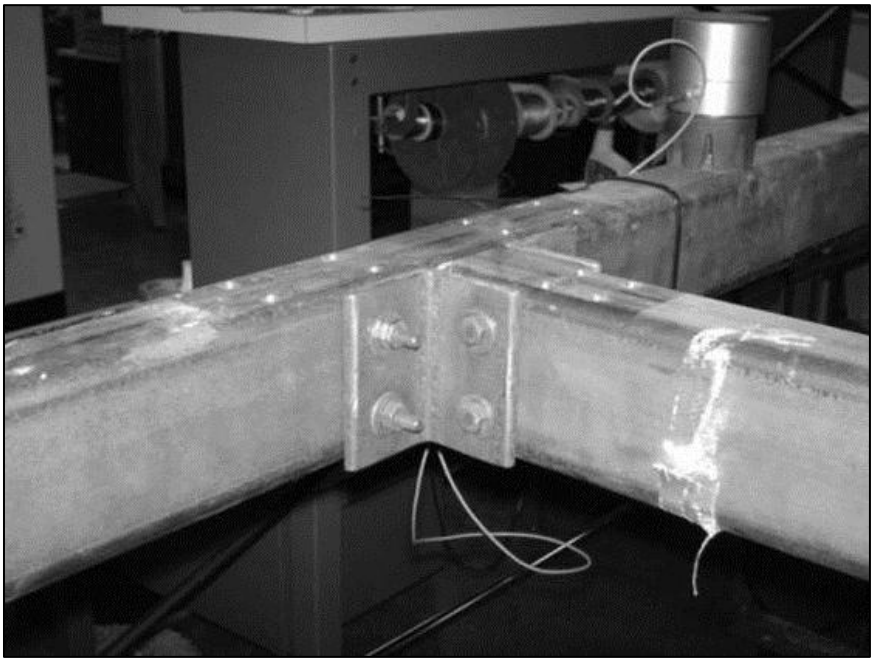

Figure 4-12: Connection Type II: Gusset Plate Removed

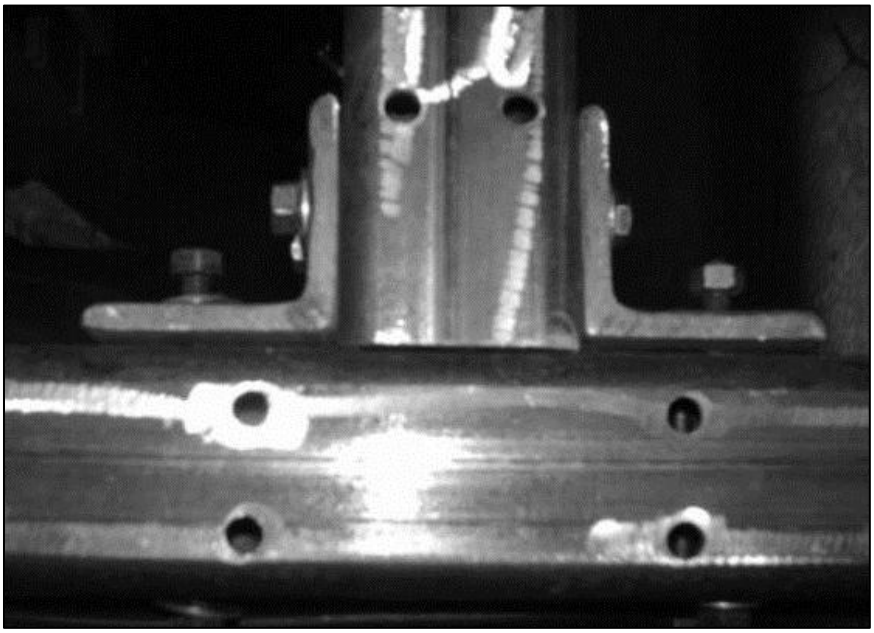

Figure 4-13: Connection Type III: Gusset Plates Removed and Remaining Bolts Loosened

The ability of modifying a global structural feature, the support stiffness, in addition to modifying a local structural feature, the connection stiffness, provided a thorough test bed for the development and validation of the MM St-Id method. Overall, a set of six structural configurations were designed incorporating the various modifications described in Sections 4.5.1 and 4.5.2 and are shown in Table 4-1.

Table 4-1: Structural Configurations

Structure	Support	Connection
1	S	I
2	S	II
3	S	III
4	N	I
5	N	II
6	N	III

CHAPTER 5: A PRIORI FINITE ELEMENT MODEL OF A GRID STRUCTURE

This chapter presents the details associated with the construction and error-screening of two FE models developed to simulate the behavior of the grid structure. In addition, a discussion of the initial model building selected and the results of the subsequent parametric studies are also presented.

5.1. A Priori Modeling for St-Id

An effective a priori finite element (FE) model is a critical step within any St-Id application, and is depend upon both a complete conceptualization of the structure (especially its critical behavior mechanisms) and sound heuristics. Within conventional St-Id applications, the FE model is used to identify a set of uncertain parameters that exert non-negligible influence over the desired performances. This input forms the basis for the experimental design which is developed principally to inform the uncertain model building blocks. Additionally, in conventional St-Id, the model is also used to identify response levels to ensure sufficient signal-to-noise ratios, to ensure sufficient safety factors are maintained during the experiment, and to provide estimates of response to allow for real-time data interpretation.

While the MM St-Id approach remains consistent with conventional St-Id in the need for an a priori model, the manner in which the a priori model is actually used is distinct. Rather than simply performing parametric studies that vary sensitive parameters to assess their effect (either in a single degree of freedom or multiple degree of freedom manner), the MM St-Id approach samples for a set of model building blocks to identify sensitive

modeling attributes and the resulting responses. While the model building blocks may simply be parametric values, they may also represent modeling decisions (e.g. how mechanisms are simulated), model resolution and dimensionality, element selection, and simulation software among other. The key distinction here is that the MM St-Id approach recognizes that not all modeling uncertain can be attributed to uncertainty associated with parametric values, and that higher-level model building blocks may be required.

5.2. A Priori SAP2000 Finite Element Model

The initial FE model (Figure 5-1) was constructed in SAP2000 (SAP2000 2009), which is a common structural engineering simulation software. The primary goals of this model were to (1) support a modal test to characterize the grid structure, and (2) to provide a means to error screen the more refined FE model developed in Strand7 (Strand7 2010) (see Section 5.3). The following sections provide the details of the various aspects of the model.

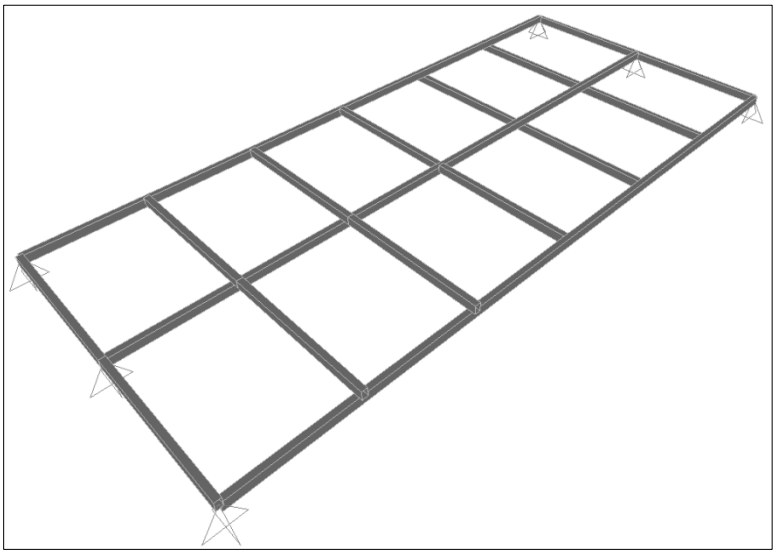

Figure 5-1: SAP2000 FE Model of Grid Structure

5.2.1. Model Geometry

The geometry of the grid structure was developed using the original design drawings as well as direct measurements to ensure accuracy. A geometric model was first developed that placed nodal points at the geometric center of each point on the grid where members framed together. These points were then connected by lines that coincided with the centerlines of both longitudinal and transverse members in their un-deformed position.

5.2.2. Element Selection

The model utilized space frame elements (Figure 5-2) to represent both the longitudinal stringers and transverse members. These elements have six degrees of freedom at each of their end nodes. The mass matrix of the model was generated with a lumped mass

formulation, where the mass from the element is distributed equally as a nodal mass to its end nodes. Shear deformation was neglected in this analysis due to the nature of the structure analyzed, in that it is primarily a flexural structure with little effects of shear deformation. The initial and coarsest mesh investigated consisted of twenty-one nodes, connected by 32 space frame elements.

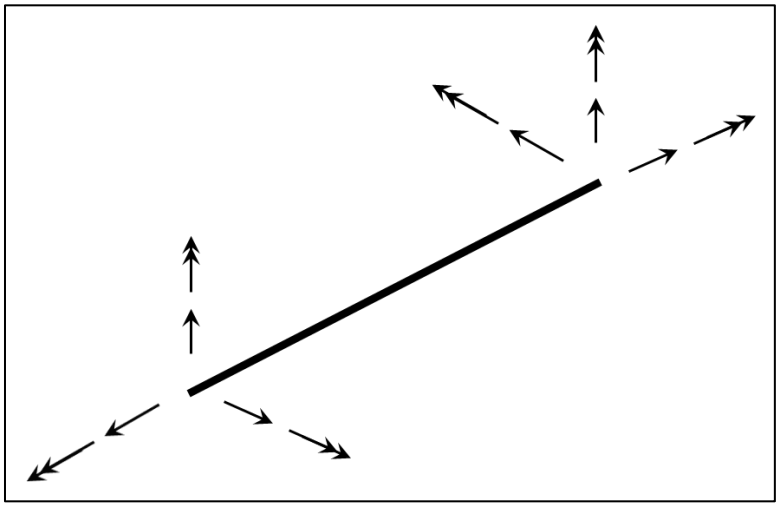

Figure 5-2: Typical Space Frame Element with 6 Degrees of Freedom per Node

5.2.3. Material and Section Properties

The structural grid is constructed from standard Grade 50 steel. Table 5-1 provides the material properties employed within the model, which come from the associated ASTM standard (ASTM A913).

Table 5-1: Material Properties of Steel

E	29,000 ksi
ν	0.3
G	11,154 ksi
ρ	490 pcf

The space frame elements were assigned section properties of the HSS 3x2x3/16 member according to the AISC manual current to the period of time when the material was acquired (as shown in Table 5-2). It is important to note that although the manufacturing of such sections remained unchanged, due to the inherent variability of the process, current design codes began to report lower bound section properties (area and wall thickness for HSS tube sections) as opposed to nominal section properties. The current design codes (AISC 13th ed.) state that the wall thickness of the HSS tube can vary by up to 10% due to manufacturing tolerances specified by ASTM standards. While this may be appropriate for new design, the use of lower bound properties within a St-Id application will bias the results and could be highly misleading during the experimental design phase.

.

Table 5-2: Section Properties of the HSS3x2x3/16

A	1.64 in^2
I_{xx}	1.86 in^4
I_{yy}	0.977 in^4
J	2.16 in^4
m	5.59 lb/ft

5.2.4. Boundary and Continuity Conditions

The connections between transverse and longitudinal members were modeled as continuous. The localized increase in stiffness of both the longitudinal and transverse members due to the finite connection size and bolted gusset plates was not taken into consideration. That is, no increased stiffness or rigid offsets were employed at the element ends for this a priori model.

The additional mass of the plates, clip angles and bolts at each connection were estimated and applied as nodal masses. This included the addition of 12 lb at each interior connection, 8 lb at each exterior connection, and 6 lb at each corner connection. Following the experiment, a single type of each connection was removed from the model and weighed, which confirmed the magnitude of the point masses added to the model for subsequent applications. In addition, the mass of the accelerometers (2 lb) employed during the dynamic test were also added as point masses to the nodal points of the grid. No additional mass for the cables was included in the model.

The boundaries of the three longitudinal members along one end of the grid were represented as rollers (with the transverse and vertical displacements restrained), while the longitudinal members along the other end were represented as pins (with all translational displacements restrained). All of the restraints were applied at the space frame element node, thus the vertical offset between the centerline of the member and the support was ignored. In addition, the vertical flexibility of the supporting pedestals and the support assemblage (see Chapter 4) was also ignored.

5.2.5. Mesh Convergence

A mesh convergence study was carried out to ensure that an appropriate number of elements were utilized for the a priori model. The convergence was carried out by starting with a model which represented a single physical member with one finite element, Model A. This model consisted of 17 elements with 21 nodes. SAP2000 allows for mid-element intersections with adjacent members without needing to discretize the main element, which was utilized in this model. The model was then discretized by dividing each element where an intersection occurred with an adjacent beam element. This model, Model B, resulted in a total of 32 elements and 21 nodes. This was further discretized by dividing each element in half, resulting in 64 frame elements and 53 nodes for Model C. Model D was generated by further dividing each element in half, resulting in 128 frame elements with 117 nodes.

Convergence was determined by tracking the model's prediction of natural frequencies for each level of discretization. When the model predictions stabilized within an

acceptable tolerance, the mesh was considered converged. For the a priori model, it was noted that after Model C, the frequency predictions did not change by more than 3% and was determined to be satisfactory for the a priori analysis.

5.2.6. Error Screening

The a priori model was error screened by performing a series of analyses and examining the results to ensure all results are expected and reasonable. A detailed flowchart describing this process is shown in Section 5.3, however will be described here in brevity. A static analysis was carried out to ensure that the structure had symmetric dead load reactions, thus confirming that no duplicate members exist and that member section properties were assigned correctly. A simple hand computation of the grid structure's dead load was compared to the sum of the dead load reactions to ensure that the total dead load was not errant.

In addition to analyzing the dead load reactions, the dead load displaced shape of the grid structure was carefully analyzed to confirm that no unintended breaks or discontinuities existed within the structure. This type of phenomenon would arise from missed member connections or improperly assigned boundary conditions.

In addition to the dead load static analysis, a modal analysis was also processed to confirm that the structure exhibited no unintended breaks or discontinuities. Modal analyses tend to accentuate this type of behavior, where it might not be easily identifiable

within a dead load analysis, because a missed end connection creates a very flexible cantilevered member and is obvious within the modal analysis.

5.2.7. Dynamic Simulation Results

The dynamic analyses of the model consisted of computing the frequencies, mode shapes and scaling factors in order to support the experimental study. The key issues were (1) to establish the frequency band of interest, (2) to identify nodal points in various modes (to avoid in the instrumentation), and (3) identify important modes from a flexibility standpoint to ensure these are properly captured.

The eigenvalue analysis algorithm employed in SAP2000 is based on an accelerated sub-space iteration algorithm. This approach computes the eigenvalues iteratively until the calculated value for each frequency meets predefined convergence criteria. This approach is referenced within the SAP2000 user's reference manual to the work in Wilson and Tetsuji 1983.

The results of the dynamic analysis are provided in Table 5-3 and in Figure 5-3 through Figure 5-12. The first ten modes were used in subsequent experimental design for identifying the location of impact locations because these modes account for more than 99% of the static flexibility of the grid structure. In total, 13 modes were computed, but since the vertical response of the structure was of primary interest, all lateral and longitudinal modes were ignored.

Table 5-3: SAP2000 A Priori Finite Element Model Frequency Predictions

Mode	Frequency (Hz)	Description
1	4.2716	First Vertical Bending
2	8.4319	First Torsion
3	17.001	Second Vertical Bending
4	22.787	Second Torsion
5	31.134	First Butterfly
6	37.618	Third Vertical Bending
7	40.015	Second Butterfly
8	44.893	Third Torsion
9	63.819	Third Butterfly
10	56.493	Fourth Vertical Bending

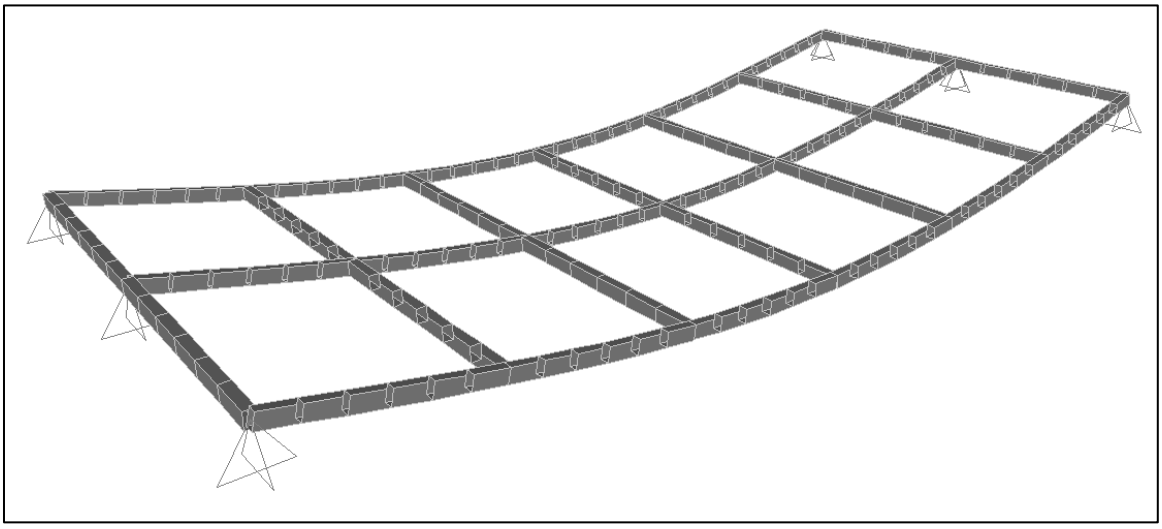

Figure 5-3: SAP2000 Mode 1 (First vertical bending)

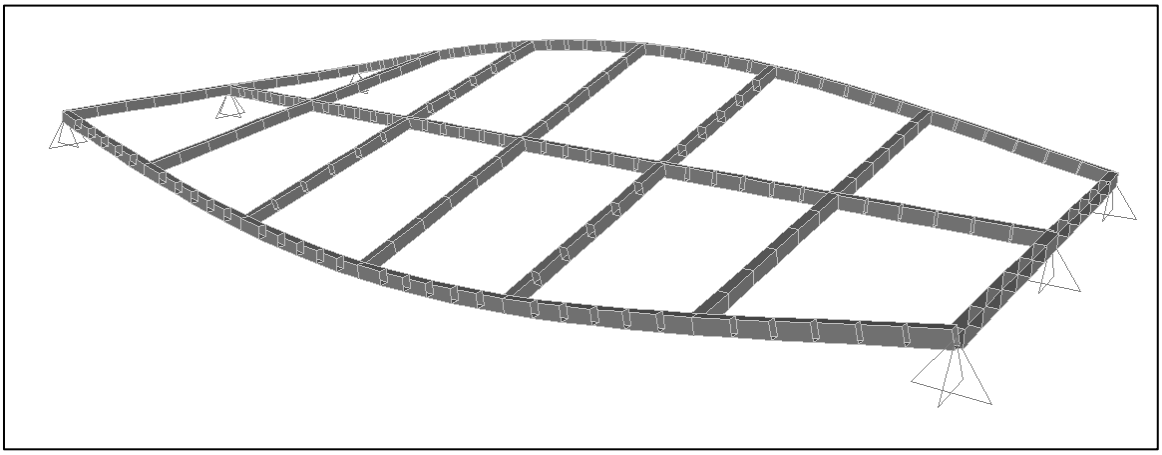

Figure 5-4: SAP2000 Mode 2 (First torsion)

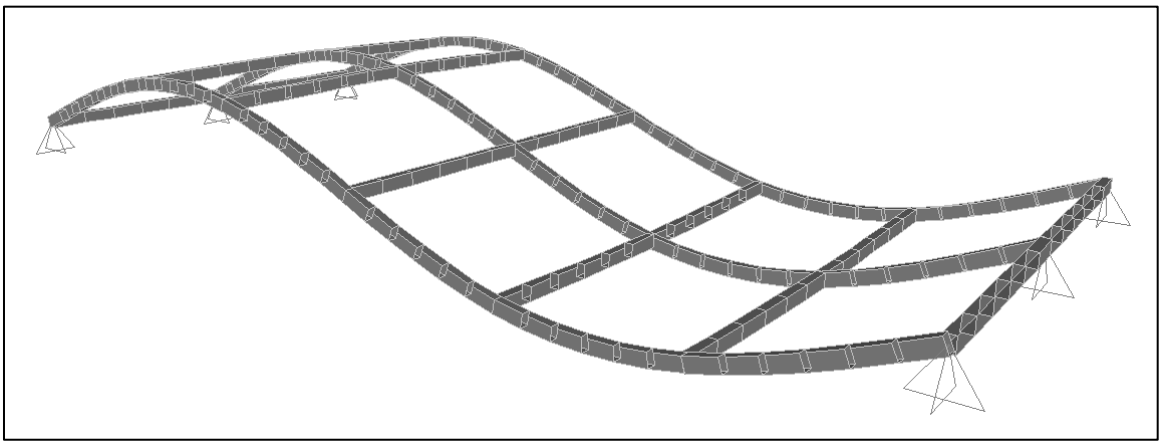

Figure 5-5: SAP2000 Mode 3 (Second vertical bending)

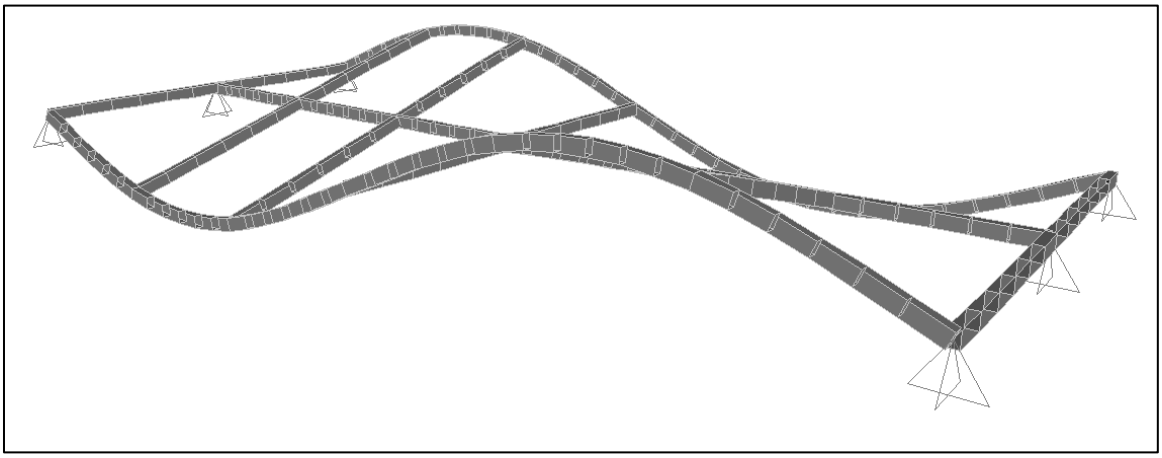

Figure 5-6: SAP2000 Mode 4 (Second torsion)

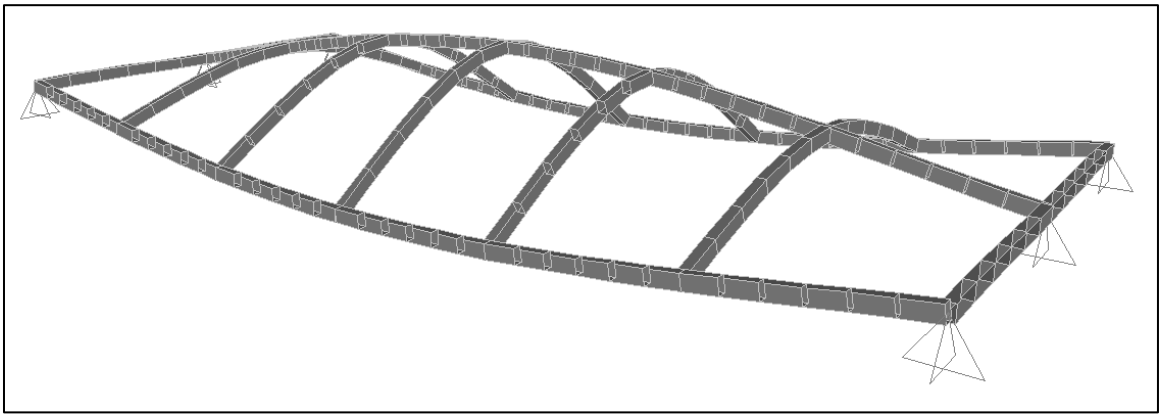

Figure 5-7: SAP2000 Mode 5 (First butterfly)

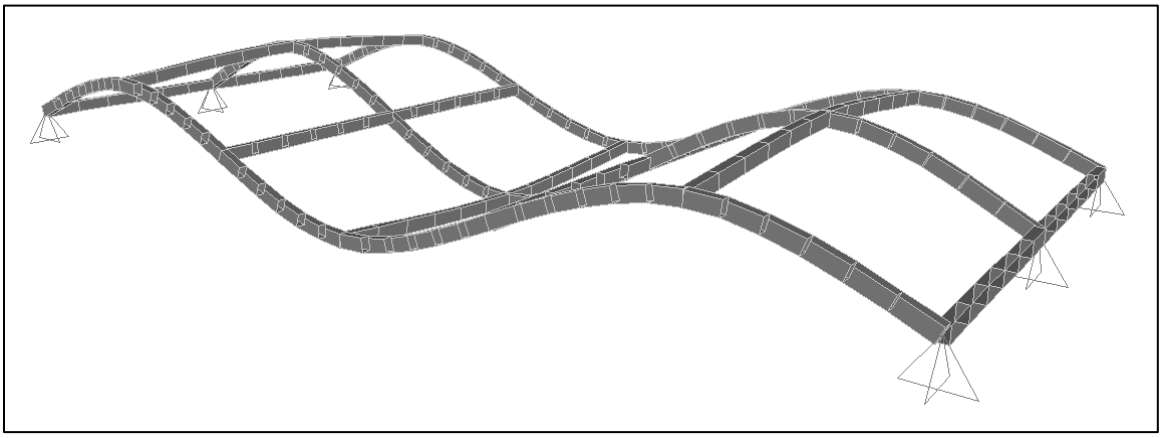

Figure 5-8: SAP2000 Mode 6 (Third vertical bending)

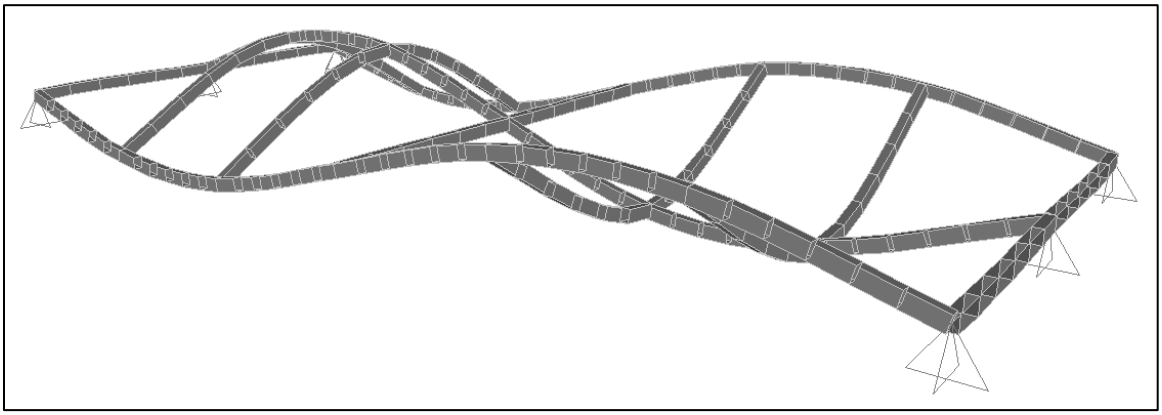

Figure 5-9: SAP2000 Mode 7 (Second butterfly)

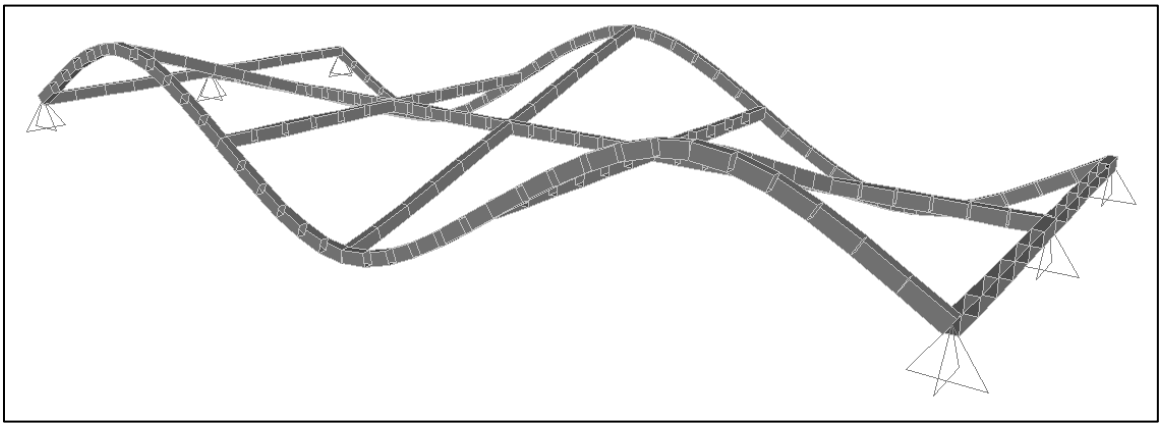

Figure 5-10: SAP2000 Mode 8 (Third torsion)

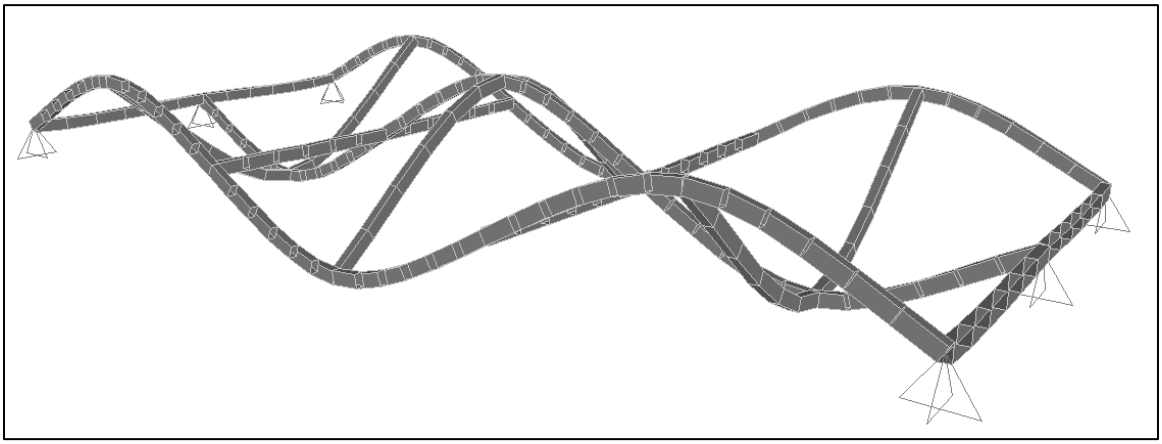

Figure 5-11: SAP2000 Mode 9 (Third butterfly)

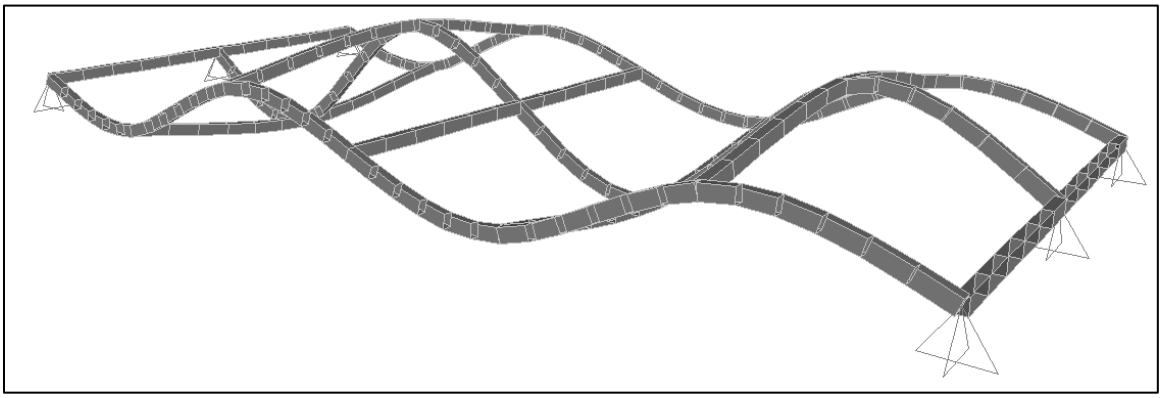

Figure 5-12: SAP2000 Mode 10 (Fourth vertical bending)

5.2.8. Static Simulation Results

A linear static analysis was used to verify that the anticipated loading was both sufficient enough to provide an acceptable signal-to-noise ratio during the experiment as well as ensuring that the maximum loads would not yield the structure. The anticipated displacements and expected signal-to-noise ratios are listed below for three load cases (Table 5-4). As shown, the signal-to-noise ratios all well exceed the noise level of the displacement transducers, and the load level of 200lb was deemed sufficient.

The maximum stress under a mid-span load of 200lb was also computed to verify that the structure would not be permanently damaged or yielded. The SAP2000 model did not have the ability to directly compute stress so the axial force, P, bending moment, M, and section properties of area, A, distance from neutral axis to extreme fiber, y, and moment of inertia, I, were output from the model and used to compute the maximum fiber stress according to the following equation (Eq. 5-1).

$$\sigma = \frac{P}{A} + \frac{My}{I} \qquad \textbf{Eq. 5-1}$$

After computing the maximum stress with the previous equation, 3.7ksi under a load of 200lb, the loading level was approved for use in the experimental program.

Table 5-4: A Priori Displacement Prediction with Signal-to-Noise Ratios

	200lb at Node 3		200lb at Node 11		200lb at Node 19	
Node	Δ (in)	Signal to Noise	Δ (in)	Signal to Noise	Δ (in)	Signal to Noise
3	-0.381	76.11	-0.271	54.18	-0.135	26.91
4	-0.398	79.61	-0.315	63.07	-0.157	31.35
5	-0.314	62.70	-0.271	54.18	-0.138	27.61
10	-0.248	49.52	-0.284	56.78	-0.222	44.41
11	-0.271	54.18	-0.339	67.77	-0.271	54.18
12	-0.222	44.41	-0.284	56.78	-0.248	49.52
17	-0.138	27.61	-0.271	54.18	-0.314	62.70
18	-0.157	31.35	-0.315	63.07	-0.398	79.61
19	-0.135	26.91	-0.271	54.18	-0.381	76.11

5.3. Finite Element Base Model for MM St-Id

As previously discussed, the a priori FE model for the grid structure was constructed in SAP2000 and used for experimental design. While SAP2000 is powerful and reliable FE analysis software, it is limited by its inability to interact with outside software, a feature

that is necessary for a method that needs to automatically manipulate, solve and extract results from many FE models. The software used to write and run the main algorithms of the MM St-Id method is MATLAB, so FE software capable of interacting with MATLAB was desired and one that was found to be capable of this was Strand7.

5.3.1. Model Construction Process

The initial FE model for the MM St-Id analysis was constructed within best practice approaches, which were developed over the course of the author's and colleagues' experiences at Drexel University and taught as part of multiple undergraduate courses. The detailed best practice approach developed is discussed for a complex constructed system in Chapter 12; however since the model for the grid structure is relatively simple compared to more complex constructed systems, a simplified error screening flowchart applicable to the grid structure is presented (Figure 5-13).

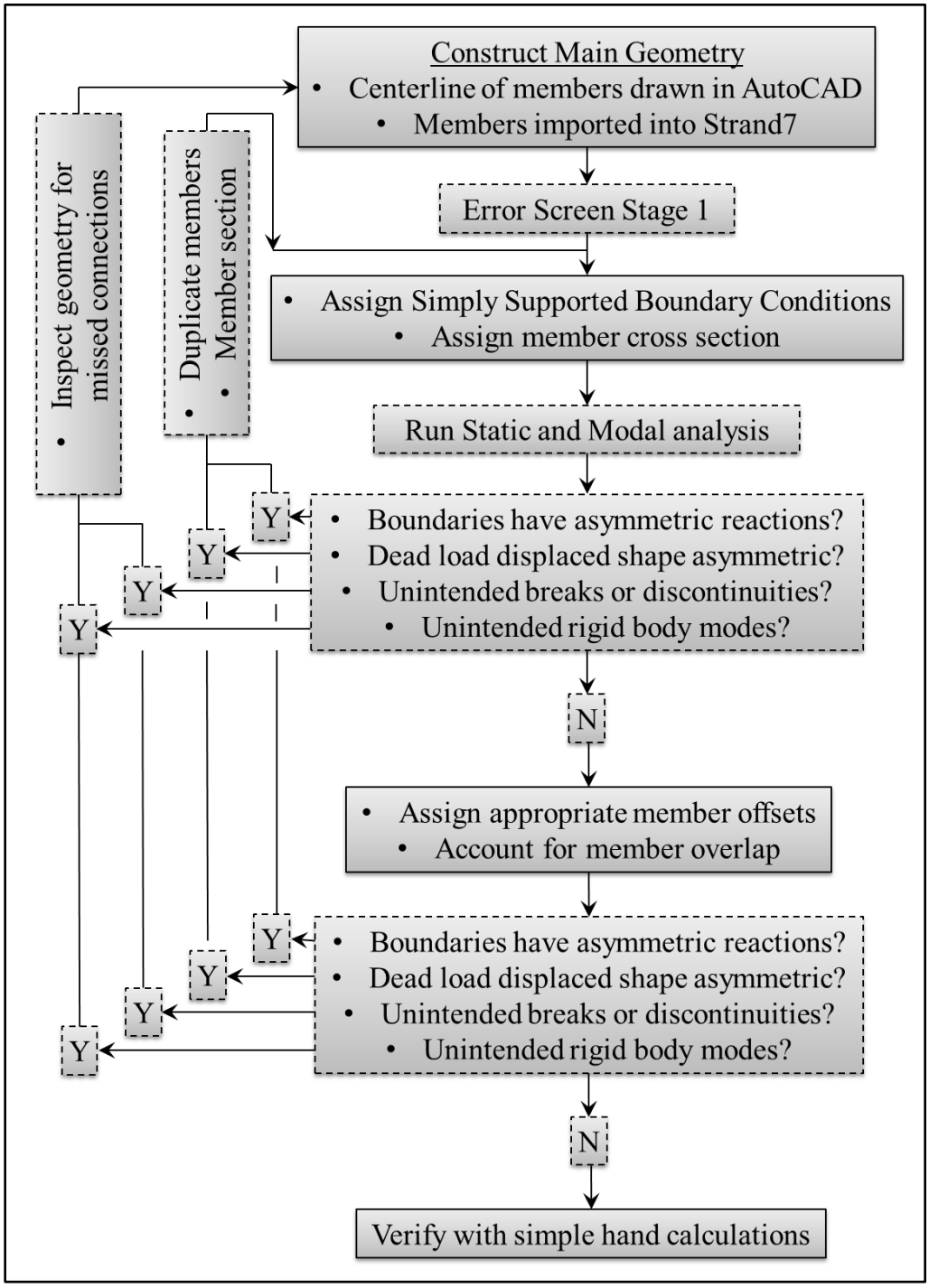

Figure 5-13: FE Model Error Screening Flowchart

5.3.2. Geometry

Since the geometry of the grid structure had already been developed for the SAP2000 model, as discussed in section 5.2.1, this step within the model construction process was not necessary. However, since different FE analysis software was being used, software compatibility was validated with benchmark studies to ensure that the intended geometry was conceptualized in the Strand7 software interface.

5.3.3. Element Selection

The elements selected for use within the Strand7 grid FE model primarily consisted of Beam2 elements, with one node on each end of the element consisting of six degrees of freedom per node (three rotational and three translational). Strand7 allows for the formulation of consistent mass matrices within the FE model, and this was implemented for this analysis. Shear deformation was neglected due to the grid serving primarily as a flexural structural system with negligible shear effects.

5.3.4. Material and Section Properties

The material and section properties assigned within the Strand7 FE model were consistent with those listed in Table 5-1 and Table 5-2.

5.3.5. Boundary and Continuity Conditions

When the initial round of error screening was complete (verifying geometry), the model was then refined to more appropriately represent the physical structure. The localized stiffness increase due to the gusset plates at each connection was modeled as an increase in the top and bottom flange widths of the HSS section along those locations (Figure 5-14). The transverse members were shortened so that they would not overlap the longitudinal members, double-counting mass at those locations. To maintain compatibility, fully rigid links were used to connect the ends of the transverse elements to the longitudinal elements (Figure 5-15).

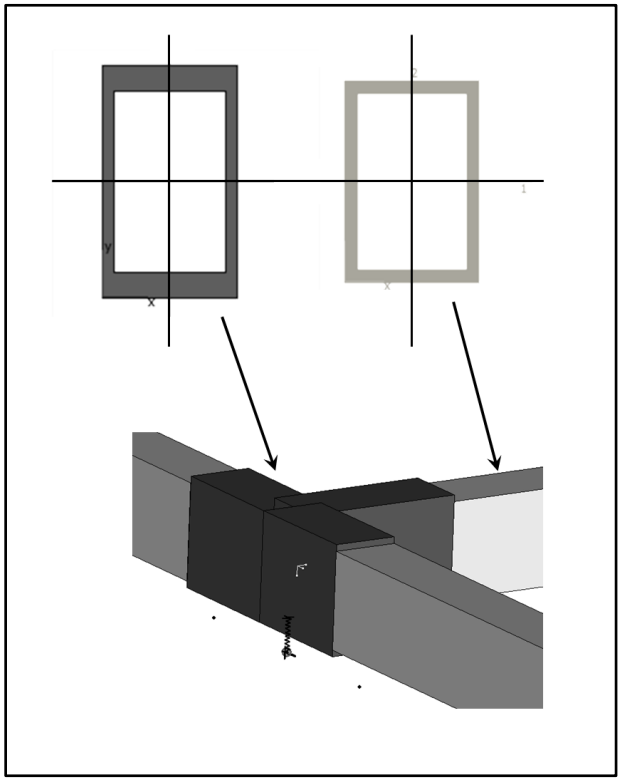

Figure 5-14: Typical Cross Sections for Elements within Connections (L) and Standard Members (R)

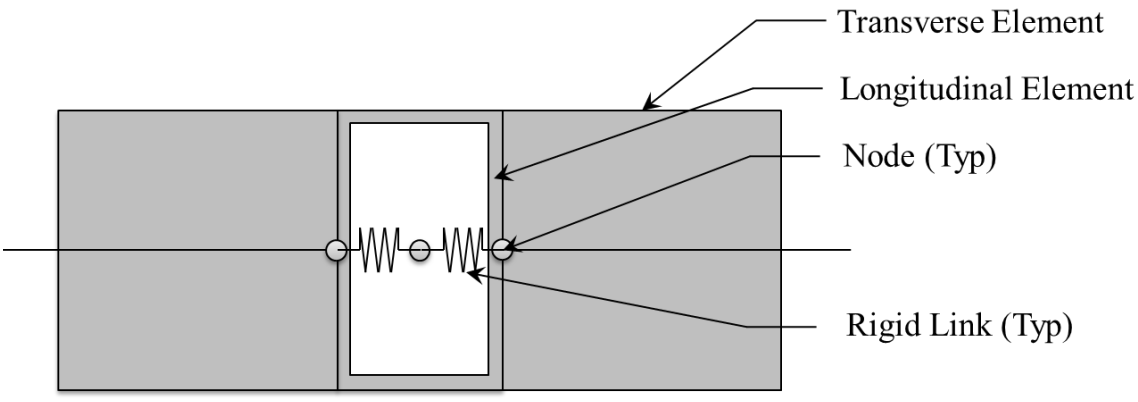

Figure 5-15: Detail Showing Connection of Transverse Elements to Longitudinal Element via Rigid Links

Due to the design of supports of the grid, the longitudinal members do not rotate about their neutral axis, as is assumed with a simply supported configuration. To account for this within the model, a vertical offset of 2.75” was assigned to all elements. This offset accounted for half of the beam depth (1.5”), the bottom gusset plate (0.2”) plus the depth of the bearing plate (1.05”), as seen in Figure 5-16.

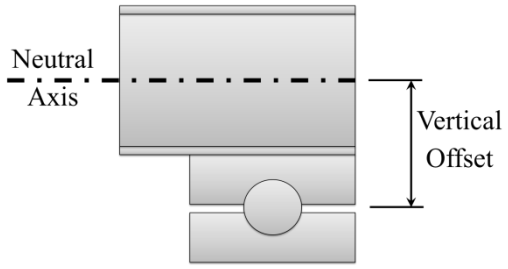

Figure 5-16: Bearing Detail Showing Vertical Offset

As previously mentioned, after all experimental work was complete a single connection of each of the three types was completely removed from the grid and weighed carefully. The mass which wasn’t taken into account in the model by increasing the flange width near the connections was added as a nodal mass able to participate in all degrees of freedom. Also, rotational mass effects were computed since the mass of the plates is located far from the neutral axis of the members and assigned as nodal rotational mass in the model. Additionally, the weight of the accelerometers used during the dynamic

impact test, to be discussed in Chapter 6, was accounted for within the model as nodal masses.

5.3.6. Mesh Convergence

The last FE modeling consideration to explore was the discretization of the grid elements. Strand7 requires one beam element between every two nodes, unlike some FE analysis software which allow connections along one beam element. This requirement made the basic FE model have 98 beam elements, with a total of 115 nodes. Three levels of discretization from this base model were evaluated for stability in their prediction of Modes 4 through 7, four high order modes achieved in experimental measurements (Figure 5-17 - Figure 5-20). These modes were selected since they have large changes in curvature, and would be sensitive to a change in the number of elements (as opposed to a simple static loading, which would not be sensitive to this level of discretization). It is shown that the predictions have stabilized after a discretization level that split each beam in half. An FE model computation of each of the modeshapes used for these sensitivity plots is shown next to each sensitivity curve.

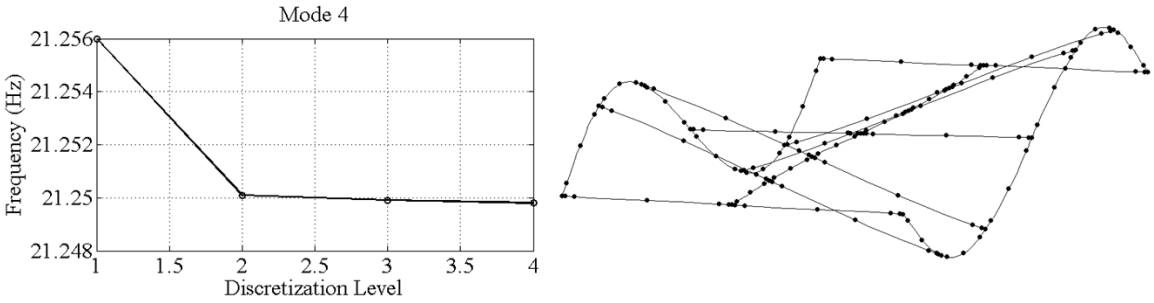

Figure 5-17: Mode 4 Convergence (L) and Mode 4 Shape (R)

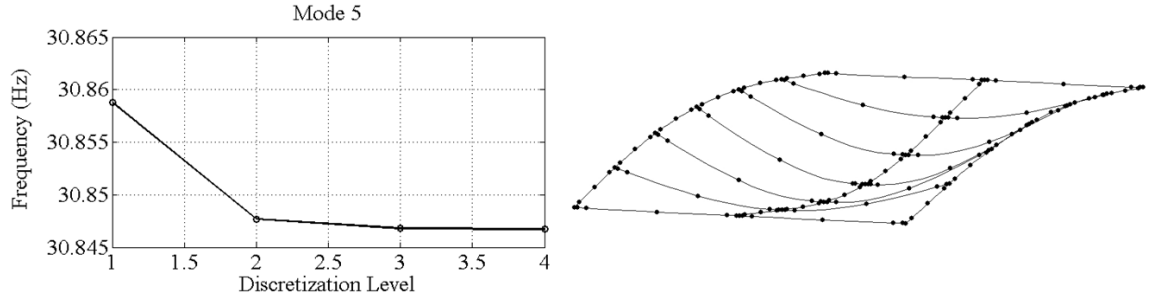

Figure 5-18: Mode 5 Convergence (L) and Mode 5 Shape (R)

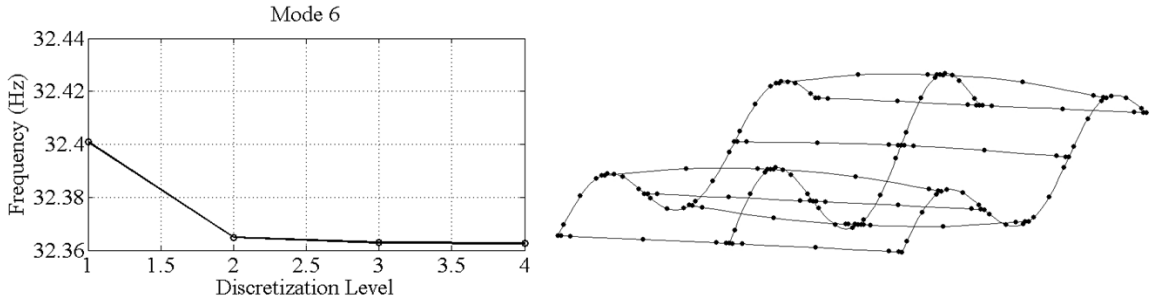

Figure 5-19: Mode 6 Convergence (L) and Mode 6 Shape (R)

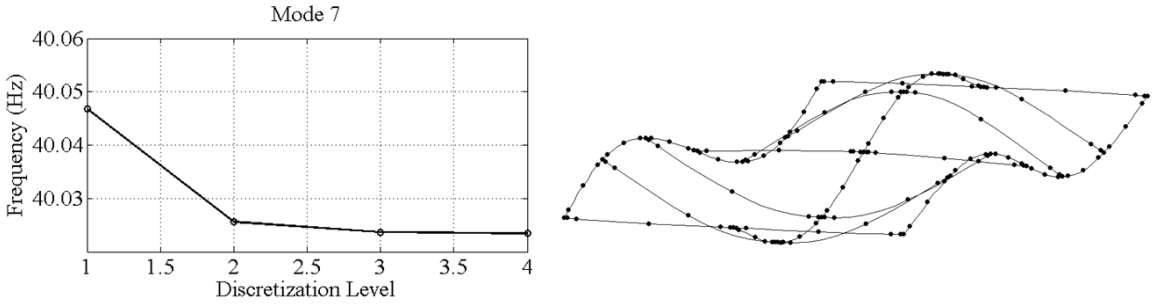

Figure 5-20: Mode 7 Convergence (L) and Mode 7 Shape (R)

Once the base model for the development and validation of the MM St-Id method was fully error-screened and evaluated for proper discretization, the next step in the process is to choose appropriate model building blocks. The final base model for the study is shown in Figure 5-21.

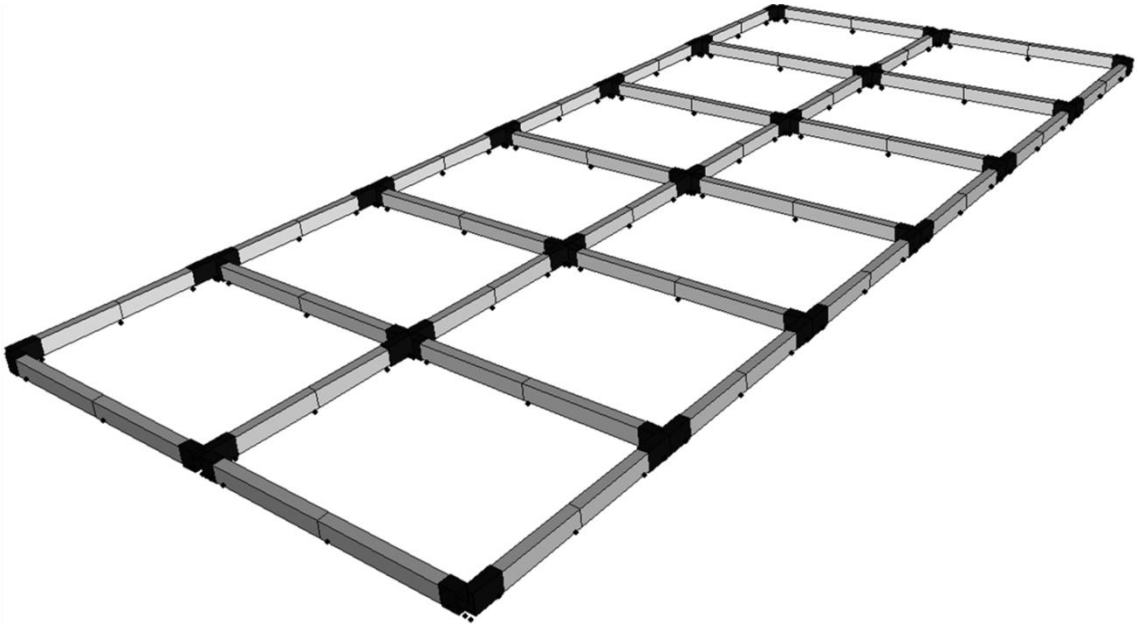

Figure 5-21: FE Model of the Grid Structure

5.3.7. Error Screening

The model was screened for errors in multiple stages. The first stage of error screening occurred after the base model had been imported into Strand7 and nominal cross sections, boundary and continuity conditions were applied. Three analyses were run on the model to screen for errors: 1.) dead load static analysis, 2.) uniform load surface static analysis, and 3.) modal analysis. The current form of the model is symmetric with respect to the geometry and member assignments. Therefore, if the boundary reaction forces did not exhibit symmetric magnitudes or the dead load caused an asymmetric displaced shape then the model was screened for duplicate members and nodes. Additionally, each member was checked for appropriate property assignments.

The model was also screened for missed end connections by inspecting the modal analysis results, since members only connected on one end tend to have exaggerated modal displacements during modal analyses due to their localized flexibility. This phenomenon can sometimes be missed in a dead load analysis. An additional way of highlighted missed connections used was the application of a uniform load surface in each coordinate direction. This type of loading also accentuates any missed connectivity assignments.

Once the refined modifications were made to the FE model, the same error screening approach was repeated, to ensure that the modifications did not compromise compatibility conditions or the symmetric nature of the grid. Simple hand calculations were then used to double check the reliability of the initial FE model. The hand calculations consisted of computation of total dead load and an estimate of maximum deflection due to a 1 kip point load at mid-span. The hand checks are only meant to be in the ball park of the model results and, especially as the model gets more complicated, should only be expected to be reasonably close.

The simple hand calculation (shown below) used to estimate the deflection of the grid under a 1 kip load at mid-span is from basic structural analysis theory for the deformation of a simply supported beam. In order to simplify the grid structure into a simply supported beam representation, it was assumed that the load was equally distributed among the three longitudinal stringers, thus allowing for a summation of each member's inertia. The displacement estimated by hand (Eq. 5-2) was -1.79" at mid-span, while the FE model predicted a displacement of -1.76". In this case, where the simple calculation

should have been less than the model prediction, considering equal load sharing was assumed, the additional stiffness from the connections was not accounted for by hand, but was in the FE model. With this simple error screening method, the model is justified as being reasonable, in terms of its stiffness.

$$\partial = \frac{PL^3}{48EI} \qquad \textbf{Eq. 5-2}$$

Before the model was modified to include the stiffness effects of the gusset plates or sensors, the mass of the structure was computed by hand and with the FE model. In this case, the dead load from the model and the dead load computed by a hand calculation were less than 1% different. However, additional sources of mass needed to be accounted for within the model. Accounting for structural mass is an extremely important step, and must be done with care. The extraneous masses for the grid included: connection masses (plates, bolts and angles), sensors (including magnetic mounting base), and coaxial cables. Each of these mass types was assigned to a unique load case, so that the total reactions could be used to double check the total additional mass for each case.

5.4. Selection of Model Building Blocks

The second step within the MM St-Id framework the identification of key building blocks. Building blocks can be conceptualized as any uncertain decision that an informed user makes during the process of building an FE model. For example, is it more

appropriate to use shell elements or solid elements to represent a roadway deck? What should be used as the elastic modulus for concrete if core tests show a significant variance throughout the structure? The building blocks are not limited to classical model parameters, but rather aim to encompass all modeling uncertainty.

5.4.1. Global Model Building Blocks

For the grid structure, the selection of building blocks was approached from a global viewpoint and then narrowed in on a more local viewpoint. The structure was first viewed from a very global perspective: What is supporting the grid? When the support system was more closely examined, it was realized that the grid was not a simply supported structure but that it was being supported by a flexible steel plate, supported on each corner by steel angle columns which were then bolted to the floor via a connection plate on the floor. The pedestals supporting the grid are effectively springs, and are certainly not infinite in translational stiffness, as pins represent. The first building block then added to the analysis is a vertical spring, K_v, at the six boundary locations. Not only is this appropriate for the grid when the steel pins are installed, but even more so when the neoprene pins are installed and an even more flexible support is created. This building block was modeled in Strand7 as translational nodal springs in the vertical direction.

In addition to the uncertainty associated with the vertical stiffness at the boundaries, it was also not immediately clear how to represent the longitudinal restraint to the grid support locations. Due to the design of the bearings, there is a longitudinal resistance as the grid is moved in a longitudinal direction to the pin's interaction with the machined

groove in the bearing plates. This also represents a substantial uncertainty, because this longitudinal spring is acting at a distance of 2.75" from the neutral axis of the beam, inducing a rotational resistance at the supports. The second building block is then the longitudinal stiffness, K_l, at each of the support locations. To create a stable model within the FE analysis, one side of the grid was restrained in the longitudinal direction, while the opposite three supports were modeled with nodal translational springs in the longitudinal direction.

5.4.2. Local Model Building Blocks

The first two building blocks represent global uncertainties associated with the grid structure. Without any further uncertainty at this level, the focus of identifying building blocks was narrowed onto the grid structure itself. At this level, one should question whether compatibility or continuity conditions might create appreciable uncertainty with respect to the identification of the structure.

For the grid, the only break in continuity is at the junction of transverse and longitudinal members. These connections certainly qualify as uncertain with respect to the amount of rotational and translational stiffness they provide. The stiffness of the gusset connection is broken into two building blocks: K_{r1} and K_{r2}. These building blocks correspond to the two main connection types seen on the grid structure, and labeled as connections I and II in Chapter 4. Connection I is the typical interior connection and has two transverse members framing into it, where Connection II has only one transverse member.

5.4.2. Material Model Building Blocks

Finally, the search for building blocks was narrowed even further to the makeup of the members themselves. One general question to ask is what uncertainty is associated with the material properties of steel? While it is known that the elastic modulus of steel is almost a deterministic, it is well published that coefficients of variation on the elastic modulus range anywhere from 1% to 7.5%. Therefore, E_s becomes the third building block. This is a building block that is beneficial to include simply because it is well known. If, for example, the MM St-Id process is heavily weighing models with an elastic modulus that is 20% higher than its established value, than this is an indicator of a problem within the method or the model. As identified in Chapter 3, this inclusion of deterministic building blocks plays a significant role in the MM St-Id method, as it provides the user with a way to "truth-check" the results.

For the purpose of this development and validation, the building blocks were limited to model parameters however it is important to recognize that this is not always the case.

5.5. Sensitivity Study of Model Building Blocks

The MM St-Id process can suffer from challenges faced in classical model updating techniques, mainly poor identifiability of building blocks. While a lack of identifiability within building blocks is accounted for within the process, it can still lead to inefficient candidate model selection by sampling over regions where there is little influence on the likelihood or objective function. In order to ensure that only influential ranges building

blocks are included within the analysis, sensitivity studies were carried out for each of the identified building blocks.

5.5.1. Sensitivity Study Objective Function

The error function utilized in this sensitivity study is shown in Eq. 5-3.

$$obj = \sum_{i=1}^{n} \left[100 \left(\frac{f_{ana(i)} - f_{\exp(i)}}{f_{\exp(i)}} \right) + 100\left(1 - MAC(\varphi_{ana(i)}, \varphi_{\exp(i)}\right) \right] \qquad \textbf{Eq. 5-3}$$

This objective function is referred to as a sum of percent difference error function formulation. The terms $f_{ana(i)}$ and $f_{\exp(i)}$ represent the analytical and experimental frequencies, respectively, of the i^{th} mode, and similarly the function MAC represents the Modal Assurance Criterion (MAC) value computation between the analytical and experimental modeshapes, $\varphi_{ana(i)}, \varphi_{\exp(i)}$ respectively, associated with the i^{th} mode. The equation for the MAC value is formulated below (Eq. 5-4) and represents the degree of consistency between two vectors of mode shape coefficients. MAC values range from 0.0, representing no consistency between shapes, to 1.0, representing perfect consistency.

$$MAC\left(\varphi_{ana(i)}, \varphi_{\exp(i)}\right) = \frac{\left|\varphi_{ana(i)}{}^{T} \cdot \varphi_{\exp(i)}\right|^{2}}{\varphi_{ana(i)}{}^{T} \cdot \varphi_{\exp(i)} \cdot \varphi_{\exp(i)}{}^{T} \cdot \varphi_{ana(i)}} \qquad \textbf{Eq. 5-4}$$

5.5.2. Automated Model Analysis with MATLAB and Strand7

The ability to automatically manipulate Strand7 FE models within the MATLAB environment lends itself greatly to the overall MM St-Id method, as well as for simple investigations, such as sensitivity studies. To demonstrate the communication between MATLAB and Strand7 for the purposes of the sensitivity study, a flowchart was developed and presented in Figure 5-22.

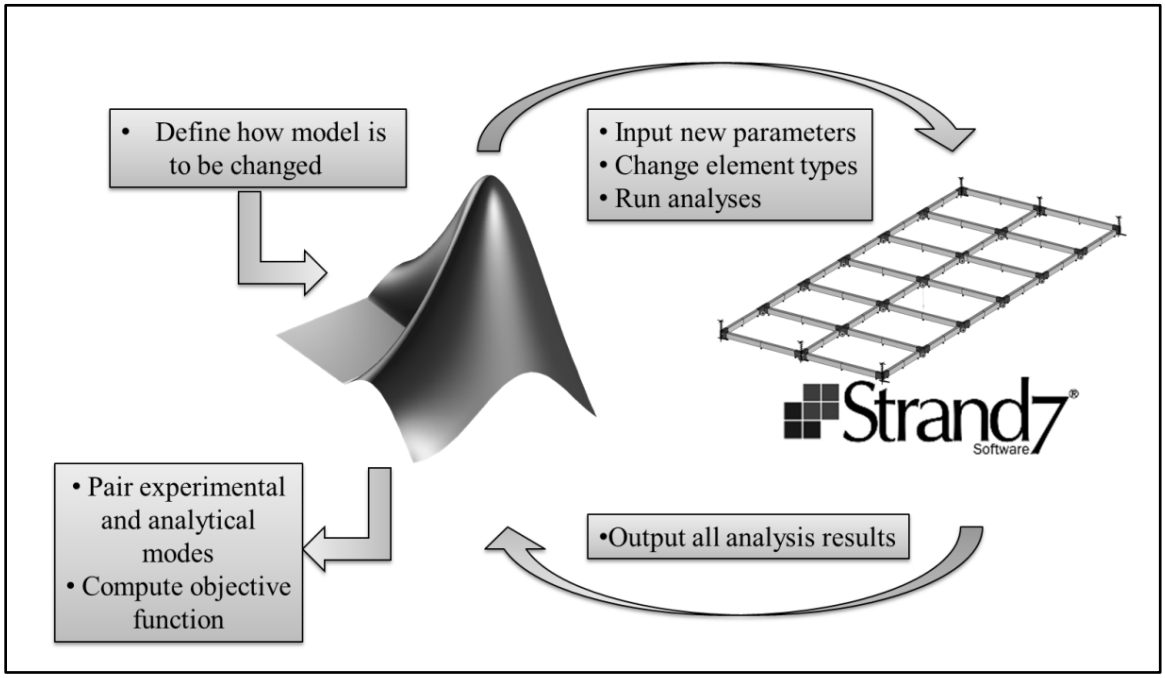

Figure 5-22: Flowchart Demonstrating MATLAB/Strand7 Communication

5.5.3. Selection of Initial Building Block Bounds

The sensitivity study was carried out within the bounds of each building block as listed in Table 5-5. The bounds were selected through a trial and error approach, until it was seen that each building block became relatively stable beyond a certain level. These sensitivity studies were used to then define the ranges over which each of the building blocks would be samples for comparative studies for MM St-Id methods.

The elastic modulus of steel is parameterized as a normalizing constant applied to the nominal value for steel, E_o = 29,000 ksi. The bounds selected for steel range from 70 % to 130 % of its nominal value and a total of fifteen evenly spaced samples were generated

between these bounds. The building block representing both vertical and longitudinal springs were studied between bounds of 0 to 1,000 kip/in by generating evenly spaced samples over a logarithmic axis. Finally, the building blocks representing interior and exterior connection stiffnesses were formulated in terms of percent rigidity within the connection.

The formulation for computing the percent rigidity in terms of the rotational spring, K_r, and the rotational stiffness of the element adjacent to the node, $\frac{3EI}{L}$, is shown below (Eq. 5-5 and Eq. 5-6), where *RF* represents the rigidity factor. The equation is also simplified in terms of K_r. It can then be seen that as *RF* approaches 1, the rotational stiffness asymptotically approaches infinity (rotation fully fixed). Conversely, as *RF* approaches 0, the rotational stiffness also asymptotically approaches 0 (rotation fully released) (Figure 5-23). This factor is convenient because it linearizes a building block with infinite bounds.

$$RF = \frac{K_r}{K_r + \frac{3EI}{L}} \qquad \textbf{Eq. 5-5}$$

$$K_r = \frac{3EI}{\left(\frac{1}{RF} - 1\right)L} \qquad \textbf{Eq. 5-6}$$

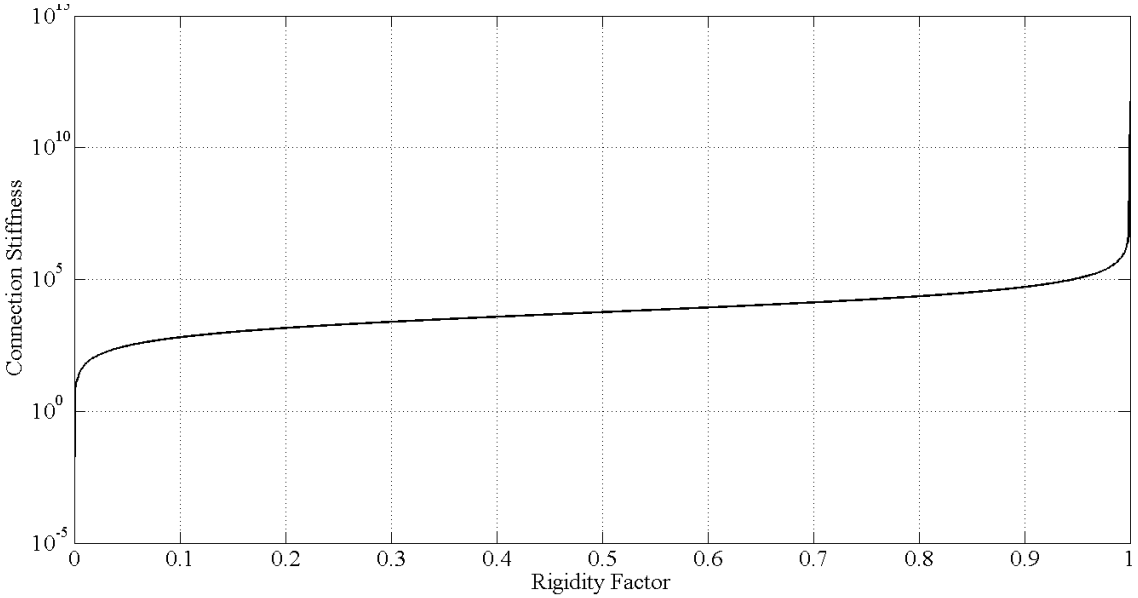

Figure 5-23: Connection Stiffness as a Function of Rigidity Factor

Table 5-5: Bounds used for Sensitivity Study

Building Block	Lower Bound	Upper Bound	Samples	Spacing	Scale
E	0.7 E_o	1.3 E_o	15	Even	Linear
K_v	0 kip/in	1000 kip/in	15	Even	Logarithmic
K_l	0 kip/in	1000 kip/in	15	Even	Logarithmic
K_{r1}	0%	100%	15	Even	Linear
K_{r2}	0%	100%	15	Even	Linear

The sensitivity curves were plotted for examination of the most sensitive regions of each building block (Figure 5-24 - Figure 5-43). Upon examination of the sensitivity studies, the building blocks all appeared to heavily influence the objective function of the FE model. Additionally, the sensitivity studies all appear to be reasonable in terms of what information they are conveying. For instance, the sensitivity plots for E over all structures (Figure 5-24 - Figure 5-27) shows a minimum objective function value of approximately $E=E_o$, which is reasonable.

Also, Structures 1 and 2 had smallest error levels at high vertical spring constants (Figure 5-28 & Figure 5-29) while Structures 3 and 4 appeared to have the least errors over a small range of lower stiffness values (Figure 5-30 & Figure 5-31), reflecting the less stiff neoprene support. For all four structures, the least errors associated with the longitudinal springs occurred when the spring value was small (Figure 5-32 - Figure 5-35). Also, all four structures exhibited a tendency to have both rotational connection stiffnesses at rigid levels (Figure 5-36 - Figure 5-43).

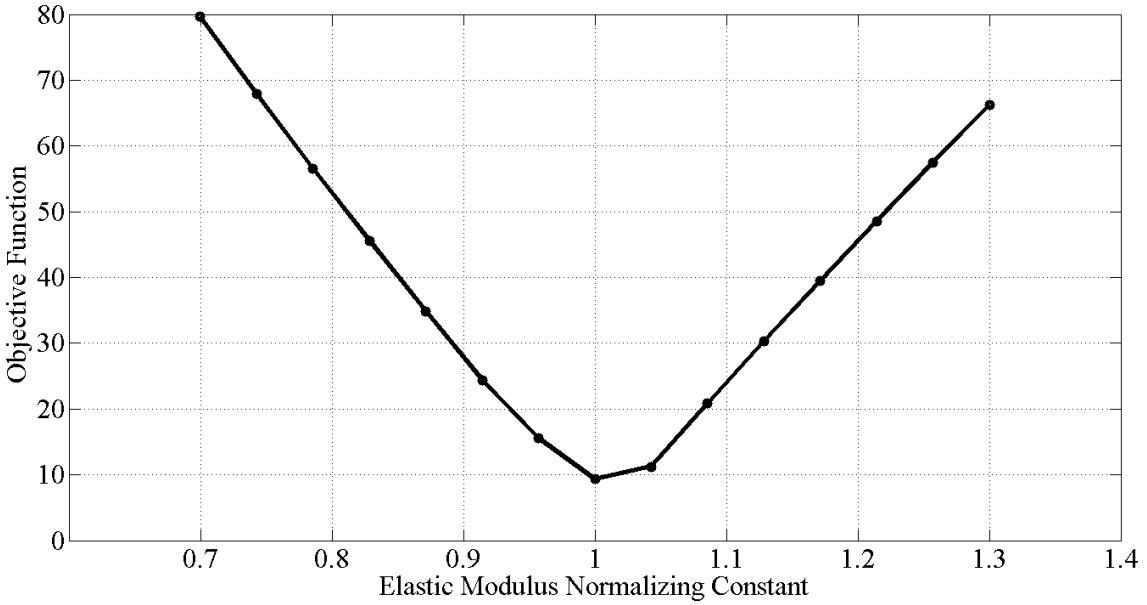

Figure 5-24: Structure 1 Sensitivity Study of Elastic Modulus

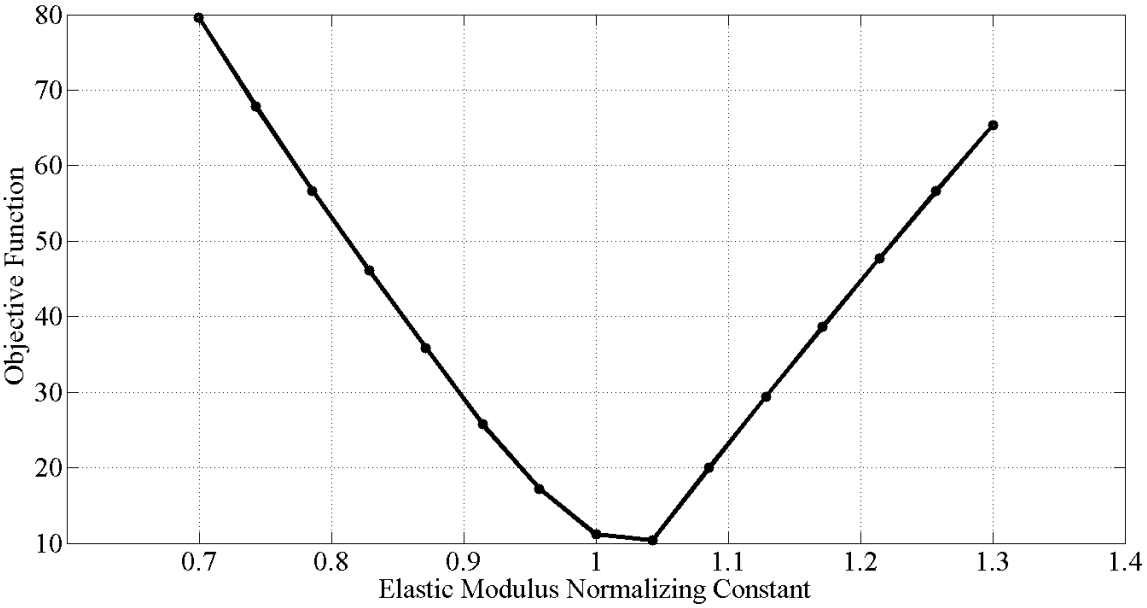

Figure 5-25: Structure 2 Sensitivity Study of Elastic Modulus

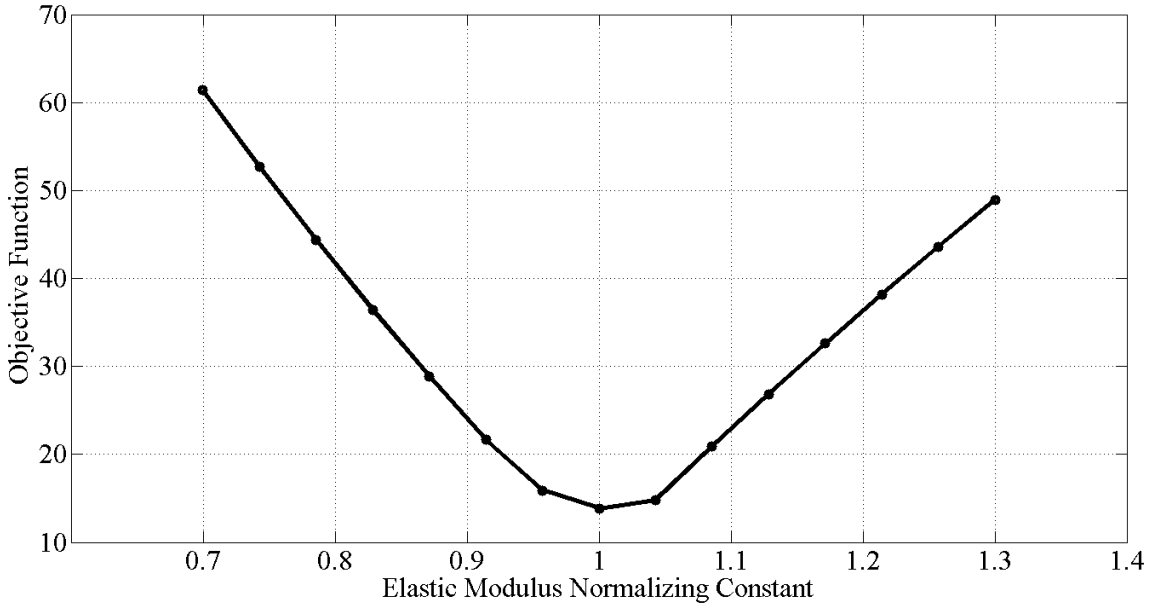

Figure 5-26: Structure 3 Sensitivity Study of Elastic Modulus

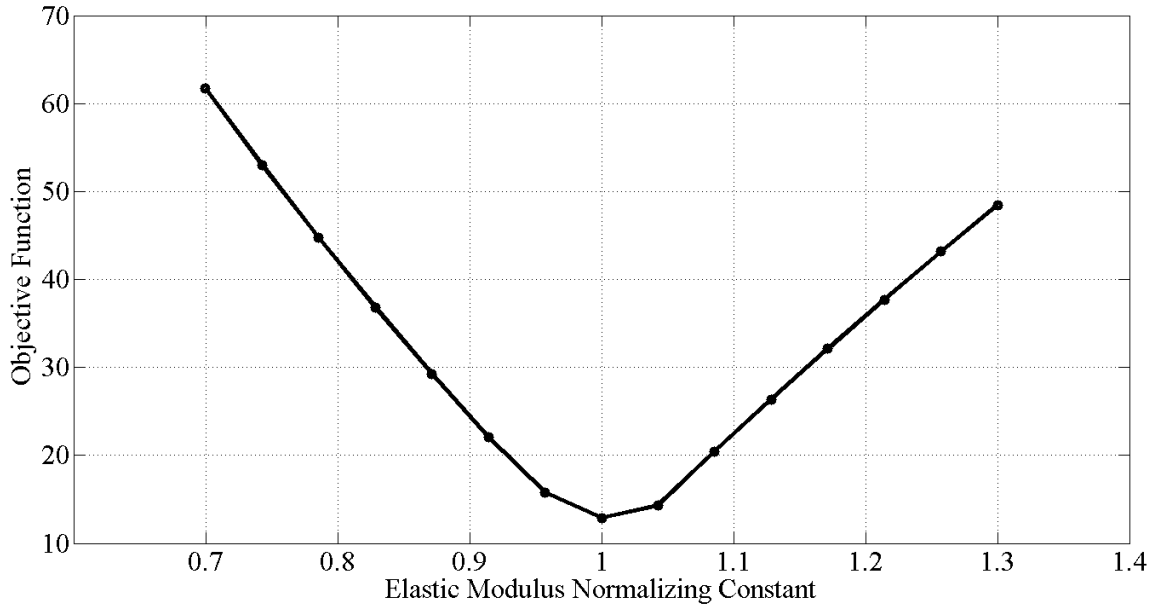

Figure 5-27: Structure 4 Sensitivity Study of Elastic Modulus

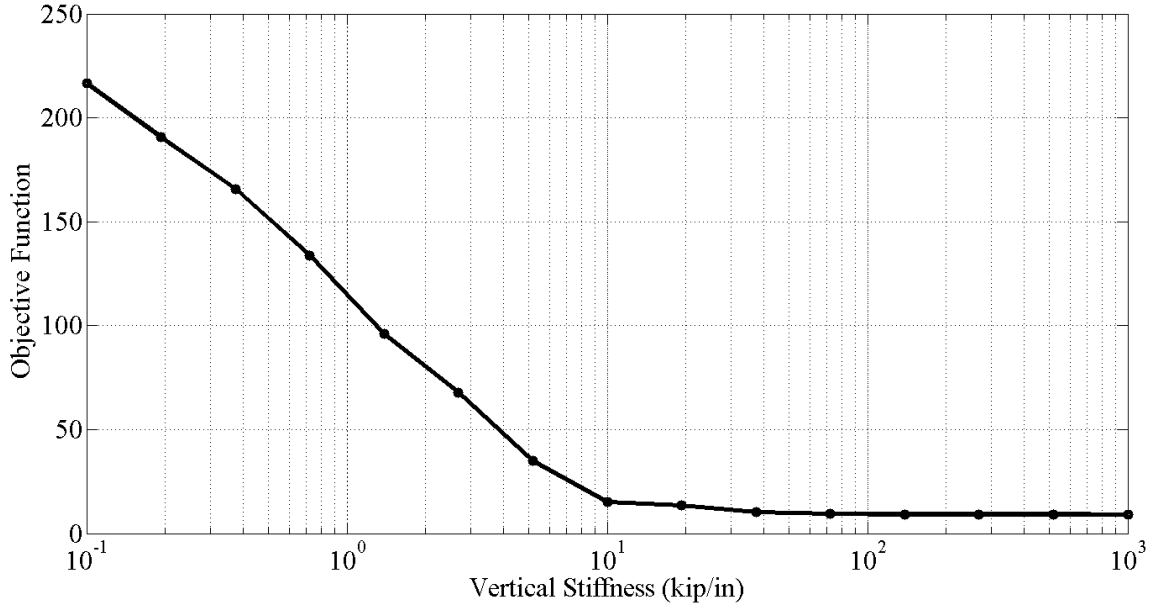

Figure 5-28: Structure 1 Sensitivity Study of Vertical Stiffness

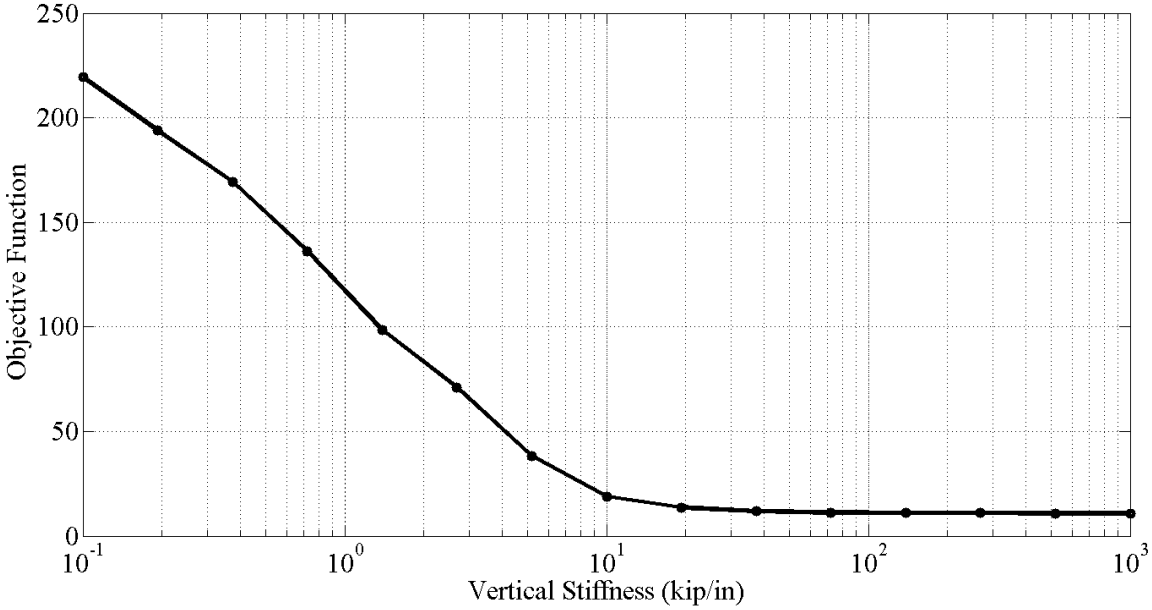

Figure 5-29: Structure 2 Sensitivity Study of Vertical Stiffness

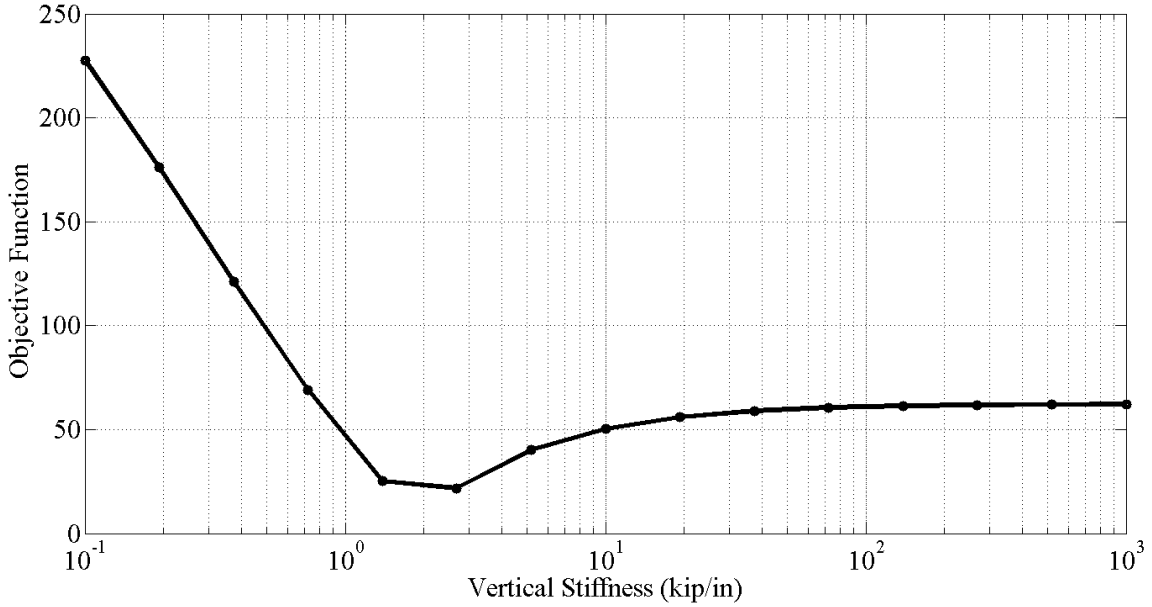

Figure 5-30: Structure 3 Sensitivity Study of Vertical Stiffness

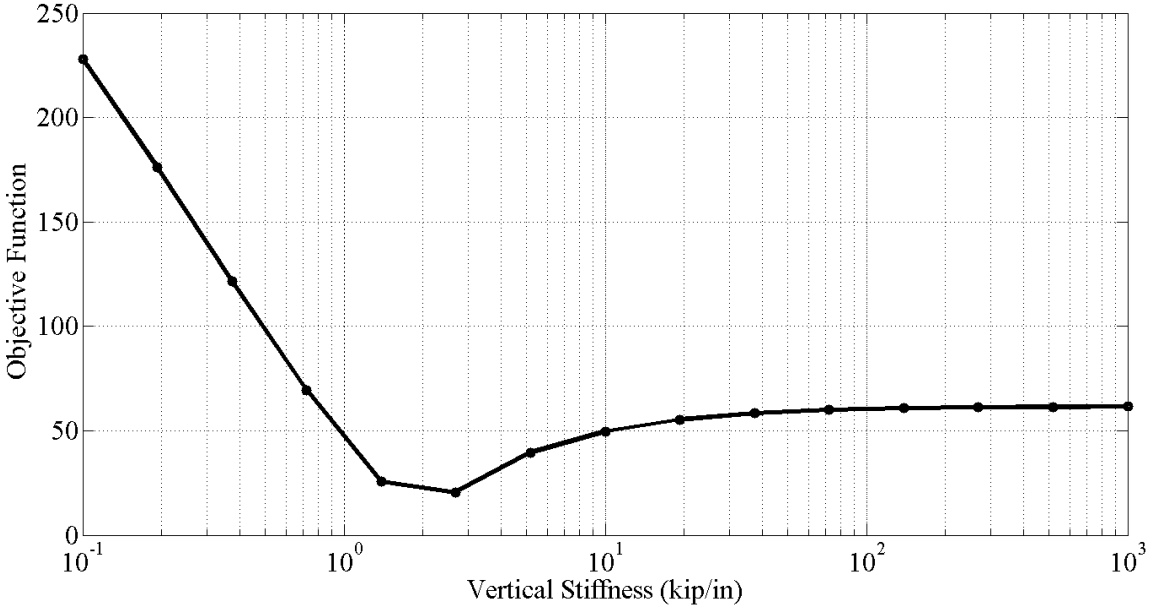

Figure 5-31: Structure 4 Sensitivity Study of Vertical Stiffness

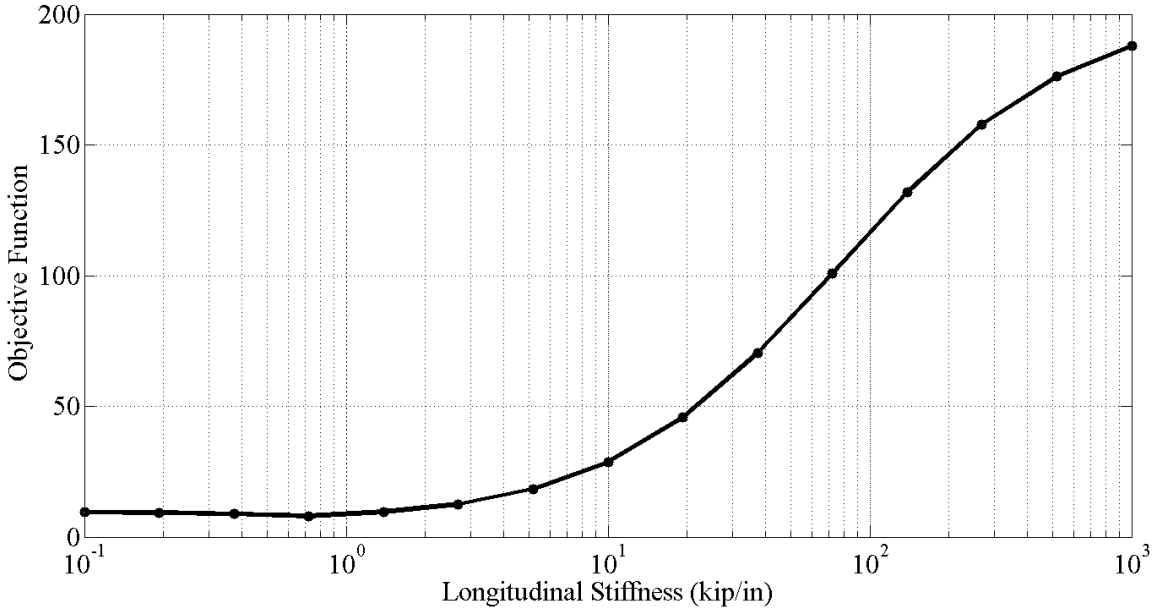

Figure 5-32: Structure 1 Sensitivity Study of Longitudinal Stiffness

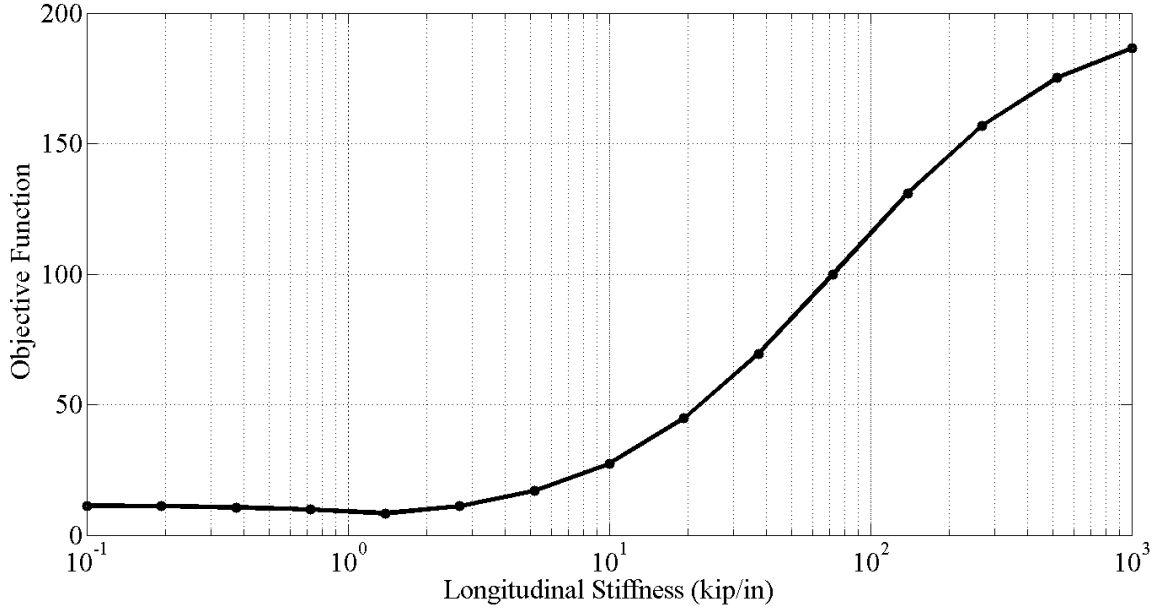

Figure 5-33: Structure 2 Sensitivity Study of Longitudinal Stiffness

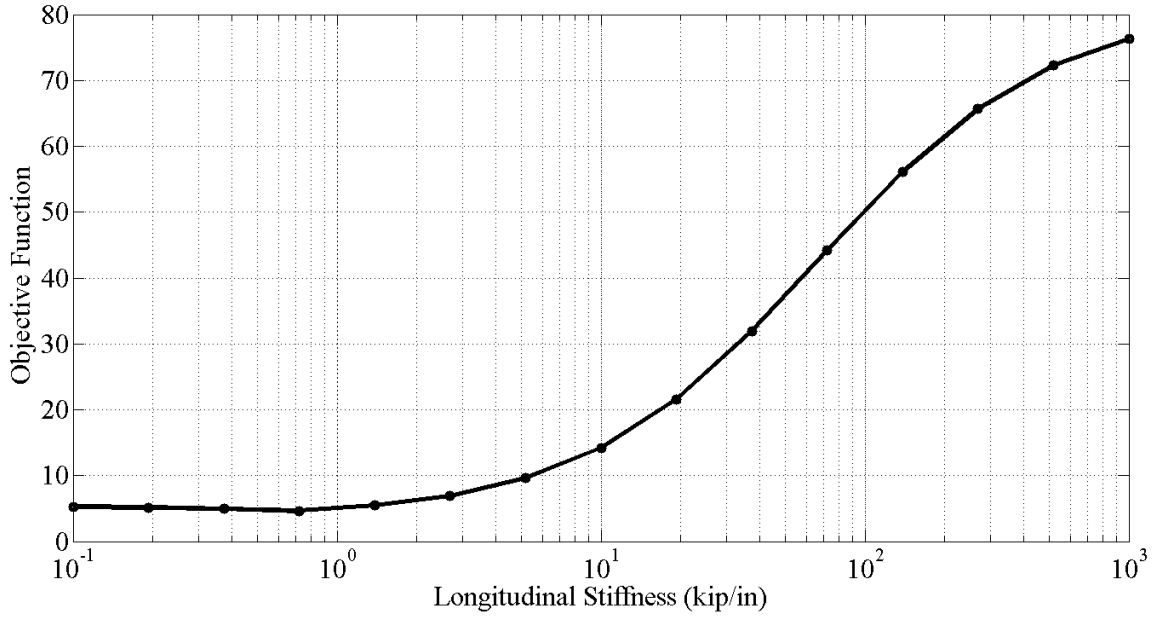

Figure 5-34: Structure 3 Sensitivity Study of Longitudinal Stiffness

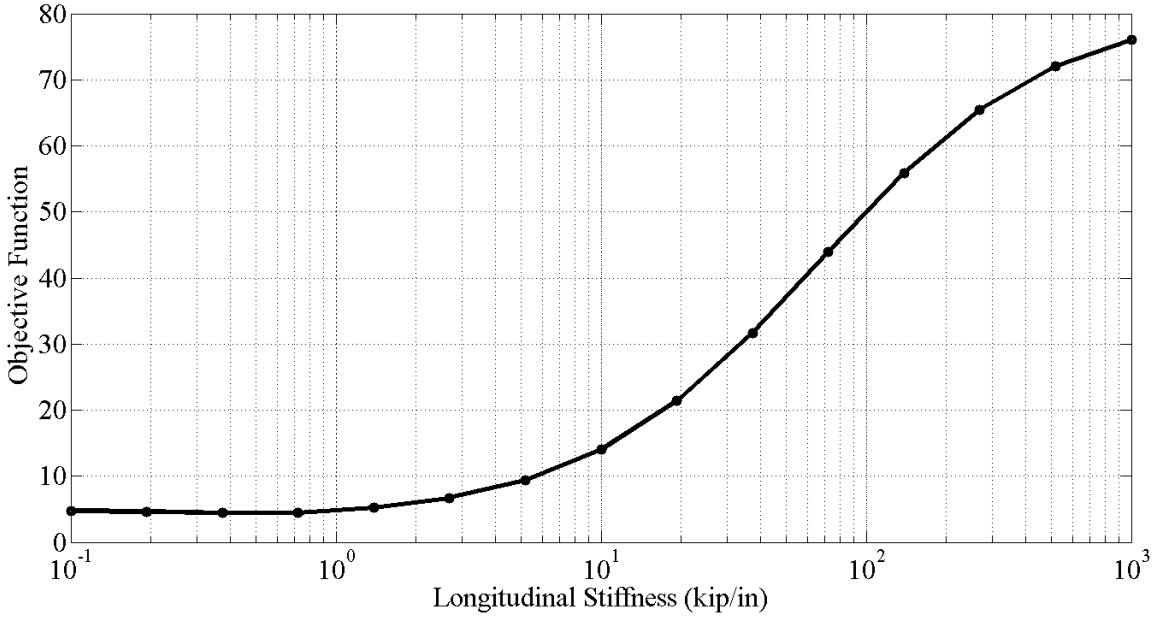

Figure 5-35: Structure 4 Sensitivity Study of Longitudinal Stiffness

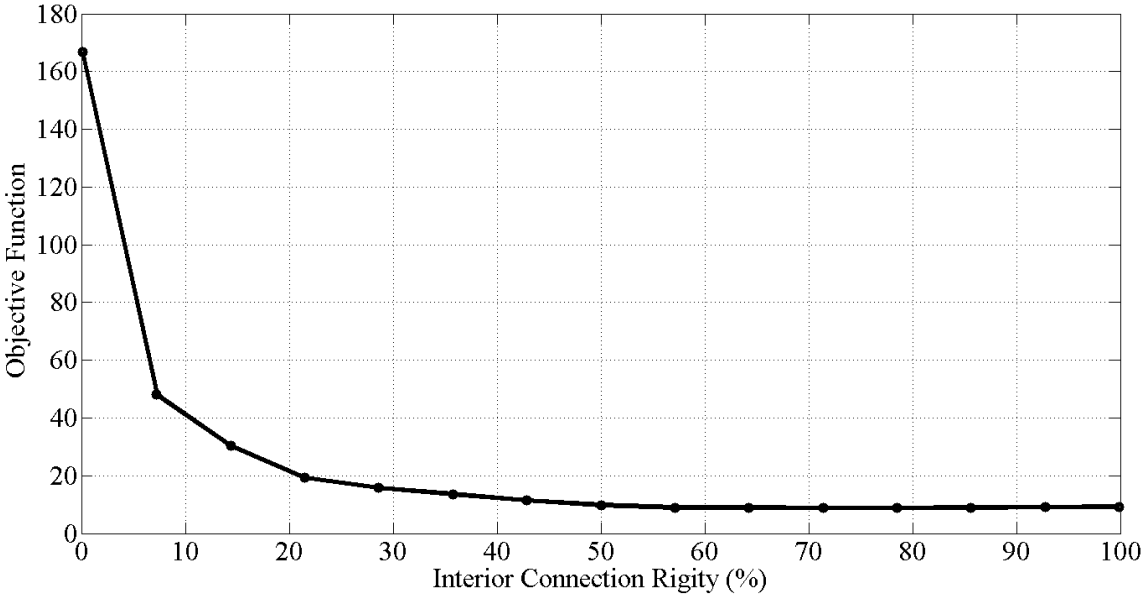

Figure 5-36: Structure 1 Sensitivity Study of Interior Connection Rigidity

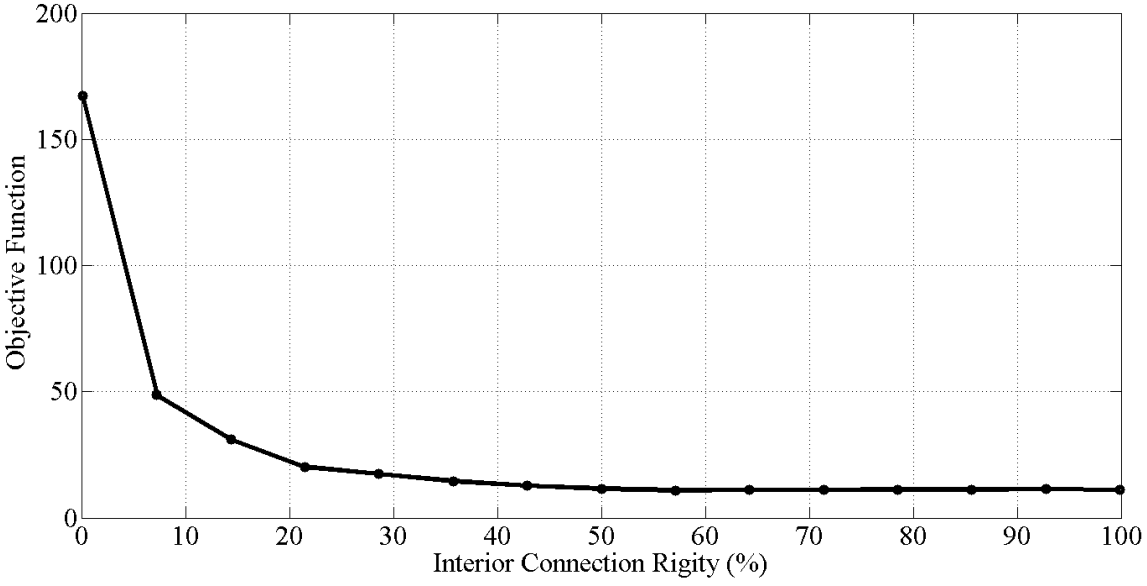

Figure 5-37: Structure 2 Sensitivity Study of Interior Connection Rigidity

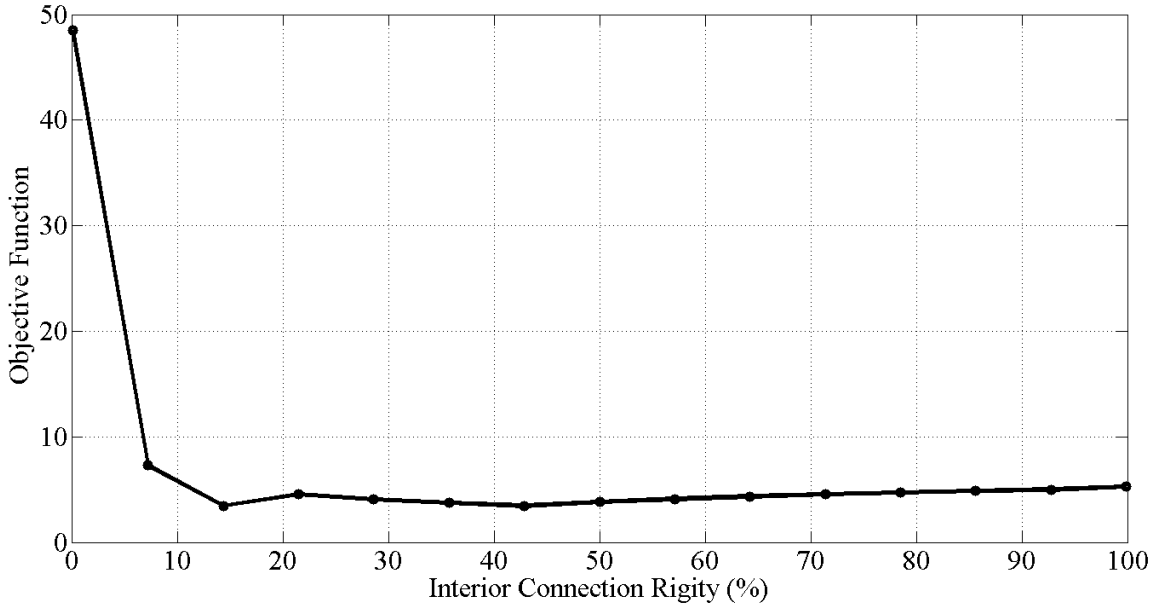

Figure 5-38: Structure 3 Sensitivity Study of Interior Connection Rigidity

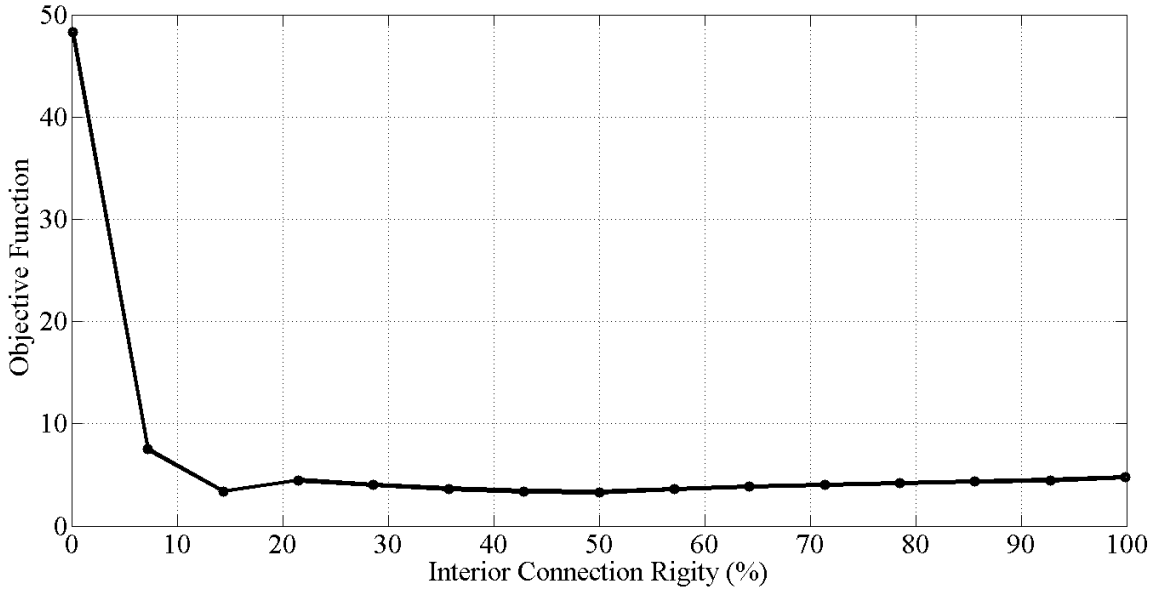

Figure 5-39: Structure 4 Sensitivity Study of Interior Connection Rigidity

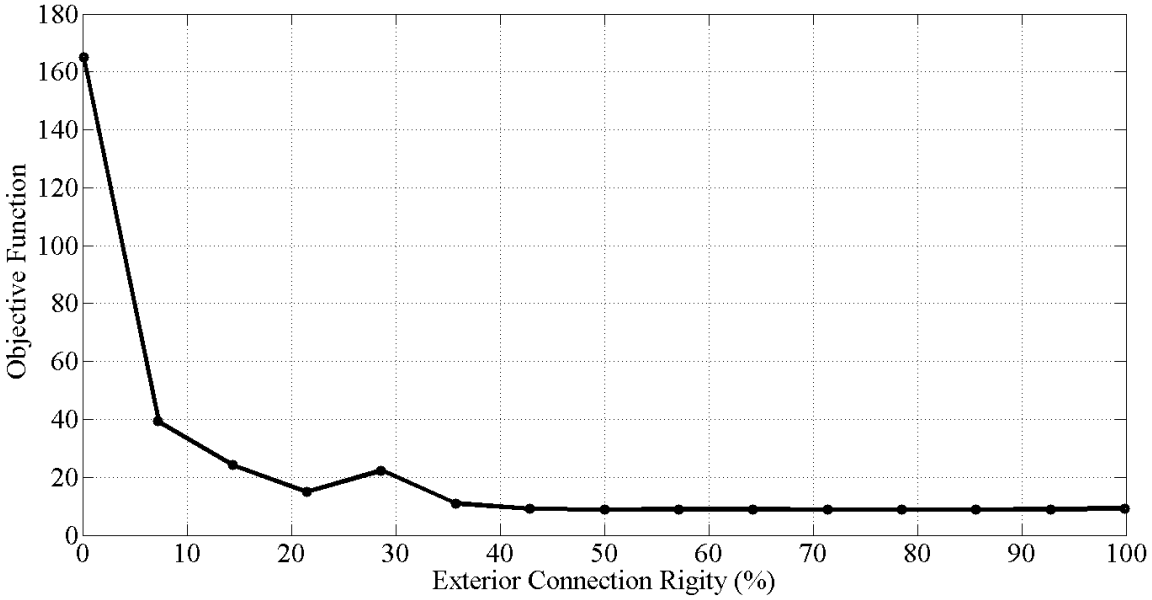

Figure 5-40: Structure 1 Sensitivity Study of Exterior Connection Rigidity

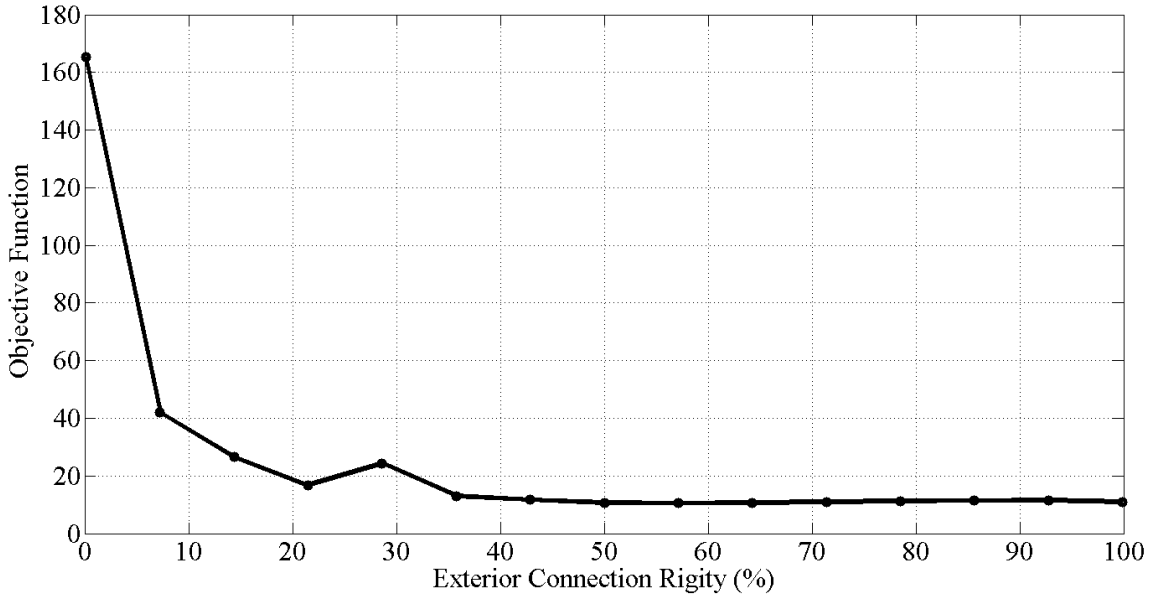

Figure 5-41: Structure 2 Sensitivity Study of Exterior Connection Rigidity

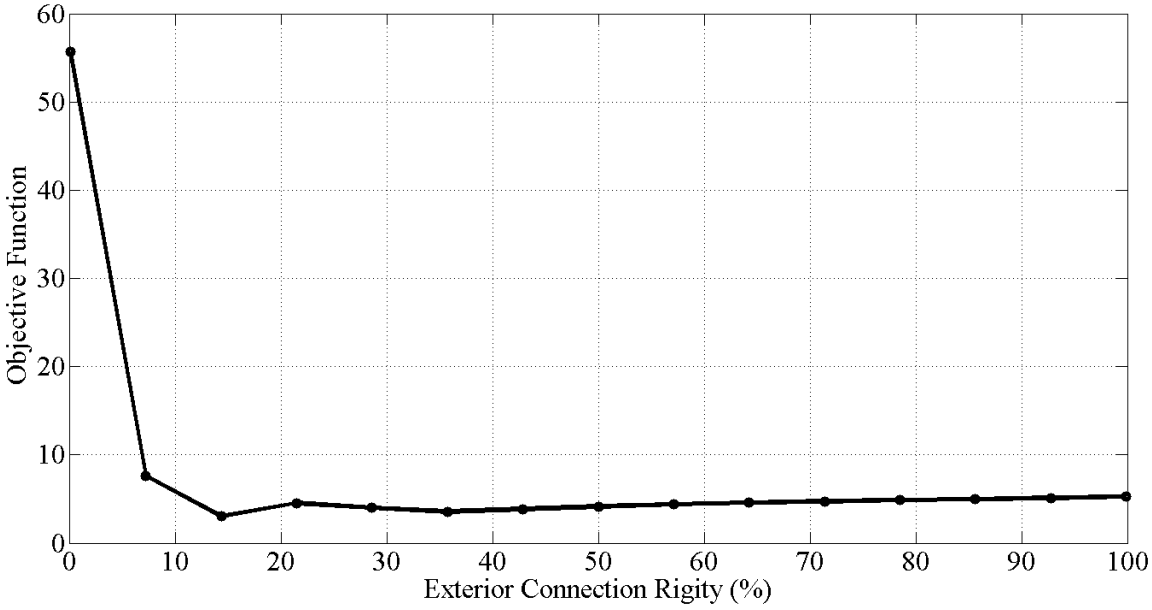

Figure 5-42: Structure 3 Sensitivity Study of Exterior Connection Rigidity

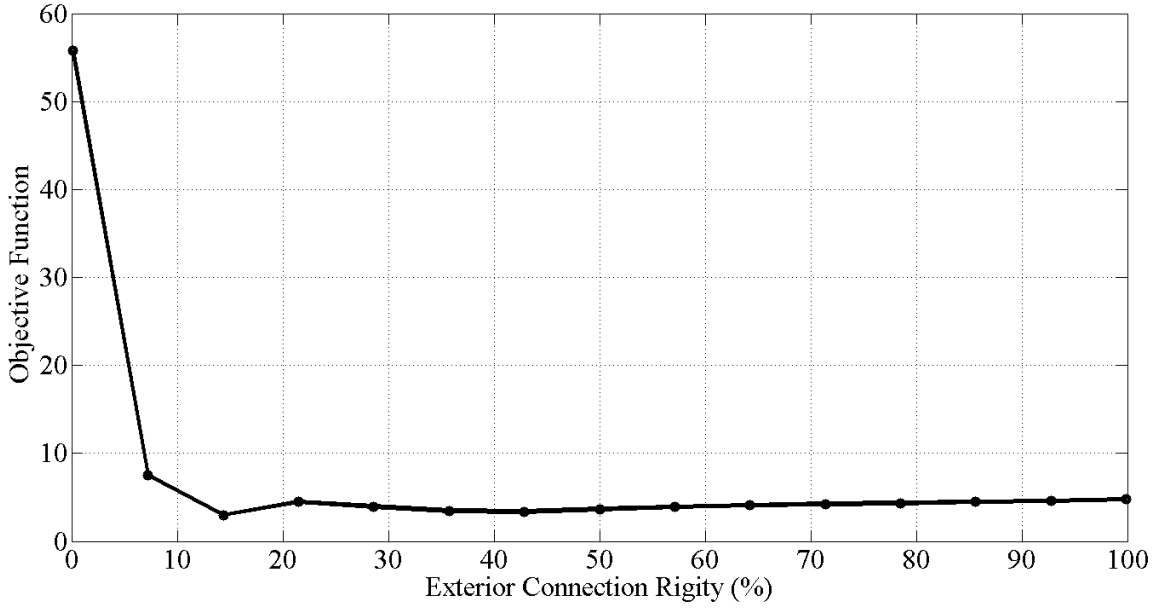

Figure 5-43: Structure 4 Sensitivity Study of Exterior Connection Rigidity

The sensitivity study was informative in that the building blocks were shown to be both influential and reasonable as well as providing for the selection of a more narrow range for each building block. At this stage, the first three steps of the MM St-Id method have been completed and all preparatory work has been finalized. Chapter 6 will discuss the design of the experimental program and the results of the measurements.

CHAPTER 6: EXPERIMENTAL TESTING OF THE GRID STRUCTURE

In order to provide detailed and high quality information for the purpose of developing and validating the proposed MM St-Id method previously outlined, two main types of experimental testing programs were designed for the grid structure. The first experiment carried out was a ‘best practices’ multiple input-multiple output impact test to determine the modal parameters (frequencies, mode shapes, etc.) and their variability. The second experiment was a -static load test aimed to capture both the static displacement/strain responses and their variability under know loads.

6.1. Multi-Reference Impact Testing of the Grid Structure

Multi-reference impact testing (MRIT) was first introduced by (W.G. Halvorsen 1977) as a testing technique to estimate the modal parameters of mechanical systems. The technique was developed following the development of Fast Fourier Transformation (FFT) analysis in the 1960s. In the 1990s, Aktan et al. (Aktan, Farhey et al. 1996; Aktan, Farhey et al. 1997; Aktan, Catbas et al. 1998) began applying this testing technique to bridges and showed that it was a practical and cost-effective alternative to traditional load testing. Of particular interest, was the use of the modal parameters to directly estimate static displaced shapes, which engineers were familiar assessing and had a great deal of intuition and related heuristic knowledge.

It is important to recognize that modal parameters are inherently global measures of response. That is, they do not depend greatly on the properties of the structure in the vicinity of where measurements are taken, but rather they are sensitive to the overall

behavior of the structure (boundary conditions, load paths, mass, stiffness, etc.). The analogous static response is displacements, which are also global in nature but are quite difficult to obtain on civil structures due to the lack of a reference frame (e.g. measuring the vertical displacements of a bridge over water). In contrast, the use of impact testing employs gravitational acceleration as the reference frame and thus overcomes this problem in a very cost-effective manner.

Two independent MRIT applications were carried out on the grid structure for unique research applications at different points in time, allowing for verification of the results obtained by the implementation described in this thesis. The second MRIT application on the grid structure utilized sensors, cables, data acquisition system and analysts which differed from the main work described herein. The original application was carried out on July 18, 2007 while the second application was carried out on June 22, 2011. This independent application of MRIT will be presented for comparative purposes, but the results from the original MRIT application will be utilized in the remainder of the thesis. The original impact testing will be labeled Test 1, while the subsequent impact test will be labeled Test 2.

6.1.1. Sensor Specifications and Calibration

The sensors used for Test 1 consisted of PCB-ICP type, Model 393C, seismic accelerometers with a measureable range of +/- 2g. To excite the structure, a PCB Model 086C20 medium size instrumented impact hammer (Figure 6-5) was used with a firm rubber tip at the locations highlighted in Figure 6-3. The accelerometers were calibrated

in a laboratory setting by utilizing an independently calibrated dynamic load cell and a large mass. By affixing the accelerometers to the mass, one at a time, and striking the load cell, which is affixed to the opposite side of the mass from the accelerometer, it is then possible to use rigid body dynamics and Newton' Second Law, $F=ma$, to derive the theoretical acceleration of the mass from the known mass and impact force. The measured acceleration from the accelerometer is then calibrated based upon the theoretical acceleration to obtain a scaling factor. This process was repeated five times for each accelerometer over various levels of force impacts to ensure that the entire range of the sensors was reliably calibrated. The specifications for the sensors described above are listed in Table 6-1 and Table 6-2.

Table 6-1: Sensor Specifications for PCB 393C

PERFORMANCE	**PCB 393C**
Sensitivity (± 15 %)	1000 mV/g
Measurement Range	2.5 g pk
Frequency Range (± 5 %)	0.025 to 800 Hz
Frequency Range (± 10 %)	0.01 to 1200 Hz
Resonant Frequency	≥ 3.5 kHz
Broadband Resolution(1 to 10,000 Hz)	0.0001 g rms
Non-Linearity	≤ 1 %
Transverse Sensitivity	≤ 5 %
ENVIRONMENTAL	
Overload Limit(Shock)	± 100 g pk
Temperature Range	-65 to +200 °F
Temperature Response	<0.03 %/°F
Base Strain Sensitivity	0.001 g/με
ELECTRICAL	
Excitation Voltage	18 to 30 VDC
Constant Current Excitation	2 to 20 mA
Output Impedance	<100 ohm
Output Bias Voltage	3.0 to 4.5 VDC
Discharge Time Constant	≥ 20 sec
Settling Time	300 sec
Electrical Isolation(Base)	$\geq 10^8$ ohm
PHYSICAL	
Sensing Element	Quartz
Sensing Geometry	Compression
Housing Material	Stainless Steel
Sealing	Hermetic
Size (Diameter x Height)	2.25 in x 2.16 in
Weight	31.2 oz

Table 6-2: Sensor Specifications for the PCB 086C20

PERFORMANCE	**PCB 086C20**
Sensitivity (± 15 %)	1 mV/lbf
Measurement Range	± 5000 lbf pk
Resonant Frequency	≥ 12 kHz
Non-Linearity	≤ 1 %
ELECTRICAL	
Excitation Voltage	20 to 30 VDC
Constant Current Excitation	2 to 20 mA
Output Impedance	<100 ohm
Output Bias Voltage	8 to 14 VDC
Discharge Time Constant	≥ 1400 sec
PHYSICAL	
Sensing Element	Quartz
Sealing	Hermetic
Hammer Mass	2.4 lb

The second MRIT application used PCB Model 393A-03 piezoelectric accelerometers with a measureable range of +/- 5g, with specifications shown in Table 6-3. The structure was excited with a PCB Model 086C42 instrumented sledge hammer, with specifications shown in Table 6-4.

Table 6-3: PCB 393A-03 Specifications

PERFORMANCE	**ENGLISH**	**SI**
Sensitivity (± 5 %)	1000 mV/g	102 mV/(m/s²)
Measurement Range	± 5 g pk	± 49 m/s² pk
Frequency Range (± 5 %)	0.5 to 2000 Hz	0.5 to 2000 Hz
Frequency Range (± 10 %)	0.3 to 4000 Hz	0.3 to 4000 Hz
Frequency Range (± 3 dB)	0.2 to 6000 Hz	0.2 to 6000 Hz
Resonant Frequency	≥ 10 kHz	≥ 10 kHz
Broadband Resolution (1 to 10,000 Hz)	0.00001 g rms	0.0001 m/s² rms
Non-Linearity	≤ 1 %	≤ 1 %
Transverse Sensitivity	≤ 7 %	≤ 7 %
ENVIRONMENTAL		
Overload Limit(Shock)	± 5000 g pk	± 49,050 m/s² pk
Temperature Range	-65 to +250 °F	-54 to +121 °C
Temperature Response	See Graph	See Graph
Base Strain Sensitivity	≤ 0.0005 g/με	≤ 0.005 (m/s²)/με
ELECTRICAL		
Excitation Voltage	18 to 30 VDC	18 to 30 VDC
Constant Current Excitation	2 to 20 mA	2 to 20 mA
Output Impedance	<250 ohm	<250 ohm
Output Bias Voltage	8 to 12 VDC	8 to 12 VDC
Discharge Time Constant	1 to 3 sec	1 to 3 sec
Settling Time	<15 sec	<15 sec
Spectral Noise(1 Hz)	2 μg/√Hz	20 (μm/sec^2)/√Hz
Spectral Noise(10 Hz)	0.5 μg/√Hz	5 (μm/sec^2)/√Hz
Spectral Noise(100 Hz)	0.2 μg/√Hz	2 (μm/sec^2)/√Hz
Spectral Noise(1 kHz)	0.1 μg/√Hz	1 (μm/sec^2)/√Hz
Electrical Isolation(Case)	≥ 10^8 ohm	≥ 10^8 ohm
PHYSICAL		
Sensing Element	Ceramic	Ceramic
Sensing Geometry	Shear	Shear
Housing Material	Stainless Steel	Stainless Steel
Sealing	Hermetic	Hermetic
Size (Hex x Height)	1 3/16 in x 2 3/16 in	30.2 mm x 55.6 mm
Weight	7.4 oz	210 gm

Table 6-4: PCB 086C42 Hammer Specifications

PERFORMANCE	**ENGLISH**	**SI**
Sensitivity (± 15 %)	1 mV/lbf	0.23 mV/N
Measurement Range	± 5000 lbf pk	± 22,240 N pk
Resonant Frequency	≥ 5 kHz	≥ 5 kHz
Non-Linearity	≤ 1 %	≤ 1 %
ELECTRICAL		
Excitation Voltage	20 to 30 VDC	20 to 30 VDC
Constant Current Excitation	2 to 20 mA	2 to 20 mA
Output Impedance	<100 ohm	<100 ohm
Output Bias Voltage	8 to 14 VDC	8 to 14 VDC
Discharge Time Constant	≥ 2000 sec	≥ 2000 sec
PHYSICAL		
Sensing Element	Quartz	Quartz
Sealing	Hermetic	Hermetic
Hammer Mass	12.1 lb	5.5 kg

6.1.2. Data Acquisition Specifications

The Test 1 configuration routed all accelerometer and impact hammer sensors to a data acquisition system via coaxial cables and corresponding required connectors. Each cable was run to a breakout box, which allowed for up to eight coaxial connections per box and which reduced the eight incoming coaxial cables to a single data cable. The three breakout boxes were directly connected to the data acquisition system. The data acquisition system used for the impact test measurements of Test 1 was an HP VXI Model E8401A chassis with three HP E1432A modules driven by the MATLAB based program X-Acquisition developed by the University of Cincinnati Structural Dynamics Laboratory (UC-SDRL 2004) (Figure 6-1). The specifications of the module are shown in Table 6-5.

Table 6-5: Specifications for the HP E1432A Module

ANALOG INPUT	
Channels	16
Differential Channels	16
Resolution	16 bits
Sample Rate	51.2 kS/s
Bandwidth	23 kHz
Simultaneous Sampling	Yes
Input Impedance	500 kOhm

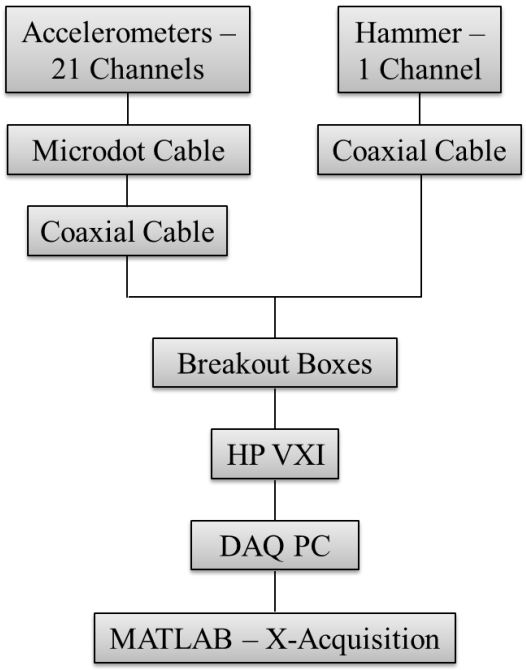

Figure 6-1: DAQ System Flowchart for Test 1

The data acquisition system used for Test 2 was a National Instruments (NI) compactRIO (cRIO) eight slot chassis equipped with six NI 9234 four channel modules with specifications listed in Table 6-6. The NI modules contain internal signal conditioning, thus neglecting the need for additional equipment, as was required during Test 1, and providing a more streamlined DAQ system (Figure 6-2). The accelerometers and impact hammer were connected directly to the cRIO modules via coaxial cables with no extra cables or connectors necessary.

Table 6-6: Specifications for Ni 9234 cRIO Module

ANALOG INPUT	
Channels	4
Differential Channels	4
Resolution	24 bits
Capable Sample Rate	51.2 kS/s
Bandwidth	23.04 kHz
Simultaneous Sampling	Yes
Input Impedance	305 kOhm

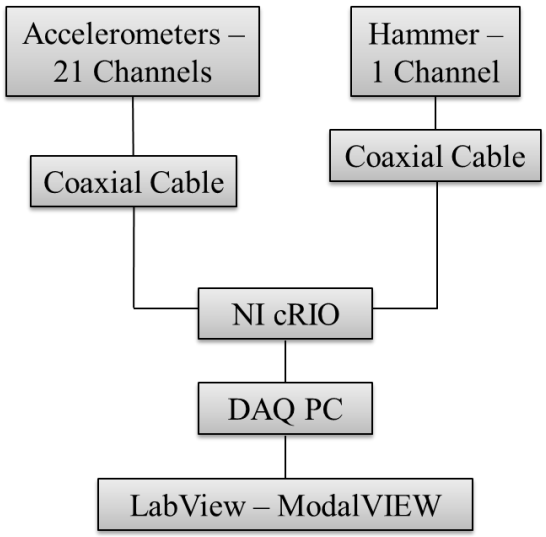

Figure 6-2: DAQ System Flowchart for Test 2

6.1.3. Instrumentation Plan

The impact test was designed with a highly discretized sensor layout, consisting of one uniaxial accelerometer per grid connection (Figure 6-3) for a total of twenty-one sensors. The accelerometers were attached to the structure with magnetic bases (Figure 6-4) and were located on the bottom plate of the connections. This configuration allowed for an impact at each connection point with the accelerometer properly positioned to accurately capture the driving point response. This level of instrumentation was chosen so that a thorough set of natural frequencies and associated well characterized modeshapes could be confidently identified based on the simulated mode shapes from the preliminary FE model and was utilized for both Test 1 and Test 2 (discussed in Chapter 5).

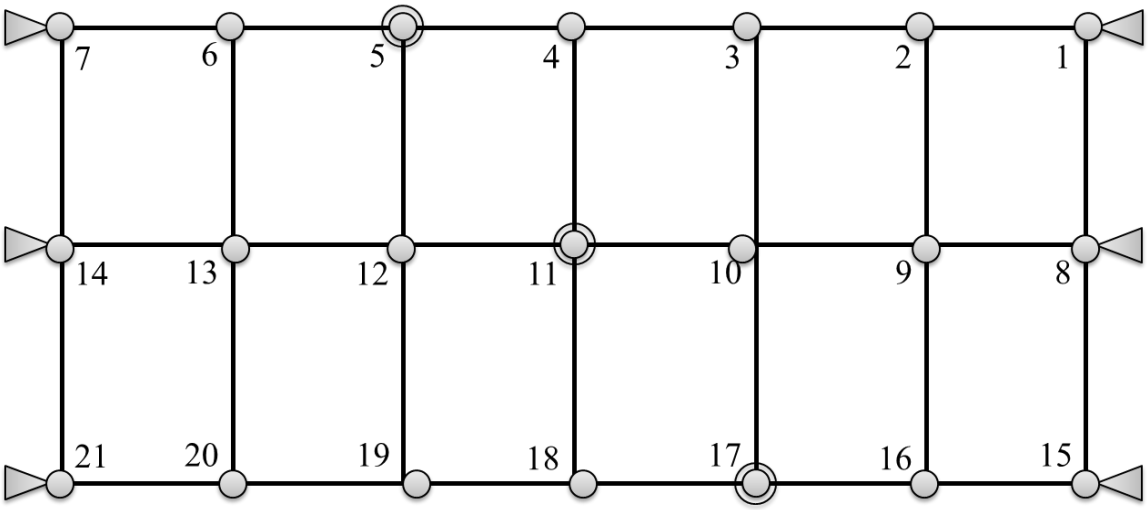

Figure 6-3: DI3 Grid Dynamic Instrumentation Plan: Output Locations (circles), Impact Locations (Double Circle) and Supports (Triangles)

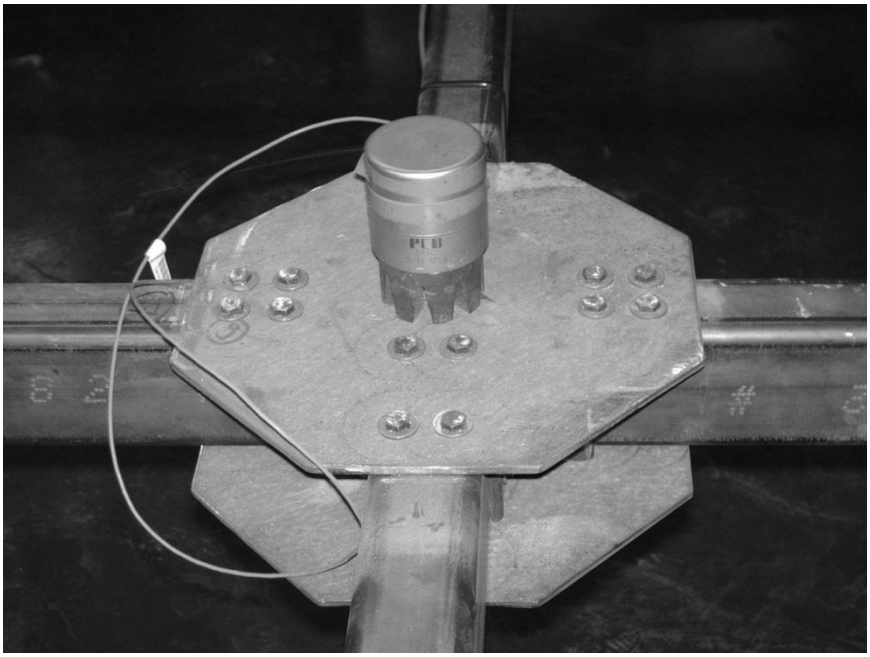

Figure 6-4: PCB 393C Seismic Accelerometer Mounted on a Magnetic Base Attached to the Grid

Figure 6-5: PCB 086C20 Medium Impact Hammer

To efficiently capture the desired modal properties, a total of three impact locations were selected to best excite the structure in all anticipated frequencies. These points were selected based on the simulation results of the preliminary FE model to ensure that each mode had non-negligible amplitudes at a minimum of two impact locations. By avoiding nodal locations of modes of interest during an impact test, a large number of modes can be excited. The impact locations used (Figure 6-3) were selected for their ability to both excite the fundamental natural frequencies and selected high order modeshapes as well as providing for the ability to check reciprocity between symmetric impact locations and were also used in both Test 1 and Test 2 setups.

6.1.4. Selection of Measurement Specifications

Preliminary testing for the Test 1 setup was conducted to determine appropriate sampling speeds and other program settings, such as windowing, for data collection and processing. Initially, sensors were sampled at 800Hz and accelerometer responses were windowed with an exponential window while the impact response was windowed with a rectangular window. After reviewing measurements from the trial impact tests, it was decided to reduce the sampling speed to 400Hz since the highest mode of interest occurred at 39Hz, well below the Nyquist frequency, discussed below, of 200Hz. Due to the low damping of the grid structure, the amount of time until the structure came to rest after each impact was significant. Therefore the reduction of sampling speed aided in reducing the amount of data collected over this period of time, while not compromising the quality of the results. A full comparison of DAQ settings implemented for Test 1 and Test 2 are described below in Table 6-7.

Table 6-7: DAQ Protocols for Test 1 and Test 2

DAQ Protocol	Test 1	Test 2
Sampling Speed	400 Hz	3,200 Hz
DAQ Software	X-Modal	ModalVIEW
Impacts per Location	5	3

The Nyquist frequency is the limit below which signal aliasing will not occur, but above which aliasing can occur. Signal aliasing occurs when a periodic signal with a very high frequency is sampled at a rate lower than its fundamental frequency. The result can be an aliased signal (Figure 6-6), where an apparent signal appears and leads to misinterpretation if not addressed. In Figure 6-6, the high frequency signal, in this case 0.9 Hz, is sampled at a rate of 1 Hz. An apparent 0.1 Hz sine wave results if the circles are fit with a sine wave, thus creating a scenario where the data could be misinterpreted. To avoid this, it is best practice to ensure that all desired frequencies are below the Nyquist frequency, defined as one-half of the sampling frequency so that aliasing can be avoided.

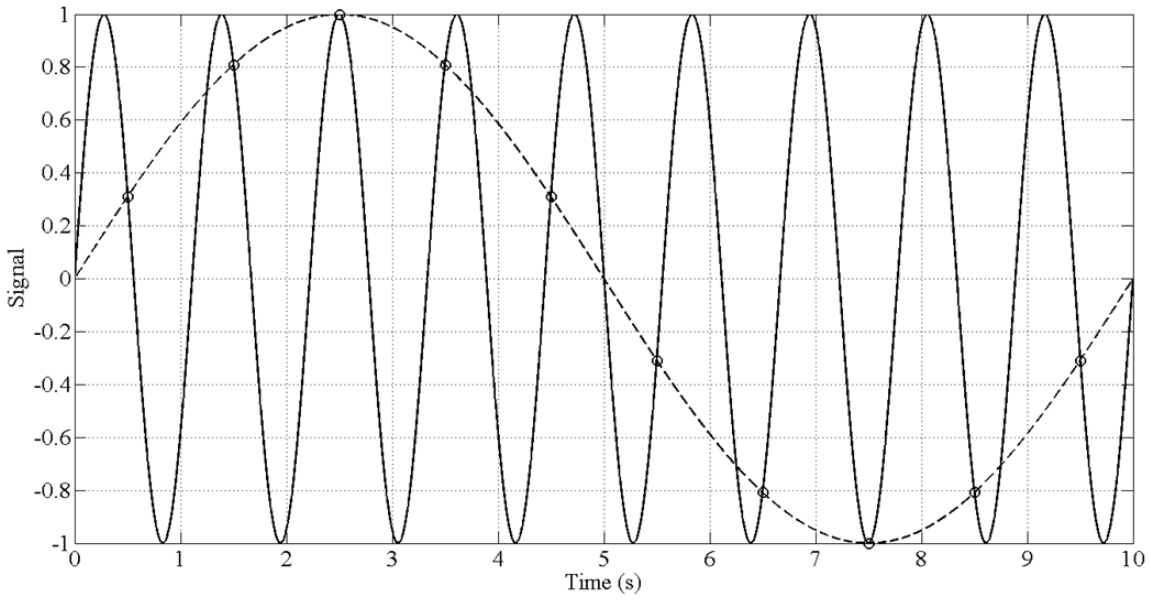

Figure 6-6: Example of an Aliased Signal

6.1.5. Execution of the Impact Test

To follow current best practice methods, each impact test was repeated five times. Frequency response functions (FRFs) were computed in real time and compared to previous impacts at each location. An FRF relates the Fourier transform of the system input to the Fourier transform of the system response (Allemang 1999). FRF generation, with the advent of computing power in the 1980's, has been the most commonly used approach to modal testing of structures with the aim of capturing modal parameters (Allemang 1999). FRFs develop the relationship between single or multiple inputs with the measured outputs of a system. The FRFs contain vast amounts of information regarding the physical properties of the structure and are typically made up of complex numbered values. The imaginary portion of the FRF contains peak responses at the location of the natural frequencies, the magnitude of which serves as the modeshape coefficient for that degree of freedom and frequency, while the real portion of the FRF has zero crossings at the location of the natural frequencies. Additionally, a 180 degree phase drop occurs at the location of the natural frequencies. These three identifying characteristics allow for thorough identification of real modes of the system.

With the development of computer techniques to compute inverse Fourier transformations (IFFT), it was possible to produce impulse response functions from the observed FRF, thus allowing for time domain analysis in addition to the frequency domain analysis.

The coherence of a set of impacts was displayed after each hit allowing the user to cancel the test and restart the set of five impacts if data quality was compromised. Coherence

represents how well two signals are related and can be used to ensure that the system is remaining linear and stationary. Following this set of standards during the impact testing, roughly 33% of the impact test sets were discarded or stopped during the set of five impacts due to a poor impact by the user.

Additionally, alarms were triggered if any accelerometer recorded a response above its specified measurement range, automatically requiring the user to restart the set of five impact tests. In this manner, significant time was saved by reviewing FRFs and coherence in real time as opposed to a later time, after the sensors and data acquisition system were shut down and removed.

6.1.6. Data Quality Assurance and Error Screening

Following the impact tests, further data quality analysis was carried out by inspecting the FRFs for reciprocity among symmetric locations. Reciprocity between symmetric locations is used to verify that the structure is behaving in a linear manner and has a symmetric stiffness matrix, consistent with structural analysis theory that the displacement at node *i* of a structure due to a unit load at node *j* is equivalent to the displacement at node *j* due to a unit load at node *i*.

Similarly, the FRF of the response at node 5 of the grid due to an impact at node 17 should be equivalent to the FRF of the response at node 17 due to an impact at node 5. The reciprocity between impacts at nodes 5 and 17 is shown below (Figure 6-7) and is shown to have excellent reciprocity. While it is seen that the FRFs do not completely superimpose one another, it is only within the regions of anti-resonance and is expected.

The regions around the poles of the frequencies do superimpose one another, and shows sufficient reciprocity.

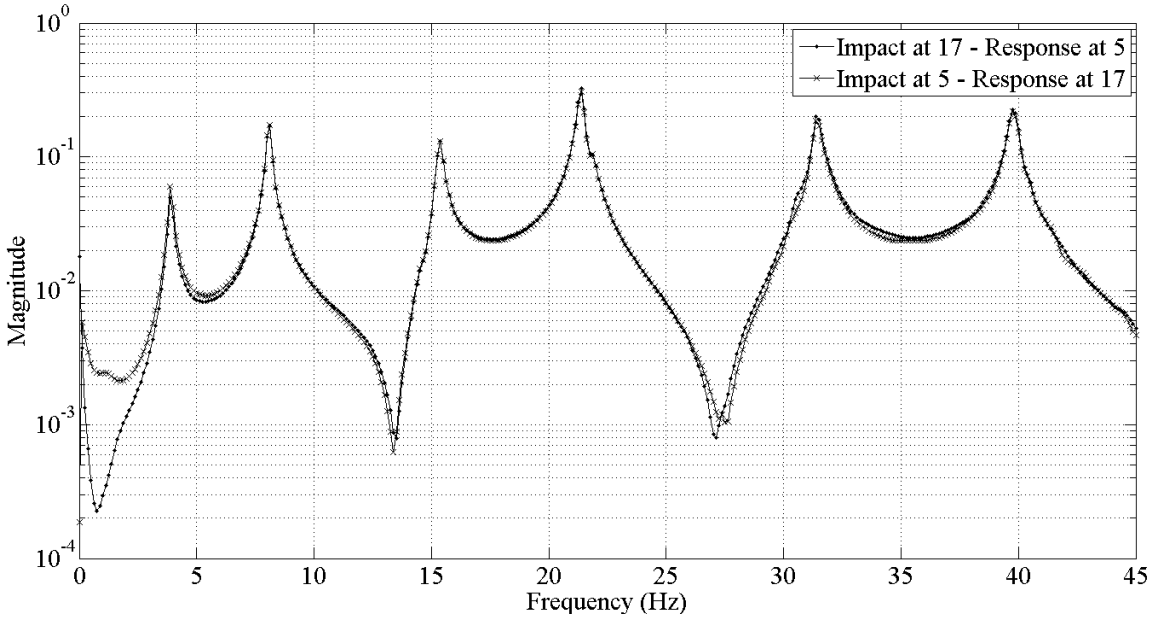

Figure 6-7: Reciprocity check for locations 5 and 17

Another tool utilized for data quality analysis was the identification of repeatability over the course of the five impacts at each location. Repeatability is the study of how consistent measurements are through estimates of modal parameters from each independent data set. An erroneous impact test could compromise the average of the five FRFs, however by inspecting the modal parameters from each individually this was mitigated. The results from one set of impacts from Test 1 at Node 5 is shown below as

an example of how repeatability can be used to ensure data quality. Note that in the results from the impact tests at this location, Mode 6 was not identified due to low excitation. The mean and standard deviation of the modal parameter estimates from the five impacts are also shown as a measure of how well each impact test was able to replicate the estimates from the other tests. In this case, the repeatability is very high, given the low deviations of the responses.

Table 6-8: Modal Parameter Estimation from Impacts at Point 5 from Test 1

	Frequencies (Hz)					Statistics	
Hit at Point 5	1	2	3	4	5	$\bar{x}$	σ
Mode 1	3.853	3.861	3.854	3.837	3.834	3.848	0.012
Mode 2	8.087	8.084	8.075	8.087	8.063	8.079	0.010
Mode 3	15.321	15.315	15.321	15.319	15.312	15.318	0.004
Mode 4	21.384	21.382	21.381	21.383	21.376	21.381	0.003
Mode 5	31.411	31.392	31.398	31.418	31.397	31.403	0.011
Mode 6	-	-	-	-	-	-	-
Mode 7	39.813	39.807	39.808	39.812	39.807	39.809	0.003

Finally, the time histories were analyzed to ensure that the signals were being sufficiently captured by the DAQ system. A common problem which can arise due to low sampling speeds is clipping, where the acceleration response appears very choppy and magnitudes of peak acceleration responses are clearly clipped. The lack of sufficient characterization

of the raw acceleration time histories can lead to further degradation of the FRFs once the time history has been transformed into the frequency domain.

6.1.7. Data Pre-processing

Acceleration and force time histories must be windowed for accurate computation of the frequency response function (FRF) associated with the impact. The computation of the FRF requires a Fast Fourier Transform (FFT) of the time histories of the acceleration response and the impact. The FFT process takes a discrete time signal and makes it periodic by repeating the time history. If the signal at the end of the time history has not damped down to a zero response level, then the FFT process can suffer from errors associated with leakage. To mitigate this error, the time history can be windowed with an exponential window to force the signal to completely damp out by the end of the time history. The window is exponential so that the nature of the structure's free response, exponential in nature, is not compromised. The effect of the windowing to the properties of the signal is not apparent in the estimates of frequencies and modeshapes, but is apparent in the calculation of damping associated with these modes as an increase in the damping for each mode. As an example of exponential windowing, Figure 6-8 shows the application of an exponential window to an acceleration time history for a separate structure in the DI3 laboratory. An appropriate window is one that minimally damps the signal over the period of the measurement time history.

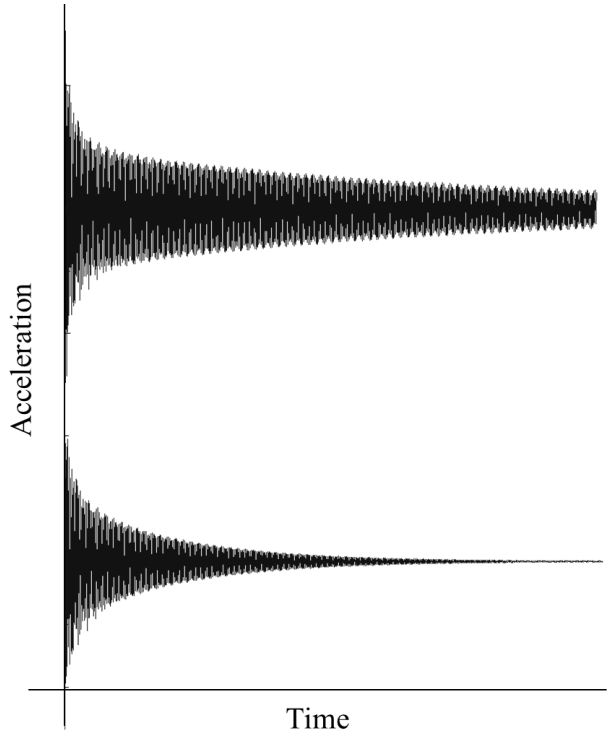

Figure 6-8: An Un-windowed Time History (Top) and a Windowed Time History (Bottom)

The force time history must also be windowed so that only the portion of time where the hammer is in contact with the structure is accounted for within the FRF calculation. Since the user of the hammer has to stop its motion after the impact, the output signal of the hammer can show a force measurement after the initial impact but is attributed to the inertia of the hammer coming to rest by the user. This type of windowing is accomplished by using a rectangular window, where the time history outside of the main impact to the structure is zero-padded and the signal during the impact period is multiplied by one. It must be noted that the user always took extreme care to not have multiple hits to the structure, and if this occurred the test was repeated. Both Test 1 and Test 2 applications

utilized exponential windows for the acceleration responses and rectangular windows for the impulse response.

6.1.8. Data Post-Processing (Modal Identification)

Once the data quality was shown to be satisfactory, the modal parameters were obtained by processing the averaged FRFs from each impact location with both the Complex Mode Indicator Function (CMIF) algorithm (Shih et al. 1988, (Catbas, Brown et al. 2004) and the Poly-reference Time Domain (PTD) algorithm (Deblauwe, Allemang et al. 1987) for Test 1 and the CMIF algorithm for Test 2. Additionally, FRFs were interpreted by hand to obtain frequencies, mode shapes and damping estimates using the "peak picking" technique for verification of the CMIF and PTD modal parameter estimation methods. Allemang and Brown (1997) provide a thorough overview of the many types of modal parameter estimation techniques available to analysts, however CMIF and PTD algorithms were chosen for their ability to identify closely spaces modes in the FRF's as well as their availability in the X-Modal software package.

The CMIF algorithm finds the singular value decomposition at each frequency line of the FRF, thus allowing for processing of multiple reference data. The algorithm produces an enhanced estimate of both the natural frequency and the magnitude of the pole for each degree of freedom. This is beneficial since manual methods of extracting frequencies and modeshapes can fall victim to issues associated with the discrete nature of the FRF and can only practically operate on one FRF at a time.

The PTD algorithm for obtaining estimates of modal parameters utilizes the time domain representation of the observed data belongs to a class of algorithms developed to analyze data corresponding to a free decay response however is also suitable to impulse response type applications. One advantage over using PTD for MRIT applications over free decay problems is that the known input provides proper scaling of the modal parameters obtained. The method works by computing an impulse response function by taking the IFFT of the FRF generated. PTD provides a benefit in that it utilizes all reference measurements in formulating the modal parameter estimates, which requires that the data be obtained by a synchronous system to ensure that time invariance does not contribute errors. The mathematical models then inputs the impulse response functions into a parameter estimation scheme which estimates the modal parameters.

6.1.9. Impact Test Results

A set of seven frequencies and modeshapes were consistently obtained among the three experimental setups corresponding to the steel supports and five frequencies and modeshapes consistently identified among the three setups corresponding to the neoprene supports. The natural frequencies are listed below for the various configurations (Table 6-10 - Table 6-13) and corresponding mode shapes are also presented (Figure 6-10 - Figure 6-33). The comparisons between Test 1 and Test 2 estimates of Structure 1's natural frequencies in addition to the comparison of CMIF and PTD estimates for all structures indicate that the frequencies selected were stable estimates of the structural proprieties. Additionally, the modeshapes from the two tests were compared by

computing MAC values for each combination of the seven modeshapes identified in Test 1. The MAC value matrix is presented graphically (Figure 6-9) and in tabular form (Table 6-9). The high MAC values (where 1.0 represents perfect correlation) along the diagonal indicate that modes 1 through 7 of Test 1 are very well correlated with modes 1 through 7 of Test 2, respectively, with no similarities along the off diagonal terms, meaning that mode 2 of Test 1 is not correlated at all with mode 5 of Test 2, for example.

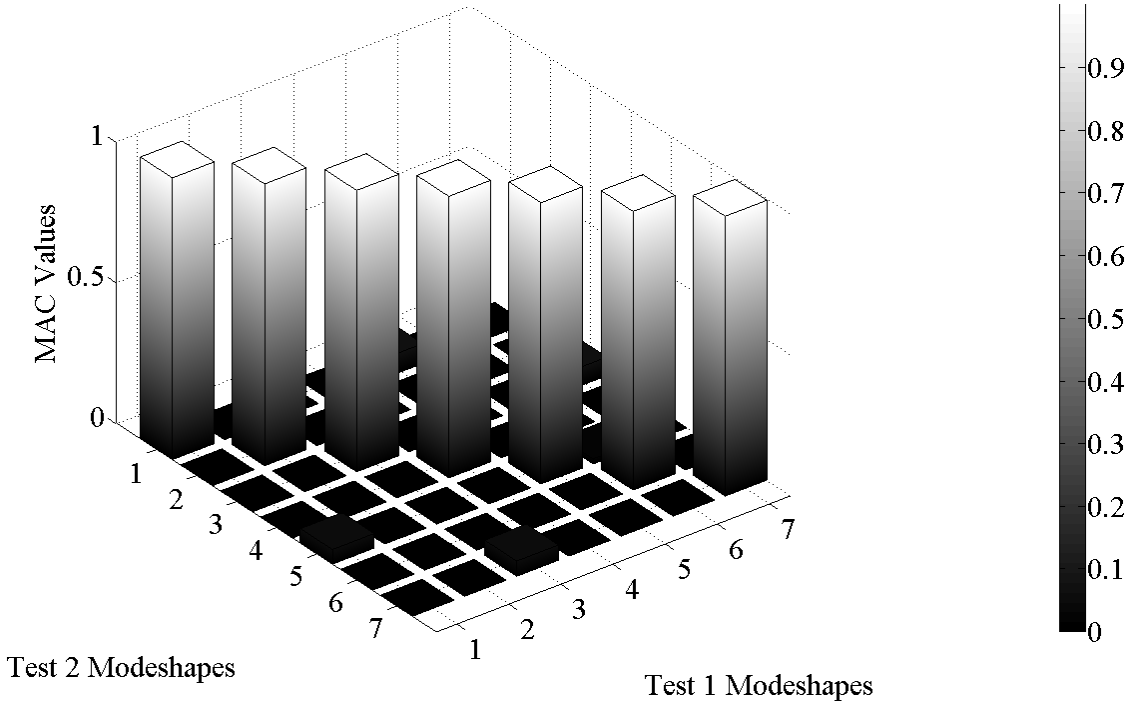

Figure 6-9: Graphical Representation of MAC Value Matrix

Table 6-9: Matrix Representation of MAC Values

	Mode 1	Mode 2	Mode 3	Mode 4	Mode 5	Mode 6	Mode 7
Mode 1	0.9995	0.0004	0.0000	0.0000	0.0705	0.0006	0.0001
Mode 2	0.0001	0.9997	0.0000	0.0002	0.0001	0.0000	0.0000
Mode 3	0.0001	0.0002	0.9983	0.0009	0.0004	0.0003	0.0658
Mode 4	0.0000	0.0006	0.0001	0.9988	0.0001	0.0001	0.0000
Mode 5	0.0517	0.0001	0.0001	0.0000	0.9976	0.0181	0.0002
Mode 6	0.0000	0.0000	0.0005	0.0005	0.0002	0.9884	0.0001
Mode 7	0.0006	0.0000	0.0539	0.0000	0.0016	0.0000	0.9928

It is noted that there was negligible change in the response of the Damage level I and Damage level II structures. However, significant changes were achieved by changing the supports from a steel pin to a neoprene pin as well as changing the connections from fully intact to partially loosened. For this reason, only the four structural configurations consisting of these modifications are considered in future use. Structure 1 will be considered as having the steel pin support and rigid connection; Structure 2 will be considered as having the steel pin supports and loosened connection; Structure 3 will be considered as having the neoprene pin support and rigid connection while Structure 4 will be considered as having the neoprene pin support with loosened connection. It should be noted that the MRIT Test 2 application only tested the Structure 1 configuration.

Table 6-10: Structure 1 Natural Frequency Estimations

Structure 1						
Mode	CMIF - Test 1 (1)	PTD (2)	CMIF - Test 2 (3)	%Δ (1-2)	%Δ (1-3)	%Δ (2-3)
1	3.851	3.888	3.926	0.97	1.96	0.98
2	8.081	8.082	8.219	0.01	1.71	1.70
3	15.320	15.334	15.378	0.09	0.38	0.29
4	21.380	21.364	21.735	-0.07	1.66	1.74
5	31.393	31.372	31.694	-0.07	0.96	1.02
6	33.022	33.018	33.370	-0.01	1.05	1.07
7	39.804	39.790	40.355	-0.04	1.38	1.42

Table 6-11: Structure 2 Natural Frequency Estimations

Structure 2			
Mode	CMIF - Test 1 (1)	PTD (2)	%Δ (1-2)
1	3.853	3.880	0.70
2	7.988	8.071	1.04
3	15.259	15.296	0.24
4	21.214	21.190	-0.12
5	27.674	27.484	-0.69
6	33.022	32.995	-0.08
7	36.158	36.368	0.58

Table 6-12: Structure 3 Natural Frequency Estimations

Structure 3			
Mode	CMIF - Test 1 (1)	PTD (2)	%Δ (1-2)
1	3.686	3.705	0.52
2	7.093	7.085	-0.10
3	12.280	12.290	0.08
4	15.882	15.894	0.07
5	30.439	30.451	0.04
6	34.633	34.613	-0.06
7	38.909	38.905	-0.01

Table 6-13: Structure 4 Natural Frequency Estimation

Structure 4			
Mode	CMIF - Test 1 (1)	PTD (2)	%Δ (1-2)
1	3.699	3.711	0.32
2	7.121642857	7.108	-0.19
3	12.29064286	12.311	0.17
4	15.70286667	15.704	0.01
5	28.01738462	28.664	2.31
6	34.20584615	34.322	0.34
7	38.517	38.433	-0.22

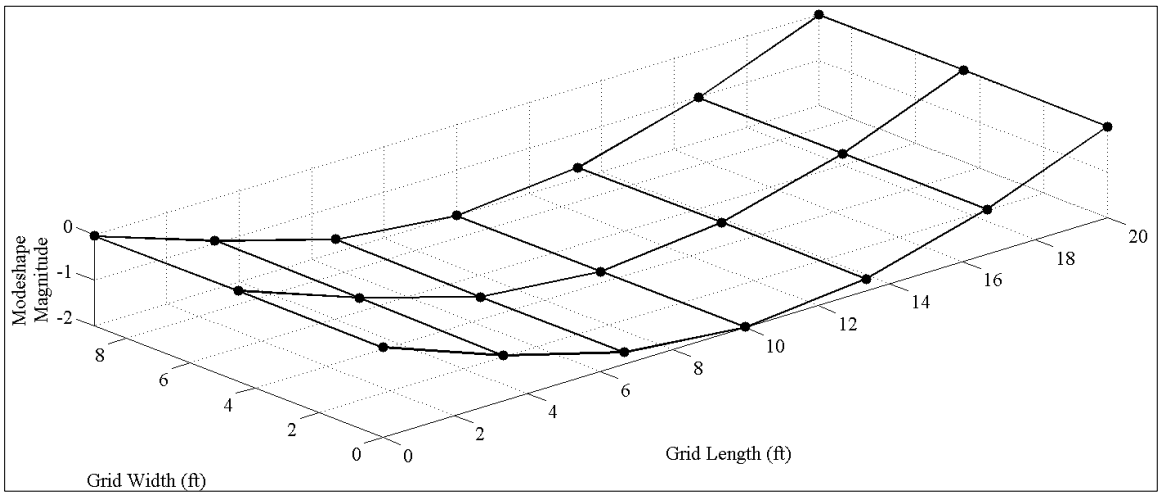

Figure 6-10: Structure 1, Mode 1 (First Bending)

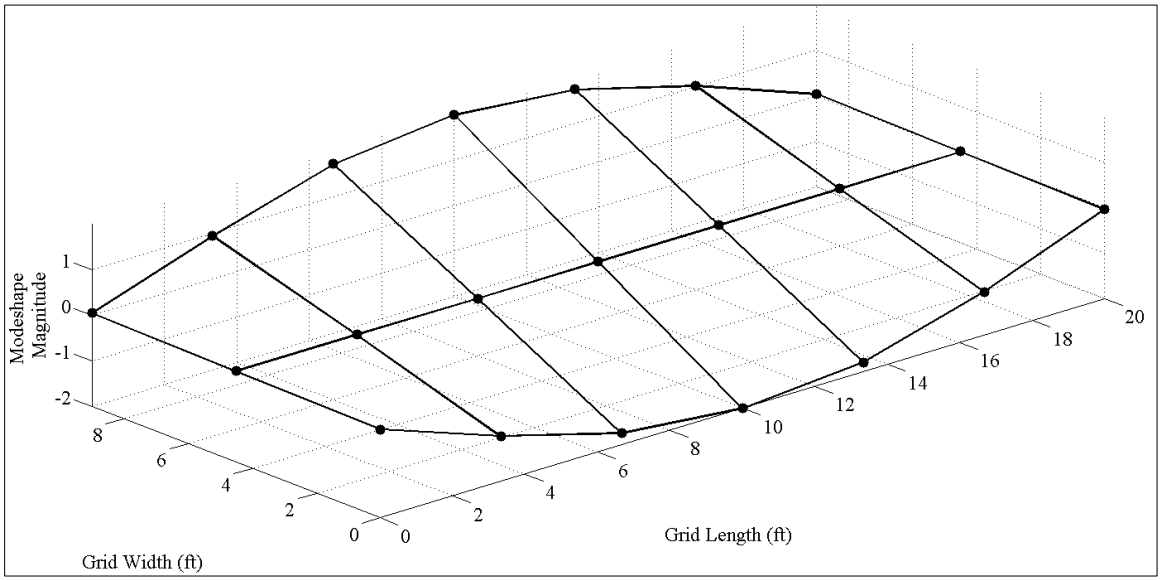

Figure 6-11: Structure 1, Mode 2 (First Torsion)

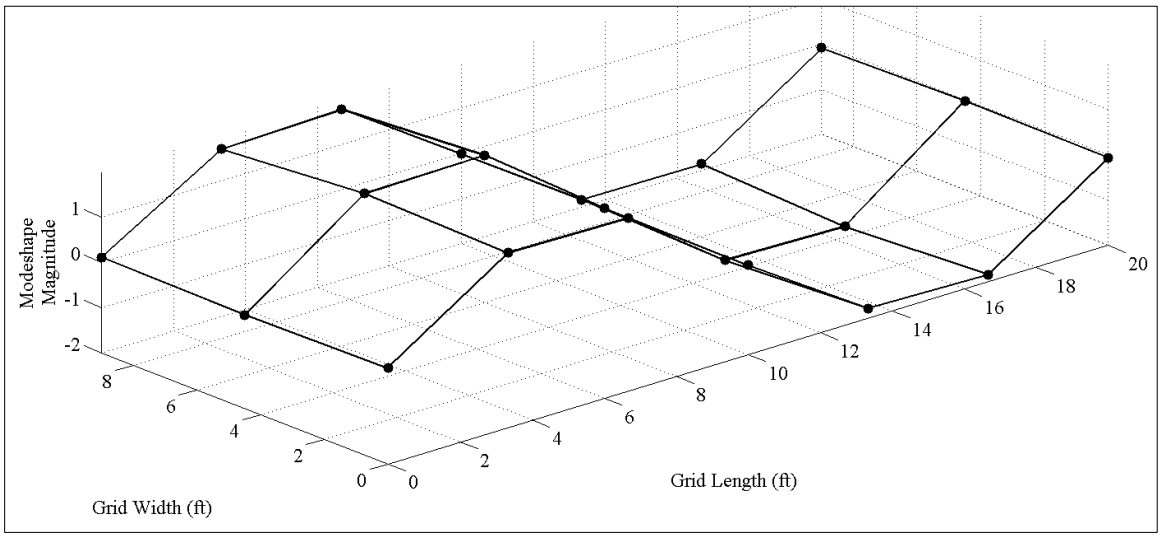

Figure 6-12: Structure 1, Mode 3 (Second Bending)

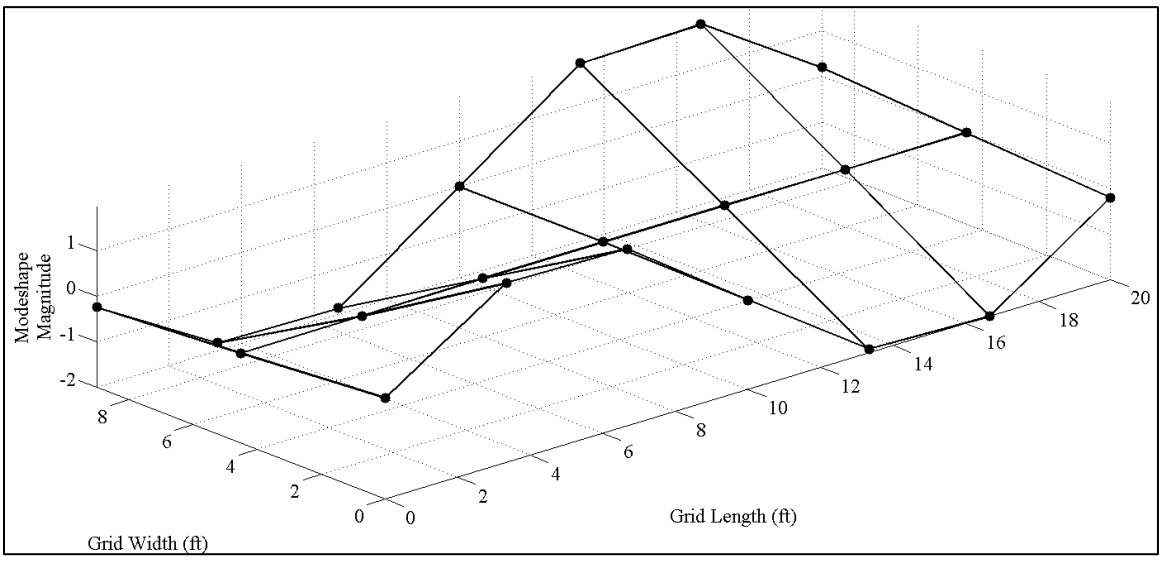

Figure 6-13: Structure 1, Mode 4 (Second Torsion)

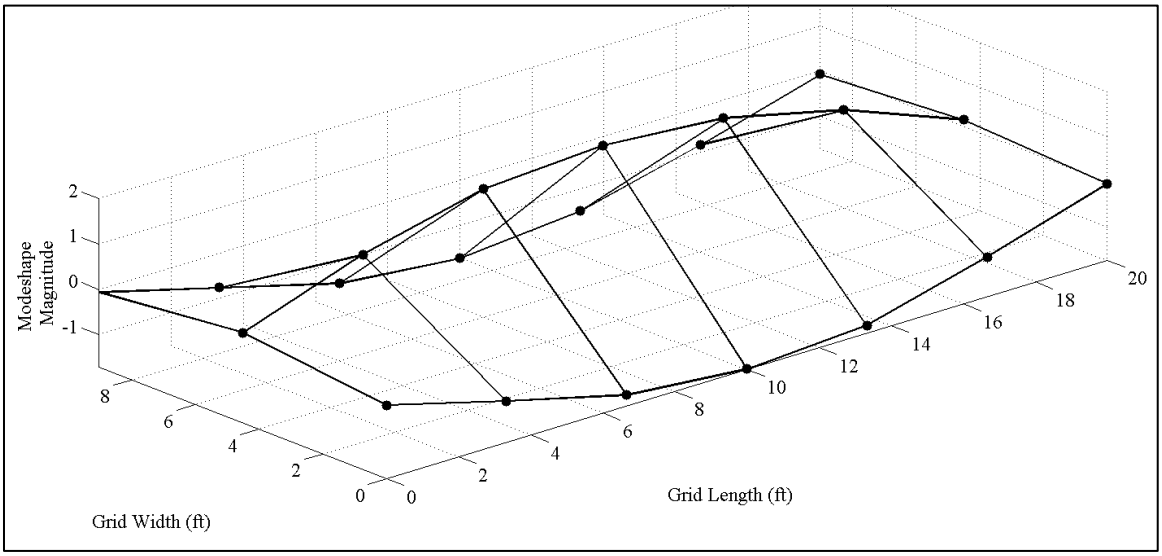

Figure 6-14: Structure 1, Mode 5 (First Butterfly)

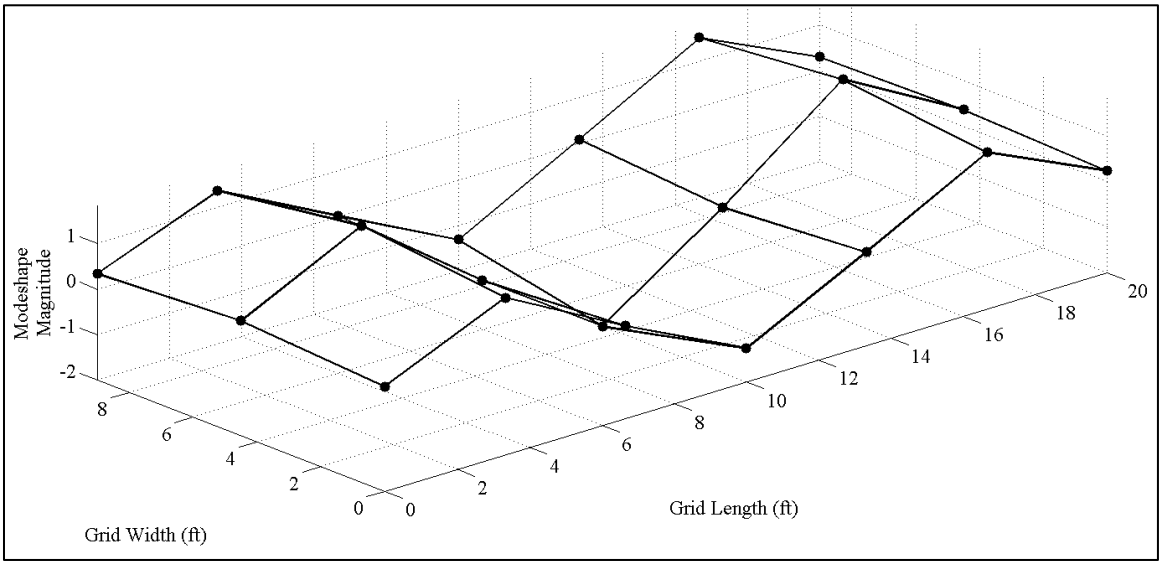

Figure 6-15: Structure 1, Mode 6 (Third Bending)

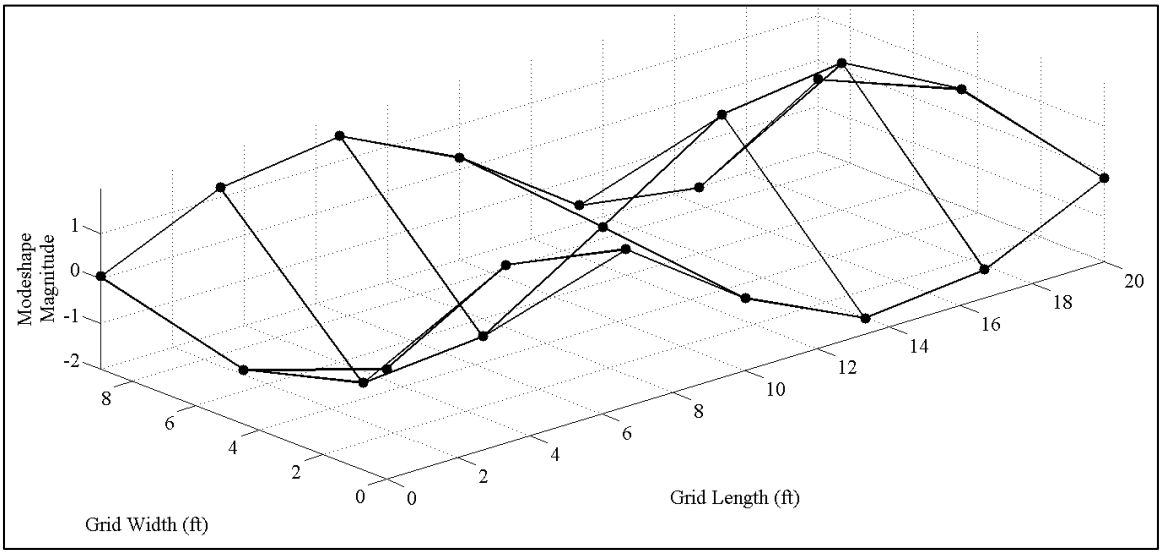

Figure 6-16: Structure 1, Mode 7 (Second Butterfly)

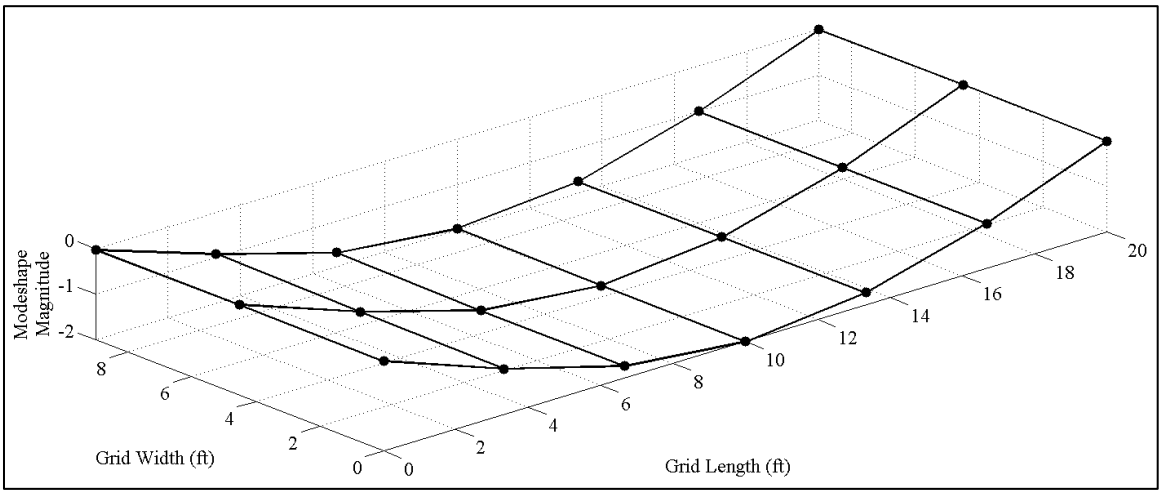

Figure 6-17: Structure 2, Mode 1 (First Bending)

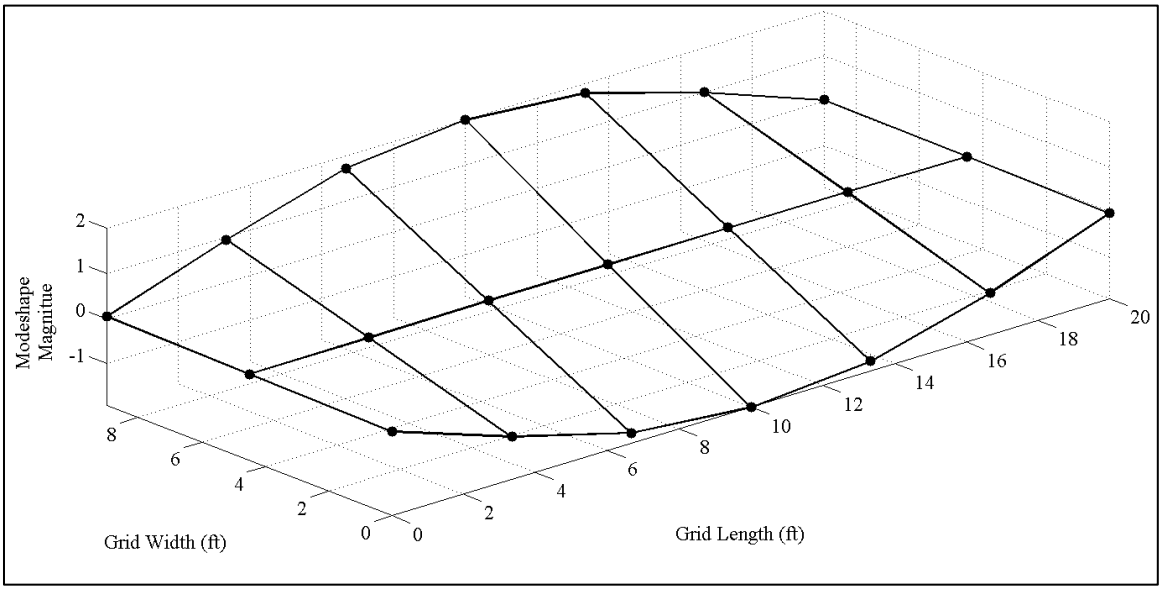

Figure 6-18: Structure 2, Mode 2 (First Torsion)

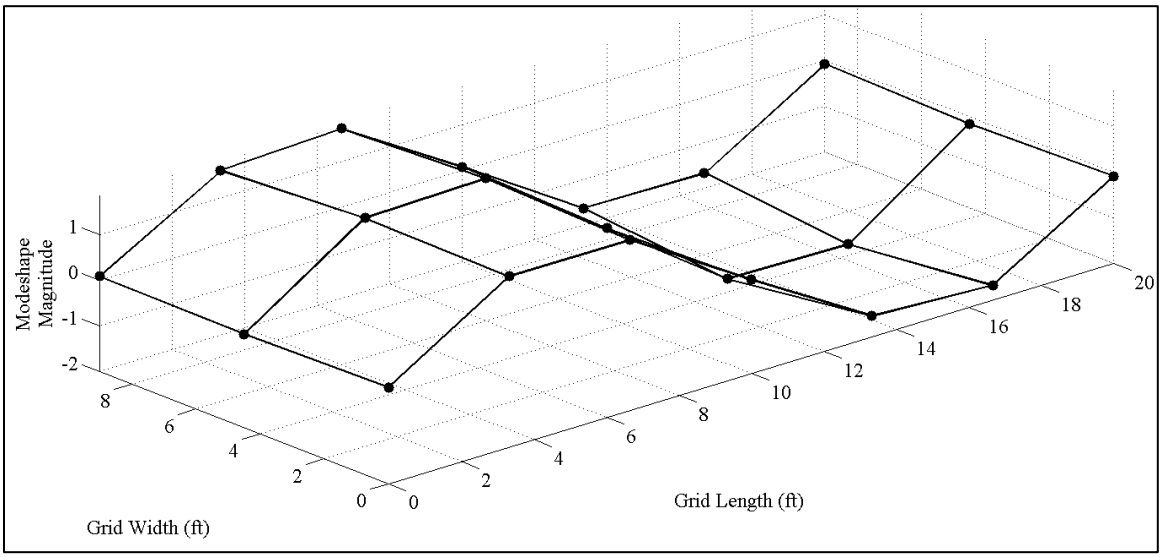

Figure 6-19: Structure 2, Mode 3 (Second Bending)

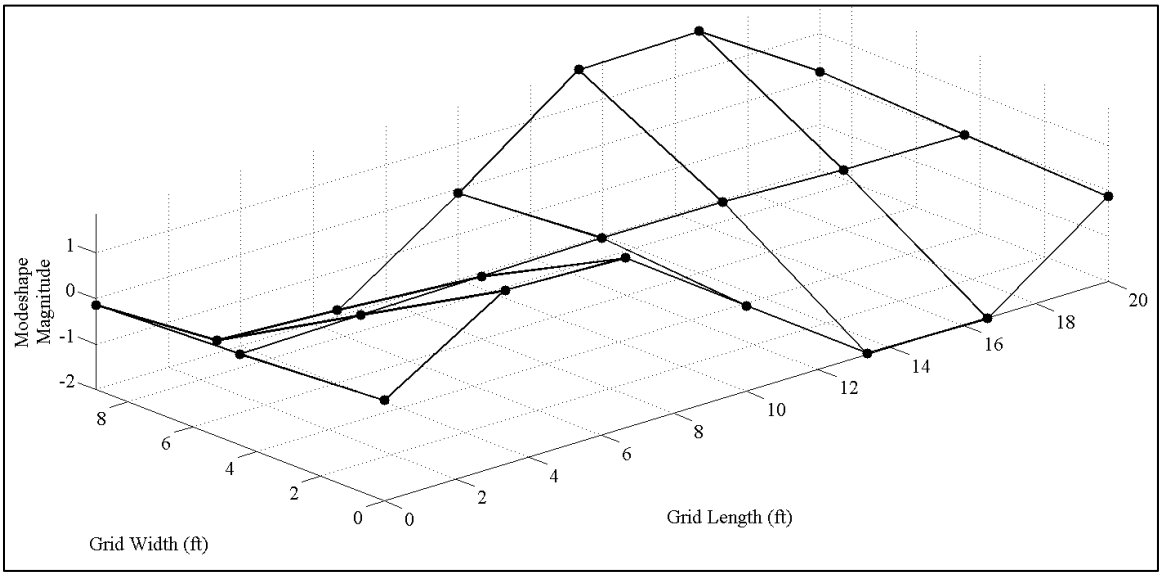

Figure 6-20: Structure 2, Mode 4 (Second Torsion)

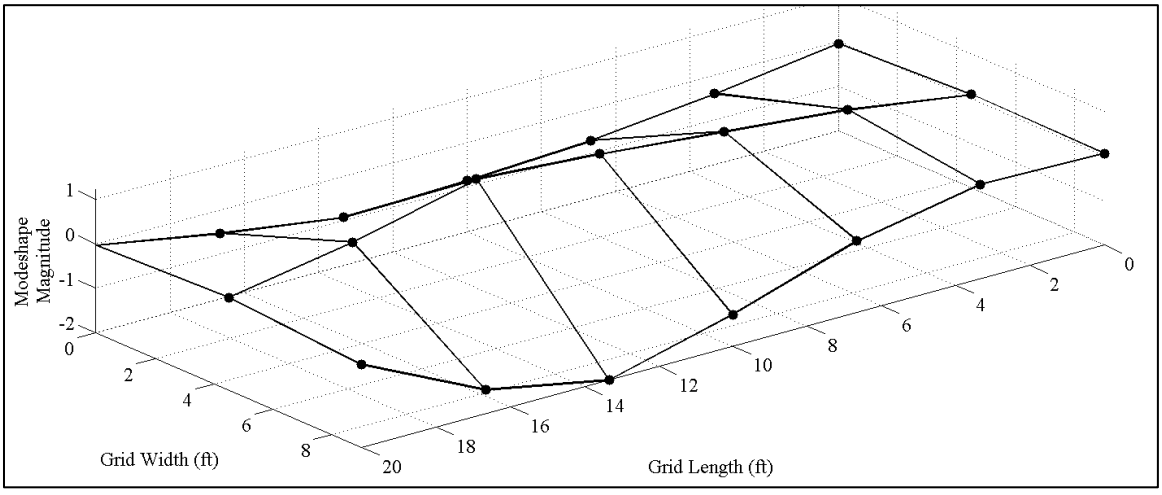

Figure 6-21: Structure 2, Mode 5 (First Butterfly)

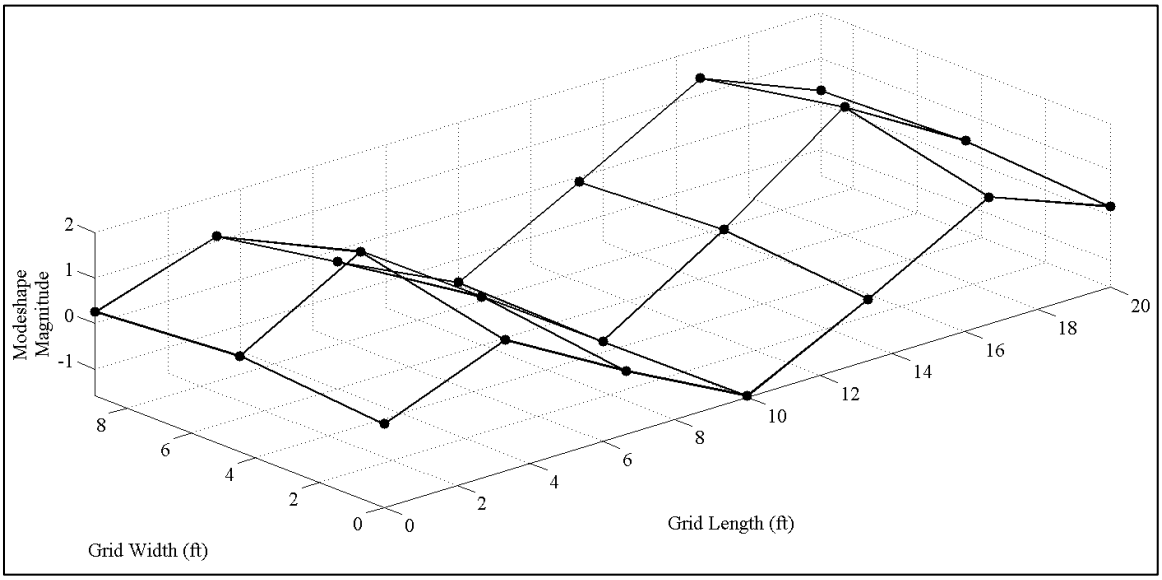

Figure 6-22: Structure 2, Mode 6 (Third Bending)

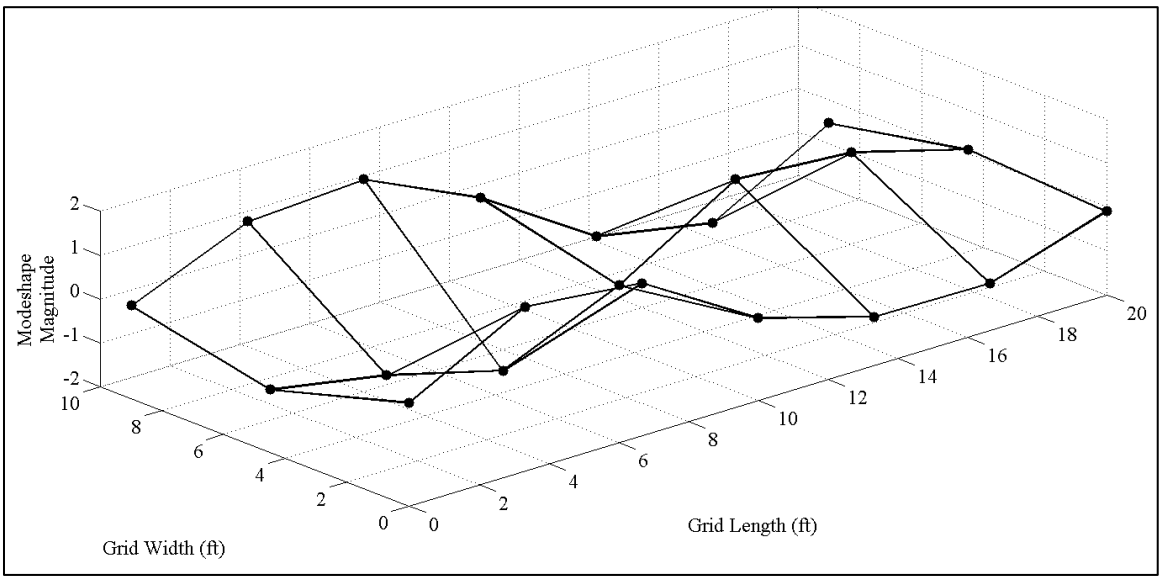

Figure 6-23: Structure 2, Mode 7 (Second Butterfly)

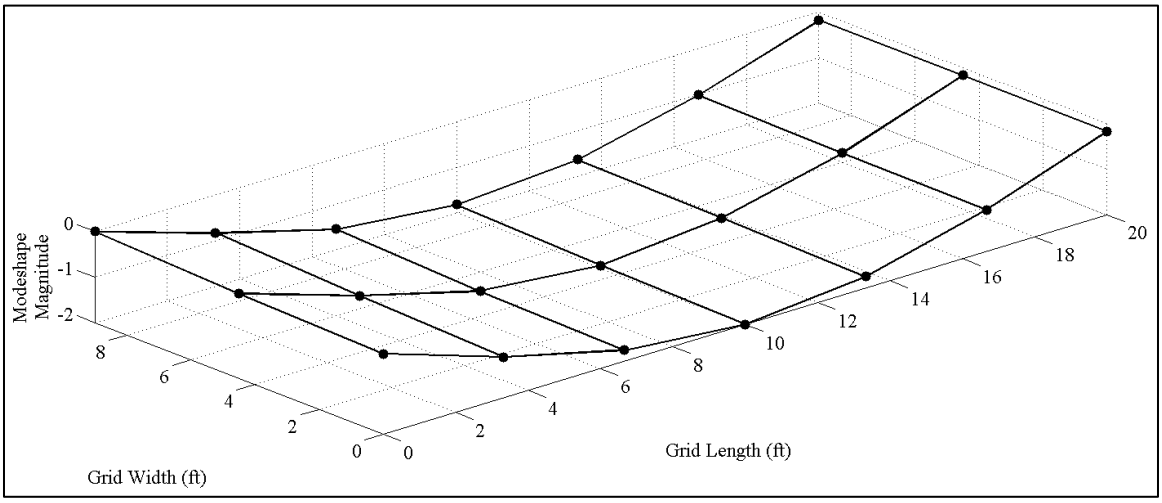

Figure 6-24: Structure 3, Mode 1 (First Bending)

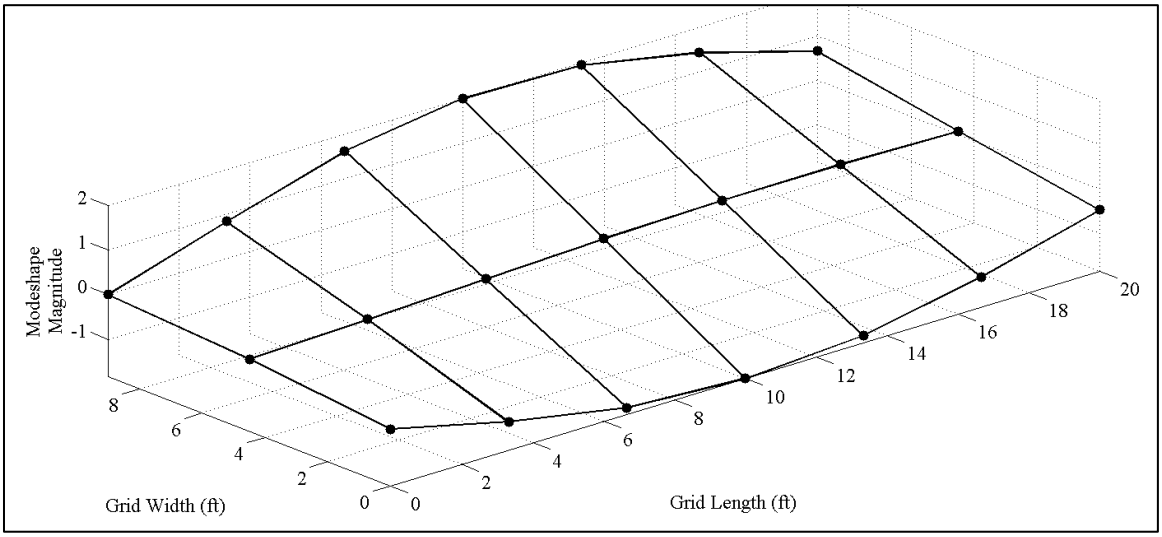

Figure 6-25: Structure 3, Mode 2 (First Torsion)

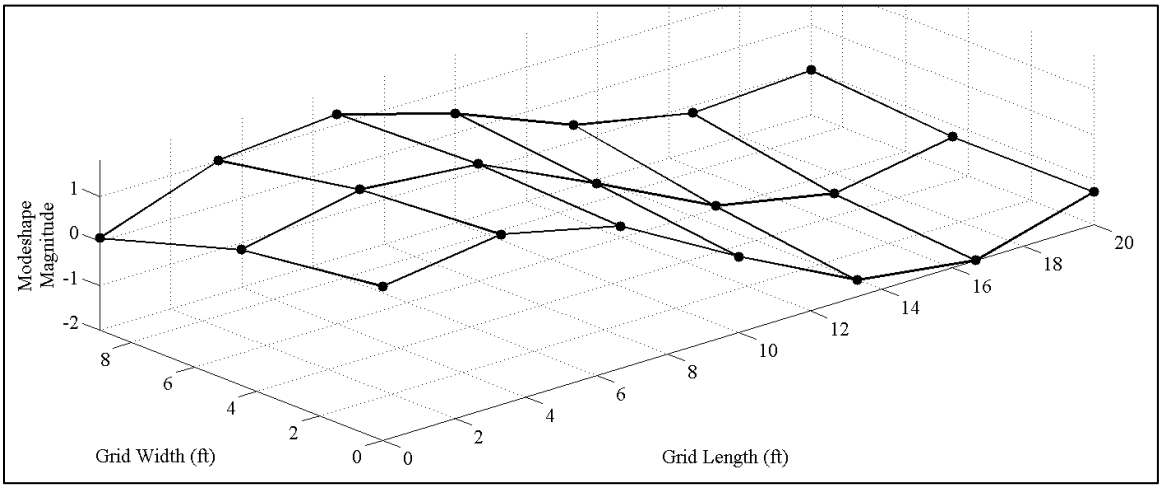

Figure 6-26: Structure 3, Mode 3 (Second Bending)

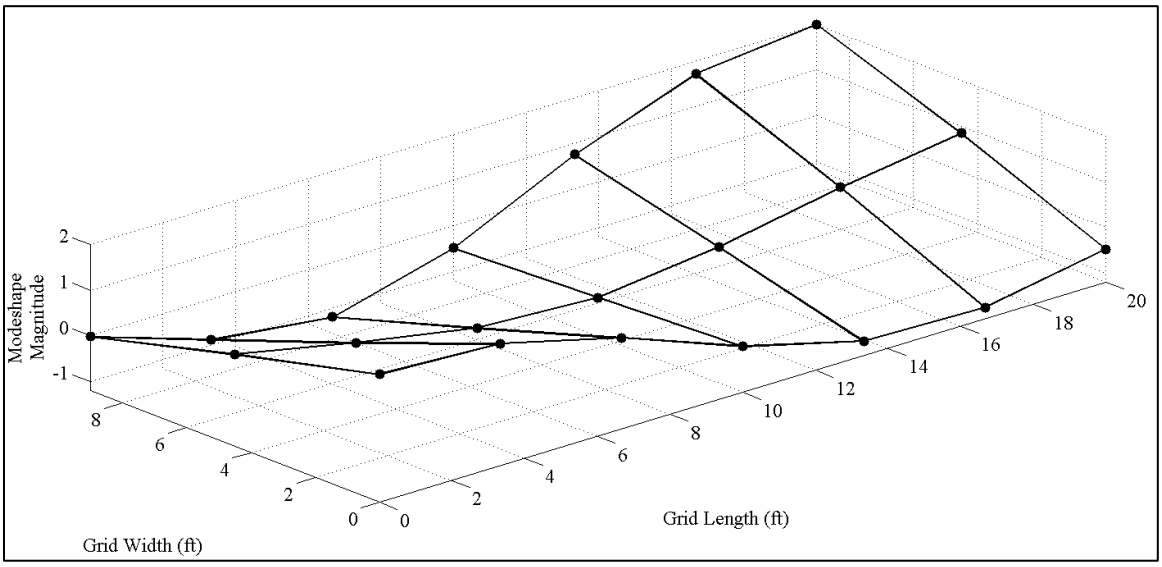

Figure 6-27: Structure 3, Mode 4 (Second Torsion)

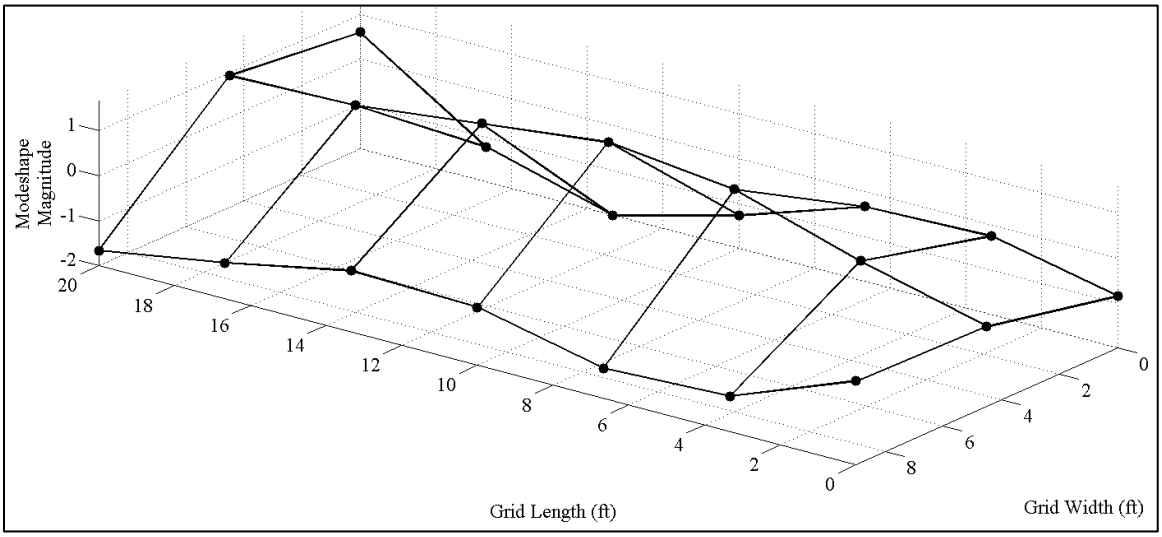

Figure 6-28: Structure 3, Mode 5 (First Butterfly)

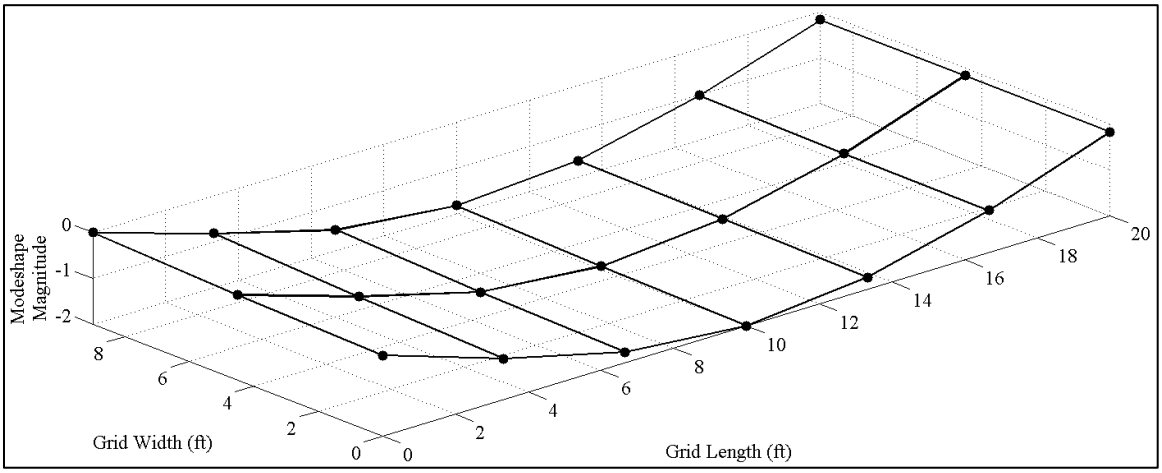

Figure 6-29: Structure 4, Mode 1 (First Bending)

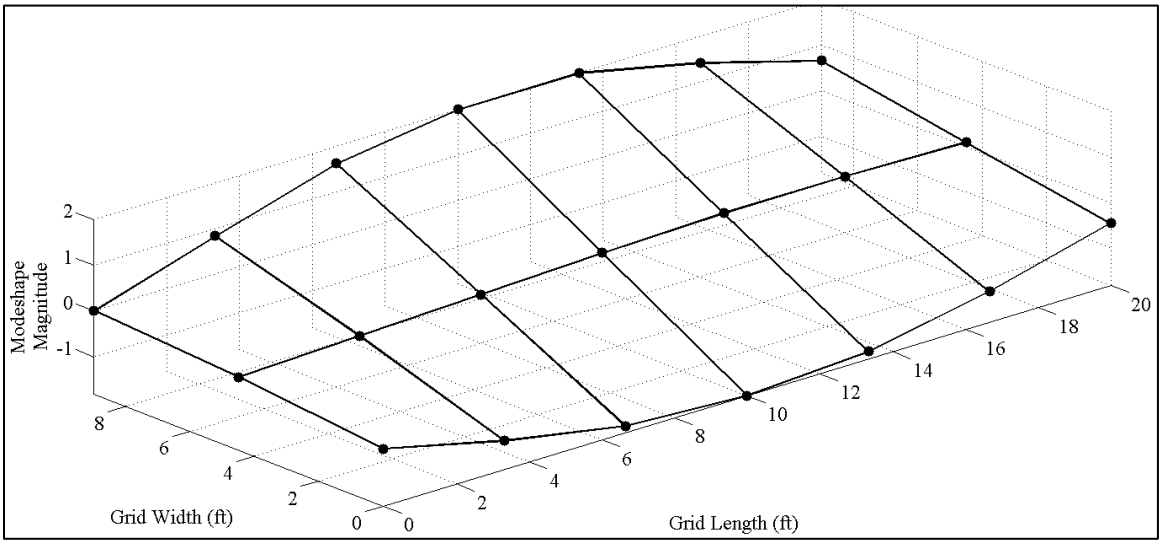

Figure 6-30: Structure 4, Mode 2 (First Torsion)

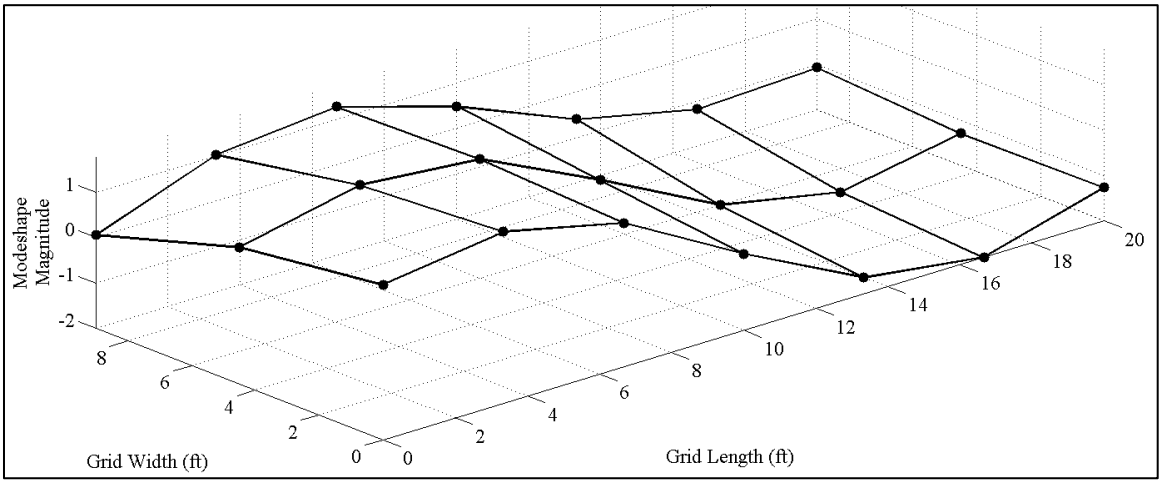

Figure 6-31: Structure 4, Mode 3 (Second Bending)

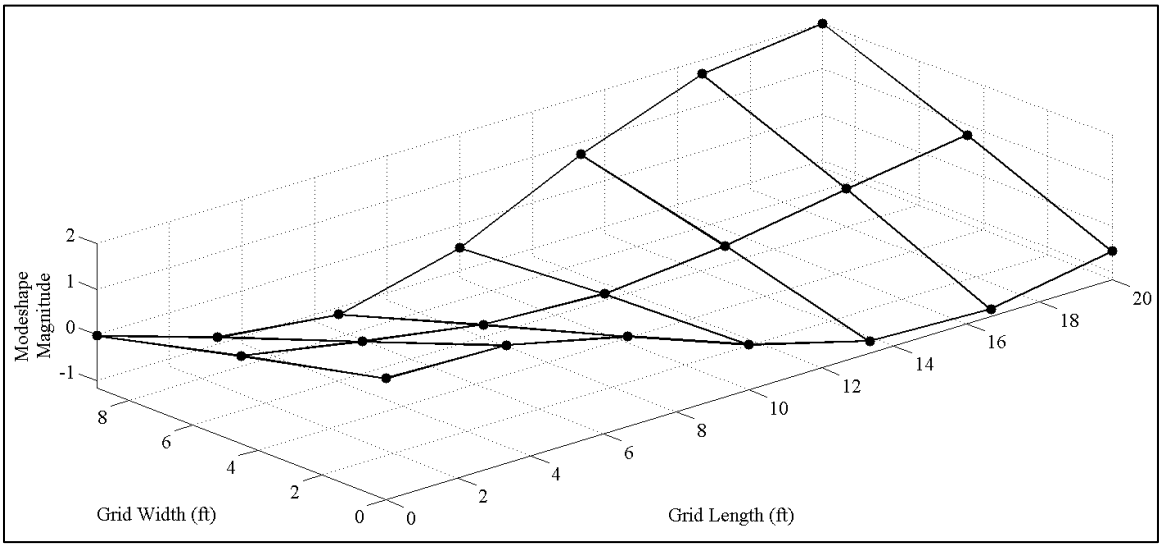

Figure 6-32: Structure 4, Mode 4 (Second Torsion)

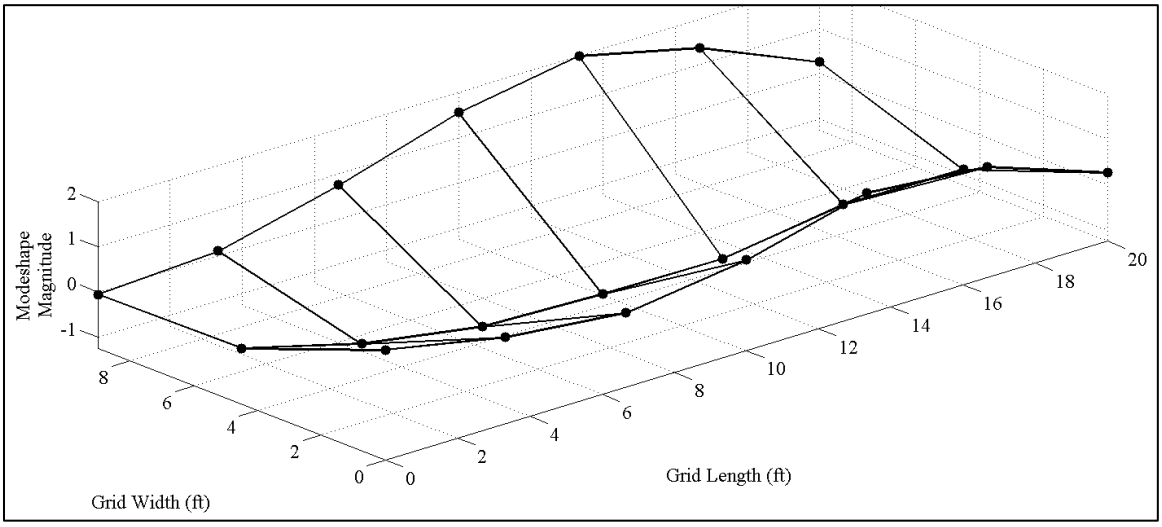

Figure 6-33: Structure 4, Mode 5 (First Butterfly)

It is noted that the major indications of change between Structures 1 and 2 and between Structures 3 and 4 is in the fifth and seventh frequencies and of the modeshapes, most obvious in Mode 5 for Structure 2. It is easy to see the location of the loosened connection by inspecting the modeshapes in Figure 6-14 and Figure 6-21. This agrees with the commonly known fact that localized changes in stiffness of a structure will not affect the global responses and fundamental frequencies as much as they will affect the local responses (e.g. curvatures in localized regions) and higher modes. In the cases of Structures 1 and 2, the fifth and seventh modes impart significant curvature into the transverse members unlike the remaining modes which primarily relate to the curvature of the longitudinal members.

The major modification of replacing the steel pins with neoprene pins had significant effects on all frequencies and modeshapes, which is consistent with the realization that a global modification to a structure will results in significant changes in the response of the structure. Due to the softened supports, the boundary nodes had increased flexibility which is apparent by inspecting the modeshapes in Figure 6-24 through Figure 6-33, more specifically modes three through five for Structure 3 and Structure 4. The data quality was also compromised with the neoprene supports, and the resulting modeshapes were in some cases, especially for high order modes, indiscernible. It is suspected that the neoprene supports acted to filter the high frequency modes by absorbing the impact energy that would have excited these modes. For this reason, only the five frequencies and modeshapes selected above will be used for subsequent work on Structures 3 and 4.

As seen in Figure 6-34, there was certainly a loss of power in the FRF of Structure 3 and the peak corresponding to Mode 7 at 39 Hz almost completely lost amplitude and was not able to be confidently identified. Only the five modes identified as being real modes of Structure 3 were saved for further analysis of the DI3 grid. Another interesting point to note from this Figure is the additional damping in the system from the neoprene supports, evident from the FRF shown below by the widened peaks visually seen with modes 2, 3, 4 and 5. The scaling of each of the peaks also changes order, indicative of the fact that the mass participation in the modes has shifted by altering the boundary supports.

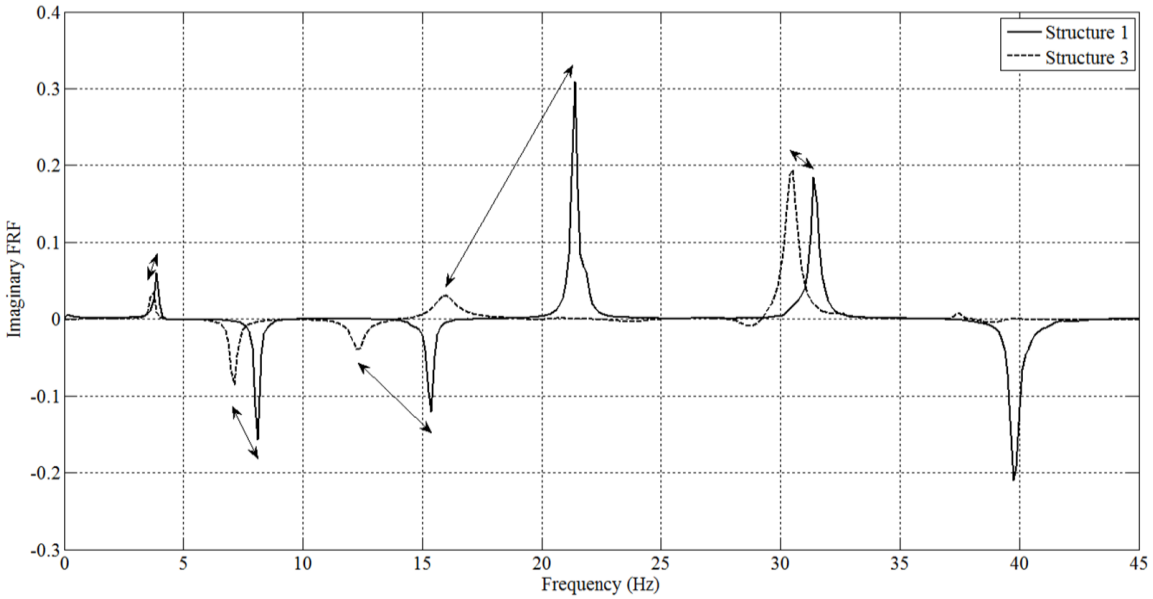

Figure 6-34: Comparison of FRFs (Imaginary Portion, Impact at Node 17 Response at Node 5) for Structure 1 and Structure 3

The reduction in frequency of the fifth mode from Structure 1 to Structure 2 was also investigated, and as shown in Figure 6-35 it is clearly seen that there is both a loss of power and an increase in damping in this mode. Both of these phenomena are justifiable considering that the loosened connection is in a high curvature region for the fifth mode and that loose fitting connections tend to increase the damping of frequencies since there is energy loss in the friction of the loose connection.

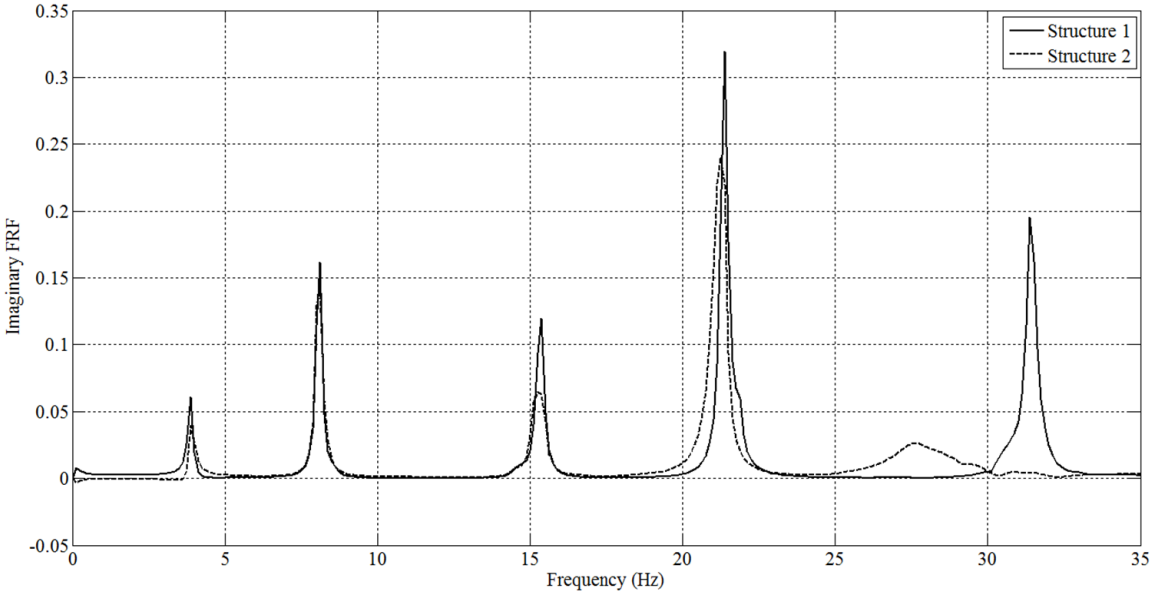

Figure 6-35: Comparison of the FRFs for Structures 1 and 2 (Imaginary Portion, Impact at Node 17 Response at Node 17)

6.2. Static Load Testing of the DI3 Grid

The goal of the static load test carried out on the grid structure was to directly measure both global and local static responses under known loads. The global responses captured were displacements of the nodal points which allow the computation of flexibility influence coefficients, while the local responses captured were flexural strains which allow the computation of strain influence coefficients. The reason for capturing both displacement and strain measurements is that by using both global and local responses the development, refinement and interpretation of the MM St-Id method can be enhanced.

6.2.1. Sensor Specification and Calibration

The displacements were measured with Celesco rotary potentiometers, Model PT8101 (Figure 6-36), while the strains were measured with encapsulated 350Ω, 2" shim length HiTec strain sensors, Model HBW-35-125-6-10GP-TR (Figure 6-38). The displacement transducers were physically attached to the grid structure using C-clamps, and the extension cable from the sensor was extended to the floor of the laboratory with high strength steel piano wire. The piano wire was anchored to the floor by fastening it to lead blocks which rested on the floor (Figure 6-37). The strain gages were attached to the grid structure with a spot welder according to vendor specifications. The specifications for the Celesco potentiometer are shown in Table 6-14.

The displacement gages were calibrated by installing them within a displacement calibration jig. The jig is outfitted with a precise control system allowing the user to input displacements as small as 0.005mm into the sensor. The observations were recorded

during a controlled displacement of the sensor over its measurable range to confirm the factory calibration factors. Due to the nature of the strain gages, in that once they are installed they cannot be removed; each sensor could not be calibrated. However, a single sensor from the batch of sensors received for the load test was installed onto a steel bar. The bar was loaded into a Tinius Olsen loading machine and put into tension while the strain readout was observed. The gage factor from the factory was thus confirmed in this manner.

Table 6-14: Celesco PT8101 Potentiometer Specifications

PERFORMANCE	
Sensitivity	200mV/V/in
Measurement Range	0 - 5 inches
Accuracy	± 0.25% FS
Repeatability	± 0.02% FS
Resolution	Infinite
ELECTRICAL	
Excitation Voltage	20 V
Input Resistance	500 Ω
PHYSICAL	
Sensing Element	Plastic-hybrid Precision Potentiometer
Weight	3lb

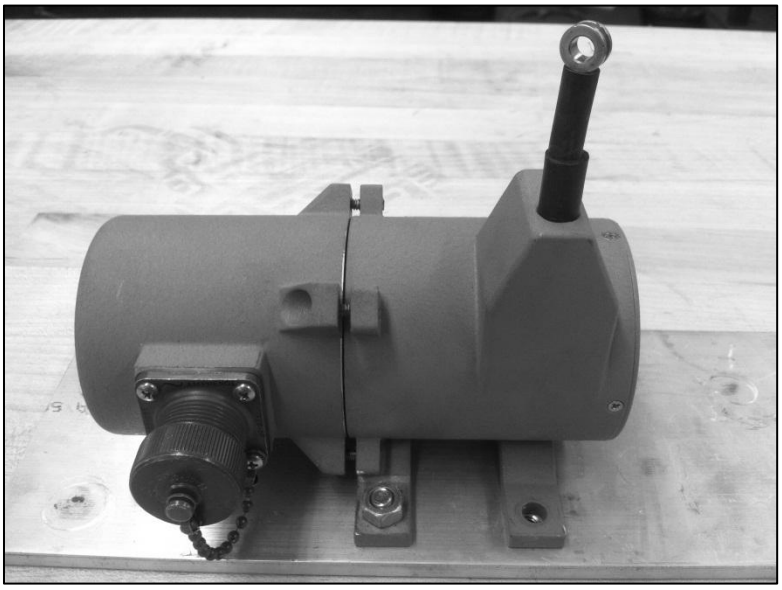

Figure 6-36: Celesco Rotary Potentiometer

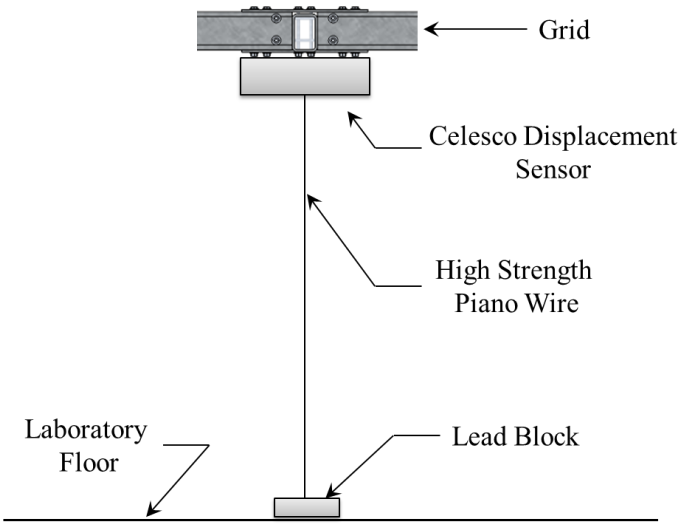

Figure 6-37: Schematic of Displacement Sensor Measurement System

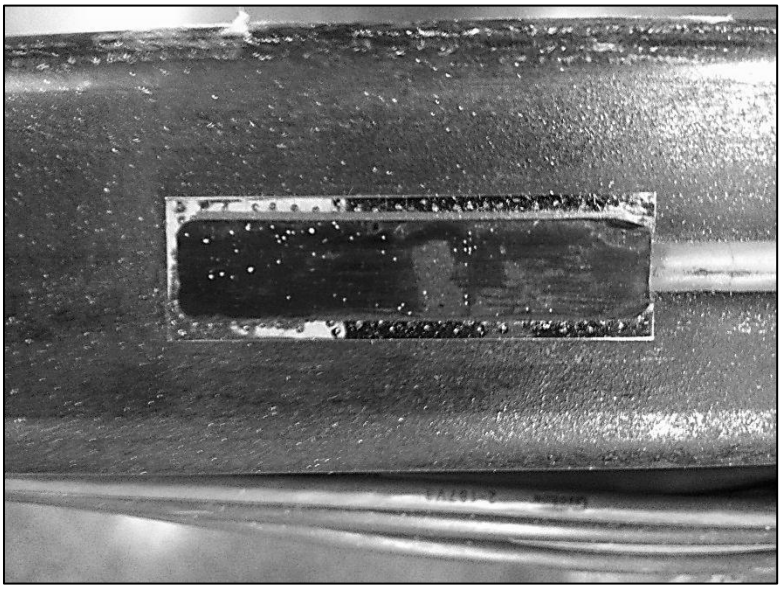

Figure 6-38: HiTec Weldable 2" Shim Length Strain Gage

6.2.2. Data Acquisition Specifications

The displacements and strains were measured synchronously with the same National Instruments cRIO data acquisition chassis as was used during the Modal test. However, different modules were used to measure the differential voltage readings from the displacement gages (NI 9239) and the quarter bridge strain measurement (NI 9236). The specifications for these modules are listed in Table 6-15 and Table 6-16. As seen in Figure 6-39, the displacement and strain sensors were connected to the data acquisition system with four-wire instrumentation cable. The cables were then fitted with military connectors and installed into custom developed data acquisition (DAQ) boxes, each capable of recording both displacement and strain sensors. The cRIO was housed within

the DAQ boxes and were synchronized with a computer that controlled all boxes over an Ethernet connection. A custom developed LabView program was utilized for measurement and recording purposes. The DAQ boxes and LabView programming were developed by colleagues at Drexel University.

Table 6-15: Specifications for NI9239 Voltage Module

ANALOG INPUT	
Channels	4
Resolution	24 bits
Sample Rate	50 kS/s
Maximum Voltage Range	-10 V , 10 V
Simultaneous Sampling	Yes

Table 6-16: Specifications for NI 9236 Quarter Bridge Strain Gage Module

ANALOG INPUT	
Channels	8
Single-Ended Channels	0
Differential Channels	8
Resolution	24 bits
Sample Rate	10 kS/s
Bandwidth	4.5 kHz
Max Voltage	29.4 mV/V
Simultaneous Sampling	Yes
Excitation Voltage	2 V
Bridge Configurations	Quarter Bridge

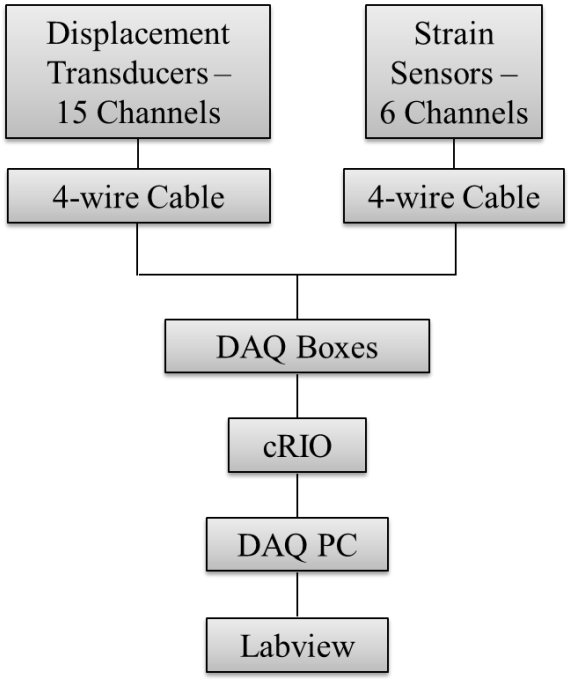

Figure 6-39: Static Data Acquisition Flowchart

6.2.3. Instrumentation

The static load test was designed to capture the full flexibility matrix of the grid structure by measuring displacements at each node, which is not a boundary, due to loads at each of the same nodes (Figure 6-40). This vast amount of testing provides a wealth of information to be used for both development and validation purposes. Strains were measured at points halfway between connection locations, to minimize local stress concentrations. The seven locations shown in the instrumentation diagram were selected to capture the load path of the grid structure for loading at various locations. The three

longitudinal members had strains measured at two complete cross sections, allowing for determination of load sharing.

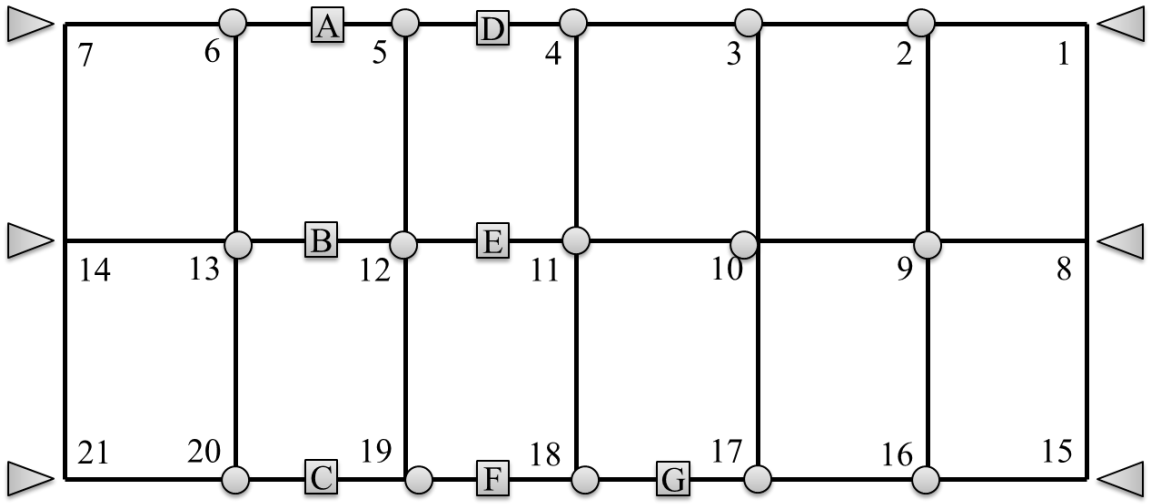

Figure 6-40: DI3 Grid Static Instrumentation Plan: Displacement Measurement and Loading Locations (circles), Strain Measurement Locations (squares), and Supports (Triangles)

6.2.4. Measurement Specifications

The sensors were sampled at a rate of 50 Hz. This sampling rate was chosen so that the dynamic effects of the first few modes of the structure could be measured and removed with sufficient data processing. As described earlier in the description of the modal test, sampling at a rate of 50 Hz allows for characterization of signals with frequencies of 25 Hz or less, which includes the most dominant global structural natural frequencies of the

grid. By measuring the dynamic effects during a static load test, the user can be confident that increased noise levels of seemingly periodic signals can be attributed to the structure and not outside noise.

6.2.5. Execution of Static Load Test

The static loads were applied with masses centered over the node in an incremental scheme. Loads were applied in 25lb increments, pausing until the structure's ambient vibrations damped out, until a total load of 200lb was achieved. The masses were then removed in the same manner. This technique was then repeated for each of the fifteen interior nodes of the grid structure for both Structures 1 and 3.

The method of applying and removing the masses was utilized so that both linearity and repeatability could be evaluated for the structure and the test. By pausing after each load interval, it is possible to later check that the incremental loads are causing proportional increases in static responses throughout the structure. Similarly, repeatability can be verified by comparing the response of the structure as load was being applied to when the load was being removed. In order for repeatability to be fairly quantified, extreme care was taken during the application and removal of loads so that the system did not experience a sudden energy input, due to a mass accidentally being dropped onto the structure for example, which might create an apparent offset in the measurements due to slippage of a connection or reseating of the structure. Figure 6-41 shows a complete time history of each of the fifteen sensors for a given load case and highlights how one could use the loading and unloading cycles to verify repeatability and linearity.

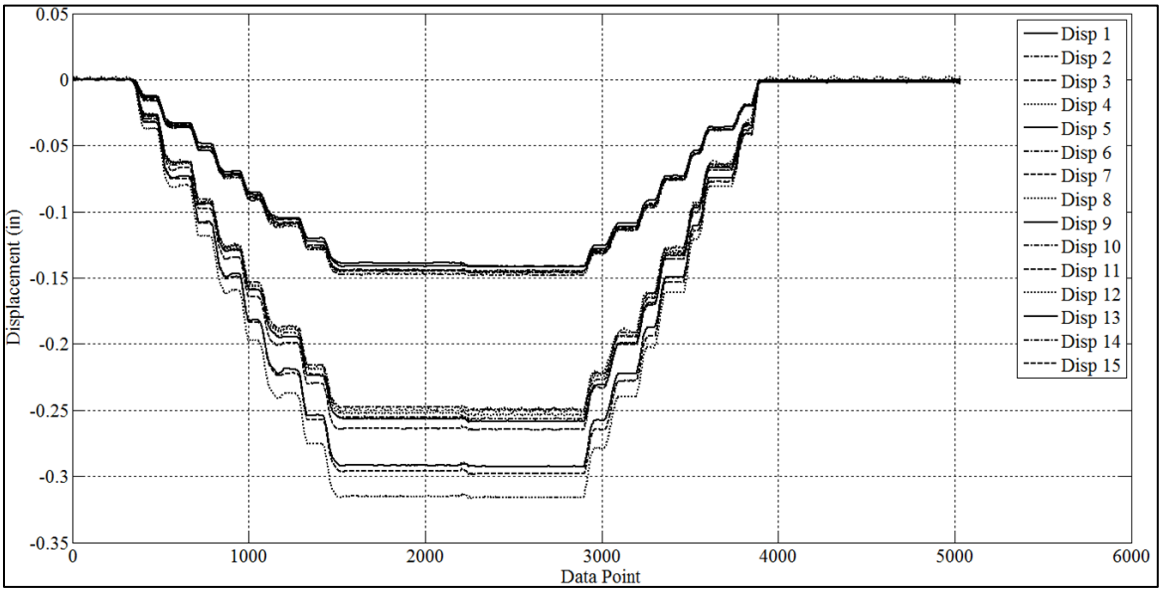

Figure 6-41: DI3 Grid Displacement Time History for Load at Node 11

6.2.6. Data Quality / Error Screening

As previously mentioned the data was checked for quality throughout the test by ensuring that the readings were repeatable from the loading and unloading stages. Additionally, strain gages are very sensitive to sources of electrical noise and interference, so time histories were examined to ensure that the noise level of the measurements were within typical ranges. For this sensor, the typical noise level for the measurements is within ± 1με. To mitigate any noise levels outside of this range, the DAQ was properly grounded and all cable shielding and DAQ components were connected to the common ground. Additionally, any power cables or power supplies were isolated from the instrumentation cables and DAQ system.

6.2.7. Data Processing

The measured data was processed using manual methods in MATLAB. The primary form of data processing carried out included filtering noise and averaging responses over a period of constant load, in addition to manual inspection of time histories for errors through plotting. A moving average filter was applied to the raw time history data to filter out measurement noise (Figure 6-42). The filter was set up to average the signal in spans of forty measurements. This span was chosen because it reduced the most noise without altering the main signal. The filtering allowed for more precise time periods to be selected, in which the structure was not vibrating, for averaging. After the time histories had been filtered to remove dynamic and loading effects, the data points were noted where steady state loading began and ended. These points then served as the limits between which data was averaged to obtain a displacement for that loading level. Once all load tests had been processed, the results were organized into tables for future reference. The results from one load case are presented in the next section.

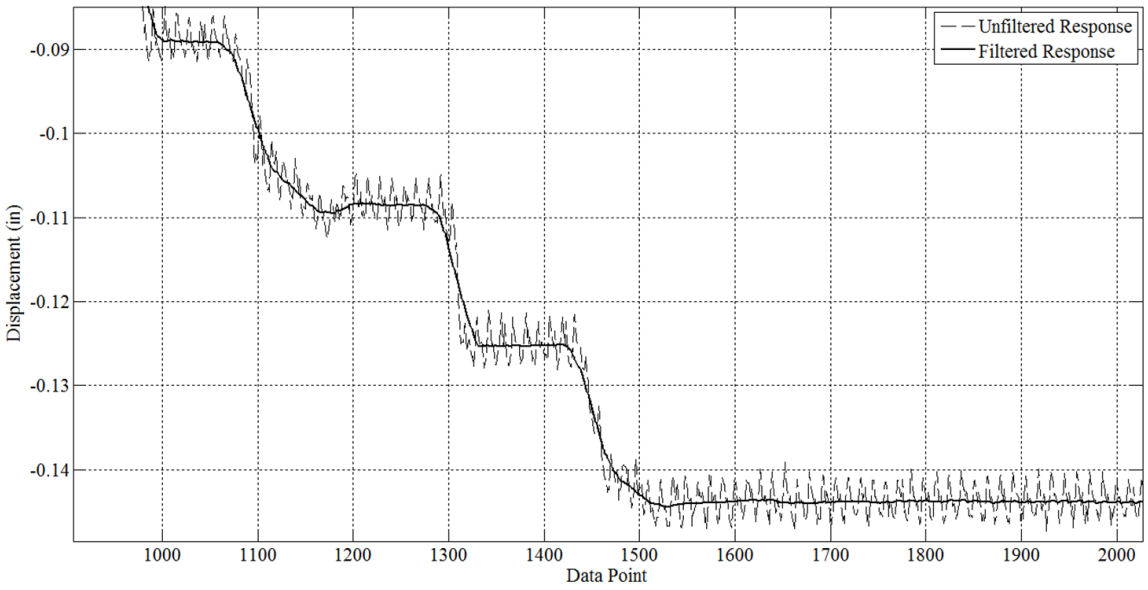

Figure 6-42: Comparison of Unfiltered Data to Filtered Data for Static Displacement Measurement

6.2.8. Experimental Results

The results from the static testing of the DI3 grid were fairly straightforward, without any unexpected responses. Multiple forms of data visualization were used to analyze the responses as well as to check for errors in the data or testing procedures. A filtered time history is shown in Figure 6-41, and demonstrates the incremental loading scheme applied during the test.

After appropriate time periods were selected and responses were averaged to obtain a single displacement for a given loading at each measured location, the responses were plotted with respect to their geometric location instead of over time to ensure that the measured response behavior is consistent with the response that is expected for a

structure of this form (Figure 6-43). Finally, after all load cases were analyzed, a Table of results was created and stored for future reference, a portion of which is shown in Table 6-17, which details the results of displacements and strains due to a load at the near mid-span Node 12.

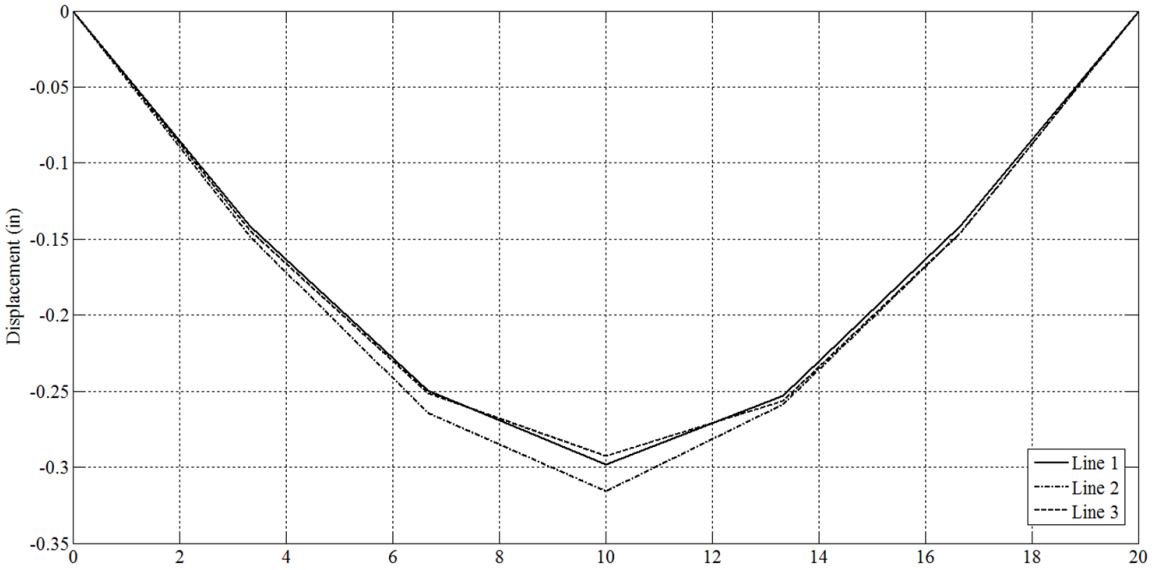

Figure 6-43: DI3 Grid Displacement Profiles for Line 1 (Nodes 1-7), Line 2 (Nodes 8-14) and Line 3 (Nodes 15-21)

Table 6-17: Measured Displacements and Strains for a Load at Node 12

Responses for 200lb Load at Node 12				
Disp 2	-0.112		Disp 17	-0.204
Disp 3	-0.203		Disp 18	-0.251
Disp 4	-0.256		Disp 19	-0.235
Disp 5	-0.233		Disp 20	-0.140
Disp 6	-0.134		Strain A	-62.923
Disp 9	-0.116		Strain B	-72.846
Disp 10	-0.210		Strain C	-62.179
Disp 11	-0.267		Strain D	-72.513
Disp 12	-0.250		Strain E	-34.333
Disp 13	-0.147		Strain F	-71.231
Disp 16	-0.115		Strain G	-71.769

CHAPTER 7: EXAMINATION OF VARIOUS SAMPLING AND WEIGHING APPROACHES

This chapter presents a study of different model sampling and model weighing strategies incorporated into Step 5 of the MM St-Id process (see Chapter 3). In total, three independent approaches were examined including (1) deterministic (Section 7.2), (2) threshold (Section 7.3) and (3) probabilistic (Section 7.4). In addition, a series of hybrid approaches that employ aspects of these three independent approaches were also examined (Section 7.5).

7.1. Assessment Scenario

To evaluate these methods, a scenario was developed in which the modal parameters obtained from the Structure 1 configuration of the grid structure (as described in Chapter 6) were considered observable responses. These responses were then used to drive the various sampling/weighing processes with the MM St-Id framework. Each model was solved for its natural frequency analysis, and its weight was computed automatically by pairing the modes based off of weighed MAC values. The MAC values were modified based on whether the modeshape was significant with respect to the measured responses. This in turn eliminated local modes erroneously being selected if by chance, its MAC value was the highest for a particular experimental mode. The formulation for the modified MAC value is shown in the equation below in Eq. 7-1, where φ corresponds to the reduced modeshape vector from Strand7 at the degrees of freedom which were measured, Φ corresponds to the total modeshape vector for the analytical mode, MAC corresponds to the MAC value between the experimental and analytical modes under

study, max corresponds to a function which computes the maximum value of its contents and abs converts that data within its contents to its positive form.

$$MAC_{ana-exp} = MAC_{ana-exp} \frac{max\left(abs(\varphi_{ana})\right)}{max\left(abs(\Phi_{ana})\right)} \qquad \textbf{Eq. 7-1}$$

By utilizing this method of modifying the MAC values for mode pairing, a local mode will not be erroneously selected as the global mode for correlation since it is penalized by the modifying factor computed above, unless that degree of freedom was specifically measured.

Once complete, the model populations (inclusive of their weights) were used to predict the static displacements and static strains of the grid. These predictions were then compared to the measured values (considered "unobservable" within the scenario) to assess the accuracy of each approach. The conclusions and recommendations developed from this study are presented in Section 7.6.

7.2. The Deterministic Approach

For this study, the deterministic approach is defined as having samples of building blocks manually selected to develop the population of candidate models, and subsequently weighing the candidate models with a percent error based objective function. The primary benefit of a deterministic approach is that it has a higher level of transparency.

That is, the user knows (and controls) exactly how the building blocks are sampled and in what manner the candidate models are formulated. For users with a sound heuristic knowledge, this type of approach may in fact prove quite efficient as the user would have some intuition about where the sampling should be focused. In addition, the straightforward percent error weighing is widely understood making this approach potentially more palatable for a wide audience of structural engineers. A potential downside of this method is the inability to explicitly consider the uncertainty associated with the modeling process and the observed measurements.

7.2.1. Deterministic Sampling

Building blocks are sampled in a deterministic manner when the generated results are not of a random nature, and the relationship between subsequent samples is explicitly defined by the user. For example, in the sensitivity studies discussed in the previous section, the samples of a few building blocks were generated by selecting bounds and then equally spacing a set number of divisions within those bounds. Additionally, for other building blocks the samples were evenly spaced over a logarithmic scale between two bounds. In the prior case, the samples are linearly related while in the former case the samples are exponentially related. Regardless of what type of relationship is chosen, the user fully defined the relationship and the quantity of samples and then generated the candidate models accordingly. An alternative to these “pre-determined” sampling approaches is one where the user manually selects model building blocks based on the previous model execution (or population of model executions). While this method is far more time

consuming it does have the ability to be quite efficient for cases were the computational expense of executing the model is significant. This potential advantage notwithstanding, the current study elected to ignore this type of adaptive deterministic approach as it depends greatly on the knowledge and insight of the user, and as such, it will never be a reliable approach in general.

To assess the deterministic approach, a full-factorial sampling of five parameters (building blocks) was carried out. Table 7-1 lists the five parameters used (see Chapter 5) together with the bounds selected based on the sensitivity studies. Due to computational time considerations, nine evenly spaced parameters were generated for each building block leading to 9^5 or 59,049 total candidate models. The samples were selected in an evenly spaced manner so as to most efficiently cover the sampling space, as determined by the sensitivity study carried out in Chapter 5. The grid structure model required an average time of roughly 6.5 seconds to compute the modal parameters and linear static analysis for three load cases. The total computation time is a necessary consideration when using a deterministic approach since the model space is being covered in a fairly dense and spread out manner. In this case, the analysis time was roughly 106.5 computation hours, a considerable amount of time given the relatively simple model and small number of building blocks. Regardless, the analysis was carried out over multiple computers and was completed in a little over one day.

Table 7-1: Deterministic Sampling Scheme

Building Block	Lower Bound	Upper Bound	Samples
E_{steel}	0.8 * E_o	1.2 * E_o	9 – Equal Spaced
K_v	1 kip/in	150 kip/in	9 – Equal Spaced
K_l	0 kip/in	30 kip/in	9 – Equal Spaced
K_{r1}	0%	100%	9 – Equal Spaced
K_{r2}	0%	100%	9 – Equal Spaced

To demonstrate how well each of the methods analyzed in this chapter samples from the model space, a matrix of plots is generated that creates scatter plots of various building block combinations on the off diagonal entries and histograms of the building block samples on the diagonal. This visualization tool helps to highlight the mapping of the model space and how efficient each approach generates models from within this space (Figure 7-1). Note that the figure appears to be missing a bin, however due to the

After inspecting the figure, it appears that the deterministic sampling scheme effectively covers the model space with a grid pattern, created by generating evenly spaced samples from each of the building block bounds. While this appears to be very effective in covering the model space, it is important to remember two key shortcomings with this specific sampling design. The first shortcoming is the large number of models needed to achieve this level of coverage. Secondly, while the model space coverage is very thorough, there are fairly large gaps within samples that might contain important information. Add this to the fact that in many cases the meaningful models may reside in a small portion of the model space, and it becomes clear that such an approach may have

a difficult time in developing reliable candidate model populations without very sound heuristic knowledge. These shortcomings are inherent to a deterministic approach and must be acknowledged when utilizing this approach.

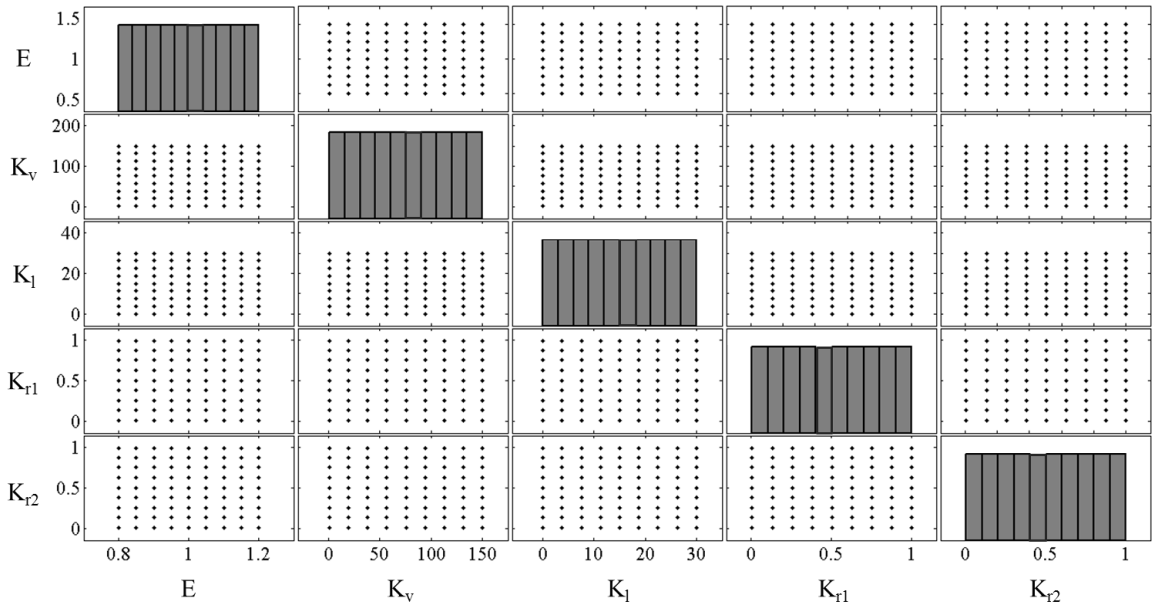

Figure 7-1: Matrix of Plots for Deterministic Sampling

During the analysis of each model, the paired frequencies, MAC values, and displacements and strains from each load case were computed and stored within a matrix structure. This results matrix was saved after each model execution to provide a backup in the event of a computer crash or corruption of the model file. Additionally, numerous

backup copies were made of the Strand7 model in the event of a corrupt file, which could occur if MATLAB is disrupted while manipulating the model.

7.2.2. Deterministic Weighing

Once the building blocks have been sampled, the models must be weighed based on their correlation with experimental observations. There were two formulations of deterministic weighing functions evaluated for their effectiveness, both being derivatives of an objective function based on percent errors of analytical and experimental quantities. The first formulation, Weighing Method 1 (WM1), consists of the product of the inverse of percent error for each observation, and is shown below in Eq. 7-2. Similarly, the second formulation, Weighing Method 2 (WM2), is the sum of the inverse of percent errors of analytical and experimental quantities and is also shown below in Eq. 7-3.

$$WM1: \qquad W_{M_j} = \prod_{i=1}^{n} \frac{1}{e_i} \qquad \textbf{Eq. 7-2}$$

$$WM2: \qquad W_{M_j} = \sum_{i=1}^{n} \frac{1}{e_i} \qquad \textbf{Eq. 7-3}$$

The term W_{M_j} represents the weight associated with model j and for each case includes e_i, the percent error associated with observation i. Although in the case of parameter identification, it is common to use the error values instead of their inverse (and then minimize the resulting objective function), in the current method a model weight is sought and thus the inverse is more appropriate as it heavily weighs models with small errors and penalizes models with large errors. WM1 represents a strict weighing, since a single large error out of the group of observations could penalize the model significantly. The second case is more conservative in that a single poorly correlated observation will not have as drastic of an effect on the model's weight since the terms are summed rather than multiplied. That is, for WM1, a large error associated with a single measurement could drastically reduce a model's weight, whereas for WM2, a very small error associated with a single measurement could drastically increase a model's weight.

Before the predictions are analyzed, the effects of the model weighing process should be visualized in a variety of methods. The first way of demonstrating the weighing process is to scatterplot the computed weights for each model number resulting from WM1 and WM2 (Figure 7-2 and Figure 7-3, respectively). To make comparisons to other methods straightforward, the sum of the model weights were normalized to one. It is seen that the WM1 weighing is stricter as anticipated and that more models have near zero weights as compared to the WM2 results. To further validate this finding, the number of models with a normalized weight above 0.001 was tabulated for each weighing methodology. WM1 was found to provide 11 models above the 0.001 threshold while WM2 was found to provide 66 models above the same threshold. The small number of models passing with this approach is also a function of the sampling implemented. It is obvious that the region

of the modeling space where the highly weighted models exist is fairly small with respect to the size of the modeling space sampled. It is envisioned that if the model space was reduced in dimension, then this method would provide a higher amount of models with appreciable weighting.

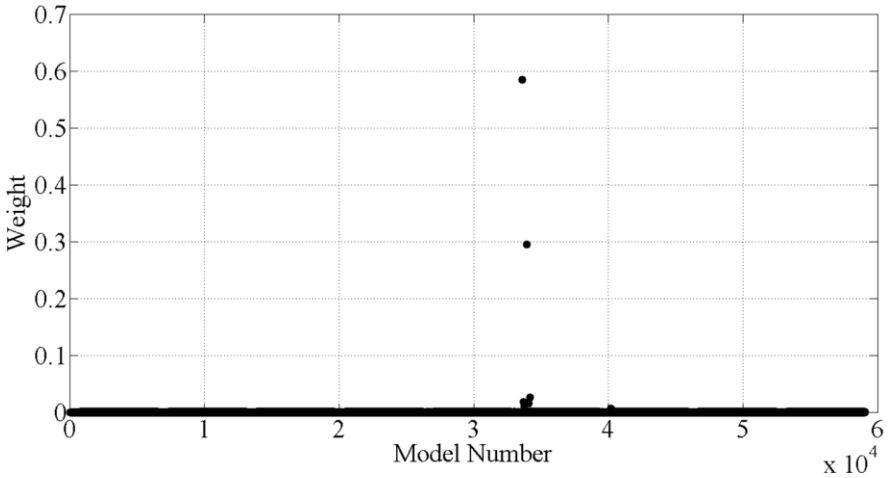

Figure 7-2: Scatterplot of Model Weights for WM1

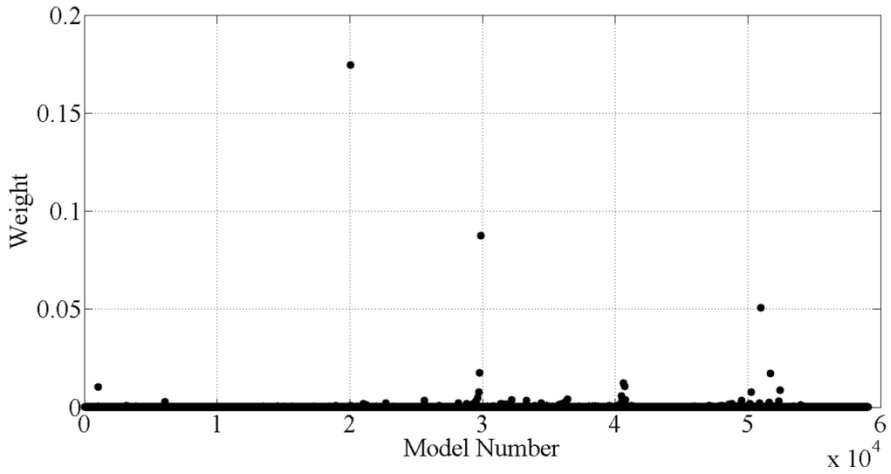

Figure 7-3: Scatterplot of Model Weights for WM2

To further investigate the effect of the different weighing approaches, the influence on the individual building blocks were assessed. To accomplish this, the weights associated with each building block value were summed across the other four building blocks. The resulting weights were plotted in a manner analogous to a cumulative probability distribution together with the un-weighted building blocks (for comparison). By plotting these results in a cumulative distribution based on each model's respective weight, it is not necessary to produce histograms which can distort the prediction distributions based on the selection of number of bins and bin width. Figures 4 and 5 show these plots for WM1 and 2, respectively.

The information contained in such plots includes the location where the most heavily weighted value of the building block exists (indicated by the largest vertical jump) and how many models have appreciable weights (indicated by whether the jumps are vertical lines or smooth curves).

For WM1 (Figure 7-4) it is apparent that only two combinations of building blocks contain the majority of the total weight (since at most there are two vertical jumps for any single building block). This is confirmed by reviewing Figure 7-2, where the majority of the weights are associated with two specific models. The building blocks that contained the largest weights from WM1 were: E = 1.05, K_v = 19.63 kip/in, K_{r1} = 0.75 and K_{r2} = 1, with K_l values of 0 kip/in and 10 kip/in. When these two models were examined in depth, it was confirmed that all frequencies and mode shapes were very close to the measurements, with the largest percent error between analytical and experimental frequencies being 2.31% and smallest MAC value being 0.9653. It appears that with the

WM1 weighing method that there is little room for error and any models that do not almost perfectly correlate with observations are heavily penalized.

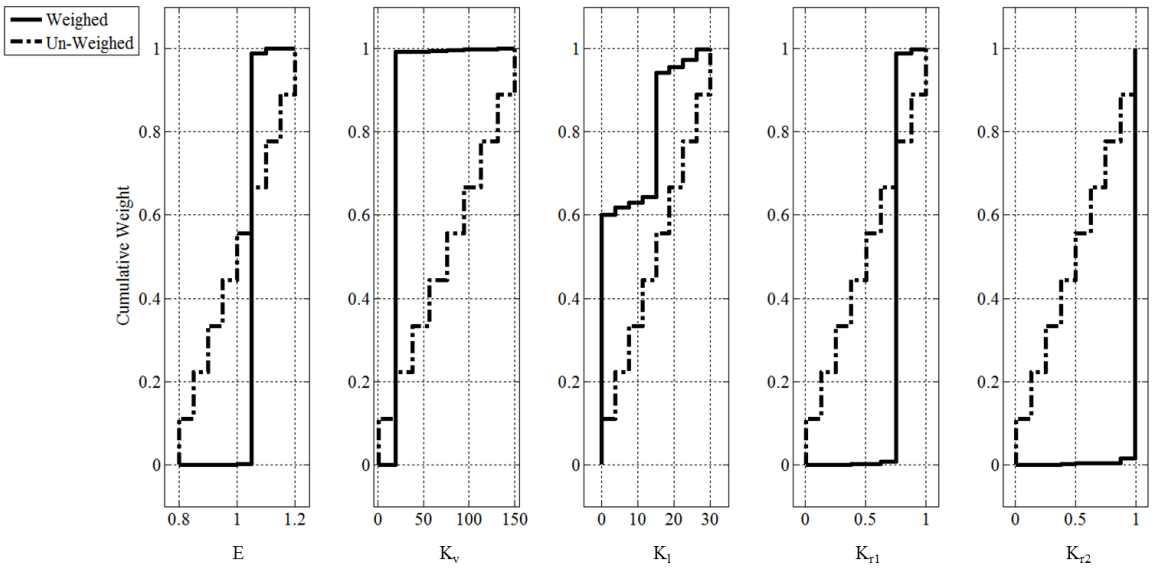

Figure 7-4: Effect of Weighing on Building Blocks for WM1

The results using the WM2 weighing approach are quite distinct from the results obtained using the WM1 approach. Where WM1 essentially reduced the model space to two building block combinations, WM2 produced variations between different building block values that were far more subtle. For example, it is not obvious from Figure 7-5 what combinations were weighed the highest using the WM2 weighing approach As previously argued, it is not the intention of the MM St-Id method to identify the building

blocks, as it is to quantify the non-uniqueness with the process. To investigate this, the response predictions from the deterministic weighing case were formulated in the same manner as the building blocks.

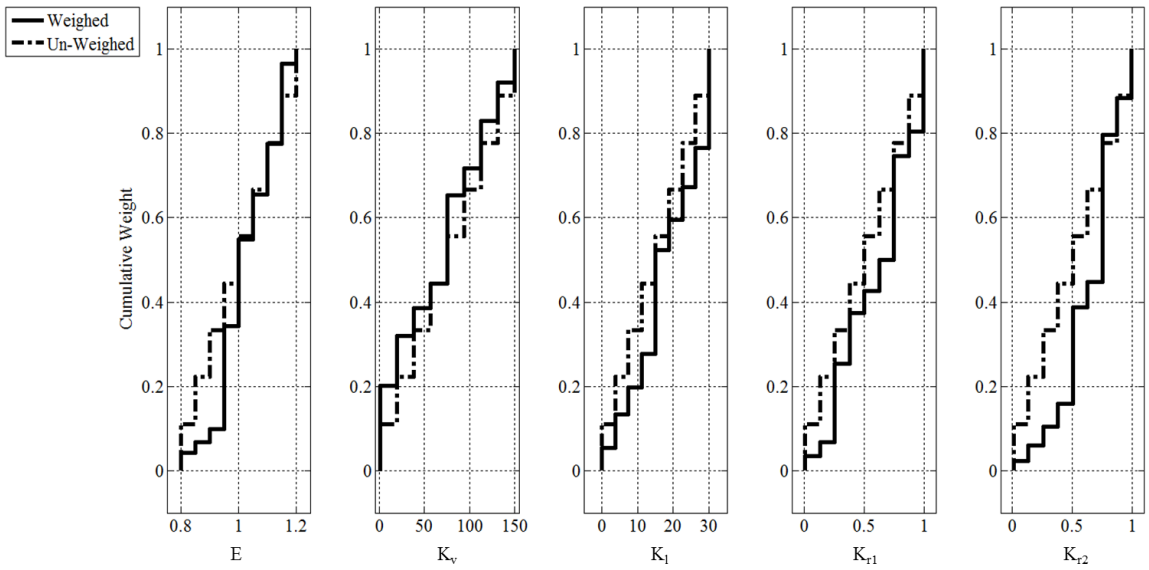

Figure 7-5: Effect of Weighing on Building Blocks for WM2

7.2.3. Deterministic Predictions

The response indices used for prediction purposes included Strain D and Displacement 11, described in Chapter 4, due to a load at Node 11, which is mid-span of the center longitudinal member. As seen in Figure 7-6 and Figure 7-7, WM1 and WM2 were both able to produce predictions which encompassed the actual measurement from testing. However, two major differences are apparent from these prediction functions.

WM1 has significantly narrowed the range of displacement predictions from {-0.1", -0.4"} to {-0.11", -0.154"} through the weighing process. While it is seen as a benefit that the method was able to reduce the range of likely displacements for a given load, it is also apparent that the measurement is on the bounds of this range and that the model at this location accounts for 60% of all model weights. The model with the next highest weight estimates a displacement that is 21% from the measured value. While it would appear that the method was only able to identify a few models which reasonable matched the observations and which then gave questionable response prediction distributions, it is also important to recall the coarse sampling scheme utilized for this approach. If a more refined sampling space was implemented, it is envisioned that the response prediction distributions would be more populated by models with appreciable weights. However, it was not apparent upfront that the model space was fairly confined to a much tighter region than what was defined.

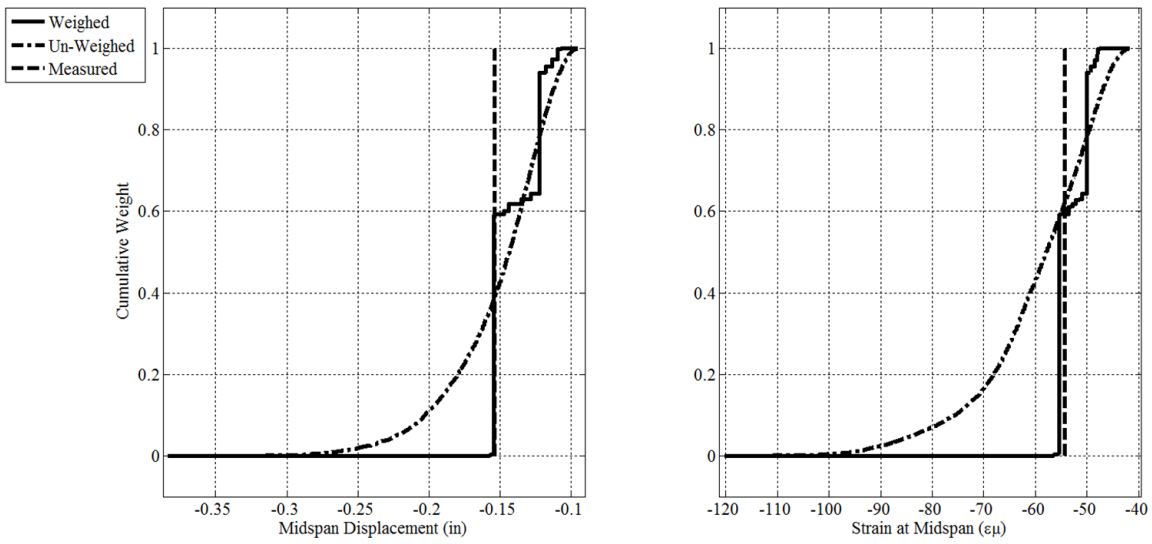

Figure 7-6: Response predictions for WM1 Weighing

In contrast, the WM2 weighing approach, as shown in Figure 7-7, was observed to be incapable of narrowing the band of likely response predictions from the equally weighed approach that does not require any experimental data. The displacement response prediction ranges went from {-0.1", -0.4"} to {-0.11", -0.25"}. While this range almost symmetrically encompasses the measurement of -0.154", and also seems to have a model with significant weight at that prediction, the bounds of likely predictions are too large to make a meaningful inference from them. If the owner of a structure was presented with the results that a critical member could experience forces +/- 30% of a central value, they would rightfully question why the time was spent to develop and analyze 59,049 models or the value of conducting an experiment to obtain measurements.

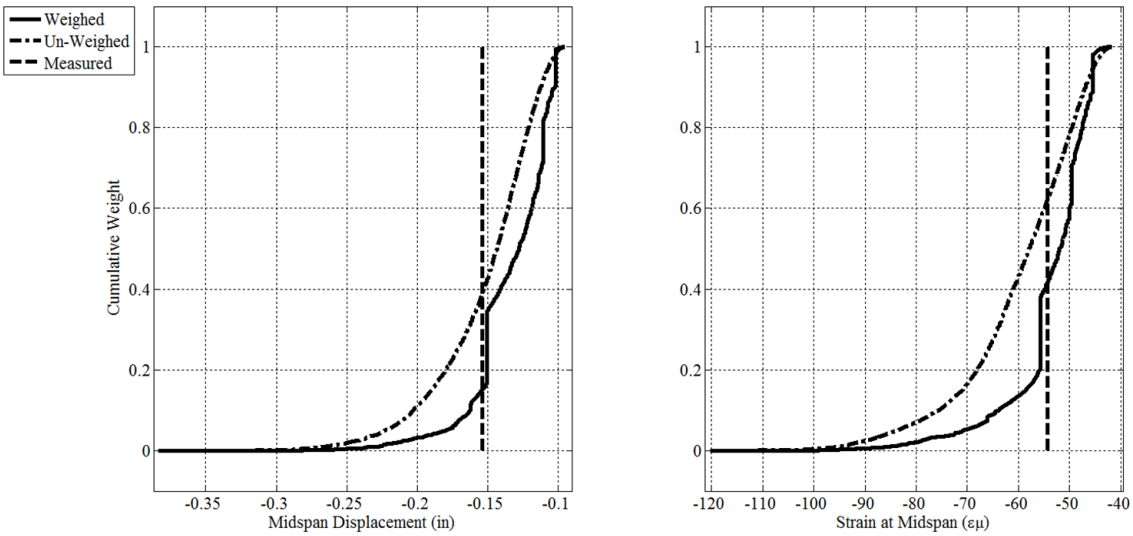

Figure 7-7: Response predictions for WM2 Weighing

While the deterministic approach to MM St-Id seems to still tend towards the selection of a single model, mostly resulting from coarse sampling of the building blocks and the lack of an appropriate weighing scheme, a clearer picture of the desired outcome is becoming apparent. A prediction distribution that is not only accurate, but provides meaningful information through bounds that can be appreciated. If the anticipated predictions are better off calculated by hand than through a MM St-Id framework, then it is clear that the method is not meaningful or at least is not being appropriately leveraged.

In summary, the primary drawbacks of the deterministic method are twofold. First, this approach lacks resolution when developing samples of the building blocks, especially without sound heuristics. As a result, even if there are many combinations within certain regions of the model space that correlate well with experimental observations, many of these combinations will be missed. This shortcoming is exacerbated by the second issue, which is that deterministic weighing lacks a rational approach to distribute weights among models. Although experience would suggest that WM1 was too conservative and WM2 was too liberal in the distribution of weighing factors, there is no basis for this judgment beyond intuition as the uncertainties at hand are not explicitly considered.

7.3. The Threshold Approach

The threshold approach to MM St-Id has been the focus of ongoing research (Robert-Nicoud, Raphael et al. 2005; Smith and Saitta 2006; Smith and Saitta 2008; Goulet, Kripakaran et al. 2010; Smith 2010), and aims to identify a set of candidate models from a larger initial model population by eliminating models based on a predetermined error

threshold. The objective of the approach is to account for uncertainties associated with all aspects of the St-Id process, and define a threshold value under which models are accepted and rejected. Models are generated with a probabilistic sampling scheme based on identified uncertain parameters. Uncertainties are tabulated when possible, and estimated using heuristics for those cases which cannot be numerically computed. This section will present a threshold technique developed through this research, based on published work of others. It was the intent of this application to best apply the methodology (as defined by the originators of the approach) in a fair and logical application to the grid structure for comparative evaluation. The sampling scheme, accounting of uncertainties and weighing of models was all done in accordance with the guidelines presented in Goulet, Kripakaran et al. 2010.

7.3.1. Threshold Sampling

The sampling scheme selected for this investigation was the Latin Hypercube Sampling (LHS) method based on the recommendations of Smith et al. (Goulet, Kripakaran et al. 2010). This sampling approach is typically used in practice to better characterize the probability density function (pdf) of interest in fewer samples than classical Monte Carlo methods, which will be discussed later. The user can also control the degree of correlation between various parameters, lending itself to uncertainty analysis. The LHS method requires the user to establish the total number of parameters, desired number of samples and the desired distribution.

The LHS method begins by dividing the parameter space into a number of bins in a random order, with the number of bins equal to the total number of samples desired. The algorithm then randomly samples within each bin, thus never repeating the same sample twice, until all have been generated. An example to assist in visualizing this process is to assume ten samples of the standard uniform distribution. Ten equal bins are generated, in this the bounds of each bin would be {0, 0.1, 0.2, …, 1.0}, and randomly organized. Then each of the bins is sampled randomly with a uniform distribution over the bounds of each.

As mentioned, an advantage to the LHS approach is that the desired pdf can be better characterized in fewer samples than classical random methods. To illustrate this point, a simple example is shown comparing Monte Carlo methods which randomly draw independent samples and the LHS method. Each method is used to generate 100 datasets of 100 samples from the standard normal distribution, with a mean of 0 and standard deviation of 1. The mean and standard deviation of each dataset is then computed to study how well the sampling scheme was able to characterize the standard normal distribution. The results are plotted in Figure 7-8, and show the mean of each dataset on the x axis and the standard deviation on the y axis. Datasets generated by traditional random methods are represented with an ‘o’, while LHS generated datasets are represented with an ‘x’. It is fairly straightforward to see that the LHS method is better able to generate samples that are characteristic of the pdf which was assigned, since the mean and standard deviation are much closer to their defined values. This does not invalidate the traditional random sampling methods, as they would eventually also converge to these results but with more samples required.

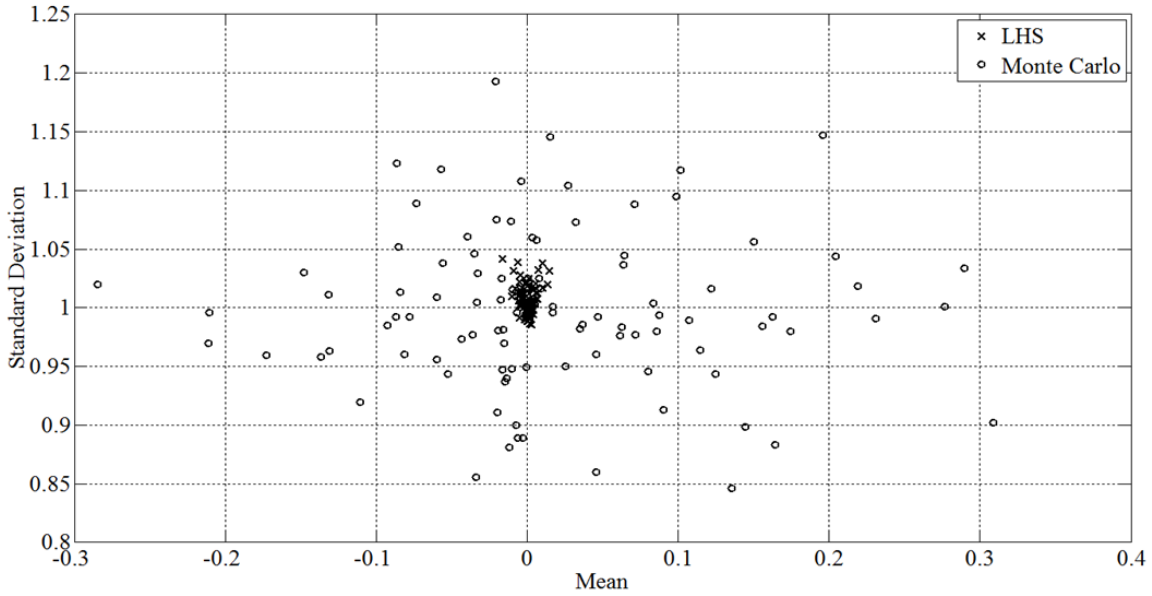

Figure 7-8: LHS vs MC Methods of Sampling

A potential disadvantage to this approach is that the total number of required samples is required upfront, however it is not straightforward to estimate how many models are needed in an a priori sense to best sample the model space so that a sufficient number of candidate models is generated. Nonetheless, the method will be applied to the grid structure to generate an initial model population of 1,000 based on the five parameters identified in the previous Sections. The Statistics Toolbox within MATLAB was used which features built-in algorithms for generating LHS designs. The same post-sampling analysis was carried out on the LHS generated models to visualize the model space coverage. As seen in Figure 7-9, the elastic modulus of steel was sampled from a normal distribution which estimates the variance seen in past analyses (Galambos and Ravindra 1978).

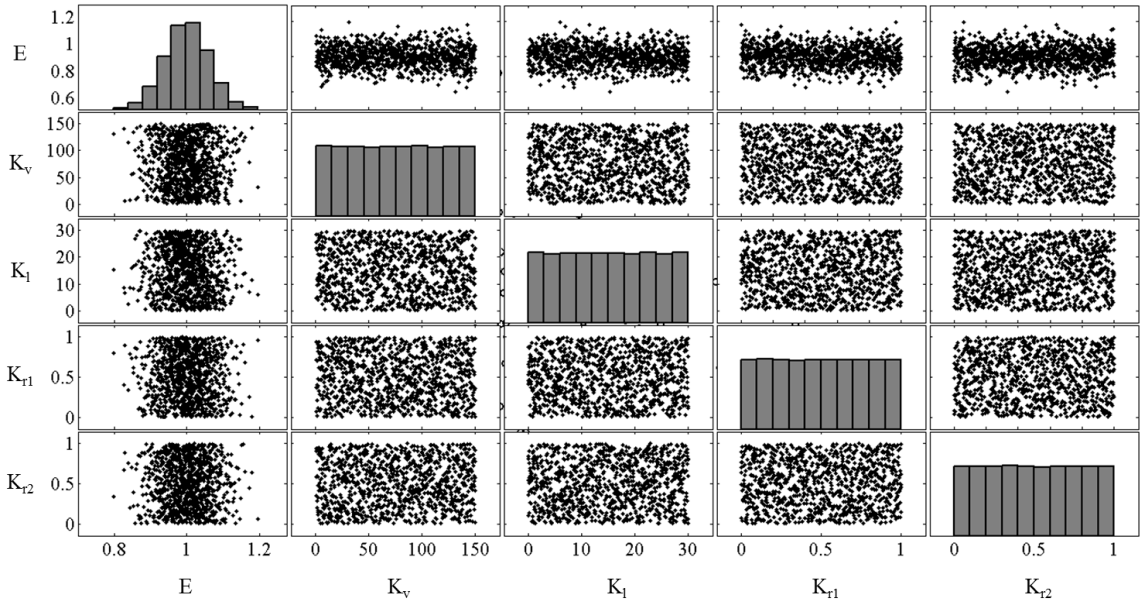

Figure 7-9: Matrix of Plots for Threshold Sampling

By comparing Figure 7-1 and Figure 7-9 it is apparent that the LHS method of generating models was much more efficient in covering the model space than a deterministic approach, even though the deterministic approach utilized almost sixty times the number of models. The systematic voids in the deterministic sampling created the potential for sensitive areas to be missed. However, the LHS design shown above has generated not only random samples that appear to efficiently cover the model space; they also characterize the distributions assigned to each parameter as demonstrated by the histograms plotted along the diagonal of the matrix of plots.

7.3.2. Threshold Weighing

The methodology employed in this weighing approach is to define thresholds for each measurement and to eliminate models that do not produce responses that fall within the thresholds for each measurement. The models that do produce responses within all thresholds are considered to be equally weighted, reflecting the claim by Goulet, Kripakaran et al. (2010) that with the uncertainties present it is not possible to distinguish between the validity of various models within the thresholds.

The threshold value for each measurement is taken as a function of pre-defined uncertainties associated with both the experimental procedure and the modeling process employed. For example, uncertainties which would be considered as part of the experimental procedure could include sensor accuracy/repeatability, data acquisition resolution, sensor installation errors, etc. Uncertainties associated with the modeling approach would include mesh refinement errors, geometric and other simplifications, and resolution issues (element selection versus desired response). For the grid structure, the uncertainties selected as being most influential on the results of the process were identified as: measurement repeatability, sensor accuracy, and sensor noise. To represent uncertainties associated with the finite element method, a single encompassing value of 5% was used based on the recommendations of Goulet, Kripakaran et al. (2010). These uncertainties and how they were implemented for all measurements in addition to the application to the natural frequency measurements are listed in Table 7-2.

Table 7-2: Uncertainty Sources for Threshold Weighing

Uncertainty Source		Uncertain Associated with Modes						
	Def.	1	2	3	4	5	6	7
Measurement Repeatability	± 3σ	1.89%	0.40%	0.07%	0.04%	0.16%	0.08%	0.06%
Measurement Noise	± 3σ	0.12%	0.12%	0.12%	0.12%	0.12%	0.12%	0.12%
Measurement Accuracy	%	0.01%	0.01%	0.01%	0.01%	0.01%	0.01%	0.01%
Finite Element Method	%	5%	5%	5%	5%	5%	5%	5%
Total		6.89%	5.40%	5.12%	5.12%	5.16%	5.12%	5.12%

The measurement repeatability uncertainties were identified by computing the standard deviation of the identified frequencies from the five impacts during the experiment. The total uncertainty then is quantified as plus or minus three times this standard deviation. Similarly, uncertainty corresponding to measurement noise was accounted for by computing the noise level within plus or minus three standard deviations and then computing what percent of the overall measured response this corresponded to. For example, the standard deviation of the noise level in the PCB 393C accelerometers, 0.0005g, was multiplied by three and divided by the maximum measurement response, 1.25g, during the impact test. This yields an uncertainty of 0.12% associated with measurement noise for the first frequency. The very low percentage seen for this uncertainty is justifiable in understanding that these impact tests were carried out in a laboratory environment on an easily excitable structure. This would be a much more significant uncertainty source for a real structure, where measurement levels are low and

sources of noise are more abundant. Finally, the last measurement related uncertainty of accuracy was identified by the vendor specifications of the sensor. To remain consistent with similar threshold weighing schemes in publications, a smeared 5% uncertainty was applied to the finite element method. Also, in this case mesh refinement was not explicitly considered as an uncertainty source since a mesh refinement study was carried out and the base model discretization was shown to be insensitive to further refinements for the first seven modes, which were used in the MM St-Id.

To translate the defined uncertainties above into a threshold band, the maximum uncertainty from those associated with measurement phenomena were summed with the maximum uncertainty from those associated with the finite element process, to obtain the final threshold values listed above. This method of summing the maximum of each uncertainty group was carried out by Goulet, Kripakaran et al. (2010) and replicated here for completeness in staying consistent with the approach.

These threshold values correspond to a band of acceptable models. For example, if a certain model predicts a first frequency anywhere within ±6.89% of the measured value for the first mode then it is accepted as a candidate model for that measurement. Similarly, if the percent difference between 1.0 and the MAC value is outside of the threshold, the model will be rejected. In order for a model to be considered as a candidate model, it must pass all threshold criteria for each measurement. In the case of the grid structure, there are 14 measurements (seven natural frequencies and seven mode shapes) and each must meet the defined threshold criteria listed above.

The 1,000 model set described in the previous section was analyzed for natural frequencies corresponding to those identified in the experiment as well as displacements and strains under static loads. Figure 7-10 shows the frequency output of each model compared to the acceptable bounds defined by the thresholds listed above. In this case, only one model passed all fourteen threshold criteria. As shown by Goulet, Kripakaran et al. (2010), when no models or only a few models pass the threshold criteria, then modifications should be implemented to generate more candidate models.

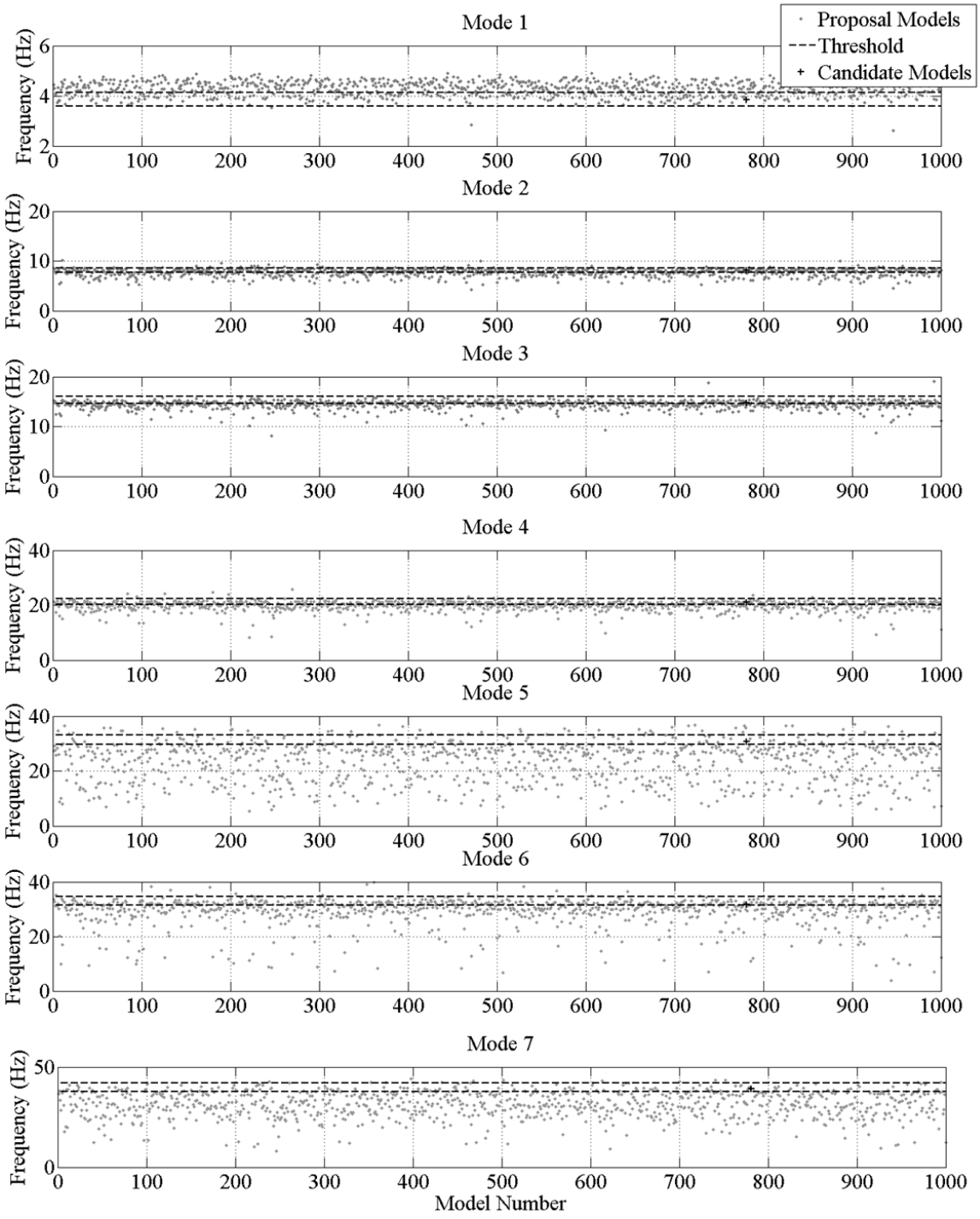

Figure 7-10: Models Plotted with Threshold Bounds for each Measurement

Towards that end, a 3,000 model set was generated in the same manner as the 1,000 model set and was analyzed for natural frequency content and static responses. Instead of providing more candidate models, in this case the 3,000 model set did not provide a single accepted candidate model. This would seemingly suggest that there is an error in the model or selection of building blocks since such a large population of models did not pass the threshold criteria. One of the major error sources an FE model can have is bias, and it would seem that there appears to be bias evident in looking at the frequency plots in Figure 7-10. However, there is no consistent bias among all modes since the first frequency has a central tendency above the threshold bounds and the remaining frequencies have central tendencies that are either within the threshold bounds or below them. Since the base model was error-screened, and there is no overarching bias present in the predictions, the model appears reasonable (particularly when one considers the very small errors found in certain models using the deterministic sampling/weighing approach discussed in Section 7.2). Instead, the quantification of uncertainties is investigated, since the thresholds imposed may be too strict in this case, and further in this chapter, the sampling methodology is investigates since once again the model space may not be efficiently sampled.

The 1,000 model set was re-weighed, however this time the uncertainty associated with the finite element process was increased from 5% to 8%. After screening each model with the new thresholds, eleven models were able to pass all threshold criteria. For comparison, the 3,000 model set provided forty candidate models, and will be used for subsequent analysis. This increase from 5% to 8% was done somewhat arbitrarily until an appreciable number of models could pass the threshold. This highlights one of the

drawbacks of this approach, in that such detail is paid to computing small uncertainties associated with measurement quality while a large, somewhat arbitrary uncertainty representing smeared errors within the finite element process is also applied. As seen previously, the 5% error initially assumed for the finite element uncertainty contributes 98% of the total uncertainty associated with some modes. However, the 8% uncertainty associated with the finite element process will be used from here to fully demonstrate the method.

7.3.3. Threshold Predictions

Threshold predictions are not generated with a specific contribution from each model, as is done with histograms for example, however the models of interest are those that define the bounds of all predictions. Thus, only the models corresponding to the minimum and maximum response prediction are used to define the bounds of response predictions. To acknowledge the 8% uncertainty used in selecting the candidate models based on frequency measurements, all candidate model predictions must also be resampled with an 8% uncertainty reflecting the translation from prediction to model and vice versa. To resample the response predictions, each response from a candidate model is treated as the mean of a normal distribution with an 8% standard deviation. This response distribution is then sampled 10,000 times for each candidate model to fully characterize the response prediction distribution. The 95% confidence interval from this sampled distribution is then found and the final threshold bounds for predictive purposes are identified. It is noted in literature (Goulet, Kripakaran et al. 2010), that the uncertainty associated with a

global model in predicting static strains is 20%. This level of uncertainty is also used in the resampling process to generate the prediction threshold bounds for comparative purposes.

In Figure 7-11 below, the cumulative weight functions for each building block is presented. Since each model is not contributing in a cumulative sense, only the building blocks which contribute the minimum and maximum building blocks are used to define the threshold bounds. A straight line is then plotted between these points to represent that each model within these bounds is equally likely. The interpretation of the building block thresholds is logical for Structure 1, with values of the elastic modulus of steel nearly centered on its normalized value, high vertical stiffness springs representing the steel supports, and low longitudinal stiffness springs representing freedom for longitudinal movement and high levels of rigidity in the connection stiffness of the two main connection types.

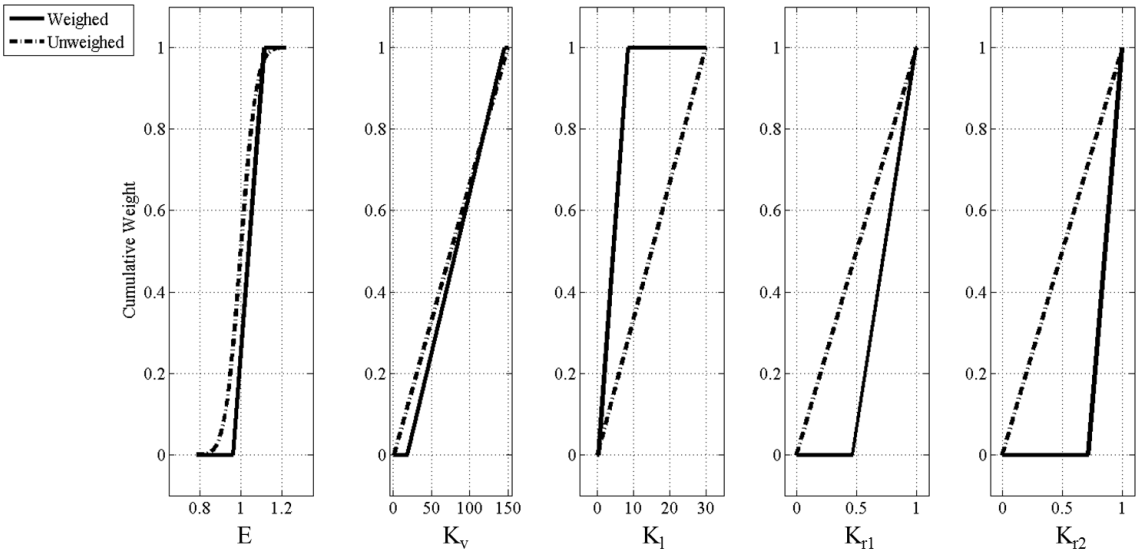

Figure 7-11: Building Block Threshold Bounds

The prediction of the response indices of mid-span displacement and strain are presented in Figure 7-12 and Figure 7-13. The first plot, Figure 7-12, shows the threshold predictions incorporating an 8% uncertainty in the ability of the finite element model to predict displacements and strains. This uncertainty was applied to the predictions by sampling the models which passed the threshold criteria with an 8% standard deviation. To best characterize the distribution, thousands of samples were generated for each model and combined with all other generated samples. This collective group of samples was then used to produce the prediction distributions seen below.

It is evident from these prediction plots that while the threshold weighing method is cutting the overall range of predictions in half, it is not distinguishing between the

roughly 99% of the models still within the threshold bounds. As a result, this approach does not appear any more justifiable than to just use the un-weighed predictions directly from the LHS analysis. It is also noteworthy that of the 3,000 models originally generated for this method, only 40 models were accepted as candidate models but yet their predictions were unable to distinguish models within the entire population. Additionally, in Figure 7-13 where the uncertainty in predicting strains was increased from 8% to 20% this inability to improve upon the un-weighed models is even more apparent.

It is envisioned at this point, that a threshold methodology of multiple model analysis would not lend itself to a decision making framework where likelihoods of specific response indices is critical, however it may be beneficial in experimental design, where the population of models is used to help design instrumentation plans.

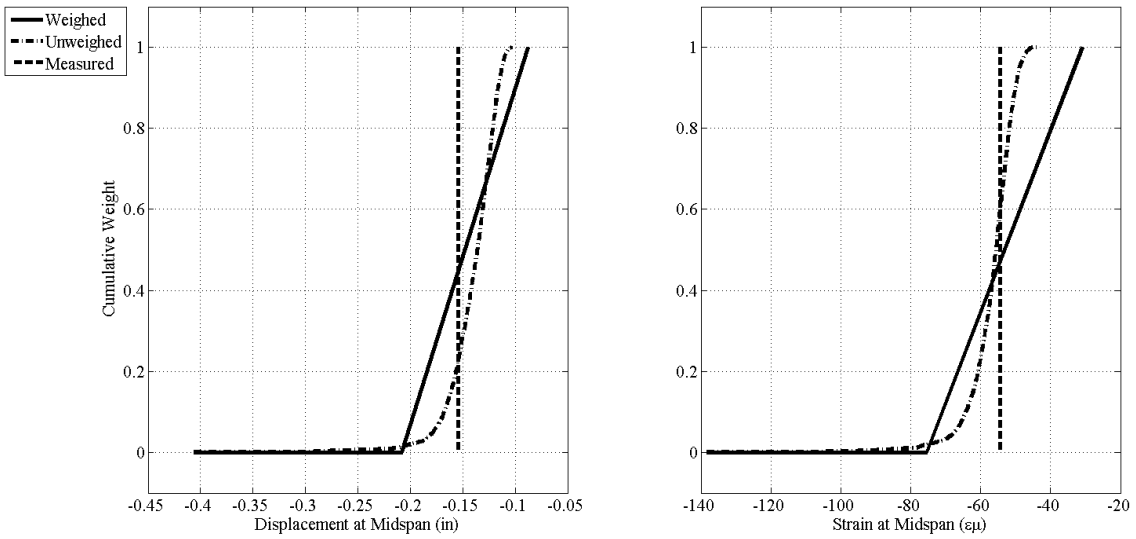

Figure 7-12: Threshold Weighing Response Predictions

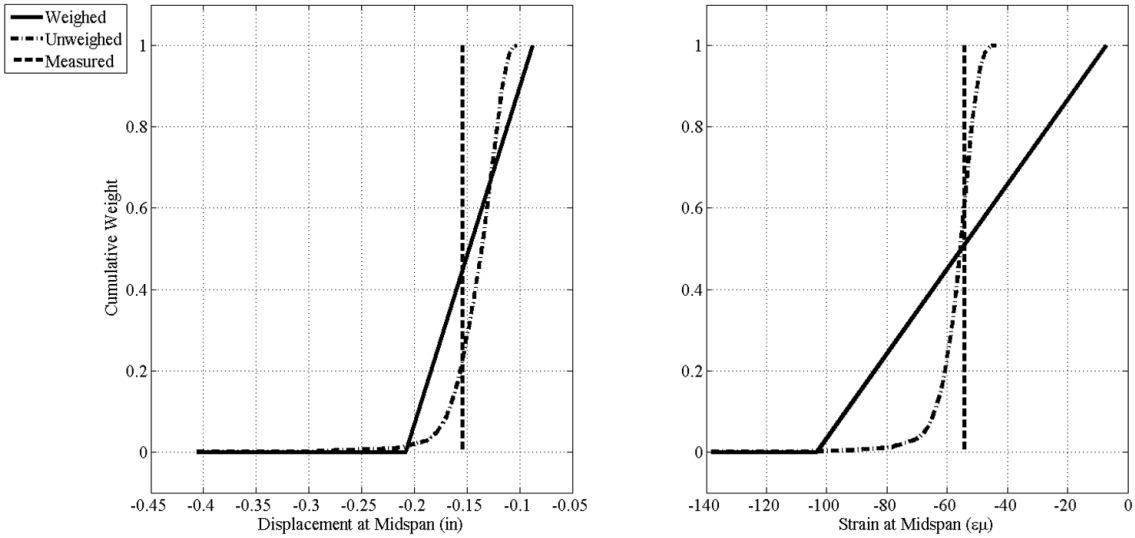

Figure 7-13: Threshold Weighing Response Prediction with 20% Uncertainty in Strain Prediction

7.4. The Probabilistic Approach

A consistent probabilistic approach to MM St-Id is defined as the use of probabilistic sampling of building blocks (either informed by a prior distribution or not) and weighing each model based on its posterior probability given the observed experimental data. A potential benefit of this method is that many advanced algorithms have been developed in other fields to efficiently draw samples from either prior distributions or directly from posterior distributions. As seen in the previous discussions on deterministic and threshold methodologies for MM St-Id, efficiency is an important consideration keeping in mind that more complicated models will require longer analysis time. In addition, the coarseness of the sampling approaches employed in these other approaches is a principle challenge as the model space of interest is likely only a small portion of the entire model

space (in some cases with significant gradients). One advantage of probabilistic sampling approaches is their ability to densely cover the entire modeling space, and in some cases seek out the regions of interest (i.e. those with strong correlation to the observed data).

7.4.1. Bayes Theorem

Before the methods of probabilistic sampling can be presented, a brief discussion on Bayes theorem used in subsequent analysis is necessary. Bayes theorem was first presented in 1763 by Richard Price, on behalf of Thomas Bayes who had passed away before publishing his work. Since its development, Bayesian inference has been widely used in fields such as artificial intelligence and expert systems, as well as decision theory, model updating, and model selection. Many disciplines utilize the tools just described, such as finance, engineering, scientific, medical and legal applications and many more. In many applications, the theorem is used to update uncertain parameters within a model to provide better estimates of those parameters. An important distinction between model updating and MM St-Id is that the end result of the method is not a single model with identified distributions for its parameters. However, in MM St-Id the analyst is provided with a set of weighed models (which do not need to be of the same dimension or form) and respective predictions to be used for engineering applications, such as hazard analyses.

The theorem described the relationship of our degree of belief in a given event before (termed prior probability) and after (posterior probability) observing some evidence or data. The likelihood function used is a key part of Bayesian probability theory, whereas

the prior probability of a certain phenomenon is updated based on learned information to generate the posterior probability with the following function (Eq. 7-4).

$$P(M_i|D) = \frac{f(D|M_i)P(M_i)}{\sum f(D|M_i)P(M_i)} \qquad \textbf{Eq. 7-4}$$

In this case, the posterior probability of a model *M* given that the information *D* has been observed, is equal to the product of the likelihood , *f(D|M)*, and the prior probability, *P(M)*, normalized by the integral of this same product over the entire model space. The key component of this expression is the maximum likelihood estimator, which is calculated in the following manner as shown in Eq. 7-5.

$$f(D|M_i) = \prod_{j=1}^{n} \frac{1}{2\pi\sigma_j^2} e^{-\frac{(x_j - u_{ij})^2}{2\sigma_j^2}} \qquad \textbf{Eq. 7-5}$$

In this computation, the likelihood of the observations given the current model is evaluated by multiplying the probability of each of the *n* number of observations, *x*, given the current model prediction. The probability of each model prediction is assumed to be normal by nature, with a mean *u* equal to the i^{th} model prediction and a standard deviation of 4%. The value of 4% accounts for uncertainties associated with the translation from physical systems to finite element models and vice versa. This specific value is based on experience in simulating measured responses of constructed and is admittedly somewhat arbitrary. As a result, the influence of this parameter on the outcome of the method will be examined and verified (see Section 7.4.4).

7.4.2. Probabilistic Weighing

The weighing methods of the probabilistic approach will be discussed first since it is a prerequisite to some of the sampling methods which will be discussed. To weigh each of the models, the posterior probability was computed using the experimental observations, model predictions and definitions of standard deviations. A normal probability density function with an inherent standard deviation of 4% was used to represent uncertainties associated with numerical errors within the finite element method. In addition, the standard deviation of each observation over the course of five repeated measurements was tabulated and added to the inherent standard deviation. The selection of an appropriate standard deviation to represent the ability of the model to make accurate predictions is paramount to the success of the method. If a standard deviation is selected that is too small, then the method will only accept models which almost exactly match the

experimental data. Conversely, if a standard deviation is selected that is too large then the method will lose the ability to discern between models and a large range of models will be accepted (analogous to simply sampling from the prior distributions and equally weighing all models). It is for this reason that the only uncertainties which can reasonably be calculated and accounted for are applied to the weighing of each model. In this regard there is no substitute for heuristic knowledge and intuition into both to both the actual behavior and simulation of constructed systems.

7.4.3. Probabilistic Sampling

There are many forms of probabilistic sampling, most of which utilize random number generators to achieve the desired statistical properties defined by the user. Two main forms of probabilistic sampling will be investigated for their potential contributions to the MM St-Id framework: (1) Monte Carlo (MC) sampling, which is a pure random sampling scheme that draws samples from prior distributions (of which the Latin Hypercube analysis previously discussed is a derivative), and (2) Markov Chain Monte Carlo (MCMC) sampling, which encompasses an entire class of sampling algorithms that over time efficiently converge to the desired posterior probability distribution.

7.4.3.1. Monte Carlo Sampling

Monte Carlo (MC) sampling (Anderson 1986; Metropolis 1987; Mosegaard 1995) was first developed within the Manhattan Project by scientists looking for ways of computing average distances neutrons travelled into various substances. The approach required the

generation of large amounts of random numbers, and with the development of computers in the 40's and 50's pseudo-random number generators became more widely used in the fields of physics and mathematics. Through the years, many implementations have benefited from using Monte Carlo methods; some as simple as simulating a coin flip or roll of a die while others are as complicated as the integration of complex multi-dimensional surfaces. It is this last use that is of interest to the MM St-Id method, as the goal of the probabilistic MM St-Id approach is to map the Bayesian probability surface of the model population. By evaluating random points for their contribution to the integral, the entire integral can be mapped, giving the analyst a clear picture of where the regions of high likelihood exist within the model space. In the long run, this estimate of the expected value of the integral will converge to the actual solution.

Also, MC methods can take advantage of assumed prior distributions and draw samples directly from them. There has been a great deal of published research on random number generators and how to select randomly from a defined distribution (Gelman, Carlin et al. 1995; Chen, Shao et al. 2000), and modern advances in computer technology have allowed researchers to easily generate large quantities of random numbers in an efficient manner.

One shortcoming of this approach is that the success of any given sample is not taken into account to produce the subsequent sample, and that samples which produce poor correlation with experimental data always have equal probability of being selected as those which produce superior correlation. In this sense, MC methods do not take into consideration the solution but concentrate on sampling the problem in a brute-force manner.

In applying the MC sampling scheme to the DI3 grid, the same five model building blocks were used as well as their bounds. However, due to the need for computation of a prior probability of each model, the building blocks had prior probability distributions assigned to them (Table 7-3). Since the elastic modulus of steel is the only building block with which any information is reliably known, it was assigned a fairly specific prior probability distribution, whereas the remaining building blocks were assigned uniform distributions over reasonable bounds.

Table 7-3: Prior Probability Distribution Assignments

Building Block	Lower Bound	Upper Bound	Distribution
E	0 E_o	2 E_o	N (1, 0.06)
K_v	0 kip/in	150 kip/in	U (0, 150)
K_l	0 kip/in	30 kip/in	U (0, 30)
K_{r1}	0	100%	U (0, 1)
K_{r2}	0	100%	U (0, 1)

The Monte Carlo sampling scheme requires that the prior probability distributions be sampled until the posterior probability of the model building blocks converge to a stable distribution and sufficiently characterize the posterior probability surface. Additionally, the response predictions should also be characterized in terms of its convergence. To evaluate whether a sufficient number of models were generated to produce a stable

distribution, convergence was assessed by evaluating the expected value and variance of the marginal posterior probability distributions for the various building blocks. Marginal probability distributions are computed by summing the probabilities associated with a certain building block value, while holding all other building block values constant. This provides a one dimensional slice of the total posterior probability surface. When these indicators have stabilized, convergence was assumed to have been reached.

The expected value, E(X), and variance, V(X), of a probability distribution are defined as shown in Eq. 7-6 and Eq. 7-7.

$$E(X) = \int_{-\infty}^{\infty} xf(x)dx \qquad \textbf{Eq. 7-6}$$

$$V(X) = \int_{-\infty}^{\infty} x^2 f(x)dx - \left(\int_{-\infty}^{\infty} xf(x)dx \right)^2 \qquad \textbf{Eq. 7-7}$$

In these equations for expected value and variance, the probability distribution, f(x), is a function of a random variable, x. In this case, f(x) represents the marginal posterior probability distribution for each of the building blocks. Since a finite number of models were generated, a continuous distribution is not possible so the discrete form of each equation was used. The expected value was used so that the central tendency of each

building block could be tracked over time. Additionally, the variance provides information on the shape of the posterior distribution over time.

The expected value of the marginal posterior probability distributions for each of the building blocks was computed over equally spaced intervals of models. Since in Monte Carlo analysis, it is not known a priori how many models are needed for convergence, the algorithm was configured to run in groups of 3,000 models. After a group of 3,000 models had been generated and executive, it was appended to the previous analysis groups and then the posterior probability of each model within the total group was computed. This approach to generating the MC models prevented an overabundance of models from being generated since they were periodically examined for convergence requirements.

To establish convergence within a set of models, twenty equally spaced intervals were identified over the entire set of models. The expected value and variance were then computed for the set of models in a cumulative manner with respect to the intervals. For example, if 2,000 models were being analyzed for convergence then the expected value and variance were computed for models 1-100, 1-200, 1-300, etc. The expected value and variance were then plotted as a function of the number of models included in the computation and examined for convergence. For the purpose of the MC model sampling, it is not a goal to have a precise estimate of the expected value and variance for each building block, so convergence was defined as when the expected value and variance stabilized to within 5%. These convergence diagrams were generated for the five building blocks of the DI3 grid structure and shown in Figure 7-14 -Figure 7-18.

In these figures, the expected value and variance are plotted against respective number of models included in the computation, in addition to the point selected as the convergence point, represented with a circle, and the 5% bounds from that point. As shown in the figures, 9,750 models were needed for all five building blocks to converge to a consistent probability distribution of weighed results.

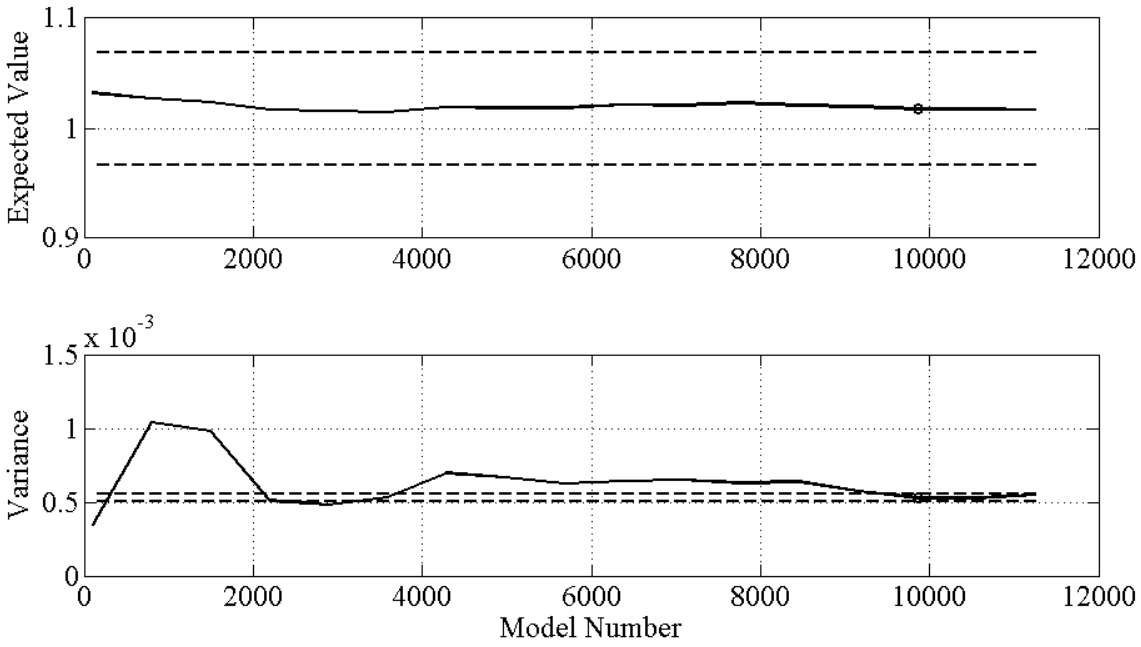

Figure 7-14: Convergence Diagram of the Building Block, E, for the MC Analysis of the DI3 Grid

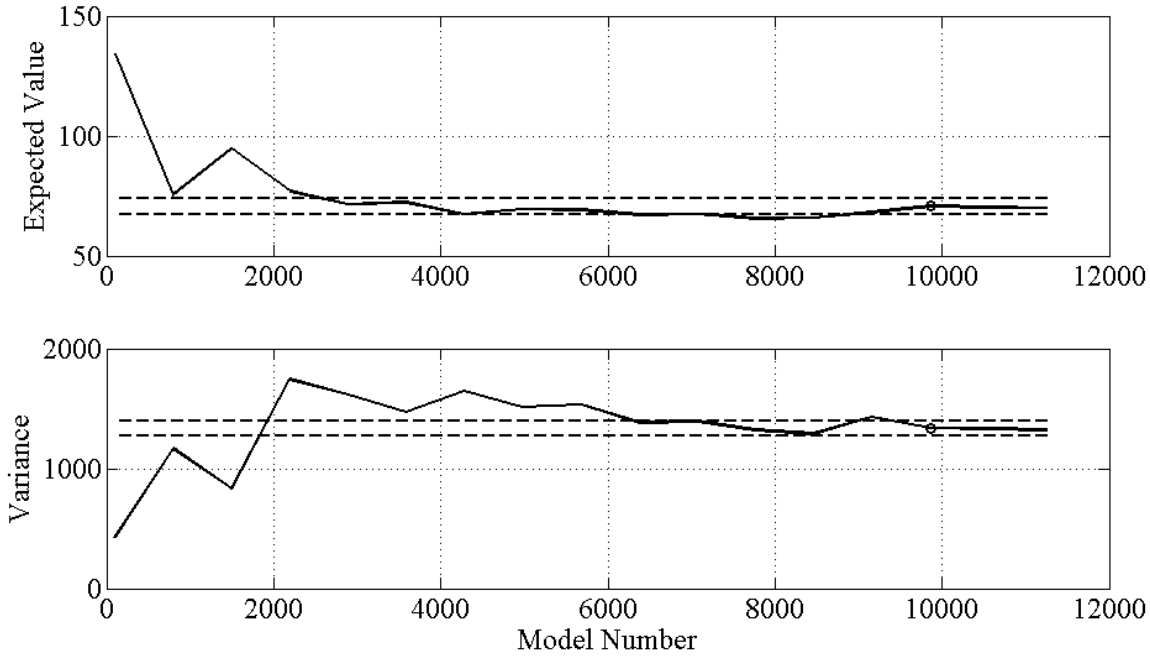

Figure 7-15: Convergence Diagram of the Building Block, K_v, for the MC Analysis of the DI3 Grid

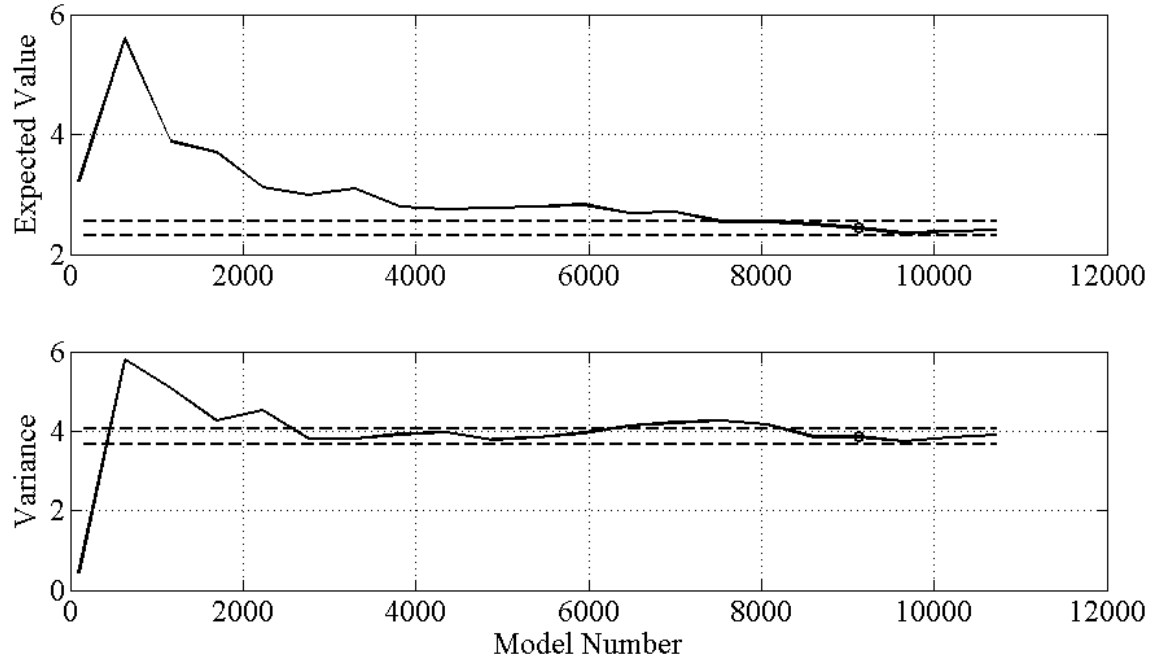

Figure 7-16: Convergence Diagram of the Building Block, K_l, for the MC Analysis of the DI3 Grid

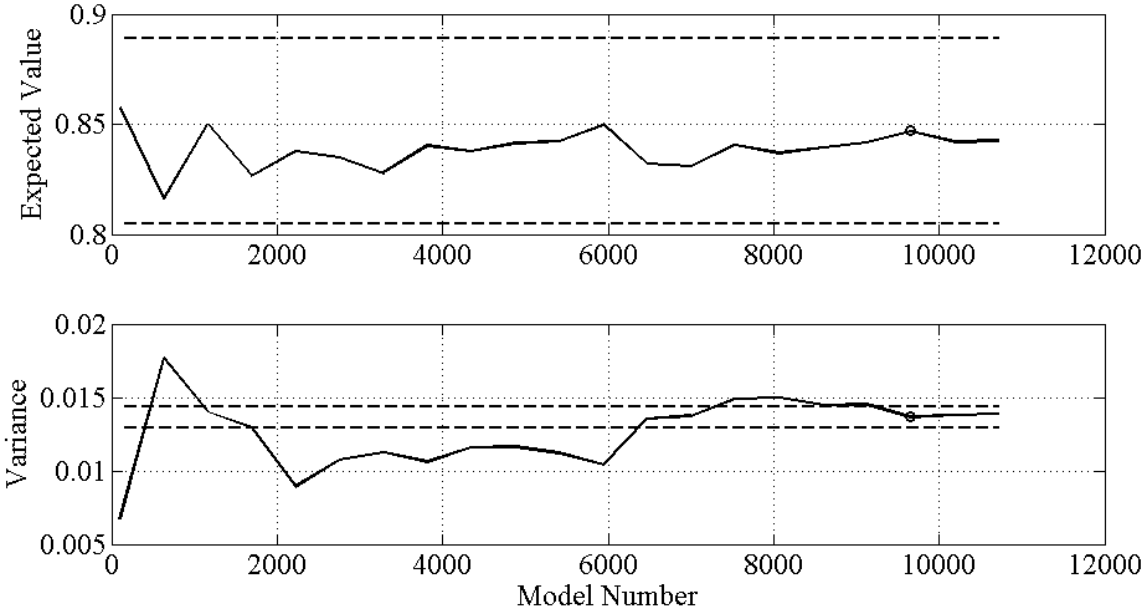

Figure 7-17: Convergence Diagram of the Building Block, K_{r1}, for the MC Analysis of the DI3 Grid

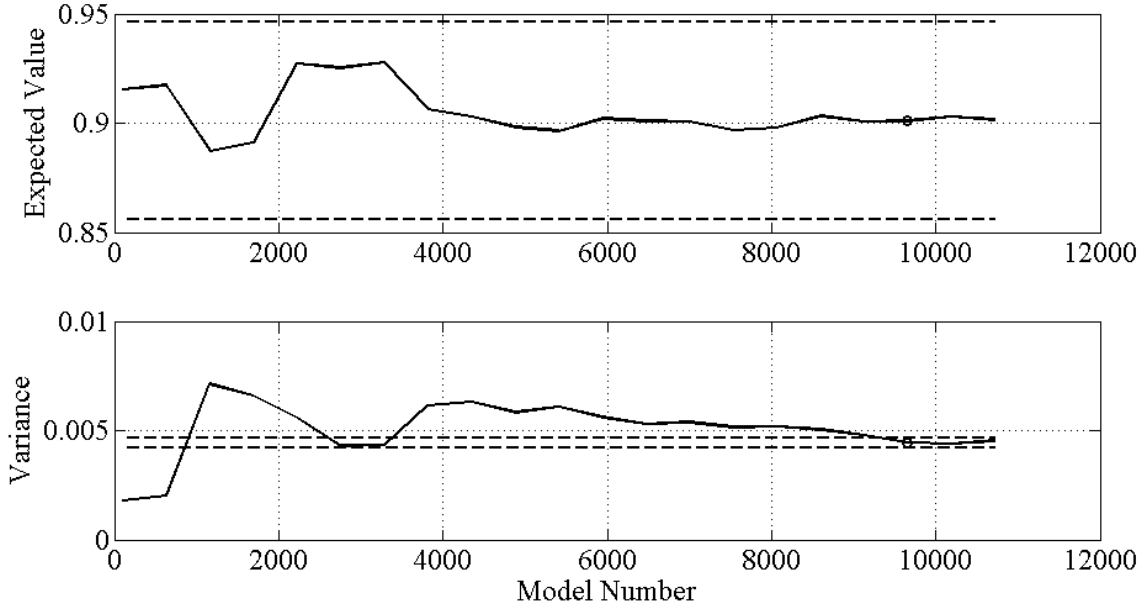

Figure 7-18: Convergence Diagram of the Building Block, K_{r2}, for the MC Analysis of the DI3 Grid

The matrix of plots, as shown in the previous sections for the Deterministic and Threshold Approaches, is shown in Figure 7-19 for the 9,750 models required to achieve convergence of using MC sampling.

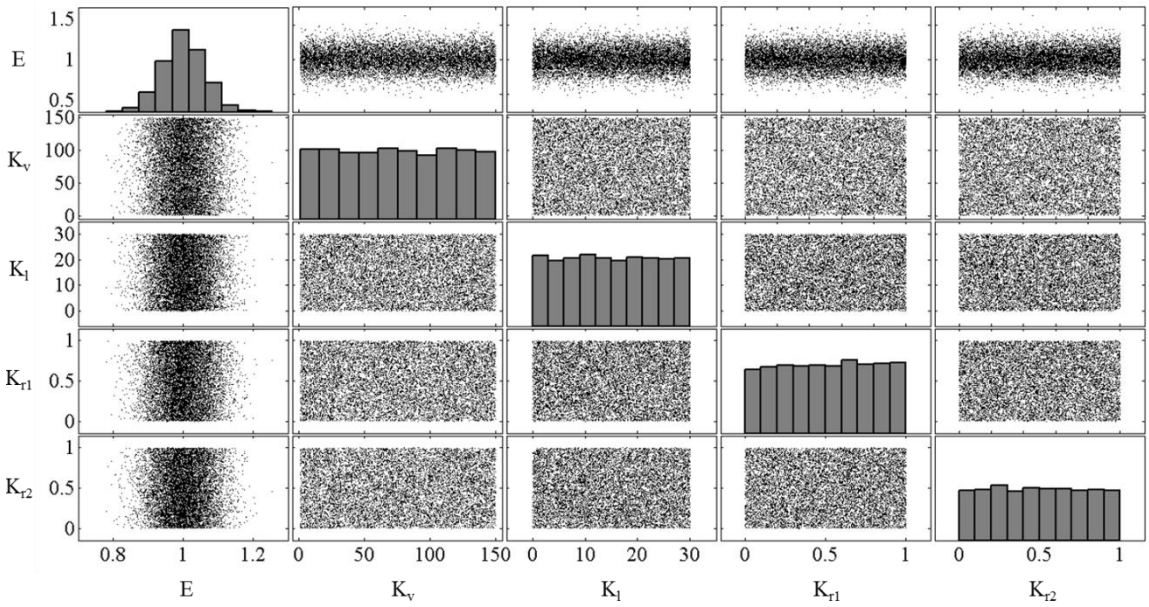

Figure 7-19: Matrix of Plots for MC Sampling

After inspecting Figure 7-19, it is clear that the Monte Carlo method has sampled the model building blocks very densely. The histograms on the main diagonal of the matrix of plots shows that the prior distributions assigned to each building block were characterized fairly well, but it is worth noting that the histograms for the uniform distributions do not appear to characterize the uniform distributions as well as the LHS

method was able to. This serves as another example, in addition to Figure 7-8, as to the benefit of LHS sampling methods on generating samples to efficiently characterize a prior probability distribution.

7.4.3.2. Markov Chain Monte Carlo Sampling

Markov Chain Monte Carlo (MCMC) sampling describes an entire class of sampling algorithms with the intent of drawings samples directly from a predefined probability distribution. This is accomplished by constructing a Markov chain with the desired probability distribution as its stationary distribution. A Markov chain is a system of mathematical transitions in which at any time a new position in the chain is only dependent on the current position. This property of Markov chains then allows the user to start the chain at any position, however the chain will still converge to its stationary distribution after a period of time, defined as the burn-in time.

Markov chains have a set of properties that are important to understand before using MCMC methods. First, a Markov chain is *irreducible*, or has a positive probability of moving to any state within the model space from its current state. Secondly, Markov chains are *ergodic*, in that they are positive recurrent and aperiodic. An aperiodic Markov chain will return to a current state at random intervals of time, and a recurrent chain has a non-zero probability of returning to the current state in a given number of steps. Finally, Markov chains in an MCMC framework are constructed so that they are reversible, or that they exhibit *detailed balance*. The detailed balance property means that it is equally

as likely to go from state one to state two as it is to go from state two to state one for all states in the chain.

Many different sampling schemes within the MCMC framework are used in different fields for various applications (Geyer 1992; Beck and Au 2002; Green 2002; Ching and Chen 2007; Glaser, Lee et al. 2007). The seminal MCMC sampling scheme is the Metropolis-Hastings algorithm first developed by Metropolis in 1953 and then generalized by Hastings in 1970 (Metropolis 1987). One main advantage of the Metropolis-Hastings (MH) algorithm is that it only needs to evaluate a function which is proportional to the desired probability density, thus in Bayesian applications eliminating the need to compute the normalizing constant.

The algorithm requires the computation of the target function $\pi(x)$, in this case the posterior probability defined above, the definition of a proposal function $q(x)$ and the selection of starting values for each parameter. The purpose of the proposal function is to generate a new sample, based on the position of the current sample. When all of these requirements are in place, the algorithm follows the following steps:

(1) Initialize x_0, the starting values for the parameters and compute the posterior probability associated with that position, y_0.

(2) For a given position in the chain, t, propose a new position, x_{t+1} in the chain by drawing a random sample from the proposal distribution and summing this number with the current position of the chain, x_t. Then compute the posterior probability associated with proposed sample, y_{t+1}.

(3) Compute the acceptance ratio α as given by Eq. 7-8. If α is greater than 1, then accept the proposed sample.

$$\alpha = \frac{\pi(x_{t+1})q(x_{t+1}|x_t)}{\pi(x_t)q(x_t|x_{t+1})} \qquad \textbf{Eq. 7-8}$$

(4) If α < 1, accept the proposed sample with a probability of α and reject the proposed sample with a probability of 1 – α.

(5) If the proposed sample is rejected, set $x_{t+1} = x_t$, and iterate steps 2-5.

There are a few parameters associated with the MH algorithm that require attention from the user. The first is the burn-in time, defined as the number of samples needed before the chain has "forgotten" it's starting value and is sampling from the target distribution. The number of samples required for the burn-in period is not known prior to the analysis and is dependent on many other factors, such as the starting position and the proposal function. Techniques have been developed to identify when convergence has been achieved (Richardson and Spiegelhalter 1996) and subsequent samples can be accepted as being drawn from the stationary distribution. For the purpose of this MM St-Id application, burn-in length was identified both visually and numerically.

Convergence was identified numerically by computing the expected value and variance of the samples over intervals of time and identifying where this expected value stabilized. Visually, the burn-in length can be identified by plotting the samples within the chain versus chain location. When the samples have stabilized both in terms of mean and variance, burn-in has been achieved. Since the visualization of the chain can be achieved

in real time during the MCMC process, it serves as a valuable tool for evaluating the MCMC method while it is running. Figure 7-20 illustrates the burn-in period during an MCMC analysis with the standard normal distribution as the target distribution and a starting position of -25.

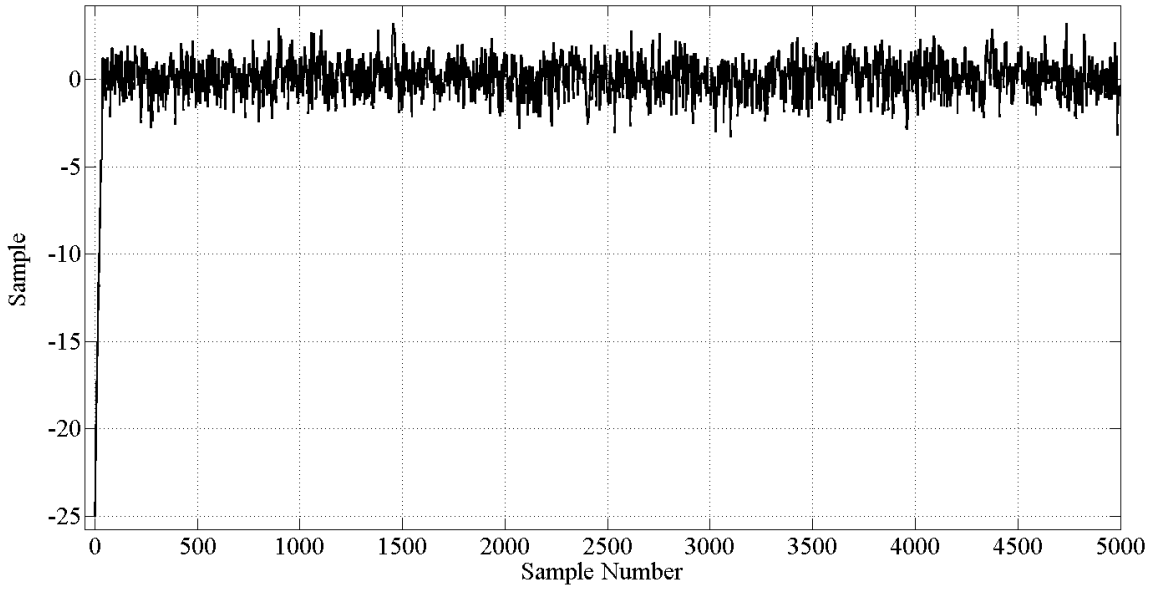

Figure 7-20: MCMC Analysis Highlighting Burn-in Period

The second decision that a user must consider is the selection of a proposal function. It is common that a normal distribution is selected due to its symmetric nature, which simplifies the computation of the acceptance ratio α. However, an important consideration to make is the variance used in the proposal function. If the proposed

moves are too large, then there will be large periods of rejected samples with intermittent jumps. If the proposed moves are too small, then the random walk nature of the algorithm is evident and the chain is mixing too slowly. An ideal proposal function variance is one that promotes rapid mixing and has an overall acceptance ratio between 25% and 50% depending on the dimensionality of the distribution (Richardson and Spiegelhalter 1996).

To illustrate how the selection of proposal functions can influence the analysis, a simple example is useful. For this example the standard normal distribution was used as the target distribution, as defined in Eq. 7-9.

$$\pi(x) = normpdf(x, 0,1) \qquad \textbf{Eq. 7-9}$$

The $normpdf(a, b, c)$ function represents a normal distribution evaluated at point a, with a mean of b and standard deviation c. Three MCMC runs were set up using three different proposal functions:

(1) Normal distribution with mean 0 and standard deviation 0.01

(2) Normal distribution with mean 0 and standard deviation 1

(3) Normal distribution with mean 0 and standard deviation 100

The results of these three MCMC analyses are presented in Figure 7-21. As seen in the figure, when the standard deviation of the proposal function is very small (Case 1), with respect to the target function, the chain is mixing very slowly and the random walk nature of the algorithm is visually apparent. However, when the standard deviation of the

proposal function is appropriate for the target distribution (Case 2), there is rapid mixing and the data appears random. Finally, when the standard deviation of the proposal function is very large with respect to the target function (Case 3), large plateaus exist where the algorithm was proposing moves too large and rejecting them very often. Large jumps are also observed, which is another telltale sign of this problem.

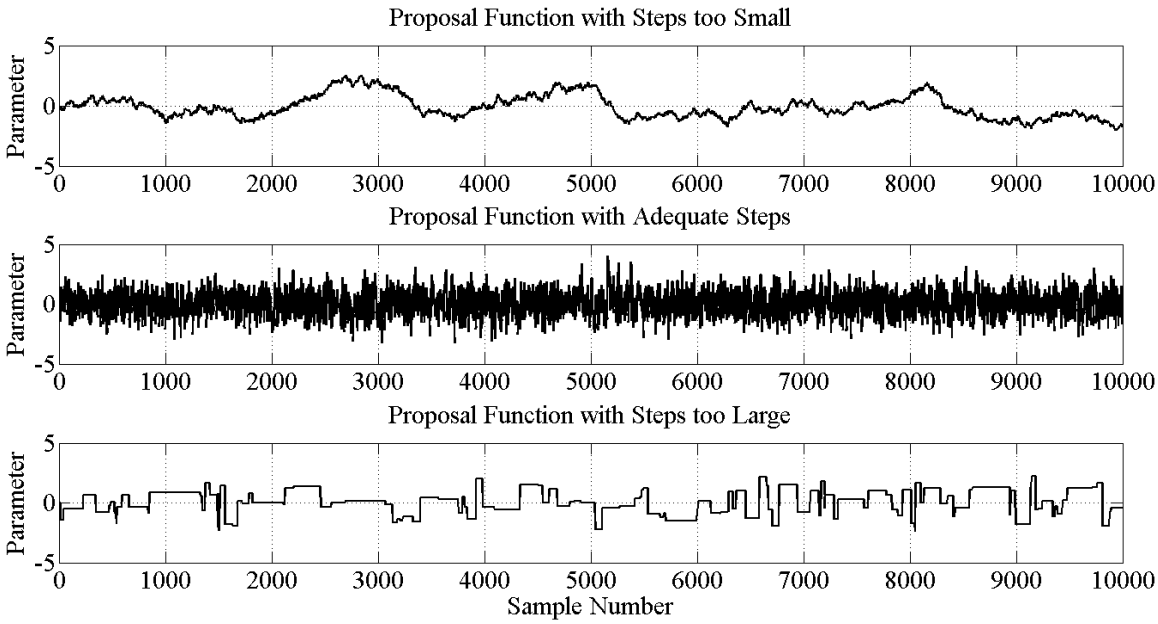

Figure 7-21: Proposal Function Study

Burn-in length and appropriate selection of a proposal function can only be verified after a significant amount of models have been run. Therefore, it is essential that an experienced user is utilizing these tools to minimize the inefficiency of the process and

time required. It is worth noting that while Cases 1 and 3 are inefficient, that over longer period time their distributions will also stabilize and converge upon the intended target distribution. Also, mitigation strategies were developed in other fields to handle such problems related to Case 1, one such strategy being the selection of periodic samples of the chain to obtain a reduced, more randomized subset of a Case 1 chain.

The Gibbs sampling algorithm was originally intended to be explored for applicability to the MM St-Id method, however after further investigation it was shown to not be applicable to the method. Gibbs sampling is mainly beneficial when the joint distribution of a probability density is not known, but the conditional distribution of each variable is known and simpler to sample from. The method very readily provides marginal distributions for each of the variables; however the focus of the MM St-Id method is not on the updated distributions of each variable but on the distributions of model predictions. Also, the method requires upfront knowledge of the full conditional distributions of each of the parameters. In the MM St-Id framework, it is more beneficial to remain with the joint target distribution (ie, the function of all building blocks), since it can easily be computed, and thus to utilize the MH algorithm.

In order to provide the most efficient MH sampling algorithm and to increase the acceptance ratio, more advanced algorithms were investigated for their potential applicability to the MM St-Id method. One method found through literature review is the Delayed Rejection – Adaptive Metroplis (DRAM) method (Haario, Laine et al. 2006). This method was developed to accomplish two main tasks: (1) update the proposal function over time to best characterize the nature of the target distribution and (2) give

regions in the model space a second chance by proposing an additional sample based on a rejected sample. These methods have been shown by the developing authors to still follow fundamental properties required of Markov chains and also have been demonstrated to provide more efficient results than the classical MH algorithm. However, the chains produced are not *true* Markov chains in that the proposed samples are dependent upon the updated proposal function. This method was explored since in many cases the simulation models will require a large amount of time for analysis, and thus the classical MH algorithm may prove exceedingly inefficient. For example, if an MCMC analysis using the MH algorithm had a burn-in length of 1,000 samples, each of which would require 5 minutes to analyze (3.5 days), then the computational effort needed to just evaluate the proposal function would be quite burdensome. In contrast, if adaptive MCMC approaches proved appropriate, then the proposal function could be updated during this burn-in period increasing the overall efficiency of the approach.

To demonstrate the ability of the DRAM algorithm in providing a more efficient approach to the MCMC analysis, the proposal function study was repeated for the three cases previously outlined. In the three cases, an initial proposal function was defined similar to the three proposal functions described above. In addition, the algorithm was set to re-evaluate the appropriateness of the initially defined, or subsequently modified, proposal function after 1,000 iterations of the target function. The results from this study are shown in Figure 7-22. For the Case 1 study, the algorithm samples the target distribution in the same manner as the simply MCMC approach previously used for the first 1,000 models. The algorithm then evaluates the success (as a function of acceptance rate) of the algorithm in covering the parameter space for the previous 1,000 models and

adjusts the proposal function accordingly for the subsequent set of 1,000 models. This change in proposal function is obvious in viewing the Case 1 samples. At the 2,000 model mark, the algorithm modifies the proposal function in one more obvious manner and then samples in an efficient manner from the target distribution, as seen in the Case 2 study above.

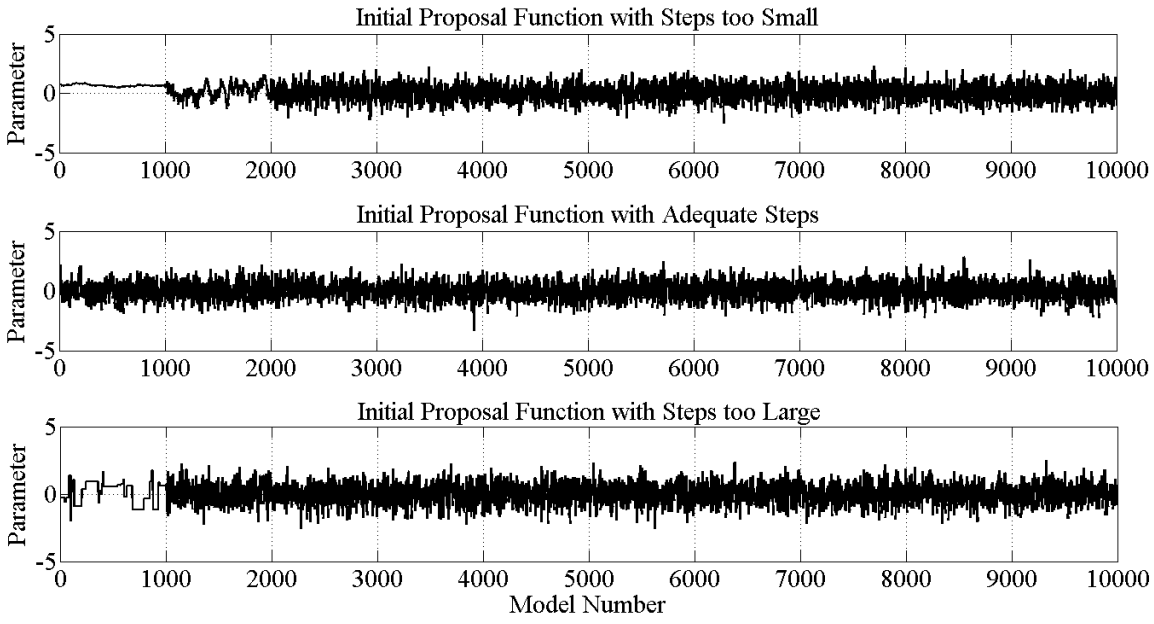

Figure 7-22: Proposal Function Study using DRAM MCMC Algorithm

The case 2 study shows that given an appropriate proposal function, the algorithm will not significantly alter the results. Finally, in viewing the Case 3 study where the proposal function was set with a standard deviation which was too large with respect to the target distribution, it is once again obvious that the DRAM algorithm appropriately modified

the inefficient proposal function into one which better draws samples from the target distribution.

To explore the application of the MCMC method to the MM St-Id approach, the analysis was carried out on Structure 1 of the grid for comparison to the other methods explored in this chapter. The same prior probability distributions used in the MC analysis were also applied to the MCMC analysis. The starting position for the chain was randomly selected from the prior probability distributions. Table 7-4 lists the initial variances of the proposal function for each of the building blocks. For those building blocks with uniform distributions, variances were selected to most efficiently cover the pre-defined range. The variance was defined as the square of half of the total range. In this manner, the MCMC algorithm will be very likely to explore the entire building block space in search of regions with high likelihood. The initial variance for the proposal distribution for the elastic modulus of steel was selected as the same variance as the original prior distribution, since it is well known.

Table 7-4: Initial Variances for Building Blocks

Building Block	Building Block Units	Initial Variance
E	Normalization Constant (*E_0 ksi)	0.06
K_v	Stiffness (kip/in)	5625
K_l	Stiffness (kip/in)	225
K_{r1}	Fixity (%)	0.25
K_{r2}	Fixity (%)	0.25

In MCMC methods, the sampling and weighing of models happens simultaneously, since the proposal of a new model is dependent on the current model. However, this section will focus on the evaluation of the sampling alone, and how burn-in and convergence were determined. The discussion of the subsequent results from this sampling will be discussed in the weighing section. Since the number of models needed for burn-in is not known in an a prior sense, it is advantageous to develop a graphical user interface to monitor the algorithm and sampling scheme to ensure efficiency and to identify errors within the algorithm or settings at an early stage. Such a graphical user interface was developed first for a simple multiple model study on a cantilever beam and then modified for the grid study. The user interface allowed for real time plotting of each building block, and once burn-in was achieved and a satisfactory number of samples were taken thereafter, the analysis could be stopped and the data was processed automatically to display prediction distributions. While this type of interface is not necessary for MCMC analysis, it aided in the efficiency of its application.

As seen in Figure 7-23, the burn-in can be visualized almost uniquely for each building block. The elastic modulus was the first to burn-in, almost immediately, most likely due to the strict prior probability distribution assigned to it. The vertical stiffness building block appears to freely roam the majority of the space between the bounds, but appeared to slightly favored the higher regions. The longitudinal stiffness building block required the most burn-in time out of the five building blocks, and this consisted of roughly 750 models. Both rotational stiffness building blocks required less than 500 models for burn-in, and also seem to tend towards the more rigid connection type. Once again, while it is not the aim of MM St-Id to identify parameters, it is still essential to make sure that they

are reasonable in the validation stage of this research. A burn-in of 750 models was selected for this analysis case, and results presented in the following reflect that selection.

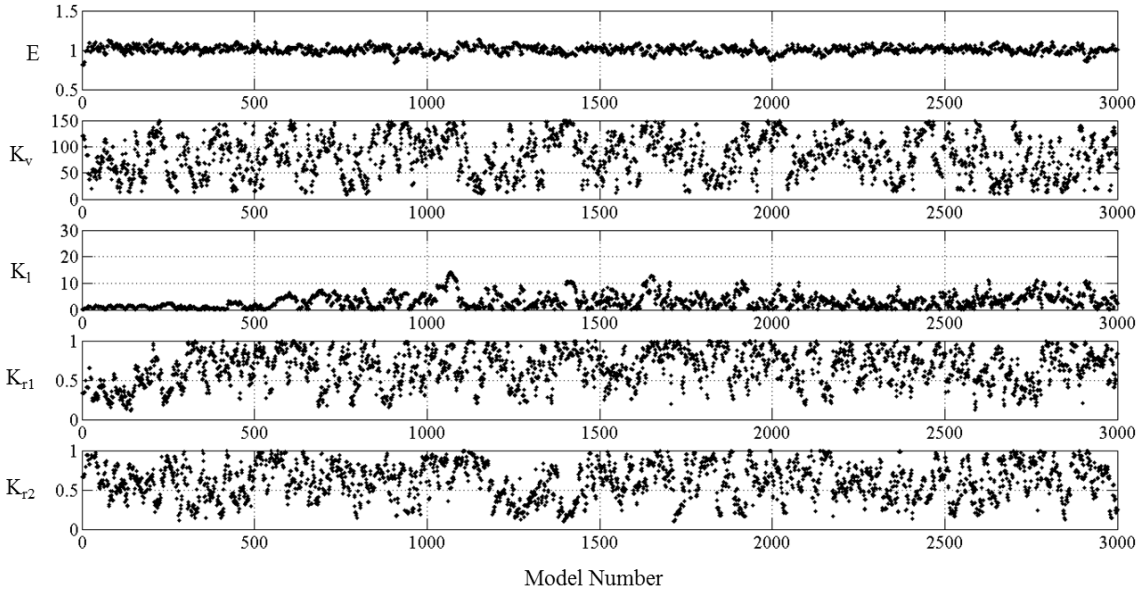

Figure 7-23: MCMC Building Block Sampling

Similar to the other sampling methods previously discussed, a matrix of plots showing how well the sampling scheme covered the building block spaces is shown in Figure 7-24. It is evident in the figure that the entire building block space (defined by the prior distributions) is not associated with appreciable posterior probabilities. The MCMC sampling scheme has efficiently targeted the high likelihood regions, and drew samples in a manner consistent with the target distribution. It is important to mention the appearance of a slight covariance between the elastic modulus of steel building block and

the longitudinal stiffness building block. The covariance is evident in that at lower samples of E, the longitudinal spring is sampled over a more broad range, to account for the reduction in stiffness by the softer elastic modulus. As discussed in Chapter 3, this would present a problem in parameter estimation or tradition St-Id approaches, however in the MM St-Id approach, this covariance is explicitly included and represented within the response predictions as an uncertainty. The next question to address is to determine the number of samples needed, post burn-in, to sufficiently characterize the target distribution.

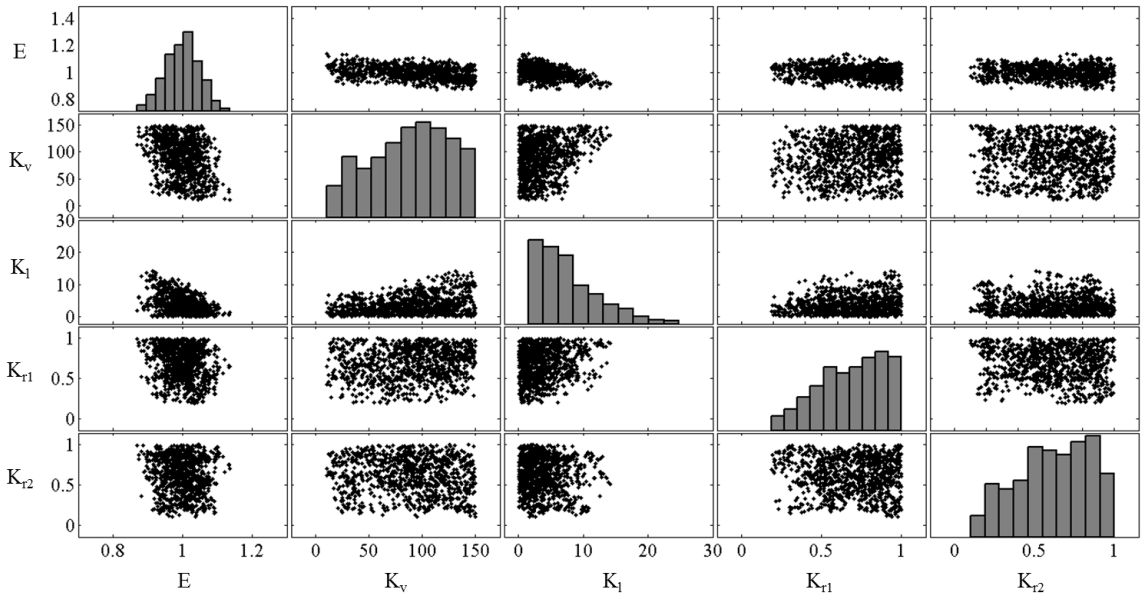

Figure 7-24: Matrix of Plots for MCMC Sampling

To determine the number of models needed, post burn-in, an analysis of the model data set, with the burn-in models removed, was conducted to evaluate the expected value and variance of the distributions as a function of the number of models included in the data set. This method is similar to the one previously described to assess convergence of the MC generated models. When the expected values and variance functions have stabilized, then a sufficient number of models have been drawn. There are multiple diagnostics available for evaluating MCMC convergence, however many have been compared and found to be difficult to implement, and have been shown to fail in detecting convergence even in simple cases (Richardson and Spiegelhalter 1996).

Some convergence diagnostics are specifically used where precise computation of the mean of parameter distributions is critical to the success of the MCMC approach. However, in the case of MM St-Id, the main interest is that the target distribution has been sufficiently characterized regardless if there are still small discrepancies in the mean of the parameters over iterations. For this purpose, and as with the MC convergence analysis, it is assumed that a sufficient number of samples were drawn when the mean and variance of groups of models do not vary by more than 5%. By using the expected value and variance, this approach implies no additional models are needed if they do not influence the expected value or variance of the building blocks.

This analysis was carried out on the MCMC generated model set to determine the appropriate number of samples needed, post burn-in and the results are shown in Figure 7-25 - Figure 7-29. As seen in these building block convergence studies, the total convergence among all building blocks is achieved after 1,300 models have been

generated post burn-in. While it may seem in some cases that the plots of expected value and variance appear to remain "jagged", it is important to take into consideration the scale of the y-axes. If these plots were generated over the entire building block space, then the convergence would be more apparent. However, for this purpose of highlighting the method of determining a convergence point, the scales were generated to best fit the data shown. These models, in addition to the 750 required for burn-in, yield a total of 2,050 models needed for the MCMC analysis of the grid structure and will be used for analysis of the model predictions.

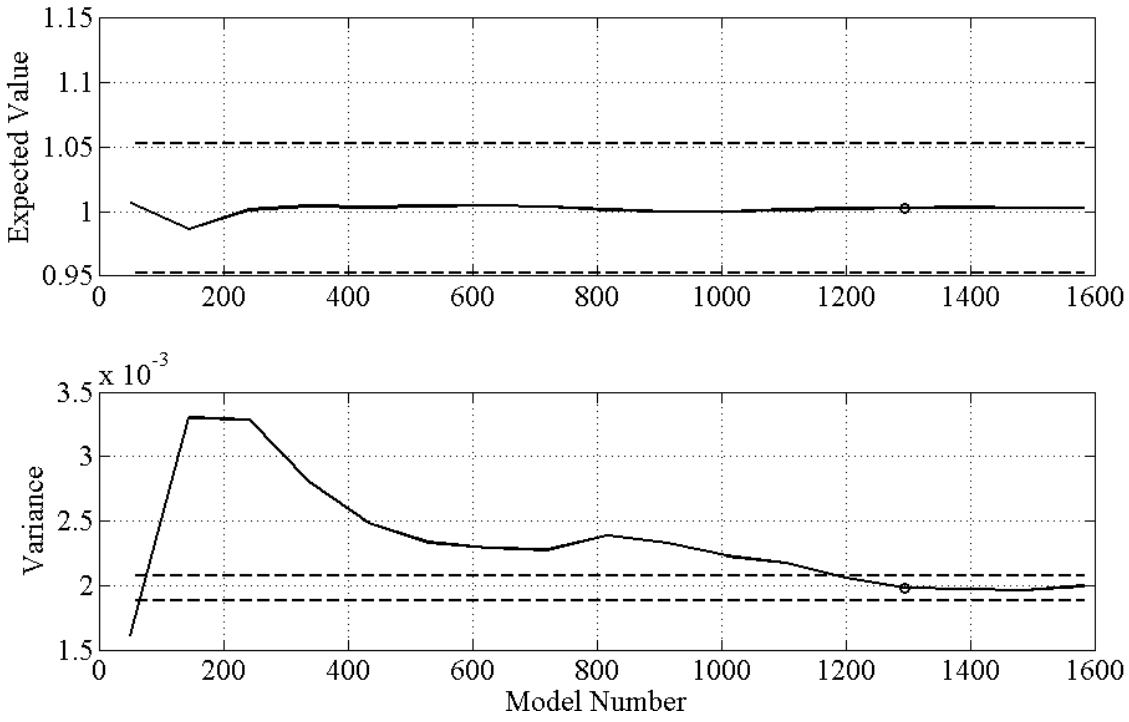

Figure 7-25: Convergence Diagram of the Building Block, E, for the MCMC Analysis of the DI3 Grid

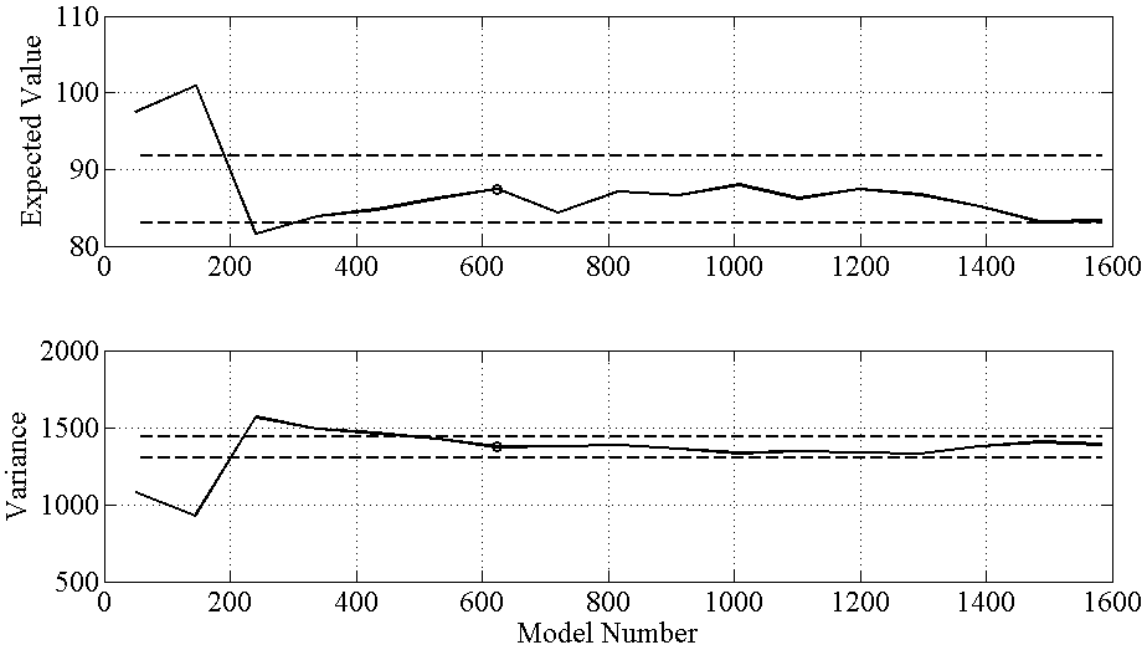

Figure 7-26: Convergence Diagram of the Building Block, K_v, for the MCMC Analysis of the DI3 Grid

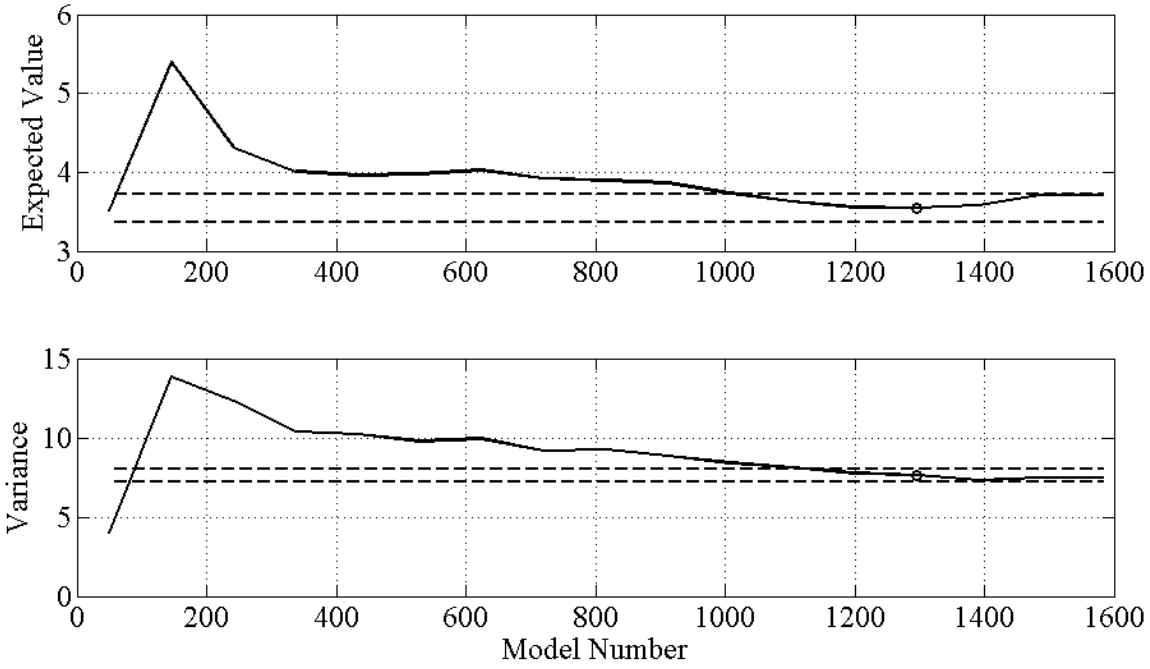

Figure 7-27: Convergence Diagram of the Building Block, K_l, for the MCMC Analysis of the DI3 Grid

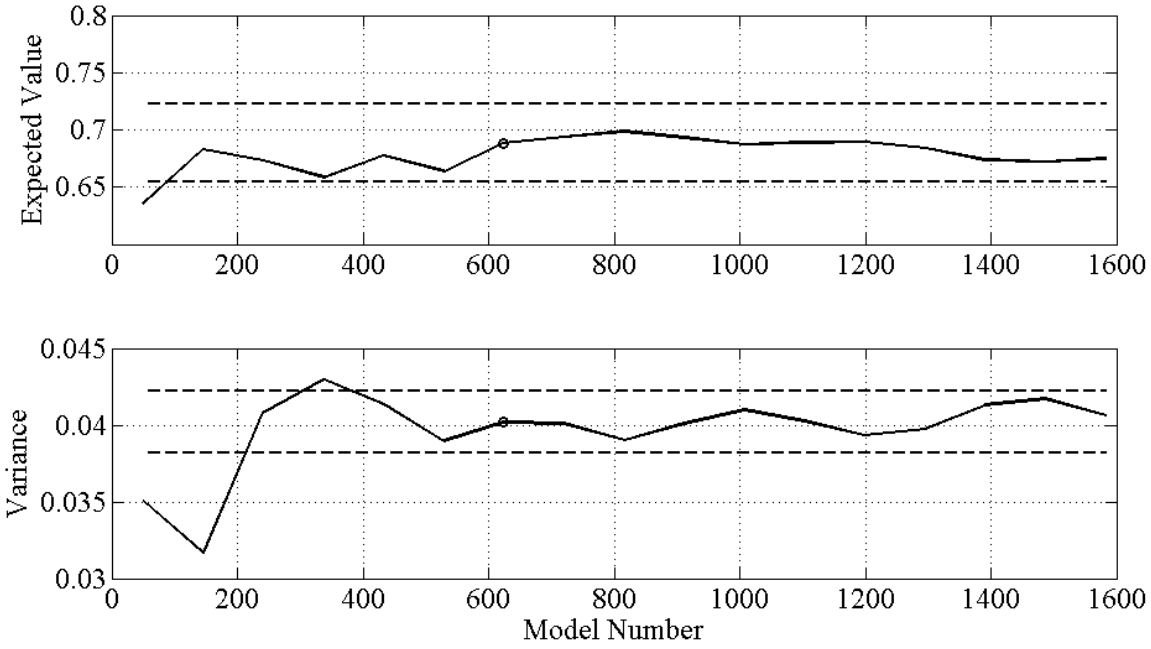

Figure 7-28: Convergence Diagram of the Building Block, K_{r1}, for the MCMC Analysis of the DI3 Grid

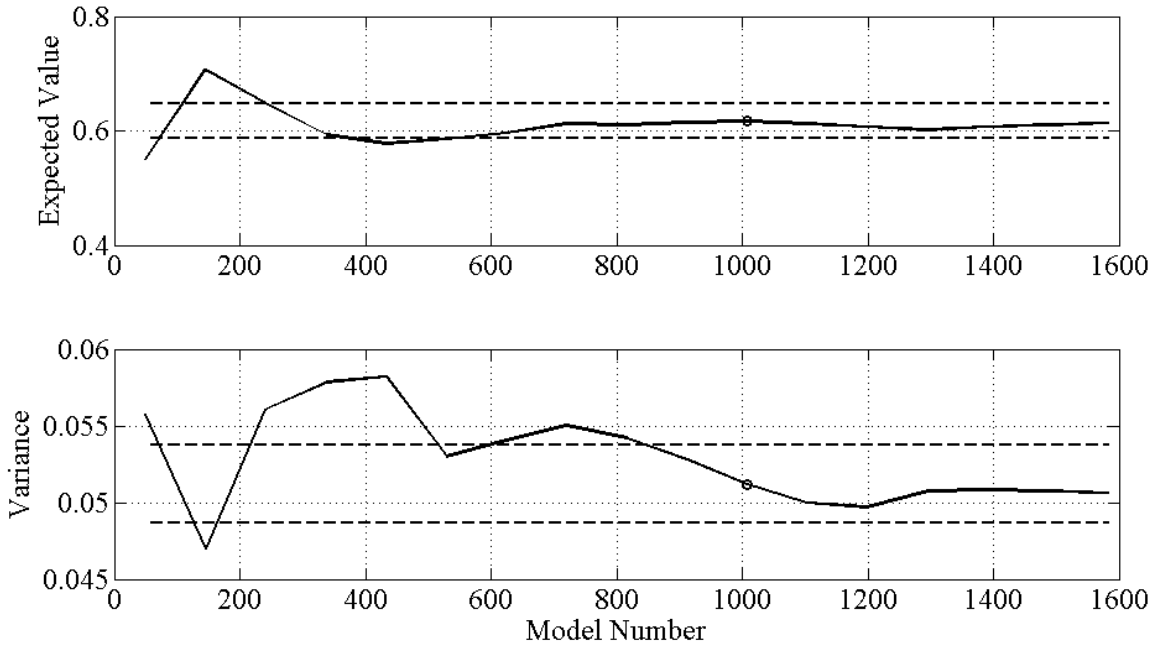

Figure 7-29: Convergence Diagram of the Building Block, K_{r2}, for the MCMC Analysis of the DI3 Grid

7.4.4. Investigation into Selection of Inherent Standard Deviation

To study the effects of the inherent standard deviation on the prediction capabilities of the MM St-Id method, wide array of values was applied as the inherent standard deviation to weigh the models from the Monte Carlo study. This study was used since the weighing process is not included in the sampling strategy, as it is with MCMC approaches. Since the MC studies simply generate candidate models based on prior information, they can be weighed multiple times in different ways, which facilitates an investigative study on the effects of selection of the inherent standard deviation.

To demonstrate the effect of the selection of the inherent standard deviation, an array of values were identified for study as shown in Table 7-5. The values in this table were selected to place the nominal value of 4% based on heuristics into context. To evaluate the effect that different inherent variability has on the results of the probabilistic weighing method, the convergence had to first be verified once again, and then all models were weighed by their respective posterior probabilities.

Table 7-5: Values Used in Study of Selection of Inherent Standard Deviation

Inherent Standard Deviation
0%
1%
2%
3%
4%
8%
12%
16%

The prediction probabilities, as with the marginal probabilities of the building blocks, were represented as cumulative probability distributions thus eliminating the need to compute histograms. Histograms can introduce a misrepresentation of data by being forced to select a bin width, where all models that fall within a particular bin have their posterior probabilities summed. The selection of the bin width and number of bins can seemingly distort the distribution. This is avoided by using the cumulative distribution as a representation since each model's unique contribution to the overall distribution is fully represented in the figure.

The posterior probabilities for each of the models were evaluated using each of the assigned inherent standard deviations to represent the uncertainty associated with the ability of the finite element modeling process to simulate the measured responses, and subsequently weighed by those probabilities. These results are presented in Figure 7-30 - Figure 7-33, and show that the selection of this standard deviation has a significant influence on the weighed results.

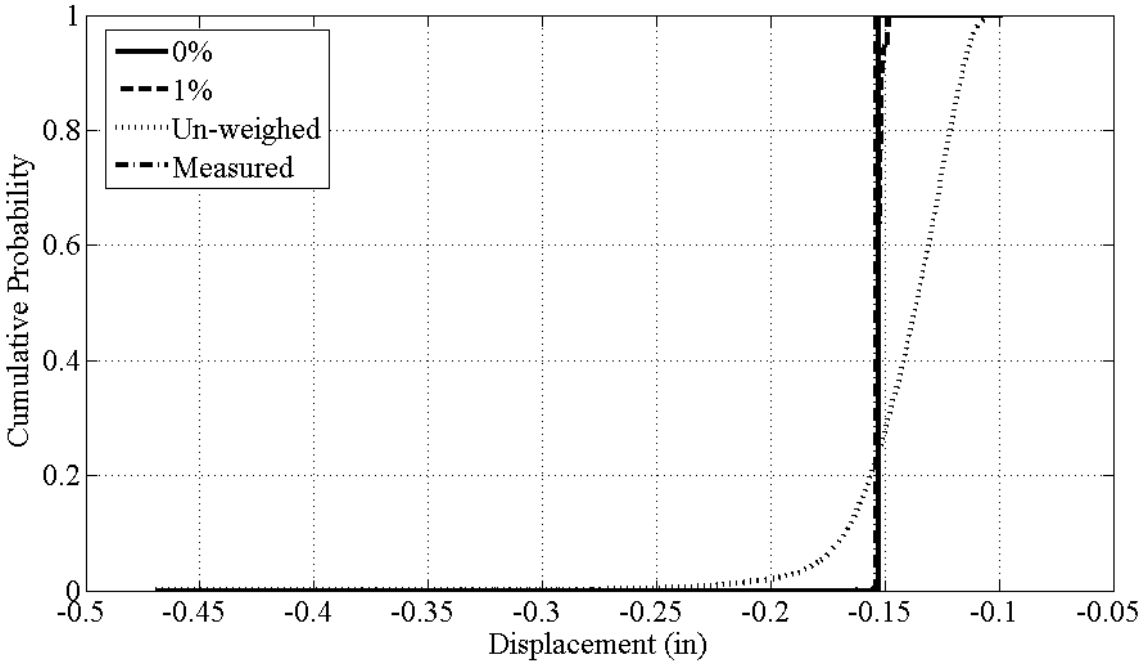

Figure 7-30: Investigation of Inherent Standard Deviation: 0% and 1% Compared Against Un-weighed Models and Observations

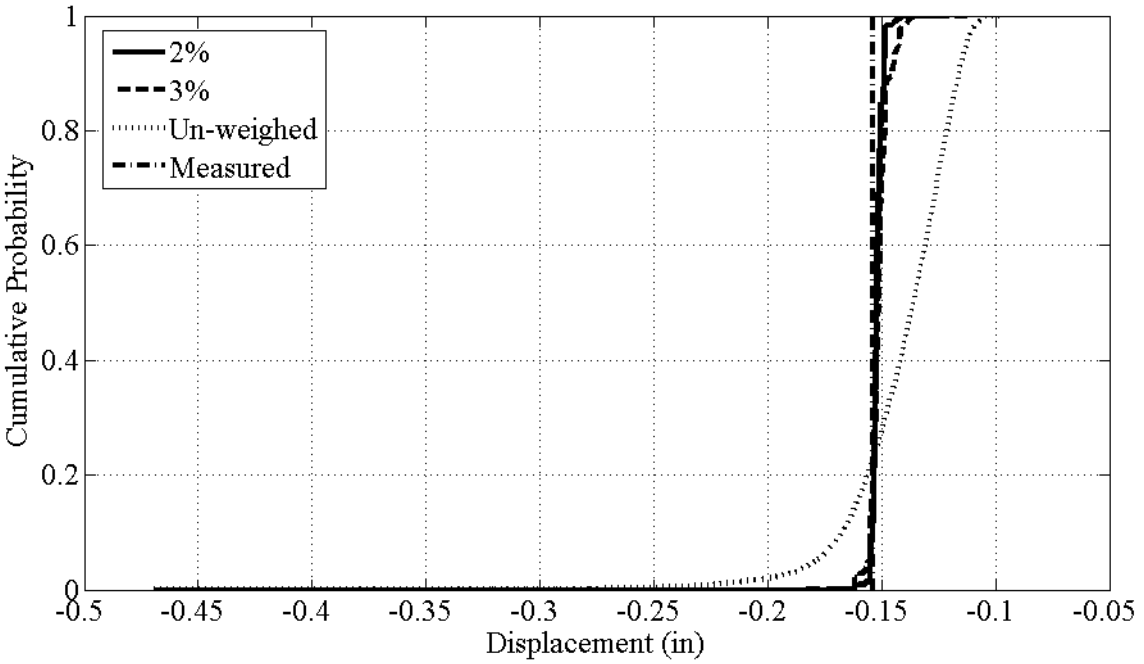

Figure 7-31: Investigation of Inherent Standard Deviation: 2% and 3% Compared Against Un-weighed Models and Observations

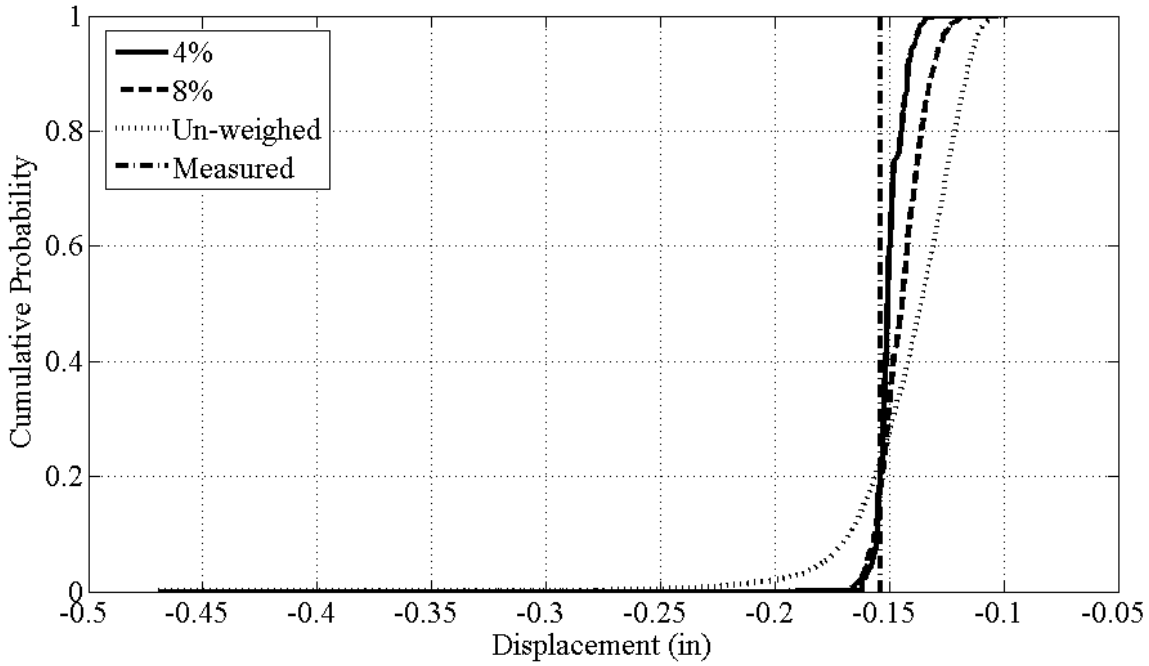

Figure 7-32: Investigation of Inherent Standard Deviation: 4% and 8% Compared Against Un-weighed Models and Observations

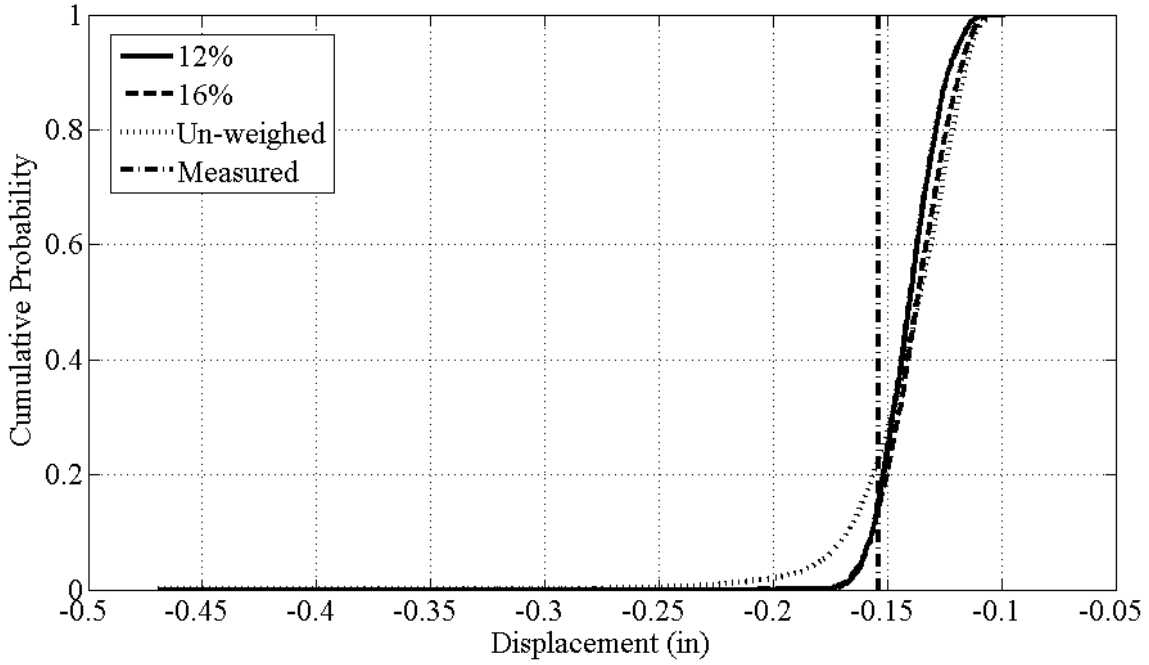

Figure 7-33: Investigation of Inherent Standard Deviation: 12% and 16% Compared Against Un-weighed Models and Observations

In review of the figures above, there is a wide distribution of responses seen. In the cases where the inherent standard deviation is 0% and 1%, the weighing scheme essentially identifies a unique model which contributes to the majority of the cumulative probability function. In the cases where the inherent standard deviation is 2% and 3%, there appears to be slightly more variability in the cumulative distribution, however there is still a very limited number of models contributing to the response.

The cases where the inherent standard deviation is 4% and 8% provide a much wider distribution, especially the 8% case. However, in the 4% case there are no sudden vertical jumps in the cumulative distribution function, which would indicate a small set of unique models contributing to the most likely response prediction. The 8%, 12% and 16% cases all become more variable and smoother as an increased number of models are contributing to the more likely regions of the prediction distribution. Additionally, as this uncertainty is increased, the method loses its ability to discern models from the un-weighed case.

From this investigation, it appears that the 4% identified in literature is an appropriate selection for an inherent standard deviation within a multiple model approach since it is the smallest value which provides a meaningful weighed response prediction, however further study into the selection of an inherent standard deviation is needed. In the case of the higher standard deviations, there is almost no need for experimental observations, let alone multiple model analysis, as the method cannot distinguish between a wide variety of models in any meaningful manner. To highlight this point, a table was constructed which displays the 95% confidence intervals for each of the distributions shown above.

Table 7-6 clearly shows the effects of selecting the inherent standard deviation on the resulting response predictions.

Table 7-6: 95% Confidence Intervals for a Mid-span Load at Node 11

	Displacement Distribution (in)	
	Upper Bound	Lower Bound
0%	-0.1527	-0.1527
1%	-0.1527	-0.1486
2%	-0.1550	-0.1486
3%	-0.1597	-0.1417
4%	-0.1604	-0.1373
8%	-0.1619	-0.1246
12%	-0.1642	-0.1153
16%	-0.1654	-0.1121
Un-weighed	-0.1941	-0.1102

Given the study into the selection of an inherent standard deviation, it is clear that the selection has a significant impact on the subsequent response predictions. In this case, the predictions were able to be compared directly to measured observations, allowing for an appropriate selection for this case. It is important to recognize that the selection of this value is also be dependent on model and structure under analysis as well as the uncertainty that the analyst wants to incorporate into the process. For parameter

identification applications, an inherent standard deviation of 0% may be most appropriate if the analyst wants to identify unique values, but this also loses the benefits of MM St-Id in general.

7.4.5. Probabilistic Predictions

The results of the two probabilistic methods must be treated individually upon examining the models generated. The Monte Carlo method generates models without taking into consideration of how well the models are performing compared to experimental data. However, MCMC methods are generating models with equal weight, since the method depends on the likelihood of each trial model. Thus, MC models must be weighed after sampling is complete and convergence has been satisfied while models generated from the MCMC method all have the same weight once burn-in has been achieved and the target distribution has been converged upon. Therefore, Section 7.4.5 has been divided into two sections to discuss the model predictions: (1) MC Predictions and (2) MCMC Predictions.

7.4.5.1. Monte Carlo Generated Model Predictions

The models generated from the Monte Carlo sampling technique are weighed after all models have been analyzed and convergence criteria have been satisfied. At this point, the response predictions are assembled by creating cumulative distribution functions. Cumulative distribution functions are computed by organizing the response indices of interest in ascending order and plotting the response against the sum of probabilities

associated with the current model and all prior models. In this manner, when all models have been incorporated into the cumulative distribution function the total probability should sum to 1.

Steeply sloped regions indicate regions which have a sharp peak in the probability density function representation, while shallow sloped regions indicate a broad and flat probability density function.

To remain consistent with the investigations into deterministic and threshold MM St-Id methods, the updated probabilities associated with the building blocks will first be shown followed by the prediction of response indices of interest, displacement and strain due to static loading (Figure 7-34).

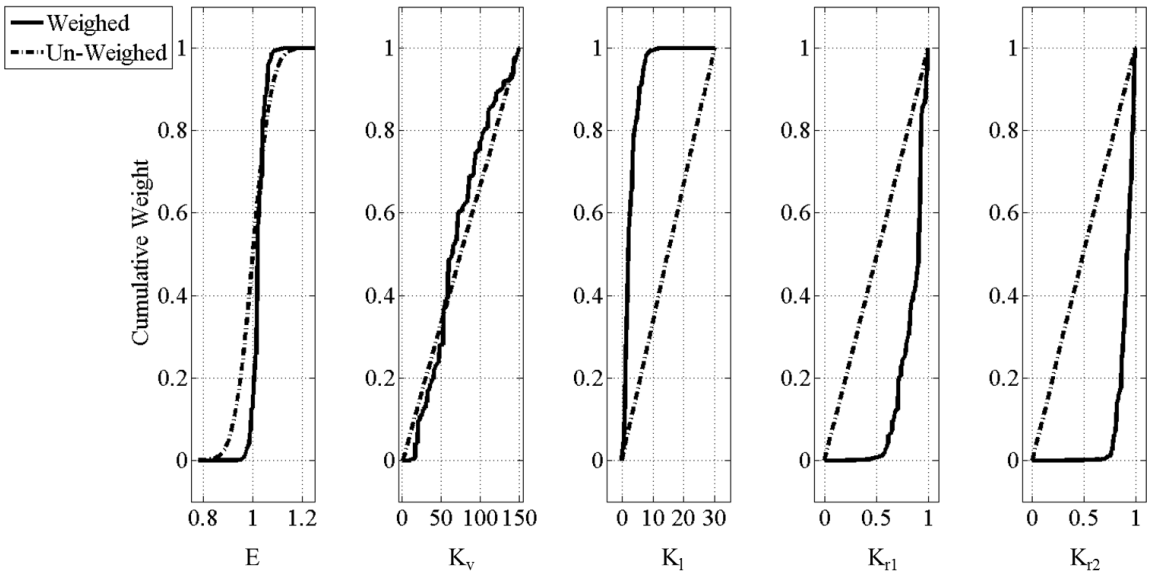

Figure 7-34: Effect of Weighing on Building Blocks for MC Analysis

As seen in the figure above, the probability based model weighing process has refined the un-weighed models to a smaller subset of likely models. The building block corresponding to the elastic modulus of steel was nearly symmetrically concentrated around a nominal value of 1.02 while the building block representing the vertical stiffness at the supports remained a broad distribution. One key difference between the un-weighed building block values and the weighed values is that the lower region of vertical stiffness has zero probability until a sufficient stiffness was reached. This agrees with the sensitivity study in that the higher stiffness values were more likely. Also, the longitudinal springs for the grid structure were most likely near zero but as high as ten kips per inch. Additionally, both stiffness connection factors tended toward the stiffest continuity condition.

The model predictions were weighed in a similar manner, and are presented in Figure 7-35. The one difference in producing model predictions for probabilistic methods is that the inherent standard deviation associated with the ability of the FE model to represent the physical structure must be taken into consideration again. Since this standard deviation was incorporated in the model's ability to match natural frequency and mode shape observations, it must also be used to represent the uncertainty in matching any independent predictions, as was done with the threshold method previously.

To incorporate the inherent standard deviation into the response predictions, the desired response from each model was resampled. The resampling was carried out by setting the model's response prediction as the mean of a normal distribution with a 4% standard deviation. This distribution was then sampled 1,000 times so that it was sufficiently

characterized. This created a vector of 9,750,000 values (1,000 samples for each of the 9,750 models) which were then used to generate the cumulative distribution functions shown in Figure 7-35. To properly account for the probability of each of the resampled models, the probabilities computed for the 9,750 models were divided by 1,000 and assigned to the corresponding resampled values. Thus, the probability was ensured to still sum to 1.0.

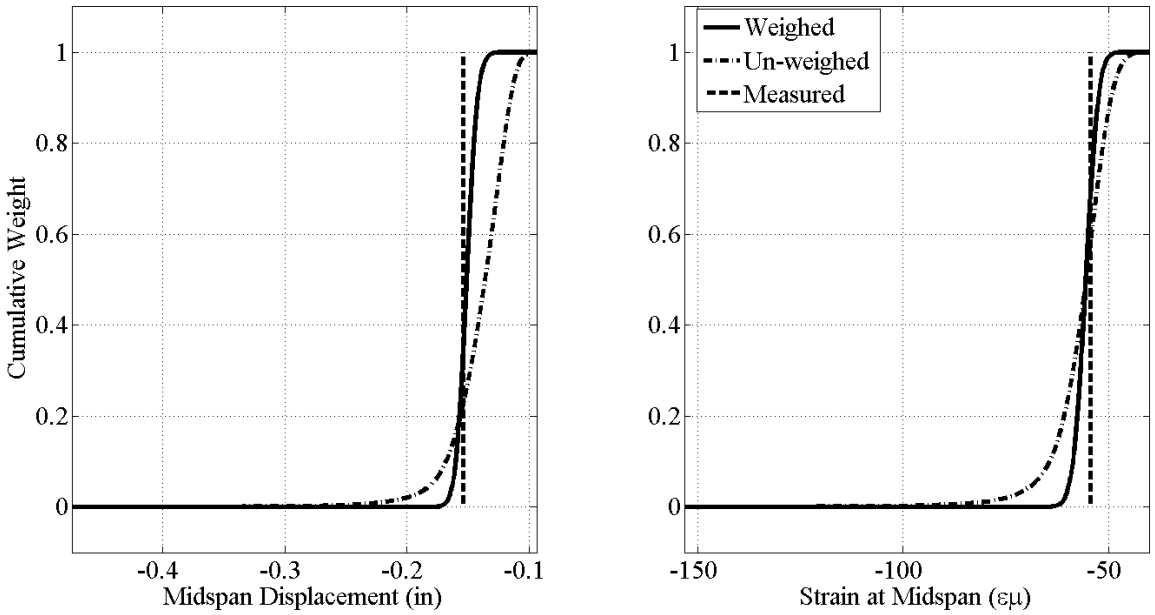

Figure 7-35: Model Response Predictions for MC Method

The results are meaningful in two regards: (1) the model space has been significantly reduced and (2) the weighed models appear to have accounted for both the observed displacement and observed strain due to a mid-span load of 100 lbs. This is an encouraging result, since being able to characterize both strains and displacements of a structure within a single model is a difficult task. However, it is fairly obvious that there are many models generated within this method which are generating predictions that are very unlikely, given the observed data (frequencies and modeshapes). The un-weighed strain predictions have over a 100 micro-strain range and displacements have a range of almost 0.4 inches. It is evident that while the method seems to have generated meaningful response distributions, there are many wasted models which do not provide meaningful information. In addition to understanding that many wasted models were generated, it is also important to note that 9,750 models were required for this analysis when comparing to the MCMC approach.

7.4.5.2. Markov Chain Monte Carlo Generated Model Predictions

As mentioned in the beginning of section 7.3.4, the models generated from the MCMC method are inherently of equal weight after the algorithm has converged and is generating models from the target distribution. Given the conclusion at the end of section 7.3.4.1 that the MC method, while able to produce weighed models which meaningfully represent the physical structure, two main disadvantages of the approach were the wasted samples in regions of low or near zero likelihood and the number of samples needed to converge to a stable analysis.

The MCMC method has already been shown to require fewer than one fourth of the models needed by the MC approach. However, the quality of the predicted responses and the updated distributions associated with the model building blocks has not been demonstrated and will be discussed within this section.

To generate the cumulative density functions for each of the model building blocks and for the model predictions, the 1,300 models generated post burn-in were first assigned equal weight, normalized so that the sum of the weights was equal to one, to be consistent with probability theory (assuming a that the model population represented the entire model space). Each of the responses and building blocks of each model were then plotted against the cumulative weight for review as shown in Figure 7-36. The plots representing the un-weighed models are simply a plot of the prior probability distribution assigned to each building block.

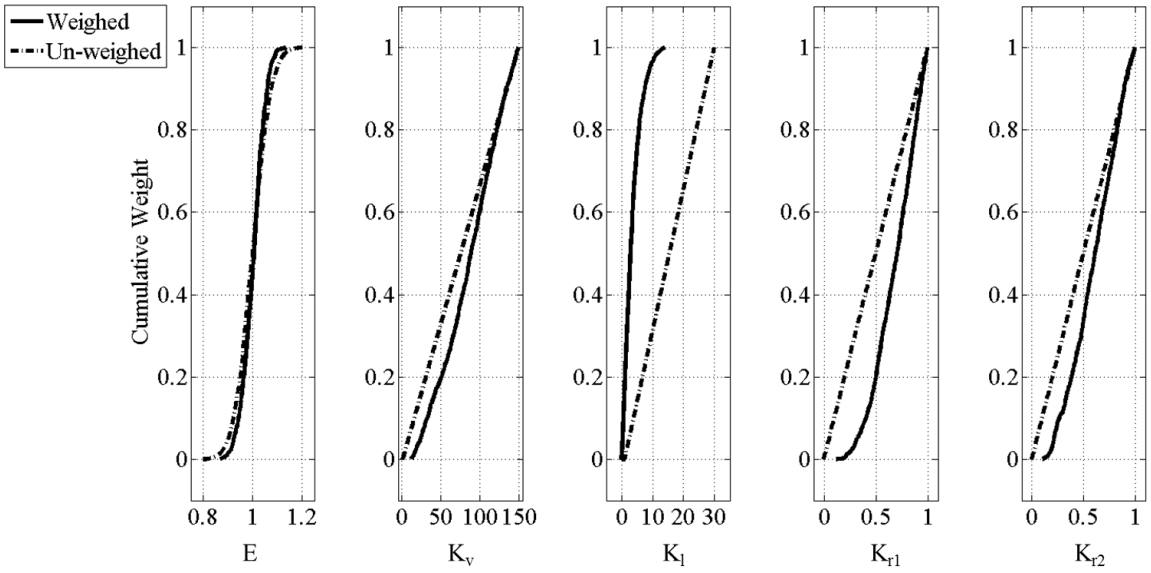

Figure 7-36: Effect of Weighing on Building Blocks for MCMC Analysis

The effects of weighing the building blocks from the MCMC method were consistent with the other approaches investigated. The building block representing the elastic modulus of steel was updated to reflect a smaller variance than assumed with the prior distribution but it was still centered at 1.0. The vertical stiffness building block was not even sampled at low values (0 – 6 kip/in), but there was a broad range of samples among the higher values. The longitudinal stiffness was also only sampled below 12 kip/in, and most of those samples were drawn near a value of 0 kip/in. Finally, the distributions for each of the two connection stiffness factors tended toward the continuous continuity condition over a relatively broad region (0.5, 1). One note to make from the building block figures is that there were very little samples in low probability regions, thus providing a better characterized posterior distribution than seen in the MC analysis.

The distributions associated with the model predictions were generated for the same displacement and strain measurements as has been presented for all cases thus far, the mid-span displacement and strain due to a mid-span load of 100 lbs. As with the MC approach, the inherent standard deviation of the finite element process must be taken into consideration with respect to the model predictions of displacement and strain (or any unobservable measurement chosen). Unlike the MC approach, each model can be resampled to reflect the 4% uncertainty. This is done by sampling the prediction made from each model one thousand times using a Monte Carlo sampling scheme. Since each model generated from the MCMC analysis is originally equally likely, each of the simulated measurements is equally likely. The cumulative distribution function of this resampled measurement data is then constructed. As seen in Figure 7-37, the MM St-Id method was once again able to account for the prediction of both strain and displacement measurements. The MCMC models do not have an "un-weighed" counterpart, since each model is inherently weighed so it is not shown in Figure 7-37.

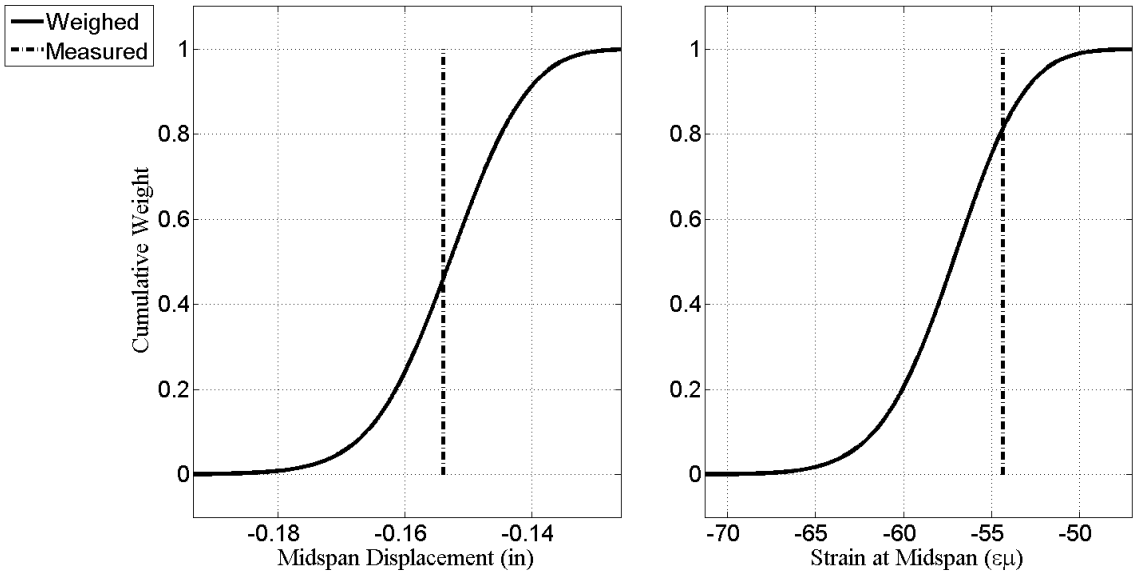

Figure 7-37: Model Response Predictions for MCMC Method

7.5. Cross-comparison of Approaches

To highlight the differences among the three main approaches described in this chapter, two special cases are considered where specific weaknesses of deterministic and threshold approaches are addressed by incorporating probabilistic techniques. These exercises demonstrate the strengths of probabilistic techniques when applied to other methods that have shortcomings. While probabilistic techniques may enhance the other two methods, there is still a clear choice made as to which method in particular should be used within the MM St-Id framework.

7.5.1. Deterministic Sampling with Probabilistic Weighing

One of the main weaknesses of deterministic sampling is its inability to effectively weigh models without developing a unique and potentially complicated algorithm for each case. To highlight the inability of the deterministic approach in effectively weighing models, the same population of models generated by the deterministic sampling scheme was weighed using probabilistic techniques. The results of this combination of deterministic sampling and probabilistic weighing are shown in Figure 7-38 - Figure 7-39.

By examining the comparison of the deterministic and probabilistic weighing strategies on the deterministic model set, it is clear that the probabilistic weighing is less prone to the influence of a single model matching observations very well. Also, it appears that the probabilistic method, because it accounts for probabilities of parameters which we know information about, is able to better characterize the building blocks after the weighing process. Where it appears that that deterministic weighing identified two models out of over 59,000 that had significant influence, the probabilistic weighing allowed more models to contribute to the updated information about the building block likelihoods.

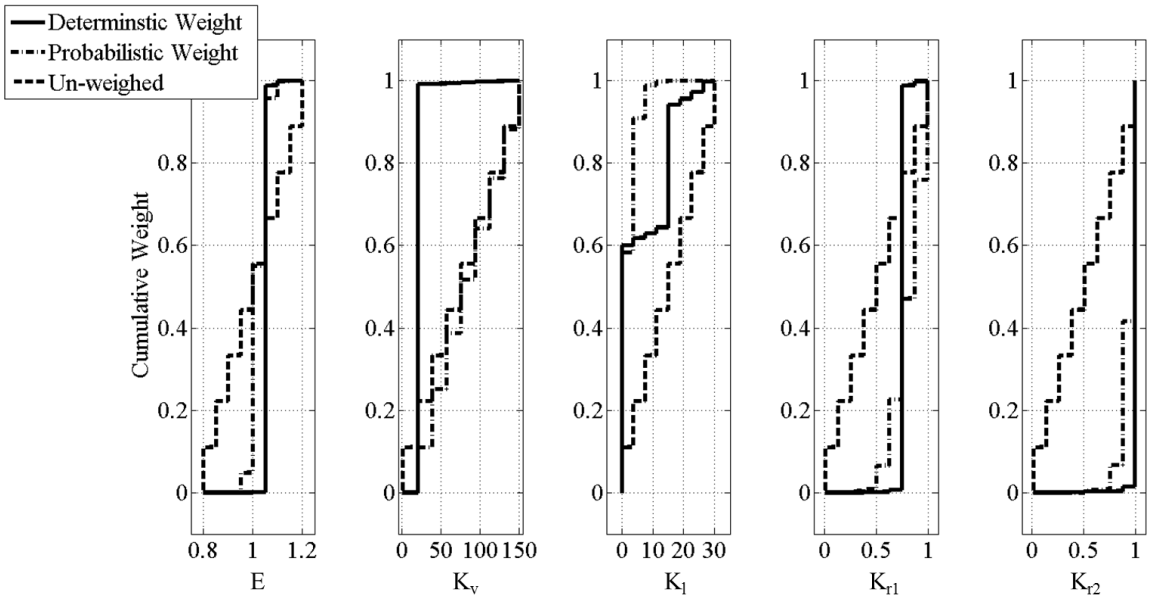

Figure 7-38: Comparison of Deterministic and Probabilistic Weighing on Building Blocks

In examining the comparison of the predictions (Figure 7-39), the ability of probabilistic weighing to allow for many models to contribute to a meaningful prediction response is evident. Where deterministic weighing clearly identified two models that contributed to most of the response, the probabilistic weighing allowed for a more defined cumulative distribution function.

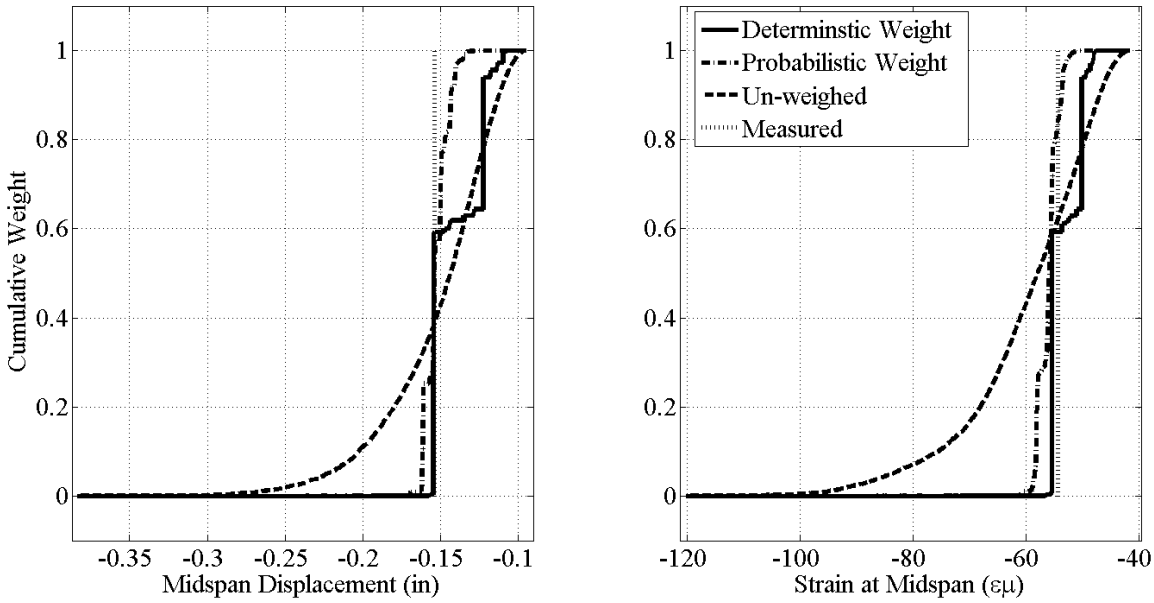

Figure 7-39: Comparison of Deterministic and Probabilistic Weighing on Model Predictions

7.5.2. MCMC Sampling with Threshold Weighing

One of the two main drawbacks identified with the threshold approach is the inefficient sampling of models. Since the Latin Hypercube Sampling method is a modification and improvement on the random Monte Carlo sampling technique, it has been greatly discussed that these approaches are inefficient in producing meaningful results and won't be discussed further.

However, one problem unique to the threshold approach encountered as a direct result of the sampling and weighing combination was the possibility of not accepting any models. It was claimed that the sampling technique, in combination with the rather harsh weighing approach, was primarily at fault since it was not producing enough models with

high enough likelihood to pass the threshold criteria. Specifically this could happen if the regions of high likelihood are not broad and are not obvious from the sensitivity studies.

Moreover, if it is observed that no models have passed the threshold then the uncertainty has to be adjusted to redefine the threshold bounds, or the sampling has to be redone. The former remedy is not entirely defendable, since meticulous efforts went into defining the uncertainties in the first place and if they are artificially increased then one might wonder what the point of the fine-tuned calculations were.

This investigation was carried out to see if indeed the number of accepted models increased as a result of using a more efficient sampling algorithm, such as the Markov Chain Monte Carlo approach. The models generated with the MCMC algorithm were weighed using the criteria developed for the original threshold approach. Then the results are re-weighed with the artificially increased threshold bounds for comparison. The results of this study are summarized in Table 7-7.

To remain consistent with the threshold weighing approach, models were generated with the MCMC method using an inherent standard deviation of 5%. Also, an inherent standard deviation of 8% was used to remain consistent with the increase in uncertainty thresholds studied in Section 7.3. The study shows that with an improved sampling scheme, the threshold method will accept more models, and make the analysis more worthwhile. By keeping the inherent standard deviation at 5%, as done previously with the threshold approach, six more models were accepted based on the same criteria defined under the threshold approach. Similarly, roughly nine times more models were

accepted when using the MCMC sampling with a larger inherent standard deviation representing uncertainty of the finite element modeling approach.

Table 7-7: Comparison of Sampling Schemes for Threshold Weighing

Sampling Scheme	Weighing Scheme	Number of Models	Inherent St. Dev. (%)	Accepted Models	% Accepted
Threshold	Threshold	1000	5	1	0.1%
Probabilistic	Threshold	1000	5	7	0.7%
Threshold	Threshold	1000	8	11	1.1%
Probabilistic	Threshold	1000	8	91	9.1%

7.6. Conclusions and Recommendations

A thorough investigation into three identified approaches to MM St-Id were carried out and presented in this chapter. To summarize and conclude the work, the three methods will be compared to highlight the key differences among them. Also, a brief discussion on the comparison of model execution efficiency is presented and finally a set of recommendations is laid out for various scenarios in which one might apply the MM St-Id.

7.6.1. Comparison of the Three Methods

In summary of the three methods outlined in this chapter, there are clear conclusions to be made. As previously mentioned, the deterministic approach effectively covers the model space in a grid pattern, however the number of model executions required obtaining this sampling is exponential with respect to the number of parameters desired. For complex structural systems, there will be many more than five parameters, and then analysis time will be much longer than that required for the DI3 grid. The coarse nature of the sampling approach, and more importantly the inability to foresee where regions of acceptable models may exist in the model space, are the primary downfalls of the approach. Both of these points highlight the ineffectiveness of a deterministic approach within the MM St-Id framework. However, there are other potential applications where a deterministic approach would be beneficial, and those will be discussed in the next section.

The threshold approach has potential weaknesses in two major areas: (1) the computation of uncertainty and (2) a defined acceptance / rejection boundary. It has been apparent in this chapter that the computations of the uncertainties which directly influence the threshold bounds have an enormous impact on the results of the analysis. It was noticed during the development of the method that much time was spent computing uncertainties associated with measurement noise and repeatability yet those contributed to only a fraction of a percent of the threshold bounds. The major contributor to the threshold bounds was the inherent uncertainty associated with the finite element process, which is a number selected by an experience user representing the uncertainty with the finite element process.

Secondly, the threshold method might be considered too strict in its weighing methods. Since there is a defined threshold through which candidate models must pass, a question must be asked: *What is the difference in the models where one passes a 5% threshold at 4.99% and one which is rejected at 5.01%?* This strict threshold also is evident in the fact that only one model was accepted out of a 1,000 model set. And due to the sampling scheme followed in this investigation, an entire separate model set must be generated and cannot be added to previous model sets in the event that no models pass the initial threshold criteria.

Finally, the probabilistic approach to the MM St-Id framework provided some continuity where there were inadequacies identified in the deterministic and threshold methods. The effectiveness of the probabilistic weighing was proven with the Monte Carlo generated model set, however the number of models needed to achieve satisfactory convergence was not ideal. Additionally, many of these models were not used towards the response predictions because they had such low posterior probabilities. A more efficient sampling method, Markov Chain Monte Carlo, was applied to the MM St-Id process in an attempt to achieve both a better picture of the posterior probability surface of the model space and to achieve this in a much smaller model set.

The MCMC sampling and weighing implementation confirmed what has been already confirmed in many other fields of science, that it is more efficient and produces higher quality results. The method is able to account for uncertainties (as does the MC method), in this case corresponding to measurement repeatability and an inherent uncertainty associated with the finite element process, in a manner that does not have a firm rejection

boundary. Instead, it is the aim of MCMC methods to always, over the long run, randomly accept models which are much inferior to those with high likelihoods. This leads to a better characterization of the posterior probability distribution. Where the threshold approach has a solid line defining it's boundary for acceptance, the MCMC approach has a weighted boundary as its acceptance criteria which accepts models according to a ratio of overall likelihood.

In examining the efficiency of each of the methods, Table 7-8 highlights the major effects of selecting each method. The deterministic approach required a vast number of models and analysis time, but fell short in its ability to effectively sample within regions that have low errors (primarily due to our lack of prior knowledge in defining the sampling areas). Now, of course one could have taken the results of this large study and changed the boundaries of building blocks, but this would then require another analysis, of equal analysis time or more. Also, the weighing applications investigated tended to either select a single small region of models or prove unable to distinguish between models.

The threshold approach, after revising the uncertainty so that models would be accepted, only accepted 1.33% of the models analyzed. Even after increasing the uncertainty so that models could be accepted, the results were unable to provide meaningful results since such high uncertainties were incorporated in the prediction of displacements and strains.

The Monte Carlo probabilistic approach utilized all of its 9,750 models; however the inefficiency of the sampling left more to be desired considering that a majority of those models contributed to near zero probability regions of the posterior probability function. The MCMC approach to the probabilistic method proved itself to be much more efficient

than the threshold method in terms of how many models used out of total models required. Additionally, the MCMC approach was able to produce meaningful prediction distributions which lend themselves directly to interpretation and prediction purposes.

Table 7-8: Comparison of the Efficiency of Each Method

Approach	Models Required	Models Used	Analysis Time (hrs)
Deterministic	59,049	59,049	98.4
Threshold	3,000	40*	5.0
Probabilistic - MC	9,750	9,750	16.3
Probabilistic - MCMC	2,050	1,250	3.4

* With increased uncertainty applied

7.6.2. Recommendations

To conclude Chapter 7, a set of recommendations will be discussed.

- The deterministic sampling approach, while inefficient for prediction purposes, could lend itself to experimental design applications where any observations are not yet known. Given a set of model building blocks, distributions of response indices of interest could be generated for instrumentation design as well as for verification of measurements during the test.

- The threshold approach could be beneficial for model analyses of preliminary experimental data, where limited observations are made. A cursory examination of model building blocks given a small set of observations lends itself to the threshold approach because the results could be used to both verify the selection of model building blocks as well as determine the effectiveness of the observations to inform the MM St-Id method in predicting unobservable responses. However, once many observations are incorporated into the process it is very likely that no models will meet the criteria laid out by the method, at which point the analyst will not be able to infer meaningful conclusions from the test.
- The probabilistic approach, specifically with MCMC sampling, should be used when a full set of observations has been made and model building blocks have been verified with sensitivity studies. Also, in applications where a well-defined distribution of unobservable responses is desired the probabilistic approach should be used.

CHAPTER 8: FURTHER DEVELOPMENT AND VALIDATION OF PROBABILITY-BASED MM ST-ID

This chapter presents an investigation into the effect that system complexity, limitations in measurements and types of measurements have on the MM St-Id approach. In addition, this study aimed to identify how to most effectively leverage the method to provide relevant predictions with respect to the observations used. This chapter is organized into four main sections: (1) Investigation into Increased Structural Complexity, (2) Investigation into Measurement Quantity, (3) Investigation into Selection of Observations, and (4) Investigation into Weighing Observations Based on the Desired Prediction.

8.1. Investigation into Increased Structural Complexity

The methods explored and developed in Chapter 7 utilized the grid structure in its Structure 1 configuration; as explained in Chapter 4, this includes steel pins and fully fixed connections. This ideal configuration was selected to aid in identifying a strategy which could provide meaningful and accurate results the most efficiently. However, the next step in the validation of the approach would be to subject a more complex structure, in terms of boundary and continuity conditions, to the approach and determine whether the approach is still as strong as it was found to be in Chapter 7.

To accomplish this, the third structural configuration of the grid structure, with neoprene pins and rigid connections, was used as the specimen for a multiple model study. The modeshapes obtained from this configuration implied that there was significant

movement of the boundaries during the test. Also, a limited quantity of five observations was made. While measurement quantity will be investigated in Section 8.2, in this case it added to the complexity of the grid structure in that less information was obtained as a function of the neoprene pins.

For consistency, the same a priori model and building blocks examined in Chapter 7 were used for this study (Steps 1 through 3). For details on the experimental testing and data collection, Step 4, the reader is directed to Chapter 6. Section 8.1.1 discusses Step 5, the sampling and weighing of model building blocks and Section 8.1.2 discusses Step 6, the generation of response predictions from the weighed models. Section 8.1.3 provides a discussion of the results.

8.1.1. Sampling and Weighing of Structure 3

As identified in Chapter 7, the most efficient sampling method within the probabilistic approach is the MCMC approach. Specifically, the algorithm utilizing the Delayed Rejection Adaptive Metropolis technique was used for this analysis. The five model building blocks representing material properties (elastic modulus of steel), boundary conditions (vertical and longitudinal spring stiffness at boundaries), and continuity conditions (connection fixity) utilized in Chapter 7 were also utilized for this study of a more complex configuration of the grid.

Table 8-1 details the bounds placed on the five model building blocks. The sensitivity studies shown in Chapter 5 indicate that the objective function for the Structure 3 configuration was most sensitive to vertical stiffness over the range of 0 to 30 kip/in. The bounds used for the Structure 1 configuration were 0 kip/in and 150 kip/in. The decrease

in the upper bound on vertical stiffness is expected, as the neoprene pin provides a softer support than the steel pins and as such the larger stiffness values cause the model to diverge from the measured responses. Otherwise, the remaining sensitivity studies indicated that the bounds for the four additional building blocks should remain the same as used in Chapter 7 and are listed in Table 8-1.

Table 8-1: Model Building Block Bounds for Structure 3 Study

Building Block	Lower Bound	Upper Bound	Distribution
E	0 E_o	2 E_o	N (1, 0.06)
K_v	0 kip/in	30 kip/in	U (0, 30)
K_l	0 kip/in	30 kip/in	U (0, 30)
K_{r1}	0	100%	U (0, 1)
K_{r2}	0	100%	U (0, 1)

Table 8-1 also details the prior probability distribution assigned to each of the model building blocks. The elastic modulus of steel was assigned a normal distribution with a nominal mean and standard deviation of 0.06. The remaining building blocks were assigned uniform distributions over their lower and upper bounds for priori probabilities. This is again consistent with the prior probability distributions used in Chapter 7.

To initialize the MCMC algorithm to sample the model building blocks, starting values were randomly acquired in a Monte Carlo fashion from their prior probability

distributions. The analysis was then set to run and monitored until convergence was achieved.

8.1.1.1. MCMC Convergence for Structure 3 Analysis

Chain convergence was first evaluated by visually inspecting the chain (Figure 8-1). It is apparent that the building blocks sampled converged to a stable pattern after 3,500 models. It is quite obvious that the sampling algorithm had a high rejection rate in the first 3,000 models and that four of the five building blocks had poor starting positions. This is apparent from the amount of movement from the initial samples, chosen randomly from the prior distributions. However, after the burn-in the samples stabilized in terms of both mean and variance.

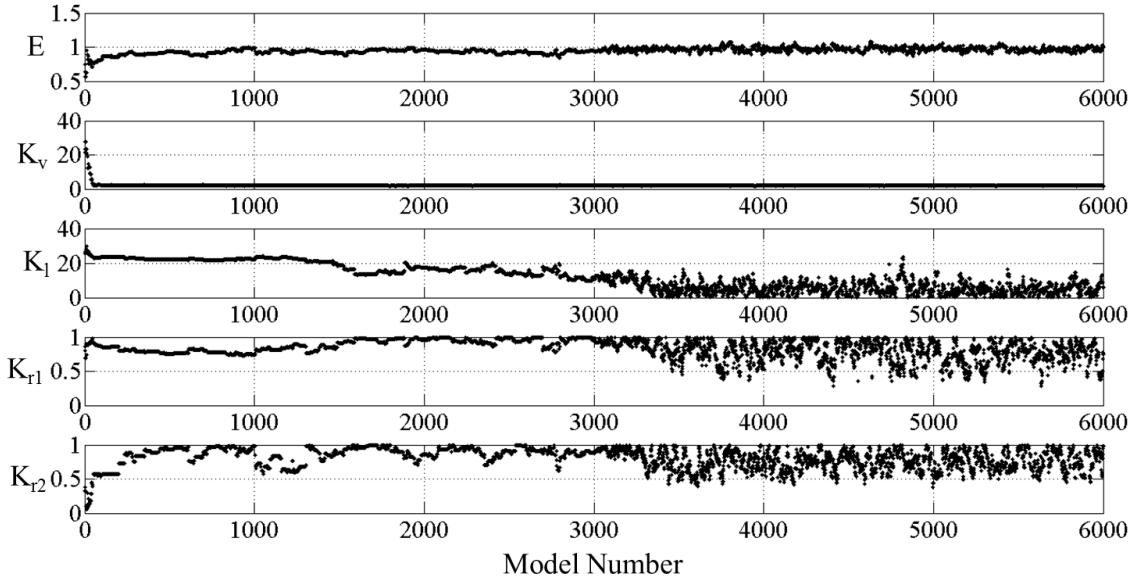

Figure 8-1: Visual Presentation of Chain Time History

After visually confirming the chain had converged to its target distribution, the chain was then visualized in a matrix of plots to inspect the distributions of each parameter as well as to examine the relationship between the building blocks. Also, the chain was analyzed to determine computationally how many models were needed beyond the 3,500 model burn-in period by computing the expected value and variance of the chain as a function of number of models (Figure 8-3 - Figure 8-7).

The histograms in the matrix of plots indicate that the vertical stiffness is fairly normally distributed about a mean of roughly 2.1 kip/in, while the longitudinal stiffness appears to be lognormal distributed. Both connection stiffnesses tended towards a rigid connection type, remaining consistent with the analyses performed on Structure 1.

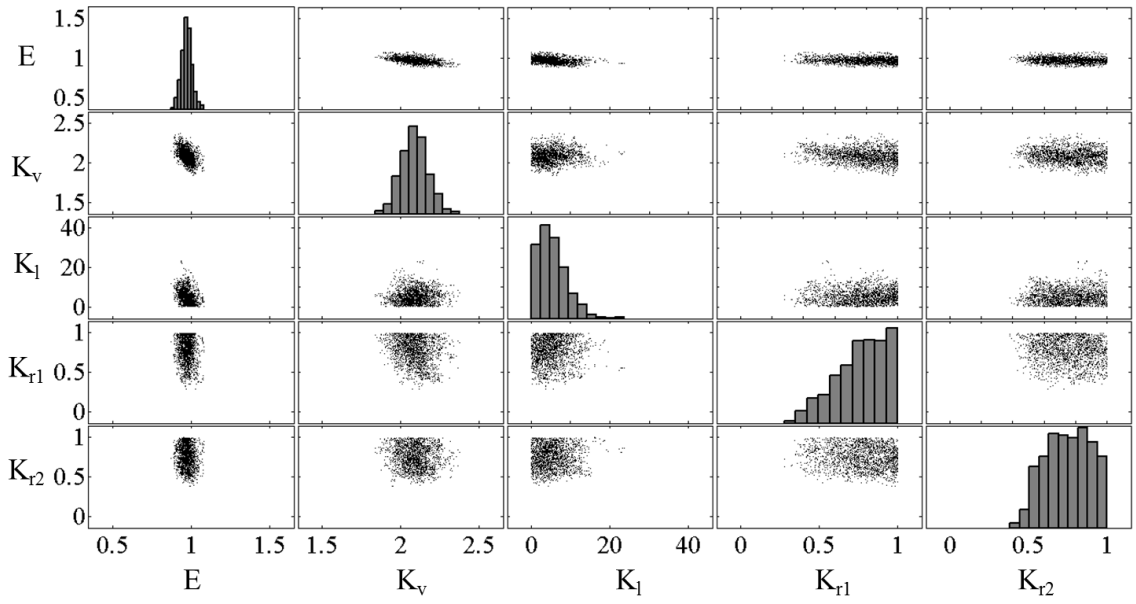

Figure 8-2: Matrix of Plots for Structure 3 MCMC Analysis

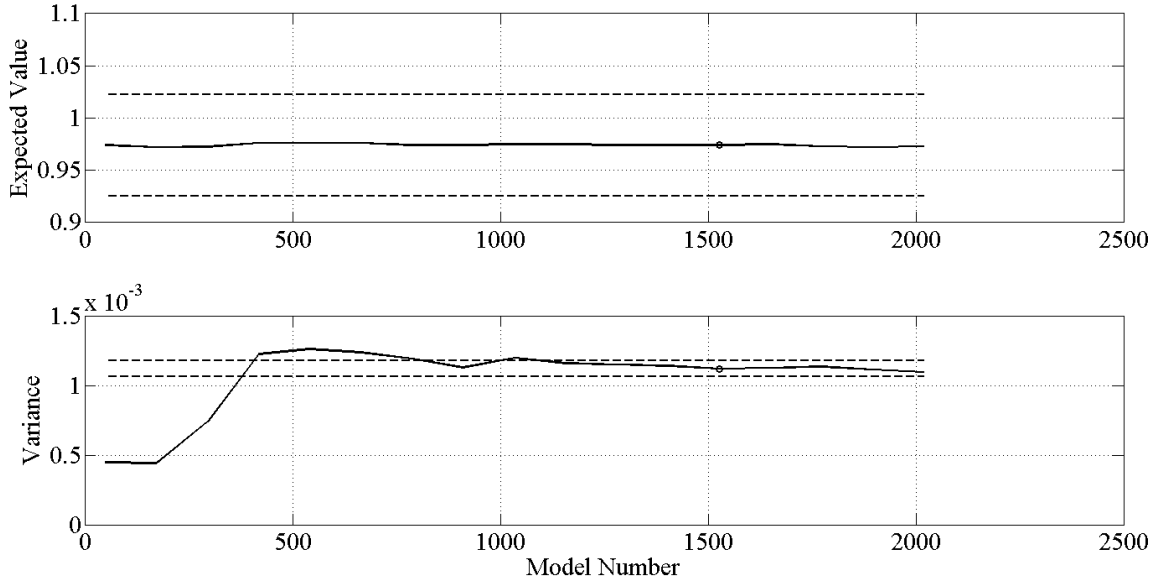

Figure 8-3: Convergence Diagram for E

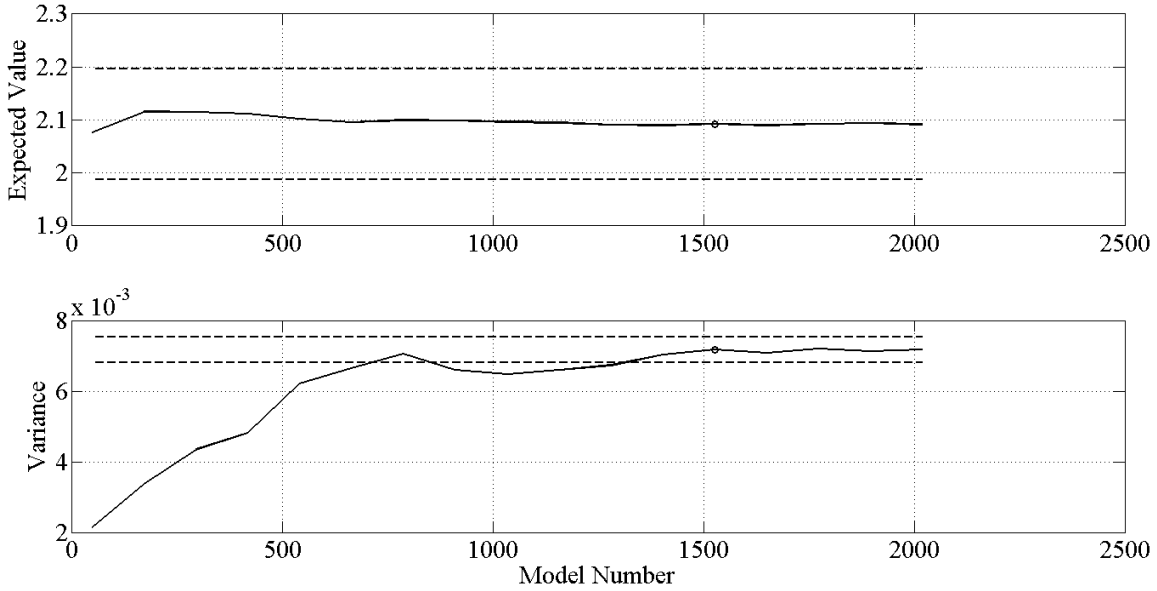

Figure 8-4: Convergence Diagram for K_v

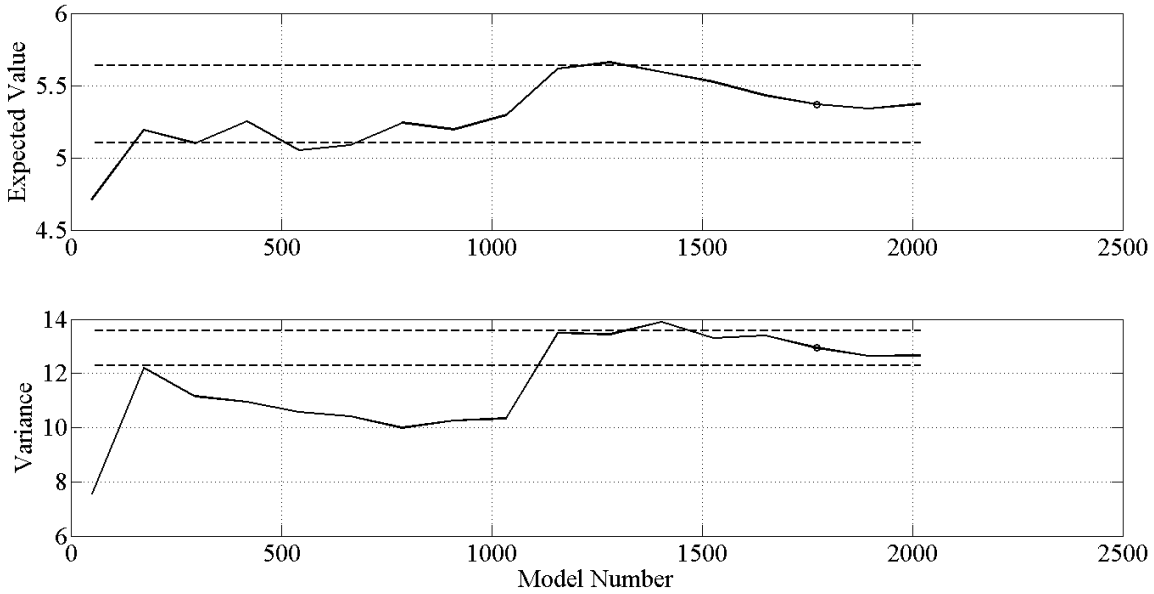

Figure 8-5: Convergence Diagram for K_l

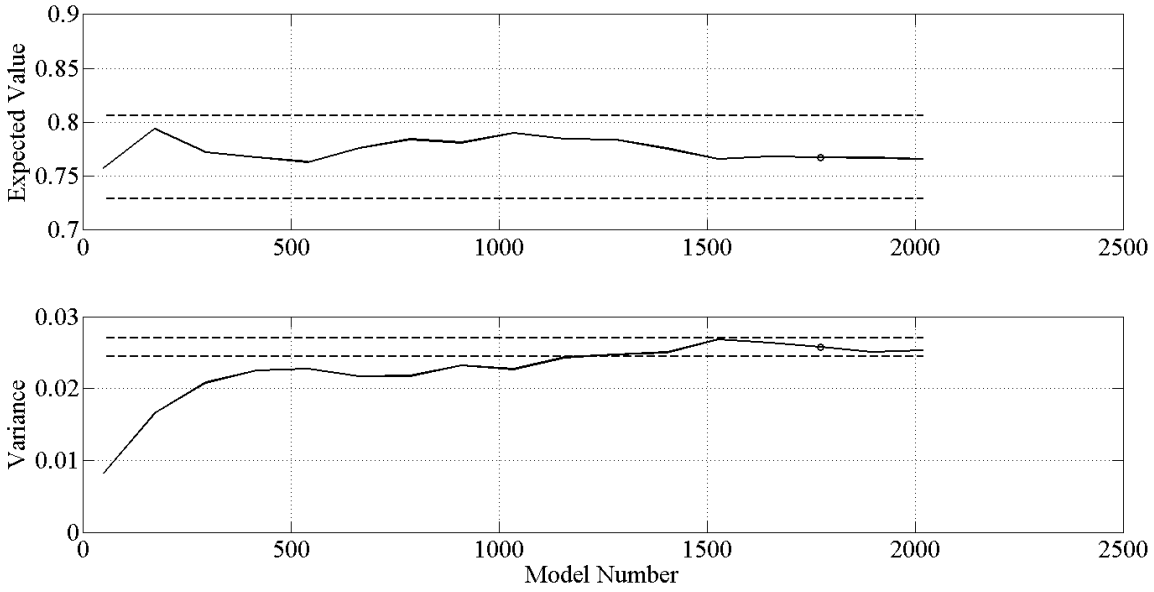

Figure 8-6: Convergence Diagram for K_{r1}

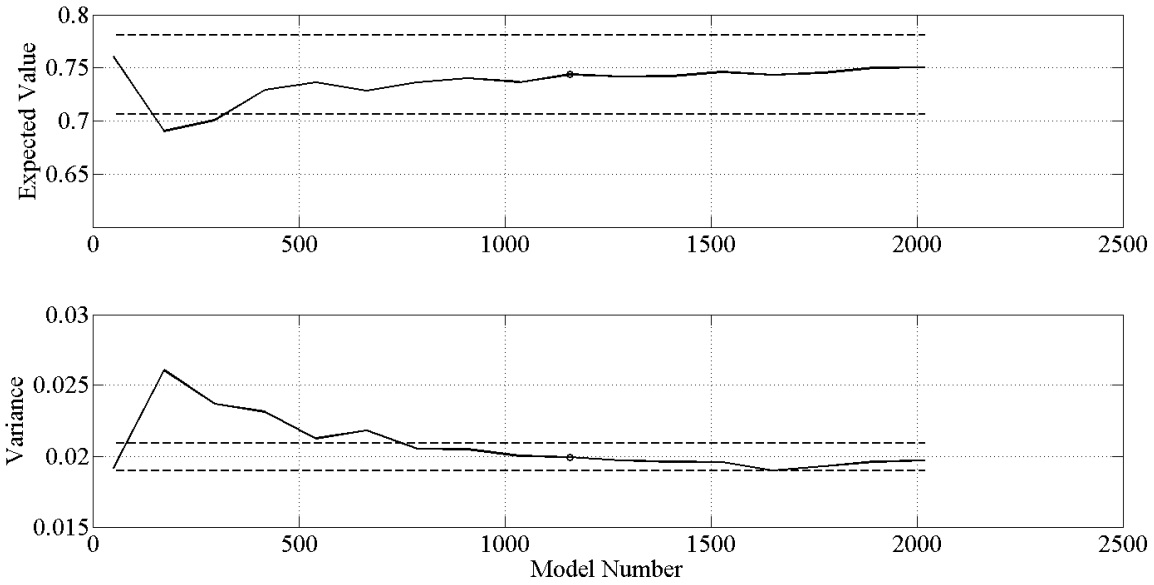

Figure 8-7: Convergence Diagram for K_{r2}

It was determined through the convergence study that an additional 1,800 models were needed post burn-in to sufficiently characterize the marginal posterior probability distributions of the building blocks. Using this set of models, response predictions were generated in a manner consistent with what was demonstrated in Chapter 7.

8.1.2. Generation of Response Predictions from Weighed Models

The response predictions for the MM St-Id analysis of the third structural configuration of the DI3 grid are shown in Figure 8-8 and Figure 8-9. First, the effects of the method on the building blocks were reviewed. There was a slight tightening on the variance of the elastic modulus, as well as a shift to the left. This apparent softening of the elastic modulus is seen due to the more flexible nature of the neoprene supports. The vertical

stiffness changed drastically, and was primarily sampled around 2.1 kip/in, while the longitudinal stiffness was sampled over the range of 0 kip/in to 20 kip/in. Both of the rotational stiffness factors tended once again towards a rigid connection.

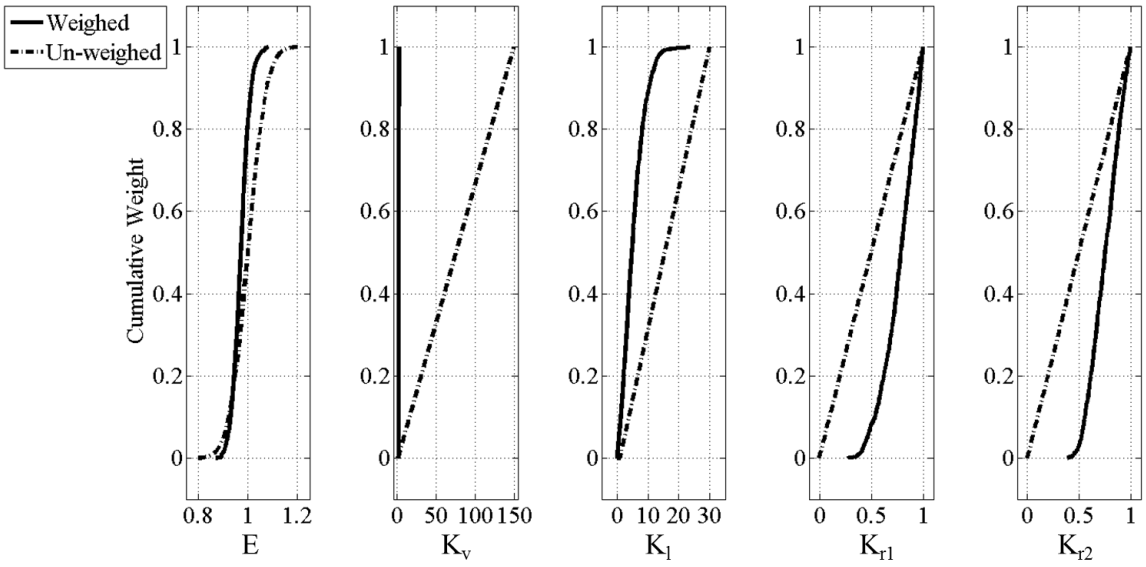

Figure 8-8: Effects of Weighing on Building Blocks

Finally, the response predictions were generated for the mid-span displacement and strain due to a mid-span load at Node 11. The response distributions were generated by sampling the predictions of each model 1,000 times with a 4% standard deviation. Both of these response prediction distributions were compared to the observed values, as

shown in Figure 8-9. It is noted that there is a substantial range seen in each distribution, and this is primarily due to the variability observed in the sampling of the vertical and longitudinal springs.

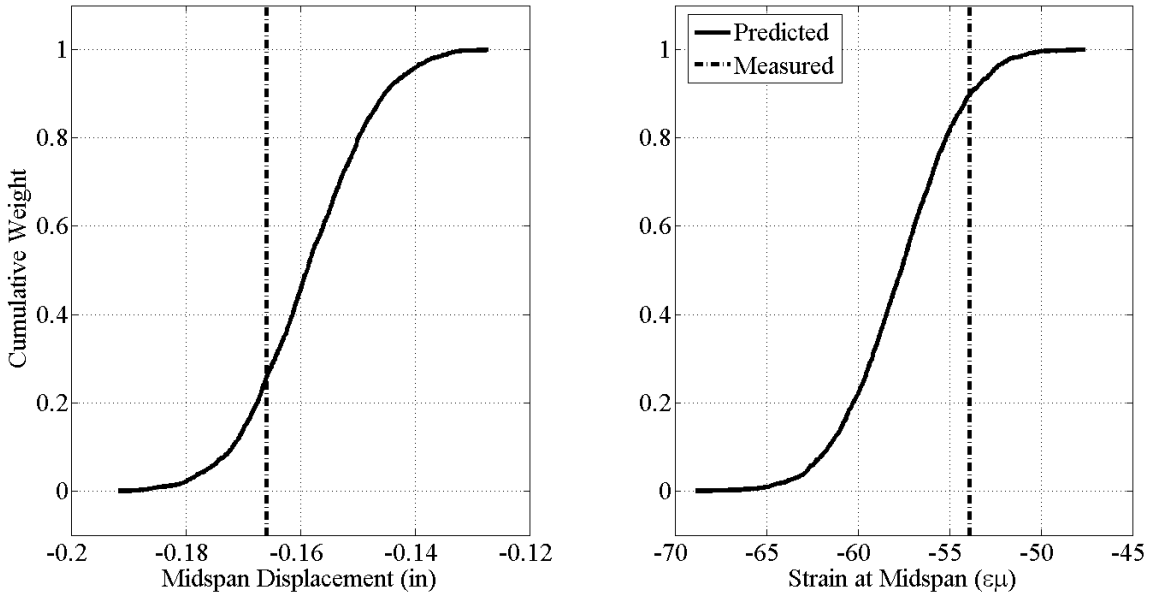

Figure 8-9: Response Predictions from MM St-Id Analysis for Structure 3

In conclusion of the study on Structure 3 of the grid configurations, the MM St-Id method was still able to both converge on the target distribution as well as provide meaningful prediction distributions, even in the presence of more complex and noisy observations (particularly the modeshapes). One important observation to make from this study is that both the number of models required for burn-in and the number of models required for

convergence post burn-in became greater with the more complex case. This is to be expected as the structures and observations become more complicated and noisier, respectively.

8.2. Investigation into Measurement Quantity

The number of observations to include in any St-Id process is always an important consideration. Ideally, more observations should lead to a more informed St-Id process and reliable predictions. However, due to the costs associated with dense instrumentation plans, access to the structure and data acquisition, the number of observations is typically limited. In addition, there likely exists a point of diminishing return where, for example, doubling the number of observations may only result in a negligible improvement of the results. Recognizing this, an investigation into the effects of limited observations was carried out on the DI3 grid structure.

To investigate the effects of measurement quantity on the quality of the predicted results, the 9,750 model set generated with the Monte Carlo sampling scheme in Chapter 7 was utilized. The Monte Carlo model set was utilized because the model population was already generated for the previous study and could be easily manipulated to provide the basis for this study. Additionally, this allowed for a consistent comparison in that the exact same models were used for the various studies.

Once again, the natural frequencies and modeshapes were selected as the observed measurements, with the aim of predicting displacements and strains due to a mid-span load. The mid-span displacement and mid-span strain response prediction distributions were generated as a function of the number of pieces of information included in the weighing analysis. A general scenario was investigated regarding the number of mode shapes included.

8.2.1. Investigation into Incremental Addition of Observations

The number of observations included in each weighing exercise is shown in Table 8-2. The group of models was incrementally weighed with each of the observations. Each included mode contained two pieces of information: (1) natural frequency and (2) modeshape. The prediction distributions of displacements and strains for each of these cases is shown in Figure 8-10 - Figure 8-11.

Table 8-2: Description of Studies for Investigation into Measurement Quantity

Trial	Observations	Modes Included
1	2	1
2	4	1, 2
3	6	1, 2, 3
4	8	1, 2, 3, 4
5	10	1, 2, 3, 4, 5
6	12	1, 2, 3, 4, 5, 6
7	14	1, 2, 3, 4, 5, 6, 7

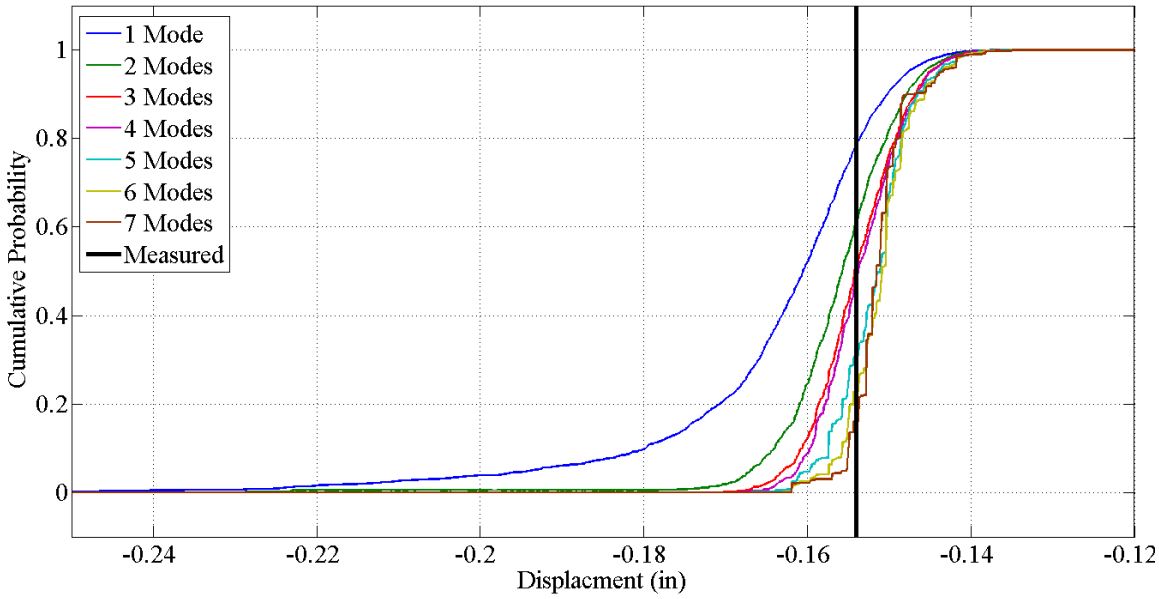

Figure 8-10: Cumulative Probability Function for the Mid-span Displacement Due to a Mid-span Load

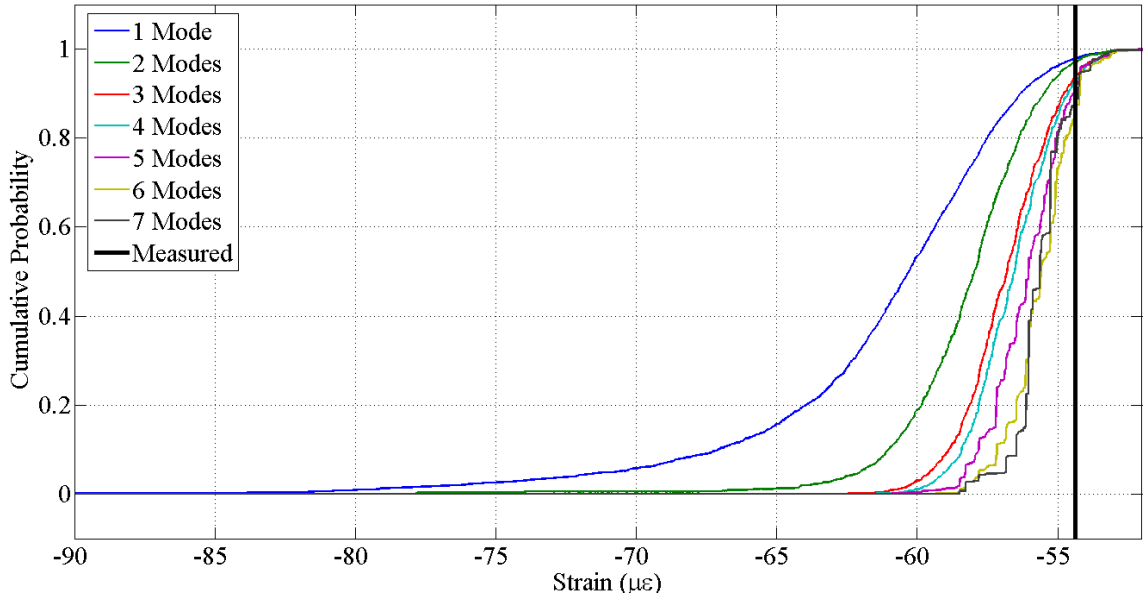

Figure 8-11: Cumulative Probability Function for the Mid-span Strain Due to a Mid-span Load

The results shown in Figure 8-10 and Figure 8-11 indicate that the response prediction functions are heavily influenced by the number of observations incorporated into the MM St-Id process. The major conclusion that can be drawn from both of these figures is that as more information is included, the variance and range associated with the predictions is greatly reduced. This is indicated by the increase in slope of the cumulative distribution functions, implying a narrower and sharply peaked probability distribution function.

This finding supports the belief that increasing the number of observations within this framework will lead to a more informed prediction. Additionally, the structure is becoming better characterized as more information is being obtained, leading to a more reliable prediction of the responses. For example, when only one mode was included as an observation the measured strain almost did not lie within the likely probability regions while the measured displacement was only 30% away from the mean of the distribution. As more information was added, the displacement and strain predictions were able to be better characterized. By the time the seventh mode information was added into the MM St-Id method, the observed displacement and strain were almost equally spaced from the means of their updated distributions, respectively, about 30%.

While this specific study shows that more information is better, in terms of response prediction, this does not mean that it will always be the case. The strains and displacements predictions were influenced by the additional information because the responses were correlated to the observations. However, if a desired response prediction which is uncorrelated to dynamic measurement observations, then additional information will not necessarily provide refined estimates of the response prediction.

8.3. Investigation into Selection of Observations

The investigation into selection of observations examines a very important decision that the user of a MM St-Id framework must select early on in the process. In some cases, as with long span structures, we are very limited in the selection of available measurements. For example, displacements are very difficult to reliably measure on a long span structure over water, however ambient vibration monitoring is relatively easy to implement. In other cases, full access may be available for any type of measurement but funds may be limited to only one type of implementation. In either case, it is imperative that an experienced user select the appropriate measurement types with a high degree of correlation to the type of prediction desired.

For example, if the desired model prediction is a seismic hazard assessment of a long span suspension structure, then a global ambient vibration test may not be the best form of observation since the foundation-tower system, critical components of a seismic analysis, are the most stiff elements of the structure and the least likely to be characterized by ambient vibrations. In that case, the structure is more readily excited in its lowest, and more flexible, modes by traffic and wind effects.

Keeping this in mind, the investigation into the effect of measurement selection on the prediction of unobservable attributes was carried out in three scenarios: (1) the use of global dynamic measurements to predict static responses, both global and local, (2) the use of global static displacement measurements to predict both local static responses and global dynamic responses, and (3) the use of local static measurements to predict global dynamic and static responses.

8.3.1. The Use of Global Dynamic Measurements to Predict Static Responses (Global and Local)

This type of investigation has been carried out in Chapter 7, but the results will be briefly presented here for comparison purposes. Using global dynamic measurements has been shown to provide very reliable predictions in terms of both global displacement responses and local strain responses for the grid structure. The main reason why dynamic measurements are so useful in St-Id applications is that they are representative of both mass and stiffness properties of the structure. In the case of the DI3 grid, there are no building blocks related to mass (ie, web thickness, density, etc.), however in other applications there may be such building blocks.

The results of using the global dynamic measurements, seven natural frequencies and seven modeshapes, for weighing the models are shown in Figure 8-12 and Figure 8-13. These results are from the 9,750 models needed for convergence using dynamic measurements as the observation. The method was able to reliably estimate probability distributions for both the local and global static response indices from a static load test, in this case a mid-span load with both responses at mid-span locations. Additionally, the updated probability distributions of the building blocks appear to be reasonable given the configuration of Structure 1.

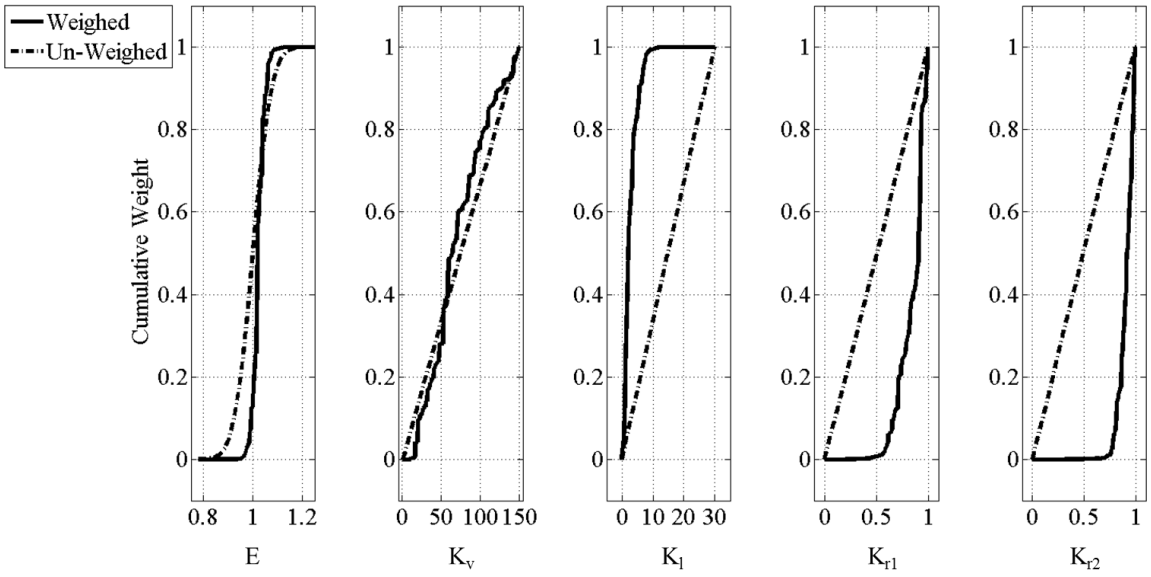

Figure 8-12: Effect of Weighing Models with Dynamic Measurements

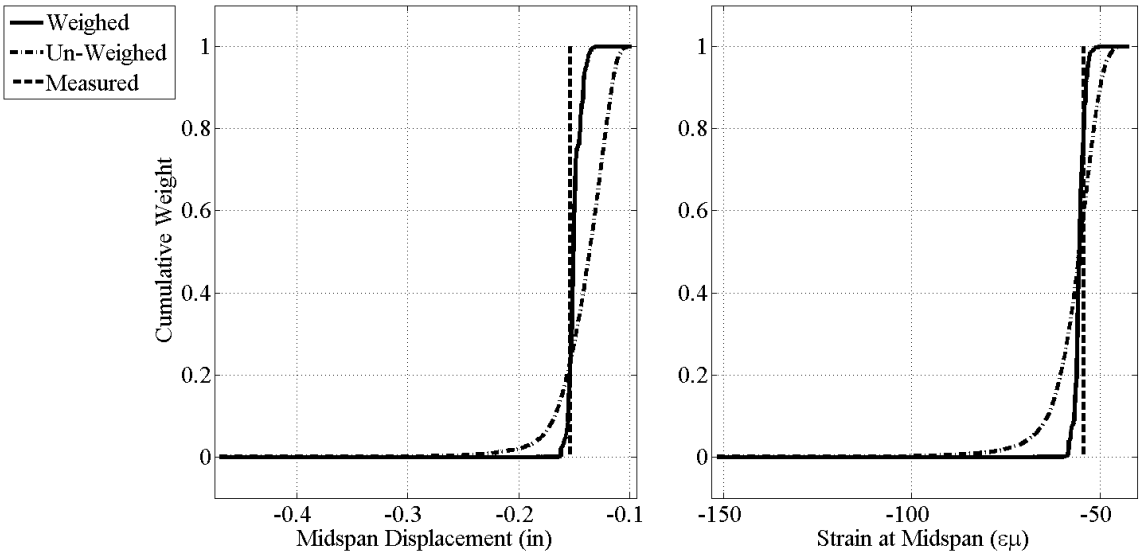

Figure 8-13: Predictions of Global and Local Static Responses Based on Global Dynamic Measurements

8.3.2. The Use of Global Static Displacement Measurements to Predict Both Local Static Responses and Global Dynamic Responses

To study the ability of displacement measurements to predict dynamic and local strain measurements, multiple displacement load cases were used. It is important to use multiple load cases so that the structure is better characterized, as shown in 8.2.1. Additionally, if only one load case were used from a static load test in which the load location coincided with a nodal point of multiple modeshapes (for example, if a load was applied at mid-span, the displaced shape would replicate that of the first bending mode and fall at the nodal point of multiple others for the DI3 grid), then the ability of that one load case to reliably predict other modeshapes is greatly compromised. However, for the purpose of comparison, initially one load case was selected which avoided as many nodal locations as possible and then three load cases were used together as the experimental observations.

For these studies, three load cases were used: (1) 100lb load at Node 11, (2) 100lb load at Node 18, and (3) 100lb load at Node 19. These three load cases were selected so that the maximum number of nodal points could be avoided for the fundamental (lower order) modeshapes. The total number of observations used in the calculation of the likelihood for each model was 45 for the three load cases. The single load case study utilized the responses due to a load of 100lb at Node 19 and comprised of 15 total observations.

Using either one or three load cases as the observed measurements, the total number of models needed for convergence from the Monte Carlo generated model set was 10,000. Note that this is very close to the 9,750 needed for the case where the dynamic

measurements were used for weighing the models. The results of the two studies will be discussed in two subsections: (1) Weighing Models with One Static Load Case and (2) Weighing Models with Three Static Load Cases.

8.3.2.1. Weighing Models with One Global Static Load Case

The measurements from the static load test of 100lb placed at Node 19 were used to weigh each of the models generated from the Monte Carlo model set. The updated probability distributions associated with each of the building blocks is shown in Figure 8-14. As seen in this figure, the updated posterior probabilities associated with the building blocks are consistent with those produced by using the dynamic data as the observations. The elastic modulus of steel was updated to a tight distribution around the nominal value for this building block, while the building block associated with vertical stiffness was updated to reflect a broad distribution over the higher stiffness values. The longitudinal stiffness building block was updated to reflect a low stiffness value while both of the connection stiffnesses yielded posterior distributions reflecting high stiffness in the connections.

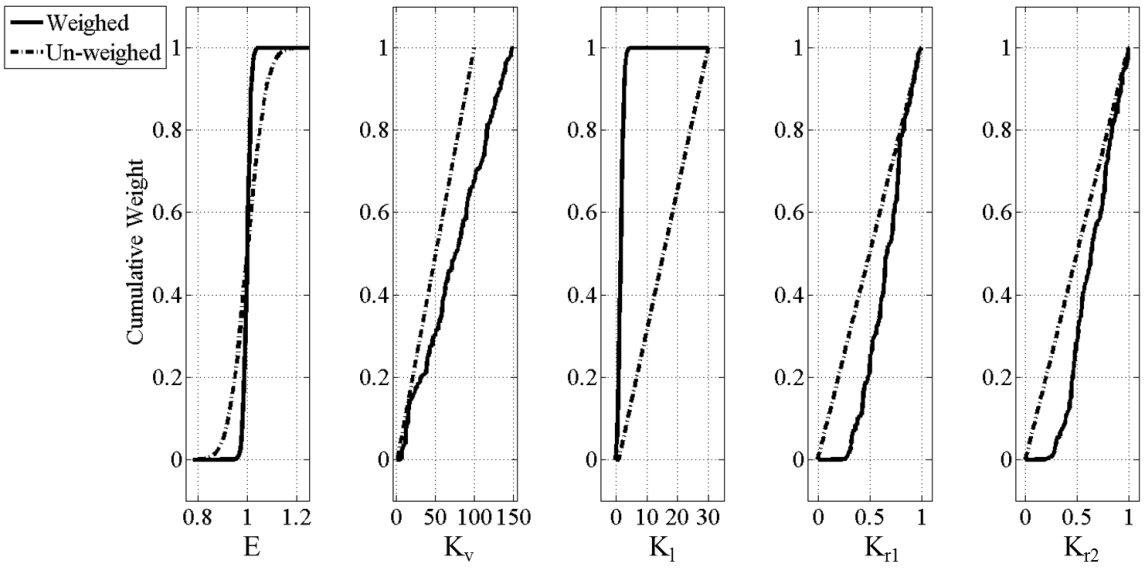

Figure 8-14: Effect of Weighing Models with One Static Load Case on Building Blocks

The predictions corresponding to these weighed models for the seven frequencies identified for Structure 1 as well as the mid-span displacement and strains due to a load of 100lb at mid-span are shown in Figure 8-15 through Figure 8-19. Also, the corresponding MAC values for the modeshape predictions are shown in Figure 8-20 through Figure 8-23.

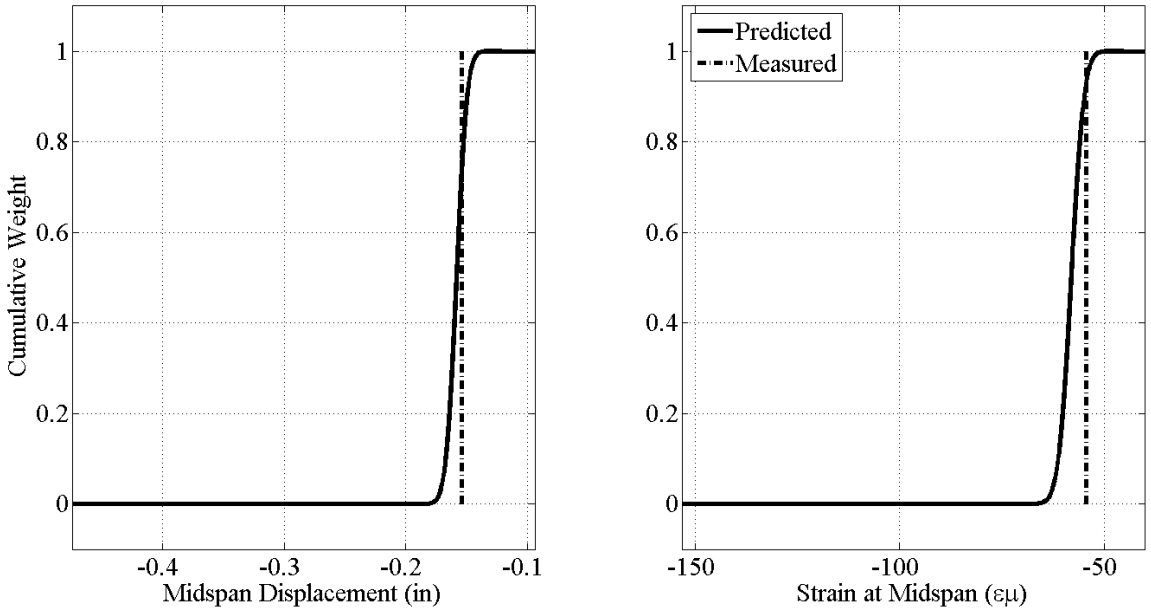

Figure 8-15: Response Predictions for a Mid-span Load

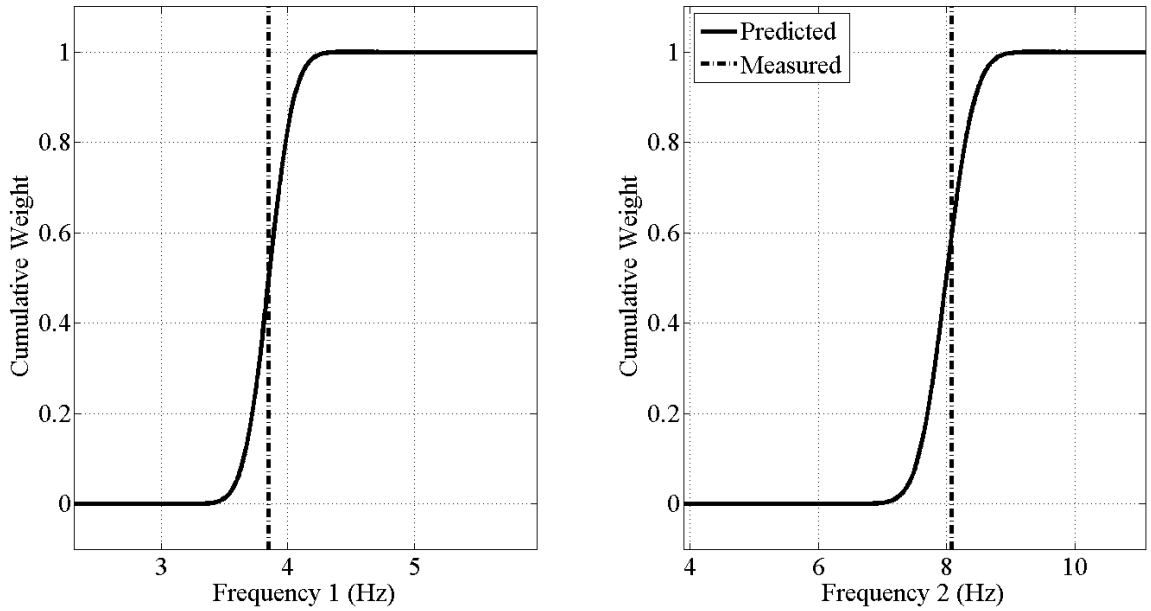

Figure 8-16: Response Predictions for Modes 1 and 2

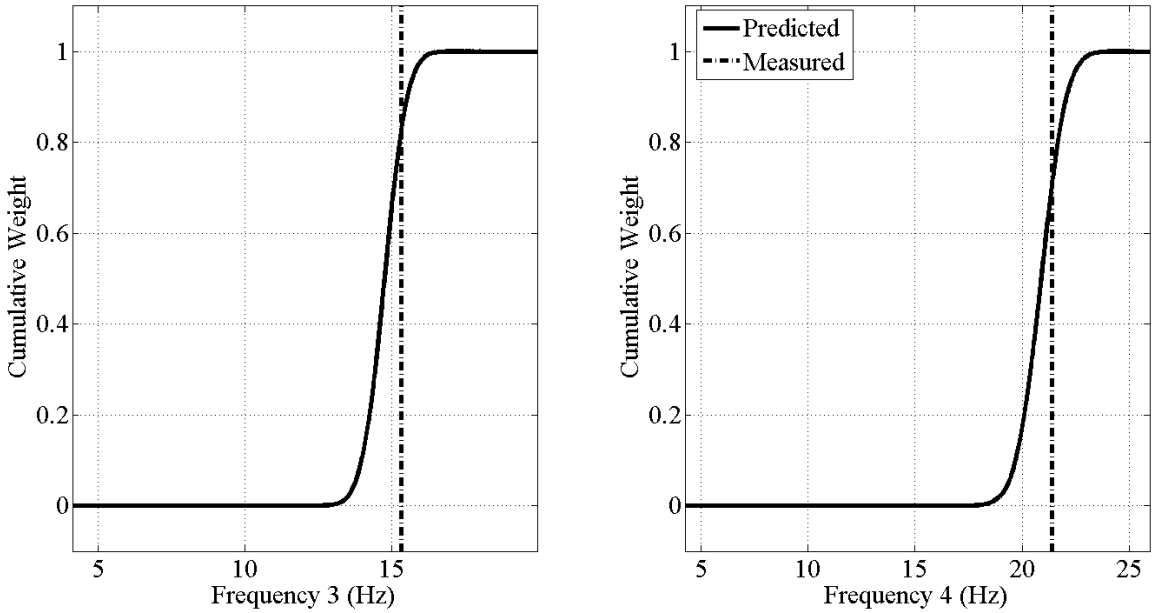

Figure 8-17: Response Prediction for Modes 3 and 4

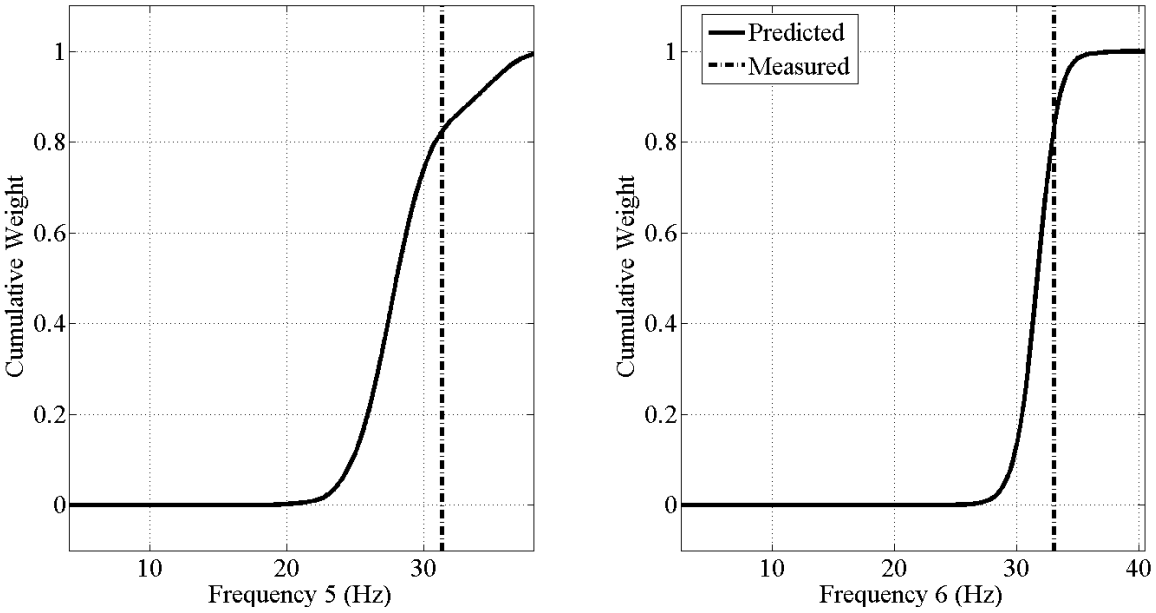

Figure 8-18: Response Predictions for Modes 5 and 6

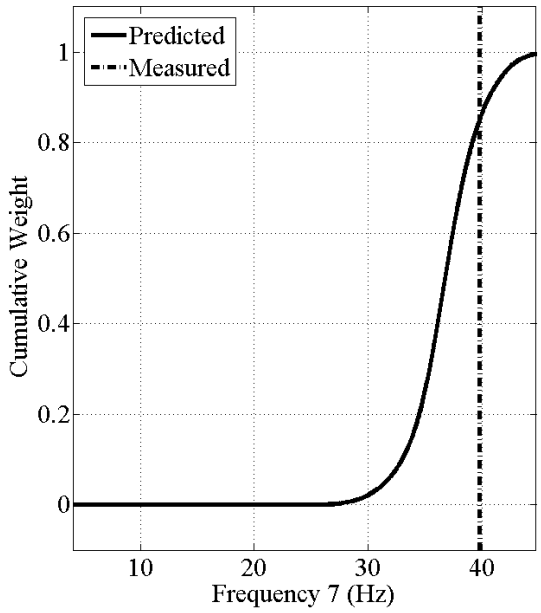

Figure 8-19: Response Prediction for Mode 7

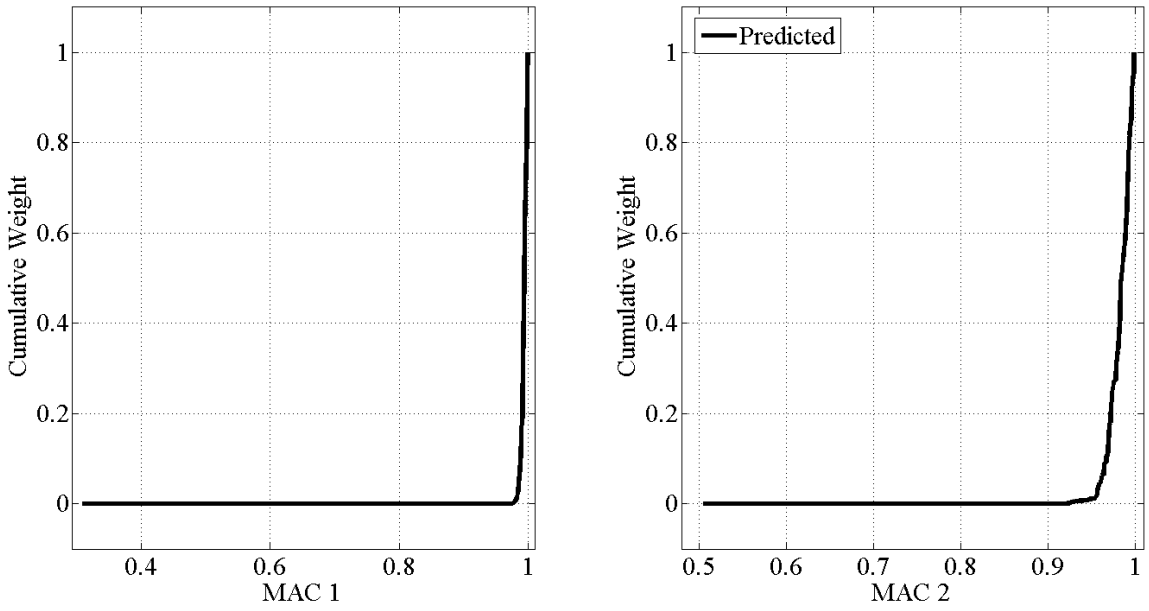

Figure 8-20: Response Prediction for Mode 1 and 2 MAC Value

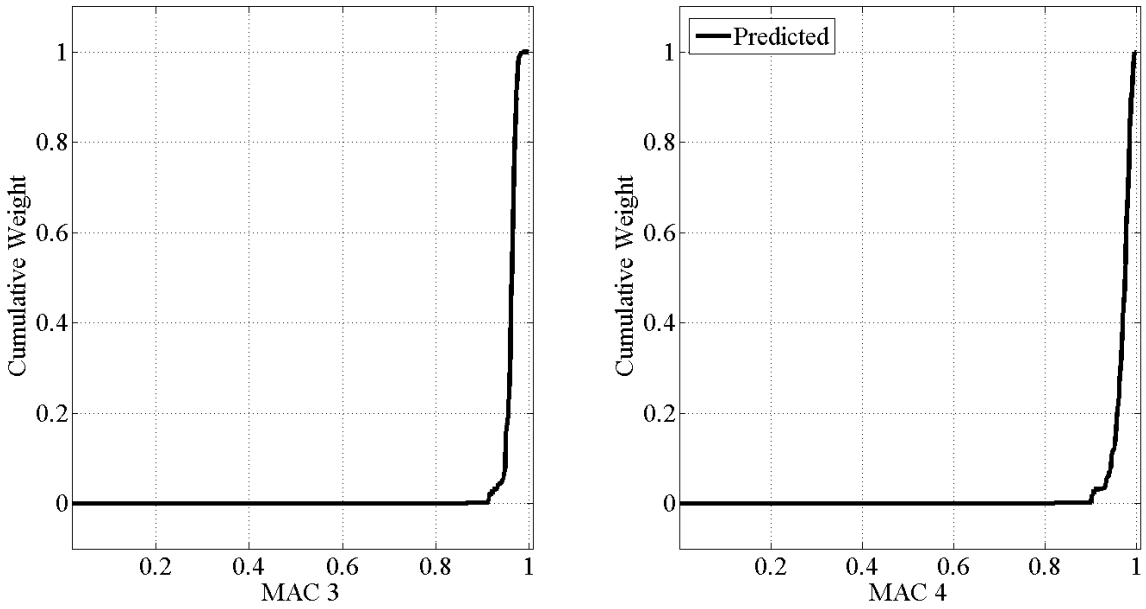

Figure 8-21: Response Prediction for Mode 3 and 4 MAC Value

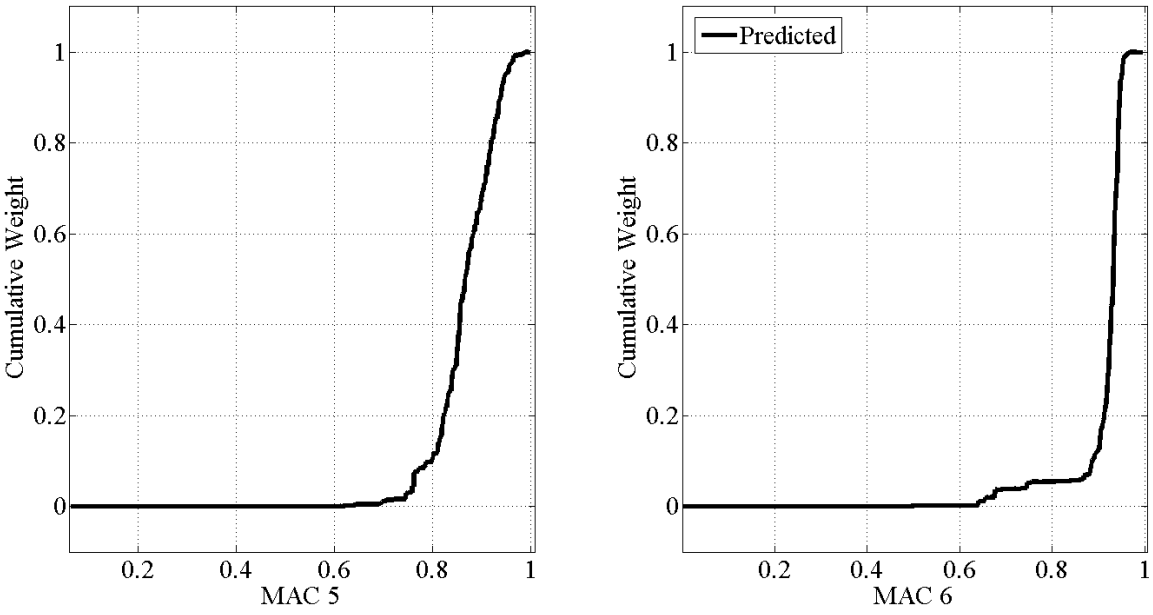

Figure 8-22: Response Prediction for Mode 5 and 6 MAC Value

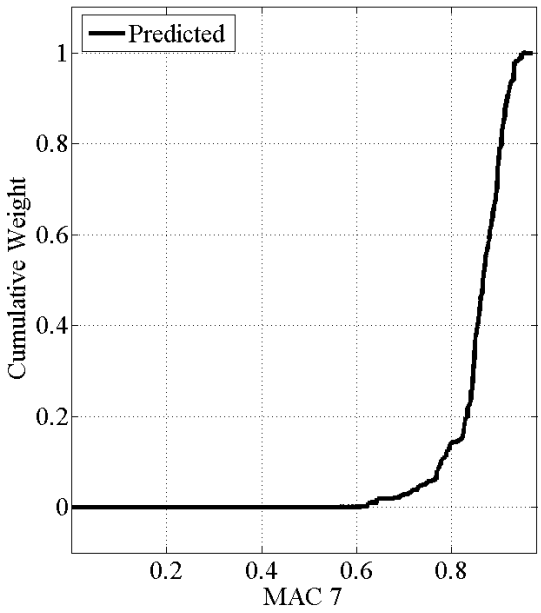

Figure 8-23: Response Prediction for Mode 7 MAC Value

Upon examining the response predictions above, it is clear that the method is able to characterize the structure in terms of all seven frequencies identified in the dynamic impact test by weighing the models with static displacement measurements. Additionally, the prediction of displacements from a separate load case appears to be very reasonable while the prediction of strains just falls within the prediction range.

8.3.2.2. Weighing Models with Three Global Static Load Cases

Additional load cases were added to the weighing of the Monte Carlo models to study the effects of including additional information when using static displacements as observed quantities. In this case, loads at Node 11, Node 18 and Node 19 were used for weighing purposes. The reason for including additional information is to better characterize the

structure by observing how it behaves under different loading conditions. Just as increasing the quantity of natural frequencies and modeshapes provided more sharp prediction distributions, it was anticipated that including additional load cases would have the same effect. The results of this study are shown in Figure 8-25 through Figure 8-33.

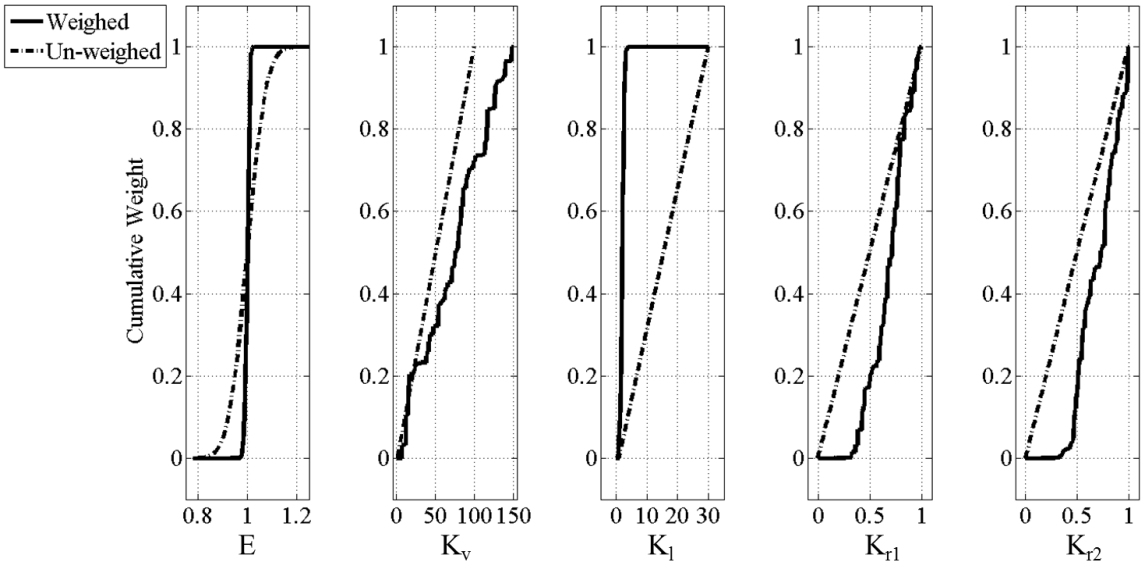

Figure 8-24: Effects of Weighing Models with Three Static Displacement Load Cases on Building Blocks

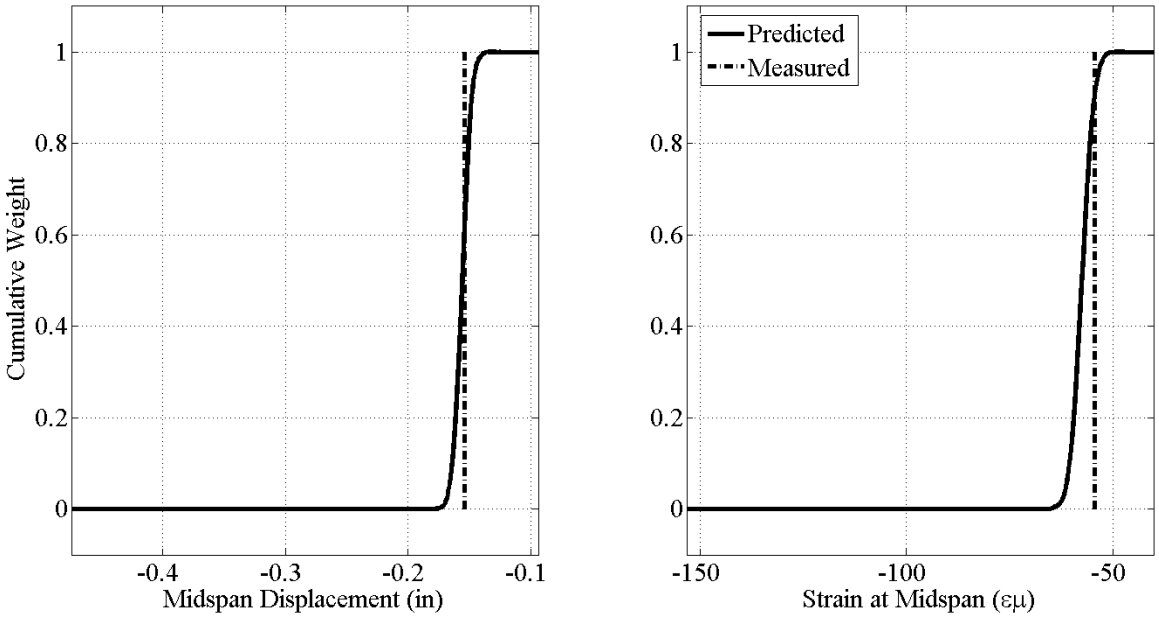

Figure 8-25: Response Predictions for a Mid-span Load

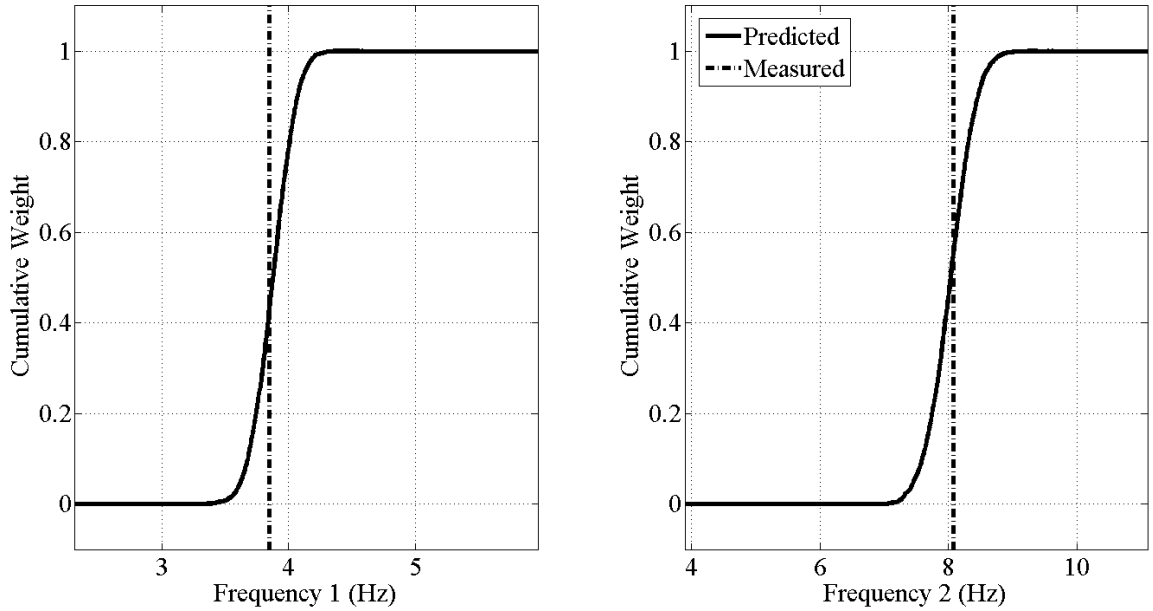

Figure 8-26: Response Predictions for Modes 1 and 2

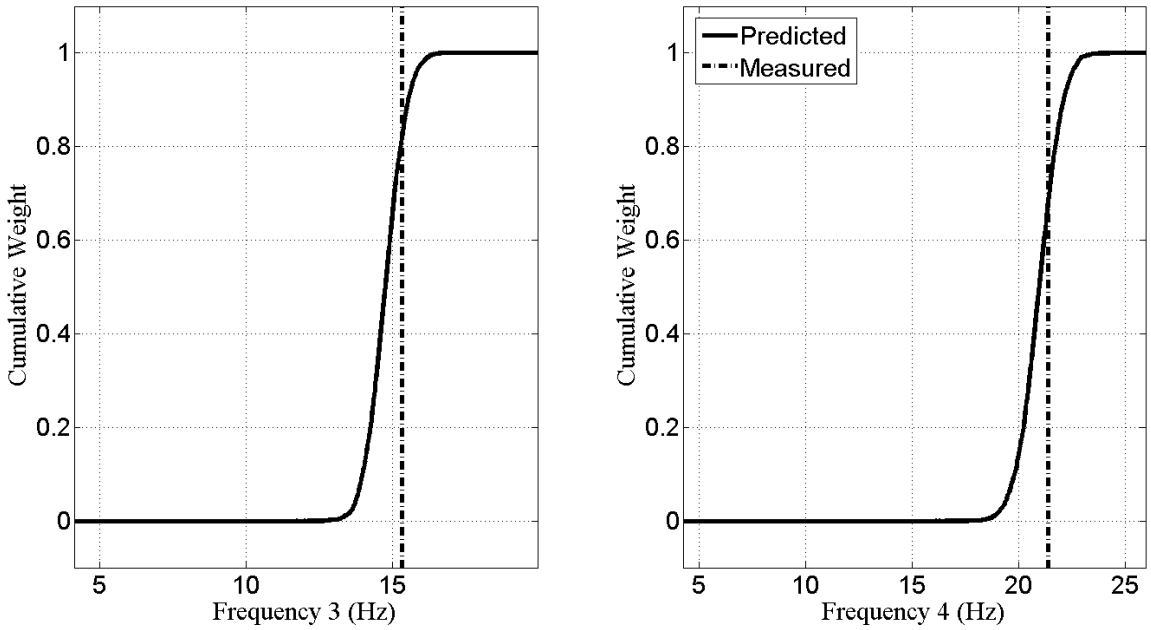

Figure 8-27: Response Predictions for Modes 3 and 4

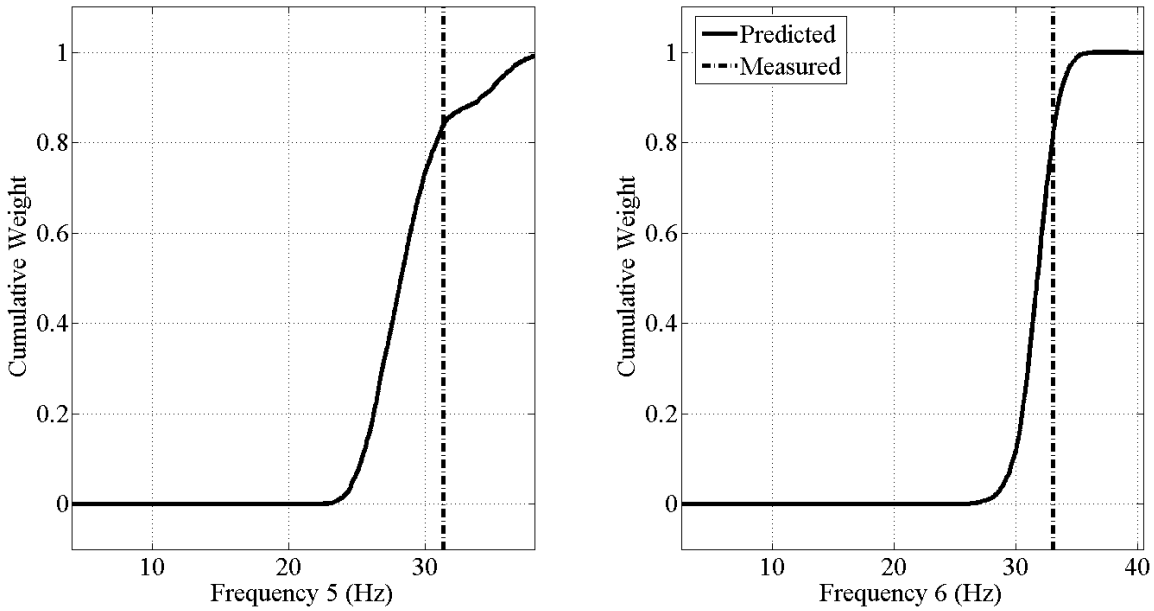

Figure 8-28: Response Predictions for Modes 5 and 6

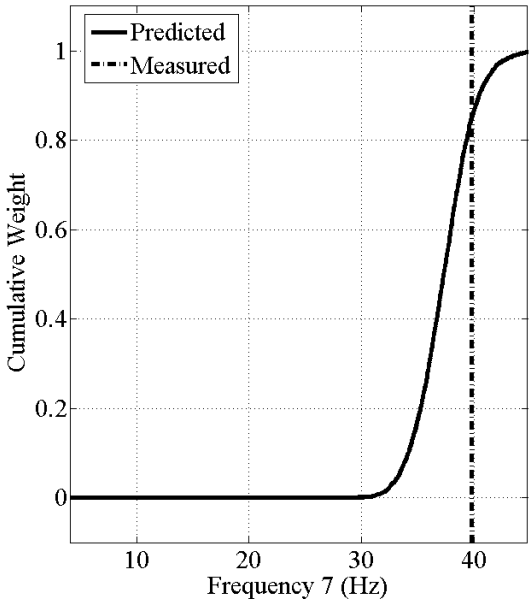

Figure 8-29: Response Prediction for Mode 7

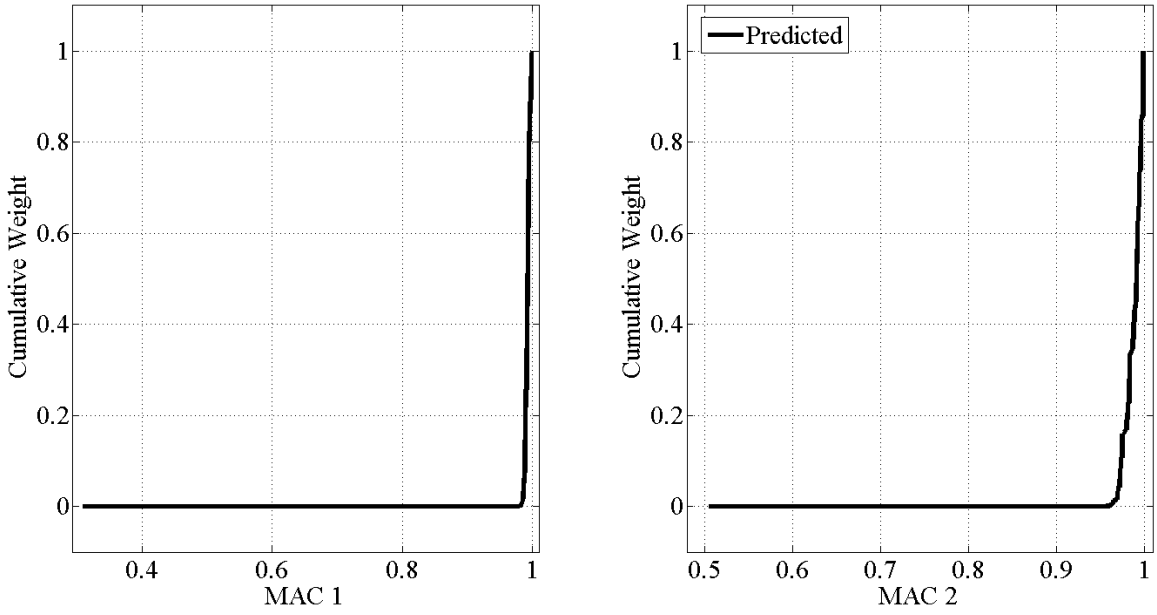

Figure 8-30: Response Prediction for Mode 1 and 2 MAC Value

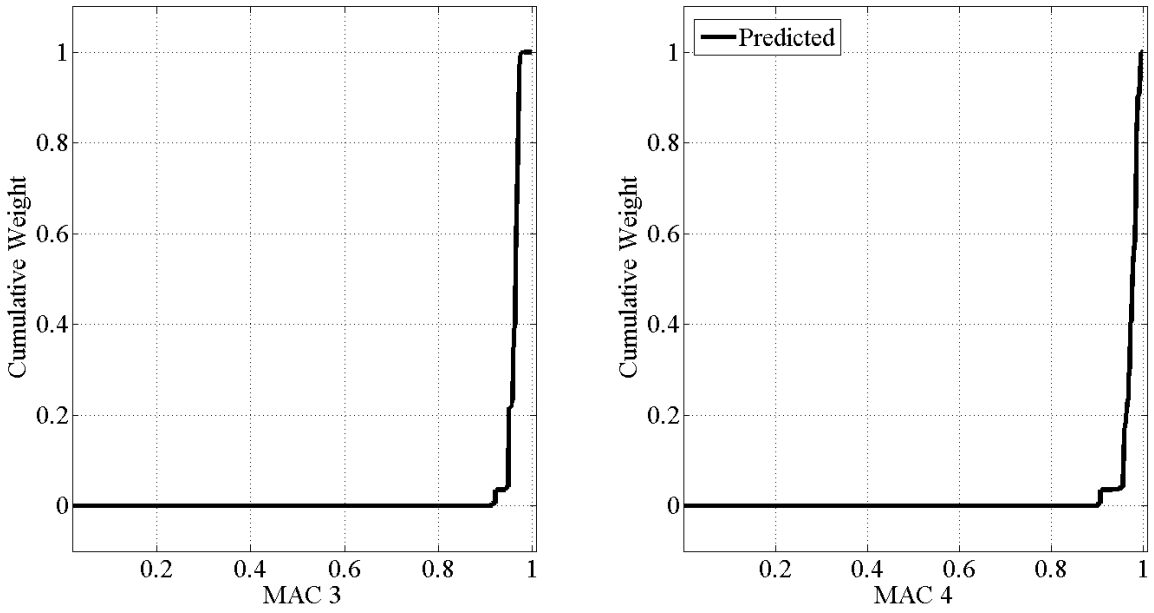

Figure 8-31: Response Prediction for Mode 3 and 4 MAC Value

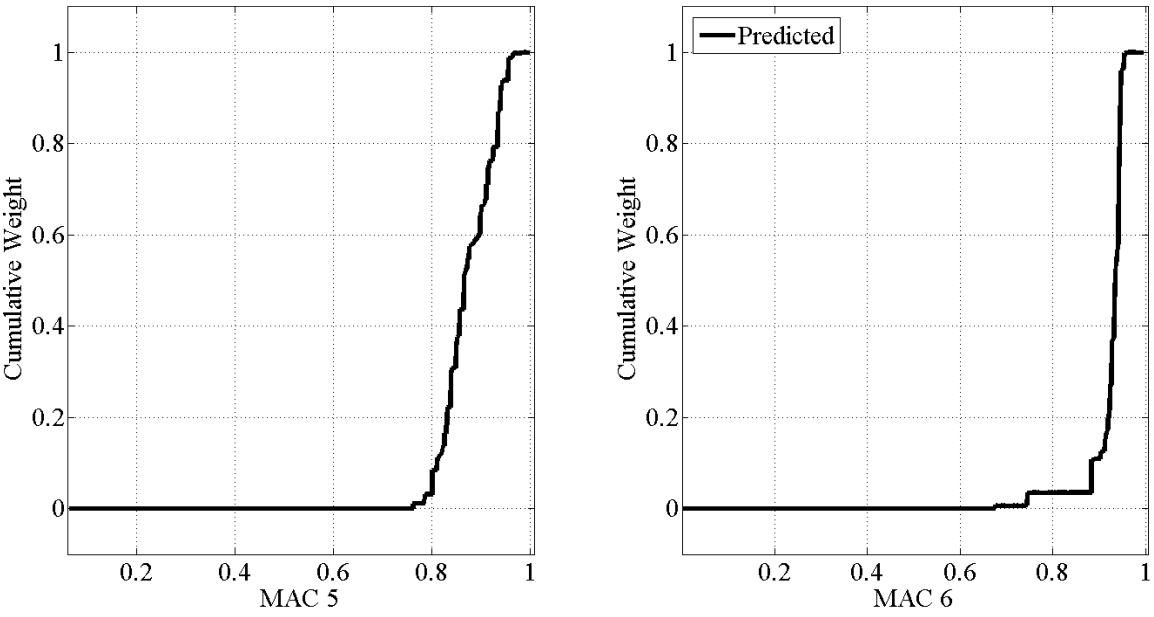

Figure 8-32: Response Prediction for Mode 5 and 6 MAC Value

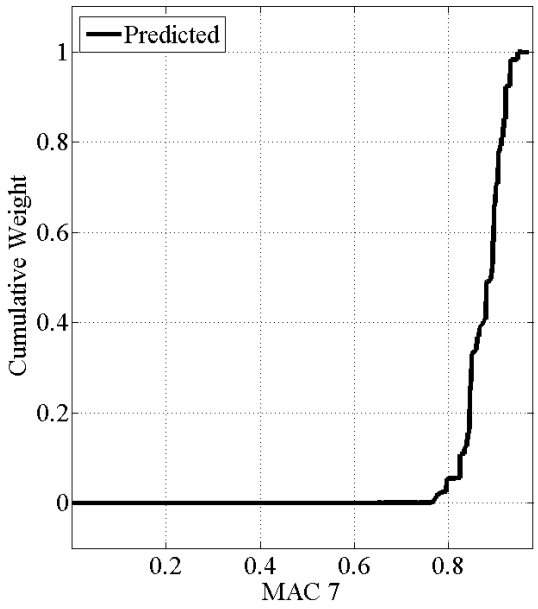

Figure 8-33: Response Prediction for Mode 7 MAC Value

Upon examining the effects of the weighing process on the building blocks, it is noted that the updated probability distributions for each of the building blocks is consistent with those seen so far: (1) a tightened posterior distribution around the nominal value of the elastic modulus, (2) a tending towards more stiff vertical stiffness, (3) a sharp reduction in the high end of longitudinal stiffness and (4) stiffened interior and exterior connections.

Initially, the effects of adding more information in the weighing process appeared to not have any appreciable effects on the predictions of strains from the mid-span load case, however the shapes of the cumulative probability functions for each of the frequencies was slightly modified by the additional information. Given the analyses from using

displacements as the observations, it appears that both the prediction of dynamic properties of the structure in addition to strains are feasible.

8.3.3. The Use of Local Static Measurements to Predict Global Dynamic and Static Responses

The final form of observational measurements commonly applied to constructed systems is the measurement of strain. This form of measurement is considered local since it is heavily influenced by localized phenomenon such as connection details (rivets, bolts, etc), changes in member direction (varied stress fields) as well as where the sensor is installed (distance from ends as well as position along cross section of member). All of these factors would lead to a hypothesis that this form of measurement would not be effective at informing global building blocks (such as vertical stiffness, in this case). This hypothesis is discussed in the following two sections.

8.3.3.1. Weighing Models with One Local Static Load Case

To remain consistent with the single load case used in 8.3.2.1, the strains observed from the load case at Node 19 were used for the single load case analysis with the strain measurements. The updated probability distributions associated with the building blocks is seen in Figure 8-34. As shown in the updated marginal posterior probabilities, there is a clear difference between using strains as opposed to other global means of measurement. Firstly, the updated distribution for the elastic modulus of steel has slightly shifted to the right and has remained fairly broad, indicating a high variance compared to

weighing with other observations. Secondly, the weighing process was not influenced by the value of the vertical springs at all. This was confirmed experimentally, when it was measured that the strains from Structure 1 and 3 were identical. This finding confirms the hypothesis that the vertical spring stiffness is not a building block which is sensitive to the strain measurement. This type of insensitive response would be captured in a sensitivity study before the analyst proceeds with the MM St-Id method. However, the longitudinal springs are now showing higher probability over a much greater range than seen before with the global means of measurement. Finally, both connection stiffnesses tended towards a rigid connection, agreeing with the other methods.

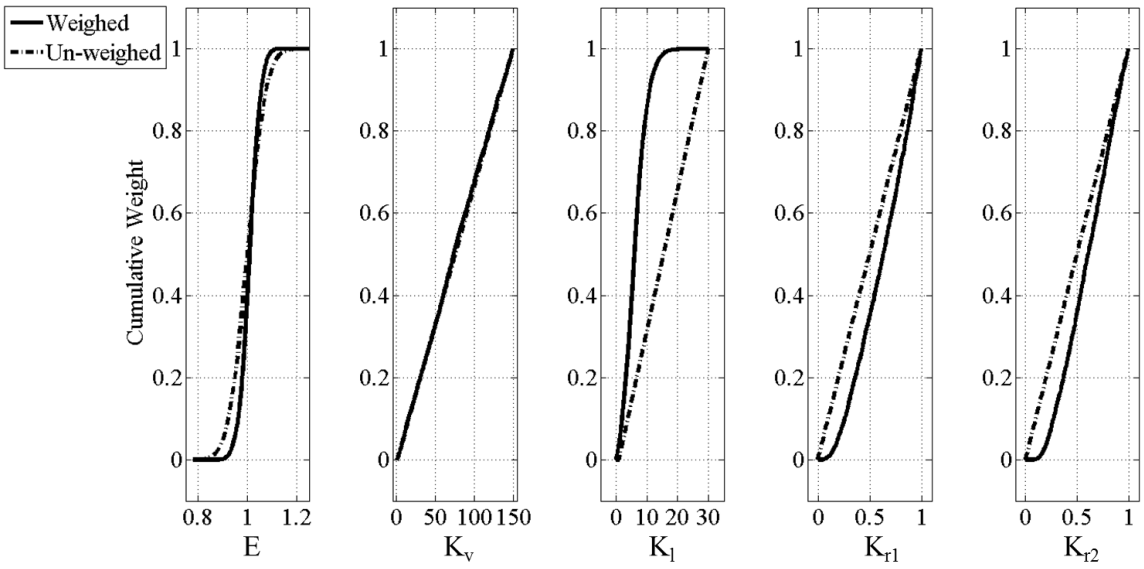

Figure 8-34: Effects on Building Blocks of Weighing the Models with a Single Strain Load Case

An important observation from the updated marginal posterior probabilities of the building blocks is that the shift of the elastic modulus of steel and the lack of an information gain in the vertical stiffness. To examine these unusual responses, the models which fell within the 95% confidence interval of the posterior probability distribution with respect to the displacement prediction at the mid-span location and with respect to the first natural frequency were studied for correlations. Correlations arise when parameters compensate for one another during a multiple model study with respect to the error function. These correlation studies were carried out by generating the matrix of plots used to examine the ability of the sampling regiments to cover the model space in Chapter 7, and are shown in Figure 8-35 and Figure 8-36.

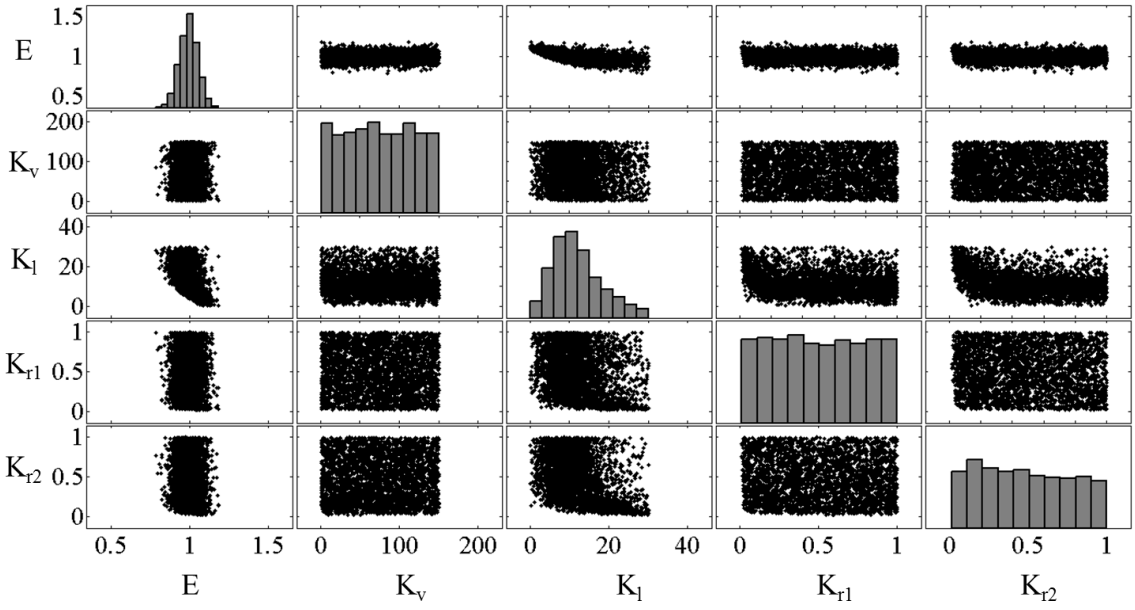

Figure 8-35: Matrix of Plots to Study for Correlations in the 95% Confidence Interval for Mid-span Displacement Predictions

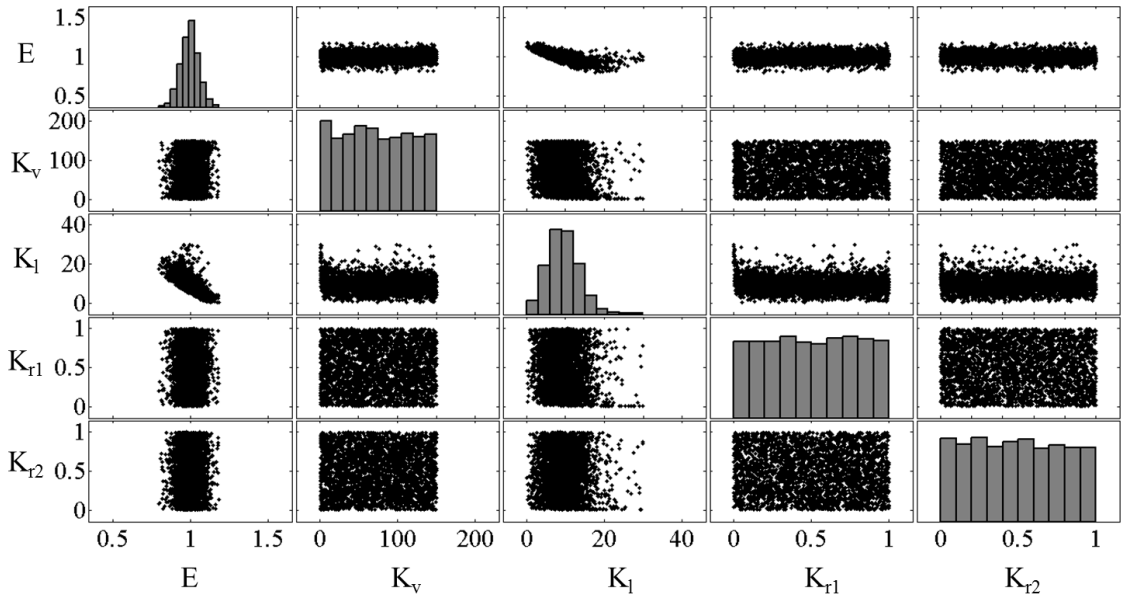

Figure 8-36: Matrix of Plots to Study for Correlations in the 95% Confidence Interval for Mode 1 Frequency Predictions

By visually examining the matrix of plots above, it is fairly obvious that a negative correlation exists with the elastic modulus of steel and the longitudinal spring at the support when examining the plots in the [1,3] and [3,1] matrix locations. This is important for multiple reasons: (1) the building blocks selected for the MM St-Id study compensate for one another when weighed by strain observations and (2) any predictions made that are not functions of the same physical characteristics as strains which were modified in the MM St-Id process (EI) will have prediction distributions with large variances. To show this, the prediction distributions are shown in Figure 8-37 through Figure 8-45.

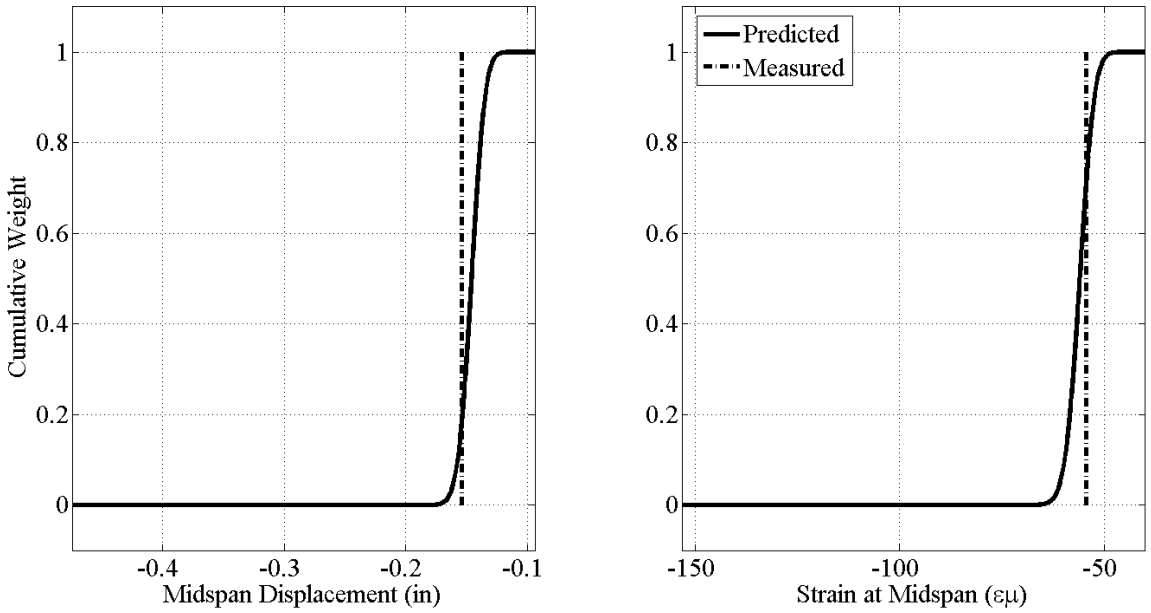

Figure 8-37: Response Predictions for Mid-span Displacement and Strain

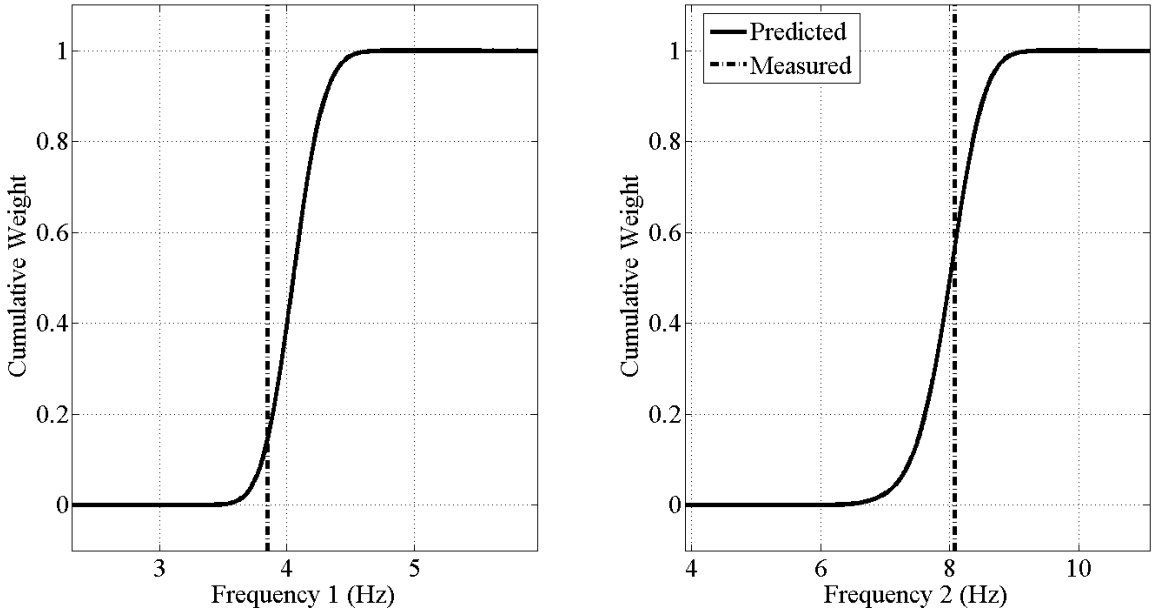

Figure 8-38: Response Predictions for Modes 1 and 2

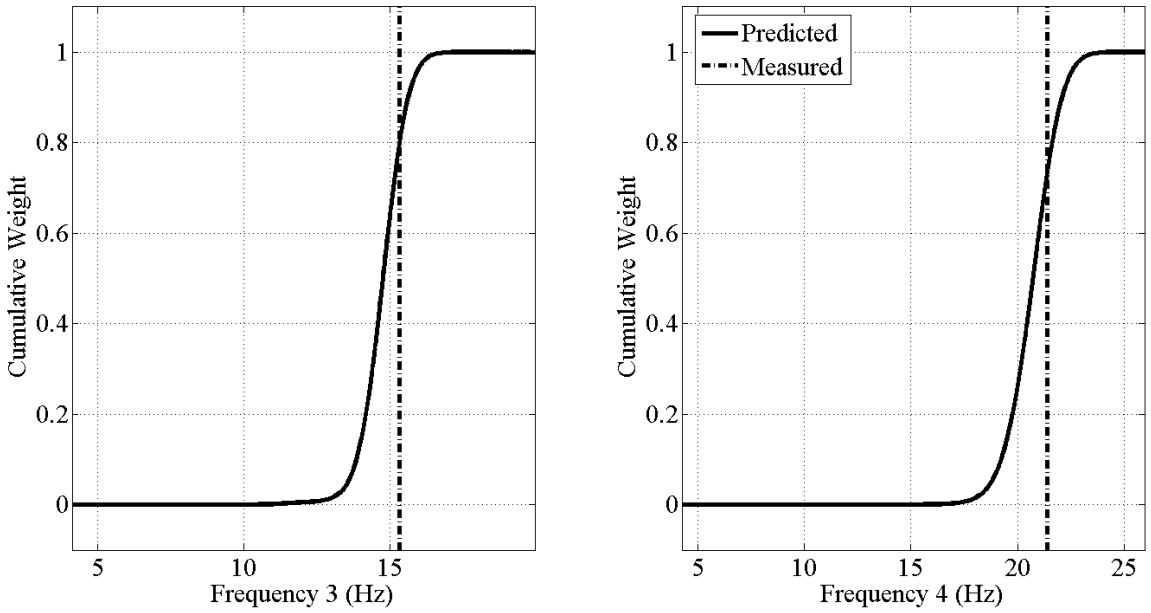

Figure 8-39: Response Predictions for Modes 3 and 4

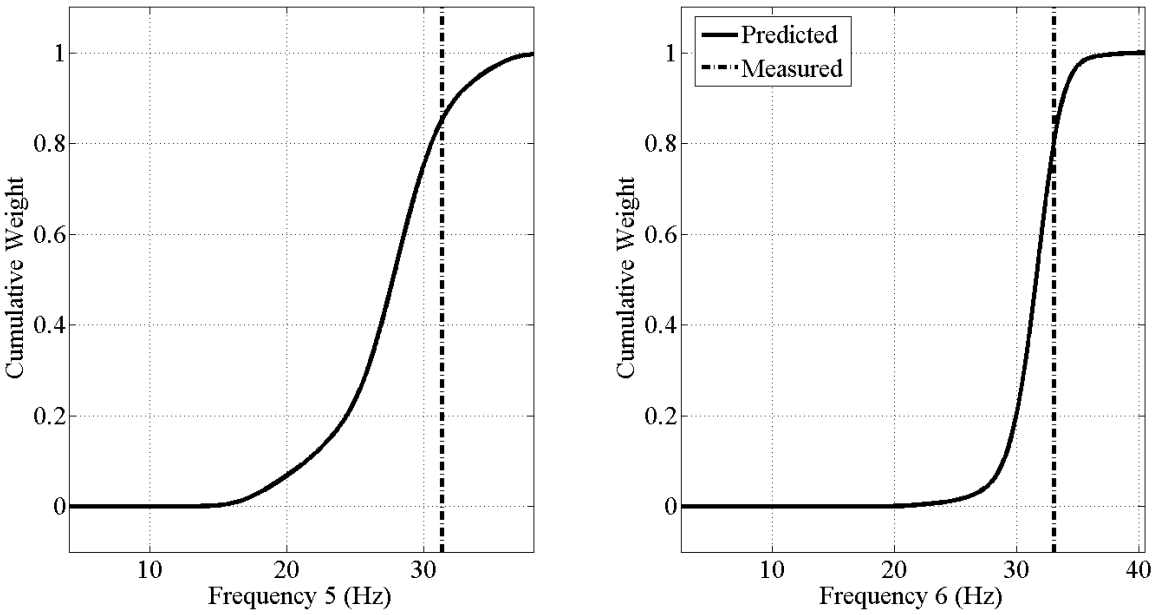

Figure 8-40: Response Predictions for Modes 5 and 6

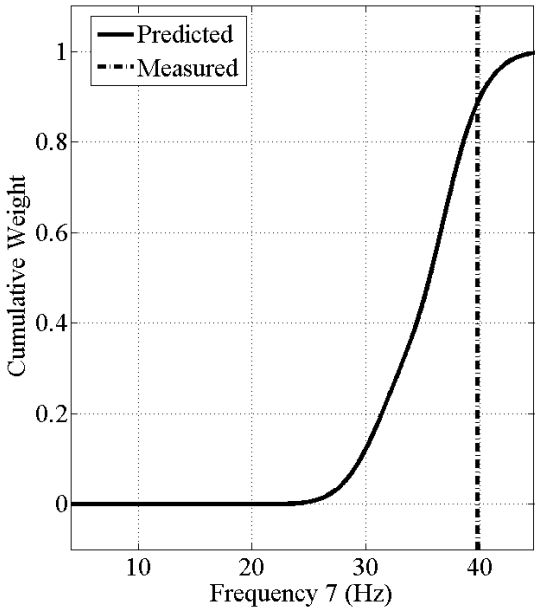

Figure 8-41: Response Prediction for Mode 7

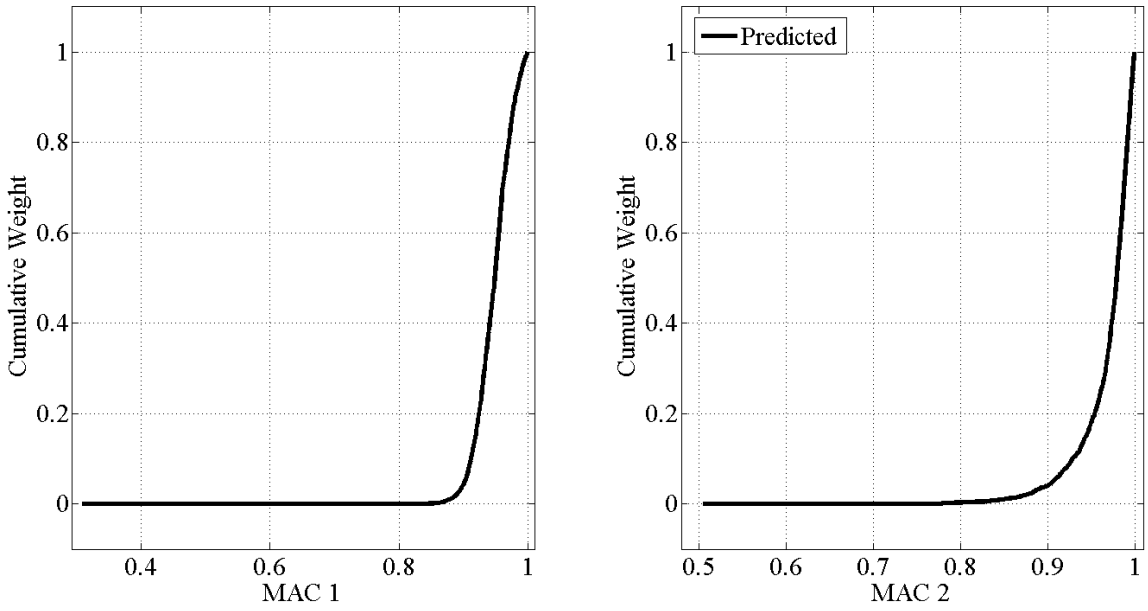

Figure 8-42: Response Prediction for Mode 1 and 2 MAC Value

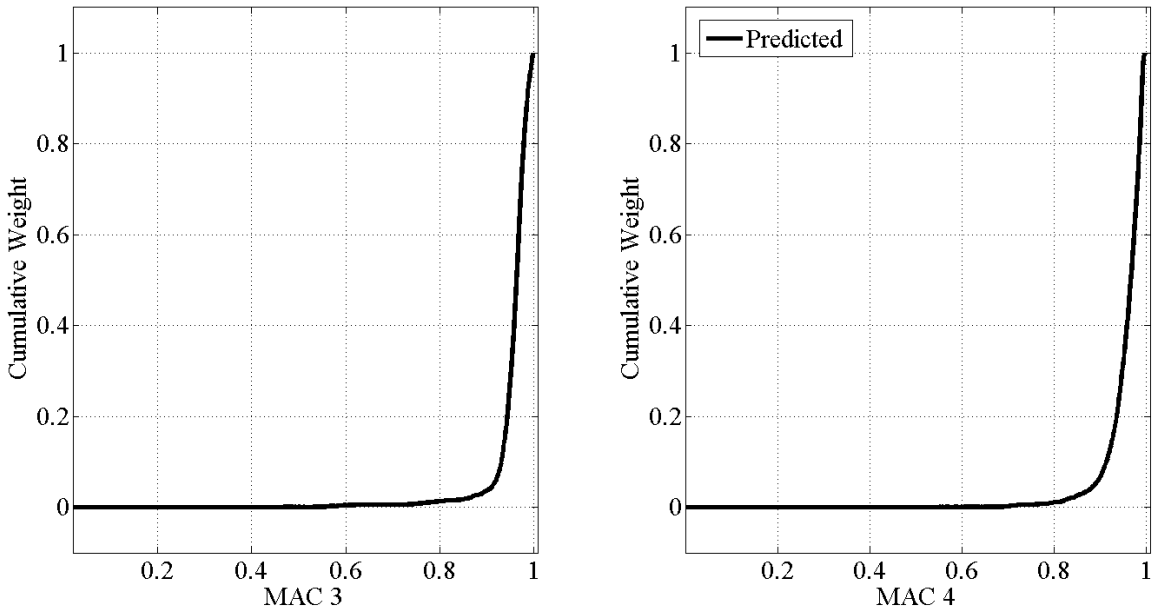

Figure 8-43: Response Prediction for Mode 3 and 4 MAC Value

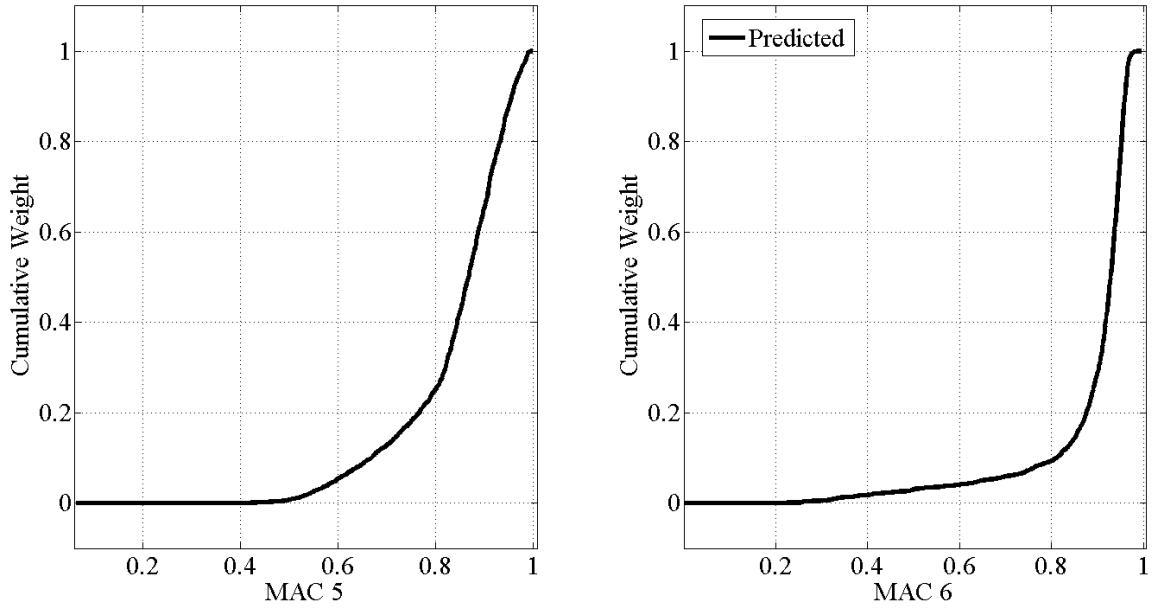

Figure 8-44: Response Prediction for Mode 5 and 6 MAC Value

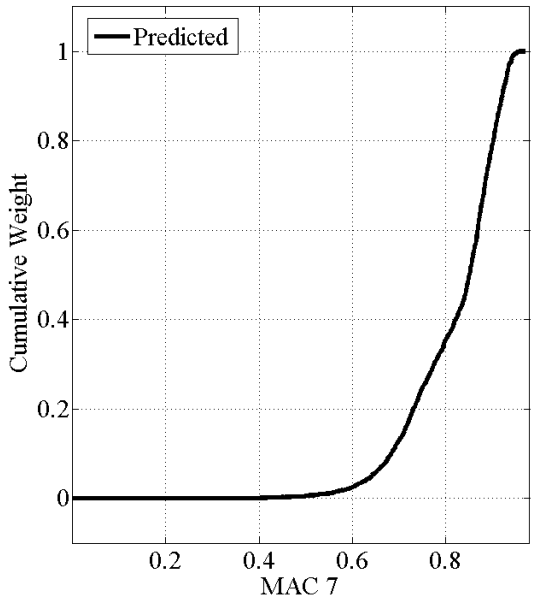

Figure 8-45: Response Prediction for Mode 7 MAC Value

The prediction distributions for displacement and strain at mid-span due to a mid-span load are fairly accurate and have a low variance. However, the predictions of the frequency and corresponding MAC values are much more variable. This is in line with the statement that when correlated building blocks exist, it is important to recognize that the structural attributes which influence the desired predictions must also be present in the structural attributes which influence the observed measurements. In this case, frequencies are heavily influenced by mass in addition to EI terms. While the updating process produces correlated values according to an EI term, they had no effect on the mass of the grid structure. Displacements on the other hand are not a function of mass, and were not affected by using strains as an updating quantity.

8.3.3.2. Weighing Models with Three Static Load Cases

To examine the effect of additional strain measurements, two more load cases were incorporated into the model weighing process: (1) 100lb load at Node 11 and (2) 100lb load at Node 18. These load cases were selected to remain consistent with those used for the study of using displacements as the observed quantity in MM St-Id. The results of using these observations on the model building blocks are shown in Figure 8-46. Once again, the elastic modulus has shifted to the right while the vertical stiffness was not influenced by the measurements at all. The longitudinal stiffness had high probability over a large stiffness range while the connection stiffnesses tended towards a more rigid connection.

The correlation between elastic modulus and longitudinal stiffness is apparent as the flexibility caused by lower values of elastic modulus can be compensated by accepting larger longitudinal stiffness values. However, at high values of E the structure is stiffer, thus any value for longitudinal stiffness will suffice. The correlation between these parameters was confirmed in the same manner as they were in 8.3.3.1. The prediction distributions corresponding to this study are shown in Figure 8-47 through Figure 8-55.

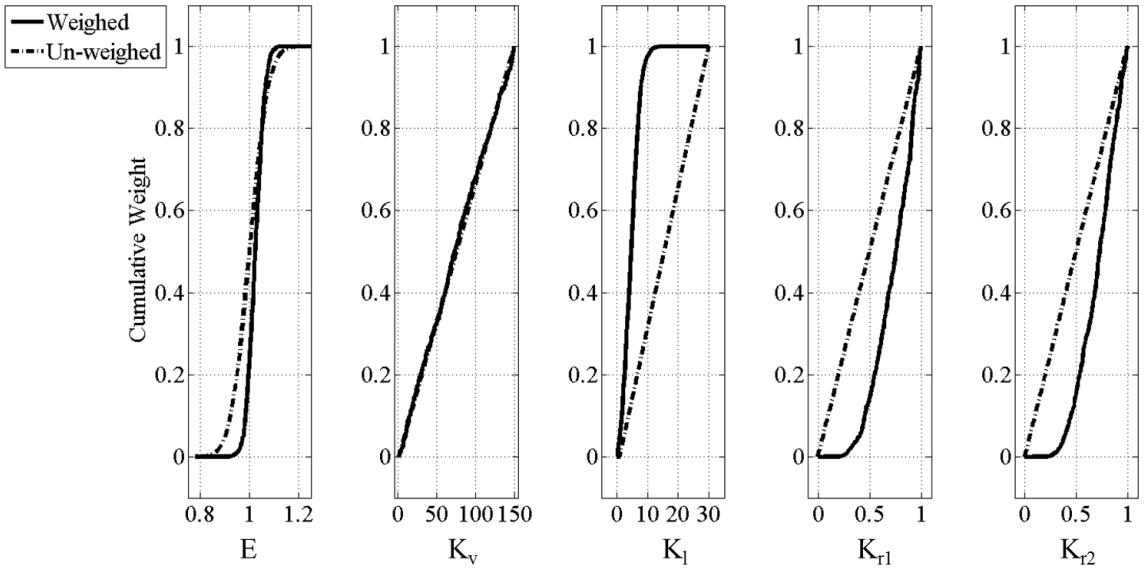

Figure 8-46: Effects on Building Blocks of Weighing the Models with Three Strain Load Cases

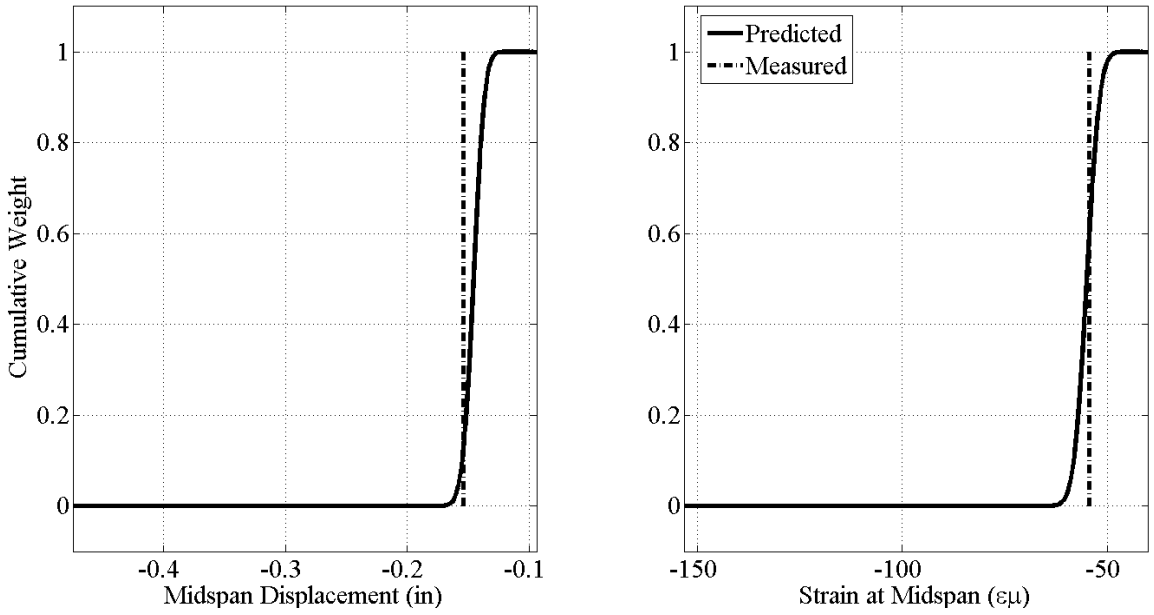

Figure 8-47: Response Predictions for Mid-span Displacement and Strain

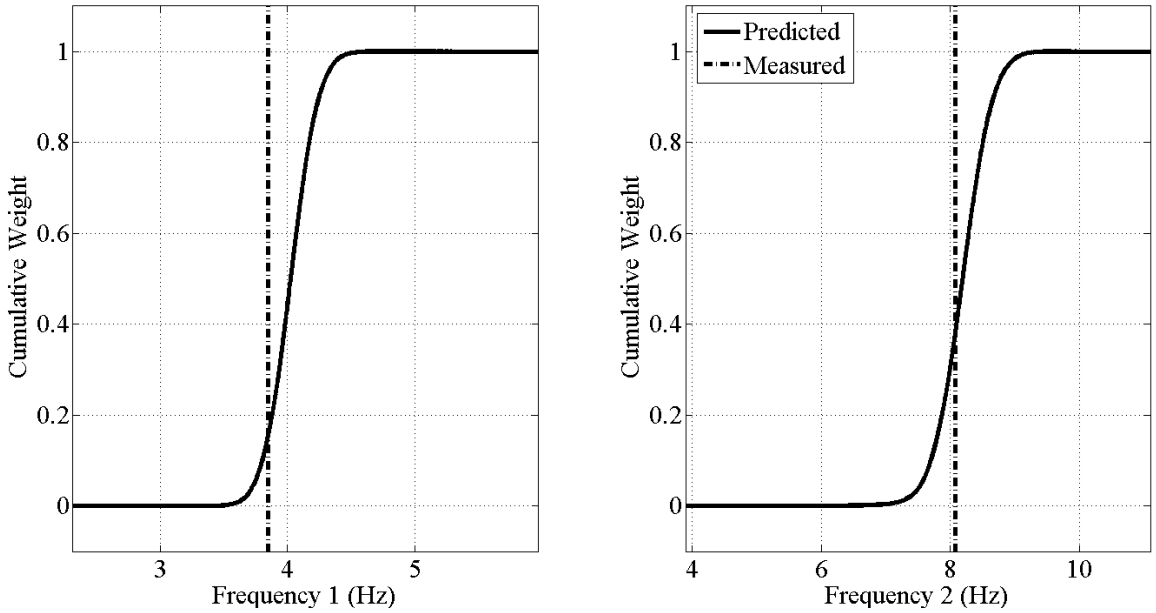

Figure 8-48: Response Prediction for Modes 1 and 2

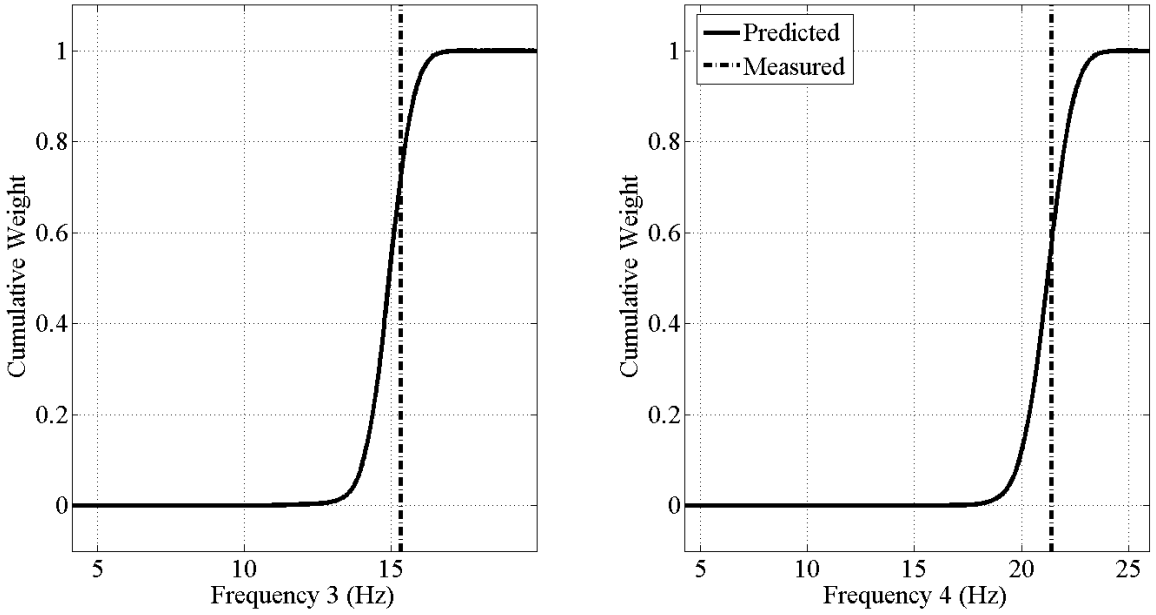

Figure 8-49: Response Prediction for Modes 3 and 4

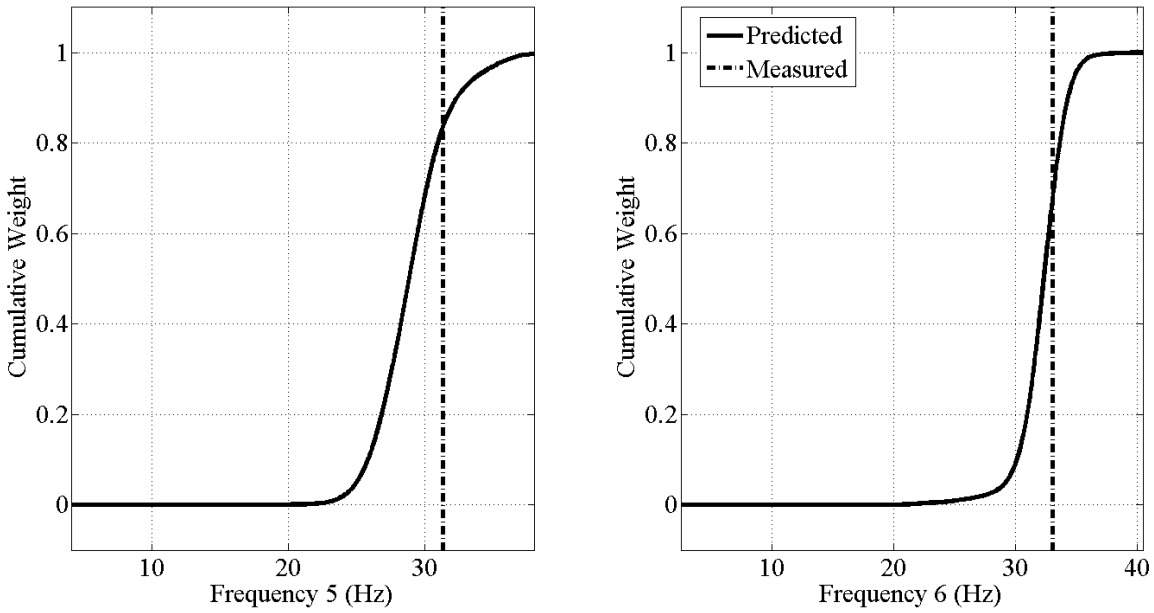

Figure 8-50: Response Prediction for Modes 5 and 6

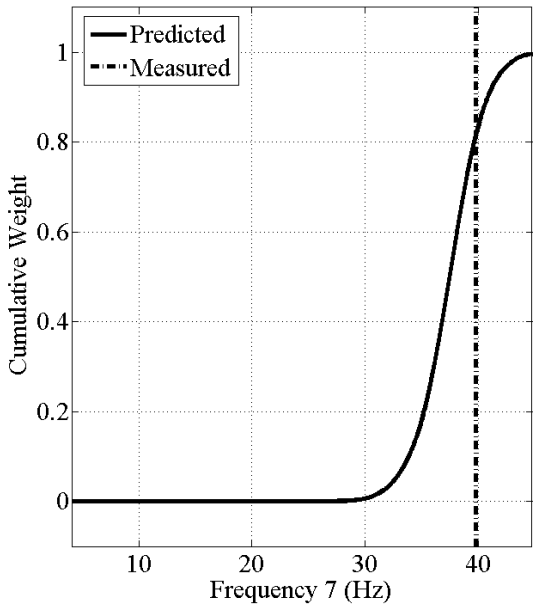

Figure 8-51: Response Prediction for Mode 7

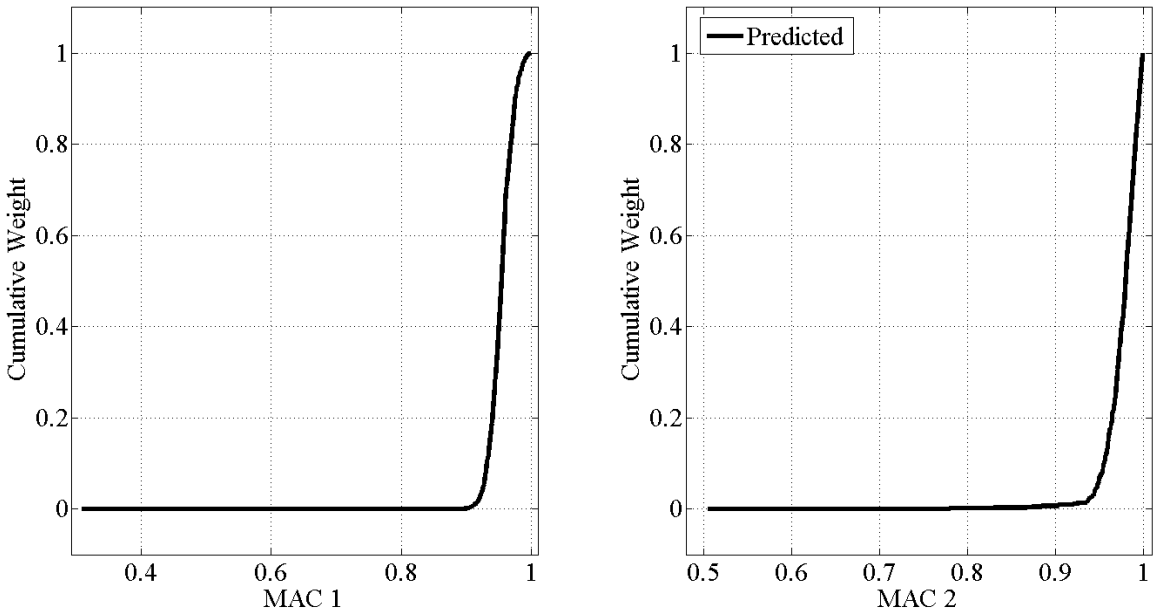

Figure 8-52: Response Prediction for Mode 1 and 2 MAC Value

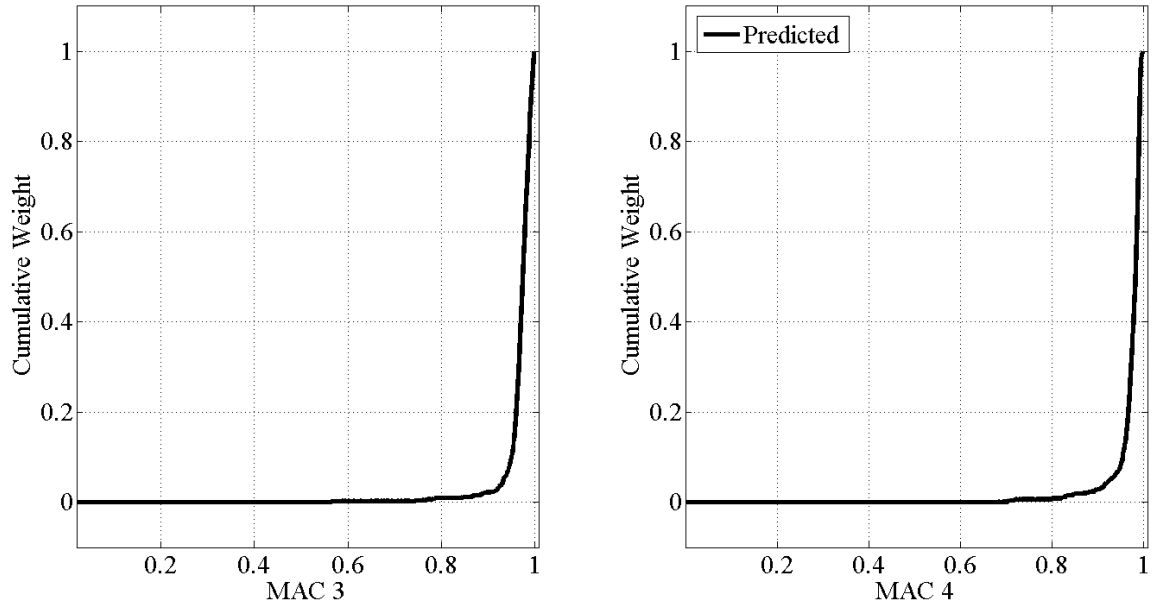

Figure 8-53: Response Prediction for Mode 3 and 4 MAC Value

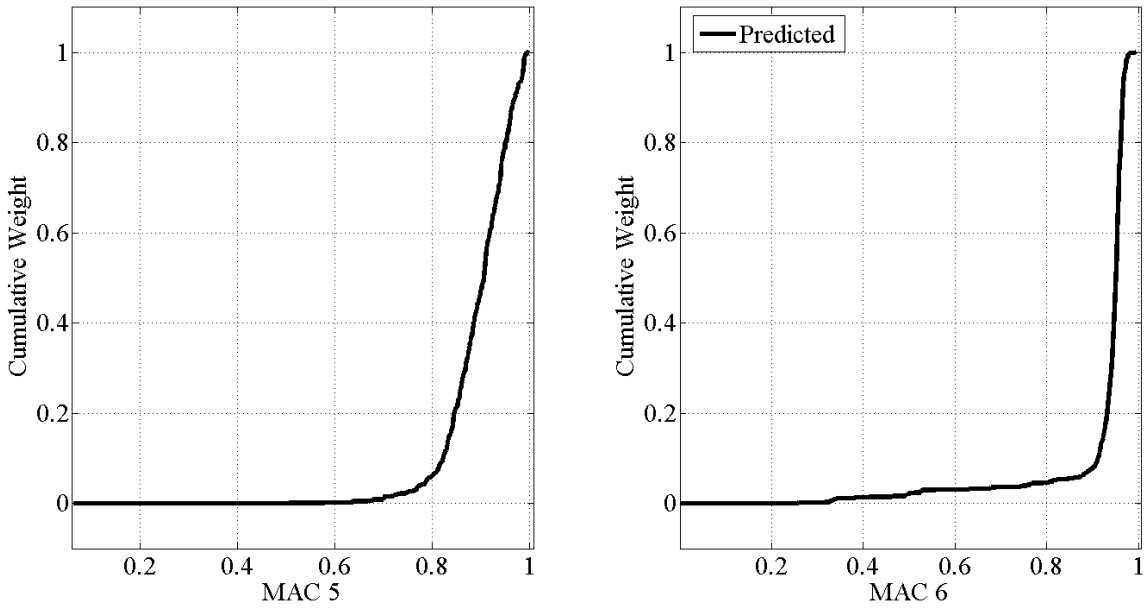

Figure 8-54: Response Prediction for Mode 5 and 6 MAC Value

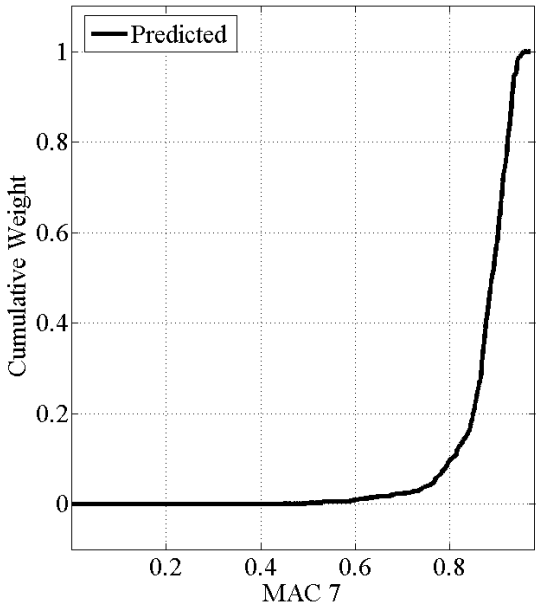

Figure 8-55: Response Prediction for Mode 7 MAC Value

As shown in 8.3.3.1, the effect of the building block correlation is evident in the frequency predictions and corresponding MAC values for the modes shown above. However, the predictions for both strain and displacement appear to be satisfactory in terms of accuracy and low variance. It also appears that additional load case information did not have an influence on this specific phenomenon; however it did slightly affect the distributions associated with strains and displacements.

8.3.4. Comparison and Conclusions on Selection of Experimental Data

When one is considering the type of measurement to make on a structure, it is imperative that the desired finite element model prediction is taken into account. It has been proven in 8.3 that the choice of experimental data has a direct outcome on the success of a response prediction, depending on the model building blocks used and the underlying mechanics of both the measurements and the desired prediction.

It is also imperative that the building blocks being used are sensitive to the measurements being used for the weighing, as shown in 8.3.3. For long span structures, due to the lack of access and a reference frame, displacements are almost impossible to measure. For that reason, long span structures are typically limited to vibration and strain measurements. Considering the inability of strain measurements to appropriately inform building blocks associated with boundaries, it is suggested that vibration data should be used for long span structures in predicting member force actions (especially dead load member actions) and global displacements.

8.4. Investigation into Weighing Observations Based on the Desired Prediction

During the process of investigating the different forms of weighing models based on various experimental observations, it was noticed that when natural frequencies were used that in some cases models were being weighed with high likelihood but which had poor predictions of the most fundamental frequency. The reason for this was found to be that other higher order modes, specifically modes five and seven of Structure 1, were heavily influencing the likelihood function. It turned out that this not only affected the quality of the models being able to match the measurements to which they were being compared, but it also affected the accuracy of the predictions of static responses, since these are also more correlated with the lower frequency responses.

At this point, it was decided that a means of weighing different experimental observations, based on what the desired predictions were, was needed. To effectively weigh the modes in a manner that would amplify the ability of the models to predict responses to static loading (displacements, strains, etc.) and to highlight the lower order modes (those which contribute most to the modal flexibility matrix), it was decided to explore an application where each observation was weighed based upon some means of physical justification. Considering that modes with high mass participation are typically captured very well with vibration testing techniques, it was first thought to weigh each mode based upon its modal mass. This approach, however, was not beneficial because the seven modes explored for Structure 1did not have varied quantities of modal mass to the degree where it would’ve had an effect on weighing each observation. The next physical quantity explored for application to observation weighing was the modal stiffness coefficient for each mode. This, however, turned out to be extremely stringent for the

first mode and greatly limited all other observations, greatly reducing the model space. Finally, it was decided to implement a means of representing both mass and stiffness in weighing each of the observations by its respective natural frequency, a function of both mass and stiffness.

In developing the weighed inherent standard deviations for each of the observations, careful consideration went into what the net effect of the modified inherent standard deviations should be for the group of observations as a whole. Much discussion went into the selection of an appropriate inherent standard deviation in Chapter 7, so it was necessary to justify how the quantity was going to be modified. It was decided to scale the inherent standard deviation based upon each observation's natural frequency in a manner where the average of all the inherent standard deviations for the observations was equal to 4%. This justifies the new values both in terms of physical meaning, since we are applying a strict requirement of matching the low order (and easily measured) modes and numerically in the sense that the 4% standard deviation is retained by enforcing the average of the group to be equivalent to this value.

The effect of the weighed inherent standard deviation is seen in Figure 8-56. It is clearly seen that by weighing the inherent standard deviation for each observation in this manner will force the MCMC algorithm to better characterize Mode 1 and subsequently relax in how well characterized the higher order modes are. This will prevent high order modes from dominating the sampling process and distorting the prediction values and deterministic building blocks. The modified values are also tabulated in Table 8-3.

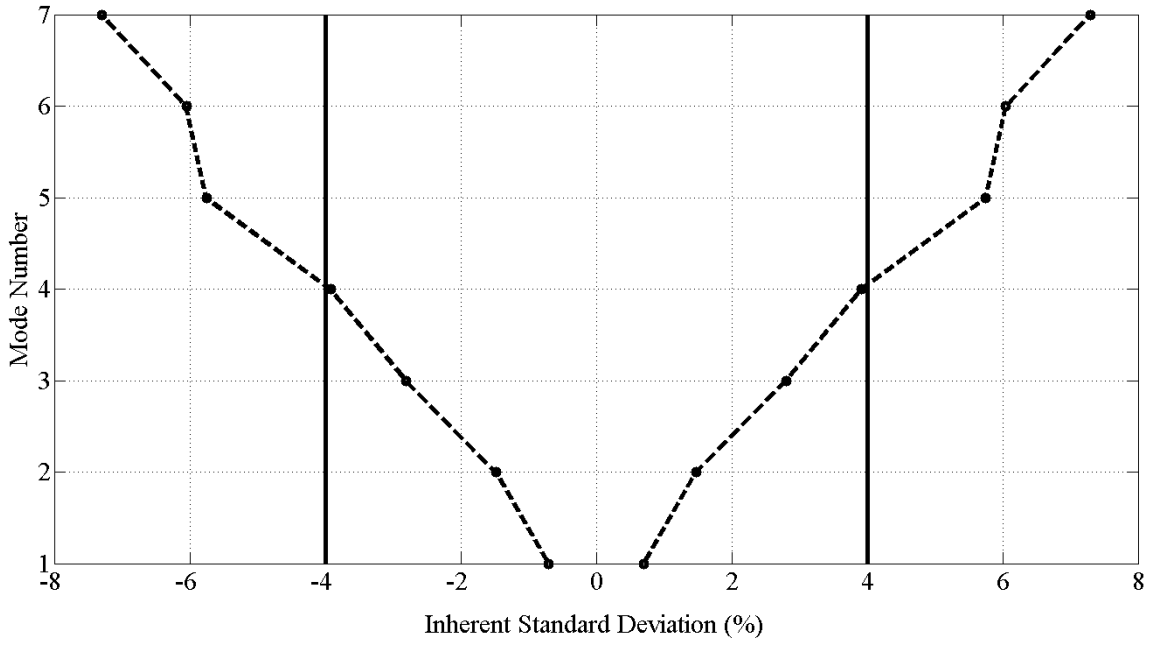

Figure 8-56: Modified Inherent Standard Deviations for Each Mode Compared Against 4% Value Used for Each Mode

Table 8-3: New Inherent Standard Deviations for Each Observation (%)

	Inherent Std.
Mode 1	0.7025
Mode 2	1.4774
Mode 3	2.8056
Mode 4	3.9167
Mode 5	5.7529
Mode 6	6.0510
Mode 7	7.2939

To highlight the effects of these weighing factors generated for the grid, a thorough MCMC analysis was carried out and compared to the results from Chapter 7.

8.3.4.1. Effect of Weighing Factors on MCMC Response Predictions to Static Loading

For this study, the set of measurements from Structure 1 were used as the observations in the probabilistic weighing process. The same five building blocks used thus far were also incorporated. The main goal of this section is to present the effects of applying the modified inherent standard deviation within the MCMC framework. First, the un-weighed standard deviations were used to generate a chain of models and corresponding prediction distributions. Then, the weighed standard deviations were applied and a separate chain of models was generated with its corresponding prediction distributions. The comparison of the sampling histories from these two analyses is presented in Figure 8-57 and Figure 8-58 while the weighing of the model building blocks for the weighed likelihood function is shown in Figure 8-59. It should be noted that the standard deviations reflecting the variability in the impact testing measurements were still added to the modified inherent standard deviation values defined above.

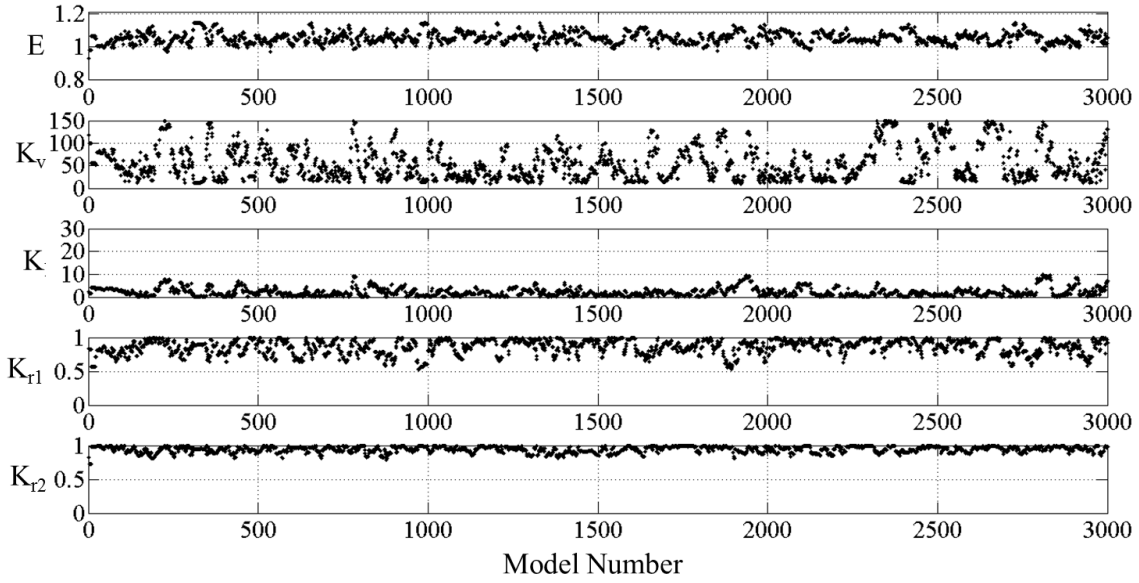

Figure 8-57: MCMC Samples Generated from the Modified Inherent Standard Deviation

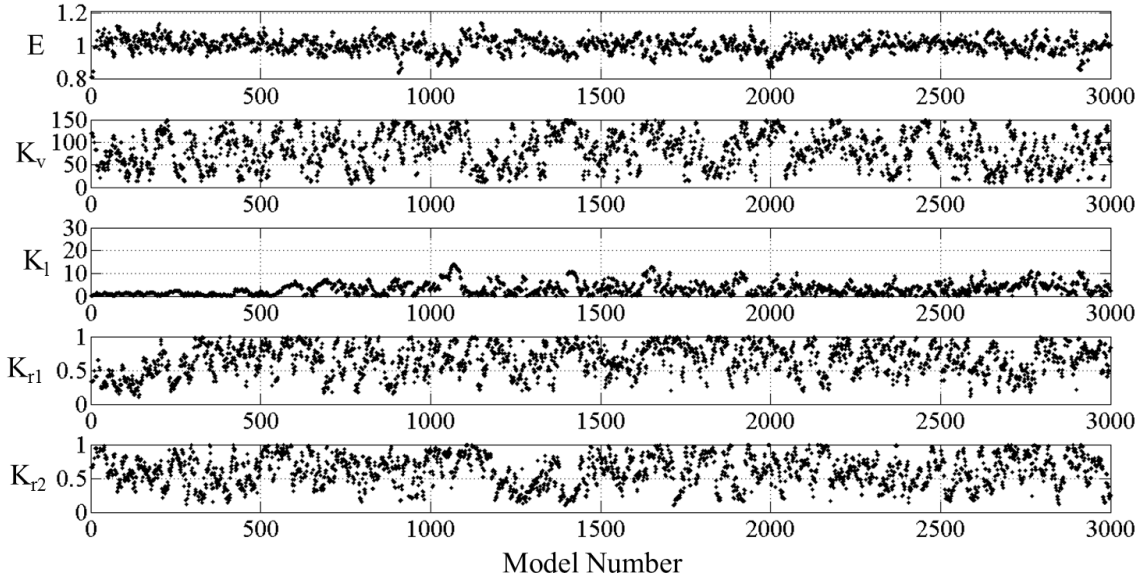

Figure 8-58: MCMC Samples Generated from the Modified Inherent Standard Deviation

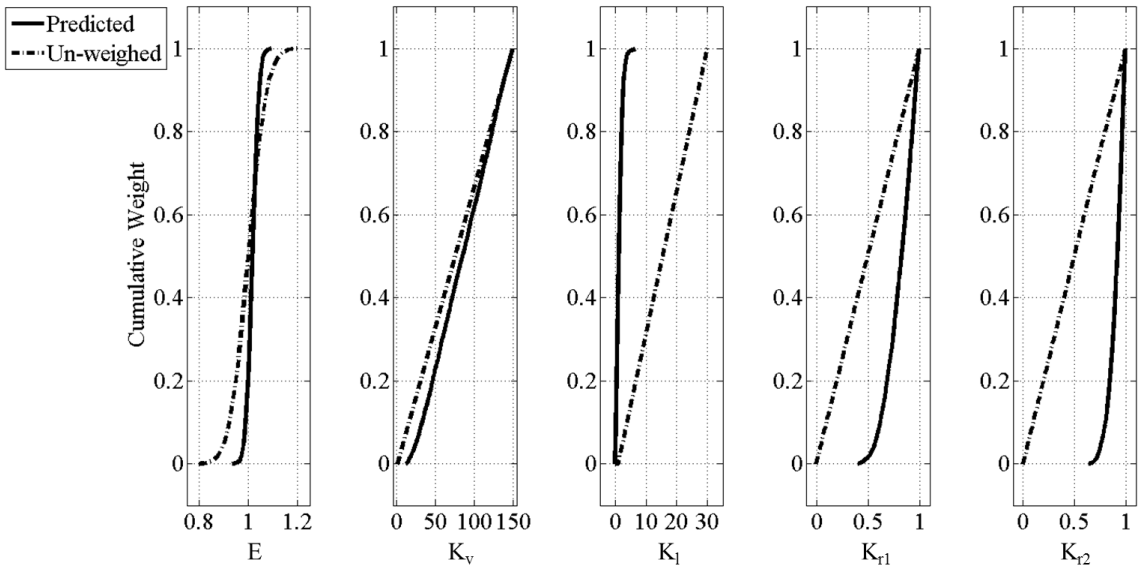

Figure 8-59: Effect of the Weighed Likelihood Function on the Model Building Blocks

As seen above, there is a great difference in the sampling of the building blocks by applying the weighing scheme described above on the inherent standard deviation. In the un-modified approach, the elastic modulus of steel is being sampled at a median just above the nominal value (as discussed in Chapter 7), while in the modified approach it is sampled around the nominal value and with a higher variance. This is seen again by looking at the marginal probability distributions for the building blocks, where it is clear that the elastic modulus of steel has shifted back to a value closer to its nominal value. In both cases, the vertical stiffness is sampled completely across its range and the longitudinal stiffness tends to be sampled near zero. The second major difference between the approaches is the sampling of the connection rigidity factors. In the un-modified approach, each factor is sampled tightly around 1.0 (reflecting the need to

match the higher order modes) while in the modified approach, the factors are sampled over a much more broad range, but still not sampled near the completely released connection type. It is evident that the modification process has had a clear impact on the sampling of models, so the next comparison drawn was the difference between response predictions and the difference between the frequencies of the sampled models (Figure 8-60 through Figure 8-64).

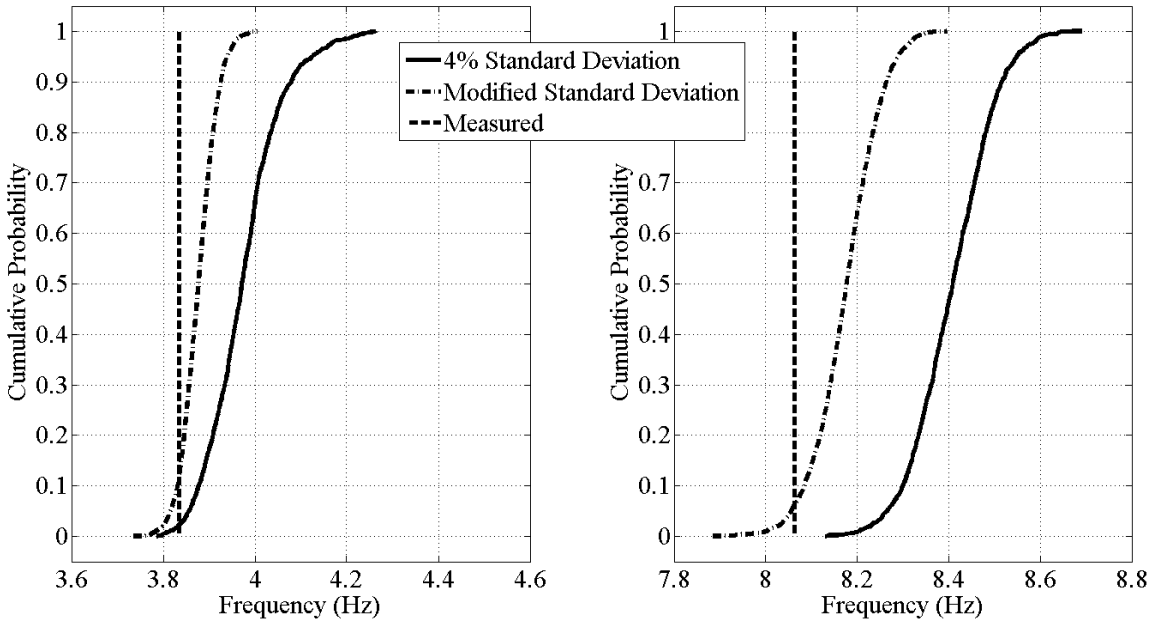

Figure 8-60: Frequency 1 (L) and Frequency 2 (R) Model Samples for Weighed and Un-weighed Standard Deviations

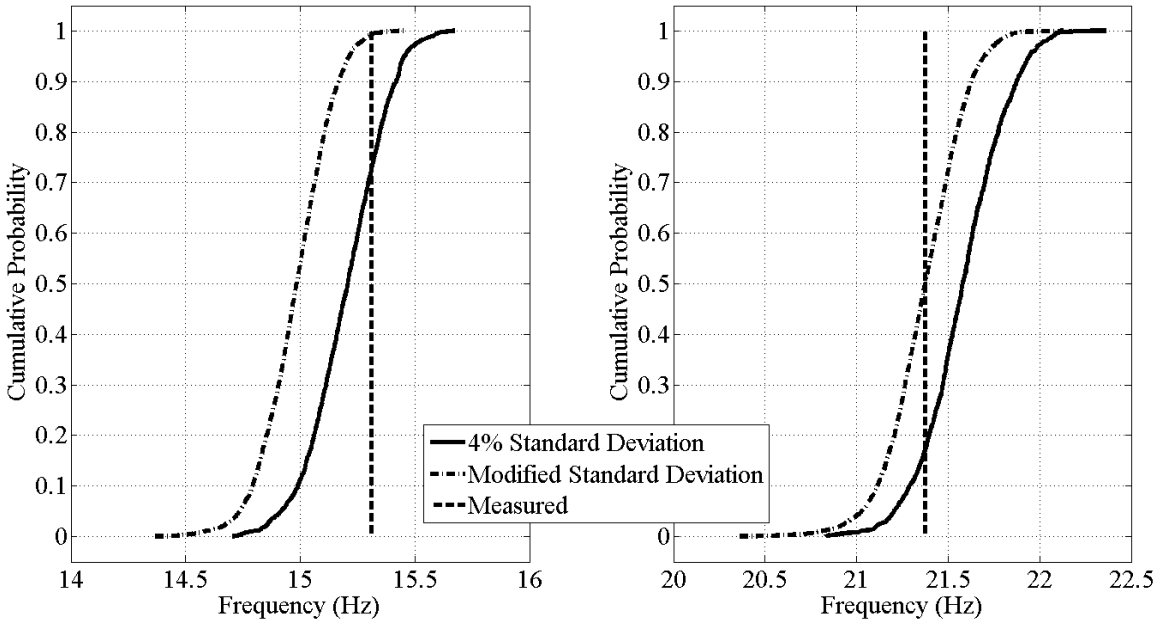

Figure 8-61: Frequency 3 (L) and Frequency 4 (R) Model Samples for Weighed and Un-weighed Standard Deviations

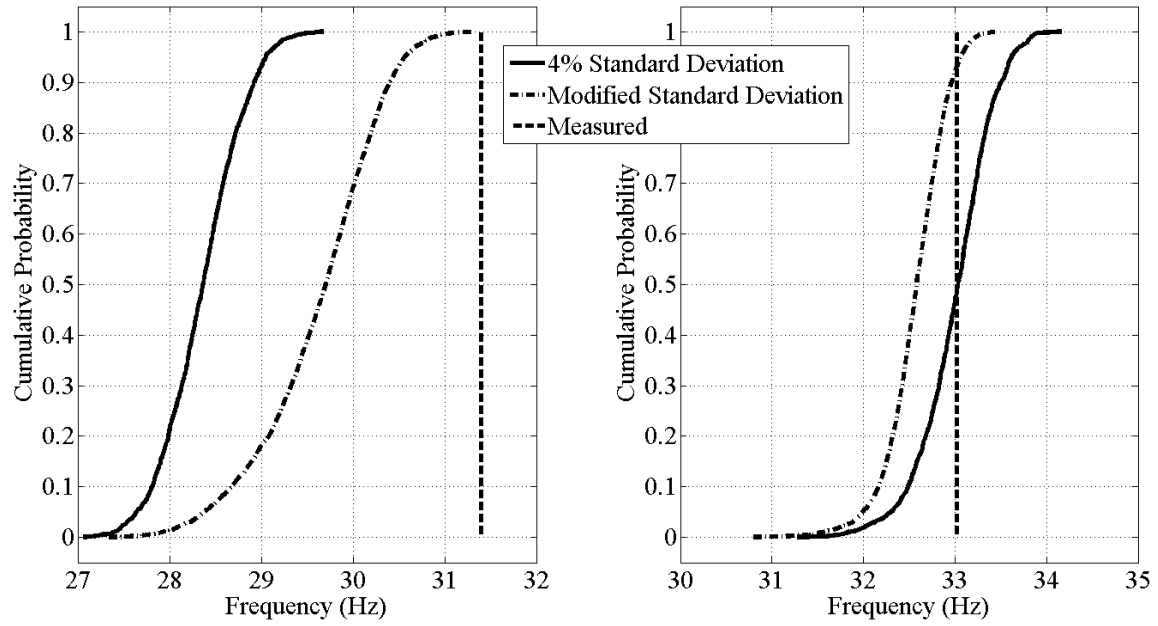

Figure 8-62: Frequency 5 (L) and Frequency 6 (R) Model Samples for Weighed and Un-weighed Standard Deviations

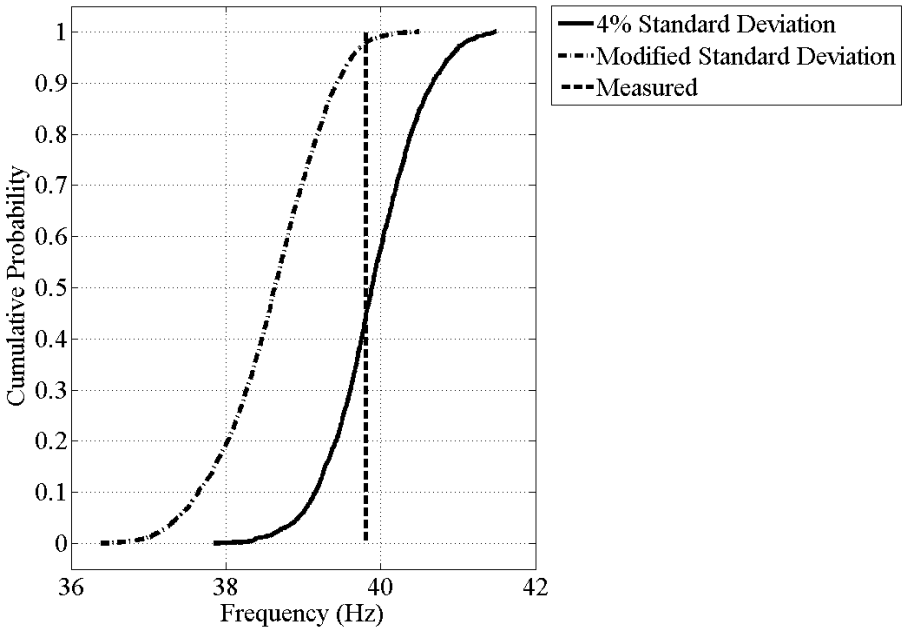

Figure 8-63: Frequency 7 Model Samples for Weighed and Un-weighed Standard Deviations

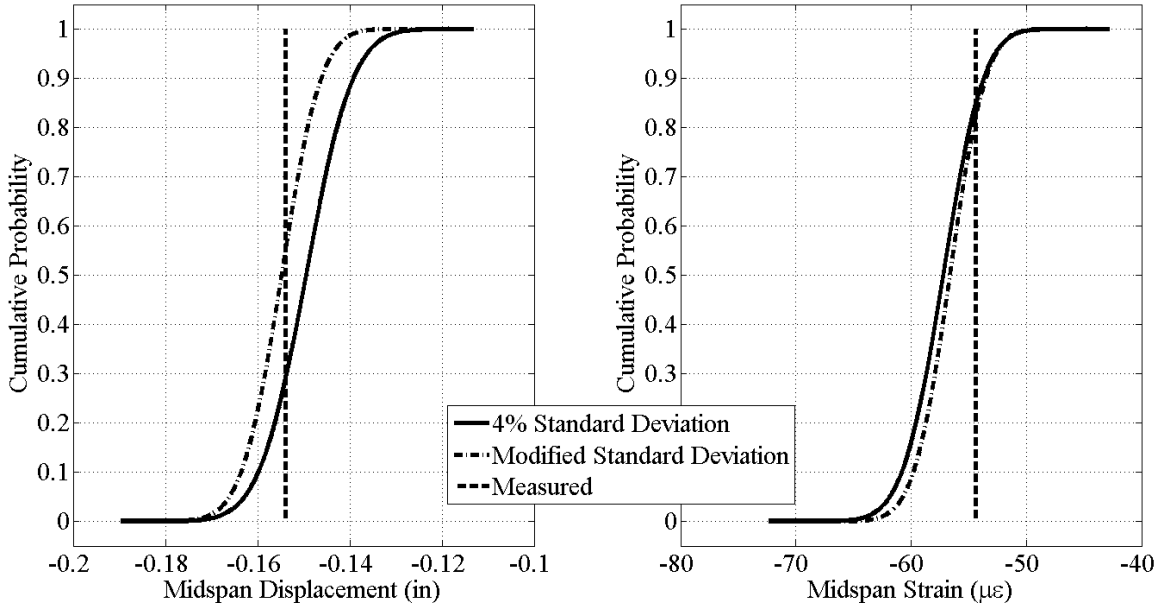

Figure 8-64: Mid-span Displacement (L) and Mid-span Strain (R) Model Predictions from a Mid-span Load for Weighed and Un-weighed Standard Deviations

The effect of the modified inherent standard deviations for each observation, based upon physical relationships, is clear and very effective in inspecting the above figures. In two cases (Mode 2 and Mode 5) the MCMC sampling approach outlined in Chapter 7 did not even characterize the measured frequencies at all. After weighing the inherent standard deviations based upon each mode's natural frequency, all of the distributions representing the frequency content of the accepted model set shifted, in some cases closer to the experimentally observed value and in other cases away from it. However, the important point to make is that collectively, the ability of the model set to characterize all seven natural frequencies improved tremendously.

Finally, in inspecting the prediction of strains and displacements, two key observations were made: (1) the distributions improved in their ability to predict the measured responses, and (2) the prediction distributions have much lower variance than the case with un-weighed inherent standard deviations. This critical finding highlights the fact that the analyst using the MM St-Id approach can specifically tailor the analysis to enforce more important information (or more reliably captured information) more stringently than less reliably captured information. It is important to recognize the fact that the inherent standard deviations representing each of the observations were not weighed arbitrarily, however were weighed in a manner which had a physical relationship to the problem being analyzed and retained an average inherent standard deviation of 4%, maintaining the overall uncertainty in representing this problem. It is envisioned that many weighing strategies could be implemented within a MM St-Id framework depending upon the type of observations employed and the desired outcome. In this example, the frequencies and modeshapes were weighed in a manner which better predicted global static responses.

However, it is possible that by weighing high order modes more stringently and low order modes less stringently, applications such as damage detection could be employed within a MM St-Id framework since it is known that damage is more readily identifiable in high order modes where the shapes are more sensitive to localized changes in stiffness. The intent of this section is to not develop a damage detection algorithm, but to demonstrate the wide range of applicability of the MM St-Id approach in general, thus the damage detection example will not be further evaluated, but recommended for further research.

CHAPTER 9: REVERSIBLE JUMP MARKOV CHAIN MONTE CARLO APPLICATION TO MM ST-ID

The fundamental idea of the Multiple Model Structural Identification method was to be able to infer certain responses using simulation models and experimental observations in a rational and quantitative way in the presence of uncertainty. This method has been introduced and developed in the previous chapters; however there has not been a discussion on the validity of one model building block set versus another. Until this point, these types of analyses would have to be done separately, and then compared at the end, if possible. What was lacking was a single method able to explore different model forms (resolution, element type, software package) in addition to different forms of building block spatial resolution.

To accomplish such a desired result, it was necessary to implement a method which was able to sample model building blocks of different dimensions. A dimension of a model building block set to this point has been defined as the number of model building blocks sampled to generate the model space. For example, the grid thus far has had a building block dimension of five (E, K_v, K_l, K_{r1}, K_{r2}). There were multiple assumptions with this configuration of building: (1) the vertical stiffness of the boundaries was the same for all six supports, (2) the longitudinal stiffness was the same for all six supports, and (3) the distribution of the two rotational stiffness factors was consistent and representative of the actual physical grid model.

In a traditional MCMC approach, these assumptions have to be accepted upfront. However, an advanced approach was developed which allows for trans-dimensional

moves within the model space. This approach, which has been termed Reversible Jump Markov Chain Monte Carlo (RJMCMC), was first implemented by (Green 1995) and utilized mainly in, but not limited to, Bayesian model selection problems (Ching and Chen 2007). In many of these applications, there were either a set of accepted (yet distinct) models that could describe a similar phenomenon, or a series of different ways that a base model could be parameterized. For example, within the field of weather forecasting it is common to use many different formulations of meteorological models to develop the likelihood of weather events. However, this begs the questions: which model is more (or the most) appropriate? For the grid structure, this translates into a question such as: Is a unique vertical stiffness at each support required or can these parameters be lumped together? When there is not enough information in an a priori sense to properly inform this decision, the use of RJMCMC methods to sample a set of plausible models can be quite useful.

9.1. Introduction to RJMCMC Methods

A common challenge in statistical problems is that the number of unknowns is often an unknown itself (Green, Hjort et al. 2003). This realization led statisticians to develop a sampling method capable of not only sampling a model with defined unknowns, but one which could generally sample any model M_k with parameter vector θ_k where k denotes the model indicator. Each of these models is not defined as a set of different building blocks, as models have been defined thus far, but can be defined as having different dimensions of parameter vectors.

The general framework for the RJMCMC was developed within the Metroplis Hastings sampling algorithm. As described earlier, the MH sampling algorithm describes a class of samplers within a MCMC problem. New samples are generated from proposal distributions and accepted or rejected according to certain criteria. After a certain number of samples (termed the burn-in period) all subsequent samples are considered to be drawn directly from the target distribution.

In the RJMCMC methodology, the same basic principle is held, except instead of drawing only a proposed sample, the algorithm also proposes a dimension move. A dimension move would then literally move from one model form (perhaps a model with five building blocks) to another (perhaps with ten building blocks). Additionally, a dimension move could consist of a change of model form, or software in addition to spatial resolution of building blocks. This proposed move and corresponding proposed sample within that model is then analyzed according to defined criteria and either accepted or rejected. Once again, if a move is rejected the algorithm remains at the current position and tries again. This process is repeated until the sampling has converged on the target distribution of the model space, now multi-dimensional.

Some key differences in RJMCMC sampling and traditional MCMC sampling is that the acceptance probability has been modified to maintain the properties of proper Markov chains. Also, transformation matrices need to be constructed to jump from one dimension to another. For example, if one model had a single building block representing the vertical support stiffness for the grid and a second model had six unique building blocks

representing the six vertical support stiffnesses, then a transformation between each of these models needs to be formulated.

An advantage of adopting this type of sampling scheme is that the burn-in period for highly parameterized models could be drastically reduced. If multiple levels of building block spatial resolution are represented in various base models, then the less parameterized models could be used to account for a majority of the burn-in period and then if the more parameterized model becomes more likely with certain independent building blocks, then it will reach that point in a far shorter period than if traditional MCMC had been used for that case.

A second advantage seen is that not only can different spatial resolutions of building blocks be represented, but different model forms altogether can be explored. For example, a solid element model, shell element model, frame element model and another frame element model analyzed in a separate FE software package could all be incorporated into one analysis. By taking all of these factors into account, this approach is attempting to reflect the true uncertainties at play and then infer immeasurable responses/attributes in a rational manner.

9.2. Framing the Grid in a RJMCMC Framework

This section will provide a detailed explanation of the implementation of the RJMCMC method. To aid in this explanation, the implementation of this method to the DI3 grid study will be discussed in detail. This section will be divided into 5 subsections: (1) selection of base models and assignment of building blocks, (2) development of

algorithm for sampling and computing acceptance probability, (3) development of dimension transformation equations, (4) preparation of finite element models, (5) monitoring analysis.

9.2.1. Selection of Base Models and Corresponding Building Blocks

The first phase within an RJMCMC approach is to conceptualize the various base models to be used in the analysis. A base model is defined as a set of fixed dimension building blocks, meaning that a single base model serves as the foundation for sampling of a set of building blocks. The number of base models selected depends on the amount of uncertainty placed on the type of model, spatial resolution of building blocks, or number of building blocks in general.

The grid finite element model was considered sufficiently represented with frame elements, so including an analysis with shell or solid element models would not be necessary. A main form of uncertainty with the grid model was in the spatial resolution of various building blocks. Namely, the distribution of building blocks representing vertical stiffness, longitudinal stiffness, and the connection rigidity factors, were initially idealized as being consistent over the locations where they were assigned. However, there is no prior knowledge that would necessarily enforce this type of building block assignment; until this point a dense resolution of building blocks was seen as being unnecessary given the great number of model executions it would require.

Three base models, A through C, were identified for the grid, all variations of different refinement of the initial five building blocks used to this point. These models are

described in terms of their building block dimensions in Table 9-1 and presented visually in Figure 9-1 through Figure 9-3.

Table 9-1: Base Model Building Block Assignments for RJMCMC Analysis

	Instances of Building Blocks				
Model	E	K_v	K_l	K_r	Total
A	1	1	1	2	5
B	1	2	3	4	10
C	1	6	3	12	22

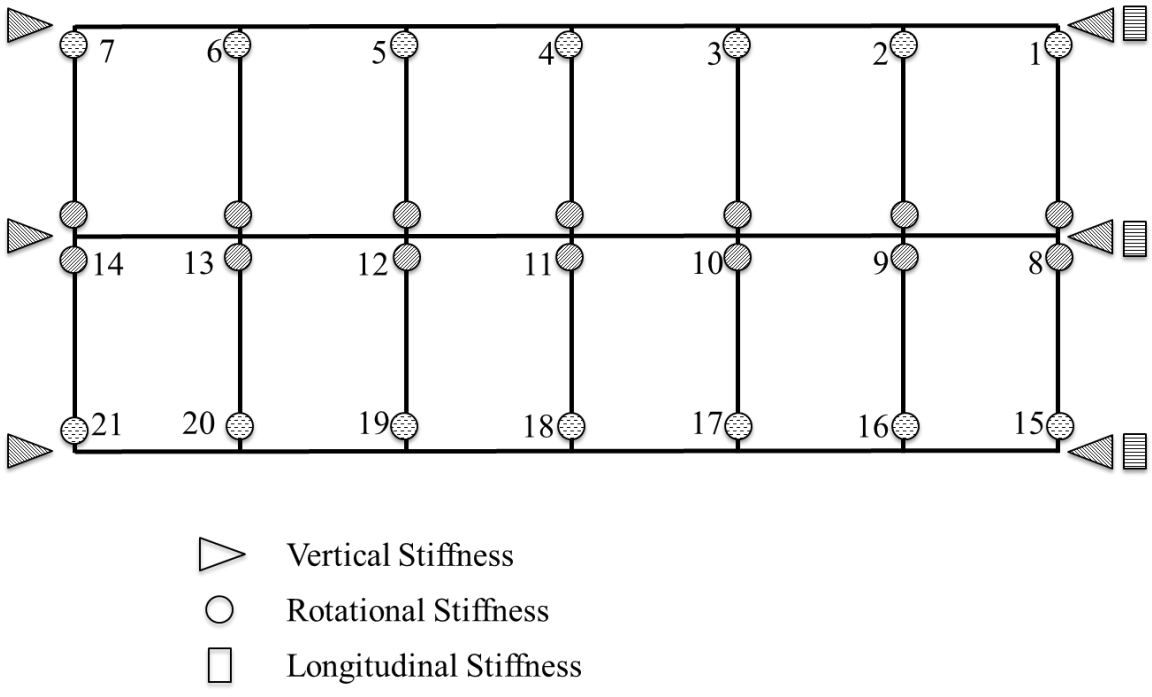

Figure 9-1: Configuration for Base Model A

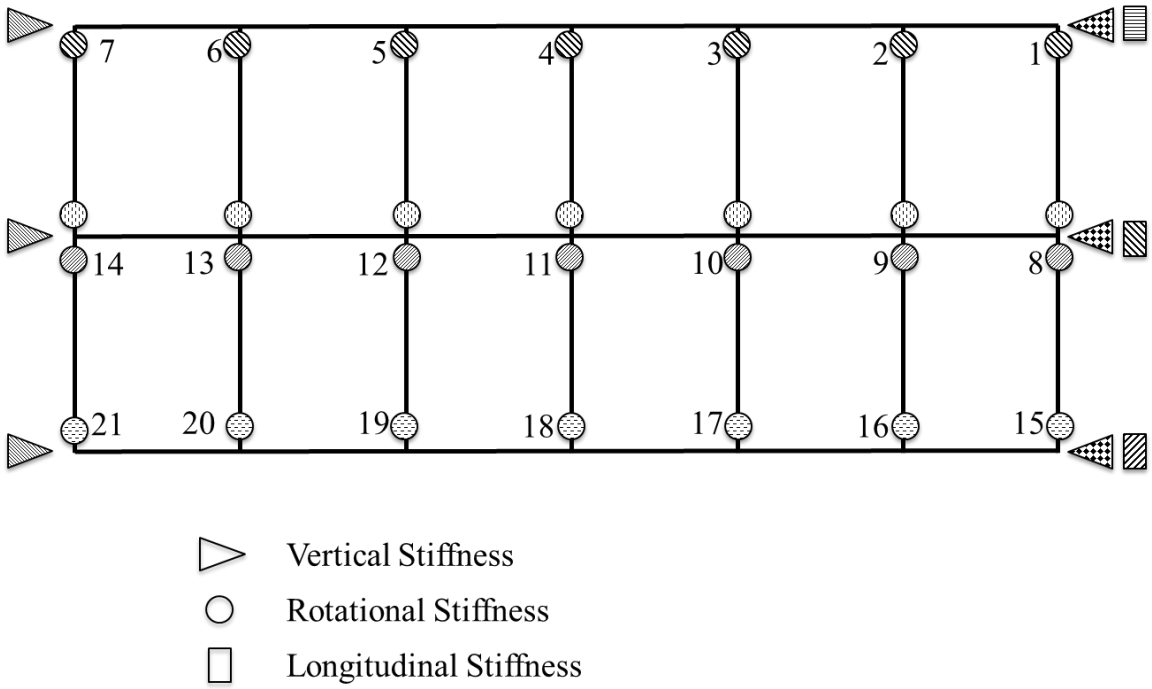

Figure 9-2: Configuration for Base Model B

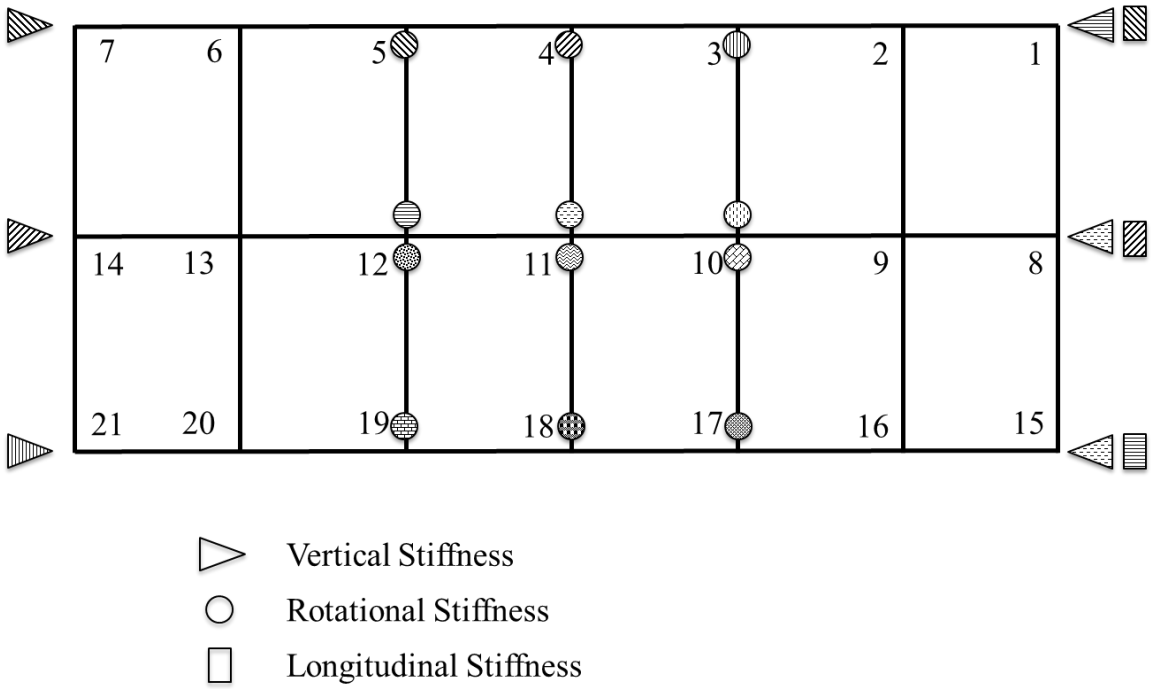

Figure 9-3: Configuration for Base Model C

As seen in the figures above, the three different base model configurations consist of a variety of spatial distributions for a set of the building blocks. Configuration A is the standard five building block model used thus far in development purposes. Configuration B explores the effects of allowing independent longitudinal springs at the supports in addition to splitting the vertical stiffness building block into two independent groups.

The third configuration, base model C, considers independent sampling of each of the building blocks at the supports in addition to a reduced set of independent rotational stiffness factors. Configuration C by far has the most freedom in terms of being able to match the experimental observations by manipulating the building blocks. However, in an a priori sense, it is not sure that this level of building block discretization is needed.

9.2.2. Development of Algorithm for Sampling and Accepting Models

Once the base model configurations have been identified, the next step required in the RJMCMC analysis is to configure the algorithm for sampling both the models and building blocks. The overall steps for the algorithm are listed below:

1.) Initialize each of the chains (one for each model) with random starting values.
2.) Randomly select an initial model and analyze with chain starting values.
3.) Evaluate likelihood of model and store predictions.
4.) Automatically accept first model.
5.) Propose a change to the model indicator variable.
6.) If the same model is selected, analyze model.
7.) If a new model is proposed, transform the variables to the proper dimension and analyze.
8.) Compute the acceptance probability and determine whether to accept or reject.
9.) If accept, store chain samples and repeat steps 5-10.
10.) If reject, retain previous values of chain and repeat steps 5-10.

While this list seems fairly straightforward, there are distinct differences within the theory of RJMCMC that has not been needed so far in the traditional Metropolis Hastings algorithms used thus far. The first major difference is the proposal of a change in the model indicator variable. The second major difference is the transformation of variables to different dimensions, while the third major difference lies in the computation of the acceptance probability for each model. Each of these three major differences will be discussed in detail, with supporting theory from literature, in three subsections.

9.2.2.1. Proposing a Change in Model Dimension

In standard MCMC practices, a proposed move is typically only in the form of a change in the model building blocks. However, with RJMCMC methods, the proposal is a two-step process. First, a change in the model indicator must be proposed, and then based on that selection a new sample is proposed. The next section will discuss how a sample is generated in a different base model from the current base model, however this section will discuss how this change is proposed and how a new sample is generated if the same model form is proposed from the current model.

There have been contributions towards the development of efficient proposal schemes within a RJMCMC framework; however a proposal scheme was developed to have the properties desired for this application. The proposal scheme was developed to have two main features: (1) for any given position within the chain, the algorithm has a 68.2% (one standard deviation) chance of staying in the current model, and (2) for any given position within the chain, the algorithm has equal probability of jumping to any other base model.

The probability of a jump can therefore be defined as equal divisions of 32.8%, depending on how many total base models exist.

For the DI3 grid model, there are a total of three base models. At each position within the chain, there is a 68.2% chance of staying within the same model and a 16.4% chance of jumping to either one of the remaining base models. This is advantageous because the algorithm is promoting an increased probability of gaining information within the same model before jumping to a separate model form. The success of this approach will be evaluated in the results of the analysis of the DI3 grid.

To implement this sampling and proposed model jumping, an indicator was assigned to each model and tracked throughout the process. If model A was selected as the initial model and accepted, its indicator would be centered within a standard normal distribution. The remaining indicators were then placed on the tails of the standard distribution, adjacent to the region assigned, one standard deviation, to the current model indicator. A random number was then drawn from a standard normal distribution, and if this number fell within the regions associated with any of the three models then that would define the proposed move.

This same sampling scheme could be implemented for more than three models fairly straightforward as well. Instead of a two dimensional standard normal, a multivariate normal distribution is implemented. The current model is assigned a region encompassing a region with probability equal to 68%, as done previously, and the remaining models are assigned regions of equal probability outside of one standard deviation of the mean. It should be noted that while a probability of staying within the current model was defined

as 68% for the DI3 grid, this is able to be modified by the user based on desired input. Additionally, in this case each model is given equal likelihood of being jumped to. In an a priori mind frame, this is reasonable since it is not clear upfront which model is more likely. However, the user can modify the probability that a given model is selected if, for instance, the analysis time is much longer than the other models and it is at the point where it is prohibitive to the method. This type of scheme was implemented for the three grid models as a demonstration tool in Figure 9-4.

In this demonstration, the current model is taken as Model A. All samples represented by a period represent the case where the algorithm would stay within the same model. All circles represent the case where a move to Model B would be proposed and all crosses indicate the case where a move to Model C would be proposed. It is easy to see that using this type of formulation lends itself easily to the case where many base models exist, as the exterior region is divided amongst the models where a move is to be proposed.

As each sample is generated, the algorithm will need to be able to identify which region (which model) is associated with that sample. For this demonstration, the region was identified by determining the distance from the origin, by square root sum of squares, as well as the angle from the positive x axis. Any model falling within the distance defined by the user will signify that the proposed model will stay in the current base model. Any samples falling outside of this region will then by identified by its angle from the positive x axis. The various proposed base models would need to have a region defined in terms of angles as well. In this case the two regions were defined by two 180 sectors.

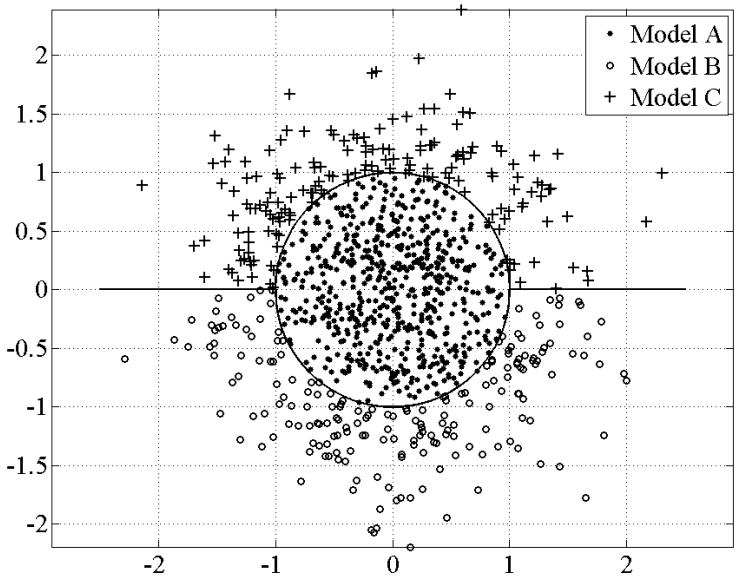

Figure 9-4: Monte Carlo Simulation of Sampling from a Current Position in Model A

When a sufficient sampling scheme has been defined, the next step within developing the RJMCMC sampler is to define how the building blocks from one model will be transformed into building blocks for another model while losing as little information gained as possible.

9.2.2.2. Development of Transformation Equations

The success of the RJMCMC method relies heavily upon the ability to meaningfully transfer samples between model forms. As mentioned, one of the potential benefits of this approach is that lower parameterized models could be used to more quickly inform

highly parameterized models. However, the ability of such an application to accomplish this requires an efficient transfer of information learned in one model to another proposed model form.

In order to transform a set of building block samples from one dimension to another, a series of transformation equations must be generated. There are many ways of transforming variables from one dimension to another, but a specific pattern was followed in this chapter. The transformation equations utilize random numbers termed jump variables. These variables modify the building block sample in one model space randomly as it is transferred into another dimension. This is done to ensure rapid mixing, for if the exact same set of samples were transferred into another dimension, there would be very little information gained. The jump variables are drawn from a distribution similar to the proposal distribution for the traditional MCMC approach. They are then formulated within the transformation equations in changing the sample dimension.

For this implementation, a consistent approach was used in generating the transformation equations. For building blocks such as the elastic modulus of steel, the transformation equation is straightforward and is equal to the addition of a random variable. However, for building blocks which change dimension, care must be taken in constructing meaningful jump equations.

The equations for jumping from Model A to Mode B are listed below in Eq. 9-1 through Eq. 9-10.

$$E_B = E_A + u_{a1} \quad \textbf{Eq. 9-1}$$

$$K_{v1B} = K_{vA} + u_{a2} \quad \textbf{Eq. 9-2}$$

$$K_{v2B} = K_{vA} + u_{a3} \quad \textbf{Eq. 9-3}$$

$$K_{l1B} = K_{lA} + u_{a4} \quad \textbf{Eq. 9-4}$$

$$K_{l2B} = K_{lA} + u_{a5} \quad \textbf{Eq. 9-5}$$

$$K_{l3B} = K_{lA} + u_{a6} \quad \textbf{Eq. 9-6}$$

$$K_{r1B} = K_{r1A} + u_{a7} \quad \textbf{Eq. 9-7}$$

$$K_{r2B} = K_{r1A} + u_{a8} \quad \textbf{Eq. 9-8}$$

$$K_{r3B} = K_{r2A} + u_{a9} \quad \textbf{Eq. 9-9}$$

$$K_{r4B} = K_{r2A} + u_{a10} \quad \textbf{Eq. 9-10}$$

As seen in these transformation equations, generating samples for Model B from a sample of Model A, a unique random variable is used for each building block in Model B. An important requirement of RJMCMC is that the transformation equations must meet dimension-matching criteria, in order to preserve the reversibility of the process. This dimension matching requirement is as follows: dim (θ_A) + dim (u_a) = dim (θ_B) + dim (u_b). This dimension matching requirement ensures that the transformation matrix is invertible, thus guaranteeing that the reverse transformation is possible.

As seen in the equations listed above, there are ten random variables used with the five model building blocks for Model A. This gives a total dimension of the transformation of

fifteen. Considering there are only ten equations on the left-hand side, an additional five equations are needed to represent the random variables of the reverse process. While it may seem that a computed number is not random, this computation is only used to verify that the process is reversible, and that there is a positive probability of eventually returning to the same sample over the long run. Additionally, these reverse jump variables are used in the computation of the acceptance probability.

To compute the equations for the remaining five variables, the equations for the reverse transformation must be defined. Then, using linear algebra and substitution the five equations for the random variables needed for the transformation above can be computed. These are the only equations for random variables that need to be generated, as those needed for the reverse transformation can be found by inverting the transformation matrix for the forward transformation. With this in mind, it is recommended that the transformation from the most model with least building blocks to the model with the most building blocks is done first. This ensures that the fewest number of equations need to be solved for, while those associated with the reverse process need only to be checked for validity.

The equations for the reverse transformation were designed so that in any instance where multiple building blocks were being condensed to a single building block, the mean was taken of the multiple building block set and then summed with a random variable. This technique can be seen in the reverse transformation equations listed below in Eq. 9-11 through Eq. 9-15.

$$E_A = E_B + u_{b1} \quad \textbf{Eq. 9-11}$$

$$K_{vA} = \frac{1}{2}(K_{v1B} + K_{v2B}) + u_{b2} \quad \textbf{Eq. 9-12}$$

$$K_{lA} = \frac{1}{3}(K_{l1B} + K_{l2B} + K_{l3B}) + u_{b3} \quad \textbf{Eq. 9-13}$$

$$K_{r1A} = \frac{1}{2}(K_{r1B} + K_{r2B}) + u_{b4} \quad \textbf{Eq. 9-14}$$

$$K_{r2A} = \frac{1}{2}(K_{r3B} + K_{r4B}) + u_{b5} \quad \textbf{Eq. 9-15}$$

As shown above, the building blocks which were divided into multiple representations in Model B have been averaged and summed with a random change to generate the building blocks for Model A. Note that K_{r1B} and K_{r2B} correspond to K_{r1A} in that they both represent the exterior connection types, while K_{r3B} and K_{r4B} correspond to K_{r2A} in that they both represent the interior connection types. It is important to ensure that the transformation equations physically make sense; otherwise little is gained from the process.

Now that the reverse transformation equations have been generated, the five equations for the random variables for the forward transformation can be found using algebra and substitution. These equations are listed below in Eq. 9-16 through Eq. 9-20.

$$u_{a1} = -\frac{1}{2}u_{b1} \quad \textbf{Eq. 9-16}$$

$$u_{a2} = -\frac{1}{2}u_{b2} - \frac{1}{2}u_{b3} \quad \textbf{Eq. 9-17}$$

$$u_{a3} = -\frac{1}{3}u_{b4} - \frac{1}{3}u_{b5} - \frac{1}{3}u_{b6} \quad \textbf{Eq. 9-18}$$

$$u_{a4} = -\frac{1}{2}u_{b7} - \frac{1}{2}u_{b8} \quad \textbf{Eq. 9-19}$$

$$u_{a5} = -\frac{1}{2}u_{b9} - \frac{1}{2}u_{b10} \quad \textbf{Eq. 9-20}$$

As mentioned previously, the equations for the random variables of the reverse process will be computed by inverting a matrix representing the above transformation equations. However, this matrix will be constructed in the next section, during the computation of the acceptance probability. The equations corresponding to the remaining transformations will be presented in a similar manner as above.

The transformation from Model A to Model C is done with a total dimension of twenty-seven, equal to the sum of each model's dimensions. The equations for the building blocks are listed below in Eq. 9-21 through Eq. 9-42. The equations for the jump variables were constructed in the same manner as above, but will not be shown for brevity.

$$E_C = E_A + u_{a1} \quad \textbf{Eq. 9-21}$$

$$K_{v1C} = K_{vA} + u_{a2} \quad \textbf{Eq. 9-22}$$

$$K_{v2C} = K_{vA} + u_{a3} \quad \textbf{Eq. 9-23}$$

$$K_{v3C} = K_{vA} + u_{a4} \quad \textbf{Eq. 9-24}$$

$$K_{v4C} = K_{vA} + u_{a5} \quad \textbf{Eq. 9-25}$$

$$K_{v5C} = K_{vA} + u_{a6} \quad \textbf{Eq. 9-26}$$

$$K_{v6C} = K_{vA} + u_{a7} \quad \textbf{Eq. 9-27}$$

$$K_{l1C} = K_{lA} + u_{a8} \quad \textbf{Eq. 9-28}$$

$$K_{l2C} = K_{lA} + u_{a9} \quad \textbf{Eq. 9-29}$$

$$K_{l3C} = K_{lA} + u_{a10} \quad \textbf{Eq. 9-30}$$

$$K_{r1C} = K_{r1A} + u_{a11} \quad \textbf{Eq. 9-31}$$

$$K_{r2C} = K_{r1A} + u_{a12} \quad \textbf{Eq. 9-32}$$

$$K_{r3C} = K_{r1A} + u_{a13} \quad \textbf{Eq. 9-33}$$

$$K_{r4C} = K_{r1A} + u_{a14} \quad \textbf{Eq. 9-34}$$

$$K_{r5C} = K_{r1A} + u_{a15} \quad \textbf{Eq. 9-35}$$

$$K_{r6C} = K_{r1A} + u_{a16} \quad \textbf{Eq. 9-36}$$

$$K_{r7C} = K_{r2A} + u_{a17} \quad \textbf{Eq. 9-37}$$

$$K_{r8C} = K_{r2A} + u_{a18} \quad \textbf{Eq. 9-38}$$

$$K_{r9C} = K_{r2A} + u_{a19} \quad \textbf{Eq. 9-39}$$

$$K_{r10C} = K_{r2A} + u_{a20} \quad \textbf{Eq. 9-40}$$

$$K_{r11C} = K_{r2A} + u_{a21} \quad \textbf{Eq. 9-41}$$

$$K_{r12C} = K_{r2A} + u_{a22} \quad \textbf{Eq. 9-42}$$

The equations for the reverse transformation, from Model C to Mode A are listed below in Eq. 9-43 through Eq. 9-47.

$$E_A = E_C + u_{c1} \quad \textbf{Eq. 9-43}$$

$$K_{vA} = \frac{1}{6}(K_{v1C} + K_{v2C} + K_{v3C} + K_{v4C} + K_{v5C} + K_{v6C}) + u_{c2} \quad \textbf{Eq. 9-44}$$

$$K_{lA} = \frac{1}{3}(K_{l1C} + K_{l2C} + K_{l3C}) + u_{c3} \quad \textbf{Eq. 9-45}$$

$$K_{r1A} = \frac{1}{6}(K_{r1C} + K_{r2C} + K_{r3C} + K_{r4C} + K_{r5C} + K_{r6C}) + u_{c4} \quad \textbf{Eq. 9-46}$$

$$K_{r2A} = \frac{1}{2}(K_{r7C} + K_{r8C} + K_{r9C} + K_{r10C} + K_{r11C} + K_{r12C}) + u_{c5} \quad \textbf{Eq. 9-47}$$

The equations for the transformation from Model B to Model C are listed below in Eq. 9-48 through Eq. 9-69. The total dimension of this transformation is thirty-two, equal to the sum of dimensions of Model B and Model C.

$$E_C = E_B + u_{b1} \quad \textbf{Eq. 9-48}$$

$$K_{v1C} = K_{v1B} + u_{b2} \quad \textbf{Eq. 9-49}$$

$$K_{v2C} = K_{v1B} + u_{b3} \quad \textbf{Eq. 9-50}$$

$$K_{v3C} = K_{v1B} + u_{b4} \quad \textbf{Eq. 9-51}$$

$$K_{v4C} = K_{v2B} + u_{b5} \quad \textbf{Eq. 9-52}$$

$$K_{v5C} = K_{v2B} + u_{b6} \quad \textbf{Eq. 9-53}$$

$$K_{v6C} = K_{v2B} + u_{b7} \quad \textbf{Eq. 9-54}$$

$$K_{l1C} = K_{lB} + u_{b8} \quad \textbf{Eq. 9-55}$$

$$K_{l2C} = K_{lB} + u_{b9} \quad \textbf{Eq. 9-56}$$

$$K_{l3C} = K_{lB} + u_{b10} \quad \textbf{Eq. 9-57}$$

$$K_{r1C} = K_{r1B} + u_{b11} \quad \textbf{Eq. 9-58}$$

$$K_{r2C} = K_{r1B} + u_{b12} \quad \textbf{Eq. 9-59}$$

$$K_{r3C} = K_{r1B} + u_{b13} \quad \textbf{Eq. 9-60}$$

$$K_{r4C} = K_{r2B} + u_{b14} \quad \textbf{Eq. 9-61}$$

$$K_{r5C} = K_{r2B} + u_{b15} \quad \textbf{Eq. 9-62}$$

$$K_{r6C} = K_{r2B} + u_{b16} \quad \textbf{Eq. 9-63}$$

$$K_{r7C} = K_{r3B} + u_{b17} \quad \textbf{Eq. 9-64}$$

$$K_{r8C} = K_{r3B} + u_{b18} \quad \textbf{Eq. 9-65}$$

$$K_{r9C} = K_{r3B} + u_{b19} \quad \textbf{Eq. 9-66}$$

$$K_{r10C} = K_{r4B} + u_{b20} \quad \textbf{Eq. 9-67}$$

$$K_{r11C} = K_{r4B} + u_{b21} \quad \textbf{Eq. 9-68}$$

$$K_{r12C} = K_{r4B} + u_{b22} \quad \textbf{Eq. 9-69}$$

Finally, the equations describing the transformation from Model C to Model B are listed below in Eq. 9-70 through Eq. 9-79.

$$E_B = E_C + u_{c1} \quad \textbf{Eq. 9-70}$$

$$K_{v1B} = \frac{1}{3}(K_{v1C} + K_{v2C} + K_{v3C}) + u_{c2} \quad \textbf{Eq. 9-71}$$

$$K_{v2B} = \frac{1}{3}(K_{v4C} + K_{v5C} + K_{v6C}) + u_{c3} \quad \textbf{Eq. 9-72}$$

$$K_{l1B} = K_{l1C} + u_{c4} \quad \textbf{Eq. 9-73}$$

$$K_{l2B} = K_{l2C} + u_{c5} \quad \textbf{Eq. 9-74}$$

$$K_{l3B} = K_{l3C} + u_{c6} \quad \textbf{Eq. 9-75}$$

$$K_{r1B} = \frac{1}{3}(K_{r1C} + K_{r2C} + K_{r3C}) + u_{c7} \quad \textbf{Eq. 9-76}$$

$$K_{r2B} = \frac{1}{3}(K_{r4C} + K_{r5C} + K_{r6C}) + u_{c8} \quad \textbf{Eq. 9-77}$$

$$K_{r3B} = \frac{1}{3}(K_{r7C} + K_{r8C} + K_{r9C}) + u_{c9} \quad \textbf{Eq. 9-78}$$

$$K_{r4B} = \frac{1}{3}(K_{r10C} + K_{r11C} + K_{r12C}) + u_{c10} \qquad \textbf{Eq. 9-79}$$

\These sets of transformation equations detailed above describe all possible transformations within the DI3 grid RJMMC analysis. There are a total of nine possible moves overall, three consisting of proposing a model within the same base as the current model and six consisting of those described above. The probability distributions for the random variables generated for the transformation process are the same as the proposal distributions for each of the parameters are outlined in Table 9-2. Also listed are the bounds applied to each of the building blocks.

Table 9-2: Proposal Distributions for Each Building Block Type

Building Block	Lower Bound	Upper Bound	Proposal Distribution
E	0 E_o	2 E_o	N (0, 0.05)
K_v	0 kip/in	150 kip/in	N (0, 10)
K_l	0 kip/in	30 kip/in	N (0, 1)
K_r	0	100%	N (0, 0.05)

Now that the transformation equations and required random variable distributions and proposal distributions have been defined, the next step within the RJMCMC framework is to define how the acceptance probability is to be computed each iteration of the algorithm.

9.2.2.3. Computation of the Acceptance Probability

As the RJMCMC algorithm proposes dimension moves and draws samples within various models, the proposals must be evaluated for acceptance by computing the acceptance probability. This acceptance probability is defined as shown in Eq. 9-80.

$$\alpha = min\left(1, \frac{\pi(x')\, j_m(x')\, g'(u')}{\pi(x)\, j_m(x)\, g(u)} \left|\frac{\delta(x', u')}{\delta(x, u)}\right|\right) \qquad \textbf{Eq. 9-80}$$

In the computation of the acceptance probability, $\pi(x)$ represents the prior probability computation of the model at *x*, $j_m(x)$ represents the probability of the move type *m* when at *x*, and $g(u)$ represents the probability of the random variables used in the process. Finally, the Jacobian of the transformation must be computed and is shown in a more detailed equation seen in Eq. 9-81.

$$\left|\frac{\delta(x', u')}{\delta(x, u)}\right| = \begin{vmatrix} \frac{\delta t_{x'}(x,u)}{\delta x} & \frac{\delta t_{x'}(x,u)}{\delta u} \\ \frac{\delta t_{u'}(x,u)}{\delta x} & \frac{\delta t_{u'}(x,u)}{\delta u} \end{vmatrix} \qquad \textbf{Eq. 9-81}$$

In the Jacobian defined above, t_x represents the transformation of the variable *x*. To aid in the explanation of the computation of this Jacobian, the matrix of the partial

derivatives for the transformations from Model A to Model B, and then from Model B to Model A are shown below in Table 9-3 and Table 9-4.

Table 9-3: Matrix of Partial Derivatives for the Transformation from Model B to Model A

	E_B	K_{v1B}	K_{v2B}	K_{l1B}	K_{l2B}	K_{l3B}	K_{r1B}	K_{r2B}	K_{r3B}	K_{r4B}	u_{b1}	u_{b2}	u_{b3}	u_{b4}	u_{b5}
E_A	1	0	0	0	0	0	0	0	0	0	1	0	0	0	0
K_{v1A}	0	0.5	0.5	0	0	0	0	0	0	0	0	1	0	0	0
K_{l1A}	0	0	0	0.33	0.33	0.33	0	0	0	0	0	0	1	0	0
K_{r1A}	0	0	0	0	0	0	0.5	0.5	0	0	0	0	0	1	0
K_{r2A}	0	0	0	0	0	0	0	0	0.5	0.5	0	0	0	0	1
u_{a1}	0	0	0	0	0	0	0	0	0	0	-1	0	0	0	0
u_{a2}	0	0.5	-0.5	0	0	0	0	0	0	0	0	-1	0	0	0
u_{a3}	0	-0.5	0.5	0	0	0	0	0	0	0	0	-1	0	0	0
u_{a4}	0	0	0	0.67	-0.33	-0.33	0	0	0	0	0	0	-1	0	0
u_{a5}	0	0	0	-0.33	0.67	-0.33	0	0	0	0	0	0	-1	0	0
u_{a6}	0	0	0	-0.33	-0.33	0.67	0	0	0	0	0	0	-1	0	0
u_{a7}	0	0	0	0	0	0	0.5	-0.5	0	0	0	0	0	-1	0
u_{a8}	0	0	0	0	0	0	-0.5	0.5	0	0	0	0	0	-1	0
u_{a9}	0	0	0	0	0	0	0	0	0.5	-0.5	0	0	0	0	-1
u_{a10}	0	0	0	0	0	0	0	0	-0.5	0.5	0	0	0	0	-1

Table 9-4: Matrix of Partial Derivatives for the Transformation from Model A to Model B

	E_A	K_{v1A}	K_{l1A}	K_{r1A}	K_{r2A}	u_{a1}	u_{a2}	u_{a3}	u_{a4}	u_{a5}	u_{a6}	u_{a7}	u_{a8}	u_{a9}	u_{a10}
E_B	1	0	0	0	0	1	0	0	0	0	0	0	0	0	0
K_{v1B}	0	1	0	0	0	0	1	0	0	0	0	0	0	0	0
K_{v2B}	0	1	0	0	0	0	0	1	0	0	0	0	0	0	0
K_{l1B}	0	0	1	0	0	0	0	0	1	0	0	0	0	0	0
K_{l2B}	0	0	1	0	0	0	0	0	0	1	0	0	0	0	0
K_{l3B}	0	0	1	0	0	0	0	0	0	0	1	0	0	0	0
K_{r1B}	0	0	0	1	0	0	0	0	0	0	0	1	0	0	0
K_{r2B}	0	0	0	1	0	0	0	0	0	0	0	0	1	0	0
K_{r3B}	0	0	0	0	1	0	0	0	0	0	0	0	0	1	0
K_{r4B}	0	0	0	0	1	0	0	0	0	0	0	0	0	0	1
u_{b1}	0	0	0	0	0	-1	0	0	0	0	0	0	0	0	0
u_{b2}	0	0	0	0	0	0	-0.5	-0.5	0	0	0	0	0	0	0
u_{b3}	0	0	0	0	0	0	0	0	-0.33	-0.33	-0.33	0	0	0	0
u_{b4}	0	0	0	0	0	0	0	0	0	0	0	-0.5	-0.5	0	0
u_{b5}	0	0	0	0	0	0	0	0	0	0	0	0	0	-0.5	-0.5

The determinants of both of these matrices, as well as for all transformation functions developed earlier, are equal to 1.0. This is convenient since the transformation function itself will not affect the acceptance probability. It is important to keep in mind that because linear equations were used, the computation of the partial derivatives is fairly straightforward. However, if higher order functions are used for the transformations, the Jacobian will become much more complicated to compute.

An important consideration to make is the contribution of prior probabilities in the computation of the acceptance probability. Model C has twenty-two building blocks in total, but only one which has a prior probability distribution reflecting actual prior knowledge (elastic modulus of steel). When the prior probability of Model C is computed assuming that all values of vertical stiffness are assigned 75 kip/in, longitudinal stiffness assigned 1 kip/in, all rigidity factors are at 100% and the elastic modulus of steel is at it's nominal value of 1.0 E_o, the prior probability is 2.251 E-17. For a configuration of Model A with the exact same values for each building block, the prior probability is 0.0015. Considering the prior probability is included in the computation of the acceptance probability, in order for a model to have a significant probability of jumping to C from A, it would have predict responses which are over 6E13 times more likely than the predictions in model A. This clearly presents a problem, and has been addressed in literature.

One way of addressing the issue of prior probabilities governing the model selection is to scale each of the prior probability distributions for the building blocks so that the ranges cover the standard uniform distribution. This then creates a scenario where only the

building blocks which represent prior knowledge contribute to the prior probability of the model. This is important for another reason, mainly that the goal of the RJMCMC implementation within the MM St-Id framework isn't necessarily to select the best model form, but it is to account for the uncertainty in selecting the model form. If the algorithm is developed to never accept any models from highly parameterized models, then the implementation of the RJMCMC approach is useless.

At this point the transformation equations have been developed and the framework for computing the acceptance probability has been developed. The next step within the RJMCMC framework is to prepare the finite element models for the analysis.

9.2.3. Preparation of Finite Element Models

In the case of the DI3 grid analysis, each of the three models used within the RJMCMC framework are the same base model developed in Chapter 5. However, the main difference is that each model has different building blocks being sampled. The major distinction between the three models is Model C, which has fully rigid connections near the supports, but variable connections near the center of the span. Three unique copies of the base model were made and separately analyzed to ensure there were no errors. Also, backup files were made for each model in case of an abrupt error which would terminate the process in the middle of a model execution.

In a more general sense, it would be at this stage that the user is developing the many different kinds of models to be used within the analysis. For example, it is feasible to include a shell, solid and frame element model (or any combination of the three element

types) within the analysis. Care must be taken that each model is individually error screened using best practice approaches. Also, if different software packages are being used then it is important to make sure that the same types of settings are selected for each analysis type. Such settings that could affect the predictions of different software packages include: (1) shear deformation, (2) consistent mass formulation of the mass matrix, (3) solution of the eigen problem and (4) material properties. There are many other settings that could vary between software packages, however these are some of the ones that typically have different default settings. It is important that the user be familiar with the software package before any type of MM St-Id implementation is used.

9.2.4. Monitoring the Analysis

During any MCMC analysis, it is important to monitor the sampling process to ensure that there are no errors within the algorithm, the model modification codes or in the parameters set to the algorithm (such as proposal distribution settings). Things to consider while monitoring an RJMCMC analysis include: (1) whether proposal are being accepted in each model form, (2) what the overall acceptance ratio is (which serves as an indicator of the appropriateness of the proposal distributions) and (3) the time history of each of the chains through the current sample. By monitoring these features of the process, time can be saved by preventing analyses from running in which errors are present.

9.3. RJMCMC Analysis of the Grid

When analyzing the RJMCMC analysis results, multiple levels of convergence must first be investigated. First, the sampling algorithm must converge on a stationary distribution for selecting base models. Then the convergence within each model's chain must also be analyzed for convergence properties. In presenting the results, two sections will describe: (1) analysis of convergence and (2) presentation of results.

9.3.1. Analysis of Convergence for RJMCMC Sampling

As previously mentioned, the analysis of convergence for RJMCMC sampling must be evaluated on two fronts: the convergence of base model selection, and the convergence within the base models' chains. The chains will be evaluated for convergence in a similar manner as has been used to analyze convergence for classical MCMC sampling. However, to determine when the algorithm has consistently sampled across the models, the acceptance probability associated with each base model was computed as a function of the number of models included in the analysis. Overall, 18,000 models were generated and analyzed through the RJMCMC method for the grid study.

As seen in Figure 9-5, the acceptance probability for the different base models appears to converge after roughly 9,000 models. It is also noteworthy that the acceptance probabilities for each model, initially defined in the algorithm as being equally likely, have converged to a distribution over the model indicator space that tends towards the simplest models. The final acceptance probability for Base Model A, the five building block set, was 0.42, while the acceptance probability for Base Model B, the ten building

block set was 0.32 and finally the acceptance probability for Base Model C, the twenty-two building block set, was 0.26.

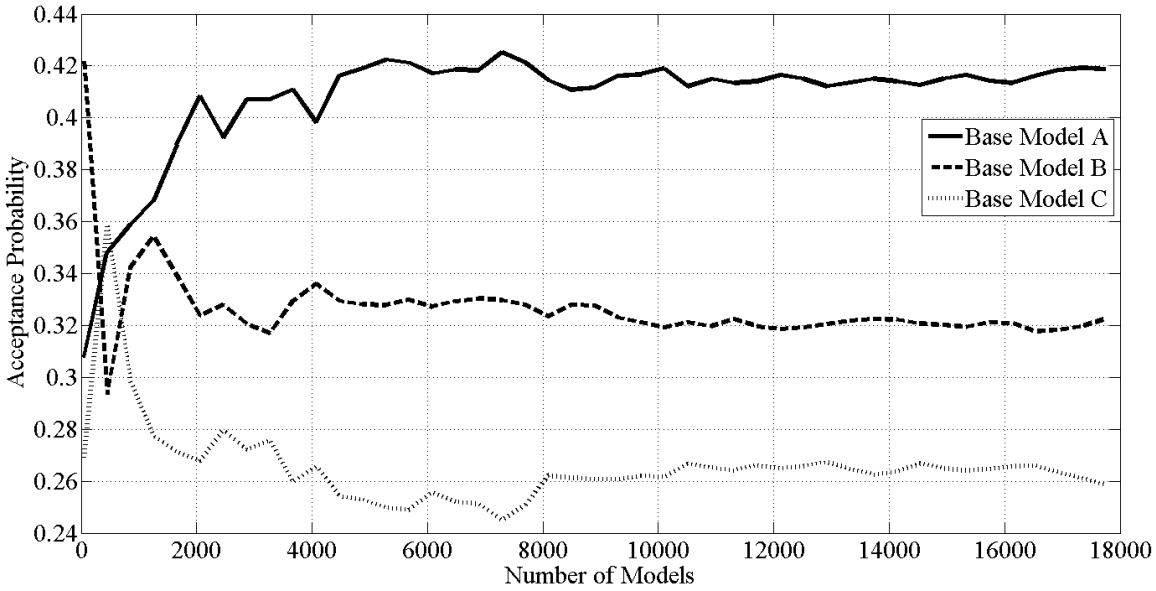

Figure 9-5: Convergence Study for Base Model Selection

In interpreting the results of the final acceptance probabilities, it is reasonable that the simplest models finished with the highest acceptance probabilities since there was no observations included that could distinguish between the base models. For example, if one of the supports was completely removed from the grid and the same analysis was run, then it would be expected over time that Base Model C would have the highest acceptance probability since it could match the experimental observations the best. However, with inherently global building blocks, that in nature do not vary significantly

in their properties, the algorithm samples the simplest model form the most since it is more likely that there is a uniform spatial distribution of the building blocks.

To analyze the convergence of the individual chains associated with each of the base models, the same approach was taken as explained in Chapter 7. The expected value and variance of the distributions of each building block was computed as a function of the number of models included in each of the base models' chains. These quantities were then plotted against the number of models included and analyzed for where both the expected value and variance converged to a stable value. By following this approach, the number of models needed for convergence within each base model is shown in Table 9-5. Also shown is the total number of accepted models within each chain. The interesting result shown from the convergence analysis of the individual chains for each base model is that the number of models needed for convergence for the base models with higher building blocks is lower than what is needed for the five building block case. As hypothesized, the base model with lower number of building blocks performs most of the burn-in, while the base models with higher numbers of building blocks are sampled less frequently, but at likely samples. This feature of the RJMCMC analysis is shown to lend itself greatly to cases where one model may require a long analysis time. That specific model could be assigned a low initial sampling probability and over time as the entire algorithm burns-in, could then be sampled more.

Table 9-5: Convergence Analysis of Base Model Building Blocks

Base Model	Models Needed for Convergence	Total Models Accepted
A	2,192	2,857
B	1,700	2,201
C	1,666	1,764

9.3.2. Response Predictions from RJMCMC Analysis

The response prediction distributions were once again produce for a mid-span displacement and strain due to a mid-span load. The predictions from all three base model analyses were combined to generate a single probability distribution for each of these response indices (Figure 9-6). As seen in these distributions, the method once again produced distributions which characterize the physical structure very well. Both the displacement and strain measurements fall within meaningful portions of the cumulative distributions functions below.

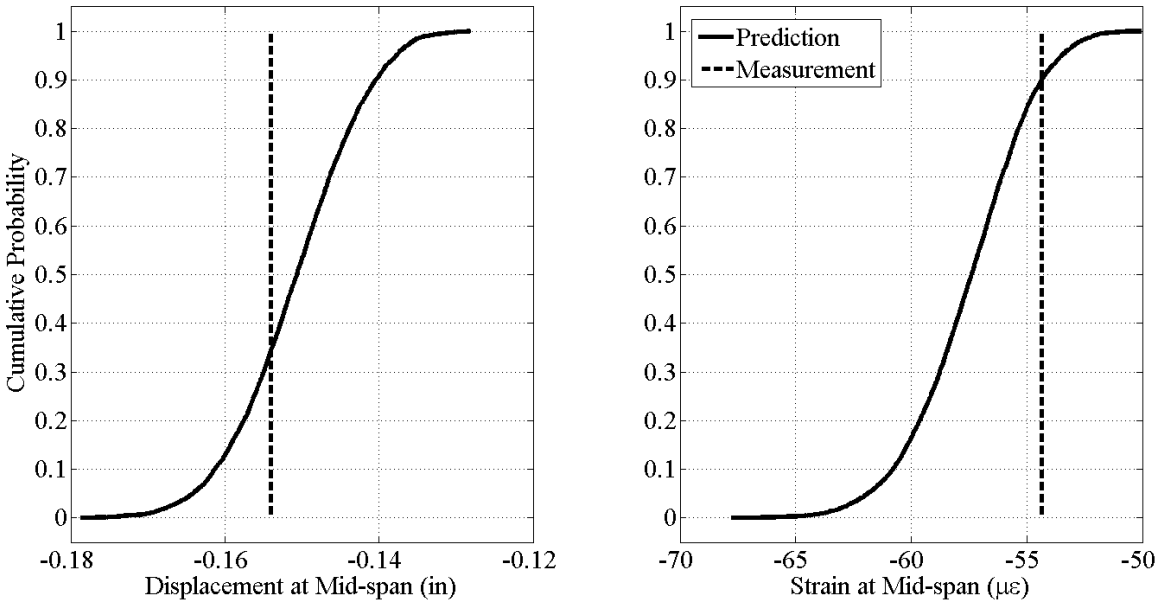

Figure 9-6: RJMCMC Response Predictions for Mid-span Load

An alternative way of presenting the results from an RJMCMC analysis is to highlight the contributions from each of the base models. It is apparent from Figure 9-7 that the three base models provided similar distributions in terms of their response predictions, however such a presentation could be useful to highlight the difference between base models that are fundamentally different (element type or software package).

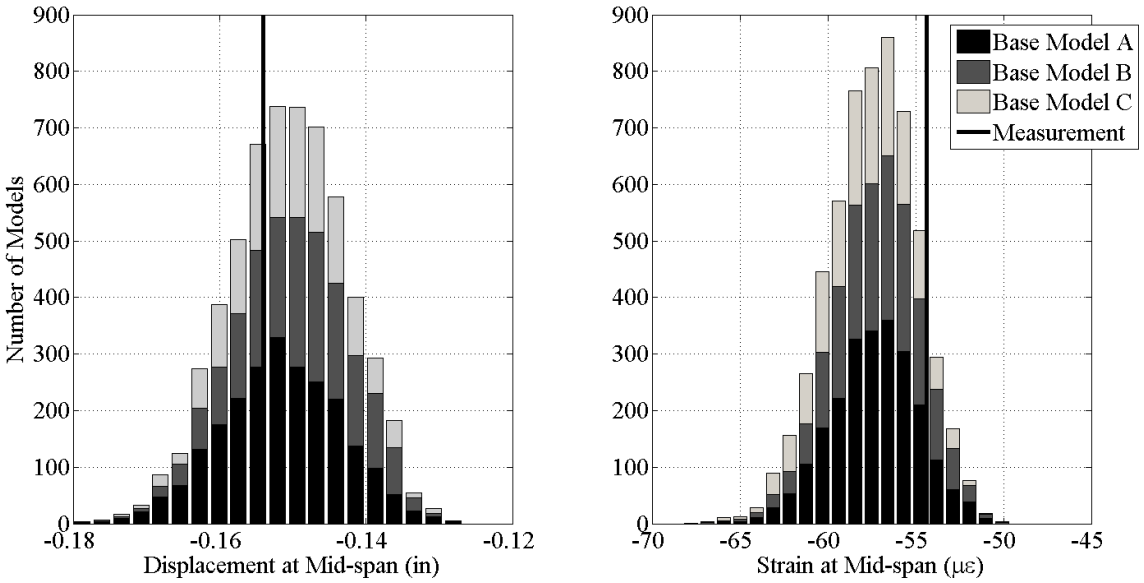

Figure 9-7: RJMCMC Response Predictions for Mid-span Load Showing Base Model Contributions

Overall, the RJMCMC analysis method highlighted and explained in this chapter has been proven to be very useful in its application to the MM St-Id approach. By incorporating such an analysis technique, there is no limit to the types of models explored in generating response predictions for a physical structure. However, the advantage of this method does not come without challenges. Specifically, the jump equations and computation of the transformation matrices can be very challenging, so it is important that an experienced user carries out an analysis on a complex system of base models and building blocks. It is highly encouraged, from the author's experiences, to begin with simple case studies, such as a cantilever beam or other simple structure, to ensure that the algorithm is performing as expected. Once a solid understanding of the method is achieved, then an analysis of a more complicated model can confidently be attempted.

CHAPTER 10: IMPLEMENTATION OF MM ST-ID ON A CONSTRUCTED SYSTEM

The MM St-Id approach has been developed and validated in Chapters 4 through 7 and has been shown to be applicable to advancements specifically relating to the desired outcome in Chapters 8 and 9. All of this work had been completed on the DI3 grid for its transparent structural system in addition to its ability to be modified in ways that create less than ideal observations. While the developed approach was shown to provide a great amount of insight into the Structural Identification process of the DI3 grid, the method needs to be applied to an actual constructed system to determine whether the approach is feasible in real world applications.

As part of a separate research project, Drexel University began a relationship with the Burlington County Bridge Commission (BCBC) to develop and implement a structural health monitoring system on its two signature long span structures: the Burlington Bristol Bridge and the Tacony Palmyra Bridge. The bridges both span the Delaware River and connect New Jersey to major corridors leading into Philadelphia, Pennsylvania. These two bridges generate revenue for the BCBC by tolling traffic traveling from New Jersey into Pennsylvania. The Burlington Bristol Bridge was identified to receive the first implementation of the Structural Health Monitoring efforts due to concerns from the owner and engineer of record and was selected to be the first major constructed system to be analyzed with the MM St-Id methods developed thus far.

This chapter will discuss the history of the Burlington Bristol Bridge, how the relationship between Drexel University and the BCBC was developed, and why the bridge was selected for thorough health monitoring.

10.1. The History of the Burlington Bristol Bridge

The Burlington Bristol Bridge (BBB) (Figure 10-1) was constructed starting on April 1, 1930 and was first opened to traffic May 1, 1931. The bridge replaced a long running ferry which provided transportation across the Delaware River between the towns of Bristol, PA and Burlington, NJ. The road supported by the BBB is designated as PA 413 and NJ 413 and consists of two lanes of vehicular traffic. The bridge was originally owned and operated by the Burlington Bristol Bridge Company; however in 1948 the bridge was purchased by the Burlington County Bridge Commission (BCBC) for $12.4 million.

Figure 10-1: The Burlington Bristol Bridge

The bridge consists of many different structural forms as it spans the Delaware River. In New Jersey, the approach spans consist of multi-girder spans and a single deck truss span. Two tower spans, steel through-truss structures, house massive concrete counterweights which balance the main 540’ steel through-truss lift span. This main span allows for a vertical clearance of 61’ at high tide in the closed position and 138’ at high tide in the open position. The Pennsylvania approach consists of three steel deck truss spans and stringer spans to return Rt. 413 to Pennsylvania grade.

The BBB was slated for replacement during two separate occasions. The first occurred in over the period from 1963 to 1980 when a replacement span (which would have become part of the proposed I-895highway) was planned. The bridge had two design alternatives, but ultimately lost support from both the Pennsylvania and New Jersey Departments of Transportation after a decade of debate.

The second attempt at replacing the BBB came in 1987 as the BCBC revealed plans to build a new fixed span. This attempt at replacing the structure ultimately lost support due to multiple factors: (1) the Pennsylvania Department of Transportation refused to support the approaches required for the new structure, (2) mayors from both Burlington and Bristol feared that the span would require the destruction of many homes and businesses and finally, (3) a poll in Burlington County for the replacement of the bridge failed to garnish enough votes for approval.

The multiple failed attempts at replacing the BBB highlight a challenge commonly seen with today's infrastructure owners: the need for indefinite preservation. The need to preserve the nation's critical and signature structures is driven by multiple factors. The first and most prominent factor is the cost of replacement. Infrastructure owners face steep prices in constructing new structures and in demolishing the existing structure. In the case of the BBB, the BCBC actually had the financial capabilities to replace the bridge but fell victim to the high socioeconomic costs.

Another controlling factor which influences infrastructure owners' decision on replacement versus preservation is the lack of property to build a new structure. Since most of the aging long span structures were built in the early 1900's, communities and

businesses flourished around the bridge due to ease of access to new markets. The many long span structures connecting Manhattan to adjacent cities highlight this dilemma, as the construction of new structures would require the demolition of large amounts of developed land. In the case of BBB, this was one of the fears with building a new structure. The two proposed structures would have required more extensive right-of-way acquisitions since a fixed span structure would require a greater area to bring the roadway back to grade.

Over the course of the history of the BBB, the need for indefinite preservation was demonstrated again and again. Today, the BCBC has accepted indefinite preservation of their signature structures as the reasonable path forward. However, in order to ensure that the structures can continue to support the traffic demands they face, rigorous inspection and maintenance plans, especially in the case of movable spans, are required. To this end, the BCBC recognized the potential that Structural Health Monitoring offered and set out to incorporate the appropriate technologies that could assist in the daily and long term operations of their structures.

10.2. Development of Relationship between Drexel University and the BCBC

During emergency inspections following the collapse of the I-35 bridge in 2007, several weld flaws in floor beam retrofits, installed in the 1950's, were identified. As part of a study to determine whether it was necessary to remove the connection where the weld flaws were occurring, Drexel University was contracted to perform detailed instrumentation around the flawed welds and unflawed welds and monitor their

performance during a crawl speed load test carried out by others. After the load test and subsequent analysis was complete, the BCBC was able to save money by confidently knowing that the connection details did not need to be removed. The BCBC recognized the benefits that Structural Health Monitoring (SHM) had to offer in terms of analyzing and evaluating their existing structures and began a long term contract with Drexel University to monitor the signature structures.

The goals of the long term project were to develop appropriate instrumentation to monitor the structures for key response indices, construct and calibrate finite element models for load ratings and finally to design and implement long term monitoring of critical actions. Aside from the monitoring of the flawed welds and connection details, the BCBC did not initially specifically request any type of measurements to be made on the BBB or TPB. While this left much freedom for the design of a SHM system, it also required the implementation of an efficient monitoring system that was not cost prohibitive due to too many sensors. The experimental program designed and carried out for the Burlington Bristol Bridge will be discussed in detail in Chapter 13.

10.3. The Selection of the Burlington Bristol Bridge as a Candidate for MM St-Id

The Burlington Bristol Bridge was identified as a prime candidate for validating the MM St-Id techniques developed on the DI3 grid for multiple reasons. First, after the study of the floor connections was complete, the BCBC's engineer of record requested that Drexel University provide an independent load rating analysis of critical member of the lift span. This required the construction of a preliminary finite element model as well as obtaining

cursory experimental measurements to verify the ability of the model to predict the most basic observations obtained. In this process, the finite element model was updated manually in an iterative fashion by comparing the model predictions to the first vertical and lateral natural frequency of the lift span and tower spans. These limited measurements were used since it was a cursory study.

During this process, multiple models were found which equally matched the experimental data, but offered differing pictures of the rating of the structure. In one case the rating was below 1.0, which is unacceptable, while in the other case the rating was well over 1.0. However, in comparing the models to the data, there was no way of identifying which model was more appropriate. This raised the question: if two models exist that match the data equally well but offer varying predictions, how many other models exist that do the same? This question drove the research on the BBB and its experimental design.

The second reason for selecting the BBB for the MM St-Id study was that multiple sources involved with the bridge (police, maintenance and engineers) reported a long existing phenomena that the New Jersey (NJ) tower span vibrated more than the Pennsylvania (PA) tower span, even though they were symmetric structures. This seemingly baffling response characteristic of the bridge was verified by Drexel University staff in field visits, as it is obvious to anyone standing on the structures. However, this phenomenon was identified from the beginning as being a critical question to answer.

A third reason for selecting this bridge for the MM St-Id study was the familiarity achieved through the floor system study in 2007. The three weeks of field work allowed researchers the opportunity for full access to the structure and plans. The plans will be further described in Chapter 11; however it will be shown that reading and interpreting the plans was very challenging as they were scans of original documents from 1930. There was a considerable effort placed on documenting and verifying the information within these plans.

These fundamental reasons served as the motivating criteria for selecting the BBB as a candidate for MM St-Id. The full MM St-Id process was then applied to the structure, in addition to specific monitoring applications requested by the BCBC and their engineer of record. The conceptualization of the structure, construction of an a prior finite element model, experimental program and eventual MM St-Id analysis will be discussed in the subsequent chapters.

CHAPTER 11: CONCEPTUALIZATION OF THE BURLINGTON BRISTOL BRIDGE

The first step in the MM St-Id process is the conceptualization of the structure. This is a very important step as it drives the question to be answered and thus serves as the foundation for the entire method. To fully conceptualize a structure, a field visit is necessary to obtain photographs of existing conditions, connection details, bearing details, foundation conditions, and roadway layout. After becoming familiarized with the structure, it is necessary to obtain all available and relevant documentation. This includes original design drawings, if available, inspection reports, structural rehabilitation plans, and documentation on accident history, typical vehicular usage and other significant past events. The next step within the conceptualization process is to translate the plans and photographs into a three dimensional computer aided drafting (CAD) rendering, where members are modeled with one-dimensional representation. This process not only provides a useful geometric model, it also forces the user to thoroughly read and inspect all the plans for details about the structure, and to identify and reconcile any conflicting or missing information. Finally, after an accurate geometric model is complete, it may be necessary to develop more detailed three dimensional CAD models where specific elements of the structure are modeled to exact geometric replication. Once these steps have been completed, the analyst is in a position to both identify and offer a qualitative ranking of all relevant hazards and vulnerabilities that may be examined and quantified throughout the St-Id application.

To discuss the conceptualization of the Burlington Bristol Bridge, this Chapter is divided into five sections: (1) Site Visits, (2) Collection of Structural Documentation, (3)

Development of a Geometric Model, (4) Development of Geometric Models for Specific Structural Components, and (5) Identification of Hazards and Vulnerabilities.

11.1. Site Visits

Several site visits were made to the BBB over the course of this study. The following sections detail the three most valuable of these visits, including: (1) Initial visit, (2) A visit to account for the structural mass, and (3) A visit to document the various bearings.

11.1.1. Initial Site Visit on August 16, 2007

The BBB was first visited as part of the project focusing on the floor connection details of the tower spans. During this site visit, the research team was allowed to walk the length of the bridge so that close up photos of the structure and connection types could be obtained (Figure 11-1). By visually inspecting the structure before looking at construction plans, it is easier to navigate the plans for specific information. This is especially true in cases where the original design drawings are deteriorated and difficult to read. Also, specific structural conditions can be assessed, such as: the load path of the structure, how members were constructed (rivets, bolts, welds), level of corrosion, condition of paint, roadway alignment and travel lanes, among many others.

For the BBB, it was noted during the first site visit that the structure was composed of built up steel members connected with rivets (Figure 11-2). It was also noted that a large machine house existed in the middle of the lift span (Figure 11-3). During the cursory

inspection, minimal levels of corrosion were noticed and the current condition of the paint was fair, with some areas of cracked paint or exposed older layers of paint. After walking the length of the structure, the research team was given access to a shoreline area where the underside of the superstructure could be photographed and visually inspected from a distance (Figure 11-4). It was at this location that the load path of the entire structure could be clearly identified. The load paths of each of the main structure types will be described in detail in four subsections.

As traffic travels along the length of the span, it crosses over four main structural forms on the BBB: (1) stringer spans with a concrete deck supported by steel columns, (2) deck truss spans with concrete filled grid deck supported by reinforced concrete piers, (3) through-truss tower spans with concrete filled grid deck supported by reinforced concrete piers and (4) a through truss lift span with an open grate deck whose dead load is balanced by concrete counterweights and live load is supported by reinforced concrete piers.

Figure 11-1: Drexel University Research Team during First Site Visit

Figure 11-2: Documentation of Member Construction and Connection Details

Figure 11-3: Burlington Bristol Bridge Machine House at Mid-span of Lift Span

Figure 11-4: Documentation of Load Path

11.1.1.1. Structure Load Path of Stringer Spans

The load path of the approach stringer spans (Figure 11-5) is fairly straightforward and can be conceptualized through a visual inspection of the structure. The roadway deck is supported by a set of cross beams that run perpendicular to the direction of the travel lanes. These cross beams are in turn supported by longitudinal stringers. The stringers then frame into floor beams, which are supported by steel columns. This is the typical load path for all stringer spans on the north and south approaches of the bridge.

Figure 11-5: Stringer Spans of the South Approach

11.1.1.2. Structure Load Path of Deck Truss Spans

The load path for the deck truss spans (Figure 11-6) is considerably different. The concrete-filled grid deck is supported by steel cross beams, which are supported directly by the top chord of the truss. The Warren style truss supporting the roadway is supported

on either end by reinforced concrete piers. The truss is composed of steel I-shape sections with riveted gusset plate connections and is designated as fracture critical, where non-redundant members are present.

Figure 11-6: NJ Deck Truss Span

11.1.1.3. Structure Load Path of Tower Spans

The tower spans (Figure 11-7) serve two main purposes: to support the roadway running through the truss along its bottom chord, and to support and house the massive concrete counterweights in addition to supporting the dead load of the lift span. The load path for the roadway supported by the tower spans consists of five main elements (Figure 11-8).

The concrete filled deck which carries the traffic loads is supported by steel I-section purlins running perpendicular to the direction of traffic. Those purlins sit on top of steel I-section stringers running parallel with the direction of traffic. The stringers are framed into steel I-section floor beams running perpendicular to traffic. The floor beams frame into the bottom chord of the tower span trusses at each panel point. Overall there are nine panel points on the tower spans. The loads are then distributed through the truss and distributed to the earth through the reinforced concrete piers on either end. The truss members consist of a variety of built up steel sections riveted together with gusset plate connections.

The weight of the counterweights and the lift span are supported by tower section of the truss. The main vertical columns of the truss consist of heavily built up steel members and carry the bulk of the load of the counterweight and lift spans. The tower section of the truss braces this main column over its 140’ height.

In the 1950’s the floor system of both tower spans was reinforced due to perceived vibration problems. The floor beams were strengthened by welding a steel T-section along the bottom flange, as seen in Figure 11-8. Additionally, the stringer connections were made continuous by welding a steel plate across the top flanges of adjacent stringers (e.g. a continuity plate) that required a hole to be cut through the web of the floor beam. In addition, this retrofit welded steel shims in the gap between the bottom flange of the stringer and the web of the floor beam (Figure 11-9). It was this connection which suffered weld flaws, and was the focus of the original testing on the bridge.

Figure 11-7: The NJ Tower Span

Figure 11-8: Floor System for the Tower Spans

Figure 11-9: Modifications to Tower Span Stringer Connections

11.1.1.4. Structure Load Path of Lift Span

The load path of the lift span is very similar to the load path of the tower spans (Figure 11-10). However, the lift span floor system was not stiffened as the tower span floor system was and the deck consists of a different structural component. The traffic on the lift span is supported by a steel grid deck (Figure 11-11). The grid deck was not an original feature of the structure, but was completely replaced in 1994. A steel grid is ideal for long span structures since it is considerably lighter than a concrete equivalent. A considerable drawback to the open grid decking is the exposure of the floor system to weather and salt, which can cause advanced corrosion.

The decking used on the BBB lift span has a total weight of 29 pounds per square foot. The deck is supported by three longitudinally oriented stringers, which frame into floor beams. The floor beams run perpendicular to the direction of traffic and are connected to the trusses at the bottom chord panel points. For the lift span, there are a total of twenty-one panel points. The truss then distributes the loads out to the supports and to the reinforced concrete piers at either end.

Figure 11-10: Floor System of the Lift Span

Figure 11-11: Steel Grid Deck on the Lift Span

The purpose of the initial site visit was to become familiarized with the structure and overall load carrying mechanisms utilized. After documenting these features, the design drawings and plans could be more easily interpreted and translated into CAD drawings.

11.1.2. Site Visit for Accounting of Structural Mass

Over the course of the bridge's 80 year history, there have been many modifications and additions or replacements made to various components and it is critical that all sources of dead load are accounted for. The load ratings of long span structures are typically

governed by the dead load forces within the members. It is for this reason that extra care was taken in accounting for the various sources of extraneous mass (i.e. mass above and beyond structural components). The BBB provides a unique opportunity in its analysis in that the total dead load of the lift span is known quite accurately. As part of its regular maintenance program, the counterweights and lift span interaction must occasionally be tested for its state of balance. In other words, it is possible to tell how well the counterweights are balancing the weight of the lift span so that the motors driving the openings are not overworked.

The balancing operations of the lift span were carried out using multiple types of evaluation. One method of determining the state of balance in the structure was to measure the torque in the drive shafts opening the bridge and noting when the direction of torque changed. In the report generated by the engineer who carried out this test, an estimate of total weight was also stated. A separate means of quantifying the total weight within the lift span was carried out by performing harmonic testing on the cables supporting the lift span. By vibrating the cables and measuring the resonant frequencies of the response, the total force within each of the sixty-four cables could be computed. Finally, one could compute the mass of the counterweights as a simple estimate of the weight of the span based upon the geometry of the overall concrete and reinforcing steel contained within, as noted on the original plans.

The original contract drawings specify the weight of the lift span to be 2,532 kips. This weight tabulation consists of the following categories, as detailed in the drawing: Sidewalk, Floor system, Handrail, Bracing, Machinery & etc at Midspan, and Trusses.

This weight was then used for the design of the counterweights, which the plans for also specify the weight breakdown of steel and concrete in each of the counterweights. The main changes to the lift span since these original contract drawings consisted of the removal of the original steel plate deck and its replacement with a steel grid deck as well as some modifications to certain floor system members.

In July of 2006, Modjeski & Masters (M&M) performed a cable tension test on the sixty-four counterweight cables which suspend the lift span counterweights. This report provided a detailed analysis of not only the estimation of the total dead load, but also a distribution of the load over the sixty-four individual cables. The cable tensions were determined by measuring the harmonic frequencies of the cables and assuming a length and unit weight. The harmonic frequencies were obtained through a simple modal analysis operation known as peak-picking, and verified through the presence of higher order harmonics at integer multiples. From this study M&M reported that the total dead load of the lift span was 2,631 kips.

In September of 2007, Gresham Consulting Engineers were hired to perform balancing test on the counterweight-lift span system. They measured the torsional strain in the drive shafts of the four main gear boxes as a function of span position. They then calculated the imbalance between the counterweight and the lift span by comparing the forces generated in raising and lowering the lift span. They found that the overall system switched from ‘span heavy’ to ‘counterweight heavy’ at a lift height of approximately 30’ out of a total lift height of 70’. This indicates that the lift span is slightly lighter than the counterweights since the system is balanced when the lift span had more of the cable weight contributing to its total. However, the difference is very small indicating that the

counterweights represent an accurate estimation of the dead load of the lift span itself. Unfortunately, there was no note in the report detailing if any additional balancing blocks were in the counterweight at the time of the test. This uncertainty notwithstanding, the weight of the counterweight can be estimated based on the amount of steel (84.8 kip), concrete (2,249.6 kip) and initial balancing blocks (210.7 kip) specified in the original contract drawings, which totals 2,545 kip.

By carrying out a quantity take-off, in which the mass of the structure is estimated from only the drawings, the total weight of the structural elements of the lift span totaled 1,585 kips. This is roughly 1,000 kips short of the total dead load of the lift span and this discrepancy and the location of the additional mass needed to be accounted for thoroughly.

On August 7, 2008, a site visit was carried out by the Drexel University research team to quantify the extraneous sources of mass on the major spans, especially the lift span. The major sources of missing mass were found to include: the structural paint (lead based), the machine house and operator's house at mid-span with accompanying machinery (Figure 11-12), gusset plates (Figure 11-13), rivets and lattice work (Figure 11-14), operating rope stations (crow's nests) (Figure 11-15), and the sidewalk and accompanying guard rails (Figure 11-16). Detailed measurements and photos were made of these details and incorporated into the quantity take-off calculation.

Figure 11-12: Measuring Gears and Machinery within the Machine House

Figure 11-13: Photo Highlighting Quantity of Gusset Plates within a Connection

Figure 11-14: Measurement of Lattice Work and Rivets

Figure 11-15: Crow's Nest Located at Pulley for Operating Ropes

Figure 11-16: Quantifying the Guard Rail Dimensions

The final result from the site visit on August 7, 2008 was a table of dead load sources corroborated by the various testing of dead load sources by others and by the original tally of dead load by the designers (Table 11-1). The miscellaneous category in the table below accounts for such things as live load shoes, electrical conduit, cables and other non-categorical mass sources.

Table 11-1: Quantification of Dead Load for the Lift Span

Structural Component	Total DL
Truss	959.35
Floor System	626.25
Machinery	342.50
Machinery House Floor System	77.50
Gusset Plates	162.98
Paint	92.84
Sidewalk	81.00
Lateral System	84.80
Misc.	55.27
Guard Rail	42.50
Rivets & Angles	20.40
Crow's Nest	18.00
Total	**2563.38**

This level of quantification of dead load will prove to be very useful in the model building process for the BBB as an error screening tool. By using the same methodologies that were employed on accounting the mass sources on the lift span, the masses of all spans could be accounted for in the same manner. While in this particular case the total mass of the lift-span could be estimated using other methods (cable tension, counterweight dimensions/balance, etc.) this is not the case for most long-span structures. Given the large magnitude of dead load stresses and actions in long-span bridges, the accurate estimation of total mass and mass distribution for such structures is critical.

11.1.3. Site Visit to Explore Bearings

A third critical site visit was carried out for the exploration of the bearings of the spans to assist with a specific experimental design, which will be described in Chapter 13. However, in the conceptualization stage it is very important to fully explore the support conditions and document all existing features of the bearings, such as what type(s) they are, whether they appear to be frozen or functional and what level of corrosion exists.

For the deck truss spans, the trusses are supported with a pin-roller configuration. The pin, or fixed, bearings consist of heavy steel shoes meeting at a thick steel pin. The roller bearing consisted of a heavy steel rocker sitting on a steel masonry plate. Both of these bearings can be seen in Figure 11-17. These were fairly typical connections in the time period of construction for the BBB.

Figure 11-17: Pin (left) and Rocker (right) Bearings for the Deck Truss Spans

The tower spans are supported in a fixed-roller configuration as well. The bearings which support the heavy columns of the tower are rigidly connected to the piers by a massive steel plate anchor bolted into the reinforced concrete pier (Figure 11-19). The bearings supported on the non-tower end of the tower span are a rocker bearing of similar design to the rocker bearings on the deck truss spans (Figure 11-18).

Figure 11-18: Expansion Bearing for Tower Spans

Figure 11-19: Fixed Bearing for Tower Spans

The lift spans do not have a fixed bearing; however sit on top of live load shoes (Figure 11-20). The dead load of the lift span is balanced by the counterweights, so when the bridge is seated only live load forces should be transmitted through the shoes. Typically, though the balance of the span and the counterweights is adjusted so that the live load shoes are taking on a percentage of the total dead load, to prevent the span from bouncing up and down during traffic. These shoes allow for movement in either the longitudinal or lateral directions, however the lift span is prevented from excessive movement or complete dislocation by sets of guides on the adjacent tower spans (Figure 11-21 & Figure 11-22). The guides extend from the lift span to the sides of the tower spans, thus preventing a differential lateral movement altogether. Additionally, on the NJ end of the lift span, the guides are constructed in such a manner that longitudinal movement is restricted as well (Figure 11-21).

Figure 11-20: Lift Span Live Load Shoe

Figure 11-21: NJ Lift Span Guide

Figure 11-22: Lift Span Guide Located at Top Chord of Lift Span Truss

11.2. Collection of Structural Documentation

A critical stage within any St-Id process is the collection of structural documentation. Important documents to obtain are the original design drawings and specifications, subsequent reconstruction plans, inspection reports and also any available accident reports that occurred on the structure or accidents which involved the structure itself (such as an impact). This type of information will provide the user with member cross sections and geometry, as well as material properties used.

The BCBC staff and engineers-of-record provided the Drexel University research team with the following documentation:

- Original Contract Drawings
- Original Shop Drawings
- Reconstruction of North and South Approaches in 1966
- Deck Reconstruction in 1976
- Deck Reconstruction in 1988 for Approach Spans
- Deck Reconstruction in 1993 for Lift Span
- Deck Repairs – Various Years
- Inspection Reports

The records indicating any traffic accidents were not made available, as they are maintained by the BCBC police staff and are not intended to be public information. However, any information related to engineering and construction were generally available upon request.

The original design drawings are still available in hard copy form at the offices of the field engineering staff. However, all plans have been scanned and are available and transferred in electronic form so that the originals can be preserved. While having the original design drawings made available is a significant benefit to the St-Id process, the quality of the plans has deteriorated, on some drawings more than others (Figure 11-23 - Figure 11-25). Extra care had to be taken in reading and interpreting the plans so that the correct dimensions were used as well as that the correct cross section properties were assigned to members. In some cases, special site visits needed to be made to confirm uncertainties seen in the design reports due to lack of quality in the drawings.

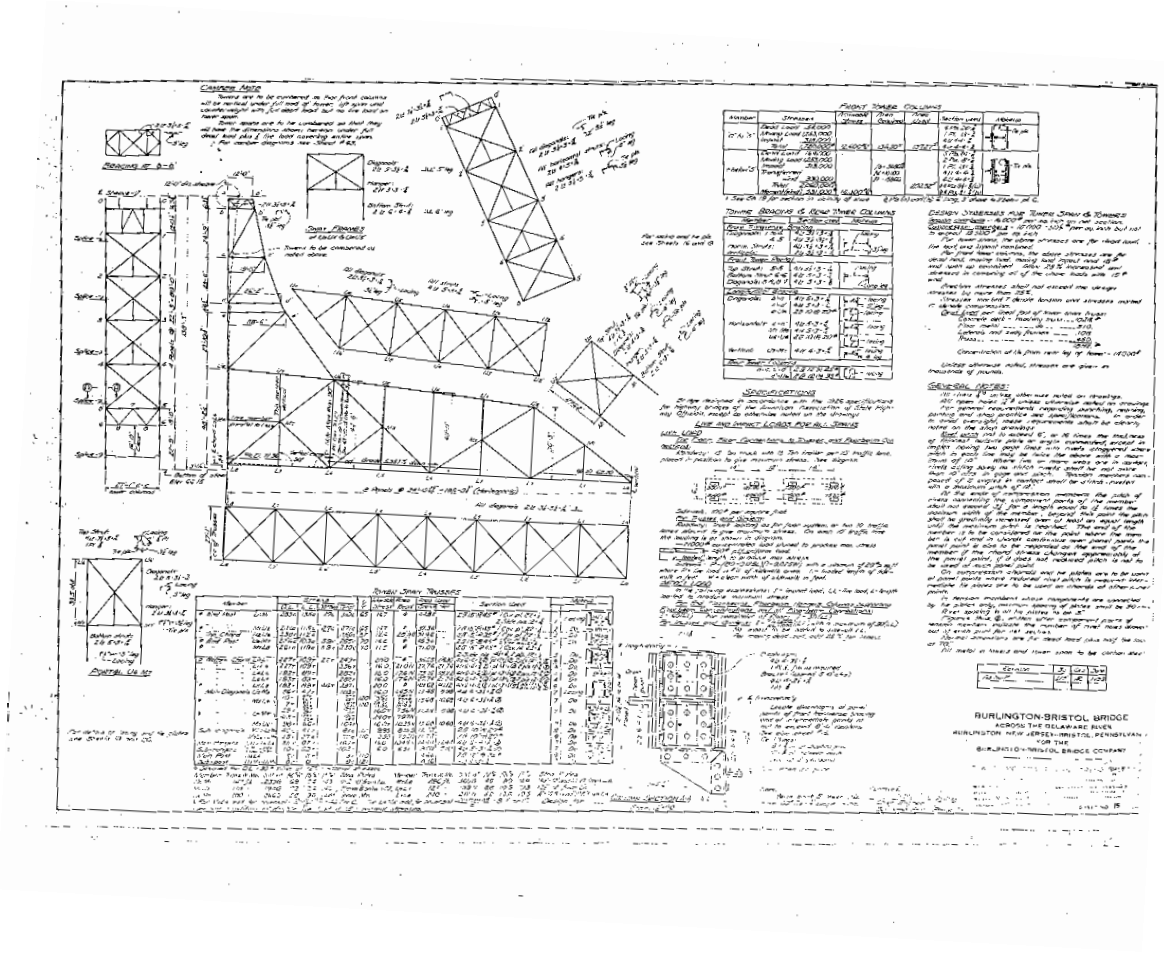

Figure 11-23: Original Stress Sheet Drawing for the Tower Spans

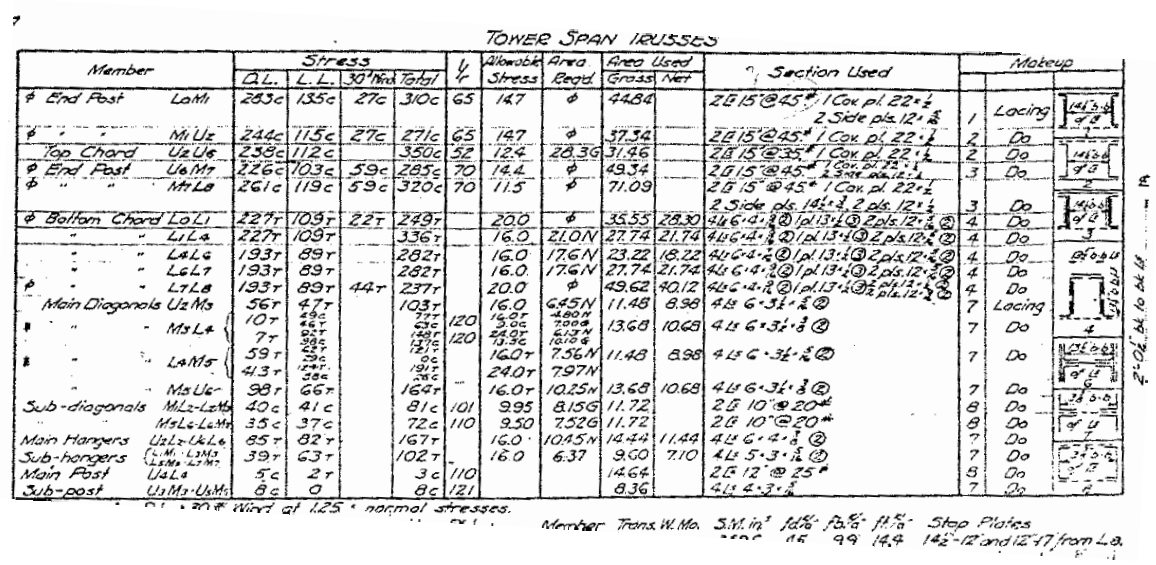

TOWER SPAN TRUSSES

Member		Stress D.L.	Stress L.L.	Stress 30 Mph Wind	Stress Total	%	Allowable Stress	Area Reqd	Area Used Gross	Area Used Net	Section Used	Makeup		
ϕ End Post	L₀M₁	283c	135c	27c	310c	65	14.7	ϕ	44.84		2 ⌊ 15" @ 45# / Cov. pl. 22" × ½ 2 Side pls. 12" × ⅜	1	Lacing	
ϕ " "	M₁U₂	244c	115c	27c	271c	65	14.7	ϕ	37.34		2 ⌊ 15" @ 45# / Cov. pl. 22" × ½	2	Do	
Top Chord	U₂U₆	238c	112c		350c	52	12.4	28.36	31.46		2 ⌊ 15" @ 35# / Cov. pl. 22" × ½	2	Do	
ϕ End Post	U₆M₇	226c	103c	59c	285c	70	14.4	ϕ	49.34		2 ⌊ 15" @ 45# / Cov. pl. 22" × ½ 2 Side pls. 14½" × ½	3	Do	
ϕ " "	M₇L₈	261c	119c	59c	320c	70	11.5	ϕ	71.09		2 ⌊ 15" @ 45# / Cov. pl. 22" × ½ 2 Side pls. 14½" × ½ 2 pls. 12" × ½	3	Do	
ϕ Bottom Chord	L₀L₁	227T	109T	22T	249T		20.0	ϕ	35.55	28.30	4 L 6" × 4" × ½ ② 1 pl. 13" × ½ ③ 2 pls. 12" × ½ ②	4	Do	
" "	L₁L₄	227T	109T		336T		16.0	21.0N	27.74	21.74	4 L 6" × 4" × ½ ② 1 pl. 13" × ½ ③ 2 pls. 12" × ½ ②	4	Do	
" "	L₄L₆	193T	89T		282T		16.0	17.6N	23.22	18.22	4 L 6" × 4" × ½ ② 1 pl. 13" × ½ ③ 2 pls. 12" × ½ ②	4	Do	
" "	L₆L₇	193T	89T		282T		16.0	17.6N	27.74	21.74	4 L 6" × 4" × ½ ② 1 pl. 13" × ½ ③ 2 pls. 12" × ½ ②	4	Do	
ϕ "	L₇L₈	193T	89T	44T	237T		20.0	ϕ	49.62	40.12	4 L 6" × 4" × ½ ② 1 pl. 13" × ½ ③ 2 pls. 12" × ⅝ ②	4	Do	
Main Diagonals	U₂M₃	56T	47T		103T		16.0	6.45N	11.48	8.98	4 L 6" × 3½" × ⅝ ②	7	Lacing	
" "	M₃L₄	10T 4.9c 46T 63c 20.5T 149T			56T 63c 169T	120	16.0T 4.80N 7.00N	13.68	10.68	4 L 6" × 3½" × ⅝ ②	7	Do		
" "	L₄M₅	7T 20.5T 12.1T 59T 3.9c 41.3T 28c			27T 63c 199T	120	24.9T 13.9c	6.13N 10.0G						
					62T		16.0T	7.56N	11.48	8.98	4 L 6" × 3½" × ⅝ ②	7	Do	
" "	M₅U₆	98T	66T		164T		24.0T	7.97N						
							16.0T	10.25N	13.68	10.68	4 L 6" × 3½" × ⅝ ②	7	Do	
Sub-diagonals	M₁L₂-L₂M₃	40c	41c		81c	101	9.95	8.15G	11.72		2 ⌊ 10" @ 20#	8	Do	
	M₃L₄-L₄M₅	35c	37c		72c	110	9.50	7.52G	11.72		2 ⌊ 10" @ 20#	8	Do	
Main Hangers	U₂L₂-U₆L₆	85T	82T		167T		16.0	10.45N	14.44	11.44	4 L 6" × 4" × ⅝ ②	7	Do	
Sub-hangers	(L₁M₂ L₃M₄ L₅M₆ L₇M₇)	39T	63T		102T		16.0	6.37	9.60	7.10	4 L 5" × 3" × ½ ②	7	Do	
Main Post	U₀L₀	5c	2T		3c	110			14.64		2 ⌊ 12" @ 25#	8	Do	
Sub-post	U₁M₁-U₅M₅	8c	0		8c	121			8.36		4 L 4" × 3" × ⅜	7	Do	

20# Wind at 1.25 × normal stresses.

Member Trans. W. Mo. S.M. in³ fd fb fa fl Stop Plates
99 14.9 14½"-12 and 12"-7 from L₀

Figure 11-24: Member Cross Section Properties and Stresses for the Tower Spans

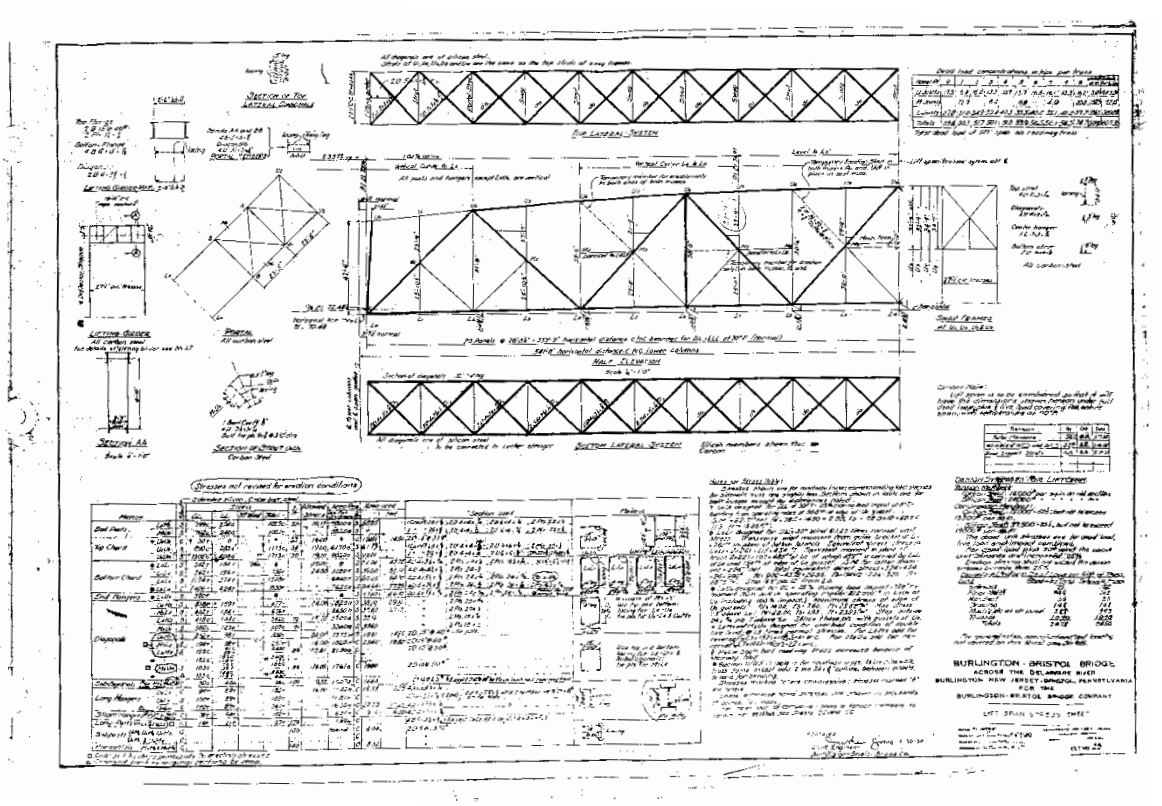

Figure 11-25: Original Stress Sheet for the Lift Span

11.3. Development of Geometric Models

After a structure has been conceptualized in terms of its physical properties, load path, and mass sources, the next step required in the MM St-Id process is to construct CAD drawings of the spans so that a full understanding of the geometry is established. A careful strategy must be employed when constructing geometric models. Considering these serve as the basis for future finite element models, careful attention must be paid to the correct location of members and structural elements. These steps will be fully explained in detail for the BBB, in three subsections: (1) Representation of Major Structural Components, (2) Representation of Secondary Structural Components, and (3) Representation of Substructure Components.

11.3.1. Representation of Primary Structural Components

The first parts of a structure that should be represented in CAD software are the major structural components. These components are done first since they typically define the overall geometry of the structure and can be completed independent of any secondary structural components. Examples of primary components for the BBB would be the main truss elements: top chord, bottom chord, diagonals and verticals of the truss. For a smaller span structure, the major structural components may consist only of a set of stringers, however even in that case those stringers define the overall geometry (in terms of both length and width).

Once the elements have been identified that are going to be modeled first in the CAD software, the user must then define how each of the members is going to be represented.

For a typical overall geometric model, members are represented as a single one dimensional line. For a structure such as BBB, this reduces the complexity and size of the CAD model and provides a more efficient template for future planning done with these drawings. Since a three dimensional member is being compressed to a one dimensional line, the user must decide on where within the cross section of each member the line will fall. For example, the line representing each member could be drawn at is geometric center, top, bottom, or any other place that is deemed appropriate. The important consideration to make is that the user should be consistent with the representation selected. If there are multiple types of representation utilized, this could lead to simple mistakes with large consequences further down the MM St-Id analysis process.

For the BBB, it was decided to model the lines of each of the members at its centroidal axis. This was done so that the cross sections could be defined in the finite element model without further modification to account for the line representing the shape not being located at its neutral axis. As mentioned, the trusses of all the major structures were drawn first in the CAD model (Figure 11-26). At this point, painstaking detail was put into checking the dimensions of members, spans and widths of the structure against the design plans discussed previously. This model was the backbone of the entire MM St-Id process, and any sources of errors were identified and mitigated at this stage.

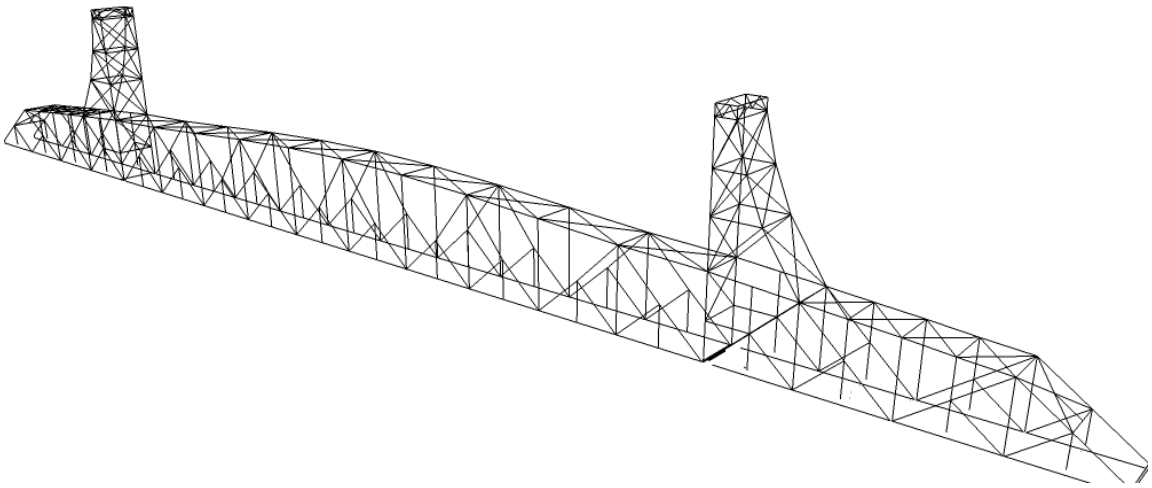

Figure 11-26: BBB CAD Model after First Stage of Completion

11.3.2. Representation of Secondary Structural Components

Once the main structural components have been represented in the CAD software, the secondary structural components can then be incorporated. Typically, the location of the secondary components is dependent on the position of the primary structural components. For example, secondary structural components would include the deck, wind bracing, floor beams, stringers, diaphragms or any other structural component that is physically connected to the primary structural components. Since roadway decks are best represented analytically as shell elements, these components were drawn in the CAD program as 3D faces, located spatially at a position equal to half of their respective heights. For the BBB, many secondary structural components exist in two main

categories: (1) floor system components and (2) truss bracing components. The entire floor system consists of secondary structural elements since they are only connected to the main truss at each panel point. Also, the truss bracing components are also secondary and include the portal bracing, which provides torsional stiffness, and the lateral bracing which stiffens the truss laterally.

All of these components were incorporated into the main CAD model (Figure 11-27), and once again all dimensions and connectivity were error-proofed and corrected if necessary. At this stage, it is not uncommon for lines representing secondary structural components to not connect to any other lines in the CAD model since each line is drawn at the neutral axis of the members. For example, if cross beams sit on top of stringers, their neutral axes are going to be separated by a distance equal to half of the height of the stringer and half of the height of the cross beam (assuming each is symmetric vertically). This lack of connection is typical in a CAD model, and will be addressed when the model is imported into finite element software, however it is more important that each member is located spatially correct.

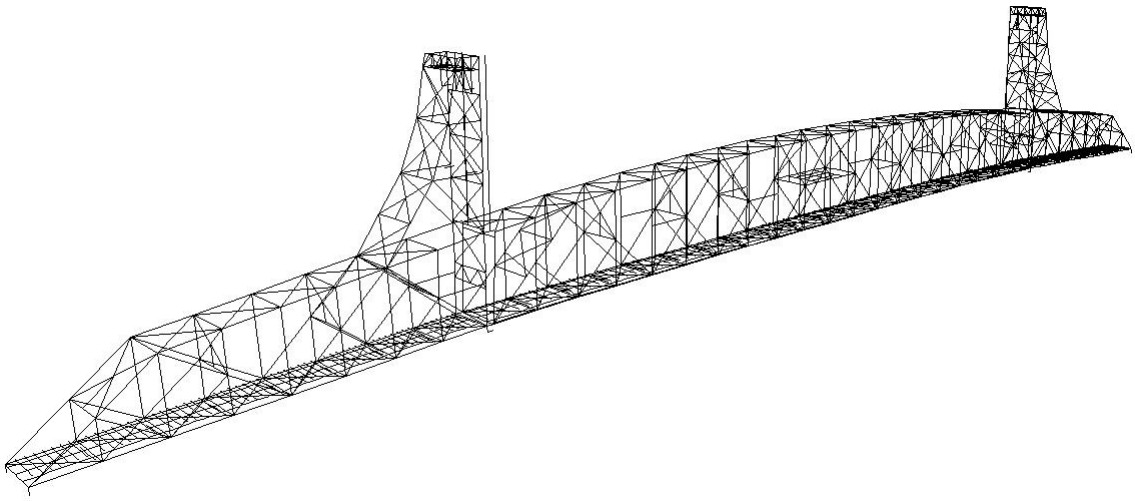

Figure 11-27: BBB CAD Model after Second Stage of Completion

11.3.3. Representation of Substructure Components

The final component of a major structural system to be incorporated into a geometric model is the substructure system. Substructure systems typically consist of a combination of piers, columns, abutments, and any other means of supporting the structure at predetermined intervals along the span.

For the BBB, there are eight reinforced concrete piers which support the NJ Truss Span, NJ Tower Span, Lift Span, PA Tower Span and the three PA Truss Spans. The seven piers which are founded on piles and are partially submerged in the waters of the Delaware River are shown below in Figure 11-28.

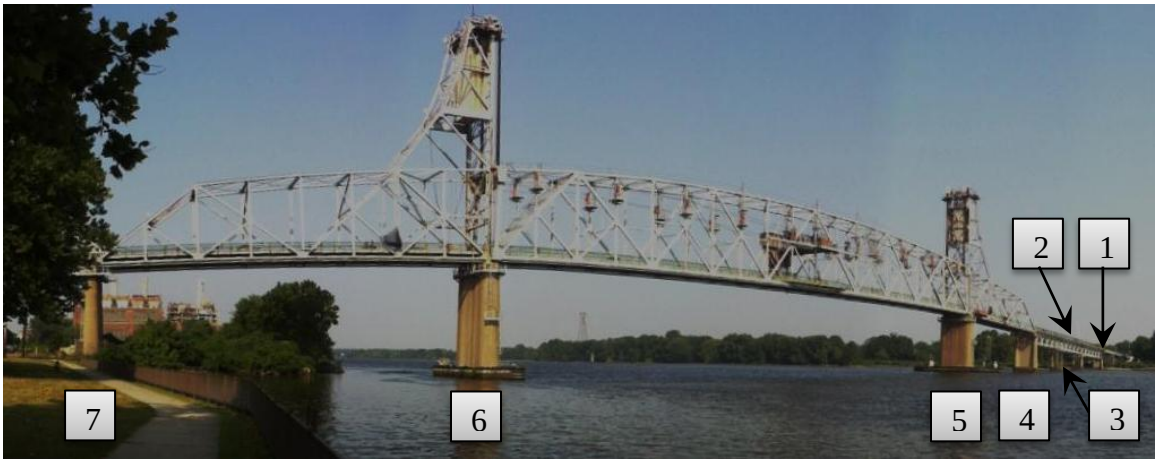

Figure 11-28: Panoramic Photo Showing Piers 1 through 7 of the BBB

Piers 1 through 7 all rest on top of timber piles which were all driven to depths so that their caps were below the mean low tide water level and there was sufficient capacity for each of the piles and soil conditions. Pier 8 is a reinforced concrete pier; however it is founded on a spread mat foundation instead of piles. The remaining supports all consist of columns with concrete foundations (Figure 11-29).

Figure 11-29: Panoramic Photo Showing Piers 7 and 8 as well as Column Supports of the NJ Approach

Each of the piers was modeled in AutoCAD as three dimensional components. These components were modeled in full three-dimensional replication for the purposes of experimental design. A three dimensional geometric replica lends itself much better to experimental design for structures such as piers since there are limitations due to access and the shape of the structure. By representing the piers exactly as they exist, an effective experimental design can be generated. Figure 11-30 shows a close-up view of the three-dimensional CAD rendering of Pier 8 which was incorporated into the overall BBB CAD model (Figure 11-31).

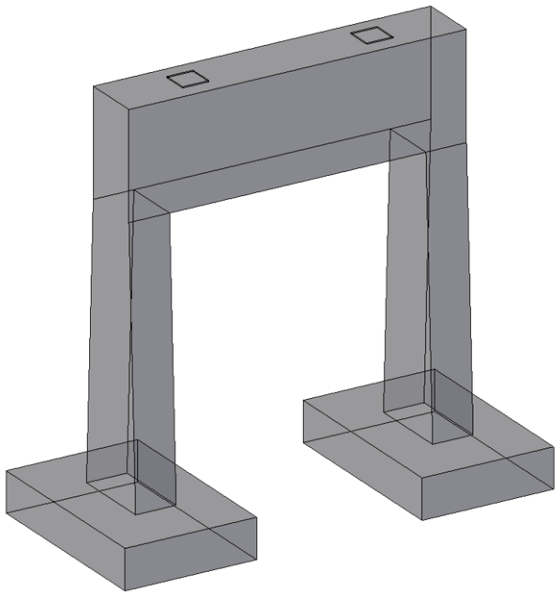

Figure 11-30: 3D CAD Representation of Pier 8

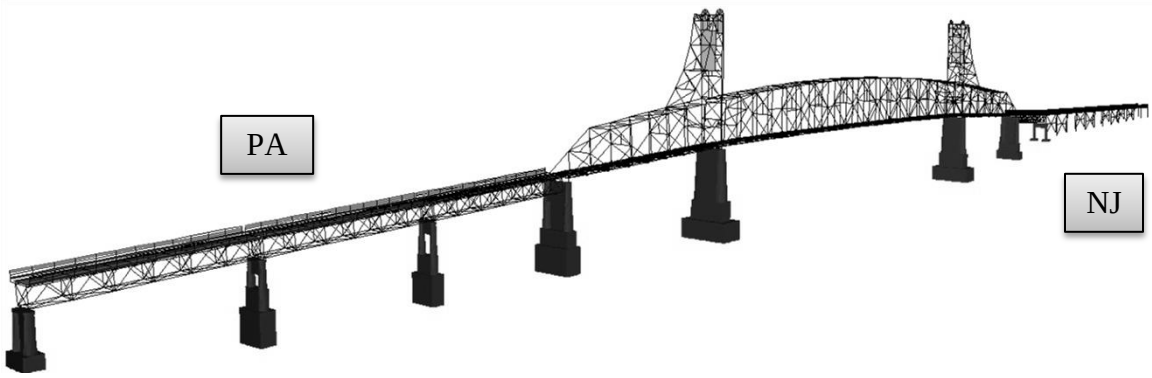

Figure 11-31: Final 3D CAD Model of BBB

11.4. Development of Geometric Models for Specific Structural Components

Occasionally it is necessary to develop more refined CAD models for experimental design or for understanding certain phenomena. In the case of BBB, two such models were made in the drafting software SketchUp. The software is commonly used in architectural applications; however it lends itself to the development of refined fully three-dimensional models for specific components as well.

The area of interest that required more detailed geometric modeling for the purposes of experimental design and learning was the top chord of the lift span at mid-span. SketchUp was incorporated to develop two models: (1) zoomed-in view of the specific location for an instrumentation plan (Figure 11-32) and (2) the role of the member in the local truss member distribution (Figure 11-33). Fine details were included in the model

such as rivets, lattice members and gusset plates. This allowed for specific instrumentation design to avoid rivet heads and for accessibility in reaching certain areas of the members.

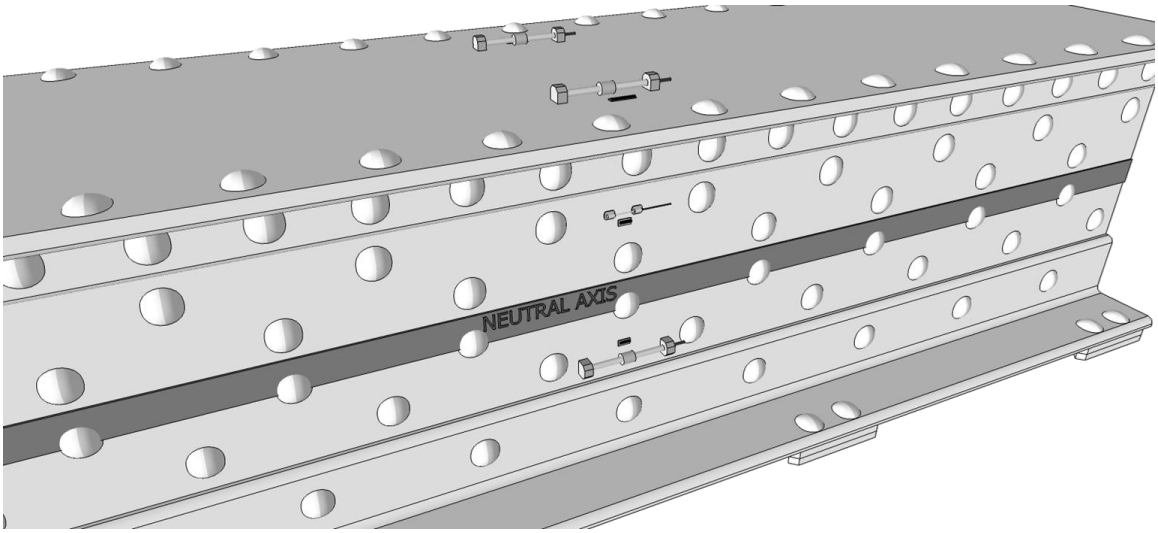

Figure 11-32: Detailed 3D SketchUp Model Developed for an Instrumentation Plan

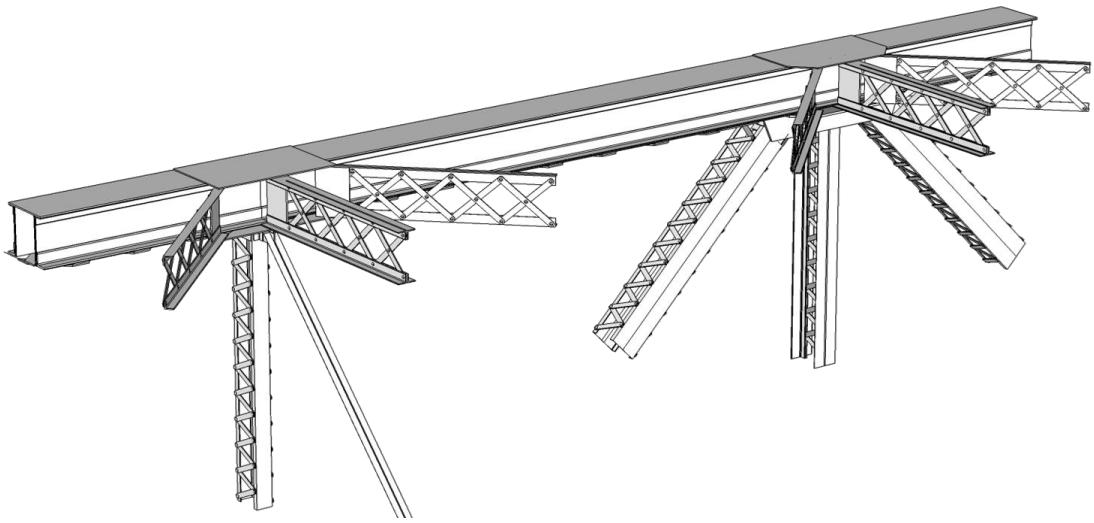

Figure 11-33: Detailed 3D SketchUp Model Developed for a Study on the Connection Details

11.5. Identification of Hazards and Vulnerabilities of the BBB

A critical step within the MM St-Id process is the identification of hazards and vulnerabilities for a given structure and the development of a set of critical questions which guide the St-Id process. The development of these questions is critical in justifying the need for the St-Id implementation, based upon a qualitative risk assessment and associated uncertainty. These hazards and vulnerabilities will define what types of analyses are run within the MM St-Id process and what the model predictions should be. For the BBB, a set of hazards and vulnerabilities were identified for the purpose of this case study.

In general, it is helpful to follow a list of limit states (Table 11-2) when generating a list of hazards and vulnerabilities. It is also important to consult experts who are familiar

with the bridge, such as long time maintenance or engineering staff, as well as experts in the fields of engineering, such as structural, geotechnical, highway, marine (if applicable), etc. Experts are also helpful in prioritizing the hazards and identifying which ones would benefit most from a MM St-Id application.

Table 11-2: Limit States for Identification of Hazards and Vulnerabilities

Limit States	
Operational	Safety
	Efficiency
Structural	Safety
	Serviceability
Geotechnical / Hydraulic	Safety
	Serviceability
Durability and Maintenance	Safety
	Serviceability

The limit states in Table 11-2 provide a starting point for any structure being analyzed for hazards and vulnerabilities, however depending on the unique application of the structure there may be other limit states which are more appropriate or ones listed above that are not appropriate for a given situation. The operational limit state governs mainly movable spans or ones where the function of the span includes some form of regular interaction to keep the structure efficient and safe, such as a structure with a moving median barrier. To that end, there are two categories of limit states within the operational category: safety

and efficiency. A set of example hazards and vulnerabilities is given below for the BBB for discussion of this point in Table 11-3.

Table 11-3: Set of Hazards and Vulnerabilities for BBB

Limit States		Hazard	Vulnerability	Failure Mode
Operational	Safety	Span Impacting Seats	Loss of Brakes	Local Buckling
	Safety	Ship Impact	Machinery Breakdown	Collapse
	Efficiency	Inaccurate Indicators	Overcautious Operator	Long Openings
	Efficiency	Thermal Expansion	Span Unable to Seat	Traffic Unable to Pass
	Efficiency	Machinery Breakdown	Span Unable to Seat	Traffic Unable to Pass
Structural	Safety	Overload	Overstressing	Collapse
	Safety	Vehicle Collision	Lack of Redundancy	Collapse
	Safety	Wind loads	Overstressing	Member Yielding
	Serviceability	Repeated Loads	Fatigue / Fracture	Loose Grid Deck
Geotechnical / Hydraulic	Safety	Flowing Water	Liquefaction	Pile Failure
	Serviceability	Flowing Water	Scour	Pier Settlement
Durability / Maintenance	Safety	Winter Maintenance	Corrosion	Costs
	Serviceability	Dynamic Impact	Excessive Vibration	Maintenance Costs

The operational limit state for BBB includes many hazards and vulnerabilities. From a safety standpoint, the hazard would need to cause a failure mode which compromises the safety of those using the structure. A hazard which would meet this criterion would be the

loss of brakes during a closing of the lift span or a vessel collision. The loss of brakes would cause the lift span structure to impact the piers at a potentially significant rate potentially inducing local buckling of the end truss members. The failure mode associated with this type of a hazard and vulnerability could be local buckling of truss members due to the impact force. A vessel collision hazard could be coupled with a vulnerability of machinery breakdown and the inability of a ship to stop in time before striking the span, resulting in a collapse of the lift span.

From an efficiency standpoint, an operational hazard could be inaccurate height indicators, thermal expansion of the lift span or even machinery breakdown. The operators of the lift span use indicators to gage how close they are to seating the structure and whether they are fully open for a given ship. If these indicators were knowingly inaccurate, the operators would be forced to move the lift span very slowly near the seating point so that the span doesn't impact the piers. The vulnerability, an overly cautious operator, would then lead to an efficiency failure mode of an extremely long opening. A long opening would then lead to more delays in traffic and a potential loss in revenue from drivers changing their route and using a separate bridge to cross the river. Similarly, if the lift span expanded due to a significant temperature gradient during the opening of the lift span, the span might not be able to seat if the joints between the lift and tower spans could not close properly, resulting in long traffic delays as well.

These types of analyses were carried out over the remaining limit states to generate the example table shown above, and will aid in the identification of what response indices

need to be generated in the MM St-Id process. To proceed forward, a set of guiding questions was developed to address a set of the risks identified in the table above:

1.) What is the elastic load carrying capacity of the lift span according to the following load levels: AASHTO codes and typical live load levels seen on the BBB?
2.) What are the most critical members in terms of load carrying capacity and load distribution for normal operating conditions?
3.) What are the most critical members in terms of load distribution (as a measure of redundancy) for lateral load cases, such as wind or vessel collision?
4.) Is the excessive vibration on the NJ Tower span due to a lack of flexural stiffness, or some other phenomenon?

While other questions certainly exist based on the tables presented above, this select group was identified as the most important based off of engineering judgment, owner and engineer-of-record input, and from overall structural conceptualization. To answer the questions outlined above, it is clear that an integrated application of experimental and analytical analysis is required. Analytical applications alone could not answer the above questions because too much uncertainty exists on the reliability of the analytical model in being able to characterize the structure in a sufficient manner to provide meaningful results. Similarly, experimental characterization alone could not answer the questions because in some cases the response indices needed to answer the questions are not able to be measured (intrinsic stresses, response due to lateral load, etc.). It is clear that a tool to

leverage analytical models informed with sound experimental observations is needed to answer the questions outlined above, and given the potential costs (failure modes) associated with some of the hazards and vulnerabilities studied it is clear that the cost of the St-Id application to the BBB is clearly outweighed by the benefits of answering the above questions.

CHAPTER 12: A PRIORI FINITE ELEMENT MODEL FOR THE BURLINGTON BRISTOL BRIDGE

The development of appropriate a priori finite element models is an essential process for any St-Id application, but especially important for the success of a MM St-Id application to a complex constructed system. In Chapter 5, a detailed discussion was given on the development of multiple a priori models for both experimental design and for MM St-Id studies for the grid structure. As with the grid, an a priori finite element model was needed for the BBB for the sole purpose of experimental design. Due to cost restrictions and level of access, only a limited number of sensors, cables and data acquisition channels were available for measuring response indices of interest on the structure so each sensor location had to be placed in areas where significant response was guaranteed. The only way to accomplish this, aside from heuristics in some cases, is to develop, error screen and leverage an a priori finite element model.

A second a priori finite element model was also developed for the BBB, however with the purpose of being incorporated into the MM St-Id framework. This model was constructed almost three years after the development of the initial a priori model, and incorporated many features of the structure which were not included in the initial model. These features were gained through significant amounts of time spent on the span, multiple site visits and continued documentation, and results from measured observations. It is common for a priori models to be both incomplete and contain mechanisms that are not representative of the physical reality of the structure. Although the term a priori has entered into standard science and engineering vocabulary, general definitions remain informative, such as: “from a general law to a particular instance; valid independently of observation” (dictionary.com);

"proceeding from a known or assumed cause to a necessarily related effect; deductive" (American Heritage Dictionary); and "based on hypothesis or theory rather than experiment" (WordNet). In the field of St-Id the label *a priori* (explicitly meaning "from the former" or "from before") is used to convey that the model was constructed prior to quantitative testing and thus only reflect the analysts understanding of the structure from visual observations and the review of legacy data.

This chapter will discuss the development of the a priori finite element model for experimental design and the development of the a priori model for MM St-Id in two main sections. However, within each section are detailed discussions on the model construction process, assignment of properties and continuity conditions, assignment of extraneous mass sources, reduction of stiffness and mass contributions for approach spans and finally a thorough error screening campaign. In addition to discussing the finite element model development, a third main section will discuss the identification of building blocks and subsequent sensitivity studies and advanced methods used for extracting modal information in an efficient manner from the complex BBB finite element model.

12.1. Model Classification

The most pertinent distinction between the numerous physics-based (PB) modeling approaches for structural identification is that of geometric resolution. The selected a priori model should be commensurate with the uncertainty that prevails as well as the precise motivation(s) for the St-Id application (see Chapter 1 for examples). The resolution and size of the model should be driven by the utility of the St-Id, available information and

heuristics about the constructed system, as well as its size, complexity and the experimental resources that are available for Step 3. Most a priori models are based on assumptions of linearity and stationarity. In general these assumptions need not be made; however, in the absence of response data from the specific constructed system, it is difficult to justify the complications associated with nonlinear constitutive relations or stochastic finite element analysis.

Starting with simpler, greatly idealized phenomenological geometric models to help conceptualize a constructed system, together with the site, soil and foundations, and then gradually increasing the detail and complexity of the model as the system is better understood is recommended. Many of the issues associated with a priori modeling are not unique to St-Id applications and different modeling approaches have been developed and discussed in literature. In any case, the utility of the a priori PB models lies in its ability to identify key mechanisms and provide an expected range of response to allow an efficient and robust experimental program to be designed and carried out. The following sections provide brief discussions and examples of the most common PB models employed as a priori models.

12.1.1. Phenomenological Models

This class of models has the lowest geometric resolution and typically consists of a few elements to describe or investigate the key response mechanisms of constructed systems (Figure 12-1). Although not a strict limitation, these models mostly employ simple one-dimensional (e.g. plane or space frame elements) and discrete elements (e.g. translational or

rotational springs, point masses). The primary advantage of this class of model is their transparency to the analyst and computational efficiency. If employed properly, such models can provide great insight into the relative impacts of various global mechanisms of the constructed system in a timely and efficient manner.

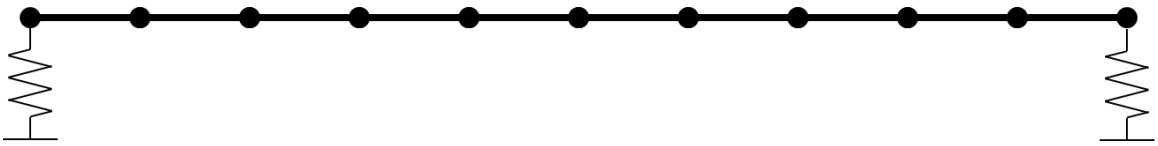

Figure 12-1: Phenomenological Model Example

12.1.2. Structural Models

Perhaps the most common class of models employed in an a priori manner to support St-Id is the structural model (Figure 12-2). These models typically employ both one-dimensional (plane or space frame elements) and two-dimensional elements (e.g. plate or shell elements). In an effort to remain consistent with the three dimensional geometry of the structure, various link elements, constraints, and rigid offsets are included. The primary advantage of these models is their ability to simulate more detailed, component-level response, and allow the impact of various member-level continuity and boundary conditions on the overall response to be assessed. In addition, they are less dependent than

phenomenological models on the understanding of the structural response by the analyst. On the other hand, their construction and error screening is far more time consuming and tedious.

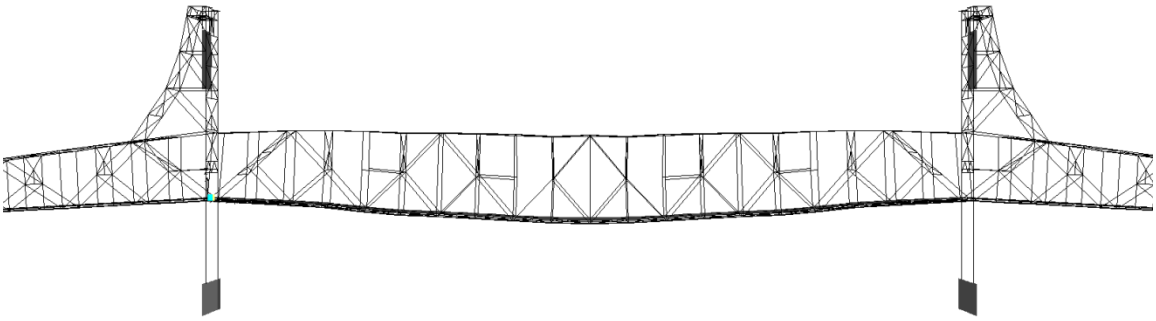

Figure 12-2: Structural Model Example

12.1.3. Finite Element Models

This class of modeling has the finest geometric resolution, and in some cases may consist of a geometric-replica model (Figure 12-3). As such, these models will employ the full range of finite elements available including three-dimensional solids. The primary advantage of this class of models is their ability to simulate the response and effect of complex structural details, connections, stress concentration, etc. The trade-off of course, is that while these models, in theory, would require less intuition and heuristics related to the response of the constructed system, they are extremely challenging to construct and error

screen in a reliable manner. In addition, the computation cost of such models makes them untenable for most constructed systems, and thus their real utility may be as a supplement/complement to a structural model. Although many commercial FE software packages are available to construct such models, they are currently not widely used in civil engineering practice.

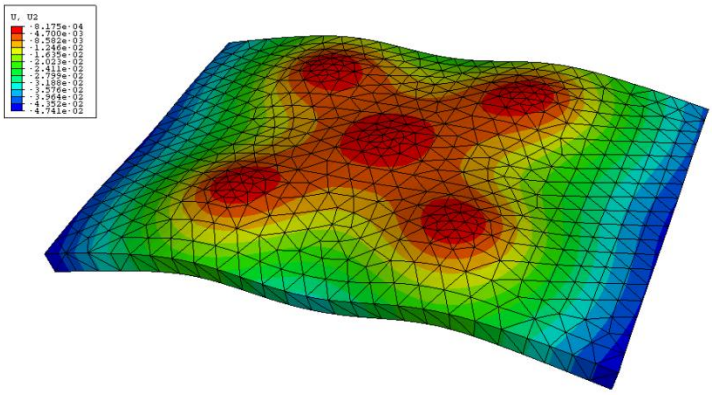

Figure 12-3: Finite Element Model Example

12.2. Selection of Model Resolution

In selecting the most appropriate model form for the BBB application, it was necessary to ensure that both the anticipated forms of measurement and identified response indices (guided by the critical questions outlined in Chapter 11) are able to be reliably computed. The model form that provided the best characterization of the structural responses of interest was a structural model, or element-level model. This type of model allowed

analysts to maintain the three dimensional geometry of the structure, calculate member level forces (to compute load ratings and stress analyses on critical members) and characterize the structure sufficiently for accurate representation of the structures' modal properties. Since the primary form of measurement for long span structures is ambient vibration monitoring, due to lack of a reference frame in measuring displacements and inability to excite the structure in a global manner for a forced impact test, it was necessary to model the BBB structure in a way which had accurate spatial resolution of mass and stiffness, but was not overly complex or computationally expensive. For global structural assessments, as the BBB, structural models are more than adequate for serving as an analytical representation. Fully three-dimensional finite element models are impractical due to the great number of elements needed in characterizing the entire structure, given current computing power and the time needed in constructing such a complex model. This is not to say that three-dimensional finite element models are not ever appropriate in St-Id applications however. For cases where specific components of the structure need finely discretized analysis, such as required by a stress concentration study, then more complex models are justified.

12.3. Overview of an Error-screening Flowchart for Development of Structural Models

The error screening flowchart utilized for complex models follows a systematic approach similar to that of the construction of the geometric model in CAD software. The first stage (Figure 12-4) consists of importing the main geometry corresponding to the primary

structural elements. For this reason, it is important to make sure that primary and secondary elements are kept on separate layers in the CAD software so that they may easily be imported separately in the FE software.

After the primary structural elements are imported, the first stage of error screening requires the assigning of temporary boundary conditions (simply supported works well) and temporary cross section properties for all members. This allows the FEM to be resolved by the software for various loading conditions. Even though the structure is not representative of the actual structure in any means besides its overall geometry, by staging the model construction and error screening process in such a manner it is possible to break the daunting task of errors screening down into stages of increasing model complexity in which the errors being screened are of increasing complexity and subtly.

Using the temporary boundary conditions and section properties the model was resolved using both static and modal analyses to allow the examination of the following properties: symmetric reactions, symmetric displaced shape, unintended breaks or discontinuities, and finally unintended rigid body modes. If any of these errors are discovered, the analyst should identify and remove the cause, which commonly include duplicate members and missed connections of elements. Duplicate members arise in the construction of the CAD geometric model. A simple copy and paste error could accidentally create two lines on top of each other, unbeknownst to the user. However, in the FEM, this duplication results in extra mass at that location and must be corrected.

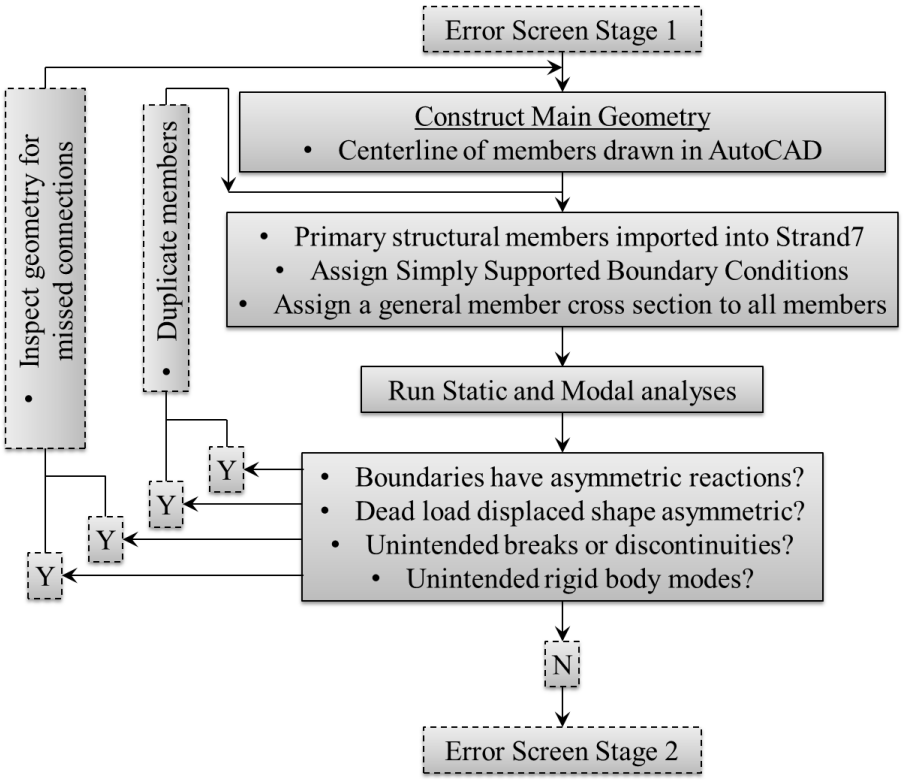

Figure 12-4: Stage 1 of Error Screening Flowchart

The second stage of the error screening process focuses on the addition of secondary structural elements (Figure 12-5). This is a critical stage, where many error sources often arise. Typically, secondary elements consist of many small elements connected together with links. It is very easy to miss a link between two elements and at the same time it is not very easy to detect its absence. By following this error screening methodology, the user has the most efficient tools available to detect such errors.

Major indicators to investigate in the second error screening stage are once again symmetric boundaries (where reasonable), reasonableness of deformed shapes due to dead load, no unintended breaks or discontinuities present in the modeshapes and no unintended rigid body modes.

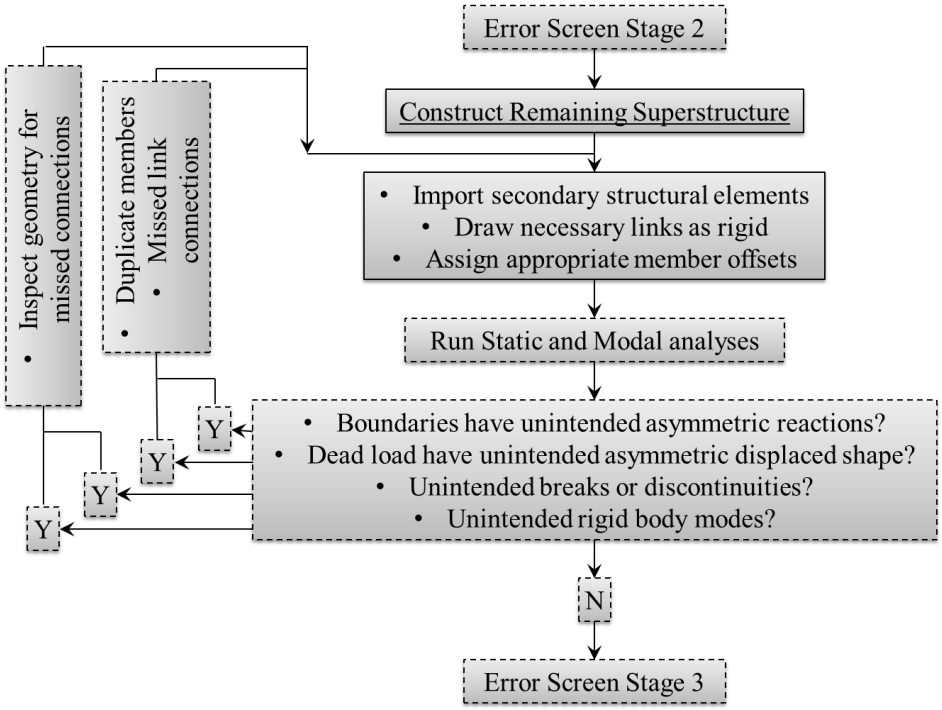

Figure 12-5: Stage 2 of Error Screening Flowchart

The third and final error screening stage (Figure 12-6) primarily involves the assignment of appropriate member cross sections and material properties as well as appropriate

boundary conditions (based on available knowledge and site visits) as well as link definitions. In FEM's for complex structures, it is absolutely essential that all errors associated with geometry and missed connections are mitigated before assigning cross sections and material properties. Many simple mistakes can be made with assigning cross sections, so it is imperative that the user is confident that the errors are not due to some other source.

Once again, the reactions are investigated for symmetry where appropriate and the displaced shapes due to dead load are carefully inspected for reasonableness. One new indicator to use at this stage is the magnitude of displacements due to a unit load and the natural frequencies from the modal analysis solver. If the period of a mode (depending on the structure of course) is such that one cycle of the vibration would take longer than is physically possible (e.g. several seconds or minutes or days or months) to complete, then there is a clear indication that errors are present. Similarly, if the period is so small that the structural frequencies are outside of the typical range for a structure of comparable span length, then the cross sections must be analyzed for correct units and accuracy according to documentation.

An easy method of error screening problems arising from assigning member cross sections is to check the material densities assigned as well as the areas of each cross section. In many cases, the areas can easily be compared against standard manuals or the design drawings. Also, the units must be checked thoroughly since the model may have been in a larger unit setting while defining the geometry of the elements and was not switched to units more commonly associated with areas and shape properties.

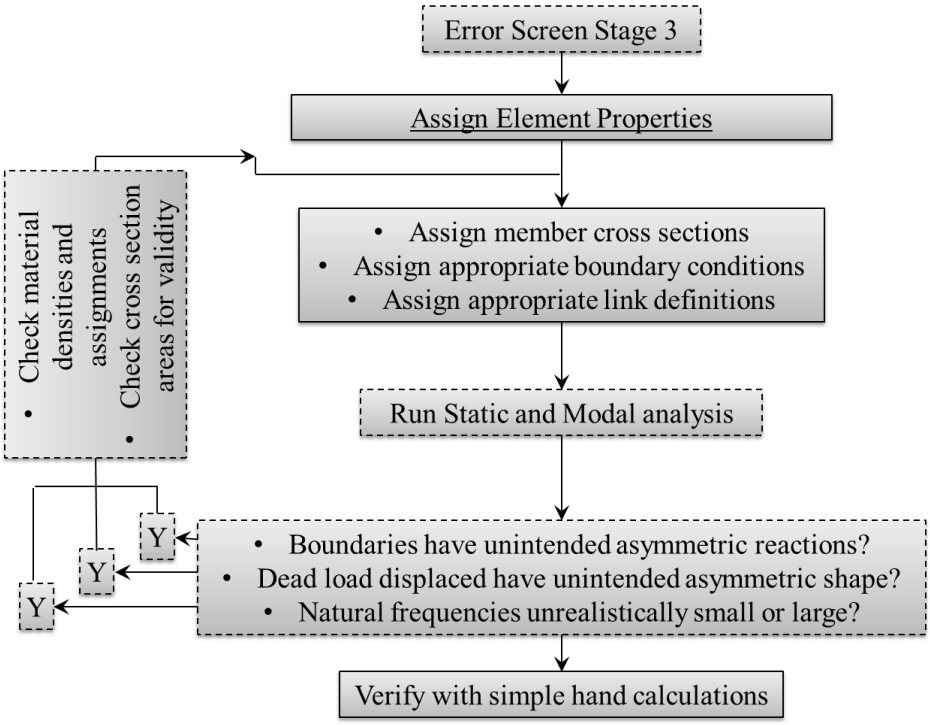

Figure 12-6: Stage 3 of Error Screening Flowchart

This overall error screening process was applied to the BBB geometric model as it was imported into SAP2000. The next three sections will describe how each of the three main error screening stages was applied to the BBB model.

12.4. A Priori Model Construction in SAP 2000

As mentioned above, the a priori model for the BBB was used to design the multiple instrumentation plans designed for the planned experimental observations, the details of which are discussed in Chapter 13. The foundation of a finite element model construction

in general begins with the development of a detailed CAD model. Finite element software packages are somewhat notorious for their ineffectiveness in building models of large and complicated structural systems. CAD programs have more user friendly tools for developing the centerline geometry, as done in Chapter 11, than most FE software packages. For this reason, the geometry generated in the CAD software was imported into the FE software and modified from that point. This section will describe the construction of the a priori model in SAP2000 with 4 subsections: (1) Overview of the Error-Screening Flowchart, (2) Importing the Geometry, (3) Modeling Local Structural Components and (4) Member Section Assignment.

12.4.1. Importing the Geometry

The CAD file developed and described in Chapter 11 was first separated into layers corresponding to primary and secondary structural elements and then imported into SAP2000 according to the error screening process outlined above. Every member was assigned the SAP2000 default beam element type with six degrees of freedom per node and all spans were assigned boundary conditions consistent with a simply supported beam.

At this stage of the BBB model, all four reactions from the lift span were equal, since the main truss is symmetric about its transverse and longitudinal centerlines. The tower span reactions were symmetric about the longitudinal axis of the bridge, however since the structure is not symmetric about its transverse axis, those reactions were correspondingly not symmetric.

Any detected breaks or discontinuities, which are amplified by examining the modeshapes for “flailing members”, were corrected by redefining their connections in the FEM. Rigid body modes tend to arise when boundary conditions are not defined correctly, and at this stage occur rarely. However, their presence would indicate a fundamental problem somewhere within the model. Another typical source of error is duplicate members. These can affect the mass of the structure significantly, especially if it is a member with a large cross section. Most FE software packages can detect this automatically, and this type of check should be carried out.

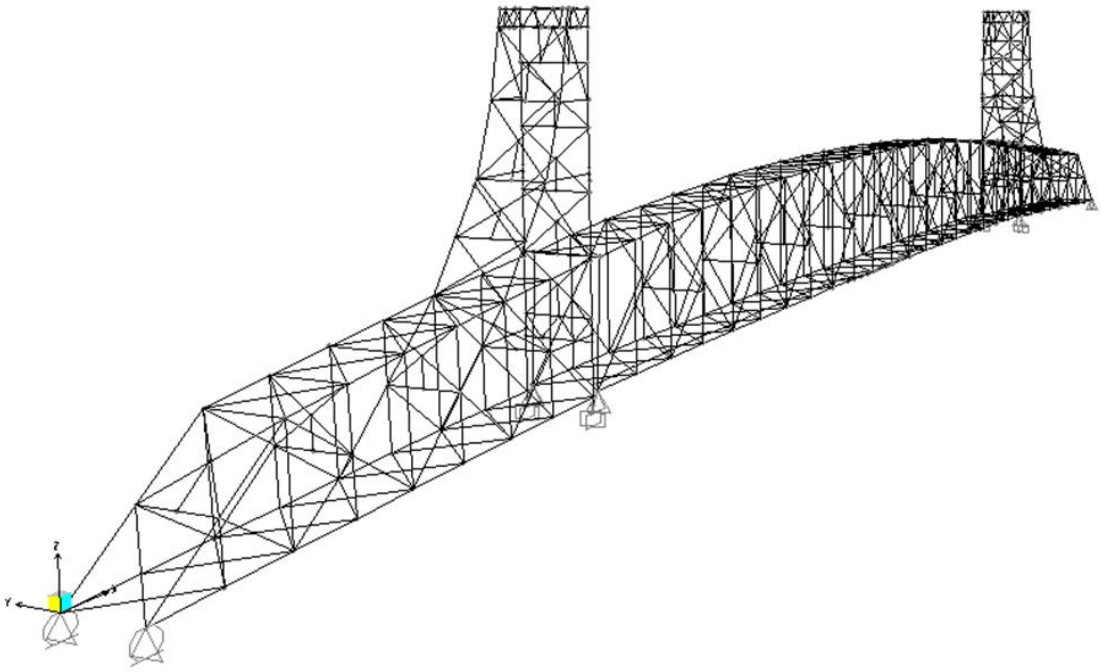

Figure 12-7: FEM after Stage 1 Error Screening

12.4.2. Modeling Secondary Structural Components

The secondary structural elements were imported into the model utilizing the same geometric reference coordinate system as the primary structural elements so that the members align exactly as they did in the CAD model. The secondary beam elements (floor beams, stringers, cross beams, etc.) were imported as beam elements with six degrees of freedom per node. The deck was imported as a four-sided shell element. The deck was temporarily assigned a unit thickness for the debugging process.

Links between members which are separated geometrically but have a physical connection in the actual structure can be either drawn in CAD and imported, or can be drawn in the FE software. In this case, the links associated with the BBB model were drawn by hand in SAP2000.

Initially, all links were defined as rigid and any member offsets which must be defined in the model were set to appropriate values as determined by the design drawings. However, when utilizing links to connect members drawn at their neutral axis, member offsets typically are not needed (Figure 12-8). Note that in Figure 12-8 the one dimensional lines representing the various members are shown as dashed lines, while the physical shapes of the members are represented with the gray boxes. The links are represented as the dark thick lines and connect the various beam element centerlines. Once the secondary elements, which once again for the BBB include stringers, floor beams, decking, and cross beams, are imported (Figure 12-9) these members are also assigned the same general cross section applied in Stage 1. The reason for this is to eliminate any simple error sources arising from cross section assignments at this stage.

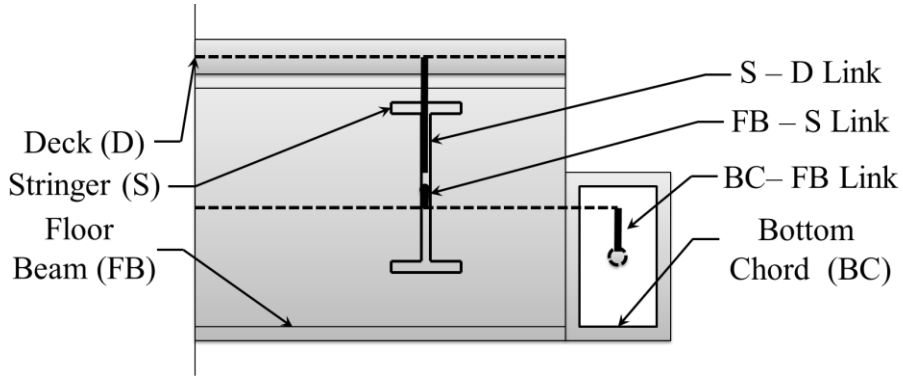

Figure 12-8: Schematic Showing Link Connectivity

The main error sources examined for after running the same static dead load and modal analysis in the FE software are missed element connections, duplicate members and missed link element connections. These can be detected by once again examining for unintended symmetric reactions. In the case of BBB, the centerline of the roadway is not congruent with the centerline of the truss thus indicating the upstream truss should have reactions which are different than the downstream truss. However, at this stage for the lift span reactions at each end of the same truss should be equal. It was expected that the reactions of the tower span at the supports closest to the towers would be much higher than those closest to the expansion bearing. This type of behavior was seen in the dead load reactions, and deemed reasonable.

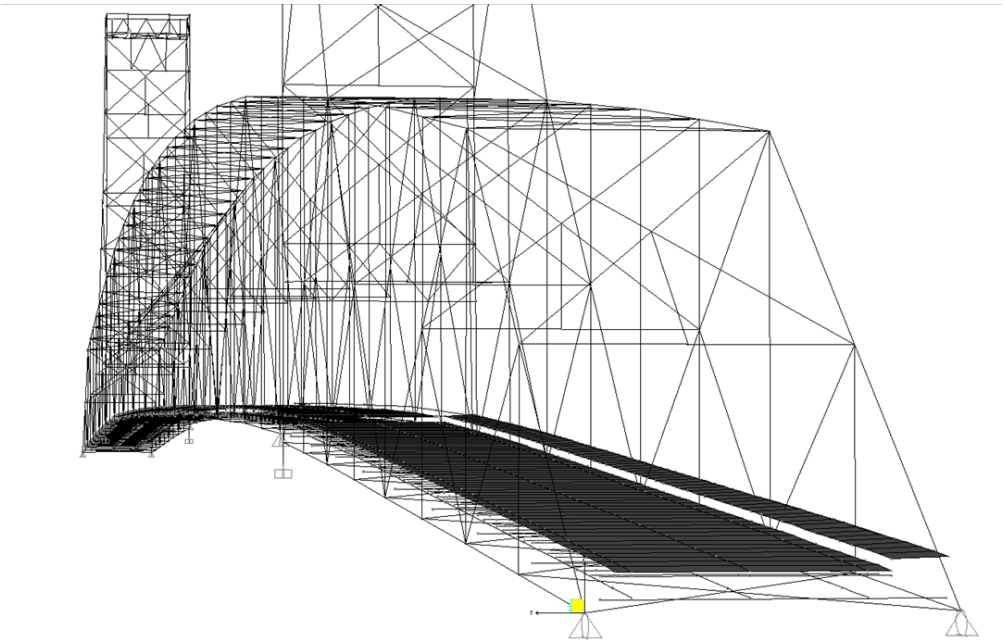

Figure 12-9: FEM after Stage 2 Error Screening

12.4.2.1. Member Section Assignment

The final stage of constructing and error screening the BBB model involved assigning the member cross sections, boundary connections and appropriate link definitions. For the BBB, the cross sections are almost all of a built-up construction, where plates, angles and/or channels are riveted together to form a more robust shape (Figure 12-10). This type of construction reflects the technology available when the BBB was built, where advances in producing rolled shapes were not available or cost effective.

Figure 12-10: Built-up Members of the BBB

To develop section properties that adequately represent such complex shapes, specific software was used to build up the independent components according to the construction plans (Figure 12-11) and develop a single cross section which includes all individual components. The software used for the a priori model to accomplish this task was called Section Builder. One clear assumption made however, is that the lattice work provides full compatibility in its connection of separate members. For example, the rightmost cross section in Figure 12-11 consists of four independent angles, as opposed to the middle

cross section which was merged to form a single shape. However, even in the case of the middle figure, the bottom two angles are not connected by lattice work. The assumption made forces the geometry of the cross section to maintain compatibility during deformation (e.g. plane sections remain plane), consistent with a linear elastic modeling approach of a fully connected cross-section, and more specifically that the spacing between members connected by lattice work to not change as well.

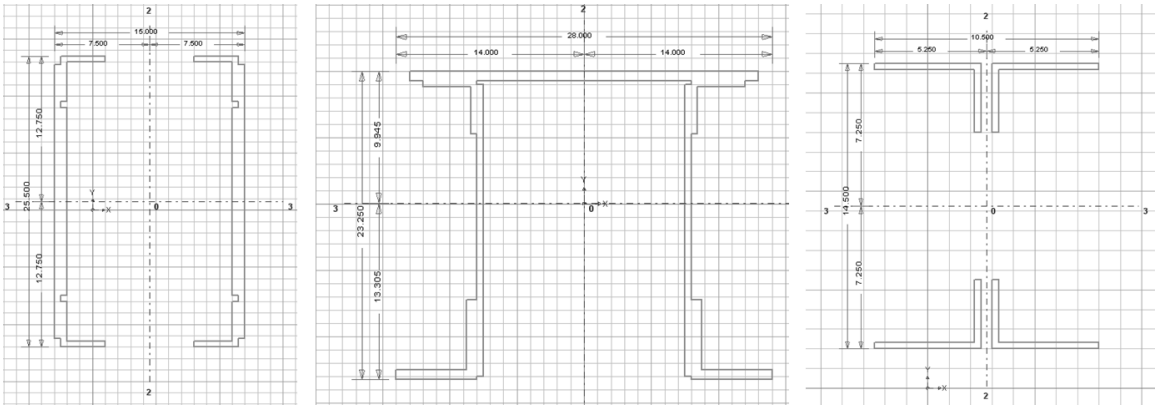

Figure 12-11: Cross Sections Assigned during Stage 3 Error Screening

12.4.2.2. Assignment of Boundaries and Link Definitions

After all cross sections were applied to the structure as specified in the design drawings, the boundary conditions were examined more closely to determine which assignments

would best represent the physical structure. After searching the plans, the best information available suggested that the tower spans should have been assigned rollers at the non-tower end and fixed supports at the tower end of the spans. As for the lift span, the lateral translational degrees of freedom were restrained; however the structure was allowed to move in a longitudinal translational direction. To make the model stable, one end of the lift span was restrained from longitudinal movement, however. All rotational degrees of freedom were released for the lift span supports, as no a priori information suggested otherwise.

All links were kept as fully rigid, since once again no a priori information was available to suggest otherwise. The major link types for the lift span consisted of:

- Bottom Chord – Floor Beam
- Floor Beam – Stringer
- Stringer – Cross Beam
- Cross Beam – Deck
- Floor Beam – Deck

The major link types for the tower spans consisted of:

- Bottom Chord – Floor Beam
- Floor Beam – Stringer
- Stringer – Cross Beam
- Cross Beam – Deck
- Floor Beam – Deck

12.4.3. Model Verification

The original a priori model was verified with two methods: (1) a simple hand calculation estimate of static member reactions and (2) a comparison of dead load to the quantities derived by hand and discussed in Chapter 11. The application of a simple hand calculation for complex structures such as the BBB is not as straightforward as it was for the DI3 grid, however with the use of heuristics to make appropriate simplifying assumptions and bound responses; it is possible to estimate the order of magnitude member actions for comparison with the model results. Additionally, the masses of the structure and the extraneous mass sources needed to be verified to ensure that they matched the tally of mass applied to the model. This is a simple error checking scheme to minimize the effects of applying incorrect masses or cross section properties.

12.4.3.1. Model Verification via Hand Calculation of Static Response

To compute a rough estimate of the displacement of the lift span due to a point load in the middle of the span, the structure needed to be simplified through additional assumptions. The first assumption made was that each truss carries exactly half of the load, thereby only requiring one to be analyzed. The second assumption made was that the truss acts as a simply supported beam and that the top chord and bottom chord members develop equal and opposite member forces. By simplifying the structure in this manner, it was then possible to reduce the truss into a beam and use classical mechanics to estimate member forces.

The moment in the center of the truss was computed for a point load at the center of a simply supported beam, as shown in Eq. 12-1.

$$M = \frac{PL}{4} \qquad \textbf{Eq. 12-1}$$

Using this computation and a span length of 537', a maximum moment of 67.125 kip-ft was applied at mid-span of the truss due to a unit point load at mid-span. This applied moment must be equally balanced by the truss. The moment reaction of the truss was computed by generating a force couple representing the distribution of force within the truss. Since it was assumed that the truss is of constant height and that the top and bottom chords have equal and opposite reactions, a simple computation (Eq. 12-2) can be made to find the axial force in the top chord of the truss.

$$HC = \frac{PL}{4} \qquad \textbf{Eq. 12-2}$$

In this equation, H is equal to the height of the truss at mid-span and C is equal to the compressive force in the top chord (or the tensile force in the bottom chord), while the right-hand side represents the applied moment. In solving for the compressive force within the top chord due to a unit point load at mid-span, it was estimated that the compressive force was equal to 1.12 kips.

In applying a unit point load to the middle of the lift span in the FE model, the top chord member actions were found to be 0.89 kips due to the unit point load. This roughly 25% discrepancy is reasonable given the assumptions made in the hand analysis and provided a sense of confidence that the model behaved as intended.

Finally, the dead load of the structure was computed in the FE model by applying a gravitational load to the entire model and summing the reactions at the boundaries. It is important that the extraneous mass sources applied in the model be included in this analysis so that potential errors within their implementation could be identified. By simply comparing the summed reactions from the model to the hand computation of mass, errors associated with incorrectly assigned cross sections or mass sources can easily be identified.

12.5. Development of a Refined A Priori Model for the BBB in Strand7

The base model in the Strand7 finite element analysis software was constructed from the framework of the SAP2000 model developed in Section 12.4. Strand7 has the ability to import SAP2000 model files directly into its workspace, however some properties such as cross section visualization do not transfer and need to be redefined. The most critical step in constructing finite element models always is in defining the geometry, so significant work was saved by being able to reuse the geometry from the SAP2000 model and only needing to reassign cross section properties. Four subsections will discuss the model construction process in Strand7, by utilizing the geometry from the SAP2000

model: (1) Development of the Geometry in Strand7, (2) Development of Continuity and Boundary Conditions, (3) Incorporation of Approach Spans and (4) Model Reduction.

12.5.1. Development of Geometry in Strand7

Once the geometry from the SAP2000 model was transferred into the Strand7 working environment, the same debugging strategy as discussed in Section 12.3 for the SAP2000 model was utilized on the Strand7 model. Small differences in the solver for Strand7 required modifications to the geometry in order to run a successful analysis. For instance, in SAP2000 if a beam element has separate elements connecting between its end nodes SAP2000 will automatically enforce compatibility between the two elements (Figure 12-12L). However, in Strand7 there cannot be interior overlapping of elements, thus each element needed to be subdivided in order to ensure that each connection between beam elements occurred at nodes for both elements (Figure 12-12R).

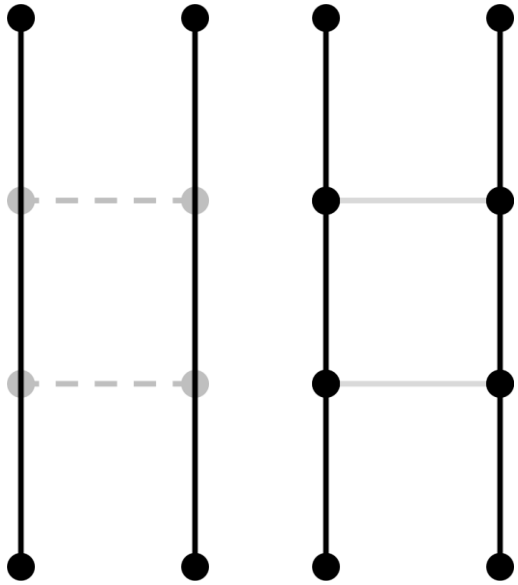

Figure 12-12: Element Connectivity for SAP2000 with Three Elements (L) and Strand7 with Eight Elements (R)

Besides the finer discretization required for ensuring appropriate connections within Strand7, there were no additional requirements in modifying the geometry from the SAP2000 model for the Strand7 framework. However, additional features of the BBB were incorporated into the model in two main groups to ensure that it represented the physical nature of the bridge. These groups consisted of adding the piers and the approach spans to the finite element model.

12.5.1.1. Addition of the Approach Spans

During the hazard identification phase, Dr. Mishac Yegian of Northeastern University, an expert in seismic vulnerability assessment, was brought to the bridge for his opinion

on the vulnerability of the piers and the potential for pile loss or deterioration. As a result of this consultation, it was decided to include all substructure and approach spans within the model in assessing the varying levels of vibration noted.

Following this realization, all models which were already built were merged into one large model. Additionally, the approach spans beyond the deck truss spans, those supported by steel columns, were also included in the model. At this point, the model construction took a large step backwards as the error screening phase had to be started from the beginning. The geometry of the approaches was first added into the AutoCAD model and then imported into the Strand7 model. Connectivity and dimensions were verified using the techniques described earlier. Finally, section properties were assigned to the approach stringer spans. The boundary and continuity conditions between all of the spans will be discussed in Section 12.2.2.

The final version of the full BBB Strand7 model of the superstructure (Figure 12-13) consisted of 6,837 beam elements and 1,910 shell elements.

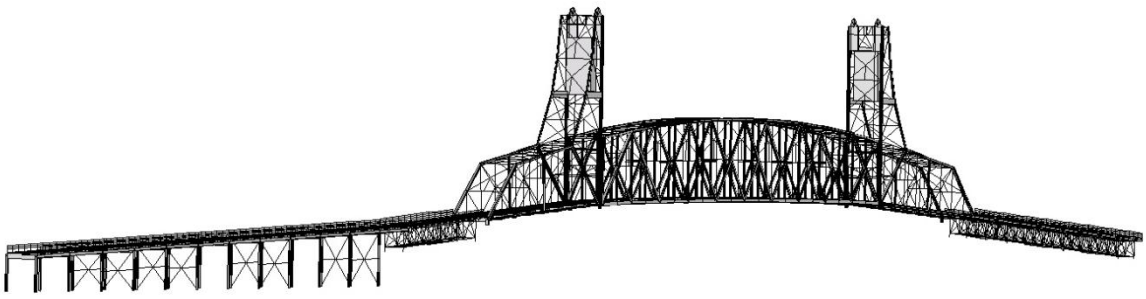

Figure 12-13: Full BBB FE Model without Piers

12.5.1.2. Addition of the Piers

In any finite element model, once the geometry is defined the next steps typically include defining continuity and boundary conditions of the model. In practice, it is not uncommon to find great attention to detail in terms of modeling the structure, however in representing the substructure some models fall short. In the initial SAP2000 model, the substructure was not included for the sake of simplicity. The boundary conditions were applied directly to the superstructure itself with no regard to the connectivity provided by the piers. However, in the more detailed Strand7 model, it was determined that including these piers was necessary.

As discussed in Chapter 11, all of the piers were modeled in AutoCAD in full three-dimensional representation. The choice to be made at this stage was which element type is most appropriate to represent the piers. Since the piers all have complex shapes, consisting of two main columns with arched walls between them, it was decided that solid elements would best represent their geometry and kinematic behavior. Of the vast solid element types in Strand7, the most simple was selected to represent the concrete piers: the tetrahedral solid element. This element, with a total of four nodes, was selected since only the global mass and stiffness contributions of the piers were desired and not specific stress concentrations within piers themselves. However, due to the capability of the software it would not be difficult to change the element type in the future if such a change was deemed necessary.

The geometry of the piers were imported into the Strand7 model by first exporting from AutoCAD the pier geometry in the ACIS file structure, which is a three-dimensional

modeling engine. This file was then imported into Strand7 as three-dimensional geometry. Tools within Strand7 allowed the geometries to be automatically meshed based on element type and maximum allowable size/distortion. The maximum element size for each pier was selected based on its ability to appropriately represent the geometry of each pier. Specific surfaces can cause problems with automatically generated meshes, such as: curved surfaces, abrupt changes in section and sharp corners. It is important that the mesh is previewed on the geometry of the object being modeled to ensure that the geometry is sufficiently represented (especially around curved surfaces).

In the case of BBB, it was ensured that all curved surfaces were reasonably represented without compromising mesh quality. Strand7 has built-in mesh checking features that detect when distorted elements were created or a successful mesh was not able to be generated, based on pre-defined quality criteria within the software. In some cases, the geometry must be refined or the maximum element size must be adjusted. After each of the piers were meshed (Figure 12-14 - Figure 12-21), the connections between the piers and the superstructure were defined.

In addition to the quantity of elements described earlier, the piers required a total of 90,018 solid elements. The total number of nodes in the final model (Figure 12-22) was 30,956.

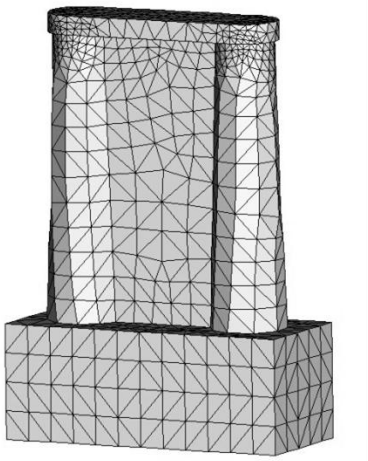

Figure 12-14: 3D FE Model of Pier 1

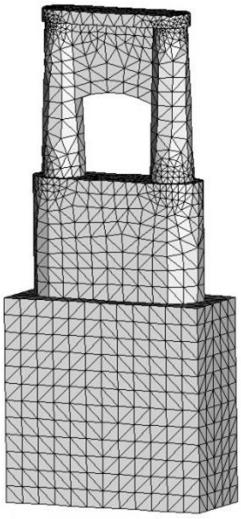

Figure 12-15: 3D FE Model of Pier 2

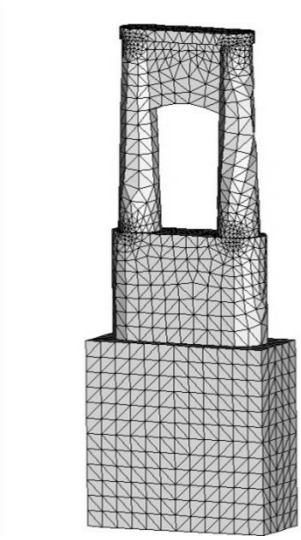

Figure 12-16: 3D FE Model of Pier 3

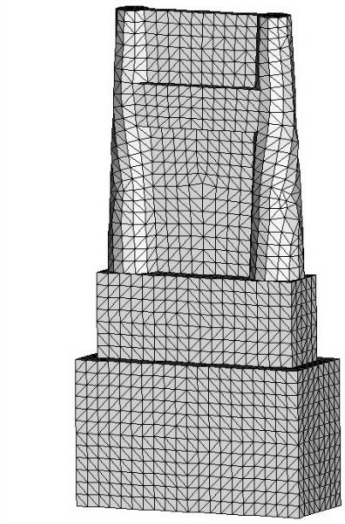

Figure 12-17: 3D FE Model of Pier 4

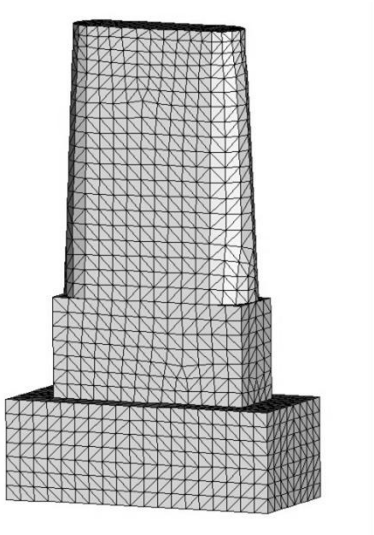

Figure 12-18: 3D FE Model of Pier 5

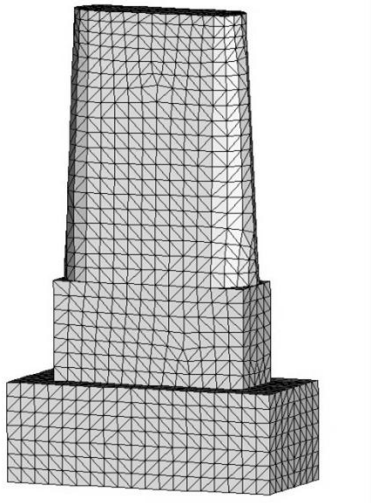

Figure 12-19: 3D FE Model of Pier 6

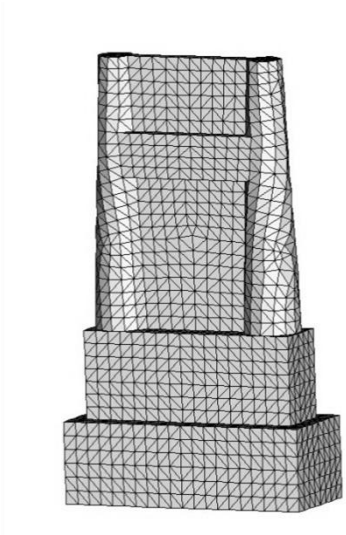

Figure 12-20: 3D FE Model of Pier 7

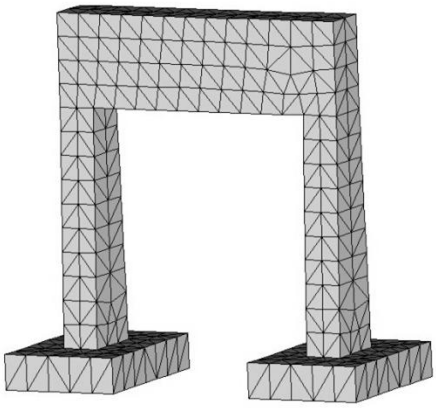

Figure 12-21: 3D FE Model of Pier 8

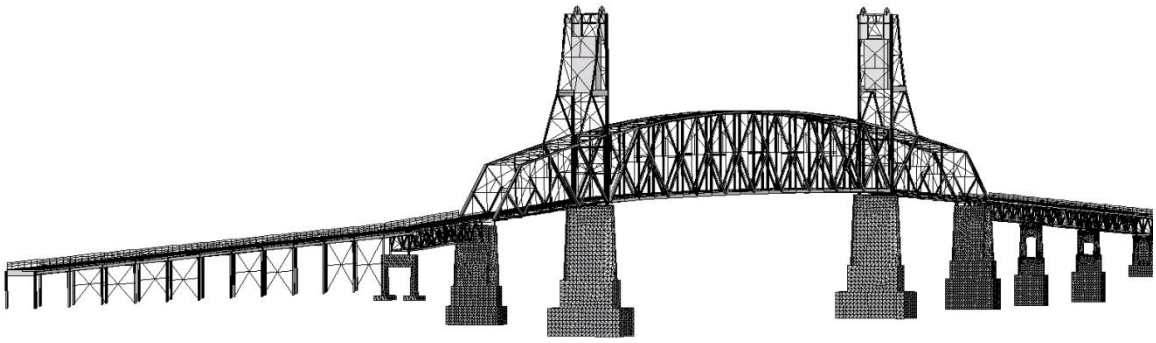

Figure 12-22: 3D FE Model for the BBB with All Geometry and Cross-sections Represented

12.5.2. Development of Continuity and Boundary Conditions

Once the geometry has been defined and member cross sections have been assigned to the finite element model, the final stages of the model construction process are the assignment of continuity and boundary conditions. In the a priori SAP2000 model, there were no continuity conditions between the spans and each was treated as either fixed, pinned or roller supported. However, the more refined Strand7 model included a much more detailed representation of the approaches and piers and required an accurate portrayal of how the spans interacted with each other and the piers supporting them.

12.5.2.1. Lift Span Supports and Restraints

The lift span is supported on each corner by live load shoes, as described in Chapter 11. These shoes do not provide any lateral or longitudinal restraint (beyond friction due to a small amount of dead load normal force and live load normal force); however provide a vertical support of live load traffic crossing the structure. The dead load of the span is mostly balanced by the counterweight. To incorporate this system, multiple components needed to be added to the finite element model: (1) a linkage between lift span and supporting piers and (2) linkages representing lift span – tower span interactions.

To attach the lift span to the piers in a manner that only vertical translations were forced to be compatible, a link was installed between the bottom chord node of the lift span and a node directly underneath the lift span on the top surface of the pier in which only vertical translations were forced to be composite (Figure 12-23). A Master-Slave link type was chosen since this was the only option within the Strand7 link element library that allowed for the individual selection of degrees of freedom to enforce between two nodes.

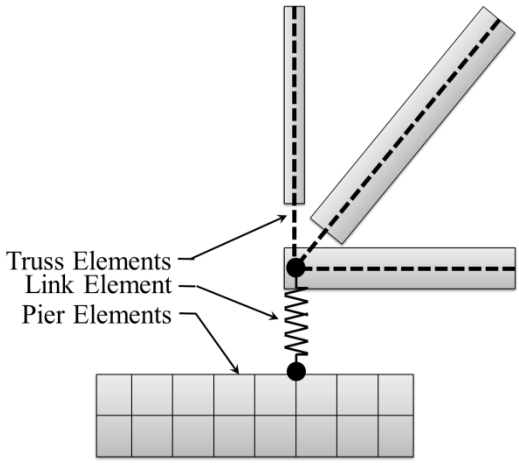

Figure 12-23: Schematic of Attaching Lift Span Truss to Pier

In addition to the live load shoes, the lift span was constructed with guides that provided some level of transverse and longitudinal restraint, as discussed in Chapter 11 but shown again for clarity. Details were constructed on the lift spans and tower spans which serve as guides while the lift span opens and closes. These guides connect the top and bottom chords of the lift span to the main columns of the tower span with four unique connections.

On the New Jersey side of the lift span, the bottom chord is restrained in a lateral direction as well as a longitudinal direction to the column of the NJ Tower span (Figure 12-24). On the New Jersey side of the lift span, the upper chord is restrained only in the lateral direction, and is free to move in the longitudinal direction (Figure 12-25). The restraints consist of large steel arms which extend from the lift span and bear against a

steel guide. These guides are periodically greased to ensure that the lift span freely moves during an opening.

Figure 12-24: Lift Span Guide for the NJ Bottom Chord Connection

Figure 12-25: Lift Span Guide for the NJ Top Chord Connection

The Pennsylvania side of the lift span has both top and bottom chords restrained only in the lateral direction to the columns of the PA Tower span (Figure 12-26 & Figure 12-27). This creates a simply supported overall boundary condition for the lift span.

Figure 12-26: Lift Span Guide for the PA Top Bottom Connection

Figure 12-27: Lift Span Guide for the NJ Top Chord Connection

To model these restraints in an effective manner, Connection elements were utilized to assign discrete stiffness values to the various degrees of freedom corresponding to the restraints. A connection element in Strand7 is a special form of a beam element in which the user assigns six stiffness values corresponding to the three translational degrees of freedom and three rotational degrees of freedom between the two nodes which the element is connected to. This element was preferred over a link to model the restraints since some “slop” does exist in these connections, and they may not be perfectly rigid. In the a priori stage however, high stiffness values were assigned to the degrees of freedom corresponding to the directions restrained in the actual structure. The connection elements were defined between the corner nodes of the truss and nodes on the columns of the tower span so that the elements were perpendicular to the vertical columns of the tower span (Figure 12-28).

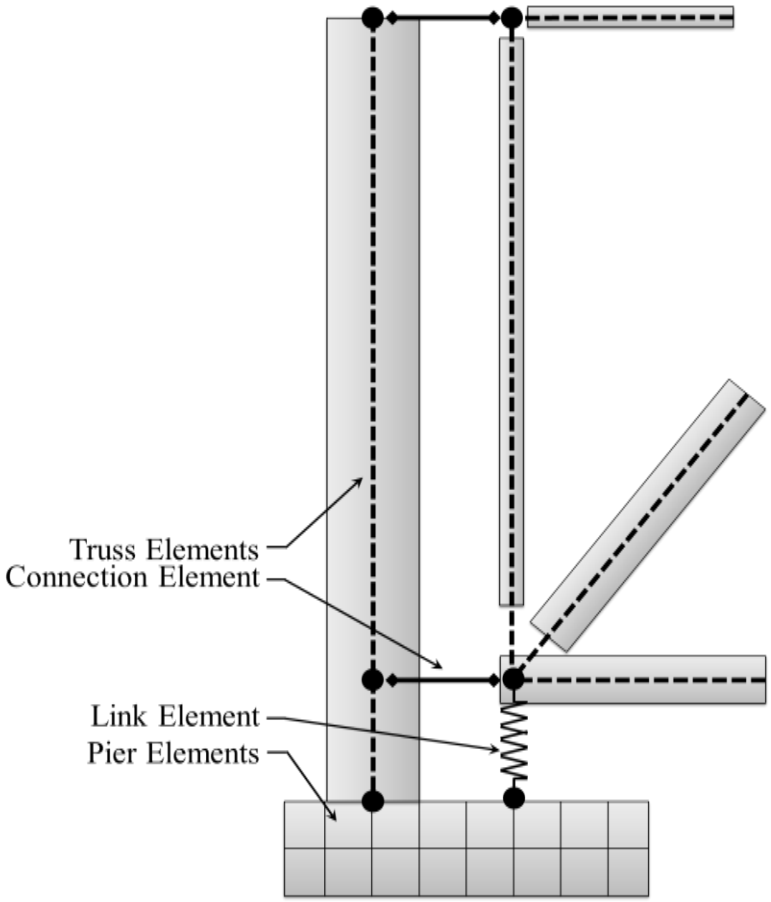

Figure 12-28: Schematic Showing Connection Element Locations

12.5.2.2. Tower Span / Pier Continuity Conditions

The tower spans, as previously mentioned, have boundaries consisting of a fixed – roller support condition. To assign a completely rigid connection between the beam elements of the tower span and the solid elements of the piers, links needed to be assigned to enforce continuity between the two different element types. Since solid elements do not have rotational degrees of freedom, it was not possible to assign a rigid connection by simply

connecting the frame element to a node on the solid elements in the pier. However, a system of links (Figure 12-29) was defined to enforce that a rotation in the column of the tower span would be transmitted to the pier cap.

By using a set of four links to connect the beam element corresponding to the tower span column to four nodes of the pier cap in the configuration shown below, it is possible to enforce continuity between the beam element and the solid elements. Each link was assigned a rigid property type with all degrees of freedom fixed.

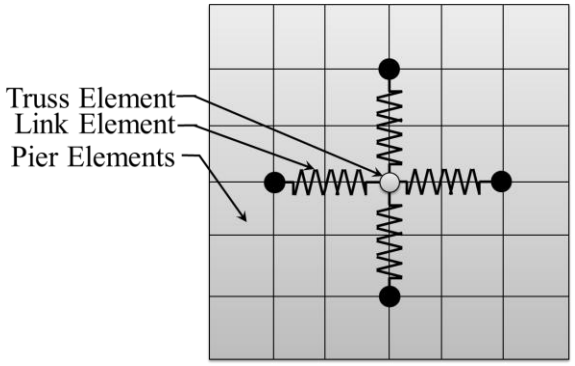

Figure 12-29: Schematic Showing Fixed Connection of Tower Span Column to Pier Cap

To create the roller support condition on the opposite end of the tower span, a similar system of links was used to connect the end post of the tower span truss to the pier cap as shown above for the fixed end. To simulate the rotational and translational releases that a

roller connection exhibits, the member end properties of the end post were adjusted. This type of model representation is beneficial for multiple reasons over a more simple representation, such as a single link with the restrained degrees of freedom assigned. By releasing the rotational and translational degrees of freedom of the end post of the truss, it is possible to also incorporate a rotational or translational spring into these released degrees of freedom to simulate a frozen bearing, which for an eighty year old structure is not unreasonable.

Four links were defined between the end post of the truss and the pier cap, as shown in Figure 12-29, and each were assigned a fully rigid link definition. Then, using beam modification tools within Strand7, the rotational and translational degrees of freedom corresponding to a roller support were fully released for the a priori model (Figure 12-30).

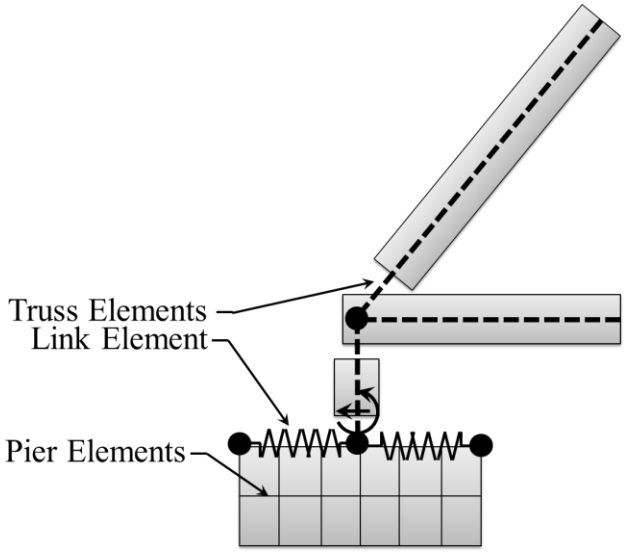

Figure 12-30: Schematic Showing the Modeled Connection for the Expansion End of the Tower Spans with Released Degrees of Freedom

12.5.2.3. Truss Span / Pier Continuity Conditions

Each of the four deck truss spans is in a simply supported boundary configuration. To model these supports in a way that accommodates the incorporation of frozen bearings, a similar approach was taken as with the expansion bearings of the tower span. The end post members on each end of the truss span were rigidly connected to four nodes on the pier cap to ensure rotational and translational compatibility. Then, the end post element itself was assigned rotational and translational releases to produce a roller or pin boundary support.

12.5.2.4. Approach Span Boundary Conditions

The approach stringer spans were originally intended to be simply supported between each of the column supports, however over the course of the lifetime of the bridge they were retrofitted to become continuous. The longitudinal stringers originally were only connected to the floor beams spanning the two supporting columns with clip angles attached to their webs. During a retrofit to stiffen the floor system, however, the top and bottom flanges of adjacent stringers were connected by welding plates to each of the stringers flanges, making them continuous.

To model this interaction, rigid links were assigned between the centerline geometry of the stringers and the floor beams, thus making the stringers continuous on either side of the floor beam. The floor beams were rigidly connected directly to the vertical support columns.

In the a priori model, no information is initially known about the foundation stiffness provided by the concrete mat foundation supporting the vertical columns, so the columns were assigned a fixed boundary condition in the FE model.

12.5.2.5. Pier Boundary Conditions

The piers spanning the Delaware River rest on a variety of soil types and stratifications. However, Piers 1 through 7 all sit on timber piles driven to appropriate depths and lengths to provide sufficient bearing capacity. Each of the pile caps is below the mean low tide level of the river, meaning that the bearing capacity should not be compromised by rotting timber.

With this in mind, each node of the bottom face of the piers in the FE model were assigned pinned boundary conditions. By assigning pinned supports to each of the nodes along the bottom face, a global fixed support is created by restraining rotation and translation of the pier along the bottom face.

12.5.2.6. Counterweight Continuity Conditions and Counterweight Cables

The counterweights housed within the tower spans are not completely free hanging. Each counterweight is fitted with a slotted piece of steel which runs along guides on the inside face of the tower span columns (Figure 12-31). The cross section of the tower span columns (Figure 12-32) shows the guides for both the lift span and the counterweights. The interaction between the guides and the channels attached to the counterweight allow for a small amount of movement, so that the counterweights are assured freedom of movement, so this interaction cannot be modeled as a rigid connection.

Figure 12-31: Concrete Counterweight with a Steel Channel Bearing Against Guides

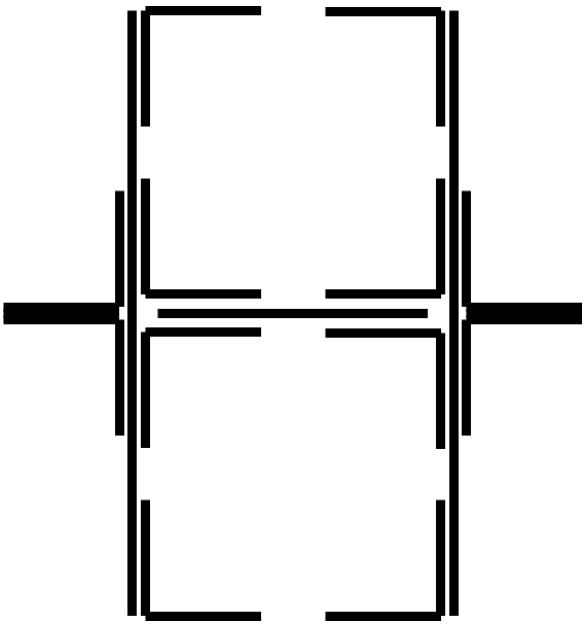

Figure 12-32: Tower Span Cross Section Showing Guides for Counterweights and Lift Span

To model this interaction of the counterweight and tower span columns, connection elements were used to define a translational stiffness between the counterweight and the beam elements corresponding to the tower span column. The freedom of the connection element to assign variable stiffness to different degrees of freedom makes it a powerful element in a multiple model study, since this will certainly serve as one of the uncertain model building blocks for the BBB.

To represent the cables which connect the counterweight to the lift span, cable elements (a special type of beam element in Strand7) were used. Since the analysis types anticipated being carried out for the BBB did not include nonlinear geometry analyses, Strand7 automatically converts the cable elements to truss elements which have only three translational degrees of freedom per node. In his manner, the cable elements will be representing the axial stiffness provided by the cable, if any, during the vibration analysis of the lift and tower spans.

12.5.3. Strand7 Model Reduction

The final constructed model for the BBB was very large and required considerable analysis time to compute the modal parameters. Considering that the anticipated measured observation for the span was identified as natural frequencies and modeshapes identified through ambient vibration monitoring, it was critical that the base model for the MM St-Id analysis can efficiently compute these responses. Originally, it was required to analyze the model for its first 500 natural frequencies in order to capture all of the global natural frequencies of interest (up through and including third torsional modes for each

span). This analysis took over 30 minutes to complete and it was evident that this would not suffice for an approach that may require many thousands of models to be generated and executed. This is one area where the MM St-Id method will only improve over time, as additional computing resources become available to speed the computation time of such complicated models. However, in this case a more refined model needed to be built so that a reasonable MM St-Id analysis could be carried out as a case study. To complete this, the model needed to be condensed in terms of stiffness and mass. The regions of the model which were condensed include the approach stringer spans, approach deck truss spans, all piers and any flexible cross bracing or other slender sections which generate local modes and decrease the efficiency of modal parameter computation. This condensation will be described in two subsections: (1) Condensation of Approach Spans and the Piers and (2) Condensation of Local Modes.

12.5.3.1. Condensation of Approach Spans and All Piers

The BBB model at this stage included all deck truss spans, the NJ stringer span approaches and every pier modeled in solid elements. One of the main contributing factors towards the half hour analysis time was the analysis of the solid elements representing the piers. Additionally, many modes of the approach spans were in the same frequency band as those corresponding to the modes of the spans of interest. For this reason, it was decided to condense the approach spans and piers into a nodal mass and spring representation.

The method in performing this type of condensation consisted of generating stiffness-based shape functions of the structures being reduced. In this manner, the stiffness coefficients at the desired degrees of freedom could directly be computed and the shape functions could be used in conjunction with the structural mass density of the structure being condensed to generate a corresponding mass coefficient at the degree of freedom of interest.

Before the shape functions or stiffness coefficients could be computed, the degrees of freedom needed to be selected which the structures would condense into. Eight nodes were identified as the locations where the approach spans and piers would condense to: (1-2) the east and west pier cap of Pier 4 (PA Tower Span Expansion End), (3-4) the east and west pier cap of Pier 5 (PA Tower Span Fixed End), (5-6) NJ Tower Span Fixed End and (7-8) NJ Tower Span Expansion End (Figure 12-33). Each nodal location has six degrees of freedom which must be accounted for in terms of stiffness and mass, leading to a total of forty-eight stiffness and mass coefficients needing to be computed.

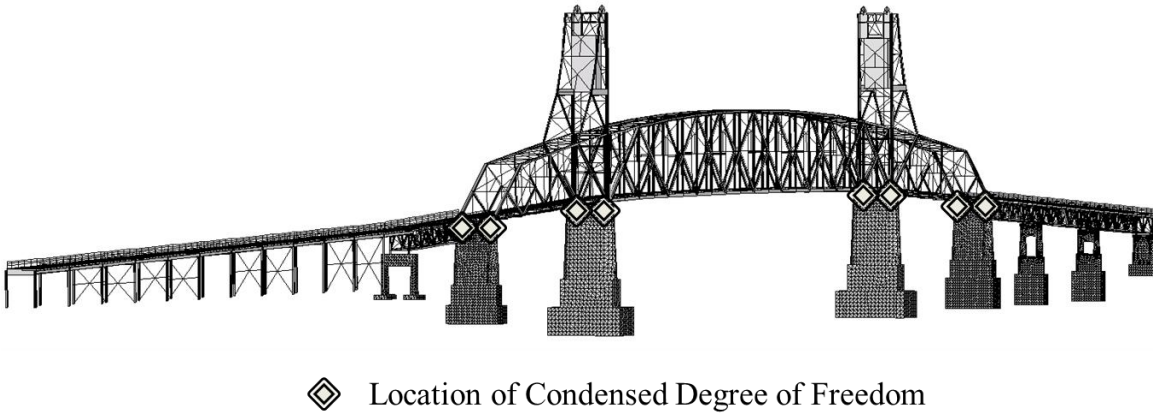

Figure 12-33: Locations of Degrees of Freedom Which Will be Representative of Approach Spans and Piers

It is clear from the selection of the degrees of freedom which the approach spans and piers will be condensed to that the deck truss spans will also be condensed from the analysis. This was decided because there are many beam and plate elements associated with these spans which increase the analysis time. Additionally, the lift span was targeted as the critical section of the entire span due to its length and its vulnerability (as it spans the shipping channel). For these reasons, the deck truss spans were also condensed from the analysis.

The stiffness coefficients were generated by first fixing all degrees of freedom and then imposing a unit displacement at the location where the stiffness coefficient is being computed. A static analysis was run, and the corresponding reaction at the location of the imposed unit displacement was equivalent to the spring force generated by that structural system. However, to eliminate any stiffness contributions of the structural systems which

are remaining in the model, those elements were removed to create a new model in which only the systems being condensed remained (Figure 12-34).

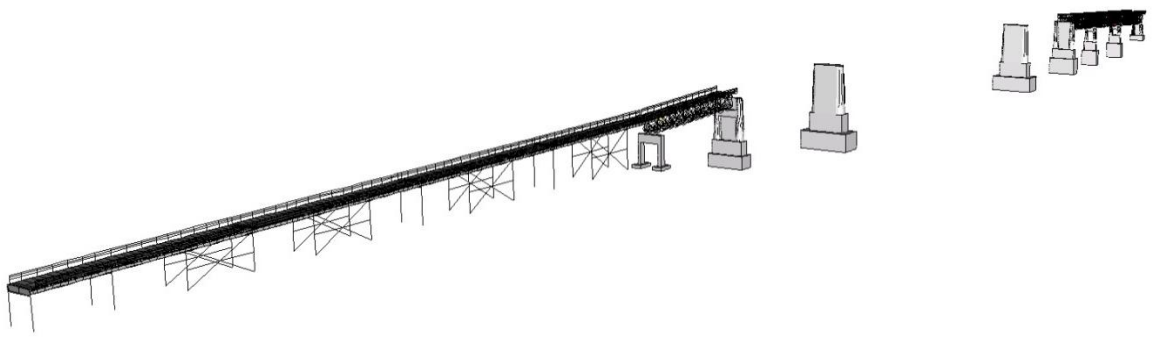

Figure 12-34: FEM Used for Condensation

The rotational degrees of freedom were the most challenging to condense, since solid elements have no rotational degrees of freedom. Instead of applying a direct unit rotation to compute the corresponding moment reaction, a series of translational displacements were applied in such a manner as to create a unit rotation about the degree of freedom of interest (Figure 12-35). The magnitude of the translational displacements depended on the geometry of the pier being condensed and the location of the applied translational displacements. Typically, eight nodes were selected around the circumference of the pier cap column, the center of which served as the degree of freedom for condensation. The center node always had its three translational degrees of freedom restrained since it served as the center of rotation. The other two nodes coinciding with the axis of rotation

were also restrained in all translational directions. The magnitudes of the applied displacements were computed using the tangent relationship of the known unit angle and the position along the pier cap from the rotational center to the application of the displacement. For the case shown in Figure 12-35, the applied exterior displacements would be equal to $\frac{D}{2}\tan 1$, where D represents the diameter of the pier cap. The result of this analysis is shown in Figure 12-36.

The application of a unit rotation about all three global axes was then repeated using the same formulation as discussed above. To compute the reaction moment from the unit rotation, the translational couples at each of the eight locations was computed with a linear static analysis and summed about the center point of the pier cap.

The unit translational displacements were applied over the same eight nodes utilized for the unit rotation computation, except that all nodes were applied the same unit displacement. This technique prevented local distortion of the elements and produced a more uniform displaced shape for the piers (Figure 12-37).

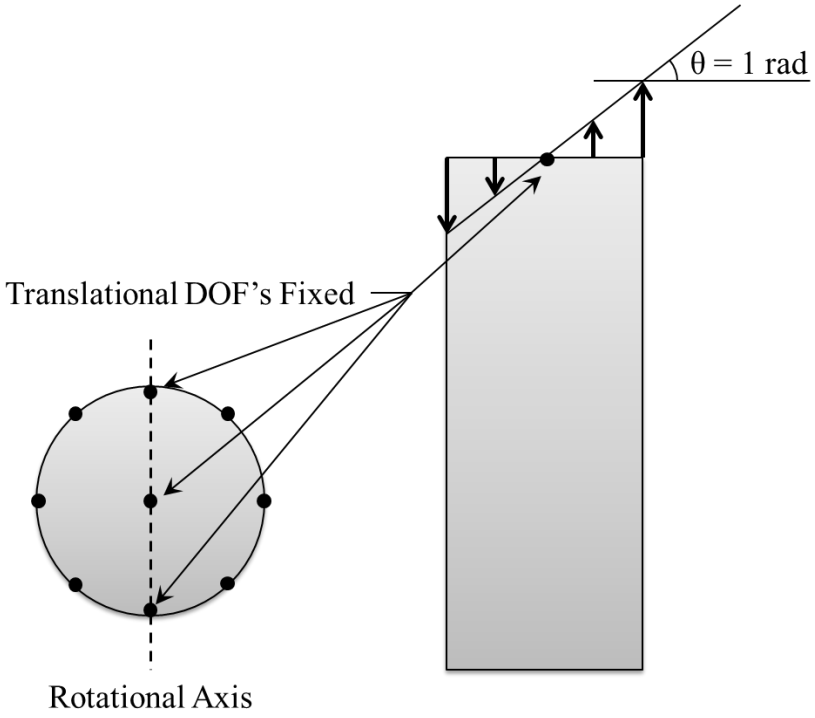

Figure 12-35: Approach to Applying a Unit Rotation to Solid Element of the Piers

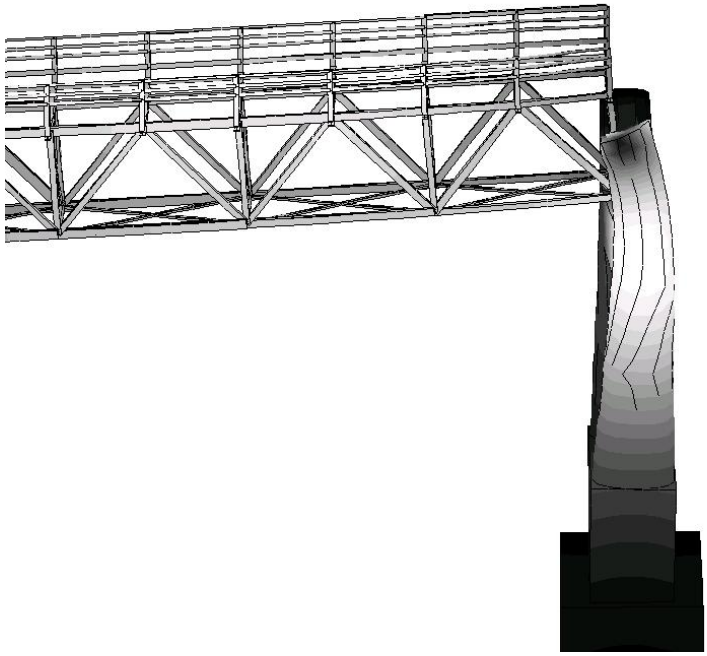

Figure 12-36: Unit Rotational Displacement of Pier Cap

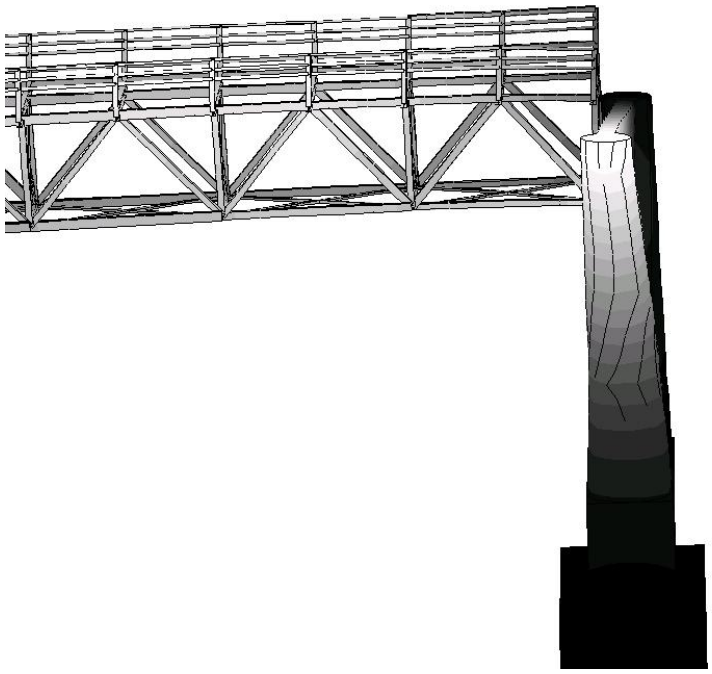

Figure 12-37: Unit Translational Displacement of Pier Cap

During each analysis of the stiffness coefficient for each degree of freedom, outlined above, the mass coefficient was also generated. The approach taken to generating the condensed mass coefficient was to use the shape function generated by the above process and multiply the coordinates of the displaced shape by the mass density of the object being condensed. The most challenging part of this analysis is the computation of the mass density and the selection of the nodes to use in the shape function.

For each pier, a vertical line down each lateral face was defined. The displacements due to the shape function were then pulled off along this line. The mass of each pier was

computed using the Strand7 attribute summary tabulation. The masses of the large rectangular pile caps were computed by hand and subtracted from the total given by Strand7. The remaining mass was that of the more complicated geometrical shape remaining. By dividing the mass of each component of the pier over their respective heights, an approximate linear mass distribution was obtained.

To compute the mass distribution of the approach spans, two lines were defined over each of the exterior stringers of the approaches. Then, the linear mass distribution of the approaches was approximated by dividing the total span weight in half and equally distributing it along the length of the span. The extra mass from the columns along the stringer approach spans were added directly to the linear mass distribution at their geometric location.

During the computation of each stiffness coefficient, the shape function for each pier and approach span defined over the lines defined above were extracted. The mass coefficient for each degree of freedom was then found by multiplying the approximate mass distribution by the shape function.

The final condensed model had all piers and approach spans removed and were represented by linear and rotational springs as well as linear and rotational masses assigned to nodes. The reduced model at this stage consisted of much fewer elements: 3,874 beams, 1,274 plates and 2,190 links. The total number of nodes was reduced from 30,956 in the original full model to just 4,506 nodes in the condensed version. This model reduction resulted in a decrease in analysis time of 25 minutes. However, there was still much room for improvement within the model.

12.5.3.2. Condensation of Local Modes

Large complex models tend to have a large amount of local modes that can increase the analysis time for the computation of the desired global modes. Local modes occur when components of the structure have the same frequency band for fundamental modes as the overall global structure. For the BBB model, global modes consisted of the natural frequencies and modeshapes associated with the lift span and tower span trusses. However, within each of these structures are smaller components that have their own vibration characteristics and create local modes.

Local modes for the BBB were found to occur mainly within the portal bracing and lateral bracing (Figure 12-38). The portal bracing consists of small angle members at every other panel point along the structure. They serve to prevent torsional racking of the lift span. The lateral bracing consists of built up members and angles bracing the top chord and bottom chords from lateral displacements. Additionally, any nodal locations with relatively flexible connecting members where a nodal mass was assigned to represent gusset plates, paint, etc. can create a local mode due to the localized mass and low stiffness.

Figure 12-38: Image Showing Portal Bracing and Top Chord Lateral Bracing

To eliminate these local modes, the weight of each element which was to be condensed was computed within the Strand7 software's Attribute Summary. The weights of each member within a group (portal bracing, wind bracing) and within a specific tributary area were summed and divided evenly among the connecting nodes, as seen in Figure 12-39. Each of these tabulated masses was then defined at the nodes as non-structural mass attributes. By defining them in this way, it was possible to separate each type of nodal masses into its own load case within the software package. This allowed for a more organized and structured framework to keep track of the nodal masses. After the mass

had been redistributed to nodal locations, the members being reduced were then assigned a mass modification factor of 0, effectively neglecting any modal contribution of these members in the natural frequency solver analysis.

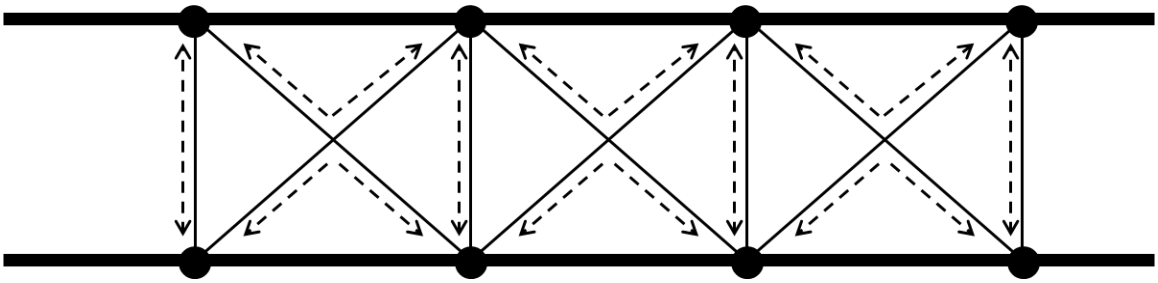

Figure 12-39: Method for Distribution of Mass to Eliminate Local Modes

During the process of relocating mass to more robust members so that local modes are reduced, it was essential to have an accounting of the structural mass before and after relocating the mass. The benefit of separating each condensed mass group into its own unique load case makes this simple since Strand7 can provide a summary of the mass of the members which were condensed, then a static dead load analysis can be computed within a specific load case to ensure that the mass added onto the structure is equivalent to the mass being zeroed out.

Once all model condensation was complete, the final analysis time for the natural frequency analysis of the BBB model was reduced to seventy seconds, a much improved reduction from the original thirty minute analysis time in the original state of the model. The linear static analysis of ten load cases was carried out to see what amount of time would be for the prediction portion of the MM St-Id process, and it was only two seconds. Overall, a seventy-five second analysis time was achieved with all data extraction taken into consideration. At the end of the reduction, it was critical to reexamine the model for errors, so another pass through the model error screening methodology outlined above was carried out. Additionally, it was important to ensure that the condensed model was representative of the original model, and that errors weren't introduced within the condensation process. This was performed by comparing the four natural frequencies of the lift span (1^{st} lateral, 1^{st} vertical, 2^{nd} vertical and 3^{rd} vertical) and two frequencies from each tower span (1^{st} and 2^{nd} vertical) (Table 12-1). By ensuring these structural parameters did not considerably become altered by the model reduction process, the reduced model could confidently be considered representative of the comprehensive model.

Table 12-1: Comparison of Full and Reduced Models

Span	Modeshape	Full Model (Hz)	Reduced Model (Hz)	%Δ
Lift	1st Lateral	0.516194	0.514896	-0.2515
Lift	1st Vertical	1.25003	1.25188	0.148
Lift	2nd Vertical	3.6224	3.67017	1.3187
Lift	3rd Vertical	4.41823	4.44187	0.5351
NJ Tower	1st Vertical	2.28967	2.29	0.0144
NJ Tower	2nd Vertical	3.84308	3.8249	-0.4731
PA Tower	1st Vertical	2.33296	2.42	3.7309
PA Tower	2nd Vertical	3.9671	3.9618	-0.1336

12.6. Identification of Model Building Blocks for the BBB

After the BBB FE model was reduced and prepared for the MM St-Id process by condensing it to have a reasonable analysis time, the next step in the method is to identify and evaluate model building blocks that represent uncertainties within the model. In the same manner as the building blocks were identified for the grid structure, the BBB model was evaluated for uncertainties on different levels: global, local and material. In considering the model building blocks, it is important to keep in mind the objectives of the MM St-Id process and what unobservable model predictions are being included in the analysis. If the model building blocks are insensitive to the measureable attributes (and thereby the information used to weigh the models) or the unobservable predictions (the desired product), then they will not benefit the process.

12.6.1. Identification of Global Building Blocks

The model uncertainties which have a global influence on the BBB model (natural frequency, load distribution, displacement, etc.) consist of two main uncertainties: boundary conditions and continuity conditions. The boundary conditions with uncertainties are the expansion bearings of each tower span. These were originally designed as a roller type bearing, however over the course of the lifetime of the structure, the degree of rotation and translation allowed by the bearing has become uncertain.

Additionally, there is uncertainty in the level of continuity between the lift span and the tower span, as well as between the tower span and the counterweight. The guides described above do not perfectly restrain the counterweights and the lift span against the tower span columns, since they need to allow vertical sliding. However, there is certainly a level of restraint provided if the counterweight or lift span engages against the guides. For this reason, the stiffness values of the connection elements between the counterweight and tower span and the tower span and lift span all serve as global building blocks.

The pier stiffness and mass contributions at the nodes representing them are common uncertainties in FE models used for updating, since they were not included in the model and little information is known in an a priori sense. However, in this case since the entire span was explicitly modeled and then condensed, the uncertainties are drastically reduced. While there may be some level of error with the computation of the reduced mass due to the approximate mass densities used, they should be minimal and were assumed to be appropriate for this analysis.

12.6.2. Identification of Local Building Blocks

The local building blocks for the BBB model were determined by examining what uncertainties could influence the model predictions only in certain areas or certain members. The most common local uncertainty is the connection stiffness provided by the gusset plates on structures. These connections are neither fully rigid nor fully pinned, so it is important to account for this uncertainty in the analysis.

There are hundreds of gusset plates on the tower spans and lift spans for the BBB and accounting for each ones rotational stiffness in a MM St-Id study is infeasible given the limited information typically available. In order to account for the uncertainty associated with the gusset plates, but keep the number of model building blocks in a reasonable range, it was decided to group the connection type into three main groups for each of the spans: (1) main truss connections, (2) portal bracing connections and (3) lateral bracing connections. It was decided to divide the connections into these groups since the size of the plates within each of the groups is relatively similar. For example, the gusset plates connecting the main truss elements together (Figure 12-40) are fairly large in comparison with those connecting the lateral bracing (Figure 12-41) and portal bracing (Figure 12-42). This strategy most effectively reduces the number of building blocks, since it is more likely that connections within each of the groups will be similar in terms of stiffness than if they had all been lumped within one single building block for each span.

Figure 12-40: Main Truss Gusset Plate

Figure 12-41: Lateral Bracing Connections

Figure 12-42: Portal Bracing Connections

12.6.3. Identification of Material Based Building Blocks

The identification of material level uncertainties is important with aged structures, since material properties may not have had the standards to that which they are produced today, or the designers may have used practices current to the period in which the bridge was constructed. For the BBB, the majority of the material used in the construction of the

superstructure was A36 grade steel with an elastic modulus of 29,000ksi and a yield stress of 36ksi. The decks of all the spans have changed throughout the years, however currently consists of the steel grid deck and a concrete filled concrete deck. From these materials, two building blocks were identified as being uncertain: (1) elastic modulus of the structural steel and (2) the elastic modulus of the concrete filled steel grid deck.

As with the grid in the verification phase of the MM St-Id method, the elastic modulus of the structural steel is included more as a measure of the success of the method to make sure that the sampling scheme is not selecting unreasonable values for the elastic modulus of steel.

12.6.4. High Level Model Building Blocks

A structure as complex as BBB also has many high level uncertainties that could be included in a MM St-Id study. For example, the construction staging of the structure could have had a great influence on the distribution of dead load stresses. Additionally, the model resolution itself is an uncertainty. Even though the best efforts were made to reduce the large FE model while still preserving its information and properties, there still could have been missing information.

The history of the BBB unfortunately does not include any information on the exact staging procedures carried out during its construction. The only documentation that exists to the knowledge of the author is a photo of the lift span being erected by cantilevering out from either end of the tower spans (Figure 12-43).

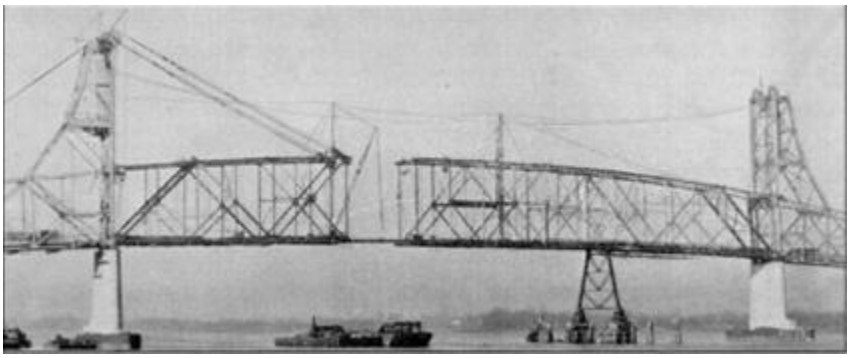

Figure 12-43: Cantilevered Erection of the Lift Span (www.bcbridges.com)

The uncertainty associated with how the structure was built remains too large to incorporate into the MM St-Id analysis with a construction staging analysis since an infinite number of construction sequences could exist. Also, while Figure 12-43 gives insight into the staging for the lift span, no information is available for the tower spans.

The uncertainties associated with model resolution for this application were also not included in the final analysis. The original model simply could not be included due to its long analysis time. In the future, this model could be included in an RJMCMC approach to MM St-Id, however this case study was focused more on the applicability of the approach in general to a complex constructed system. The ability to incorporate more complicated models is anticipated for future research however. A simpler model from the final version described in this chapter was not seen as necessary, since too much information would be lost. For example, if a 2D truss representation of the spans were created, any torsional information would be lost.

12.6.5. Building Block Sensitivity Study

A list of initial model building blocks was identified (Table 12-2) for further evaluation with a sensitivity study. Considering the long total analysis time anticipated for the BBB model, it was imperative to ensure that only sensitive building blocks were included within the approach. This was done by varying each building block over predetermined bounds (Table 12-3) and examining the effect on a simple prediction of structural responses which are related to the desired outcome of the MM St-Id.

Table 12-2: List of Model Building Blocks for BBB

Building Block	Description	Building Block	Description
1	Elastic Modulus	20	PA - Exp - DS - Lat.
2	PA - BC - US - Lat.	21	PA - Exp - DS - Rot.
3	PA - BC - US - Long.	22	NJ - Exp - US - Lat.
4	PA - BC - DS - Lat.	23	NJ - Exp - US - Rot.
5	PA - BC - DS - Long.	24	NJ - Exp - DS - Lat.
6	PA - TC - US - Lat.	25	NJ - Exp - DS - Rot.
7	PA - TC - US - Long.	26	PA - CTWT - Long.
8	PA - TC - DS - Lat.	27	PA - CTWT - Lat.
9	PA - TC - DS - Long.	28	NJ - CTWT - Long.
10	NJ - BC - US - Lat.	29	NJ - CTWT - Lat.
11	NJ - BC - US - Long.	30	Connection - Diag - Lift
12	NJ - BC - DS - Lat.	31	Connection - Diag - NJT
13	NJ - BC - DS - Long.	32	Connection - Diag - PAT
14	NJ - TC - US - Lat.	33	Connection - PB - Lift
15	NJ - TC - US - Long.	34	Connection - PB - NJT
16	NJ - TC - DS - Lat.	35	Connection - PB - PAT
17	NJ - TC - DS - Long.	36	Connection - LB - Lift
18	PA - Exp - US - Lat.	37	Connection - LB - NJT
19	PA - Exp - US - Rot.	38	Connection - LB - PAT

In Table 12-2, PA and NJ represent Pennsylvania and New Jersey respectively. BC and TC stand for Bottom Chord and Top Chord while US and DS stand for Upstream and Downstream. Lat, Long and Rot indicate lateral, longitudinal and rotational directions, respectively. CTWT stands for counterweight connections while Diag, PB and LB represent diagonal member connections, Portal Bracing connections and Lateral Bracing connections. Building blocks 2 through 18 all represent uncertainties located at the interface between the tower spans and lift span. Building blocks 19 through 25 represent uncertainties associated with the level of stiffness provided by the expansion bearings of the two tower spans. Building blocks 26 through 29 represent the uncertainties associated with the interface of the counterweights and the tower spans, while building blocks 30 through 38 represent the uncertainties associated with each of the three main types of beam element connections for each of the three spans.

The bounds shown in Table 12-3 were done in a manner to ensure that the full range of the building block was being explored for sensitivity purposes. All continuity conditions between the lift and tower spans were explored over a range from 1 to $1x10^6$ kip/in while all connection and bearing related building blocks were varied from 0% to 100% rigid connectivity.

Table 12-3: Building Block Bounds for Sensitivity Study

Building Block	Lower Bound	Upper Bound	Building Block	Lower Bound	Upper Bound
1	0.8 E_o	1.2 E_o	20	0%	100%
2	1 kip/in	$1x10^6$ kip/in	21	0%	100%
3	1 kip/in	$1x10^6$ kip/in	22	0%	100%
4	1 kip/in	$1x10^6$ kip/in	23	0%	100%
5	1 kip/in	$1x10^6$ kip/in	24	0%	100%
6	1 kip/in	$1x10^6$ kip/in	25	0%	100%
7	1 kip/in	$1x10^6$ kip/in	26	1 kip/in	$1x10^6$ kip/in
8	1 kip/in	$1x10^6$ kip/in	27	1 kip/in	$1x10^6$ kip/in
9	1 kip/in	$1x10^6$ kip/in	28	1 kip/in	$1x10^6$ kip/in
10	1 kip/in	$1x10^6$ kip/in	29	1 kip/in	$1x10^6$ kip/in
11	1 kip/in	$1x10^6$ kip/in	30	0%	100%
12	1 kip/in	$1x10^6$ kip/in	31	0%	100%
13	1 kip/in	$1x10^6$ kip/in	32	0%	100%
14	1 kip/in	$1x10^6$ kip/in	33	0%	100%
15	1 kip/in	$1x10^6$ kip/in	34	0%	100%
16	1 kip/in	$1x10^6$ kip/in	35	0%	100%
17	1 kip/in	$1x10^6$ kip/in	36	0%	100%
18	0%	100%	37	0%	100%
19	0%	100%	38	0%	100%

For the sensitivity studies, the thirty-eight building blocks listed above were grouped where appropriate into fourteen building block sensitivity studies. The list of building blocks evaluated for their sensitivity to the natural frequency analysis of the BBB model is shown in Table 12-4.

Table 12-4: Building Block Groups for Sensitivity Study

Sensitivity Group	Building Blocks	Description
1	1	Elastic Modulus
2	2,4,6,8,10,12,14,16	Lateral Lift-Tower Connectivity
3	3,5,7,9,11,13,15,17	Longitudinal Lift-Tower Connectivity
4	18,19,20,21,22,23,24,25	Tower Span Expansion Bearings
5	26,27,28,29	Counterweight Connectivity
6	30	Connection - Diag - Lift
7	31	Connection - Diag - NJT
8	32	Connection - Diag - PAT
9	33	Connection - PB - Lift
10	34	Connection - PB - NJT
11	35	Connection - PB - PAT
12	36	Connection - LB - Lift
13	37	Connection - LB - NJT
14	38	Connection - LB - PAT

The first group, elastic modulus, covered the modulus of all materials within the model. Most of the members within the reduced model are composed of steel members except for the tower span decking. This decking (concrete filled steel grid) certainly has an uncertain elastic modulus property, and was included for this reason. However for the sensitivity study it was grouped with the elastic modulus of the steel members to enforce a consistent relative change in the modulus of all materials within the model.

Each sensitivity group was evaluated at fifteen equally spaced samples between the bounds defined above. During the sensitivity process, the natural frequency solver was

used to compute the frequencies associated with the identified modes, to be discussed in Chapter 13. The experimental frequencies were used in conjunction with the computed ones to formulate an error function based on summed percent error for each frequency of the lift span and two tower spans. At this stage, if experimental frequencies are not available, the user can simply explore whether the model is sensitive to the building blocks by tracking the frequencies of interest over the bounds of the building block.

The sensitivity studies for each of the fourteen building block groups are shown below in Figure 12-44 through Figure 12-57.

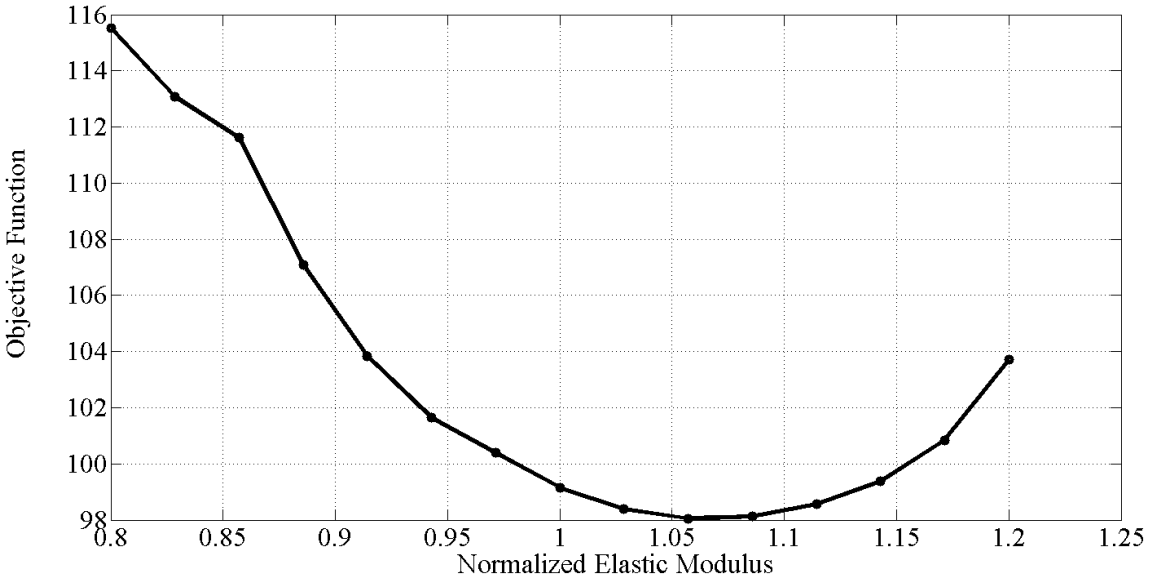

Figure 12-44: Sensitivity Study of Elastic Modulus

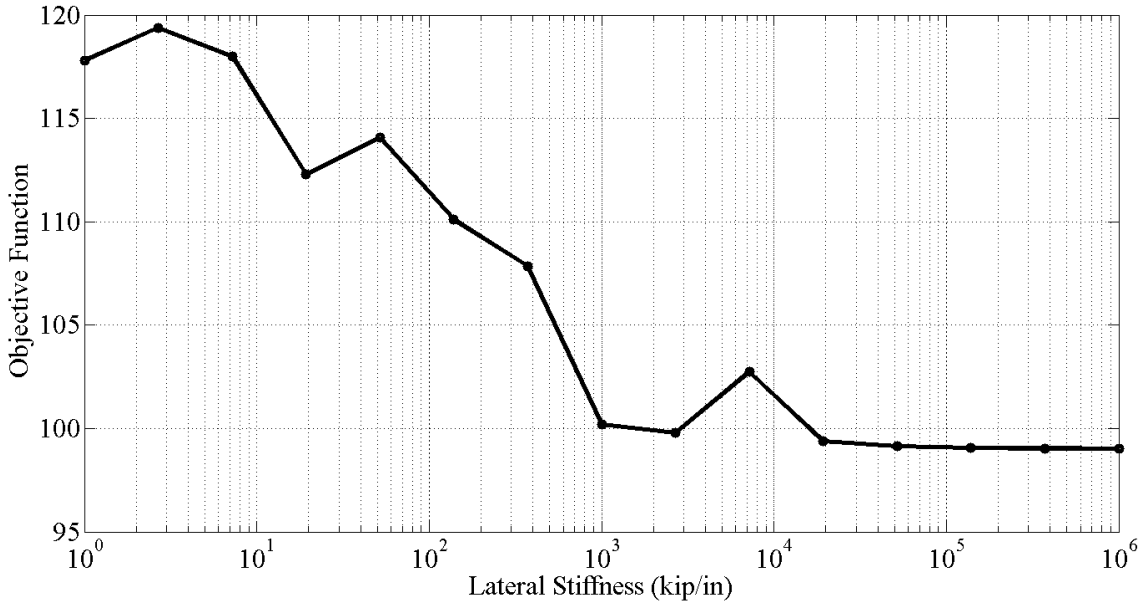

Figure 12-45: Sensitivity Study of Lateral Connection Stiffness between Lift and Tower Spans

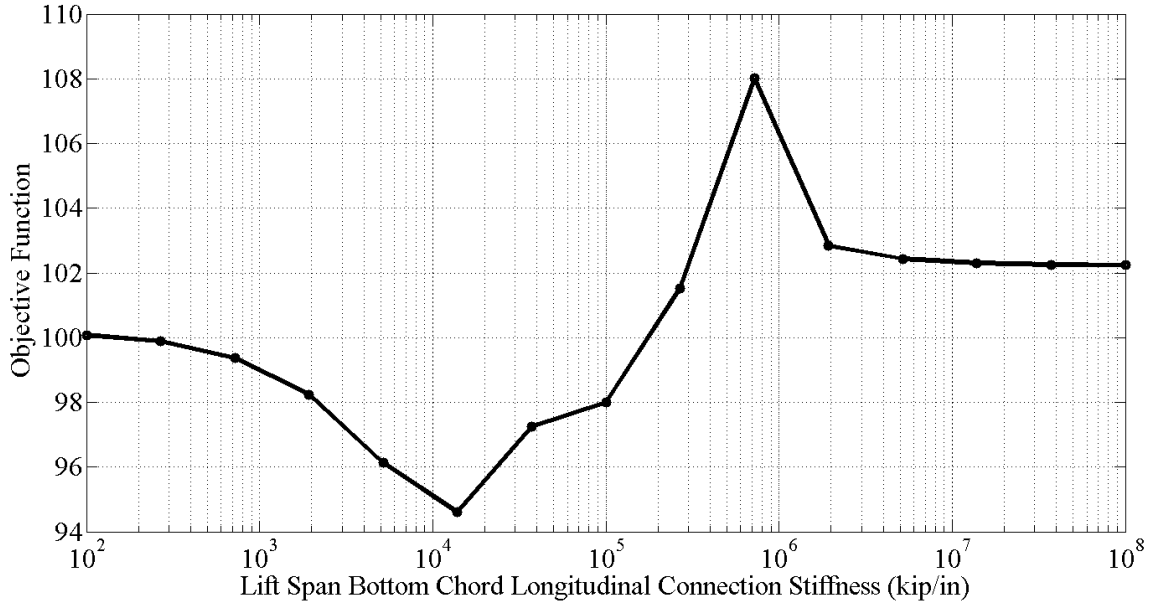

Figure 12-46: Sensitivity Study of Longitudinal Connection Stiffness between the Lift and Tower Spans

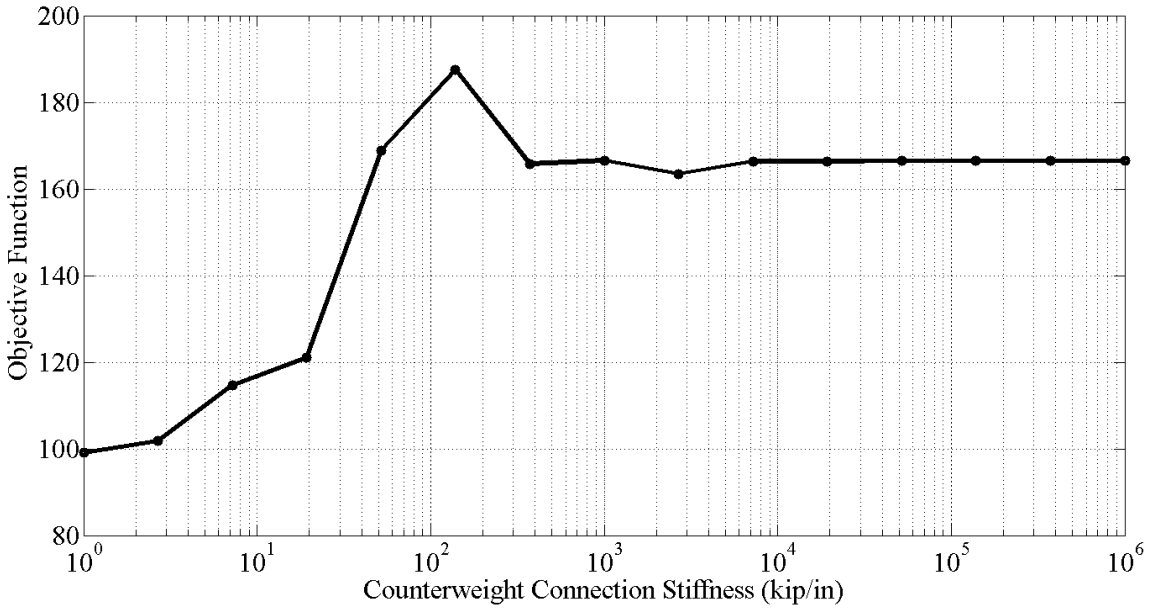

Figure 12-47: Sensitivity Study of Connection Stiffness between Counterweights and Tower Spans

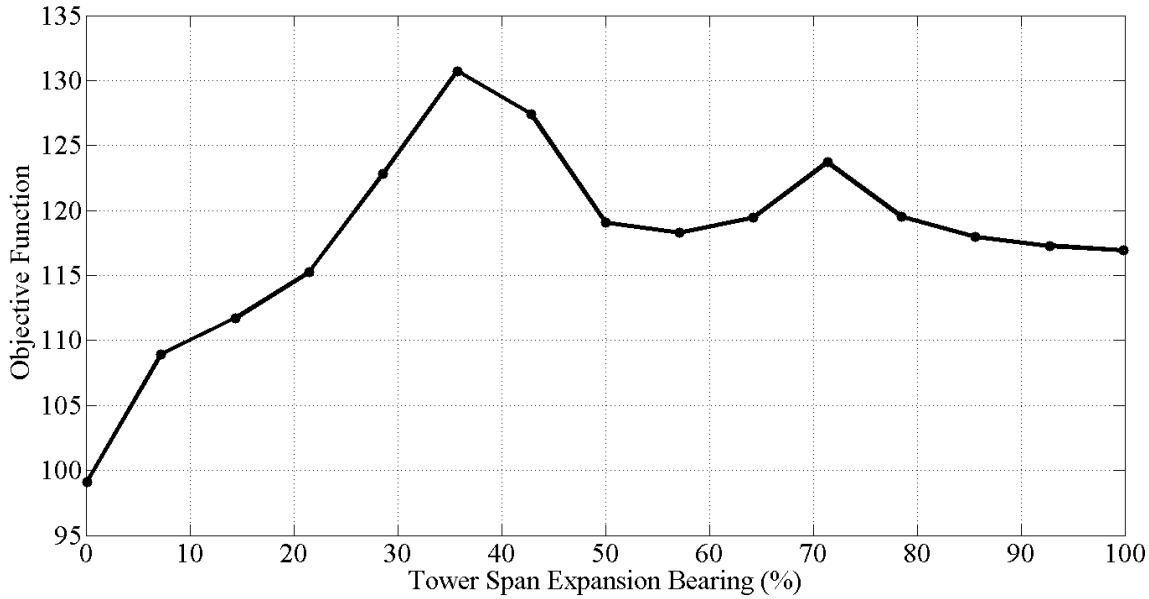

Figure 12-48: Sensitivity Study of the Tower Span Expansion Bearing Stiffness

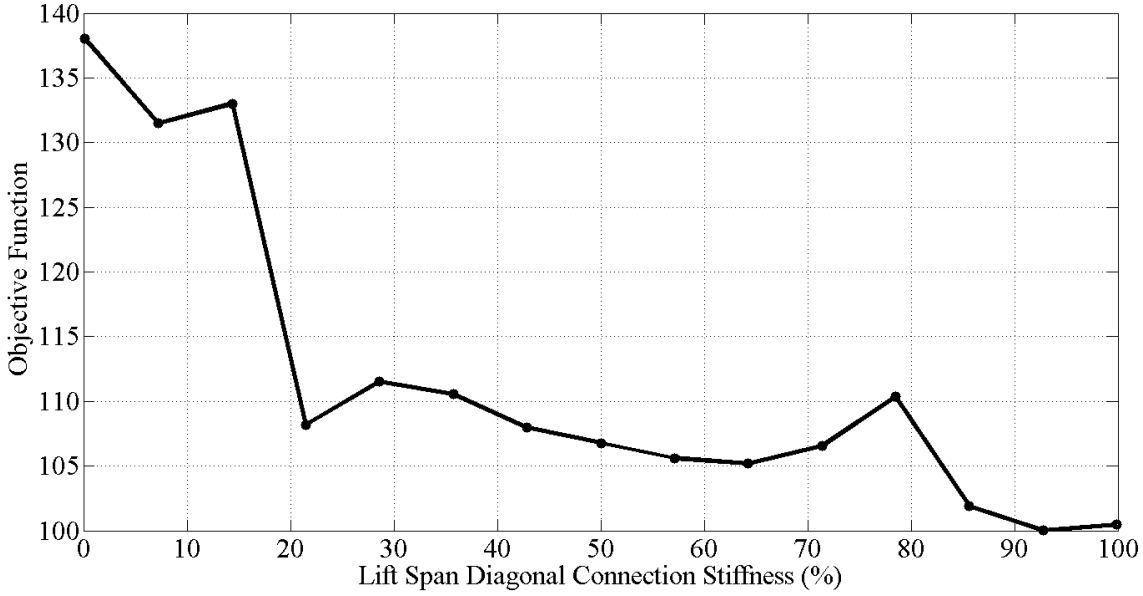

Figure 12-49: Sensitivity Study of the Lift Span Diagonal Connection Stiffness

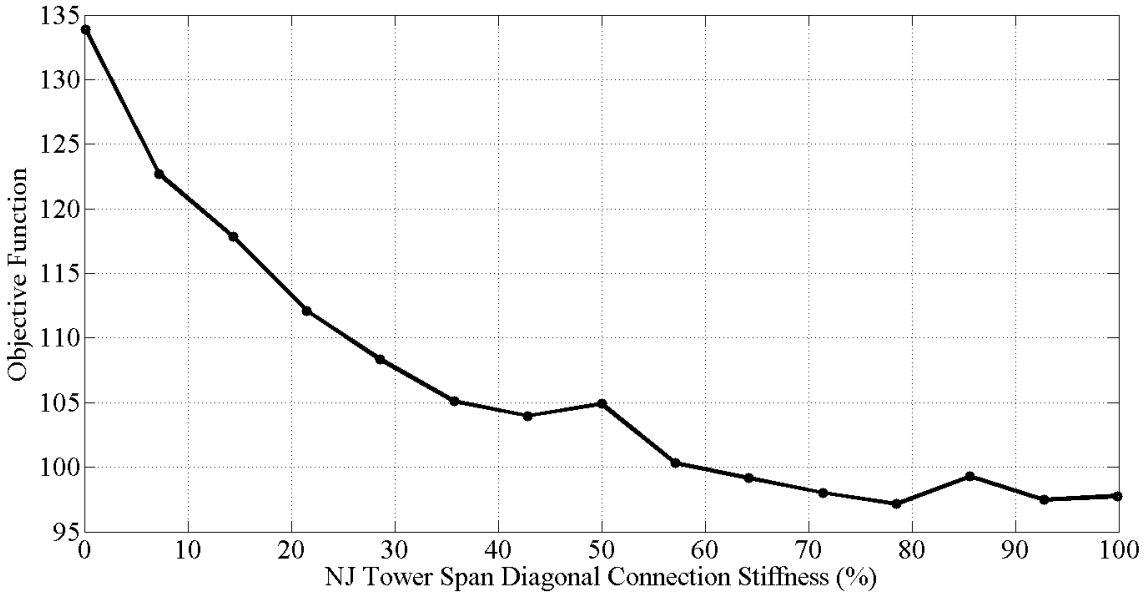

Figure 12-50: Sensitivity Study of the NJ Tower Diagonal Connection Stiffness

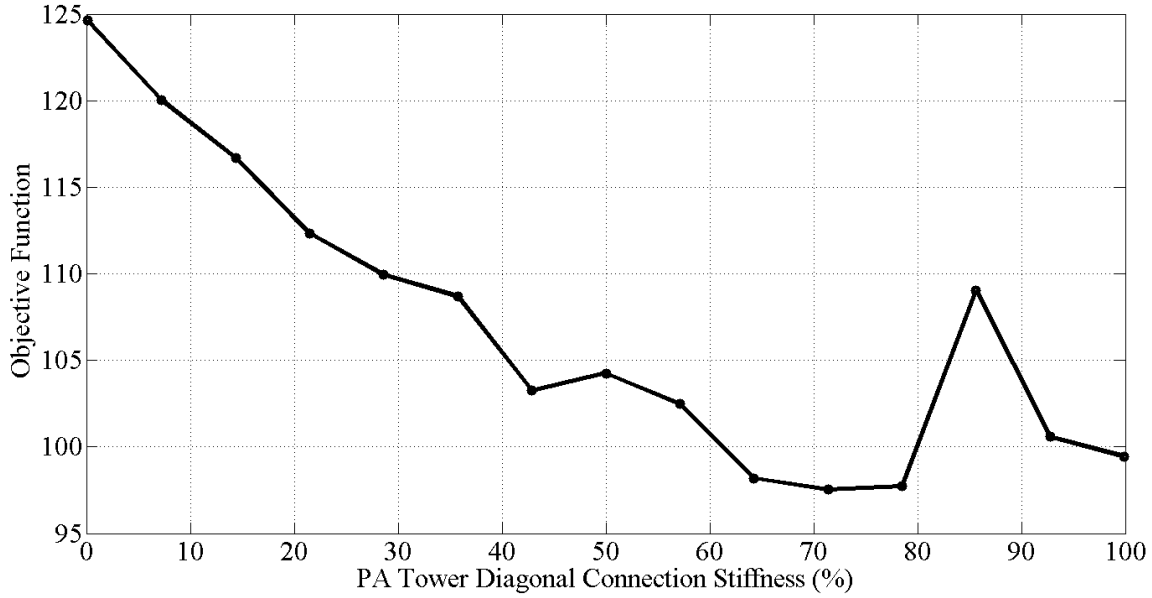

Figure 12-51: Sensitivity Study of the PA Tower Span Diagonal Connection Stiffness

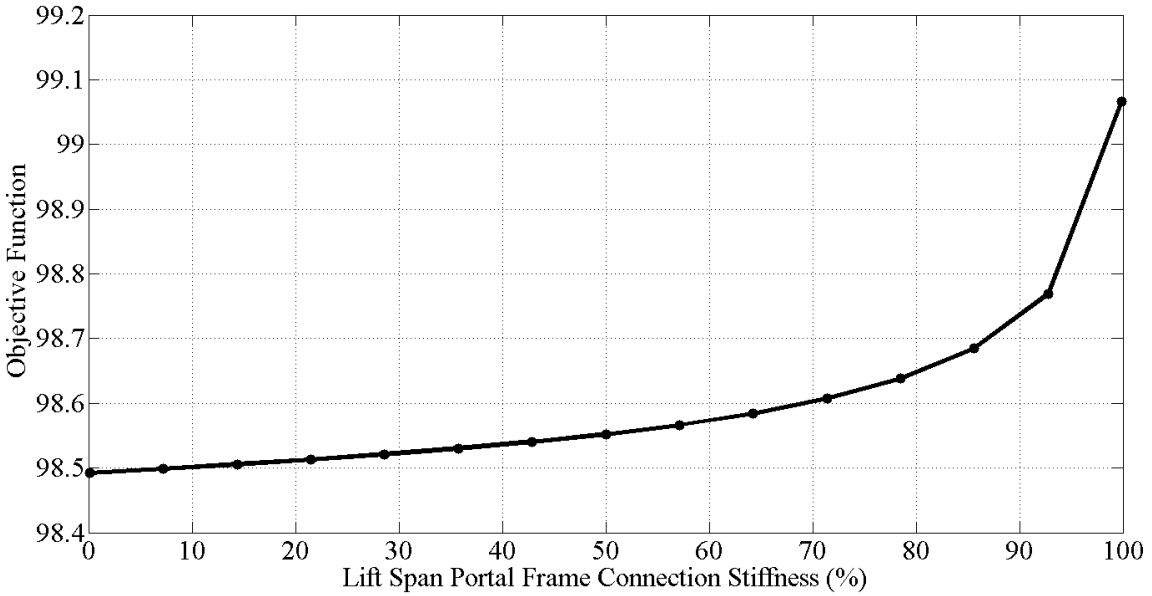

Figure 12-52: Sensitivity Study of the Lift Span Portal Frame Connectivity Study

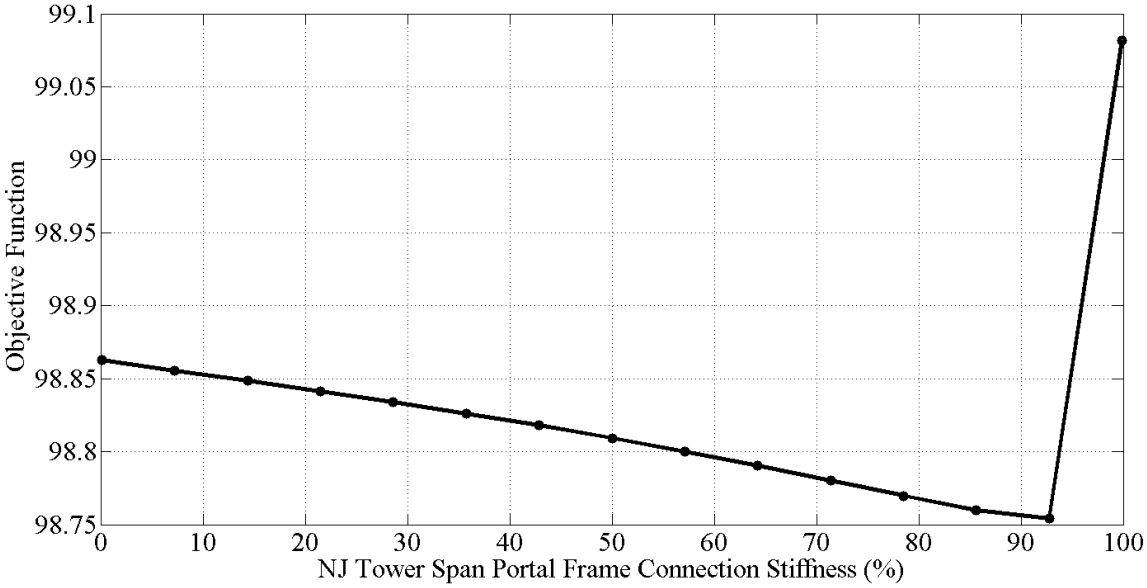

Figure 12-53: Sensitivity Study of the NJ Tower Span Portal Frame Connection Stiffness

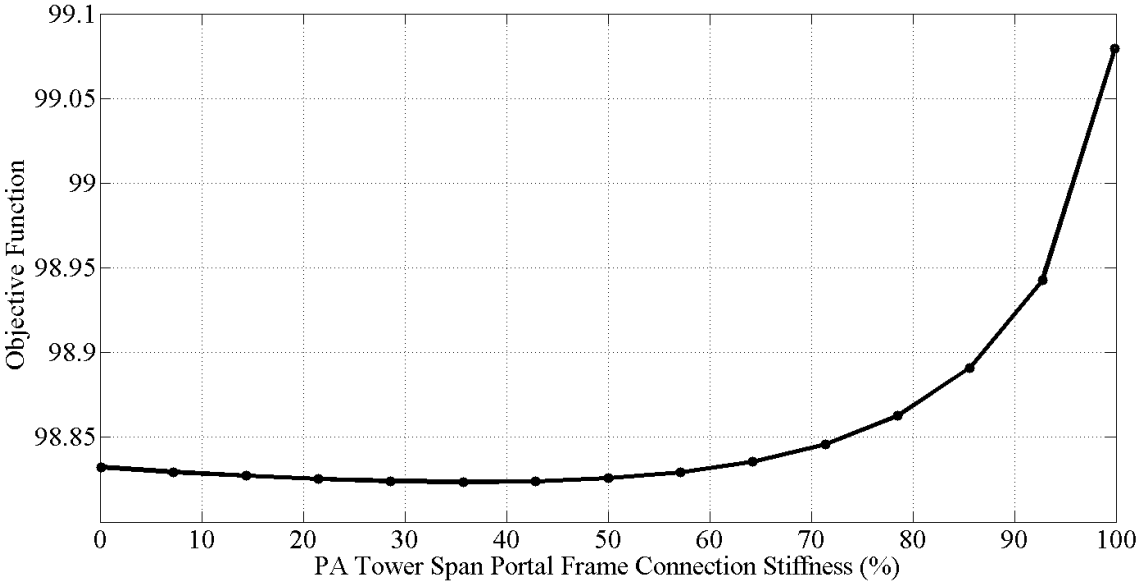

Figure 12-54: Sensitivity Study of the PA Tower Span Portal Frame Connection Stiffness

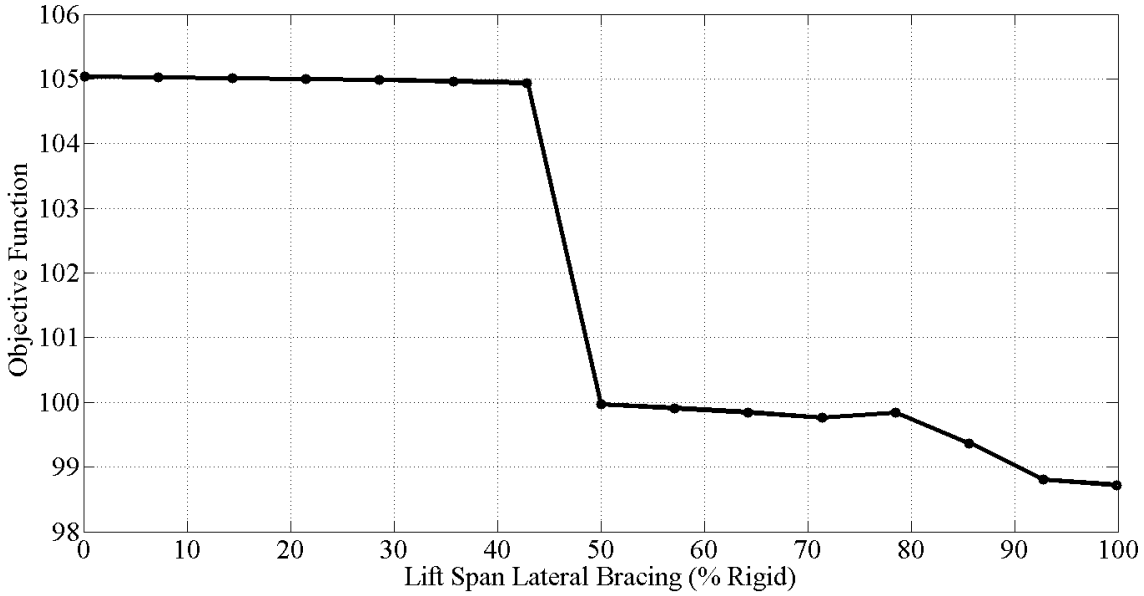

Figure 12-55: Sensitivity Study of the Lift Span Lateral Bracing Connection Stiffness

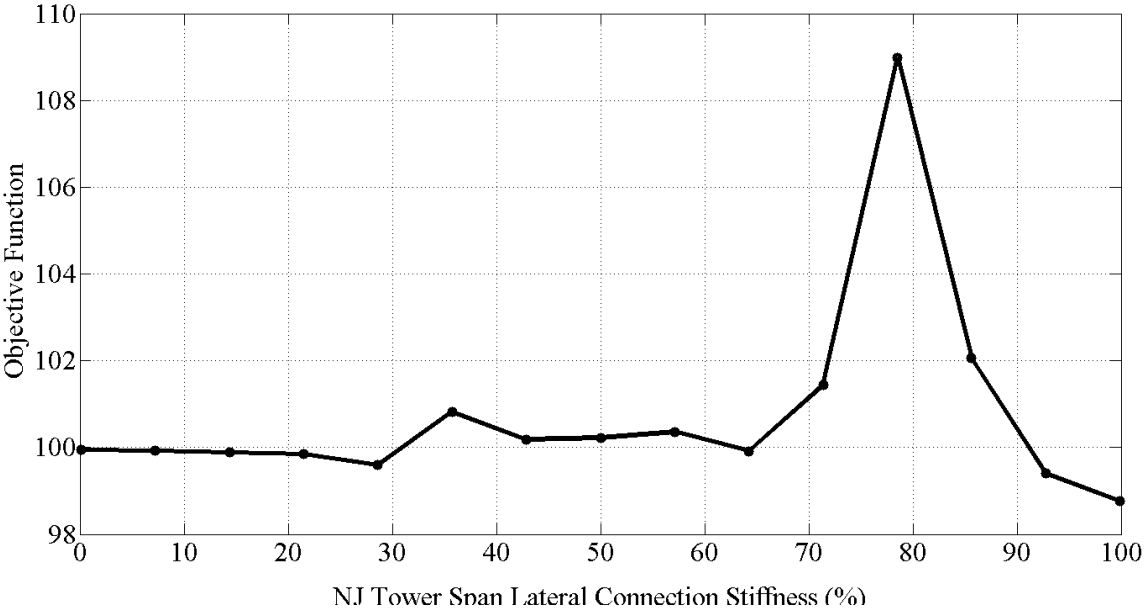

Figure 12-56: Sensitivity Study of the NJ Tower Span Lateral Connection Stiffness

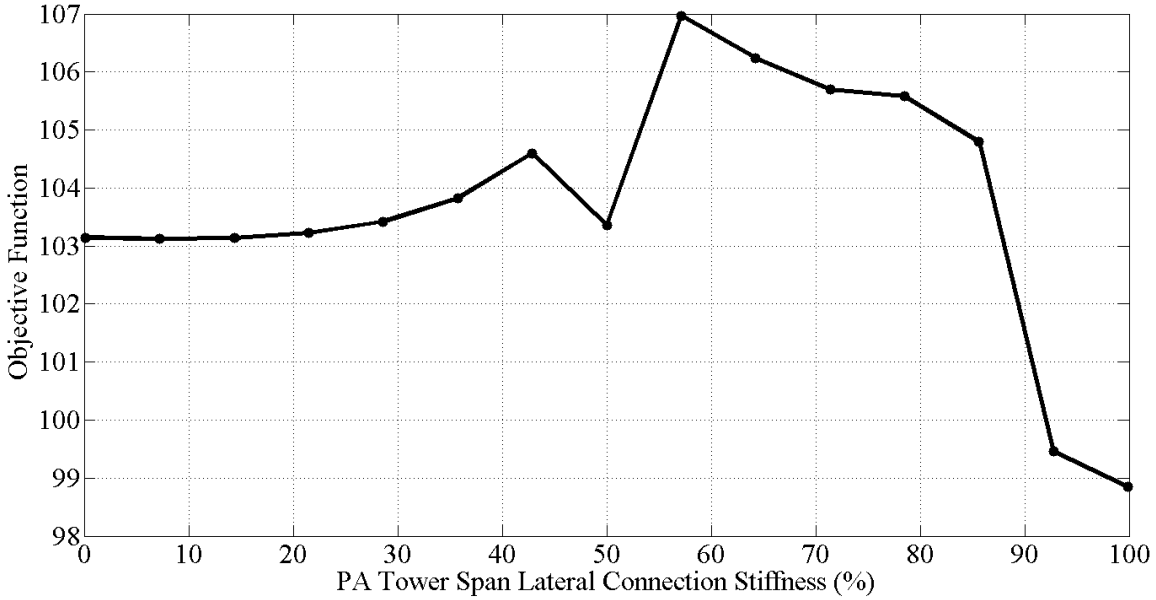

Figure 12-57: Sensitivity Study of the PA Tower Span Lateral Connection Stiffness

After examining the above sensitivity studies, it is obvious that the curves are not as smooth as those for the grid structure studied in Chapter 5. However, careful attention was paid to why these curves are not as smooth as what may be intuitively expected. One factor which was carefully monitored during the sensitivity study was the success of the mode pairing algorithm developed for the grid structure. It was noticed that repeated global structural modes existed within the Strand7 natural frequency output. However, at that time not all of the nodal masses located at flexible joints had been reassigned to stiff

nodal locations. Once this was complete, the MAC value could be used to identify the best analytical modeshape base on the experimental frequency.

Once the mode pairing process was shown to select consistent modeshapes for all twenty-one modeshapes (to be described in the next chapter), the sensitivity studies shown above were trusted. Another reason for the "choppy" sensitivity curves is that the change in objective function is not that large, thereby amplifying any non-smooth curves.

Finally, when considering the information included in the sensitivity process (lateral modeshapes, vertical modeshapes, three separate spans), it is not inconceivable that the sensitivity studies for the model as a whole is not smooth. For example, the first lateral modeshape of the lift span might be heavily influenced by the stiffness representing the lateral connection stiffness between the lift span and the tower spans, yet the vertical modes of the tower spans could be less sensitive to this same building block yet is still included in the objective function. Conversely, the NJ Tower span is heavily influenced by the modification of its expansion bearing stiffness, yet the lift span is most likely completely insensitive to this. Because the building blocks do not affect all the modes in similar manners, the objective function is not expected to be monotonic.

12.6.6. Final Set of Model Building Blocks for BBB

The sensitivity study showed that the BBB model was not sensitive at all to the change in portal frame connection stiffness. Also, in an effort to primarily reduce the number of building blocks for the first MCMC analysis of the BBB model, the lateral connection stiffness building blocks were neglected from the initial model building block set since

the amount of change in the sensitivity curve was not as substantial as some of the remaining building blocks. This does not exclude this building block permanently, as the analysis of the results may indicate that this building block should be included. An indicator which would show this as being necessary could be the poor identification of lateral modes.

However, the BBB model was very sensitive to the remaining set of model building blocks. After the site visit described above where the guides were investigated for their ability to transmit lateral and longitudinal forces between the lift span and tower span, it was decided to only have a longitudinal spring where the lift span channel completely surrounded the guide on the tower span. The final model building block set then consisted of those shown in Table 12-5. This model building block set will be analyzed with the MCMC MM St-Id approach in Chapter 14.

Table 12-5: Final Building Block Set

Building Block	Description
1	Elastic Modulus Steel
2	Elastic Modulus Concrete Deck
3	Lift Span - Tower Span Lateral Continuity
4	Lift Span - Tower Span Longitudinal Continuity at NJ BC
5	NJ CTWT Connectivity
6	PA CTWT Connectivity
7	PA Tower Span Expansion Bearings
8	NJ Tower Span Expansion Bearings
9	Lift Span Diagonal Member Connection Stiffness
10	NJ Tower Span Diagonal Member Connection Stiffness
11	PA Tower Span Diagonal Member Connection Stiffness

CHAPTER 13: EXPERIMENTAL PROGRAM FOR THE BURLINGTON BRISTOL BRIDGE

The experimental program for the Burlington Bristol Bridge was extensive and covered multiple global and local structural characterizations as well as specific owner requests. When designing an experimental program for a large and complex structural system such as the BBB, it is important to take into consideration the uncertainties of the structure and what vulnerabilities are most critical to the structure. It is also important to take into consideration any concerns of the owner or the engineer-of-record for the structure. Each sensor placed on a structure has a direct cost associated with the observation process, in terms of sensor cost and items like connectors, cables, data acquisition channels and interpretation and information extraction. The success of a monitoring application can very easily be compromised if too many sensors were used and the cost of the application was exorbitant. Similarly, the location of sensors (how will information be sent to analyst?) and the speed with which sensor is sampled (how much data must be mined to extract meaningful information?) are also significant factors which can affect the cost of the process. With these points in mind, a strategic experimental monitoring program was designed for the BBB that would most efficiently aid in answering some of the fundamental uncertainties associated with the structure.

The experimental program devised for the BBB will be discussed in chronological order to give a sense of appreciation to the task of monitoring global structural attributes in addition to answering specific owner questions. To aid in the presentation of this effort, the program was organized into 6 main sections: (1) Preliminary Vibration Monitoring, (2) Live Load Monitoring of Critical Members, (3) Design and Verification of Load Cell

Bearings, (4) Full Ambient Vibration Monitoring, (5) Design and Installation of a Laser Height Monitoring System and (6) Installation of Load Cell Bearings.

While all of the experimental observations discussed in this chapter may not be used within the MM St-Id case study, they are being included to provide a realistic perspective on the many ways technology may be leveraged to answer specific questions about a constructed system. In certain cases it is possible to directly measure responses that are required, such as the height and uniformity of the span during an opening. In these instances no model is required and thus the multiple model approach can offer little benefits. However, in other cases the desired responses or structural attributes cannot be directly measured, e.g., the rating factor or seismic vulnerability of the bridge. In these situations it is imperative that the observed responses be reliably "translated" into estimates of the immeasurable but desired responses/attributes. It is here that the developed multiple model approach can offer significant benefits over the direct use of measurements or conventional model-experiment correlation approaches. The presentation of the applications of multiple model structural identification for the BBB will be presented in Chapter 14.

13.1. Preliminary Vibration Monitoring

One of the critical components required to ensure a successful and complete ambient vibration monitoring application to a constructed system is a preliminary vibration survey to provide a picture of the dynamic characteristics of the structure and the ambient vibration environment. Some of the information that a preliminary study provides

includes acceleration magnitudes, initial estimate of fundamental natural frequencies for model error screening, adequacy of sampling speed, and ease of access. This preliminary survey can then guide the users in selecting appropriate data acquisition systems and sensors. The BBB preliminary vibration survey will be discussed in 4 subsections: (1) Instrumentation Design, (2) Field Work, (3) Data Processing and (4) Preliminary Results.

13.1.1. Preliminary Vibration Instrumentation Design and Data Acquisition

For a preliminary vibration study, an important consideration is the level of instrumentation to employ on the structure. For the BBB structure, it was decided to use no more than eight sensors on each of the spans at one time and measure data for one hour. A quantity of eight sensors was selected due to the speed and efficiency with which they could be installed, wired and recorded on each of the three main spans. It was planned to have this preliminary study complete in one day, so it was important to not have a large quantity of cables and sensors which could lead to debugging issues in the field.

The instrumentation design for each span needed to utilize the limited number of sensors in a single configuration in the most beneficial manner. For the lift span, the main goals were to identify the overall acceleration magnitude, identify the fundamental vertical and lateral frequencies and to gain insight about the degree of movement at the supports, since there was no physical pinned connection at the bearings. To this end, the instrumentation design shown in Figure 13-1 was created. All of the instrumentation

shown in this plan was installed on the sidewalk side of the lift span truss (Figure 13-2) to increase the efficiency of the deployment.

Five vertical accelerometers were installed at panel points 0, 5, 10, 5', and 0' while lateral accelerometers were installed at panel points 5, 10 and 5'. This discretization of sensors would directly inform the goals of the study and give insight to the degree of movement at the boundary as well as identify the most fundamental natural frequencies.

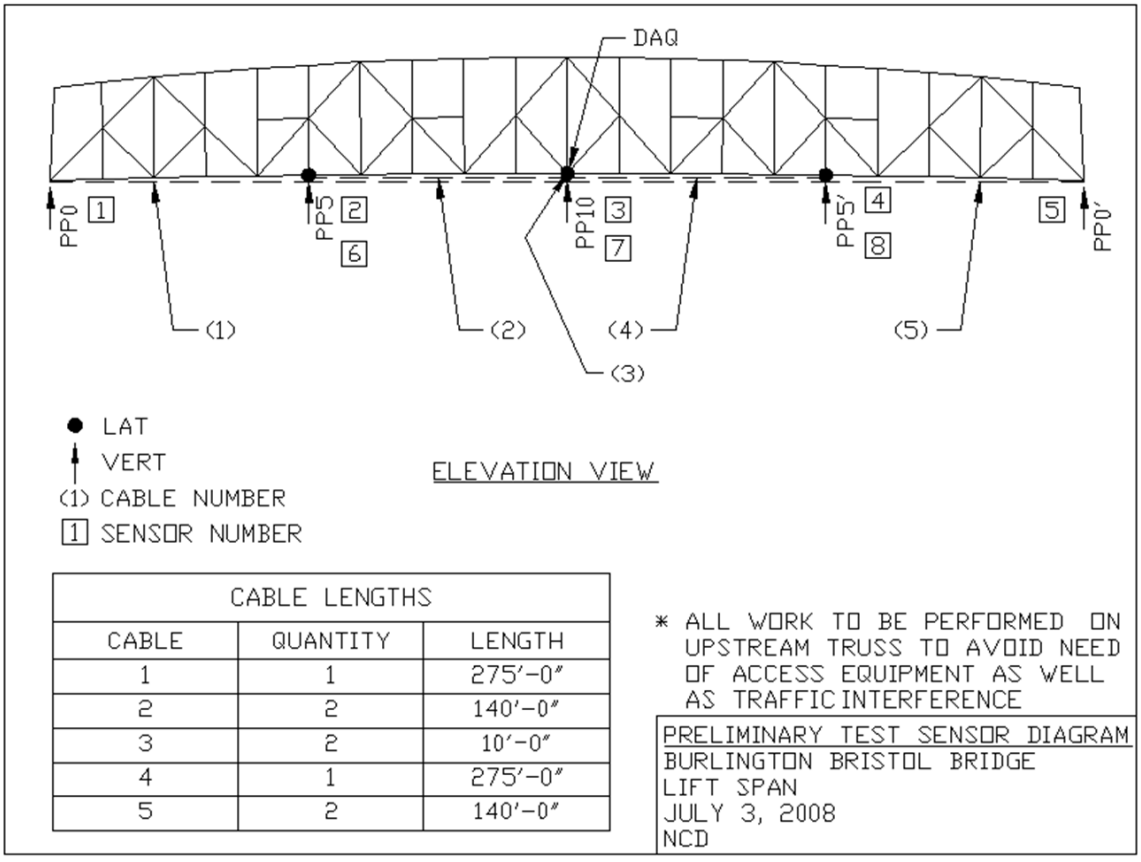

Figure 13-1: CAD Drawing for Lift Span Instrumentation Design

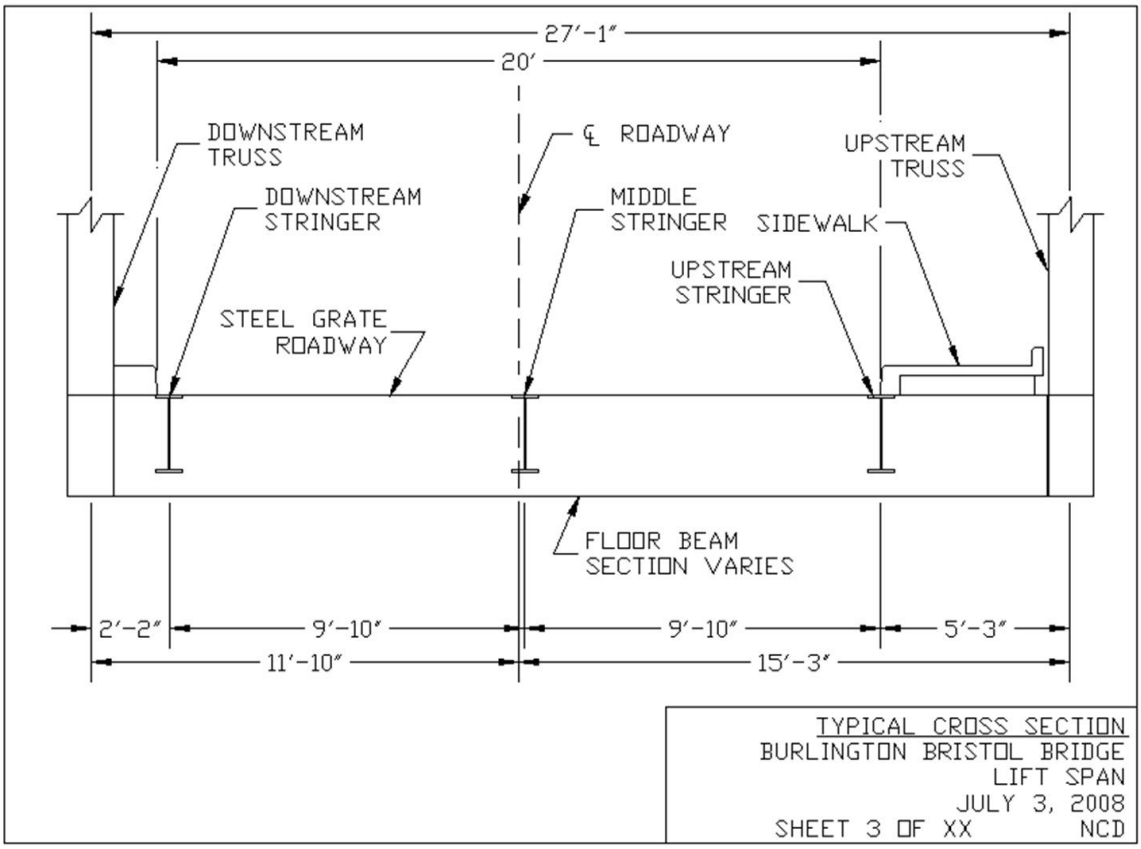

Figure 13-2: Lift Span Cross Section

The instrumentation plan for the tower spans was more challenging to devise with a limitation of eight sensors, however the use of more sensors would compromise the efficiency and ultimately the value of such preliminary ambient vibration surveys. The instrumentation design, shown in Figure 13-3, was developed to answer a set of questions specifically for the tower spans related to the degree of interaction between the towers and the roadway truss and the level of response in the vertical, lateral and longitudinal directions. It was important to limit the number of sensors along the tower since a time

consuming climb was required for deployment. Two accelerometers were installed at the very top of the tower, in lateral and longitudinal directions, while a single longitudinal accelerometer was installed at roughly mid-height of the tower. This configuration was selected to give insight into the movement of the tower in both planar directions. The five sensors on the roadway truss were once again installed on the sidewalk side due to ease of access to the span and power supply. Three vertical accelerometers were installed at panel points 2, 4 and 6 along each tower span while lateral accelerometers were installed at the bottom chord and top chord of panel point 4. It was decided to use a distribution of lateral accelerometers along the height of the tower span instead of the length to determine if there was large differential lateral movement of the span across the height due to the massive counterweight housed within the tower span.

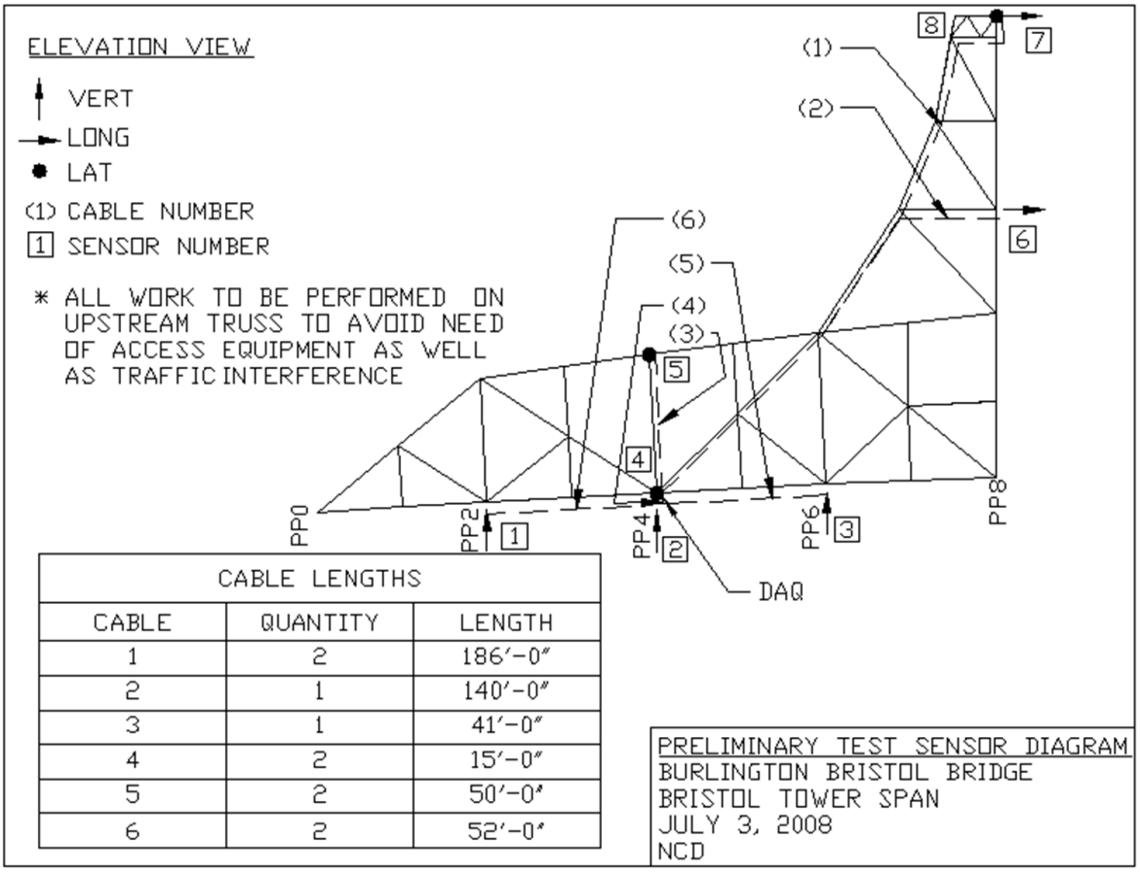

CABLE LENGTHS		
CABLE	QUANTITY	LENGTH
1	2	186′-0″
2	1	140′-0″
3	1	41′-0″
4	2	15′-0″
5	2	50′-0″
6	2	52′-0″

Figure 13-3: CAD Drawing for Tower Span Instrumentation Design (Typical for PA and NJ)

The instrumentation plan for the NJ and PA tower spans were identical to examine any differences in relative magnitude between the two spans. The approach spans were not instrumented for the preliminary vibration survey because at the time of this study, they were not considered critical to the main goals of the ambient vibration survey: calibrating a model for a more accurate load rating of the lift span.

The data acquisition used to record the eight sensors was an HBM MGCplus operated by the Catman® data acquisition software. From preliminary modal analysis of the SAP2000 a priori model, it was confirmed that no major structural modes of interest existed above 20 Hz. The Nyquist frequency associated with this bandwidth is 40Hz. However, since this is a preliminary study it was decided to sample the accelerometers at 100Hz to see how well the acceleration time history was captured.

The sensors used were the same PCB 393C seismic accelerometers used in the grid study. The cables connecting the sensors to the HBM DAQ were coaxial cables precut to appropriate lengths based on the CAD model estimates shown in the figures above.

13.1.2. Preliminary Vibration Field Work

On July 17, 2008 a Drexel University research team carried out the preliminary vibration survey on the two tower spans and the lift span of the BBB with the aid of maintenance and engineering staff provided by the BCBC. The New Jersey tower span was the first span to be instrumented with the eight accelerometers and appropriate cabling.

The accelerometers were mounted with magnetic bases to the steel truss. It was necessary to clean debris off of the surface of the truss to ensure sufficient contact between the magnets and the steel. The magnets provided enough pull force that the steel did not need to be cleaned of its paint coating before installing the sensor. All sensors on the tower spans were able to be mounted with the exception of sensor 6. The access to this location required additional harness equipment which was not readily available. This sensor was subsequently eliminated from the instrumentation plan for both tower spans.

After the eight sensors were installed in each configuration, the coaxial cables were connected to each sensor with a micro-dot cable. The cables were then run to the data acquisition locations (shown in the instrumentation schematics above). After all sensors were connected to the data acquisition, the system was configured to sample each sensor synchronously at 100 Hz for a period of one hour (Figure 13-4).

Figure 13-4: Configuring the Data Acquisition System to Record Measurements

After the measurements were complete on the NJ Tower span, the time histories of the measurements were first checked in MATLAB to ensure that the sensors were recorded and were operating properly over the course of the one hour period. Once all time histories were verified, the sensor configuration was torn down and re-set up on the lift span (Figure 13-5 - Figure 13-7).

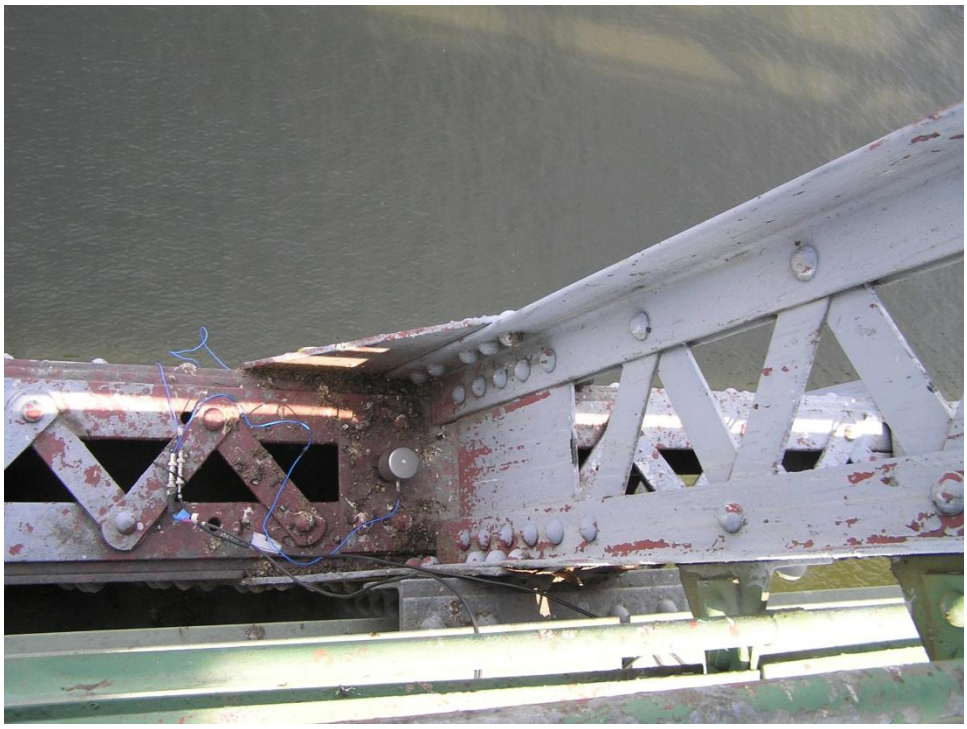

Figure 13-5: Accelerometer on Bottom Chord of Lift Span

Figure 13-6: Accelerometer Installed Above Live Load Shoe of Lift Span

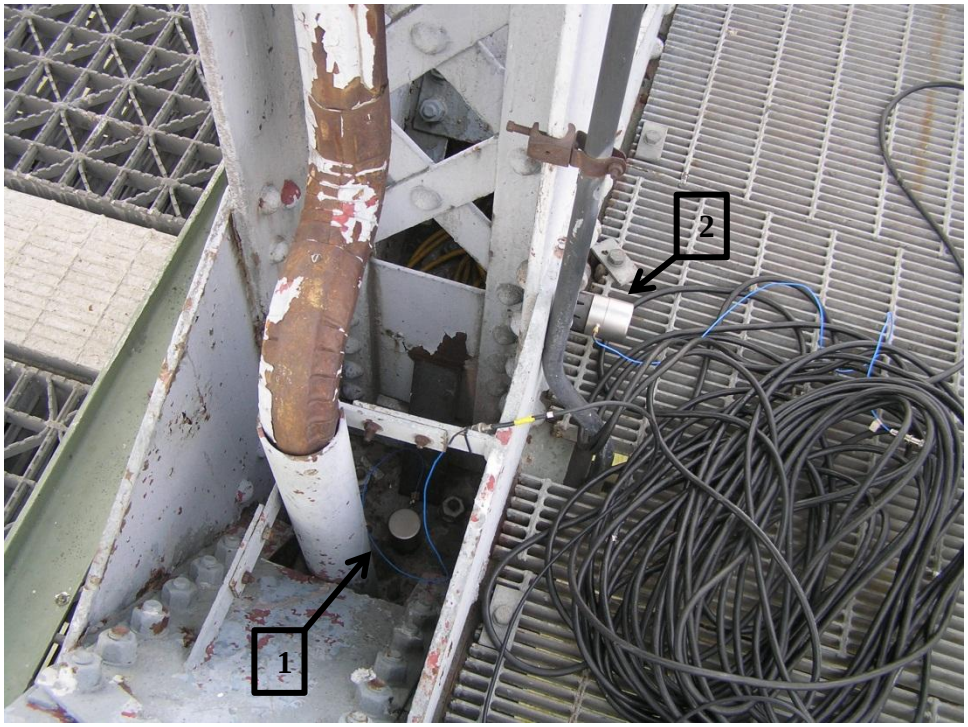

Figure 13-7: Accelerometers at Mid-span of Lift Span in Vertical (1) and Lateral (2) Directions

Once again, after the one hour period of data collection was complete on the lift span, the time histories were checked in MATLAB for errors before tearing down the setup. After the measurements were verified, the lift span configuration was torn down and re setup on the PA tower span. The Drexel team was able to install, debug measurement issues, and record for one hour a set of eight accelerometers on three adjacent spans of the BBB in one day. The ability to carry out an aggressive preliminary vibration survey such as this on the BBB was extremely beneficial for the planning of the full ambient vibration test of the spans as discussed in subsequent sections.

13.1.3. Preliminary Vibration Data Processing

The time histories for each span was plotted and inspected before each of the setups were tore down during the vibration survey. The qualities of the time histories investigated in the field included drift and signal magnitude. If the baseline acceleration of a sensor or group of sensors was drifting over time, this could indicate problems with the grounding of the data acquisition, cable noise or sensor connection issues. If this problem is identified, it is best to mitigate the source of the drift and begin the monitoring period again. The signal magnitudes were compared against one another and ensured that they were reasonable. For instance, it was anticipated that the mid-span vertical accelerometer should have a higher response magnitude than the than the vertical accelerometer located at the support. Using heuristics to perform quick verification of acceleration time histories saved both time and money by being able to guarantee data with no blatant errors.

13.1.3.1. Burlington Tower Span

The Burlington tower span was the first structure to be instrumented, and subsequently took the most amount of time since the research team needed to become familiarized with climbing the structure and running the instrumentation cables. At the end of the one hour measurement period during the data investigation, it was noticed that only six of the seven sensors were recorded. The error was found to be within the settings for the DAQ program and was mitigated; however additional measurements were not made due to the time limitation. It was also anticipated that the information lost with the one missing sensor recordings would be acquired while monitoring the similar Bristol tower span. The seven time histories for the two hour period are shown in Figure 13-8 and Figure 13-9.

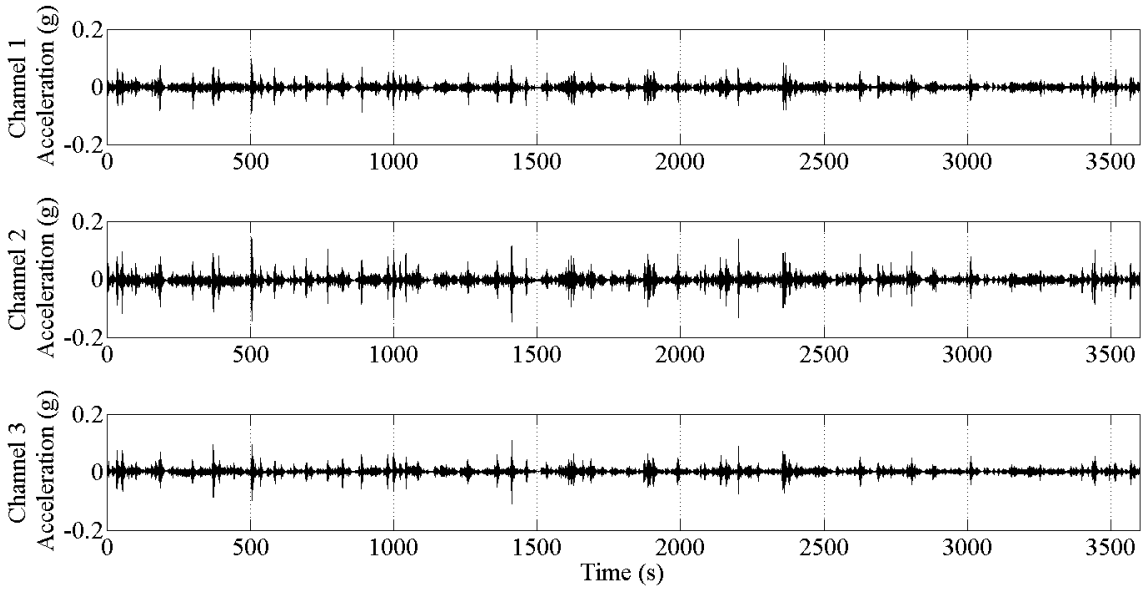

Figure 13-8: Burlington Tower Span Ambient Vibration, Channels 1-3

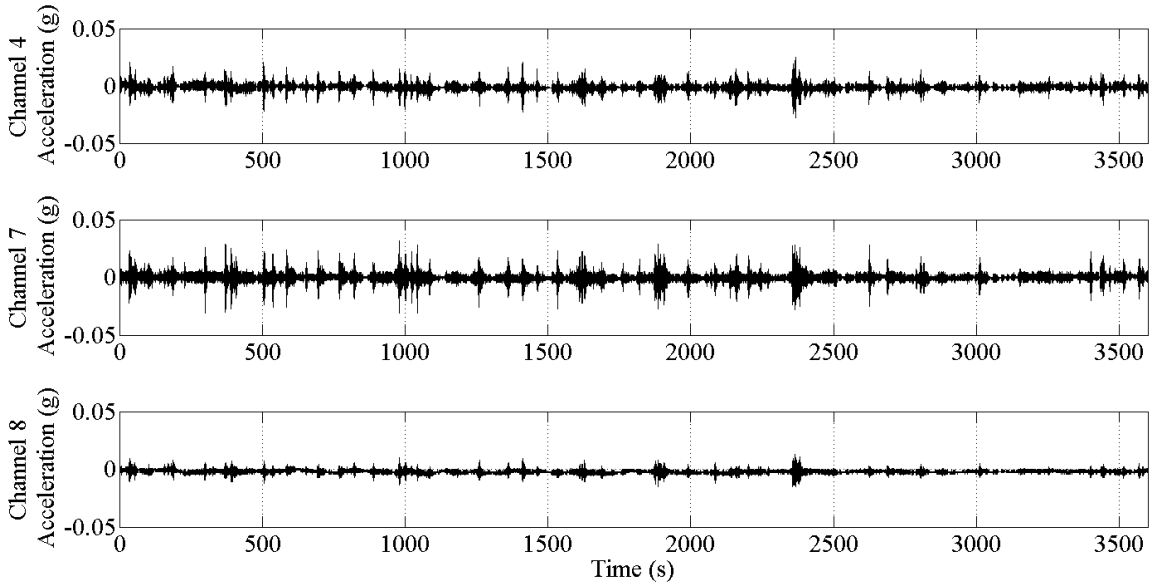

Figure 13-9: Burlington Tower Span Ambient Vibration, Channels 4-6

The time histories shown above were reasonable with respect to the relative level of response anticipated between the different locations. The three vertical measurements recorded the highest magnitude responses, with the highest at the mid-span location (approximately +/- 0.15g). The lateral truss measurement and longitudinal tower measurement recorded the next highest levels of acceleration at approximately +/- 0.05g while the lateral tower response recorded the lowest magnitude at approximately +/- 0.01g.

After the time histories were validated, the acceleration measurements could be processed to obtain the frequency content associated with the vibration. The vibration data was processed to obtain frequency content by using a built-in function with the MATLAB signal processing toolbox. The function, *pwelch*, computes a power spectral density for

the time history by using Welch's method. The method splits the data into overlapping blocks and computes the periodogram for each block. Each periodogram is then averaged to obtain the estimate of the power spectral density. Each block in the analysis is windowed with a Hamming window, also known as a "raised cosine" window. The algorithm divides the data into eight blocks of equal length and overlaps them 50%. The power spectral density (PSD) estimate was then used to investigate the frequency content of the span (Figure 13-10 and Figure 13-11).

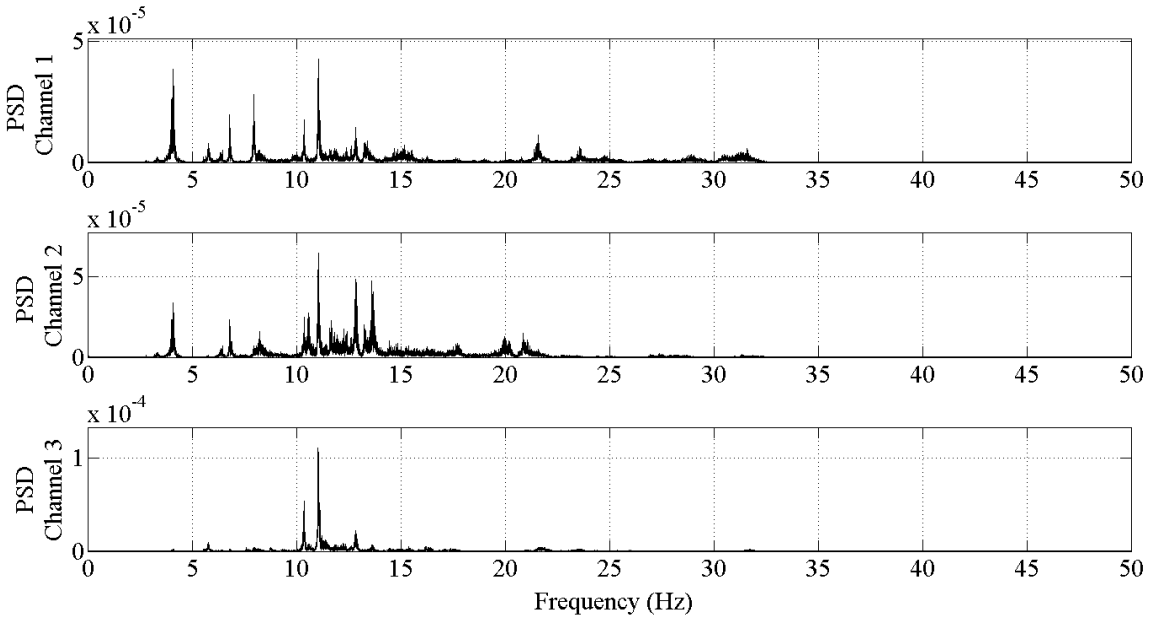

Figure 13-10: PSD for Channels 1 through 3 of the Burlington Tower Span Setup

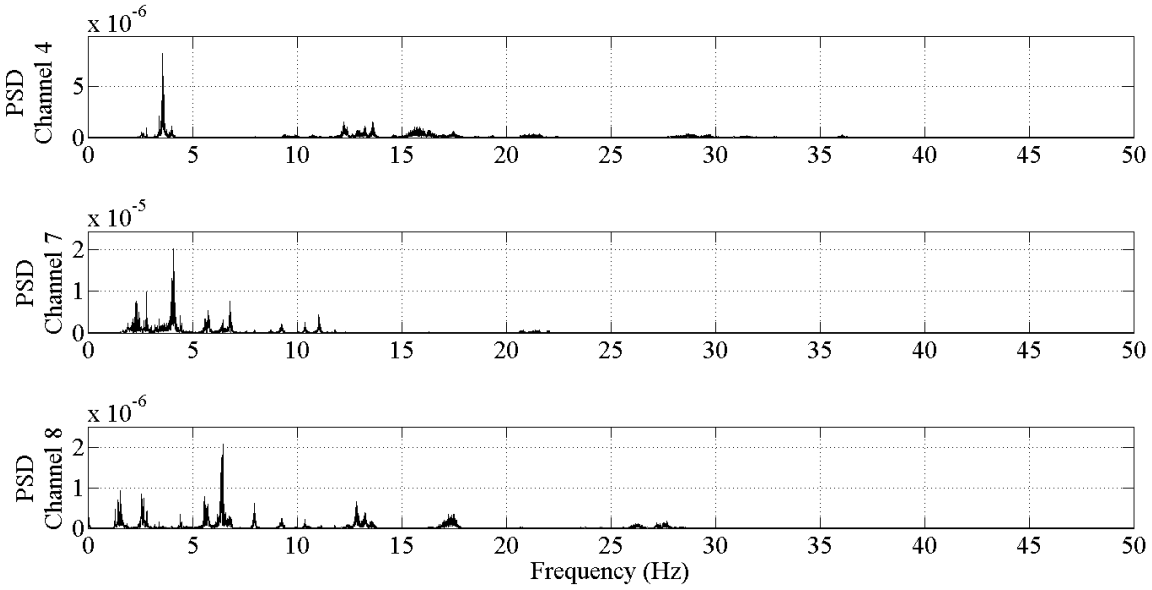

Figure 13-11: PSD for Channels 4 through 6 of the Burlington Tower Span Setup

The PSD's from Channels 1, 2, 3 and 4 (vertical and lateral span measurements) indicate a concentration of peaks within the frequency content in the band of 0-25Hz. Additionally, it can be seen that Channel 1 has more peak frequency content than Channel 2 and similarly more peak frequency content in Channel 2 than Channel 3. This can be justified by reasoning that the vertical stiffness of the expansion end of the tower spans would be less than that of the fixed tower end. Both the fixed support and the tower stiffen the truss vertically at that end.

The PSD's from Channels 7 and 8 (longitudinal and lateral tower measurements) indicate a concentration of frequency content primarily below 10Hz, with some peaks up to 20Hz.

The low frequency band of the towers is also reasonable given the considerable mass housed within the tower and the height of the tower itself.

An additional property of the time history which was important to extract for design of the full ambient vibration test is the quality of the acceleration time history. The signals have a tendency to become clipped at lower sampling frequencies and can affect interpretation of acceleration magnitude comparisons. Clipping occurs when the sampling frequency is too low to adequately capture the acceleration response. To check the time histories for clipping, it is most effective to zoom around a large response and investigate the smoothness of the curves.

The time history of Channel 2 was plotted (Figure 13-12) and a large response event was examined closely. The data points were also marked for ease of identification and to ensure that the interpolated lines did not hide a potential clipping issue. In the bottom plot of Figure 13-12, it is apparent that some clipping is occurring, specifically at 504.0s and 504.05s. While the Nyquist frequency (representative of the sine wave with the shortest period able to be captured given the sampling rate, 50Hz in this case) is twice the frequency band for this span, it is also important to be able to make acceleration magnitude comparisons between the spans, so a quality time history was also desired. While aliasing was avoided by ensuring the Nyquist frequency was above the desired frequency range, a faster sampling rate will better characterize the peaks of the sine wave. This type of investigation into signal clipping was useful in planning the full ambient vibration test.

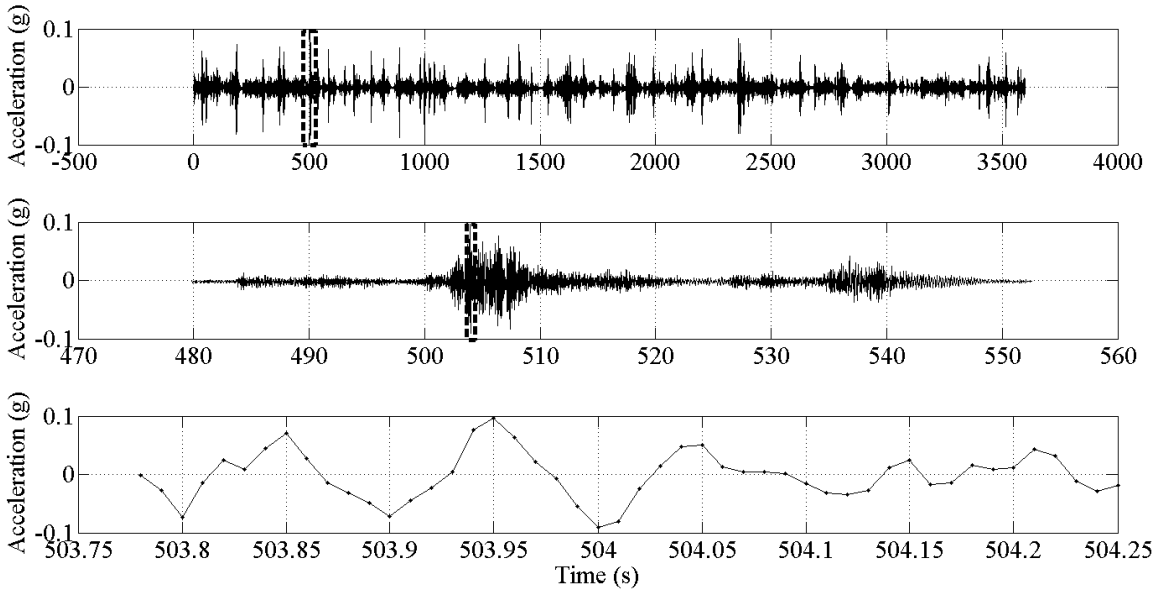

Figure 13-12: Investigation into Degree of Signal Clipping

13.1.3.2. Lift Span

The lift span time histories were examined in the same manner as was just discussed for the NJ Tower span. In this case, all eight measurement locations were able to be accessed and all channels were correctly recorded. The visual inspection (Figure 13-13 and Figure 13-14) show a maximum response level of approximately +/- 0.1g on the lift span in the vertical direction and slightly more than +/-0.05g in the lateral direction. One important note to make is that the lift span measurements were made during a period of the day when heavy truck traffic was sparse (between 12:00pm and 2:00pm). It was expected that overall maximum acceleration responses would be higher. However, the signal to noise ratio measured was sufficient. An important piece of information extracted from the time

histories is that the lift span experiences almost no vertical movement at the live load shows, indicated by the near-zero response for Channels 1 and 5.

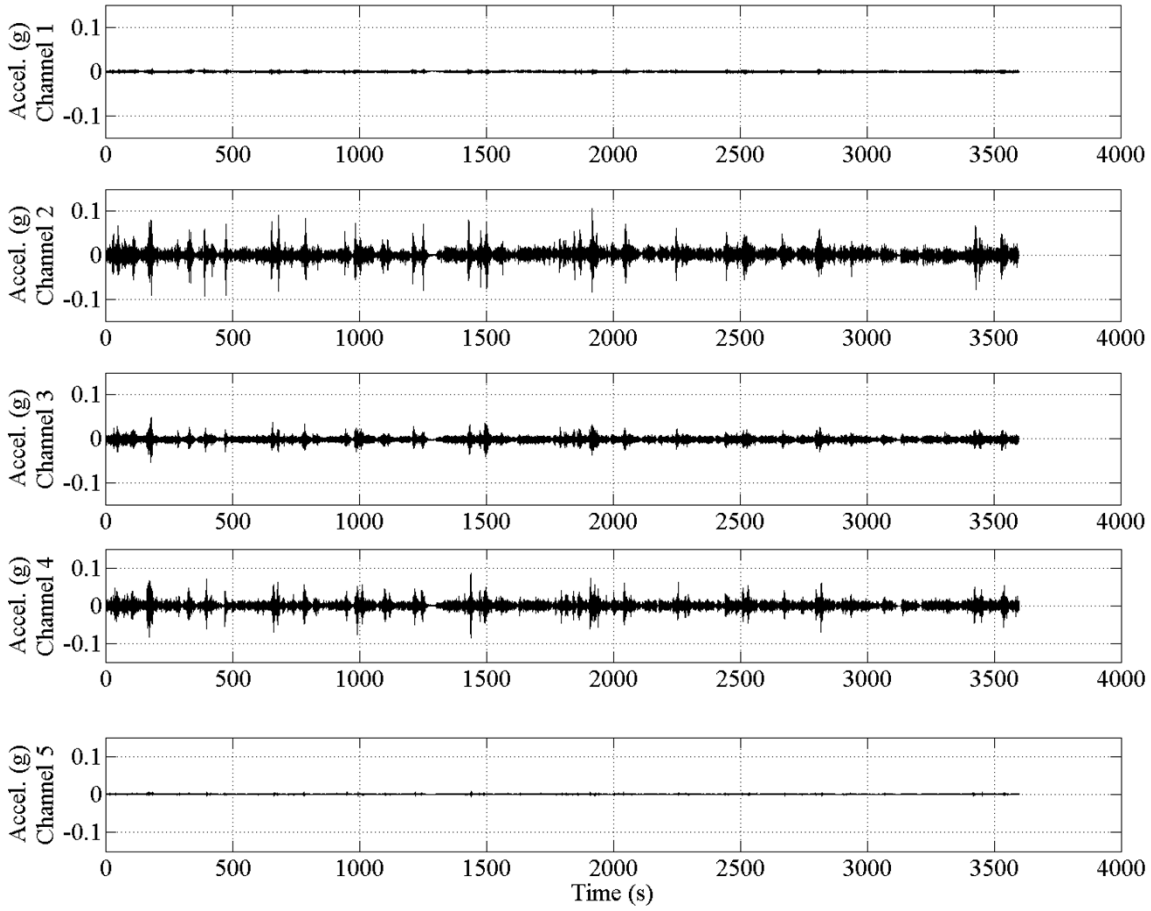

Figure 13-13: Lift Span Vertical Measurement Time Histories

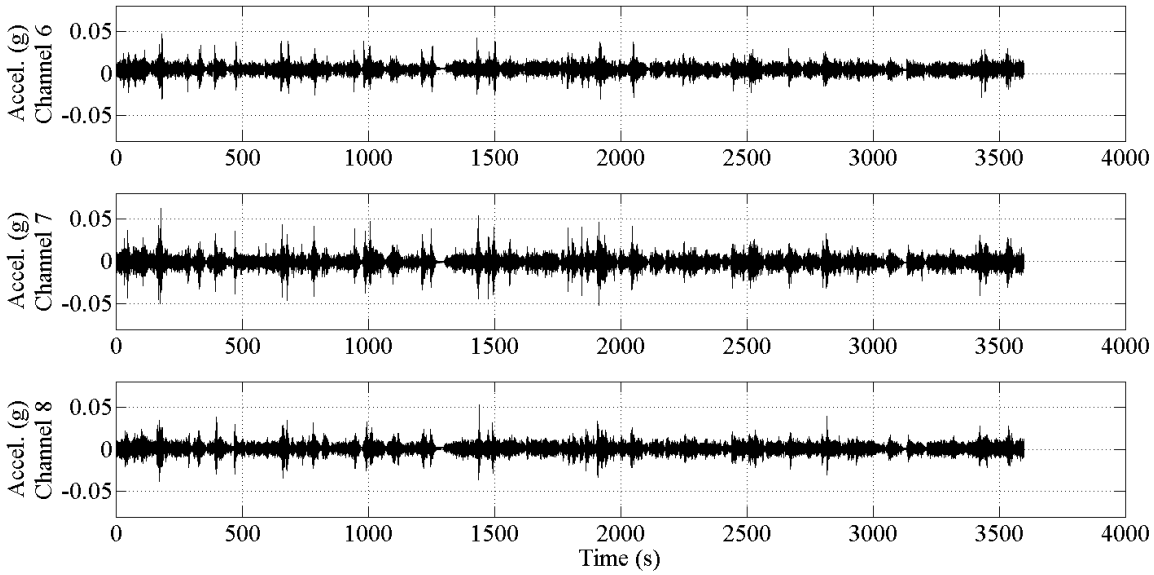

Figure 13-14: Lift Span Lateral Measurement Time Histories

The PSD's for each measurement was computed with the same approach as the NJ Tower span and are shown in Figure 13-15 and Figure 13-16.

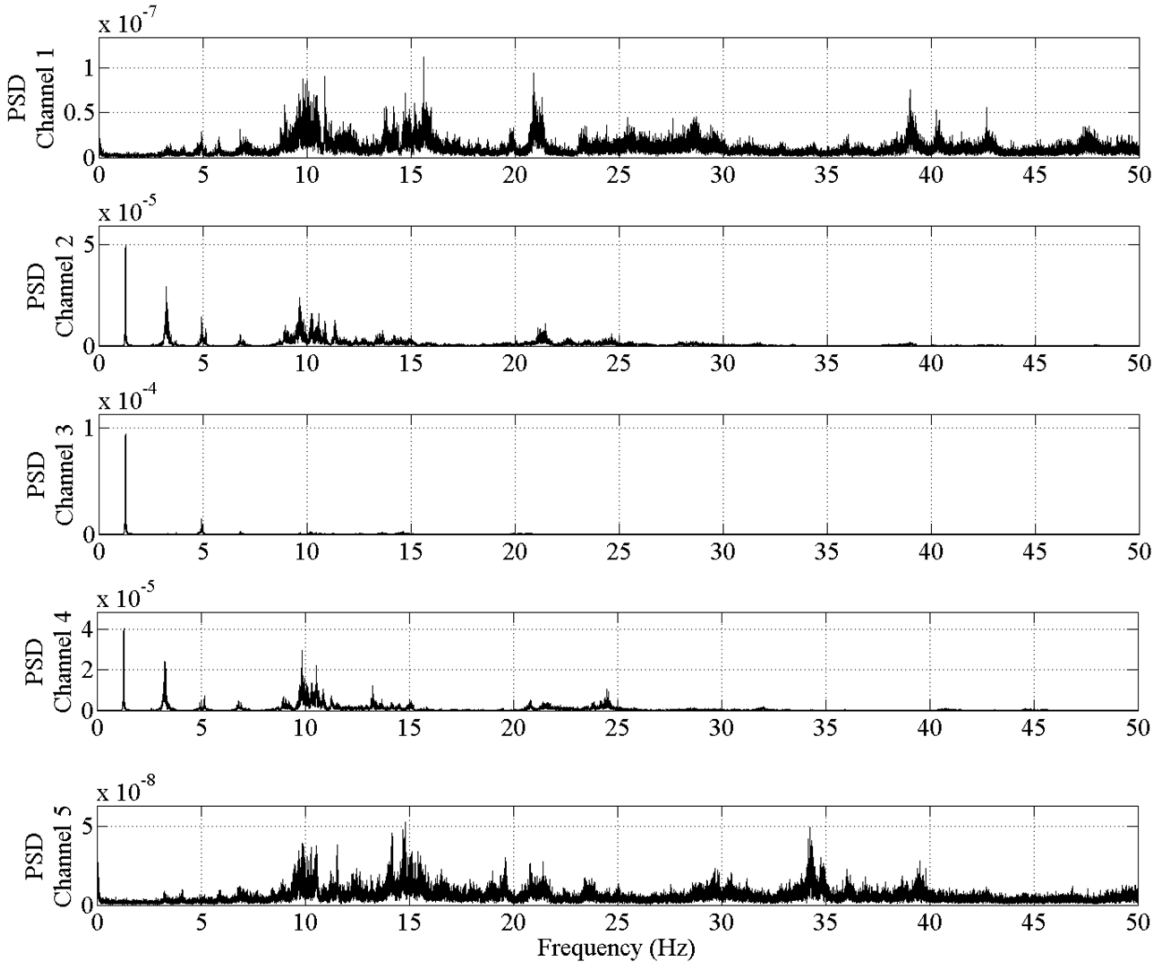

Figure 13-15: Lift Span Vertical Measurement PSD

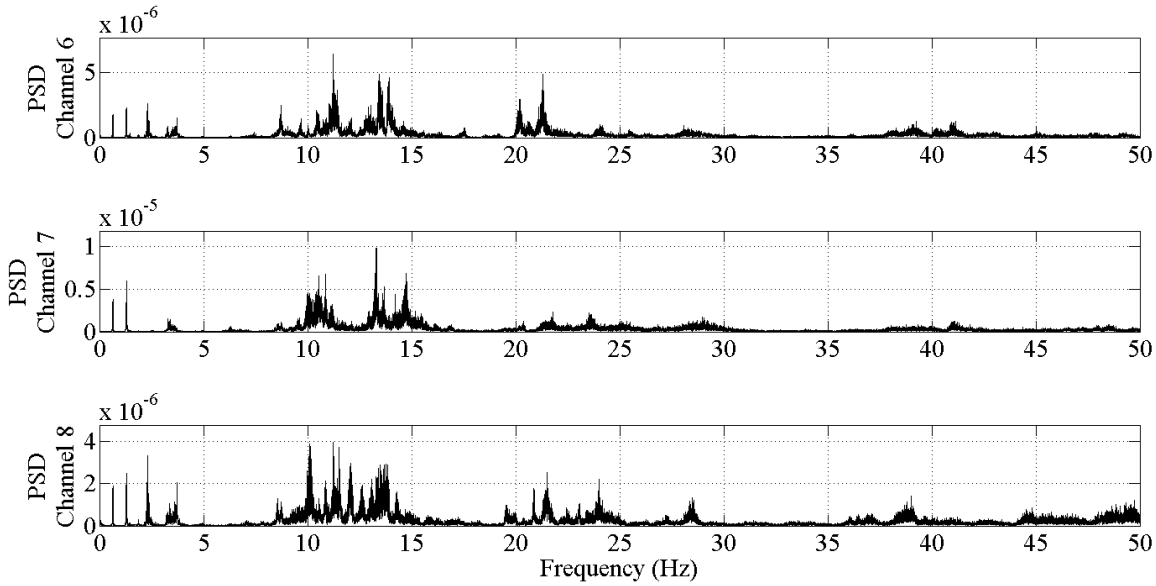

Figure 13-16: Lift Span Lateral Measurement PSD

There are clear properties of the lift span that were identified from the time history and PSD analysis of the vibration data. The first is that the vertical response at the live load shoes is negligible. This is verified by the near-zero time history acceleration and broadband noise seen in its PSD. The second property seen is that the lift span has higher magnitude vertical accelerations at PP5 and PP5', quarter span locations, than at PP10, the mid-span location. The reason why this is so was answered by looking at the PSD's of these signals. Channels 2 and 4 have a strong frequency peak at roughly 3.4 Hz where Channel 3 has no frequency peak. However, the peak at 1.29Hz is much stronger at mid-span than at the quarter span locations. The hypothesis was that the 3.4Hz frequency signal was most likely a second vertical bending mode shape, which has a nodal point at

mid-span. The vibrations from modes 1 and 2 were additively higher than the vibration at mid-span due to just the first bending mode.

The signal properties of the vertical and lateral responses of the lift span were similar to that of the tower spans. The main frequency bands ranged from 0 to 25Hz with a set of clear distinct peaks within the 0 to 5 Hz range for both vertical and lateral directions.

13.1.3.3. The Bristol Tower Span

The Bristol Tower span was setup and monitored the exact same way as the Burlington Tower Span. Once again, channel 6 was eliminated due to access restrictions on the span at the time. The time of day for the Bristol tower monitoring was roughly 5:00PM to 6:00PM. At this time on the BBB, the traffic is primarily passenger car rush hour traffic. For this reason, the time histories do not have as many sharp high response peaks, but have a more stead low magnitude vibration response due to the constant but lighter traffic. The time histories of the vertical response (Figure 13-17), lateral response (Figure 13-18), and tower response (Figure 13-19) are shown.

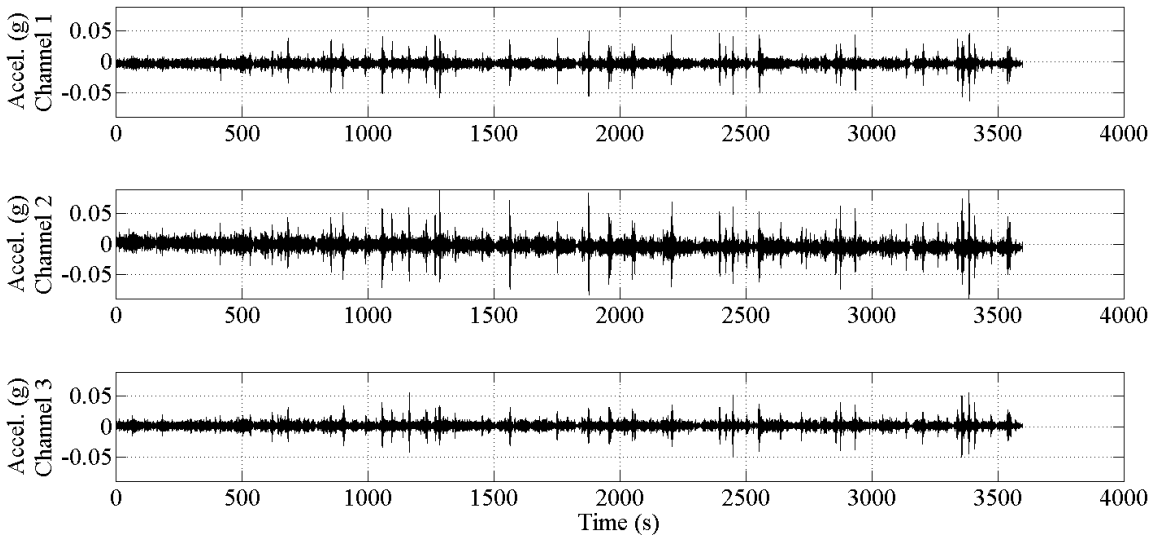

Figure 13-17: Vertical Acceleration Response of the Bristol Tower

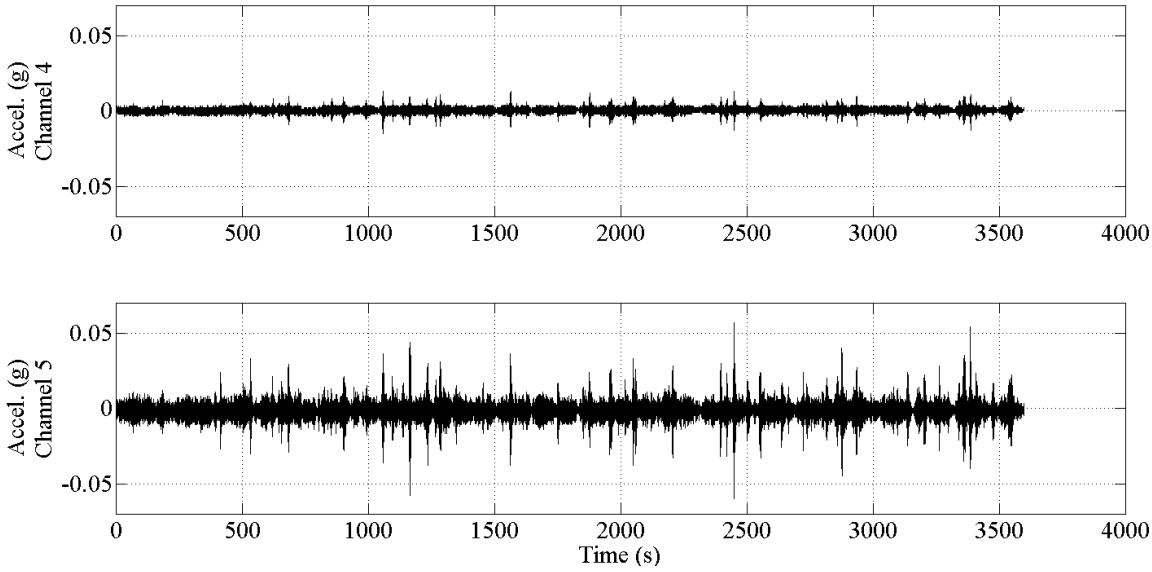

Figure 13-18: Lateral Acceleration Response of the Bristol Tower

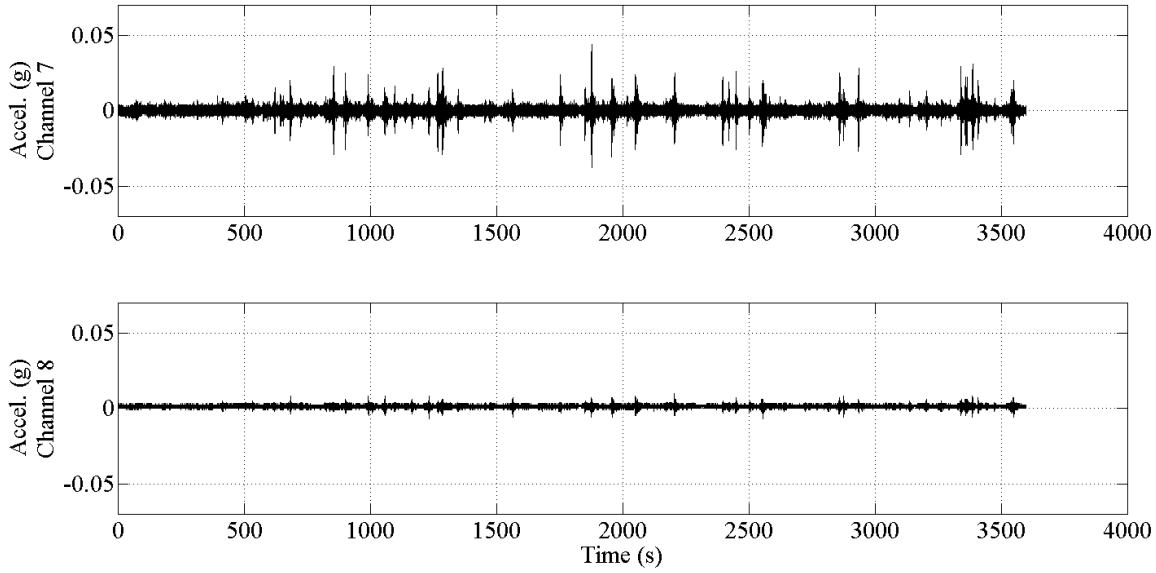

Figure 13-19: Tower Response of the Bristol Tower

After inspecting the time histories for the Bristol tower span, a similarity was drawn to the Burlington tower span: the longitudinal acceleration (Channel 7) is much greater than the lateral acceleration (Channel 8) at the top of the tower. An additional comparison that was made from the Bristol tower measurements was that the bottom chord lateral vibration (Channel 4) is much less than the top chord lateral vibration (Channel 5). One hypothesis for this was that the top chord may have been interacting more with the lateral/ torsional vibrations of the tower; however that could not be verified from this setup due to a lack of spatial resolution.

The PSD for each of the signals above was computed in the same manner as for the previous two spans and is shown in Figure 13-20 through Figure 13-22.

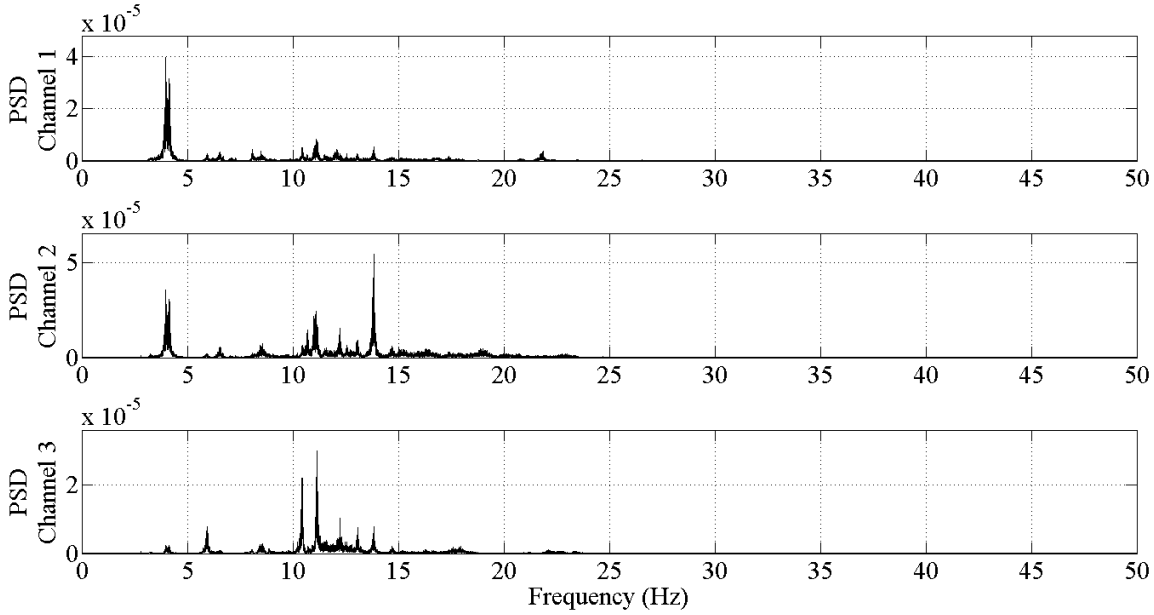

Figure 13-20: Bristol Tower Span Vertical Response PSD

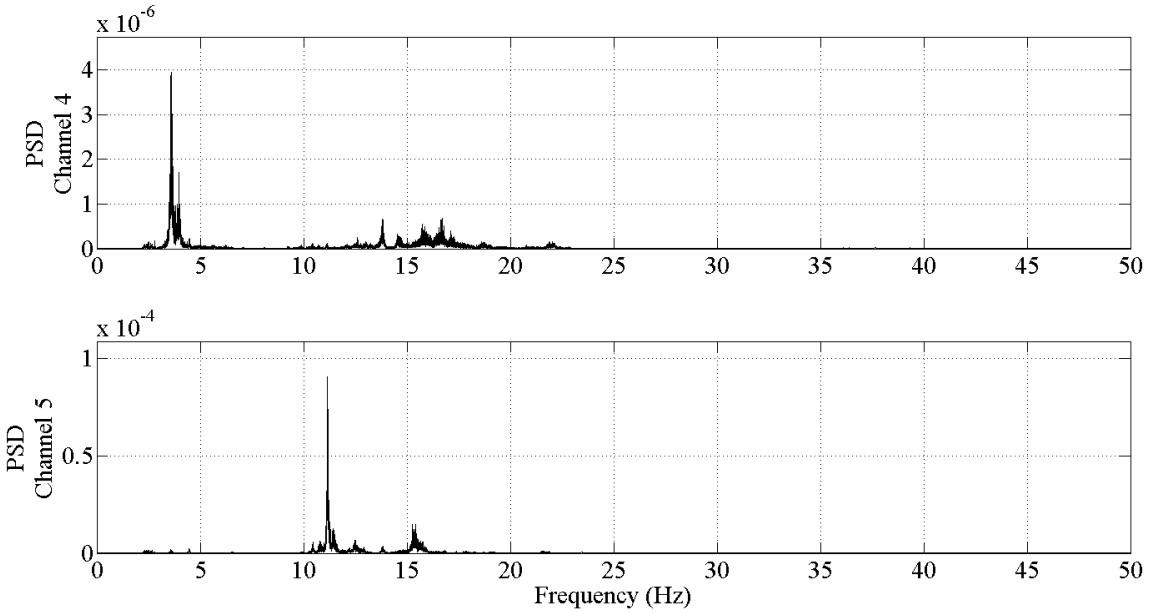

Figure 13-21: Bristol Tower Span Lateral Response PSD

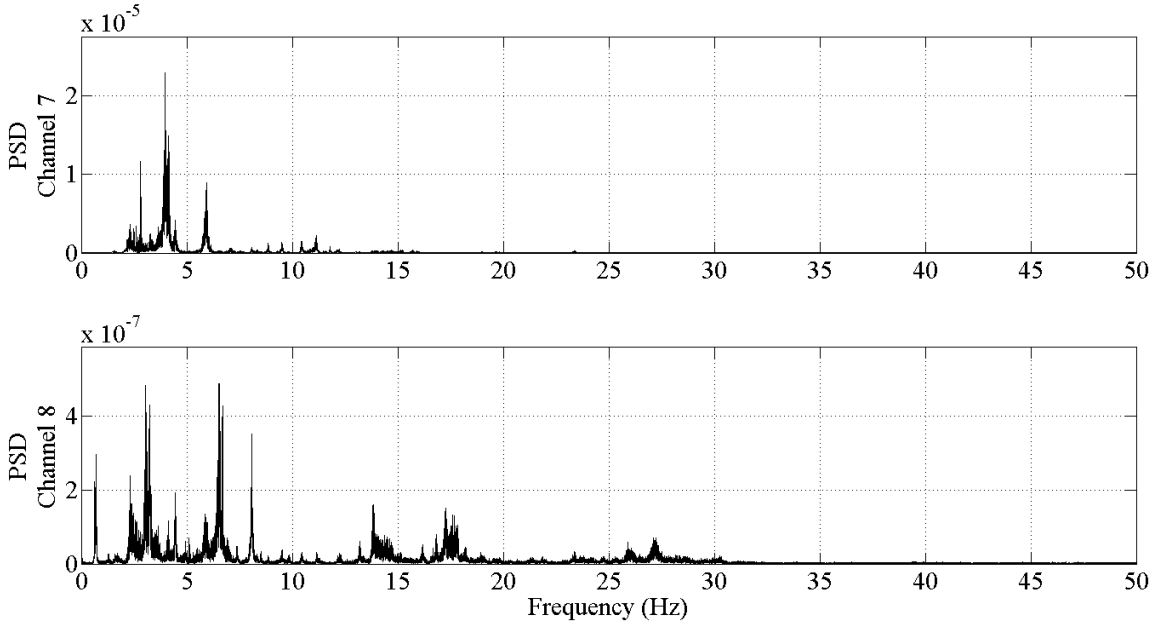

Figure 13-22: Bristol Tower Span Tower Response PSD

The frequency content of the Bristol tower span is similar in terms of frequency range to its counterpart, the Burlington tower span. It was not justifiable to make inferences about the differences in characteristics of the vibrations at this point since the two spans had greatly different excitation sources in terms of the type of traffic during the time of day in which they were monitored. However, meaningful information was able to be extracted from all tests to produce a more efficient full ambient vibration study.

13.1.4. Preliminary Vibration Results

The results of the preliminary vibration study were directly applied to the design of the full ambient vibration test. The sampling frequency of 100Hz was slated to be increased to at least 200Hz to better characterize the acceleration time history responses to provide a better means of comparing separate spans. Also, the uncertainty with the vibration properties of the spans as a function of their excitation sources was mitigated by increasing the measurement period to at least one full week day to capture the morning rush hour, which typically includes several heavy truck crossings. Additionally, the preliminary survey was useful in determining where extra access accommodations were needed so that all desired locations could be reached. The BCBC was contacted about ways to reach areas on the structure which were not readily available by manual climbing techniques and appropriate measures were taken.

While a detailed set of frequencies and mode shapes could not be generated for each span due to the sparse instrumentation plan used, an estimate of the fundamental frequency for each span was hypothesized for preliminary model correlation and shown in Table 13-1.

Table 13-1: Preliminary Estimates of Fundamental Modes for Each Span

Span	Modeshape	Frequency (Hz)
NJ Tower	First Bending	4.089
Lift	First Lateral	0.67
Lift	First Bending	1.29
PA Tower	First Bending	4.041

13.2. Live Load Monitoring of a Critical Member

The work plan discussed in this section was part of a larger effort to serve the BCBC through the development of a comprehensive, long-term preservation and renewal plan to maintain the safety and enhance the serviceability and affordability of the assets owned and operated by the Commission. The specific objective of this work plan was to gain insight into the short term and long term intrinsic action fluctuations experienced by truss members on the BBB, which were deemed critical due to low load rating factors resulting from high dead load demands. This project was directed and carried out by Drexel University research associates, and included the design of the most appropriate sensor instrumentation plan, sensor installation, data acquisition, data interpretation and corresponding finite element model construction and calibration. The intended goal was to gain a deeper understanding of the daily and seasonal demand on critical members, and to value the cost-benefit associated with any resulting recommendations to maintain satisfactory performance related to safety, serviceability/durability and operations/functionality.

13.2.1. Live Load Monitoring Project Background

On September 18, 2007 a load test was performed on the BBB in an attempt to validate a finite element model constructed by an outside engineering firm. This load test was carried out by a contracted firm and the data from this experiment was then used to calibrate a model and generate load ratings for the structure. In these ratings, it was found that mid-span top chord members of the lift span had load ratings less than 1.0 for certain trucks using the Allowable Stress Rating (ASR) approach. However, the load rating

reports were vague in their explanation of dead load sources and distribution throughout the lift span, which represents over 90% of the demand on the critical top chord members.

In the unique case of this structure, the dead load of the lift span is known very accurately, as was described in the accounting of mass in Chapters 12 and 13. The total dead load identified during these tests exceeded the dead loads estimated through conventional modeling approaches by around 50%. In the load rating report, outside engineers “backed into” the total weight of the model by simply distributing the unaccounted for dead load uniformly throughout the span.

Given the uncertainty associated with this approach, Drexel University subsequently scheduled a field visit to the bridge in an attempt to quantify sources of extraneous mass as well as their distribution throughout the span, as discussed in Chapter 12. Following this field visit, Drexel research associates were able to calculate a quantity take-off of the total dead load in the lift span very similar to the total dead load calculated through balancing procedures. These masses (i.e. connection plates/rivets, machine house, equipment, non-structural members) were incorporated into a SAP2000 model of the structure and validated through the sum of total dead load reactions of the lift span as well as through a comparison with experimental determined modal parameters.

On July 17, 2008 Drexel University research associates carried out a preliminary ambient vibration monitoring of the BBB to capture response magnitude as well as a few modal parameters of the two tower spans and lift span. In this vibration study, the first bending mode shape of the lift span (Figure 13-23) was determined to be 1.29Hz and the first lateral bending mode shape of the lift span (Figure 13-24) was determined to be 0.67Hz.

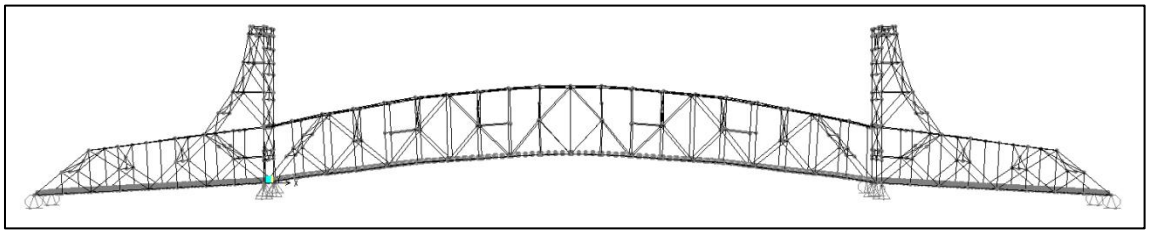

Figure 13-23: First vertical bending mode shape (1.29Hz)

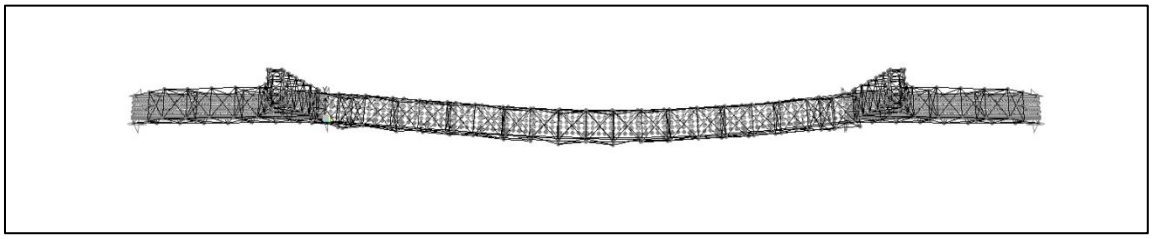

Figure 13-24: First lateral bending mode shape (0.67Hz)

Once the preliminary vibration survey was complete, a coarse model correlation could be carried out. At this point in the overall MM St-Id analysis of the BBB, the experimental design benefited more from a traditional St-Id model calibration than a more complex multiple model analysis since very little information was known about the structure. However, the preliminary SAP2000 model was calibrated to the first few modes from the preliminary vibration survey by adjusting the continuity conditions between the lift span and the tower spans. These continuity conditions were adjusted by placing links between

the two spans and adjusting the spring stiffness of the links manually until a sufficient convergence was reached for a preliminary analysis.

Upon completion of the model calibration, load ratings were generated for members deemed critical by an outside firm's preliminary load rating report. When calculating the initial ASR, it was found that mid-span top chord members had ratings of less than 1.0. However, through the process of model calibration it was discovered that multiple models provided very different load ratings for the same members, under equivalent levels of calibration success. The difference in load ratings was due to different dead load distributions generated by the varied boundary conditions assigned in the models. In one model the load ratings were around 1.7 while in another model they were around 0.7.

Due to this discrepancy in dead load distribution, further testing was necessary to provide the best set of recommendations to the BCBC. Research was carried out into vendors who could potentially measure the dead load stress in the top chord section of the lift span. A select few companies claimed to have technologies capable of measuring in-situ dead load stresses non-destructively (X-ray diffraction, ultrasonic scanning), while certain destructive tests were also available for in-situ stress determination (ASTM E-837 Hole-Drilling Method).

While these vendors were being coordinated for their potential use in this application, a monitoring system was designed to study the variation of intrinsic actions in the top chord sections. This type of instrumentation would provide crucial information such as strain variation due to traffic, which would also show the effects of possible overloaded vehicles, as well as the strain variation due to long term and ambient conditions, such as daily, seasonal and climatic events.

By monitoring these short term and long term strains, it would then be possible to see what the overall maximum and minimum imposed (traffic, weather) strains were. This was critical since the dead load stresses within the top chord member were currently estimated to be a large portion of the member's capacity, and so significant variations could have a sizeable influence over safety and serviceability performances.

13.2.2. Instrumentation Design

The designed monitoring system included various types of strain gages, instrumentation cables and a data acquisition system which would be maintained in the machinery house at mid span of the lift truss. The identified location for monitoring was at mid-span of the lift span between PP9 and PP10 (Figure 13-25), both upstream and downstream truss members. This location was the closest to mid-span of the lift truss, but also the furthest away from any connection details, which cause turbulent stress flows that make data interpretation difficult and, in some cases, unreliable.

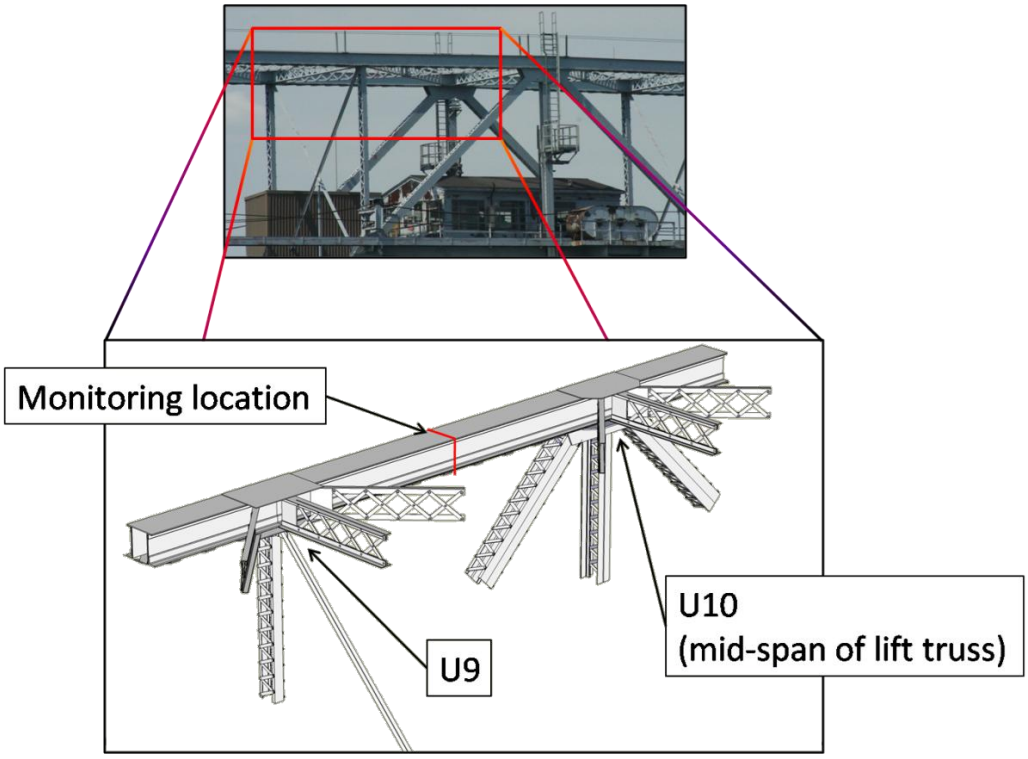

Figure 13-25: Location of Strain Monitoring Gages on both Upstream and Downstream Truss

The cables and data acquisition system would be installed to ensure minimal interference with regular maintenance and access to and around the machinery house. The sensors also would be installed on locations that minimize trip-hazards to personnel walking along the top chord member being monitored.

13.2.2.1. Sensor Selection

The strain gages were selected based on the specifications required for this monitoring system. In order to measure short-term strains, the gage must be able to read

measurements at high speeds so that peak responses, due to the transient effects of traffic, are captured reliably. Likewise, in order to monitor a certain long-term responses, gages must not "drift" and must remain accurate over long periods of time. Current strain gage technology is not yet capable of meeting these requirements with a single sensor, so a suite of multiple gages were designed to collectively meet all of these requirements (Table 13-2).

Table 13-2: Sensor Type vs Application

		Sensor Type				
		Electrical Resistance (1")	Vibrating Wire (2")	Electrical Resistance (2")	Vibrating Wire (6")	
Time	Milliseconds	■		■		Short Term
	Seconds	■	■	■	■	
	Hours		■		■	Long Term
	Weeks		■		■	
		Short	Middle		Long	
		Gage Length				

As seen in Table 13-2, the best gages for short term, high speed data collection are the electrical resistance gages. The best gages for long term monitoring are the vibrating wire gages. The reason why electrical resistance gages are not good for long term monitoring is that they tend to drift due to temperature variation from the electrical current passing through the gage, however they are more accurate and do not drift over shorter time periods and can be read at high sampling frequencies.

The vibrating wire gages are best for long term measurements, as they do not have continuous electrical current passed through them but a pulse to activate the gage over a specified time period. Due to requirements associated with processing data from this sensor, the sampling frequency for vibrating wire gages cannot be more than one measurement per second. However, since they are used in monitoring for days, weeks or even months at a time, the sampling frequency was not required to be very high. Another advantage of the vibrating wire gage is the added ability to measure temperature, so that seasonal variations due to temperature could be correlated.

It should be noted that many other means of measuring strain are available and include clip gages, fiber optic strain gages, and full bridge strain gages (such as from BDI). However, the both the full bridge and fiber optic strain gages were ruled out for this application due to the higher cost of the instruments (fiber optic and full bridge) as well as the data acquisition hardware (fiber optic). Clip gages were also ruled out for this application because they are better suited for monitoring cracks, and the geometry of the sensor made it susceptible to effects from ice forming on the sensing element.

The remaining requirements for a reliable system are related to gage length, or the length over which the strain will be measured. The longer the gage length is, the less of a

chance for local, turbulent stress flow to influence the measurements. This results in smeared strains, which are more reliable, but may not provide the resolution needed for detailed model calibration. To acquire these smeared measurements, a six inch vibrating wire sensor was used, which was the maximum length possible give the high density of rivets in the top chord members (Figure 13-26). The shorter strain gages are able to pick up strain concentrations, and while this is desirable, it does make data interpretation far more difficult. To capture localized strains, 0.5 inch electrical resistance gages were used in conjunction with two inch vibrating wire gages, to measure both short-term and long term responses.

Figure 13-26: Rivet Density of Top Chord Member

The high speed electrical resistance strain gages were manufactured by Hitec Products, Inc. The 1 in. and 2 in. strain gages (Model # HBW-35-250-6-10GP-TR) each had a nominal resistance of 350Ω. The 2 in. vibrating wire gage (Model 4150) and the 6 in. vibrating wire gage (Model 4000) each were manufactured by Geokon, Inc.

13.2.2.2. Identification of Sensor Location

In order to obtain an accurate profile of the strains throughout the cross-section of the member, as well as to measure differential stress due to heating of one side of the member due to radiation, a set of sensors must be distributed around the cross section of the member. Also, the different sensor types must be used where they are most beneficial, for the reasons listed in the previous section.

As seen in Figure 13-27, a total of twelve gages at one cross section were planned (gages shown on the web are mirrored on the opposite web). Six gages are vibrating wire type, while the remaining six are electrical resistance gages. As mentioned previously, this level of redundancy allows the same measurements to be made, but at different temporal scales.

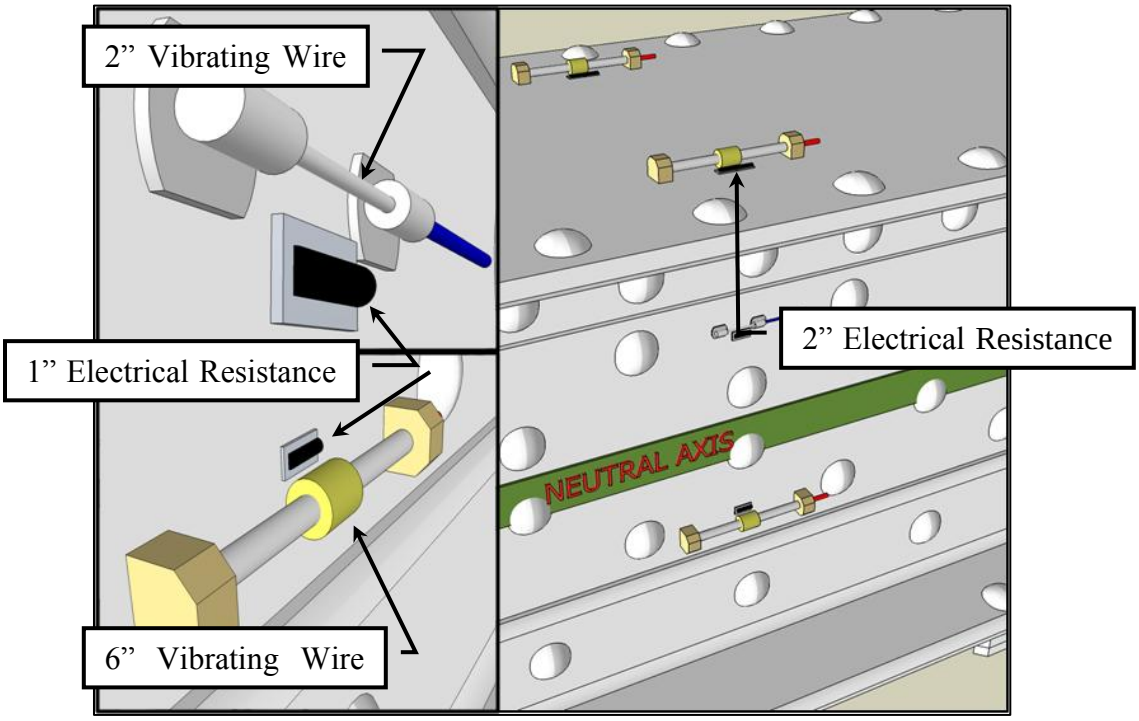

Figure 13-27: Instrumentation Plan

In addition to the twenty-four sensors included in the design above, an additional four sensors are reserved for drift monitoring purposes. An isolated steel plate was designated as a “dummy plate” and had each of the four types of sensors installed on it. This plate was then located in a shaded and unexposed area where it would not be interfered with. Over the course of time, these sensors would act as a reliability check for the sensors installed on the structure. If a drift is seen in the vibrating wire data, a means of verifying that it is a valid observation of a physical event is necessary, and not that the event is due to a data logger error or sensor sensitivity to environmental changes. If a drift is seen

across all sensors, including the dummy sensors then it can be identified that a noise or data logger issue is causing the drift. However, if the response is only seen in the sensors installed on the structure and not on any dummy plate sensors, then the user can confidently associate the reading with a physical event.

The inclusion of the dummy sensors brings the final tally of sensors to twenty-eight, twenty-four of which are on the structure and four dummy sensors.

13.2.2.3. Data Acquisition Design

To record twenty-four sensors discussed above, a data acquisition system needed to be designed which incorporated multiple features: two independent sampling rates for the different sensor types, automated triggering system, and remote control capability. After research into available data loggers at the time, it was decided with the help of sales technicians at Campbell Scientific that a CR5000 data logger would best handle the defined requirements. In order to measure the quantity and types of sensors involved with this instrumentation design, a variety of peripherals were also required. The flow chart shown in Figure 13-28 details the peripherals used and how they interface with the main data logger.

The CR5000 is powered by a dedicated power line run by the BCBC to power the electronics in the machine house. While it is convenient to have a dedicated source of power, it does not ensure that the data logger will always have a consistent power source. Outages (both intended and unintended) occasionally occur in the machine house, so a

battery backup capable of providing up to six hours of power in the event of an outage, was included in the data logger.

The data logger is able to be remotely accessed via a cellular phone modem provided by Campbell Scientific. The cell modem requires a major phone network data plan but provides a wireless means of remotely connecting to the data logger for data collection or program manipulation. Considering the travel time and effort it took to reach the data logger, having a remote access connection was crucial to the success of the application.

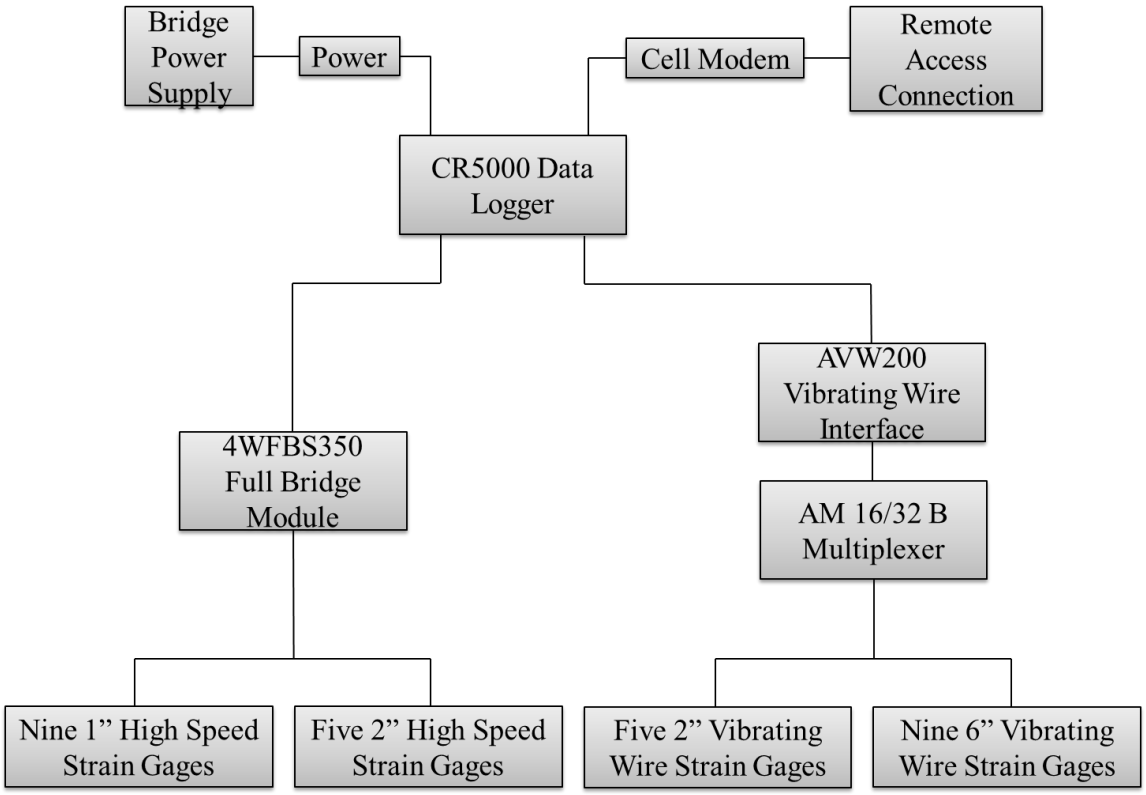

Figure 13-28: DAQ Design

The vibrating wire sensors are measured with a vibrating wire interface. This interface, Model AVW200, sends an electronic pulse to a magnetic coil in the sensor. This magnetic pulse then acts to pluck the wire which is housed within the sensor unit and induce a free vibration response. A second coil in the sensing unit then tracks the movement of this wire via a second magnetic coil which generates an electronic signal back to the AVW200. This information is then interpreted by the interface to provide the frequency of oscillation of the wire, various data quality variables and the temperature of the sensor. A downfall of the vibrating wire interface is in its limited number of available channels for measurement. The two channels included on the AVW 200 certainly are not sufficient for the fourteen vibrating wire sensors included in the instrumentation, yet it is not necessary to purchase seven AVW200 peripherals to measure all of the sensors. Rather, a single AVW200 can be used to interrogate the 14 sensors through the use of a multiplexer, the AM 16/32B.

A single multiplexer only requires one channel on the AVW200, however can read sixteen sensors with a four-wire connection or thirty-two sensors with a two-wire connection. The vibrating wire sensors used require a four-wire connection: two for the strain signal and two for the temperature signal. The multiplexer acts as a switch between the sixteen vibrating wire sensors connected to it, allowing the AVW200 to read the sensors one at a time until all have been measured. A drawback to using multiplexers in any data acquisition system is the loss of synchronous measurements, however for the vibrating wire strain gages this is not a necessity since the sensors are only going to be interrogated over long intervals of time. After the multiplexer polls every vibrating wire

strain gage, all of the stored information is then sent to the data logger for conversion to physical units and storing.

The electrical resistance strain gages do not require as many measurement peripherals since the data logger itself has twenty available channels for reading and recording differential voltage sensors. However, signal conditioning is necessary since by nature electrical resistance strain gages are naturally measured by detecting changes in the resistance of the sensor. This change in resistance is correlated with a change in the length of the sensor, and therefore the strain applied to the sensor by what it is attached to. In order to amplify a change in resistance (a very small quantity) to a voltage differential, a bridge completion module, which contains a Wheatstone bridge that amplifies the signal of the single resistor (strain gage) is required. In this case, a 4WFBS350 bridge completion module from Campbell Scientific was used. The bridge completion module provides three of the four legs of a Wheatstone bridge, with the strain gage serving as the fourth and final leg. The Wheatstone bridge is able to both amplify the signal and provide a signal in terms of differential voltage.

The data acquisition program was configured to read the vibrating wire strain gages at a rate of once every twenty minutes. It would then take approximately thirty seconds to read the entire group of vibrating wire sensors. Once the vibrating wire data was recorded, the data logger then began scanning the high speed electrical resistance gages at a rate of 50Hz. This measurement speed was selected so that the data logger would be able to sufficiently characterize the response from a vehicle crossing the span at full

speed. In order to preserve the memory of the data logger, a triggering system was developed.

A trigger variable was automatically computed by averaging the response of all six strain gages on the downstream chord. This chord was selected since most of the heavier traffic travels from PA to NJ and would receive more of the distributed load. Once the trigger variable exceeded a defined threshold value, the data logger would record the five seconds of data leading up to the trigger event and keep recording until the trigger variable dropped below the threshold value. Once the trigger variable dropped below the threshold, the data logger continued to record for another five seconds. The final threshold, 15με, was identified after the system was fully installed through a trial and error approach so that normal passenger car events were not captured, but heavier trucks were.

13.2.2.4. Sensor Installation

The sensor and data acquisition system were described in a proposal to the BCBC for approval. The proposed system was approved and on January 13, 2009 Drexel University research staff, with the generous support from engineers and BCBC staff, began the installation of the top chord strain monitoring system (Figure 13-29).

Figure 13-29: Drexel and BCBC staff during instrumentation installation

Over the course of the next two months, the installation of the top chord strain monitoring system was completed. The major tasks completed over the course of this time period include the following (See Table 13-3 for Gaant Chart representation):

1.) Manufacturing and shipment of required instrumentation
2.) Installation and debugging of all instrumentation
3.) Providing gage and cable protection by painting exposed steel and encasing cables
4.) Manufacturing and shipment of the data acquisition system and all related peripherals for sensor measurement
5.) Laboratory verification of programming and wireless communication systems
6.) Field installation of data acquisition system
7.) Finalization of data acquisition program utilized by data acquisition
8.) Preliminary data interpretation and analysis
9.) Creation of data storage techniques

Table 13-3: Gaant chart of work completed on Strain Monitoring System

Task	Dec	Jan	Feb	Mar	April
Proposal					
Order equipment, sensors and DAQ					
Field Instrumentation					
Sensor Debugging					
Laboratory Testing of DAQ					
Field Installation of DAQ					
DAQ Data Collection Regime Refinement					
Data collection					
Investigation of Large Responses					
Creation of Data Storage Regime					
Data Analysis					

The DAQ equipment was ordered before the field work began, however each piece requires factory calibration before being shipped so there was a significant lead time in its delivery. In order to not delay the project, the field instrumentation of the sensors began on January 13, 2009. In order to simplify the strain gage installation process on the sides of the top chord member, BCBC staff fabricated a bracket (Figure 13-30) to support the person installing the sensors.

Figure 13-30: Drexel, BCBC and Pennoni Staff Instrumenting the Top Chord Member

The process of installing strain sensors on the bridge begins with the removal of surface paint from the steel members. The strain gages are spot welded onto the steel, so it is important that the steel is clean of paint, rust or any pocketing which would compromise the integrity of the spot welds. As seen in Figure 13-31, the spot welds were used to fasten the shims of the strain sensors directly to the bridge as well as to install the cover plates over the 2" vibrating wire strain gage. These cover plates were required to minimize the effects of thermal radiation directly on the sensor. The strain gages were initially installed without the cables being run so that the cables would not be damaged.

Each sensor was provided with a short lead of cable which was left coiled at the sensor until the cables were run (Figure 13-31).

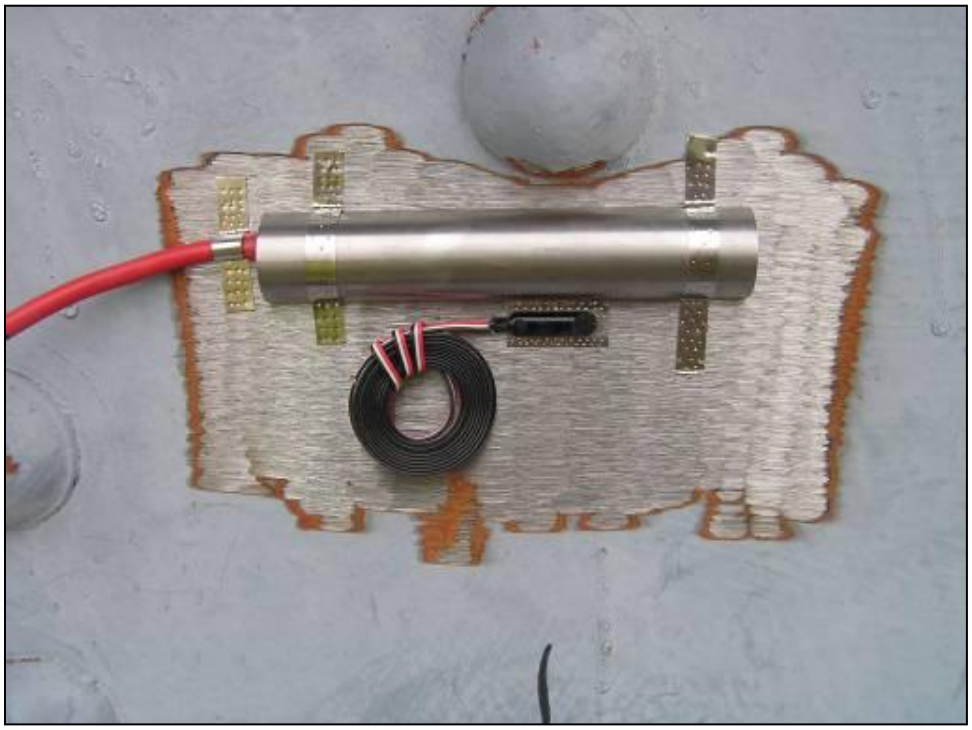

Figure 13-31: 2" Vibrating Wire Gage with Cover and1" Electrical Resistance Gage

The 6” vibrating wire gages required an arc weld to attach the mounting bases to the steel members (Figure 13-32). To reduce the risk of destroying the sensor during the welding process, a mounting bracket was installed between the tabs which were the same dimension of the sensor, but solid metal. The mounting bracket was then removed from the tabs by loosening the set screws on either mounting tab and the sensor was installed by tightening the same set screws according to manufacturer specifications. The sensing

mechanism is separate from the tube containing the wire for the 6” sensors and was attached to the tube with a pipe clamp. The 2” vibrating wire sensor was a single piece sensor which was spot welded to the steel.

Figure 13-32: 6" Vibrating Wire Gage with 2" Electrical Resistance Gage

To ensure that the installation of the sensors and removal of paint did not compromise the integrity of the steel member or introduce locations of advanced corrosion, great care was taken to paint the steel to its original color and level of corrosion protection. After the

sensors were installed, a black rust inhibiting primer was used to coat the bare steel to immediately protect it from corrosion (Figure 13-33). A final coat of paint was then applied on top of the black primer. The second rust inhibiting paint used matched the color of the bridge and was applied in two coats (Figure 13-34).

Figure 13-33: Black Rust Inhibiting Paint used to Coat Exposed Steel After all Sensors were Installed

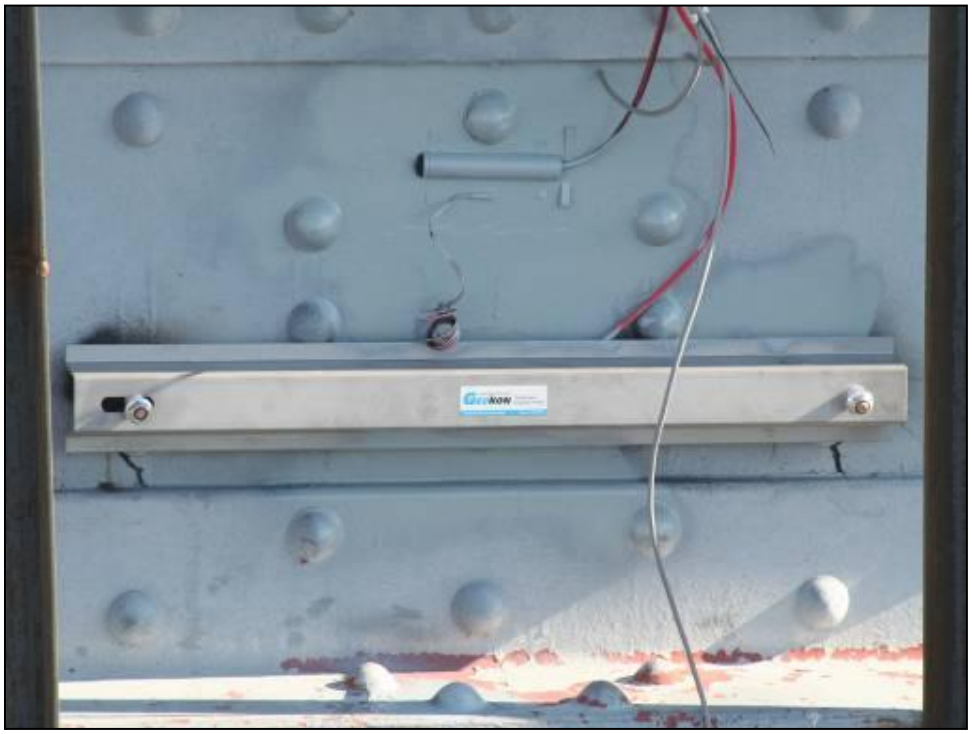

Figure 13-34: Painted Surfaces after Installation with Protective Covers Installed

The 6” vibrating wire gages required a large cover plate that was able to be removed if needed. Since the 6” gage was mounted with set screws between two steel mounting brackets, it was possible to overstrain the sensor during the installation process. By having access to the gage after the cover plate was installed, it was possible to access the sensor and reset the screws. The cover plate supplied by Geokon consisted of a sign post channel with two predrilled holes for bolted mounts. The heads of the mounting bolts were arc welded to the structure. Locking nuts were used to tighten the cover plates on to the welded bolts since the bridge experiences heavy vibration and the sign posts were directly above traffic.

After all the sensors were installed, cables were run from the sensors to the location of the DAQ within the machine house. To protect the cables against environmental conditions, a flexible conduit was wrapped around the bundle of cables coming from the sensors (Figure 13-35). Each cable bundle was installed in a location where it would not interfere with accessibility for the maintenance crews walking along the top chord.

Figure 13-35: Conduit Encasing all Instrumentation Cable

The cables were attached to the leads from the sensors by soldering each wire together and protecting the soldered joint with a heat shrink coating (Figure 13-36). The entire spliced connection was also protected with a heat shrink tube and then reinforced with multiple layers of electrical tape.

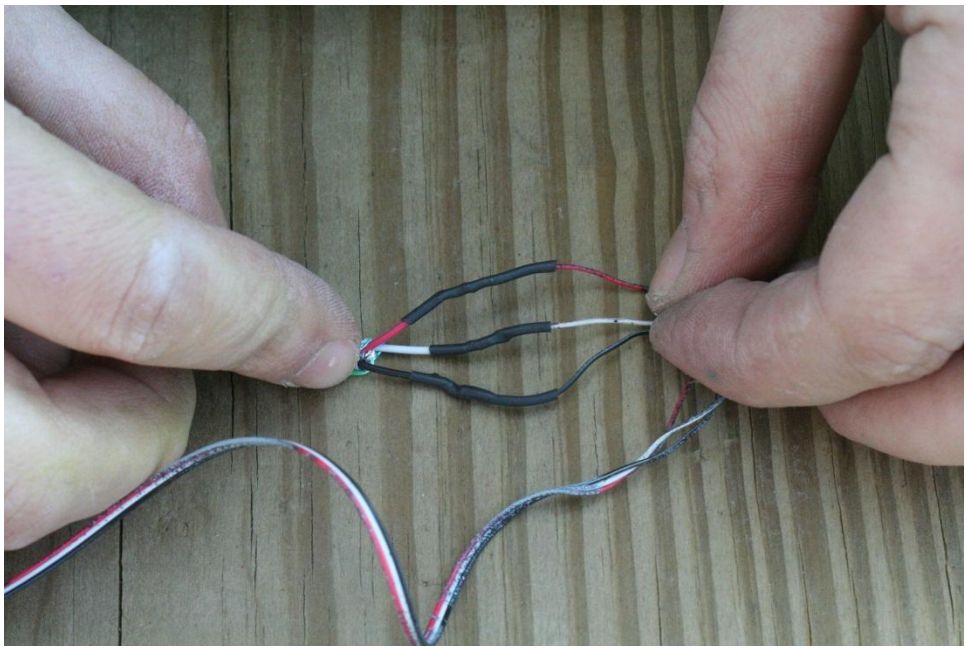

Figure 13-36: Heat Shrink Tubing Protecting the Soldered Splice Connection

The data acquisition system was received after the installation of all the sensors was complete. The cell modem interface was verified in the laboratory before the system was installed in the field to minimize debugging efforts. The programming of the data

acquisition was also performed in the laboratory and verified with extra sensors of the same type as were installed on the bridge. The DAQ system was finally installed in a permanent metal cabinet which housed all loggers and peripherals. The cabinet was able to be locked to prevent accidental power outages or damage. The programming and data triggering schemes were debugged and finalized for full operation on March 21, 2009. The system was then set to run and continuously record and stream data to Drexel University offices for permanent storage.

13.2.2.5. Vibrating Wire Strain Gage Data Analysis

Vibrating wire strain gages have another key advantage because of their long term stability, and that is the ability to stop recording the sensors for a period of time and then resume without losing the reference point for each sensor. The first measurement made on each sensor is the permanent reference point as long as no changes are made to the mounting of the sensor itself. This is beneficial when the measurements are being monitored for years, because malfunctions can cause the storage computer to stop recording or communications equipment can fail. In either case, the measurements can be resumed whenever connectivity is restored without any information loss, besides short term events which occurred during the outage.

For the BBB vibrating wire data collection, the measurements were recorded continuously for over one and a half years. Afterwards, there were large breaks in the recorded measurements as computers and systems were updated at Drexel offices. However, when questions arose due to conditions on the bridge, the data logger was

connected and the available data was downloaded. At the time of publication of this thesis, the data collection and maintenance responsibilities have been transferred to the engineer of record for continuous recording and storage of data, thereby eliminating any further gaps in the records.

The full time history of all the vibrating wire gages for the upstream chord is shown in Figure 13-37 and the time history of all the gages for the downstream chord is shown in Figure 13-38.

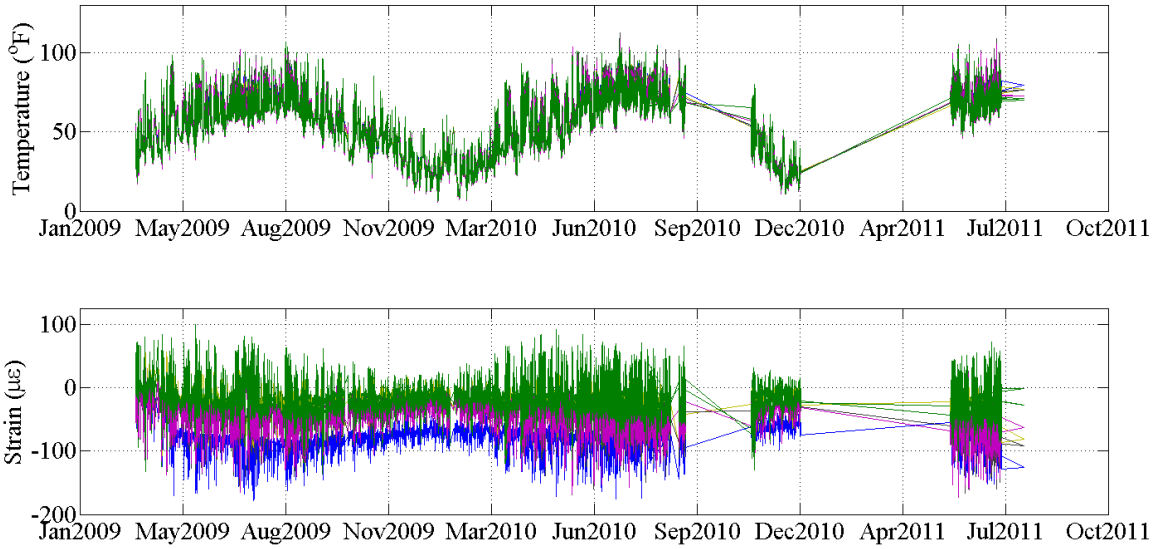

Figure 13-37: Strain and Temperature Time History for Upstream Chord Sensors

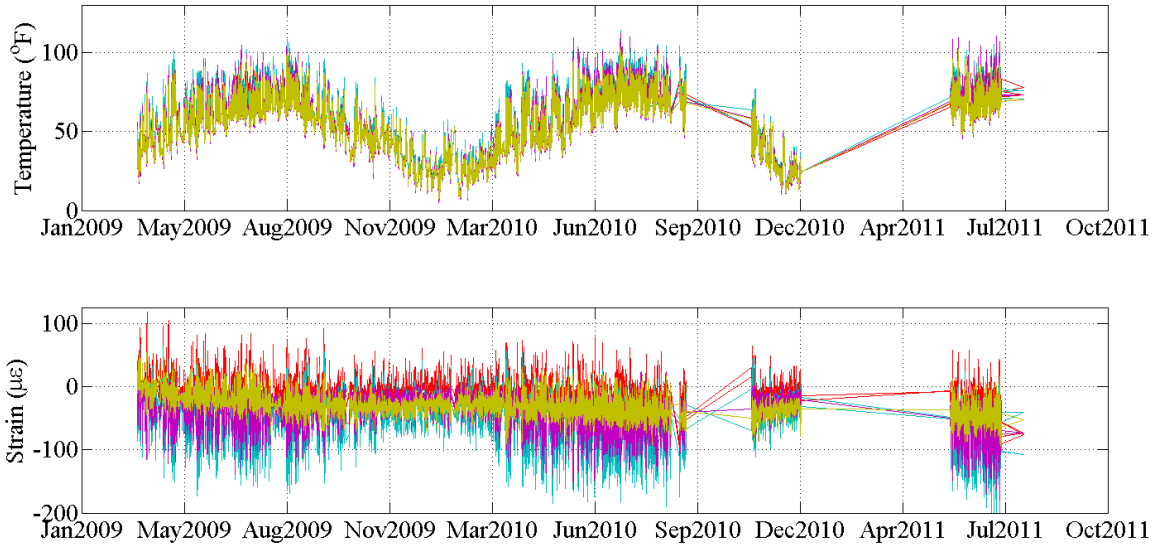

Figure 13-38: Strain and Temperature Time History for Downstream Chord Sensors

After examining the time histories, a few observations were made: (1) the daily fluctuation of strain within the top chord members is much greater in the summer months than winter months and (2) an overall increase in the amount of compression is present. The daily fluctuation of the strains of the top chord is due to the more drastic temperature changes over the summer months than the winter months. To examine a close-up view of the strain time histories, Figure 13-39 and Figure 13-40 present a ten day plot of temperatures and strains for the upstream and downstream chords, respectively. The temperature induced strains have a great effect on the top chord member, as it induces a +/- 100με strain cycle during warmer days. This information will be beneficial to engineers and researchers as a more accurate rating factor is obtained.

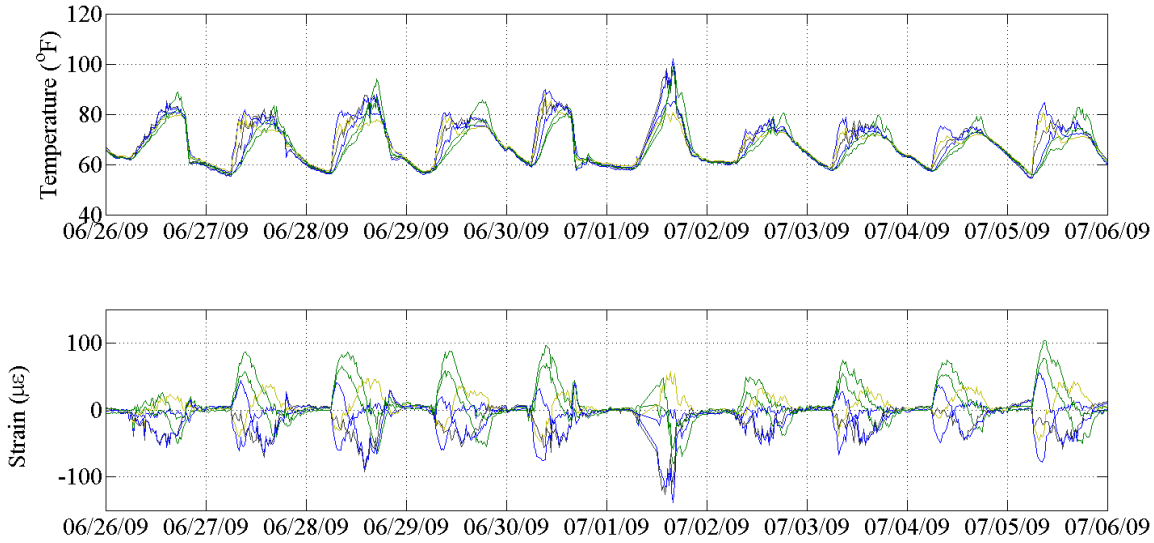

Figure 13-39: Strain and Temperature Time History over Ten Days for Upstream Chord Sensors

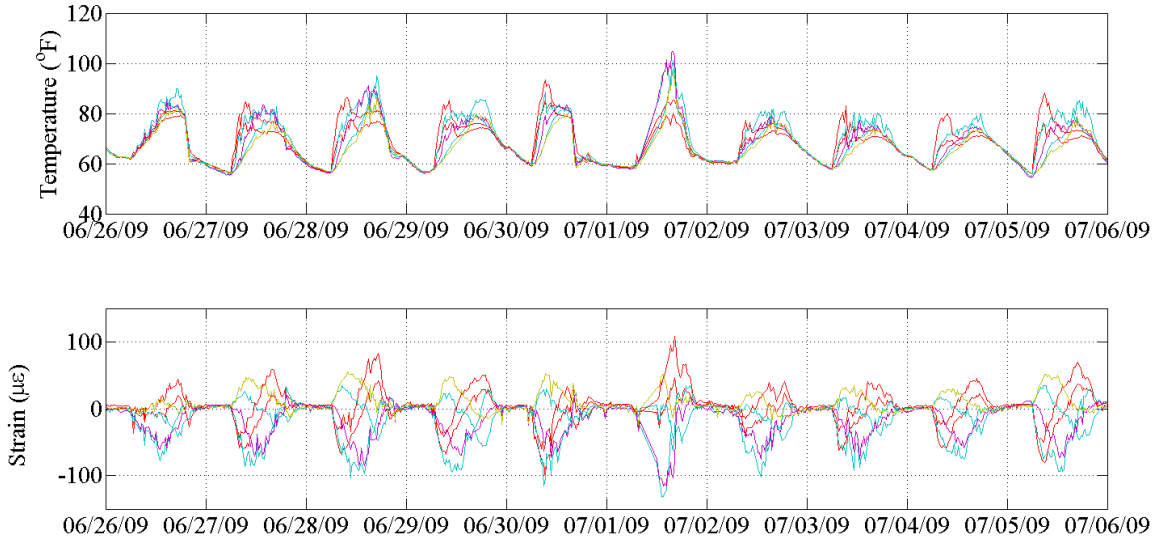

Figure 13-40: Strain and Temperature Time History over Ten Days for Downstream Chord Sensors

In addition to the information obtained about the daily and seasonal fluctuation in strains of the top chord members (an example of the temperature gradients seen on the upstream top chord member is shown in the strain profile visualizations in Figure 13-41), the monitoring system can also be used to track changes in dead load of the structure. As mentioned, it was noticed that a consistent increase in the compressive strains of the top chord members was present. The engineers of record for the bridge were contacted and an explanation was given. The lift span had a traveler system installed along its length in April and May of 2009 which consisted of two I-beam sections running along the length of the bottom chord. The total additional mass was approximately 50,000lbs, the effects of which were recorded by the strain gages.

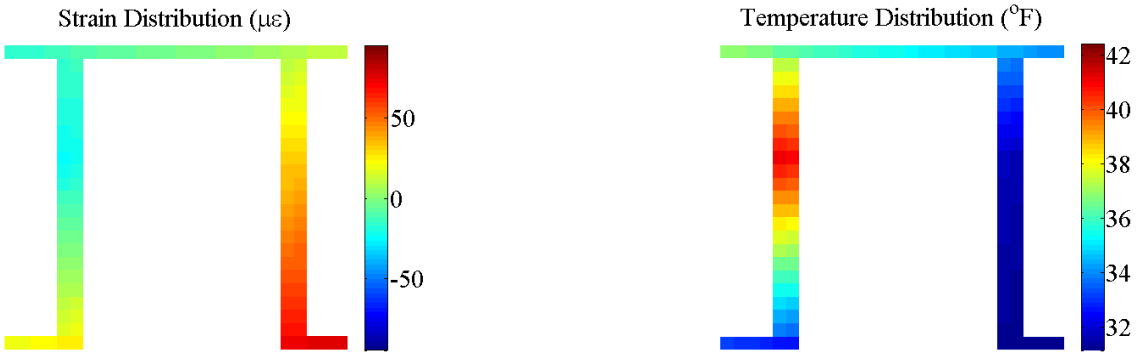

Figure 13-41: Strain and Temperature Distribution Visualization

13.2.2.6. High Speed Strain Gage Data Analysis

Upon initial review of the high speed data, it was noted that there appeared to be responses in the top chords above levels achieved by legal truck loads in the load test performed by others on September 18, 2007 in member U5-U6. Although the U9-U10 strain response cannot be directly correlated since they are not the same member, it was determined from an error-screened finite element analysis of the lift span that the top chord member U9-U10 had a legal truck strain response of approximately -30uε. These high magnitude responses seen in the data from the first few weeks of collection were very consistent over peak hour traffic, occurring most densely from 5:30AM to 4:00PM during weekdays (Figure 13-42, Figure 13-43, Figure 13-44). Note in **Figure 13-44** the signal indicating a reading of zero microstrain is the dummy sensor for the high speed strain gage group.

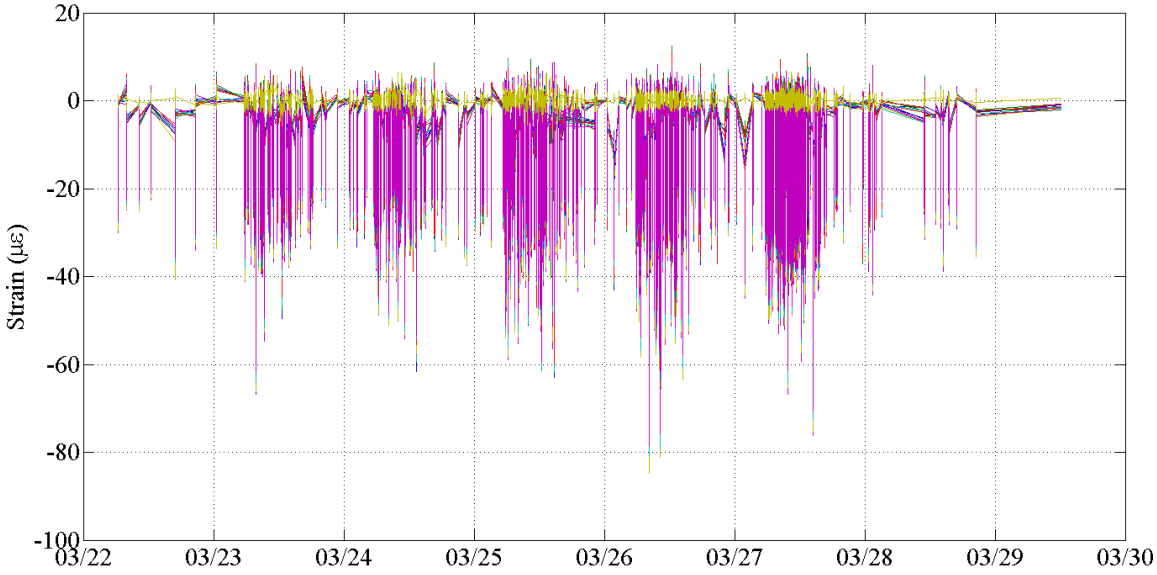

Figure 13-42: One week of high speed strain response

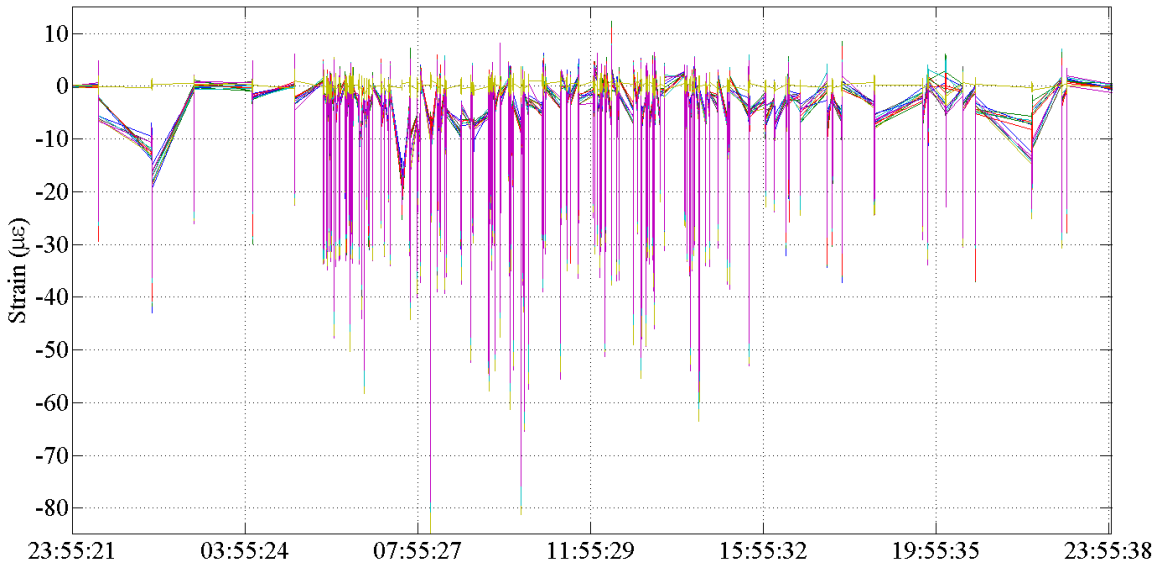

Figure 13-43: Close-up look of Strains on March 26, 2009

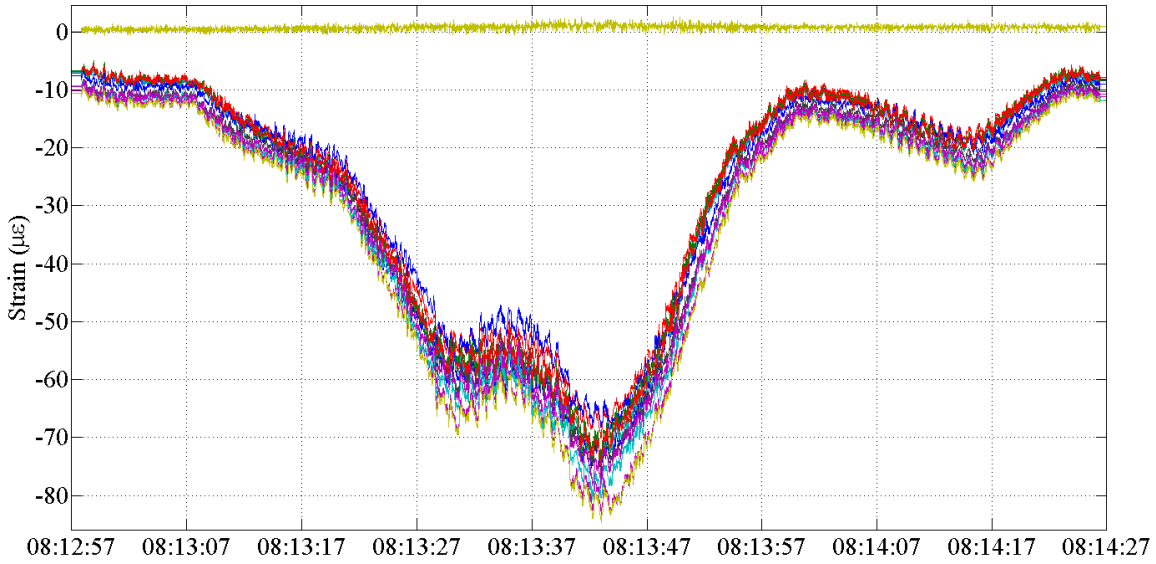

Figure 13-44: Zoomed in View of Largest Event on March 26, 2009

In an effort to understand the cause of these high magnitude responses, Drexel University research staff performed an on-site evaluation of strain response per vehicle type on March 31, 2009. This on-site evaluation consisted of monitoring the real time strain response while making note of what type of vehicle was crossing the bridge at that point in time. Photographs of the trucks correlating to the recorded strain response were also captured in an effort to understand the vehicle types, or combinations of, which produced the largest response within the top chord members. It was noted that during the course of the study, there appeared to be a large number of dump trucks crossing the bridge from PA to NJ while loaded with stone material. While it was evident that each dump truck on its own appears to be right at the legal limit or slightly higher, based on their response against the finite element model prediction, it is the combination of multiple trucks crossing the bridge at the same time which causes the high strain responses.

The following template (Figure 13-45) is an example of the largest response seen while Drexel University staff was performing this study on site. Note that this large response is caused by two loaded dump trucks following each other across the bridge. Had these trucks been more closely spaced, the response would have been even larger. Also note that in the strain plots in Figure 13-45, the ‘sawtooth’ response is due to the oscillation of the bridge as the trucks excite the low frequency vibration properties of the lift span. This determination can be made because the dynamic properties of this strain response were compared with the measured dynamic properties from the preliminary ambient vibration test and the peak frequency of vibration matched in both cases. In processing the data from the preliminary vibration survey, the fundamental frequency was calculated to be 1.29Hz, which matched exactly the dynamic analysis of the strain data.

While the source of the large responses was identified through remote monitoring and a site visit and investigation to be a combination of near legal loaded trucks, according to the SAP2000 model, it was decided to continue monitoring the strains for an indefinite period of time since the only cost associated with doing so is storing data and processing the data. Two main tasks needed to be completed at this stage: (1) load the bridge with a known load and measure the strains to determine the actual legal load strain response (calibration of the monitoring system), and (2) develop an automatic data processing algorithm to reduce data processing time.

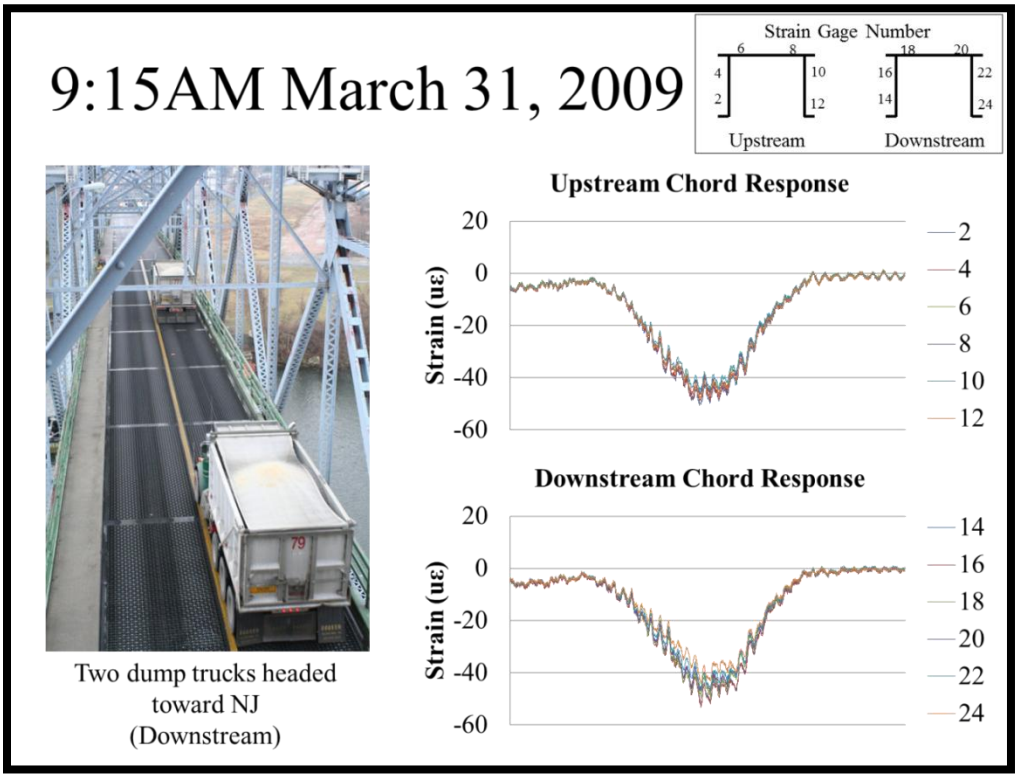

Figure 13-45: Template for Response in Each Chord Due to Truck Configuration Shown

13.2.2.7. Monitoring System Calibration

Upon reviewing the data and identifying larger than legal level truck responses occurring on a daily basis, and subsequently classifying the type and combination of various trucks which caused some of the peak responses, it is apparent that a controlled legal truck calibration was the required next course of action. The calibration allowed Drexel University research staff to produce two major components of this project: the exact legal truck strain response in member U9-U10, and an influence line of the response of chord member U9-U10 for a load anywhere on the lift span. The capability to capture these two properties of the lift span is critical to the long-term reliable interpretation of the high speed gages as discussed in subsequent sections.

In an effort to capture these measurements, the following calibration plan was carried out. The test utilized one level of truck loading crossing the bridge at two speeds: (1) a maximum speed of 5mph and (2) a speed of 35mph. The posted legal limit of the Burlington Bristol Bridge, 36 tons, was used as the target truck weight, and would be verified on site with high capacity truck scales by Drexel University research staff. In following best practices, each test was repeated for a total of six trips across the bridge; three trips in each direction. It was recommended that BCBC police officers stop traffic from crossing the lift span while the calibration truck was crossing to obtain the most accurate results. It was also recommended that the test be performed after sunset, to eliminate the effects of differential thermal radiation on the top chord member.

On July 8 2009, Drexel University Staff met with Pennoni and Burlington County Bridge Commission staff at the Pennsylvania stock yard of the Tacony-Palmyra Bridge to begin

loading the calibration truck to be used during the load test (Figure 13-46). The truck was loaded to a final total weight of 73,460 lbs (36.74 ton) using roadway millings. The individual tire weights are listed below (Table 13-4).

Figure 13-46: Loading calibration truck

Table 13-4: Tire Weight (lbs)

	Left	Right
Front Axle	7640	8160
1st Rear Axle	6480	6440
2nd Rear Axle	11740	10760
3rd Rear Axle	11260	10980

The truck was weighed by using standard digital truck scales (Figure 13-47). Upon completion of the loading, the team traveled to the Burlington Bristol Bridge and waited for approval to shut down the bridge to begin testing. The testing program consisted of the following:

1.) Three 35mph runs in the upstream lane

2.) Three 35mph runs in the downstream lane

3.) Three 5mph runs in the upstream lane

4.) Three 5mph runs in the downstream lane

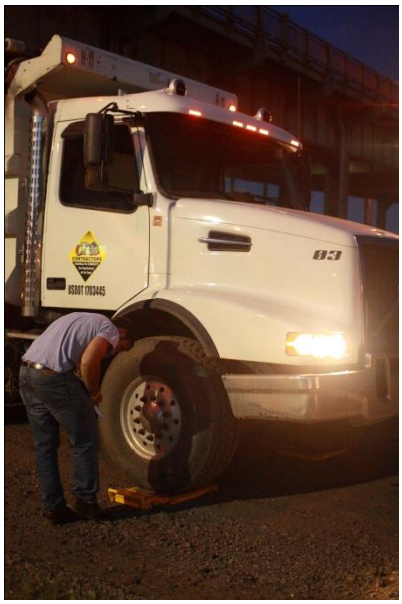

Figure 13-47: Recording Tire Weights

The high speed tests were conducted first (Figure 13-48 through Figure 13-53), and were then followed by the crawl speed tests (Figure 13-54 through Figure 13-59). During the crawl speed tests, the location of the truck was marked in the data file by having Pennoni personnel inform the operator of the data acquisition when the truck was crossing each panel point. Then a recorded variable was toggled between 0 and 1 at each panel crossing. Using this technique, influence lines can be calculated for future studies.

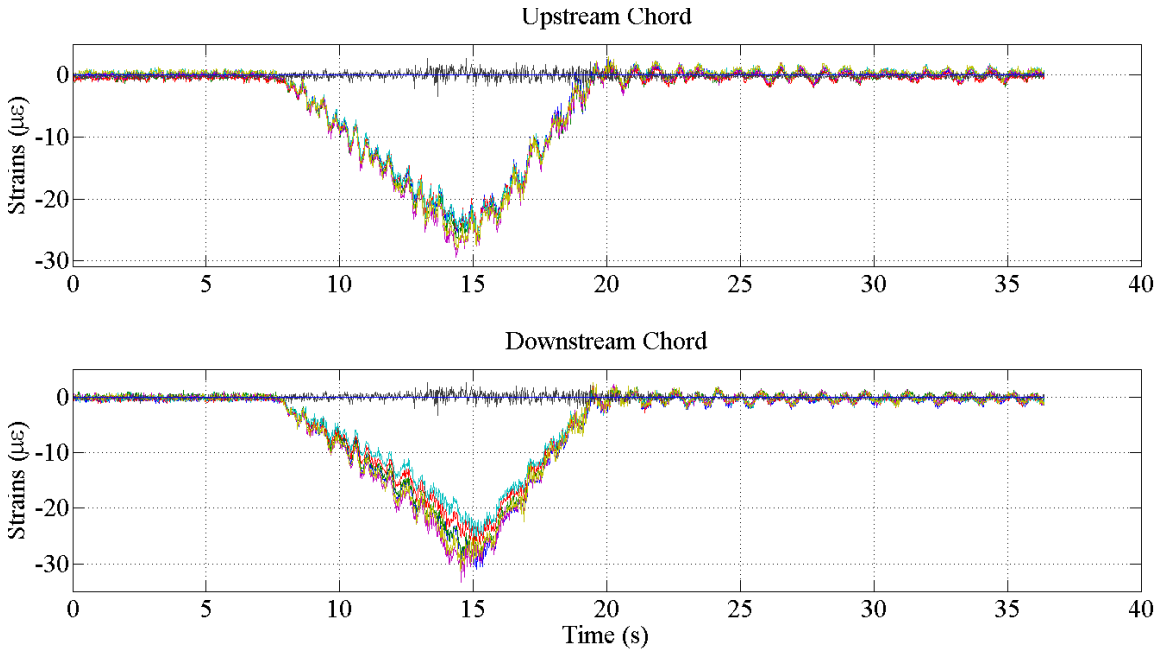

Figure 13-48: Run 1 Time History

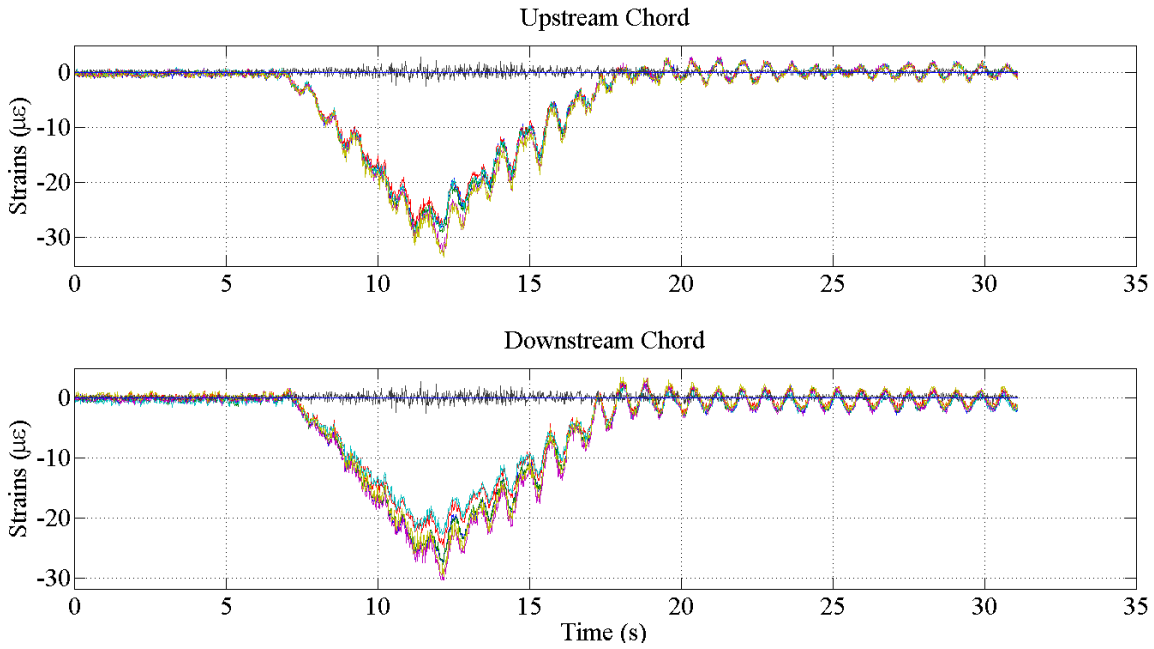

Figure 13-49: Run 2 Time History

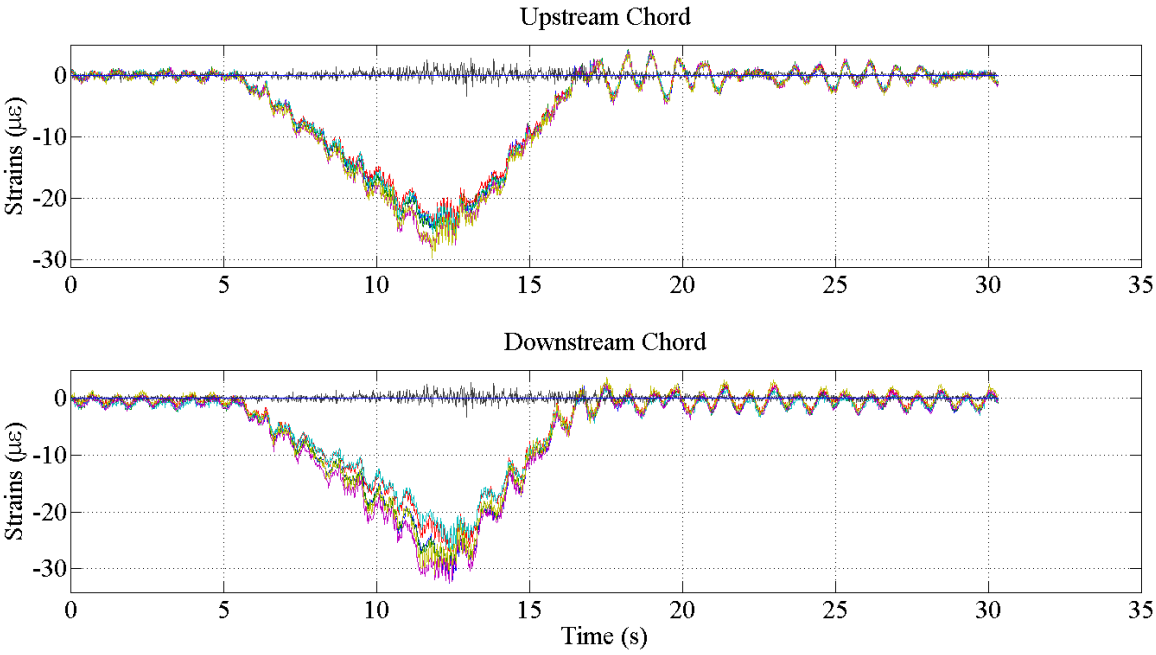

Figure 13-50: Run 3 Time History

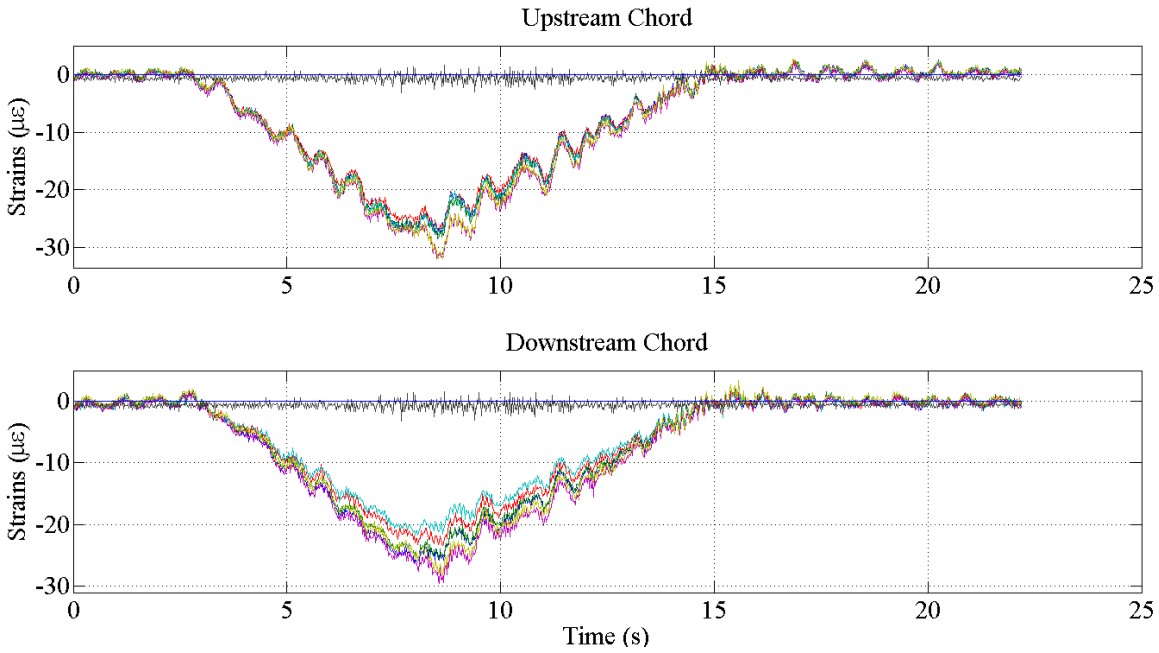

Figure 13-51: Run 4 Time History

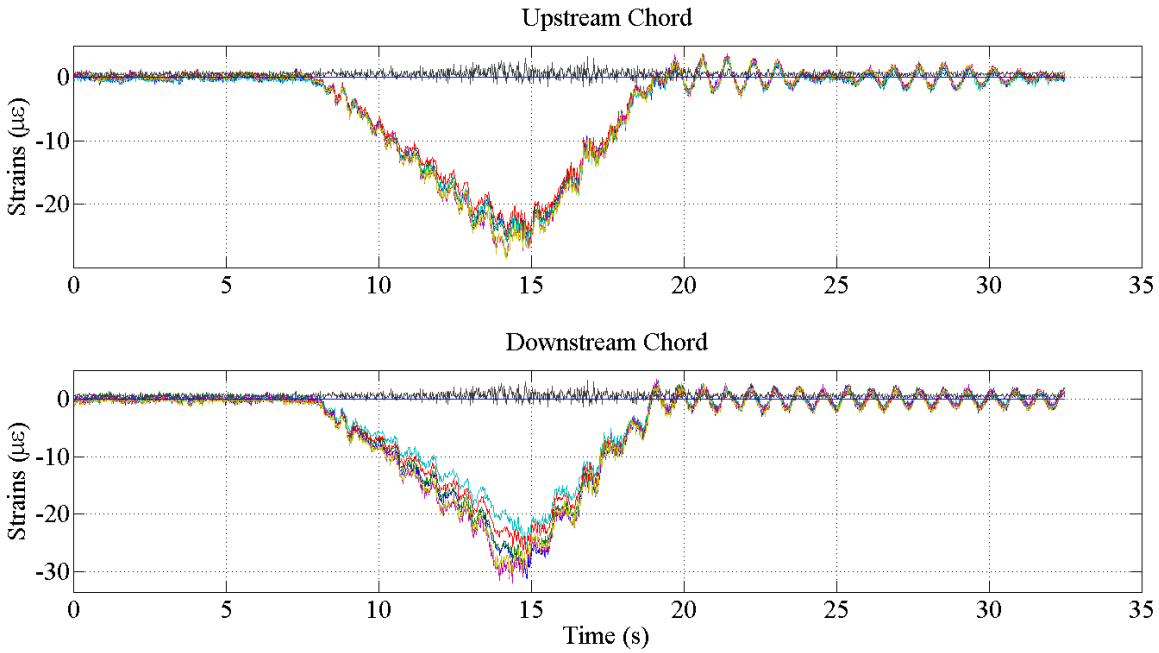

Figure 13-52: Run 5 Time History

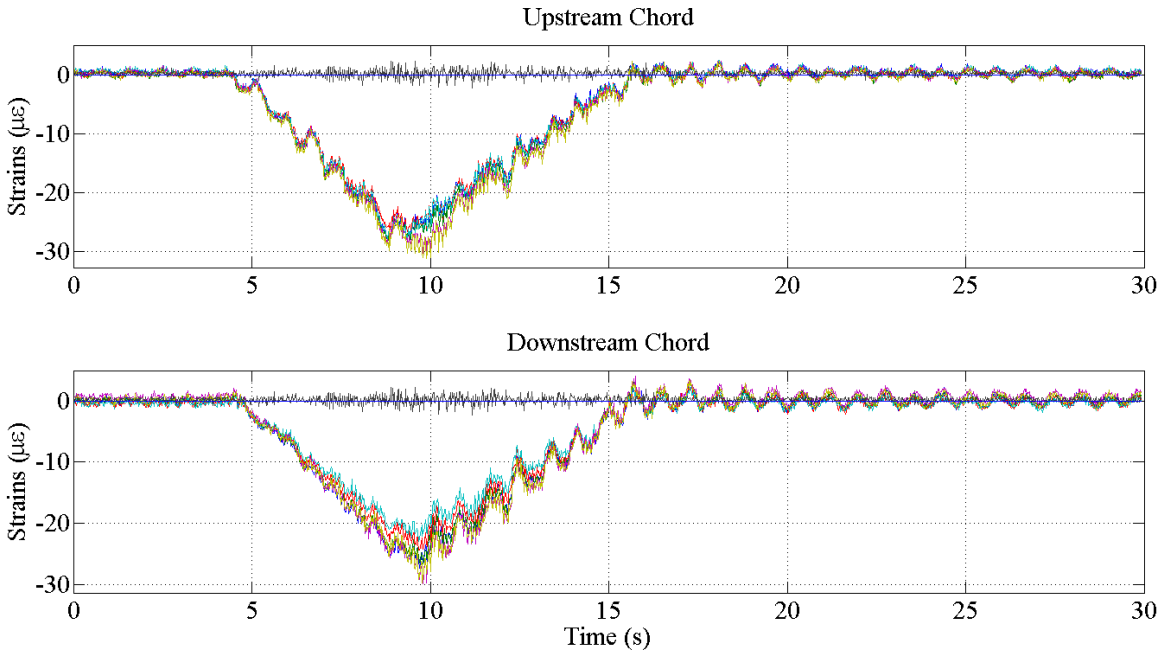

Figure 13-53: Run 6 Time History

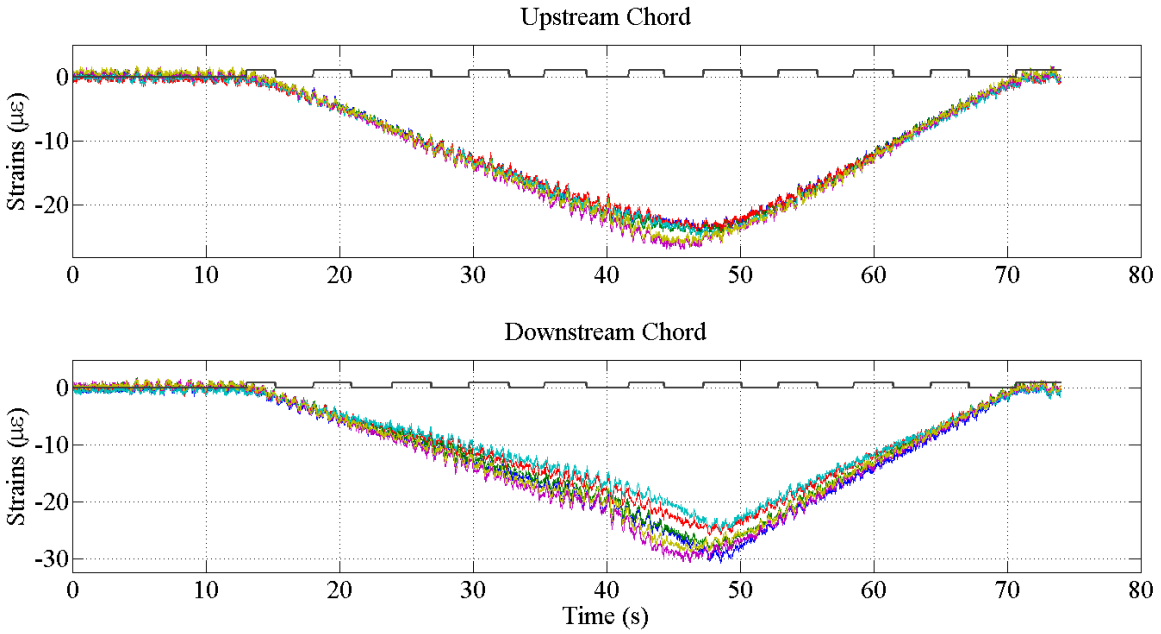

Figure 13-54: Run 7 Time History

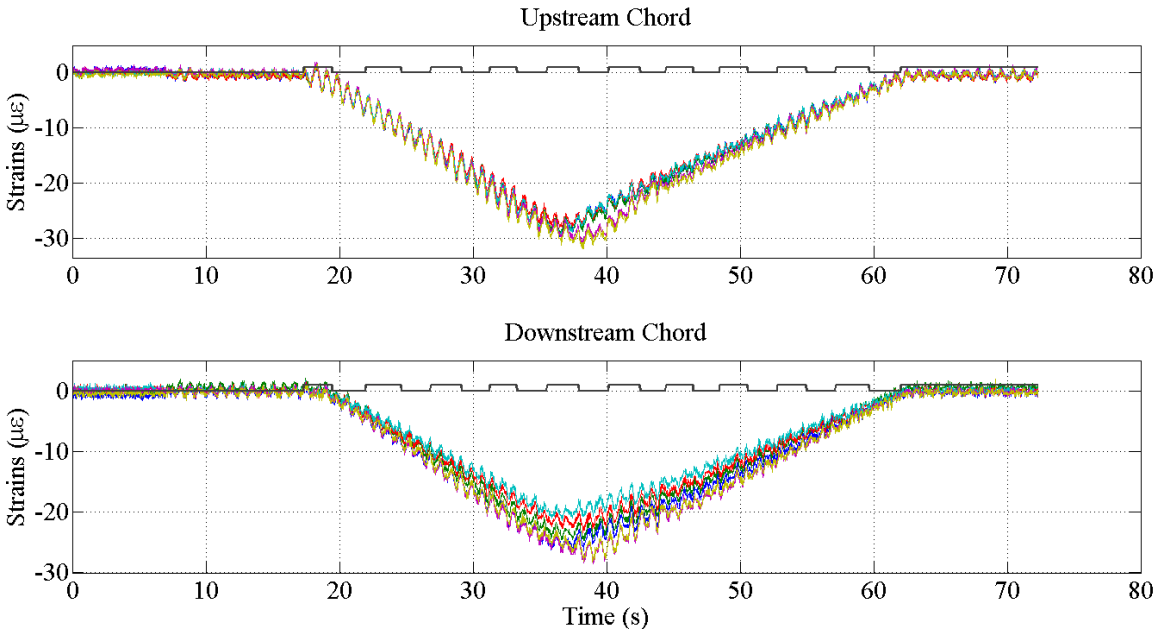

Figure 13-55: Run 8 Time History

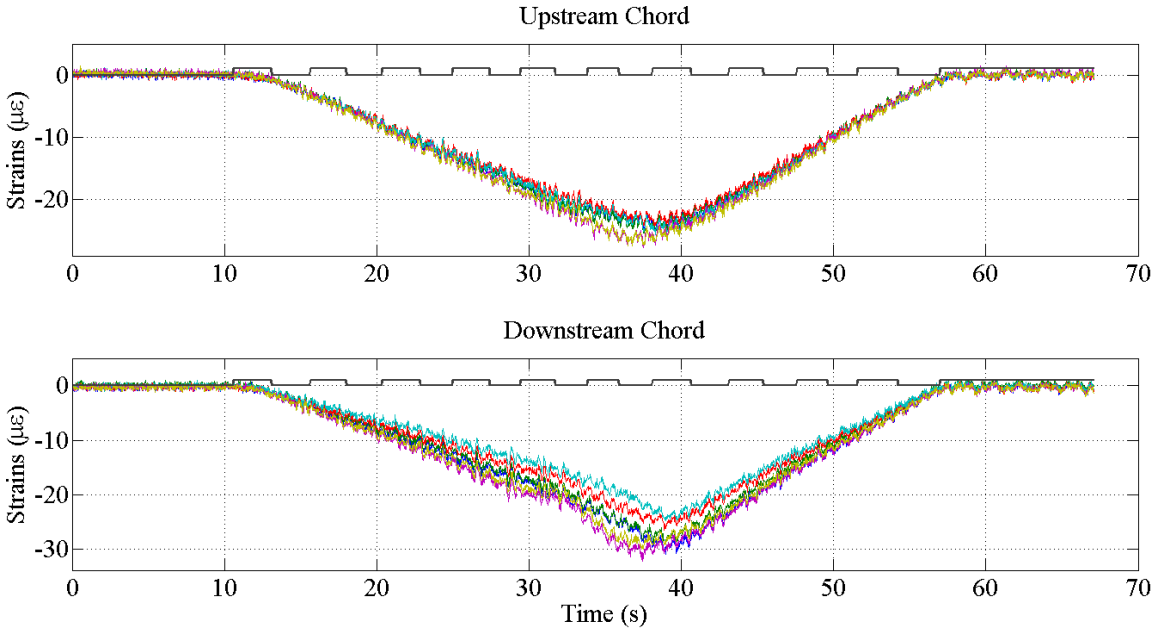

Figure 13-56: Run 9 Time History

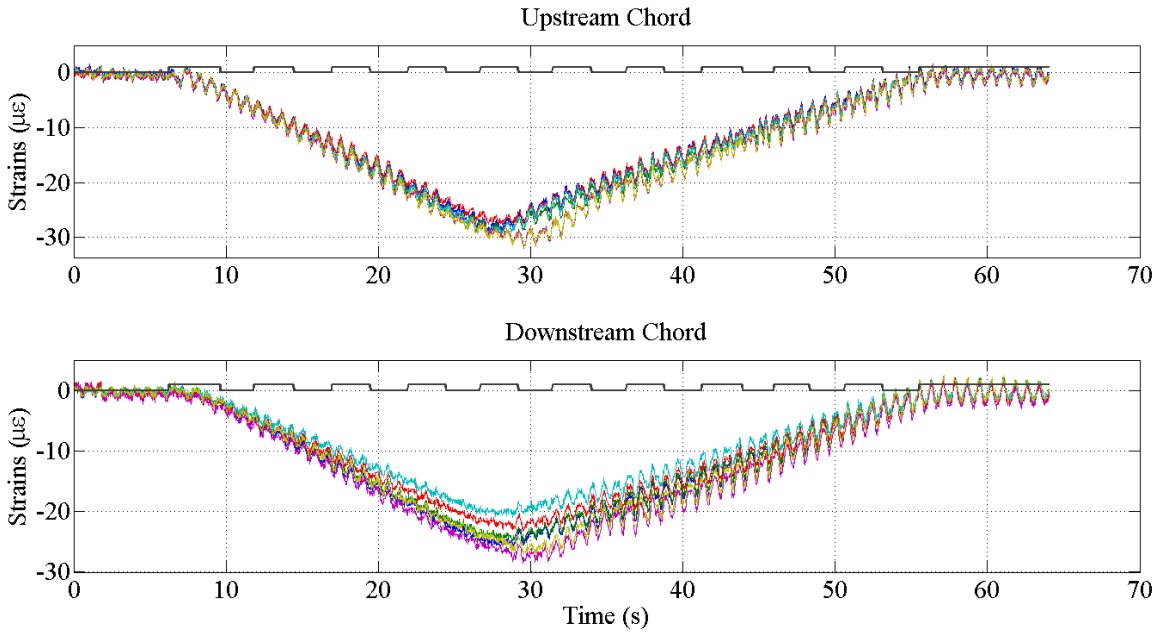

Figure 13-57: Run 10 Time History

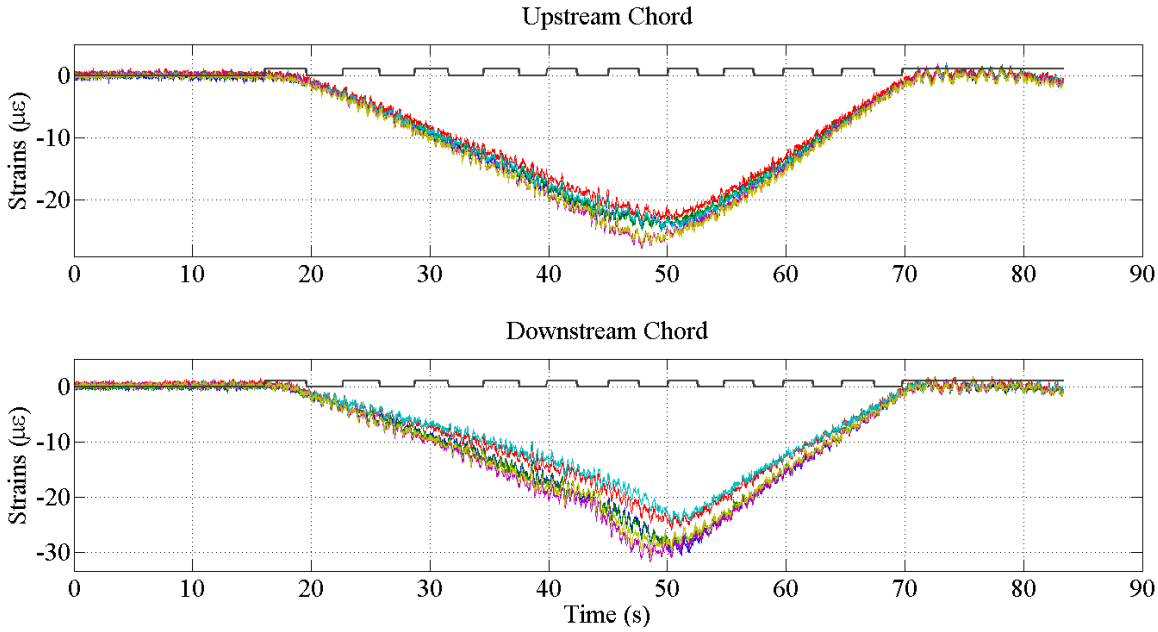

Figure 13-58: Run 11 Time History

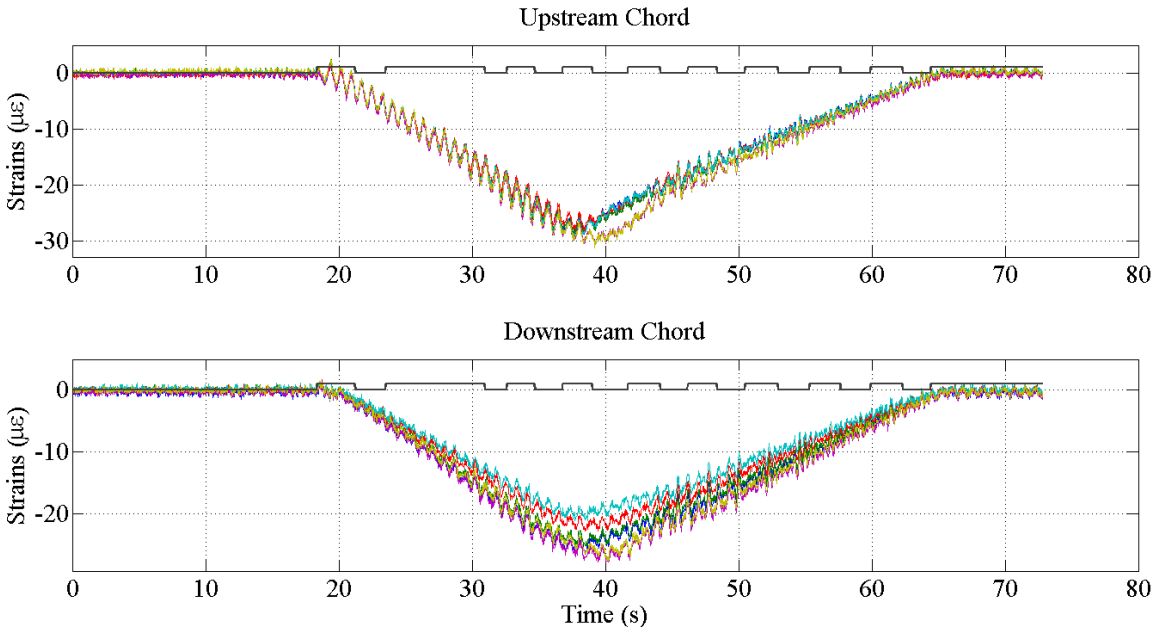

Figure 13-59: Run 12 Time History

The results of the calibration test are compared with the a priori SAP2000 model of the structure (Table 13-5), and then adjusted to calculate the response level of a legal 36 ton truck (Table 13-6). The measurements show satisfactory correlation with the model for an a priori assessment. The legal load equivalents were computed by assuming the structure was linear, and a simple linear conversion was applied to the measured truck weight.

Table 13-5: Peak Value Response (με) for all Tests Compared with SAP Model

Load Case	Truck Location	US Response	US SAP	% Δ	DS Response	DS SAP	% Δ
Run 7	DS Lane	-24.34	-23.39	4.06%	-26.97	-30.67	-12.06%
Run 8	US Lane	-28.08	-28.12	-0.14%	-23.74	-25.8	-7.98%
Run 9	DS Lane	-24.42	-23.39	4.40%	-27.15	-30.67	-11.48%
Run 10	US Lane	-28.4	-28.12	1.00%	-24.04	-25.8	-6.82%
Run 11	DS Lane	-24.25	-23.39	3.68%	-27.01	-30.67	-11.93%
Run 11	US Lane	-27.91	-28.12	-0.75%	-23.75	-25.8	-7.95%
			Average	2.04%			-9.70%

Table 13-6: Legal Load Response in Each Chord for Loading in Both Lanes

Truck Location	Chord	Legal Load Response (με)
Downstream	Downstream	-26.19
	Upstream	-22.65
Upstream	Downstream	-23.09
	Upstream	-27.23

Using the experimentally obtained values in Table 13-6, it was then possible to make real time comparisons of measurements to legal load equivalents. However, care must be taken in interpreting this type of information, as assumptions must be stated and understood regarding the legal load strain equivalents listed above: (1) the legal truck equivalent is for a specific truck type, (2) the legal truck equivalent was measured with no other traffic on the span and (3) dynamic effects of the lift span were mitigated by

having the truck traverse the bridge at crawl speed. While it at first appears that many vehicles are crossing the bridge at over-loaded levels, a detailed statistical study was carried out with the aim of conceptualizing all of the recorded live load events in a manner which could be used to identify the types of trucks crossing the bridge and whether they were overloaded or not.

13.2.2.8. Development of Automated Data Processing Algorithm

In order to process the vast amount of data collected by the top chord strain monitoring system, a thorough automated data processing algorithm was required to mine the data for triggered events and extract pertinent information such as maximum strain during event, maximum mean strain (ie, strain computed from moving average) and impact factor of each event. The algorithm was embedded within a MATLAB Graphical User Interface (GUI) and provided four main computation steps and then various visualization tools. A period of one year's worth of data was processed using the algorithm so that statistical analyses could be performed. However, the statistical analysis of the mined and extracted data will be discussed in the Section 13.2.2.9.

13.2.2.8.1. Clean Raw Strain Data

Before the data could be analyzed in an automated manner, the responses needed to be filtered to remove both the effects of measurement noise and structural vibration. This type of filtering thus allowed for the removal of dynamic effects and provided a mean strain equivalent for each event. In other words, the filtering provided a static response

equivalent of the passing vehicle. To properly filter the data, a low-pass Butterworth filter was utilized to remove any signals with a frequency above 0.5Hz. This value was selected since the fundamental vertical frequency of the lift span was established with the preliminary vibration test at 1.29 Hz. The results of the filtering are shown in Figure 13-60. By filtering the data in this manner, it is possible to use built in MATLAB functions to identify the peak strain over each recorded event.

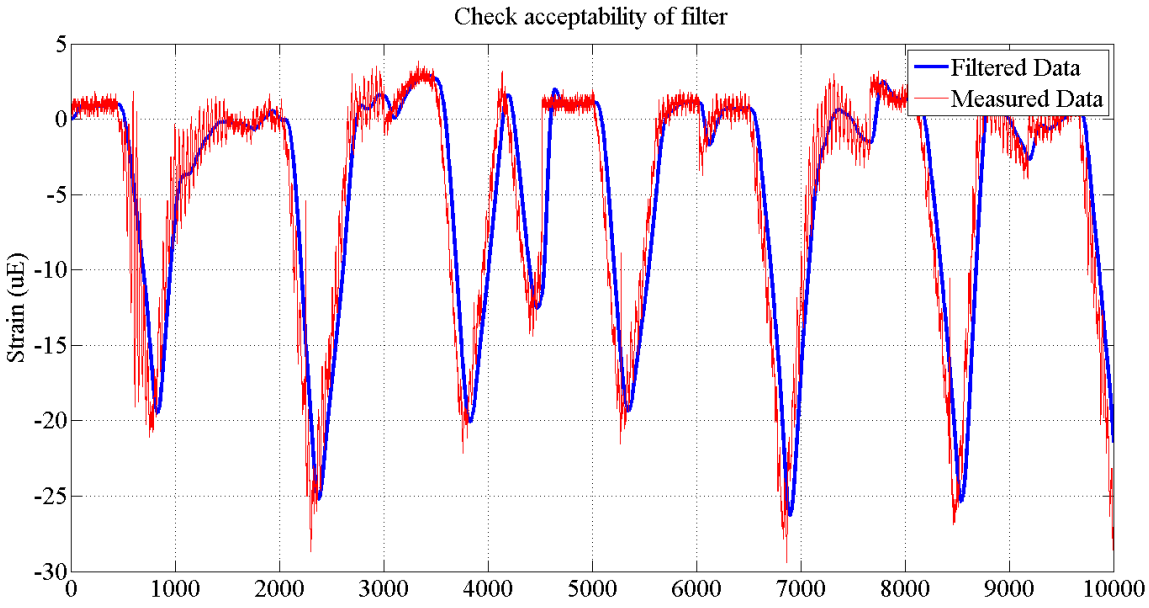

Figure 13-60: Visualization of Filtered Time History Data

13.2.2.8.2. Identify the Start and End Point in Time Histories

The raw strain data files did not contain any indication of separation between the recorded events. However, since each record contained a time stamp, it was possible to use the timestamp information to determine where a specific event began and ended. A code routine was developed which searched the time histories for a discontinuity which differed than the 0.02 second time difference related to the sampling rate. Using this methodology, it was possible to identify the bounds of each recorded event, thus allowing for analysis of the data between the identified bounds for error screening purposes and data extraction purposes.

13.2.2.8.3. Quality Analysis of Recorded Events

Due to spurious errors within the datalogger, electromagnetic interference, or other sources of noise, non-events are actually recorded and identified as triggered events by the system. The success of an automated method hinged on whether it would be able to identify these poor data quality events and eliminate them from consideration and further analysis. In order to carry out such a task, statistical properties of the recorded event were evaluated. The mean and standard deviation for each recorded event was computed automatically by the algorithm and evaluated for whether the event is good or bad, based on the dispersion of the event. Dispersion is used because a non-event would consist solely of noise oscillating around a zero strain reading. However, a true event has peaks of at least fifteen microstrain, ensuring that both the mean and standard deviation will be non-zero. By using these statistical parameters as accept / reject criteria for each recorded event, only the quality recorded events were analyzed further. A visualization of the GUI

output showing good versus bad recorded events is shown in Figure 13-61. Note that in the upper left hand corner, it is not necessarily a “bad” event which was recorded, however it is one that is not characteristic of a typical truck event, as seen in the bottom two plots. Instead this event was most likely due to traffic congestion on the bridge following an opening. Considering that the time of the event was at 8AM, this is certainly feasible given that is a typical rush hour time. Even though this was not a “bad” event, it was discarded from consideration in studying the heavy vehicle loading.

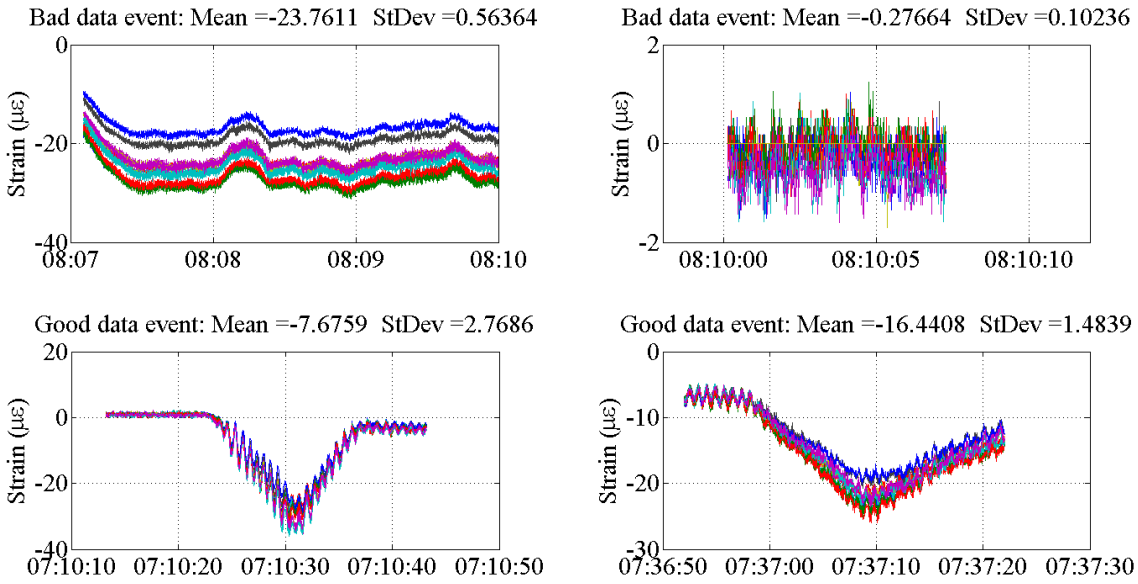

Figure 13-61: GUI Output for Data Quality Analysis

13.2.2.8.4. Extraction of Key Information from Each Recorded Event

Once the recorded events were identified and the responses cleaned, pertinent information could be extracted from the processed measurements. The maximum overall strain was identified from each data event by finding the minimum (compression is measured as negative strain) strain recording between the two times identified for each event. The static equivalent was identified by finding the minimum filtered strain, or mean strain, between each time event. Finally, the impact factor was computed for each event by dividing the raw strain measurement by the static strain equivalent. Overall, a set of 19,912 recorded, processed and mined sets of events were produced from one year's worth of data of strain measurements on the BBB for the year of January 2009 to January 2010. This extracted data was then processed with statistical analyses.

13.2.2.9. Statistical Analysis of the Triggered Live Load Strain Recordings

The goals of the statistical study were to establish: (1) an appropriate statistical model for the magnitude of heavy trucks the Burlington Bristol Bridge sees, (2) what times (time of day, day of week, month) see the most heavy truck traffic and (3) what is the correlation (if any) of impact factor to truck magnitude. To accomplish these goals, statistical analyses were utilized. A brief description of each method with standard procedures for each will be discussed in this section. The methods used to address the goals outlined above include: (1) Maximum Likelihood Estimation (MLE), (2) Akaike Information Criterion (AIC) & Bayesian Information Criterion (BIC), (3) Monte Carlo (MC) simulation and (4) SPSS statistical software for visualization and exploratory analysis (SPSS). Each will be explained and discussed.

The MLE method of fitting statistical models to data uses optimization algorithms to maximize the probability, or likelihood, of obtaining the observed data. The parameter values of interest, for example, mean and standard deviation of a normal distribution, are allowed to vary in the optimization scheme. It is also considered good practice to use multiple starting points of assumed probability models to ensure that the optimization is not becoming trapped in local maxima. This tends to happen quite often if the likelihood surface is complex and the optimization scheme is local, meaning that it is derivative based and will find only the nearest peak. For this study, relatively simple models are being used so a local optimization algorithm will be sufficient, however multiple starting points will still be used to ensure that the appropriate parameter estimates are obtained.

The objective function maximized in the MLE process consists of the product of probabilities associated with each data and their likelihood of coming from the proposal distribution. Given a vector X of data, a probability density function, $f(X|\theta)$, is assumed and used to compute the probability of each value in X. To obtain the overall likelihood of the model, the probability of each model is multiplied together, utilizing the assumption that each data is independent. Since this process typically yields very small numbers, the product of which giving a very small number, the data is commonly log transformed to take advantage of the property of log functions where the product of the log of two numbers is equivalent to the sum of log of the two numbers. The log transforms then allows for the summation of all log likelihoods, which lends itself much better to the optimization process.

Since there are very few datasets where one statistical model can be fit exactly, it is common that multiple models are explored to see which one tells the best story. This

obviously means that a standardized way of evaluating different models for their ability to fit the data, given how many observations and number of parameters are being used, is needed to refine the results from the MLE and arrive at a single model or smaller subset of models which are more appropriate. Likelihood alone cannot be used, since sometimes different numbers of parameters are used, and a method of "leveling the playing field" is needed. There are two accepted methods of assessing model fit, and these include the Akaike and Bayesian Information Criterion. The AIC method (Eq. 13-1) computes a criterion, where the smaller value is better, that is a function of the negative of the likelihood function and the number of parameters (N_p) used. This forces a model with added parameters to substantially increase the likelihood to compensate for the added expense of an additional parameter. The BIC method does this and more. Once again, the negative of the likelihood function is taken (Eq. 13-2), however this time the number of observations is included in addition to the number of parameters. The BIC function forces a model with large data sets to significantly improve the likelihood even more for each additional parameter.

$$AIC = -2\ln(L) + 2N_p \qquad \textbf{Eq. 13-1}$$

$$BIC = -2\ln(L) + \ln N_{obs} N_p \qquad \textbf{Eq. 13-2}$$

To help investigate the hypothesized correlation between impact factor and truck size, Monte Carlo (MC) simulations will be used to replicate the dataset with different properties than the actual collected one. For example, the MC simulation will be used to simulate the effects of impact factor when different levels of noise filtering are used (since filtering affects lower magnitude responses more in the computation of impact factors). This way, various ways of processing the data can be simulated before the time is spent on actually transforming the data countless numbers of times (one week to process all of the data once). MC simulations are founded on the generation of random numbers, and was conceived in the Los Alamos National Laboratory (Anderson 1986; Metropolis 1987) during research on nuclear weaponry to compute the distance neutrons travelled into various substances. Monte Carlo approaches tend to follow a similar method: (1) define the inputs, and classify what distribution they may come from, (2) sample these inputs using a random number generator, (3) carry out a deterministic computation and (4) summarize the results. For example, MC methods have been used to approximate pi, compute integrals of complex surfaces and simulate a coin flipping experiment. The details of the MC simulation used in this project will be explained in the results.

The statistical software SPSS was used for exploratory analysis, data presentation and correlation studies to be conducted within the BBB strain data. The software allows for easy manipulation of the data to present number of trucks per hour, day, week, etc. so that correlations can be made as to when the largest of the trucks are crossing the BBB. Also, correlation studies were carried out between strain response (as a direct indication of truck weight) and respective impact factors to see if the results in other studies (Kim and

Nowak 1997) can be replicated. The findings of Kim and Nowak 1997 suggest that no impact factors for short span girder structures are above those recommended by AASHTO in design and that higher impact factors are correlated with lower weight trucks. These conclusions were compared against the data from BBB.

The results presented in this section will be split into three main categories to address the three goals outlined above: (1) Data Exploration, (2) MLE – Statistical Model Fitting and (3) Correlation of Impact Factor and Truck Weight.

13.2.2.9.1. Data Exploration

In order to preliminarily investigate and visualize the data, Q-Q plots of the static strain of each truck were generated for a normal distribution (Figure 13-62) and a log-normal distribution (Figure 13-63). Q-Q plots consist of plotting the quartiles of the observed dataset versus the quartiles of a known probability distribution, thus indicating model fit.

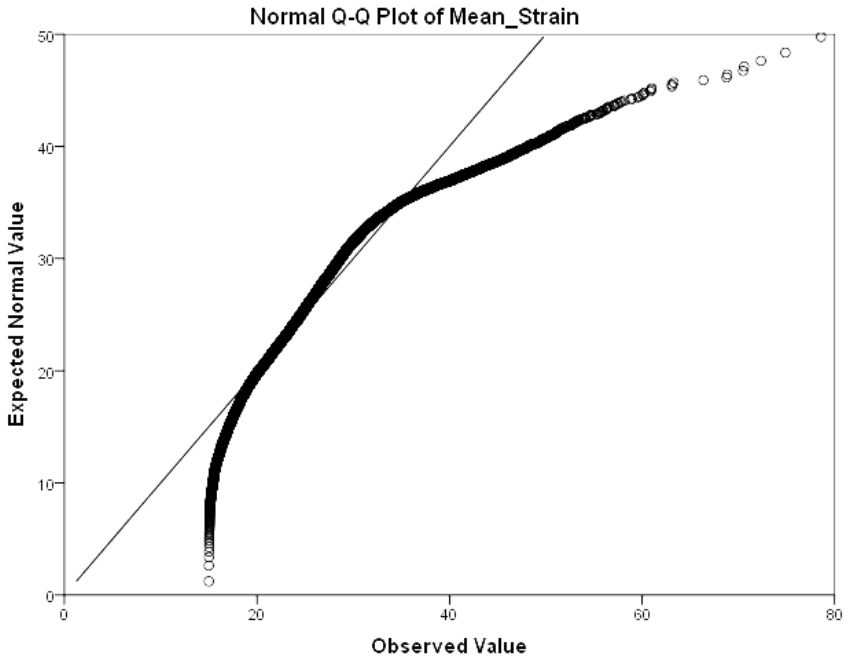

Figure 13-62: Q-Q Plot of Averaged Strain Events

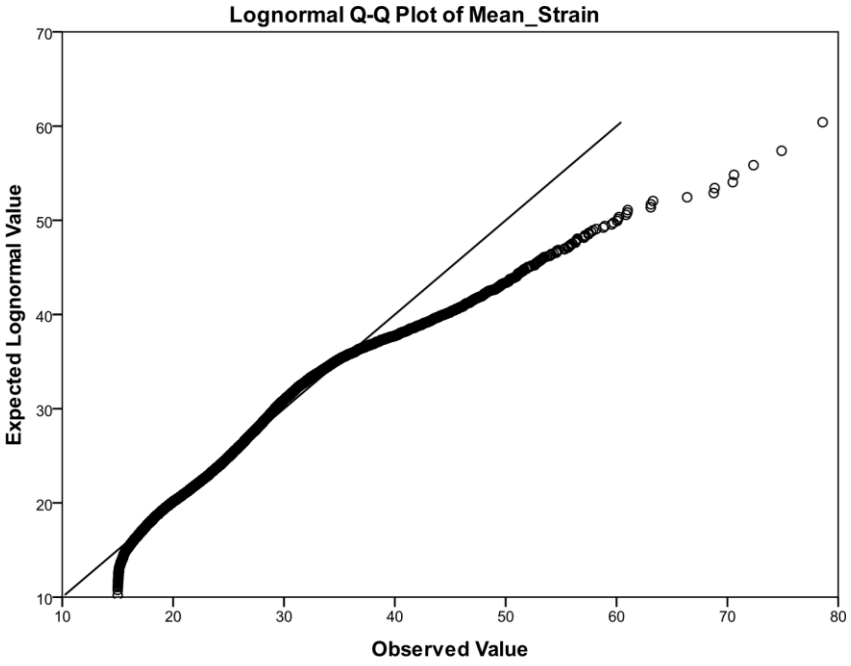

Figure 13-63: Q-Q Plot with Normal Distribution (a) and Lognormal Distribution (b)

From these Q-Q plots, it is apparent that the data is very roughly normal, however when looking at the lognormal test distribution, the Q-Q plots looks much more reasonable, but yet still leaving room for improvement. This formed the basis of the construction of a more refined statistical model, but the cause of the heavy tail still needed to be investigated with further exploration. The next exploratory analyses included box plots of static (or mean) strain events per time period (month, day, hour). These plots will give insight into why (and more importantly, when) the heavy tails are occurring, and if they can be attributed to anything in particular.

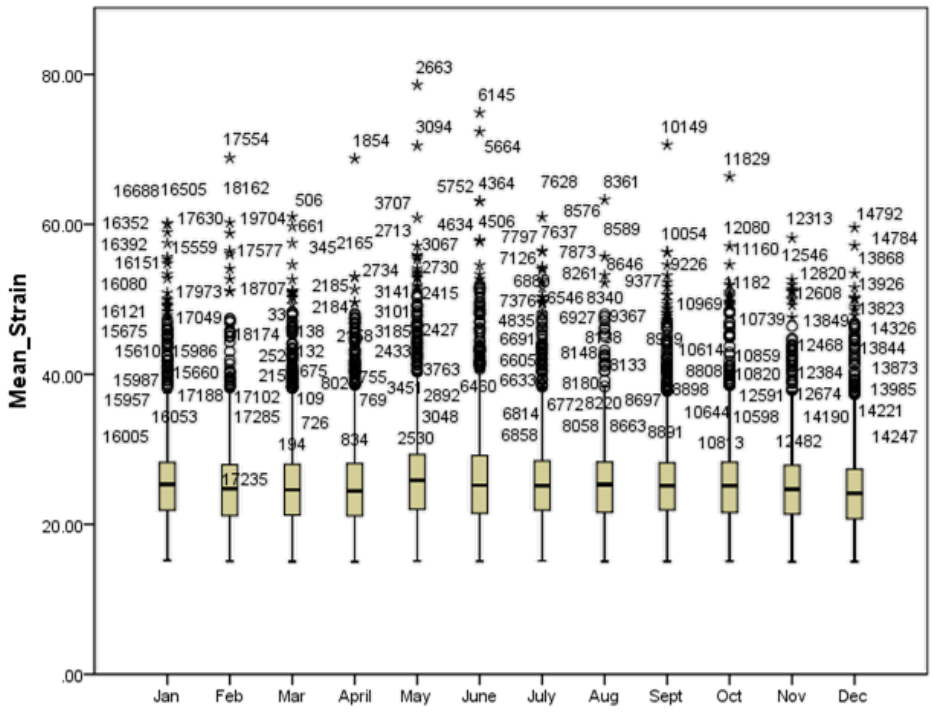

Figure 13-64: Box Plot Analysis of Static Strain Events for Each Month

The box plot analyses (Figure 13-64 through Figure 13-66) provide valuable insight into the outliers identified in the Q-Q plot analysis. It appeared that the heavy tails were attributed to a consistent set of outliers in Figure 13-64, and that the underlying distribution is fairly consistent throughout each month. The quartiles and mean do not change much over each month and the overall magnitude of the outliers is similar. This figure almost seems to suggest that two distributions are present within the data: one distribution represented by the mean identified in the box plots and another distribution to represent the group of outliers. However, at this point the outliers could not be associated with any event in particular, so further exploratory analysis was required.

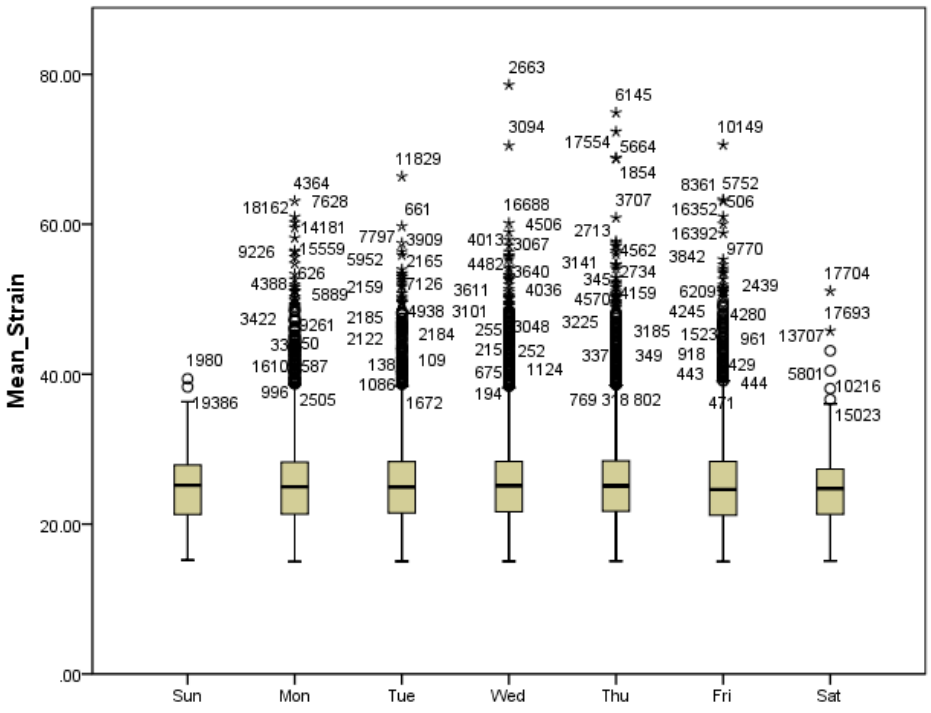

Figure 13-65: Box plot analysis of static strain events for each weekday

The next analysis carried out was a box plot representation of static strain events over each weekday (Figure 13-65). This will now concentrate the focus of the time scale in this study, since the month by month analysis was inconclusive. Figure 13-65 shows a box plot analysis that is far more insightful than the monthly analysis. In this case, it appears that the outlier events can be associated with weekdays and not weekend days. Having spent countless hours on the BBB installing various SHM systems, this plot now provides an insight into what these outlying events can be associated with: dump trucks carrying stone over the bridge from a quarry in PA to NJ (Figure 13-67). However, further analysis could be carried out to identify peak times when these trucks are crossing, to once again be compared with personal experience witnessing these heavy trucks crossing the structure.

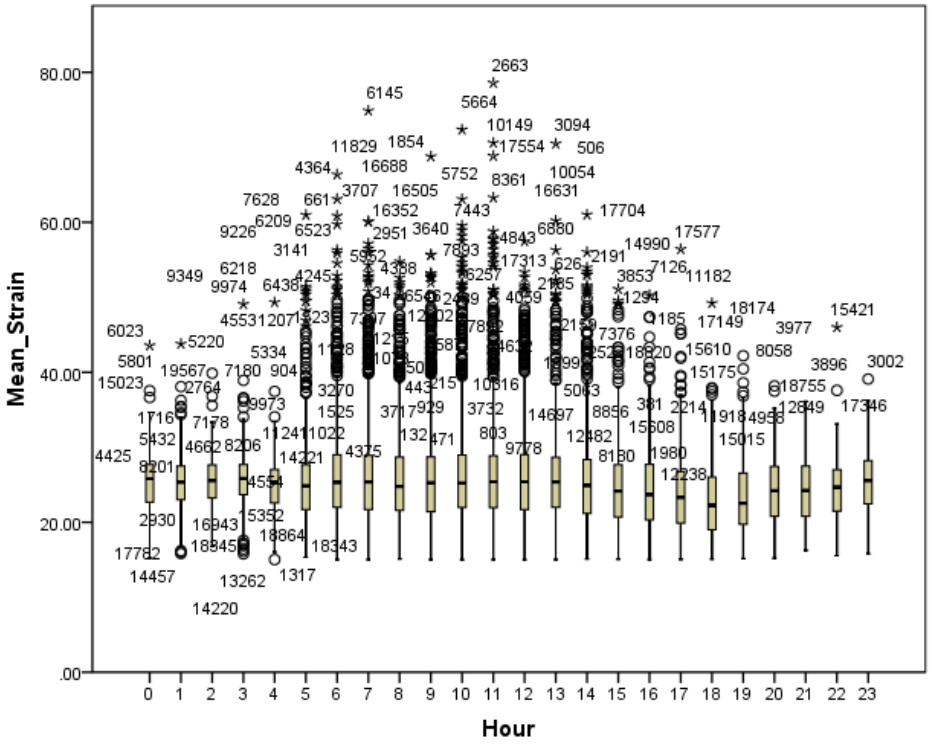

Figure 13-66: Box plot analysis of static strain events for each hour of the day

The final box plot analysis carried out was an hour-by-hour analysis of each day of the data set. This analysis shows that the majority of the outlying events occur between 5am and 2pm, once again corroborated by personal experience on the structure as to when heavy trucks (Figure 13-67) are crossing the span. This study and preliminary conclusion concluded the exploratory analysis phase of this project, and a more detailed estimation of the underlying distribution(s) of the strain events was necessary.

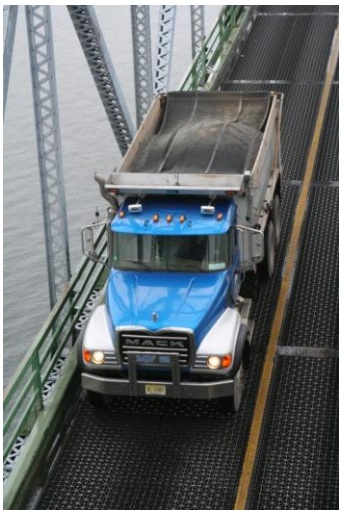

Figure 13-67: Dump trucks causing outlying events in box plot analyses

13.2.2.9.2. Statistical Model Fitting

Since the exploratory analysis resulted in a hypothesis that there appeared to be two underlying distributions in the strain event data, a set of models had to be constructed and

compared against each other to determine which one best fit the data, using both AIC and BIC methods outlined above, but more so relying on the BIC method since it has been shown to be a superior means of comparison than the AIC. Six statistical models were evaluated for their ability to represent the measured data with respective objective functions (Table 13-7).

Table 13-7: Statistical Models Evaluated for BBB Truck Events

	Number of Parameters	Dist. 1	Dist. 2	Objective Function
Model 1	2	Normal	-	$P(x) = N(x, \mu, \sigma)$
Model 2	2	Log Normal	-	
Model 3	5	Normal	Normal	$P(x) = f * N(x, \mu_1, \sigma_1) + (1 - f) * N(x, \mu_2, \sigma_2)$
Model 4	5	Normal	Log Normal	
Model 5	5	Log Normal	Normal	
Model 6	5	Log Normal	Log Normal	

During the MLE process, it was noted that both Models 4 and 5 simply converged to Model 2 (the lognormal model) with a probability of 0 and 1 for the normal and lognormal, respectively. This was interesting, but made sense when viewing the likelihoods for each individual model. The likelihood of the log normal model was much

higher than the normal model, so the MLE simply penalized the normal model with a probability of 0 and used only the lognormal model.

Using the MLE method outlined in Section 2, the following parameter values and associated AIC and BIC values are presented for each of the four distinct models (Table 13-8).

Table 13-8: Statistical Model Evaluation for Best Fit

	AIC	BIC	μ1	σ1	μ2	σ2	f1
Model 1	128294.65	128304.45	25.50	6.06	-	-	-
Model 2	-3439.68	-3423.88	24.85	1.25	-	-	-
Model 3	123943.03	123988.53	24.45	4.45	37.05	8.92	0.92
Model 6	-4211.71	-4166.21	24.45	1.22	45.4	1.15	0.97

The model with the best fit, according to both AIC and BIC (even though BIC would have been preferred if there was a discrepancy) is Model 6, the joint distribution of two lognormal distributions. This model is plotted against the observed data in Figure 13-68.

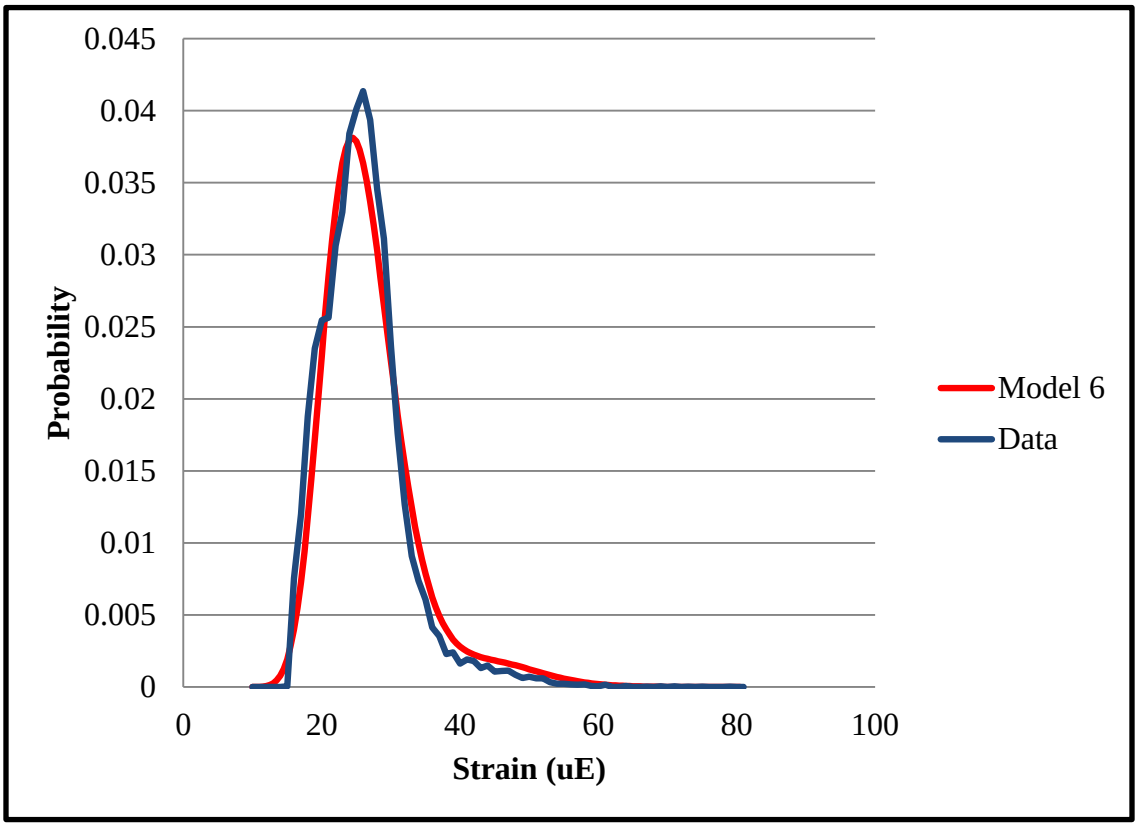

Figure 13-68: Model 6 compared with experimental data

13.2.2.9.2. Monte Carlo Simulation and Correlation Study

Finally, the impact factor study was carried out to investigate whether there was a correlation between impact factor and static strain response for each event. Initially, the impact factor and static response were scatter plotted to visually determine whether any

apparent trends might exist (Figure 13-69) and it appeared that there is a significant trend that as the truck magnitude increases, the impact factor decreases (which agrees with (Kim and Nowak 1997)). However, it was discovered that the sensor noise was not removed from the dynamic strains (where impact factor is defined as the ratio of dynamic strain to static strain), which could greatly affect lower magnitude strain response. Before all of the data was re-processed, a Monte Carlo (MC) simulation was carried out to see if this phenomenon would indeed have an effect, and if it would produce a trend similar to that seen in Figure 13-69.

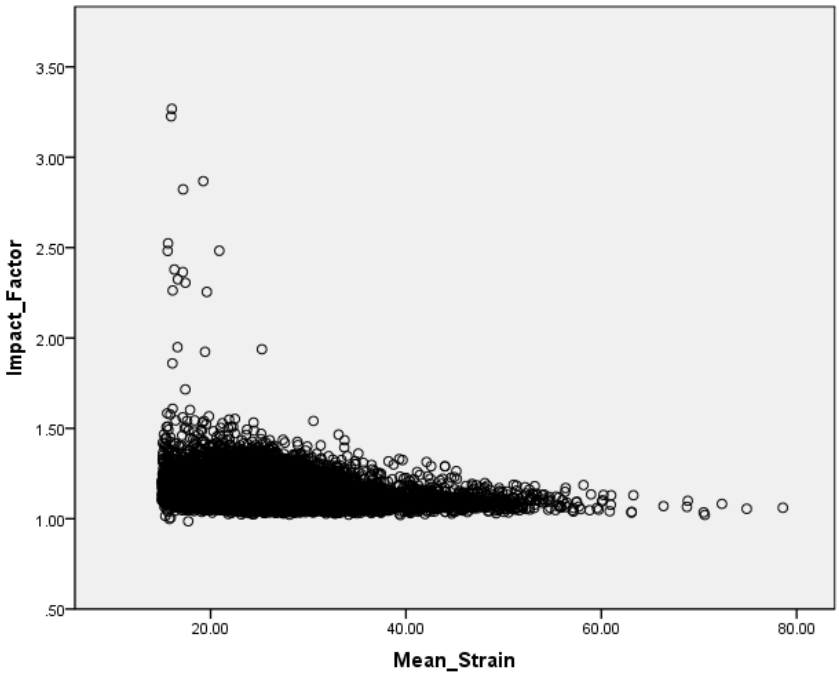

Figure 13-69: Scatter Plot of Static Strain vs Impact Factor

To carry out the MC simulation, a population of truck events was generated by randomly sampling Model 6 19,912 times to obtain the distribution seen in Figure 13-70. Then each event was multiplied by a forced impact factor of 1.2 and had random noise added to it, once again generated by MC sampling of a distribution close to that of sensor noise (normal distribution, mean = 0 and standard deviation = 0.5 uE).

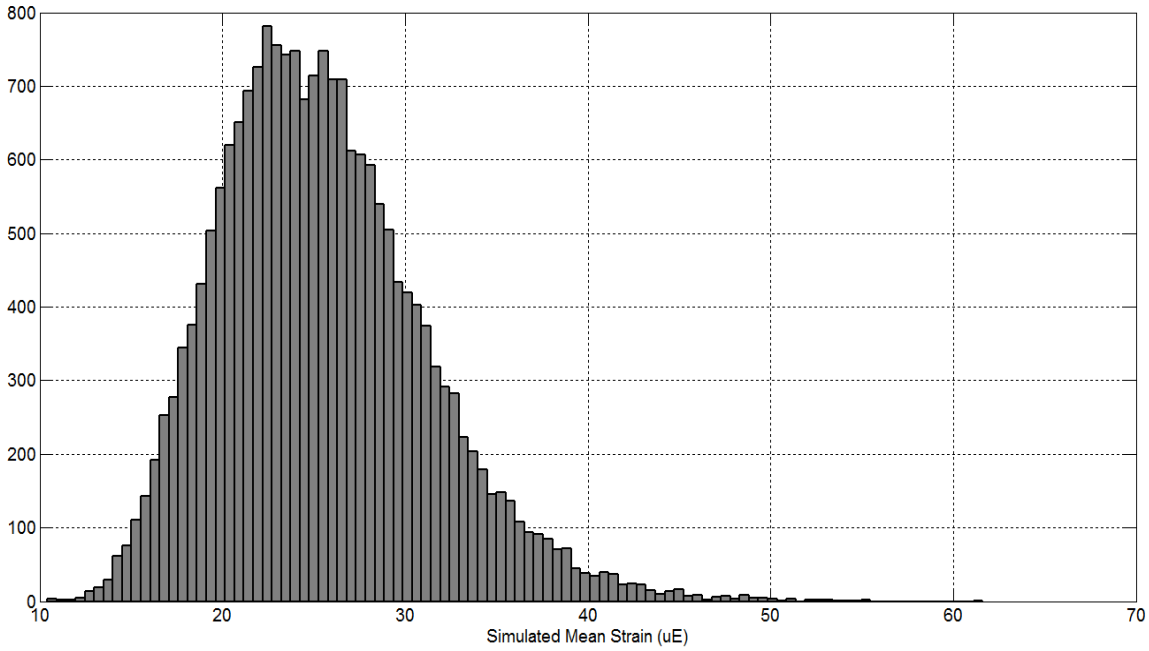

Figure 13-70: MC simulated population of truck events

If the sensor noise were to not have an effect, the impact factors should just all be 1.2 since that was the applied factor. However, as seen in Figure 13-71, this was not the case. On the left of the figure, the impact factors for events with no noise added is plotted and is simply just 1.2. On the right of the figure, the impact factors for all events with noise

added is plotted against the mean strain of the event and a trend similar to that of the experimental data is seen. This resulted in the need to reprocess the data and remove measurement noise.

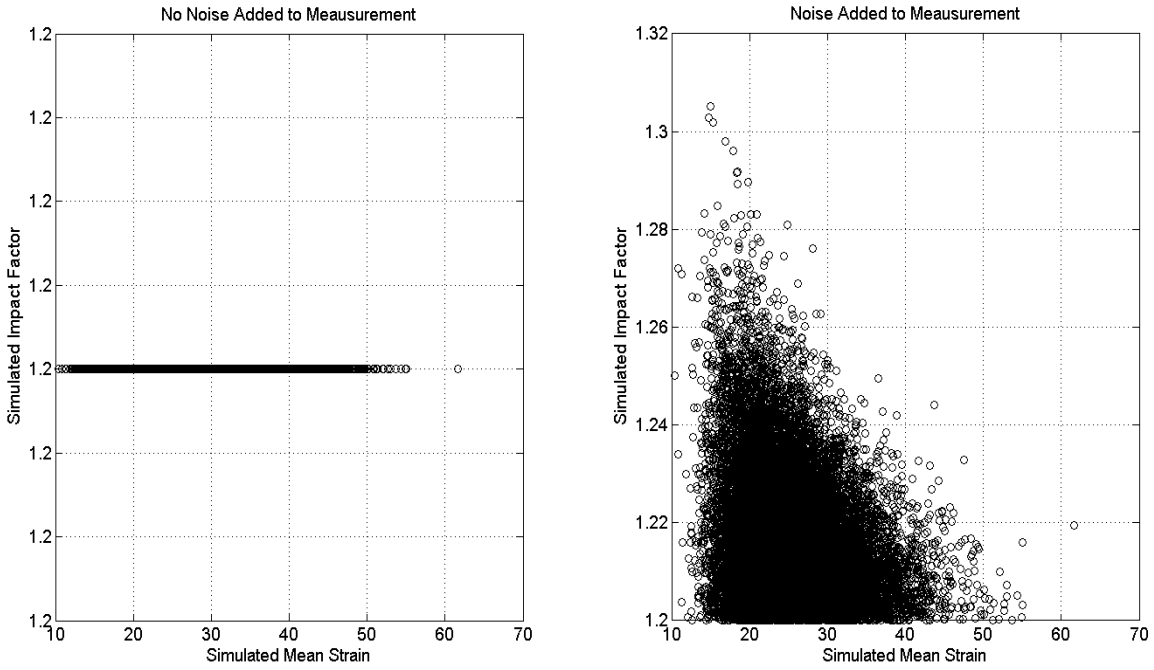

Figure 13-71: Monte Carlo simulation of the effects of measurement noise

Once the data was corrected, the impact factors were regenerated and once again plotted against their respective static strain counterparts. The trend observed previously is still present; where it appears lighter trucks impart higher impact factors than heavier trucks (Figure 13-72). Since this trend was still present, a correlation analysis was carried out to determine if these two factors are indeed correlated at all. Subsequently, from Microsoft

Excel, the linear trend r^2 value is only 0.0297 and the Pearson Correlation coefficient is only -0.172, or not meaningfully correlated (Table 13-9). Even though an apparent visual trend is noticed, there is not a statistical relationship between truck magnitude and impact factor, unlike the conclusions seen in other research. However, it is hypothesized at this stage that impact factor must be correlated with some other phenomena, not measured. Such other sources could be the shocks of the truck or the type of truck crossing the span.

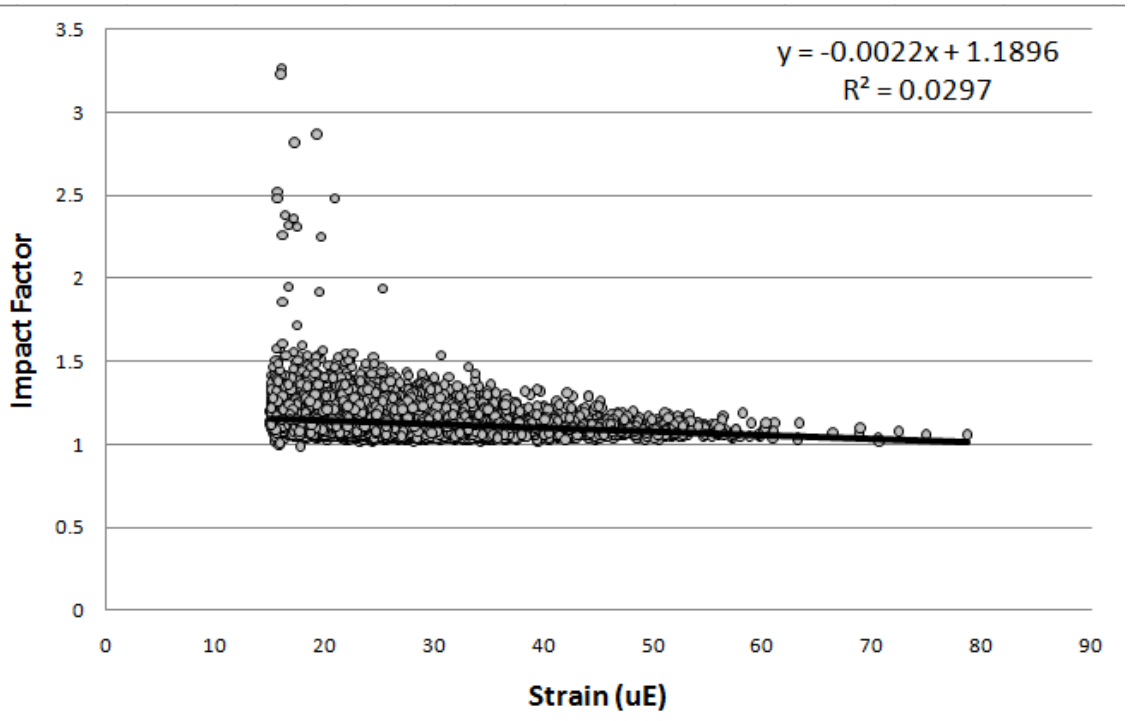

Figure 13-72: Revised impact factors with linear trend line

Table 13-9: Correlation Output from SPSS Regarding Impact Factor Study

Correlations

		Impact_Factor	Mean_Strain
Pearson Correlation	Impact_Factor	1.000	-.172
	Mean_Strain	-.172	1.000
Sig. (1-tailed)	Impact_Factor	.	.000
	Mean_Strain	.000	.
N	Impact_Factor	19912	19912
	Mean_Strain	19912	19912

The study of the BBB strain response data proved to be a very challenging and complicated study. In conclusion of the study, a set of key conclusion can be drawn:

1.) There are two distinct distributions of trucks crossing the Burlington Bristol Bridge. This was not only seen visually by studying the box plots and Q-Q plots, but in the model fitting portion of the research. Whether using normal distributions or lognormal distributions to represent each of the populations, the model which used two distributions fit the data better than the model which used only one distribution, based on BIC values. Overall, the lognormal distributions were better able to replicate the observed data than normal distributions. This statistical discovery of two distinct groups of trucks is significant, since it can be correlated with on-site experience that these trucks are of a specific type (dump truck loaded with stone) and coming from the same place (a quarry en route to NJ construction). This is information that the Burlington County Bridge Commission (BCBC), owners of the bridge, would like to know so that they could put into action a scheme designed to account for these heavy trucks. A legal truck has a strain response of -26uE and the best-fit model estimates a second population of trucks with a

mean of -45uE, or almost twice the legal limit. However, it should be noted that other traffic could be on the span while the truck is also on the span, so it is possible that the truck is of legal weight.

2.) The impact factor for each truck cannot be solely statistically correlated to its overall weight, for this structure. Considering that the impact factor vs strain response plots looked similar in other observed research, it is possible that these studies are also not correlated, even though the data has been presented in that light. There are other potential underlying conditions that may be contributing to the observed trend, such as the type of shocks that the truck is using or the specific type of truck. If information was available for correlation studies with these variables, then a more significant correlated variable could be found. However, it is clear that heavier vehicles do not have a significant impact factor, while lighter vehicles have quite a variety of impact factors.

13.3. Design and Verification of Load Cell Bearings

In an effort to remove the classification of the BBB as structurally deficient, the BCBC and their engineers of record ordered the replacement of all expansion bearings throughout the BBB. The bearings were never replaced over the lifetime of the structure, and the expansion bearings had become frozen due to corrosion and debris limiting the amount of movement in the bearing mechanism. The original expansion bearings were typical for the period of construction of the BBB, and consisted of large steel rockers (Figure 13-73).

The slated expansion bearing for replacing the aged rocker bearings was an elastomeric expansion bearing. These bearings are more commonly used in current construction practices due to their durability and functionality over longer periods of time than bearings with mechanical components. The elastomeric bearing assembly typically consists of a large elastomeric pad reinforced with steel shims at regular intervals throughout the depth of the rubber. The elastomeric pad is then bonded to steel plates on either end, the bottom plate serving as the masonry plate which is attached to a pier or support structure, and the top plate serving as the bearing plate for the structure.

Figure 13-73: Expansion Bearing on BBB

The BCBC was approached about the opportunity to incorporate sensing technology within the bearing assembly. Since the bearings had not yet been designed, the timing allowed the designers to incorporate the sensing technology selected by Drexel University into the bearing assembly. The most effective form of instrumentation to incorporate into the bearings was one which could measure the forces (axial force and bi-directional moment) experienced by the bearing during operational and seasonal demands. This type of instrumentation could be used to weigh vehicles for correlation with other monitoring systems on the BBB as well as to track how the spans are affected by differential thermal expansion throughout the course of days and months.

Drexel University research staff was then asked to identify the following: the locations for each of the bearings to be equipped with the sensing systems, specifications for the sensors to be used, a design for the adaptation of the traditional elastomeric bearing assembly and verification of the design with FE models, final design, laboratory verification of a prototype bearing, and installation methods.

13.3.1. Selection of Bearing Locations

The identification of locations in which the bearings would be equipped with the sensing technology was a critical step in the design process. Overall, there were twelve expansion bearings selected for replacement. The cost to include instrumentation was estimated and constituted a minimal percentage of the total cost of the bearing, leading Drexel University research staff to recommend that all expansion bearings be equipped with instrumentation. Additionally, one span was selected to have all four bearings replaced so

that a total weight could be measured for passing vehicles and for the span. This brought the total number of bearings to be replaced to fourteen, twelve of which were expansion bearings and two of which were fixed bearings (not allowing any translation). The instrumentation plan highlighting the location of each bearing along the length of the BBB is shown in Figure 13-74.

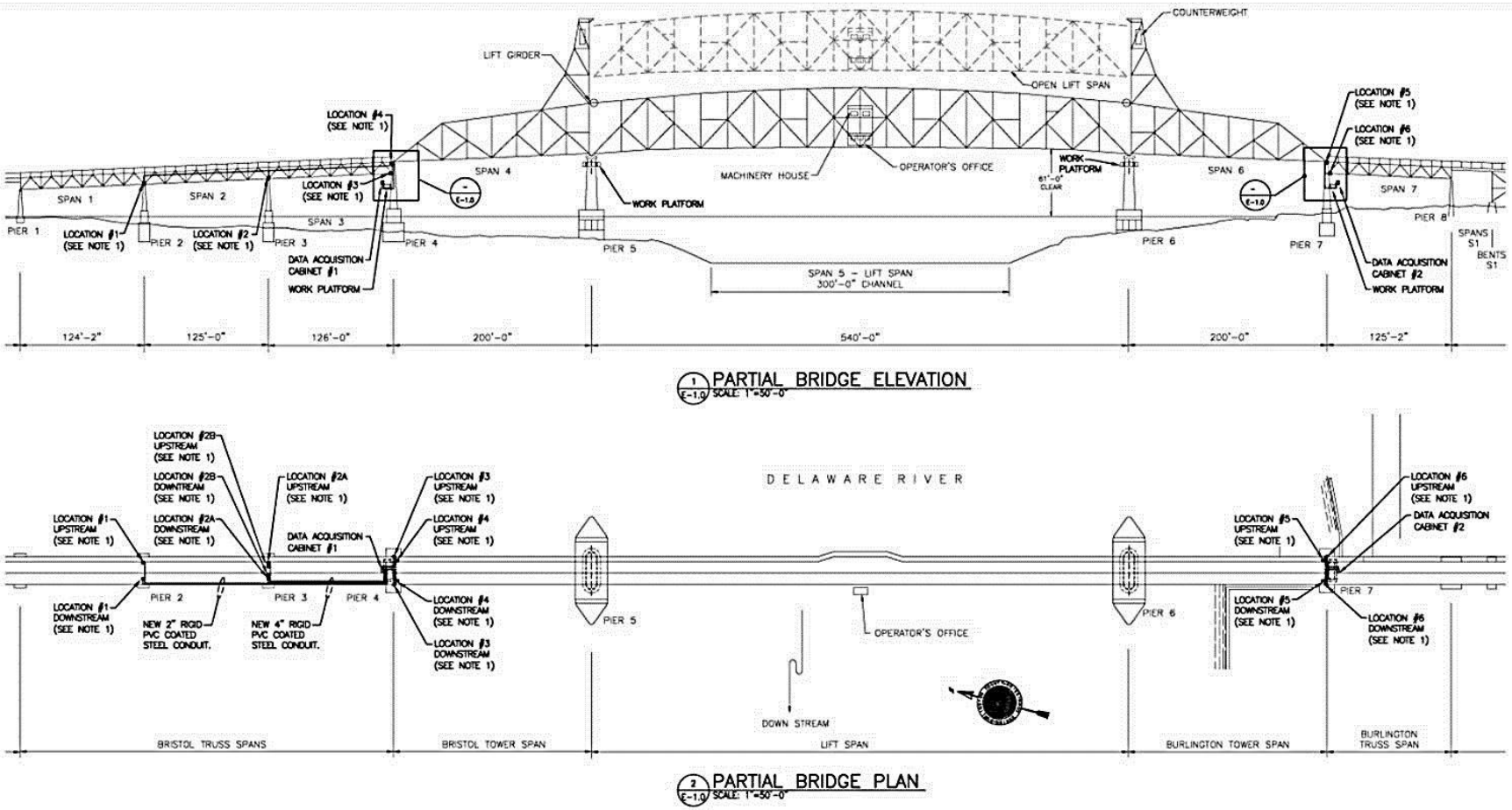

Figure 13-74: Bearing Locations for Incorporation of Sensing Technology

As shown in the instrumentation plan, each of the tower spans and each of the deck truss spans were planned to have their expansion bearings replaced. Span 2, the second deck truss approach span from PA, was identified as the candidate for having all four bearings equipped with instrumentation.

13.3.1. Designation of Specifications

The specifications for appropriate sensing technology were one of the most important steps within the process. Since the overall project was going to be bid upon by contractors, it was at their discretion to select vendors to supply all of the parts required for the bearings. However, by defining specifications about the instruments to be used, research staff was able to ensure that appropriate technology was ultimately selected.

In order to provide accurate measurements of force over long periods of time, high capacity-low profile load cells were specified as the sensor technology to be incorporated into the bearing. Due to the harsh environment that a bridge experiences, it was important that all materials used in the load cells were stainless steel and that the sensing equipment was sealed from environmental effects. Due to the potential for advanced corrosion to do electrochemical reactions with dissimilar metals, it was also required that the load cells be electrically isolated from all mild steel in the bearing assembly. This required the manufacturer to use a stainless steel on any part of the bearing which contacted the load cells or to provide some form of isolation, such as a rubber gasket, between the metals.

In order to assist with the bidding process, a prototype configuration was presented in which four load cells were used support the elastomeric bearing from under its masonry

plate (Figure 13-75). The overall bearing capacity for the tower span bearings was identified by the bearing designer as being 392 kips including dead and live load effects, while the truss span bearing capacity was 219 kips.

To ensure that the load cell system would not compromise the integrity of the bearing as a whole, it was specified that a locking system was to be incorporated into the design so that the bearing could not completely dislocate laterally. Another key requirement of the contractor was to provide an example of the load cell selected for laboratory verification.

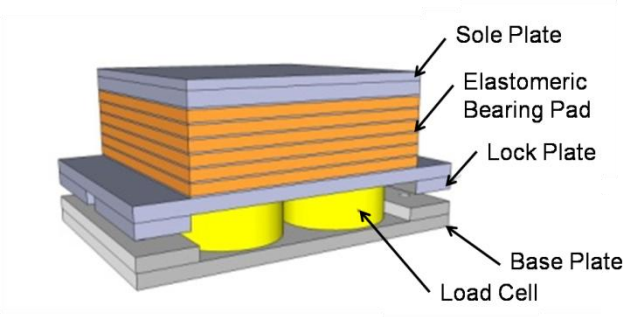

Figure 13-75: Prototype to Assist with the Bidding Process

The specific load cell specifications defined for the contractor consisted of the following:

1. Accuracy: Overall accuracy of 0.2% required, including hysteresis, linearity and repeatability.
2. Frequency bandwidth: Operating frequency of 0 – 100Hz.
3. Temperature range: Operating range of -20°F to 120°F.
4. Capacity: Operating capacity of 100 kips; safe overload of 150 kips

5. Deflection: Full scale deflection less than 0.005”.
6. Calibration: Initial calibration valid for at least five years of service with load variations from 50-100% and temperature ranges from -20°F to 120°F. All load cells should be equipped with the ability to perform periodic shunt calibrations.
7. Lifespan: Expected lifespan of 50 years
8. Material: Stainless steel
9. Connections: Military grade.
10. Dimensions: Each load cell should have a bearing area of at least 10 in^2 and a height which does not exceed 2 in and a diameter which does not exceed 10 in.

13.3.2. Preliminary Design

When a contractor was awarded the contract to construct the load cell bearings, a preliminary design was required. The contractor decided to retain the prototype design included in the bid package as the preliminary design for the bearing assembly. This configuration consisted of four load cells equally spaced between two stainless steel plates (Figure 13-76 and Figure 13-77). In Figure 13-76, the gusset plate connection of the structure has a solid rectangular steel bar inserted to serve as a jacking mechanism. This component will stay in the structure after all construction is complete to make future jacking of the structure easier in case the load cells need to be reset or replaced. The gusset plates would then be attached to the top plate of the bearing, which is adhered to the top of the reinforced rubber pad, shown in black. The bottom of the rubber pad is adhered to the stainless steel bottom bearing plate which is supported by the four load cells. The load cells then rest on the stainless steel masonry plate which is fastened to the top of the pier.

The dimensions of the rubber pads vary for the tower span and truss span bearings due to the difference in anticipated longitudinal expansion over the lifetime of the bearing. All steel plates were specified at 1” thickness.

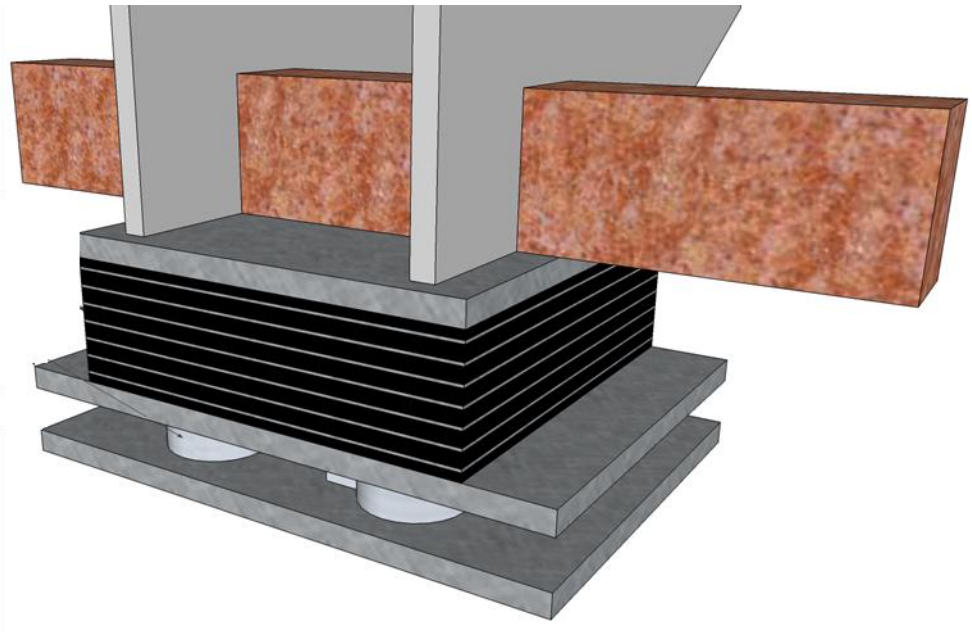

Figure 13-76: 3D CAD of Preliminary Design

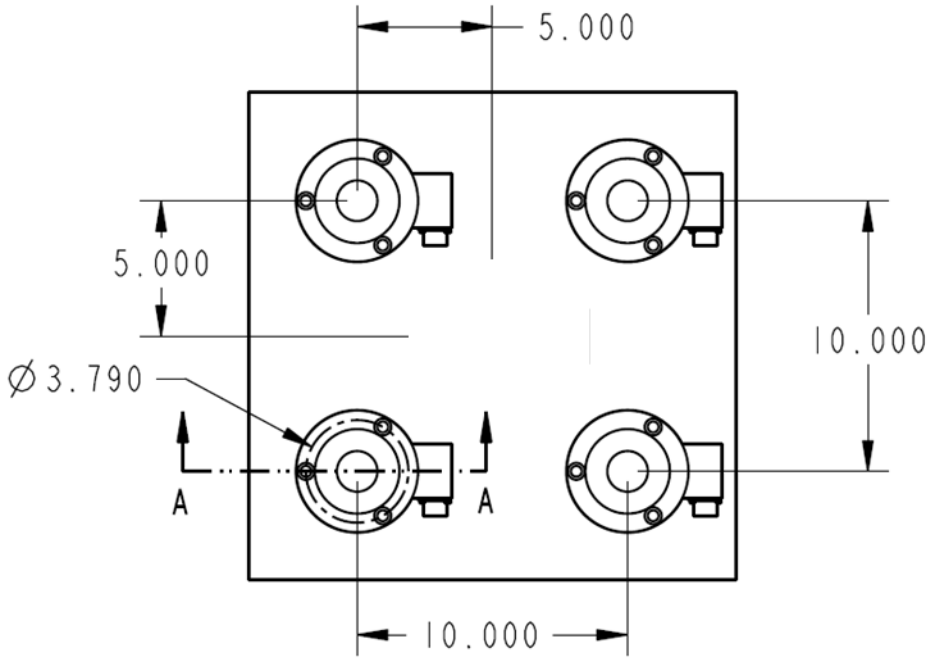

Figure 13-77: Preliminary Load Cell Configuration with the Bearing

13.3.3. FE Model Verification

The preliminary design for the load cell bearing assembly needed to be verified with a finite element model. One of the anticipated areas where concern was shown was the center of the bearing which was both unsupported and under a large amount of force. The load cells provided by the vendor did not meet the required 10 in^2, so if the preliminary design needed to be modified there were no concerns related to change orders.

The finite element model was first created by defining its geometry in AutoCAD as 3D solids (Figure 13-78). For the simple analysis of the bottom bearing plate, all of the solid components of a similar material property were intersected to form a single component. This left three main components: (1) top bearing plate and truss connection, (2) neoprene pad and reinforcement, (3) bottom bearing plate, load cells and masonry plate. The elastomeric bearing pad was modeled by having alternating rectangular components representing layers of rubber and layers of steel reinforcement. All components were then combined in the ABAQUS software by defining master-slave surfaces between the appropriate locations. For example, the bottom face of the top bearing plate was defined as the master surface and the top face of the neoprene pad was defined as the slave surface. This was repeated for all layers of neoprene and steel reinforcement as for the bottom of the neoprene pad.

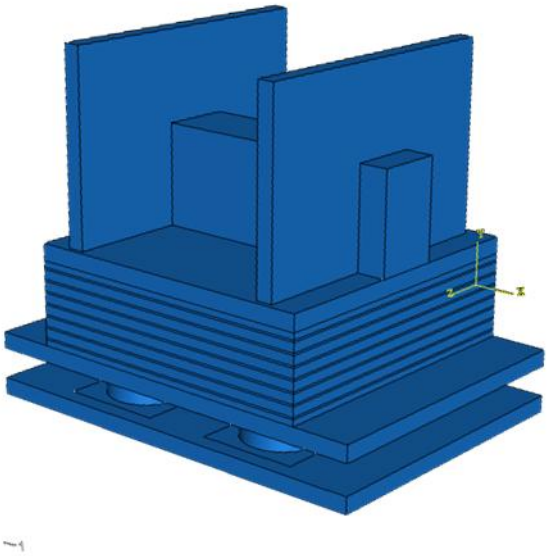

Figure 13-78: 3D CAD of BBB Load Cell Bearing Assembly

The geometry was automatically meshed with tools within the ABAQUS FE interface, with a specified element type of C3D10, a 10 node quadratic tetrahedral solid element (Figure 13-79), for all geometric regions with complex geometry. These regions included the load cells and the plates on the top and bottom of the load cells. The original concept of the top and bottom plates was to have machined pockets for the load cell to rest in so that the bearing assembly cannot completely dislocate laterally under a significant shock. These cylindrical pockets and the geometry of the load cells all had complex geometry, which a traditional brick element could not appropriately represent. However, for all other components the C3D8, an eight node linear brick element, was used.

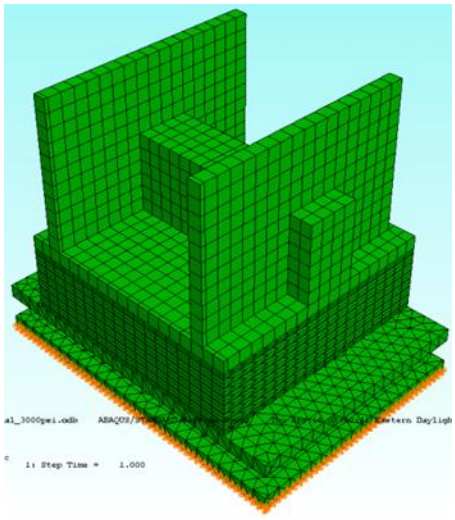

Figure 13-79: Meshed Bearing Assembly in ABAQUS

The bottom of the masonry plate was assigned as a fixed support. Loads equivalent to the design load were applied to the top faces of the elements that represented the gusset plate connections. Great care was taken to replicate the actual conditions of the loading seen in the structure, including the jacking bar which was to remain in place, so that an accurate stress profile could be generated for the bottom bearing plate. A linear static analysis was run, and the model was analyzed for stress distributions across the bottom bearing plate.

It was seen by examining the von Mises stress combination of the bottom bearing plate (Figure 13-80) that the stresses in the center of the bearing and in the regions between load cells exceeded the yield stress of the steel plate. To reduce the stress these regions, the engineers were presented with three alternatives.

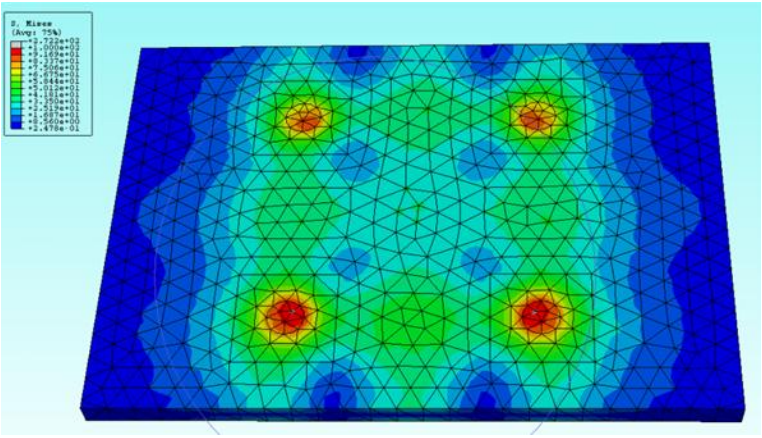

Figure 13-80: von Mises Stress Distribution for the Original Bearing Design

The three alternatives consisted of: (1) Increasing the thickness of the bottom bearing plate to 2” instead of 1”, (2) Increasing the thickness of the bottom bearing plate only in the regions of high stress, and (3) Inserting a fifth load cell in the middle of the bearing assembly to reduce the bending stress in this region. The three configurations were modeled in ABAQUS in the same manner as the original prototype design and were analyzed for the same stress distribution. The results from the three stress analyses are shown in Figure 13-81 through Figure 13-83.

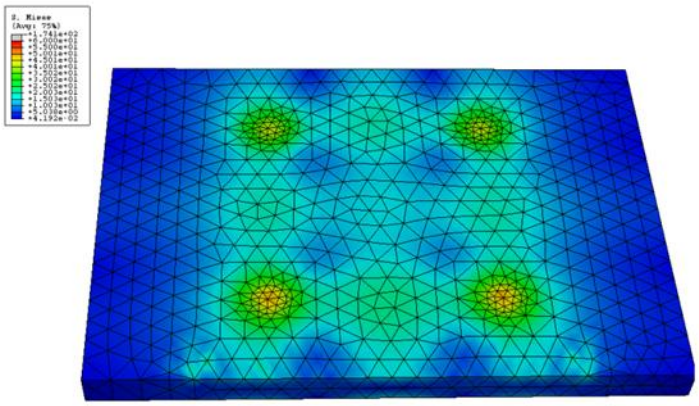

Figure 13-81: von Mises Stress Distribution for the 2" Thick Bottom Bearing Plate Alternate Design

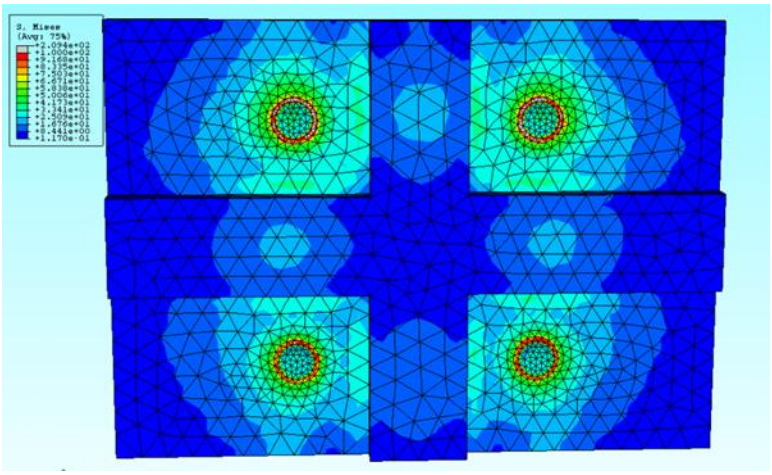

Figure 13-82: von Mises Stress Distribution for the 2" Thick Bottom Bearing Plate in High Stress Regions Alternate Design

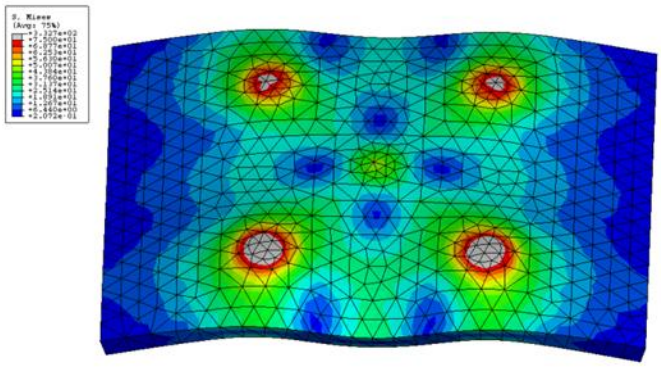

Figure 13-83: von Mises Stress Distribution for the Fifth Load Cell Alternate Design

All three design alternatives were shown to have significantly reduced the bending stresses in the center of the bottom bearing plate. However after consulting with the design engineers, it was decided that the second alternative was infeasible due to the anticipated cost of machining the plates into thickened regions between the load cells. A final stress comparison between the thickened plate and the five load cell configuration was supplied to the engineer for their final decision on which course of action to take (Figure 13-84).

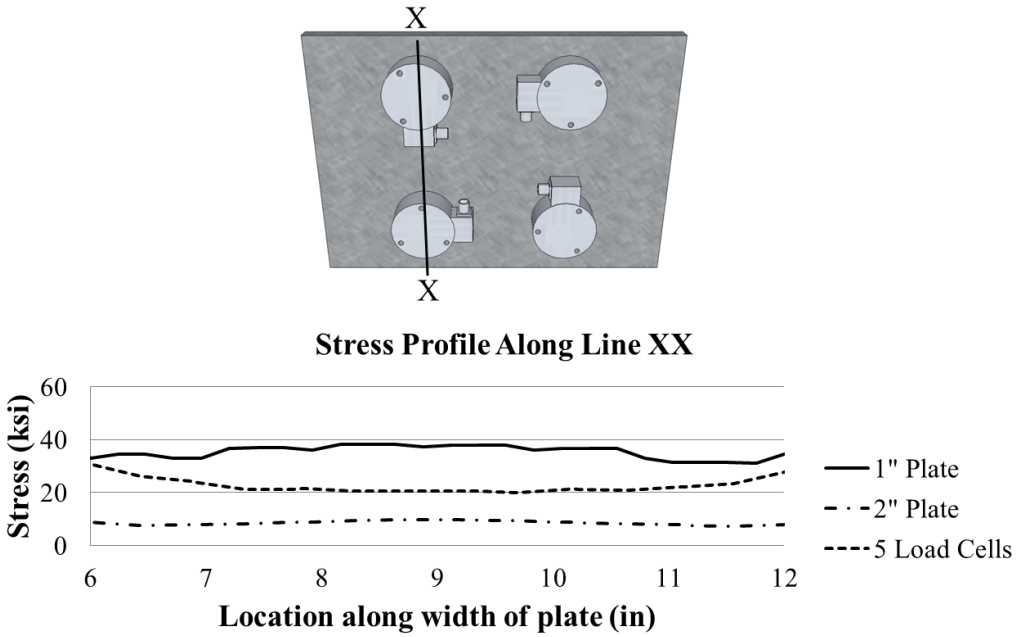

Figure 13-84: Final Stress Profile Comparison for Selecting an Alternative Design Compared to the Original 1” Plate Design

It was shown that both methods reduced the stress in the center of the plate below the yield stress for the material. The high stress towards the edges of the plots was due to the contact stresses between the top surface of the load cells and the flat surface of the bottom bearing plate.

13.3.4. Final Design

The final decision by the design engineer was to proceed with the five load cell configuration, since the extra 1” needed for the thickened plate would have to be made up by removing concrete from the top of the piers to maintain the roadway alignment. The final load cell configuration is shown in Figure 13-85.

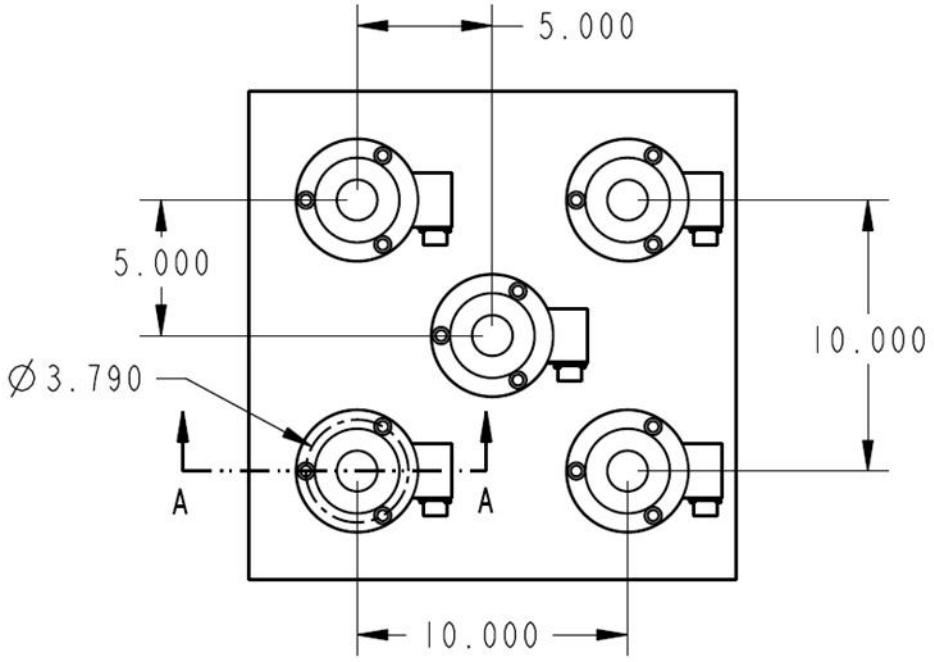

Figure 13-85: Final Load Cell Configuration

To ensure that the load cells would not move about within the bearing assembly, it was decided to machine pockets in the bottom face of the bottom bearing plate and in the top face of the masonry plate to a depth of 1/8". Then each load cell would rest within these pockets and lock the bearing assembly together (Figure 13-86 and Figure 13-87).

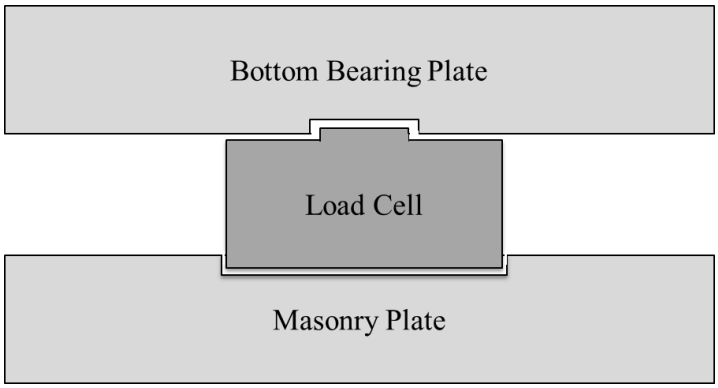

Figure 13-86: Cross Section of Load Cell Pockets

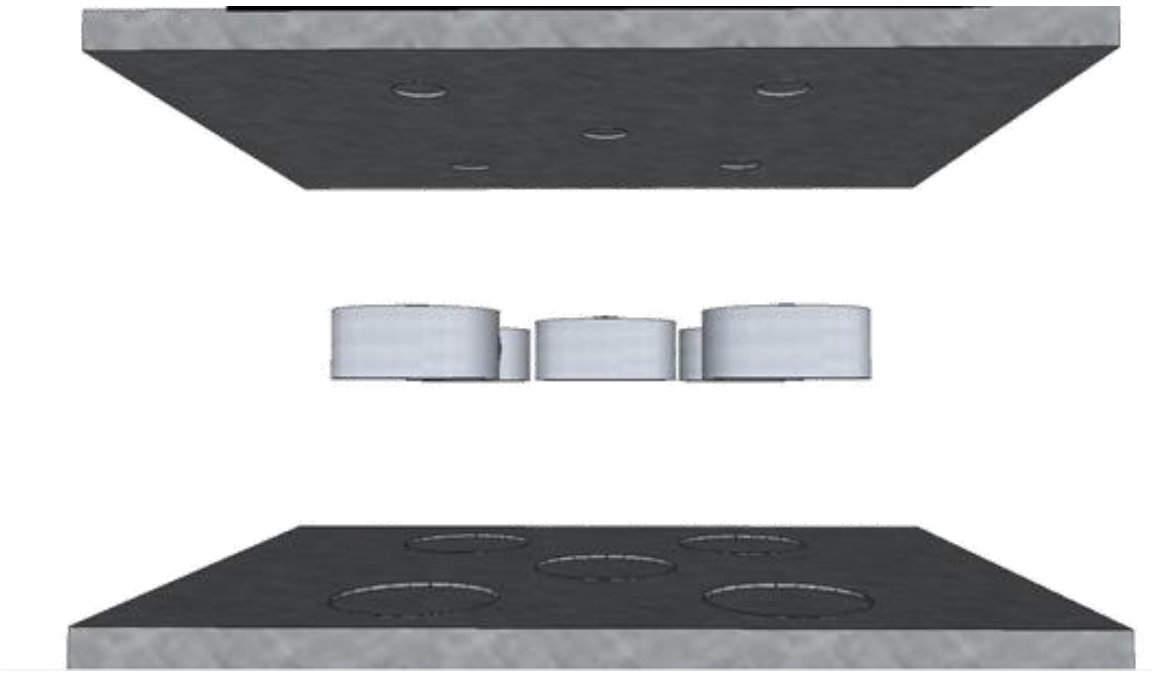

Figure 13-87: Blown-up View of the Bottom Bearing Plate (top), Load Cells, and Masonry Plate (bottom)

13.3.5. Laboratory Testing

As stated in the design specifications, it was required of the contractors to submit both the selected load cell and the prototype design for the complete bearing assembly for laboratory verification by Drexel University research staff.

13.3.5.1. Load Cell Verification

The sensor selected by the contractor for the load cell bearing assembly was manufactured by Cooper Scientific. Each load cell had a full scale range of 100 kips with a 50% safe overload. The stainless steel sensor, Model LGP 312, met all required

specifications. However, due to the nature of how the load cell is installed within the bearing assembly, it was important to verify the physical integrity of the sensor and specifically how the sensor performed under non-ideal loading conditions.

A testing regime was designed to verify that the LCP 312 load cell would satisfy the requirements of the load cell bearing. All of the tests were carried out in a Model FX-400 Forney compression machine with an built-in load cell measuring up to 400,000 lbs +/- 0.5% FS.

First, the load cell was tested cyclically in 10,000lb increments up to full range with the load applied at the center of the load cell and in a vertical direction. The second testing was also applied vertically at the center of the load cell with magnitudes that varied from 45,000 lb to 55,000 lb in 1,000 lb increments. The first test was to verify the full range accuracy of the load cell, while the second test was to verify the accuracy in an operating range of the load cell.

The second main testing carried out on the load cell was cyclic eccentric loading. This test loaded four locations of the loading button of the load cell to replicate situations where the load cell would not be ideally loaded within the bearing assembly. It was necessary that the load cell still perform in an acceptable manner, even if loaded in an eccentric manner. Each of the four configurations (Figure 13-88) was loaded in 5,000 lb increments up to the anticipated service load of 50,000 lb.

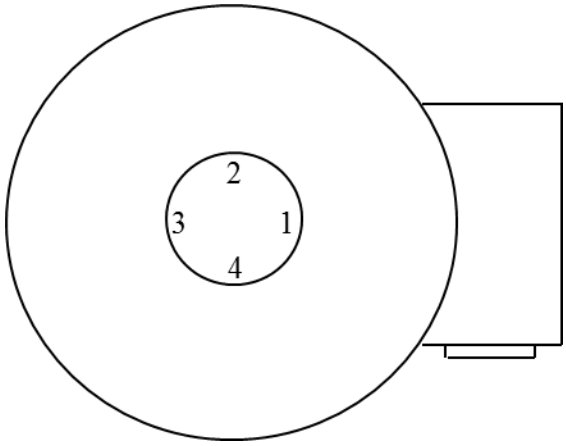

Figure 13-88: Eccentric Loading Pattern on the Load Cell Button (Plan View of the Load Cell)

The final form of testing on the load cell was to produce a shear force in the load cell unit to replicate a situation where the load cells are being sheared between the masonry plate and bottom bearing plate during an expansion or shrinkage cycle of the bridge. To replicate this type of behavior, the load cell was inclined 10° and loaded at the center of the load cell button in 5,000 lb increments up to a load of 30,000 lb.

At each load increment during all tests, the Cooper load cell and the Forney load cell readings were recorded and compared to one another. The results of the tests showed that the Cooper load cell was able to read within 2.5% of the Forney load cell for all performed tests. Given that the Forney load cell was only accurate to within 2,000lbs, the results indicate that it is possible the errors lie within the Forney machine's load cell and not the Cooper instrument. An example of each of the three main types of load testing performed on the load cell is shown in Figure 13-89 through Figure 13-91. In each of the

figures, the equation of a best fit line is presented to conceptualize the percent error between the reference load cell and the Cooper load cell.

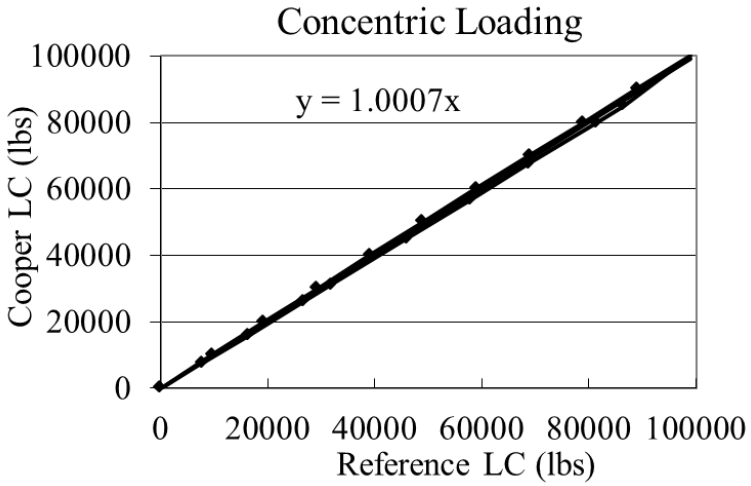

Figure 13-89: Concentric Loading of Load Cell up to 100,000lbs

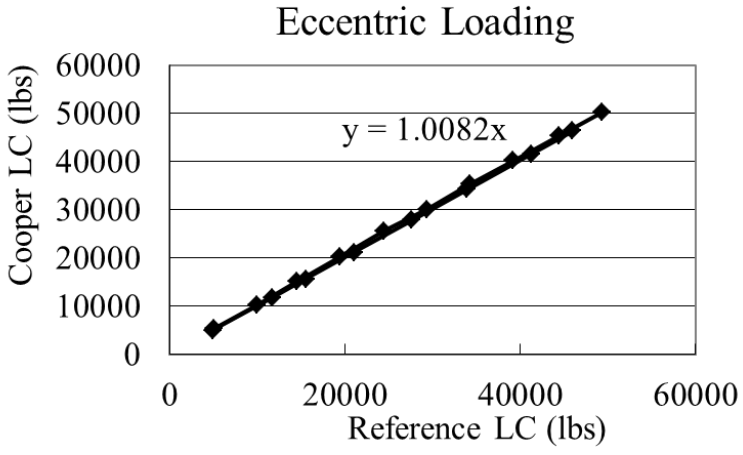

Figure 13-90: Eccentric Loading of Load Cell up to 50,000lbs

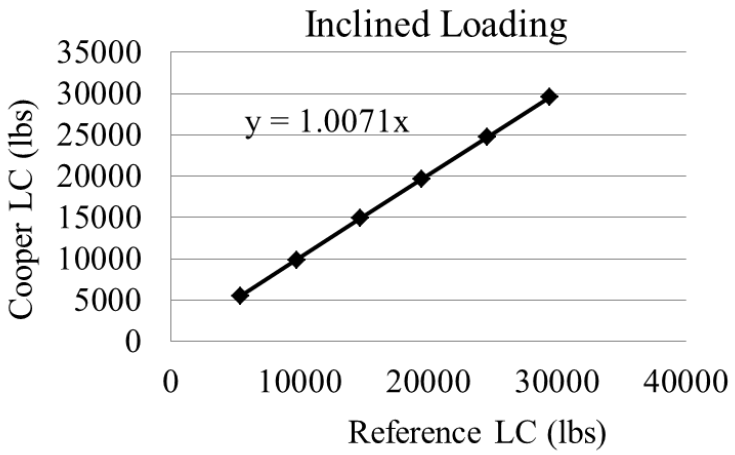

Figure 13-91: Inclined Loading of Load Cell up to 30,000lbs

Based on the testing program carried out above, the load cell was approved pending further bearing assembly testing and the contractor was instructed to manufacture the prototype bearing.

13.3.5.2. Bearing Assembly Verification

Once the prototype bearing assembly was manufactured, it was shipped to Drexel University laboratories (Figure 13-92). A loading frame was constructed in the laboratory with two actuators, capable of providing up to 440,000lbs of force. Due to the fact that one actuator was rated at 330,000lbs while the second was rated at 110,000lbs it was necessary to position the bearing assembly in such a manner as to generate pure axial

force within the bearing. This was done by ensuring the bearing assembly had zero moment and computing the necessary moment arms to each actuator. The smaller actuator needed to be three times further away from the center of the bearing than the larger actuator. To apply the load from the actuators to the assembly, a loading beam was placed across the top of the bearing in a manner consistent with how the actual bearing was to be loaded (Figure 13-93). Each actuator was equipped with internal load cells, allowing for a direct comparison between measured applied force and the corresponding measured response in the bearing.

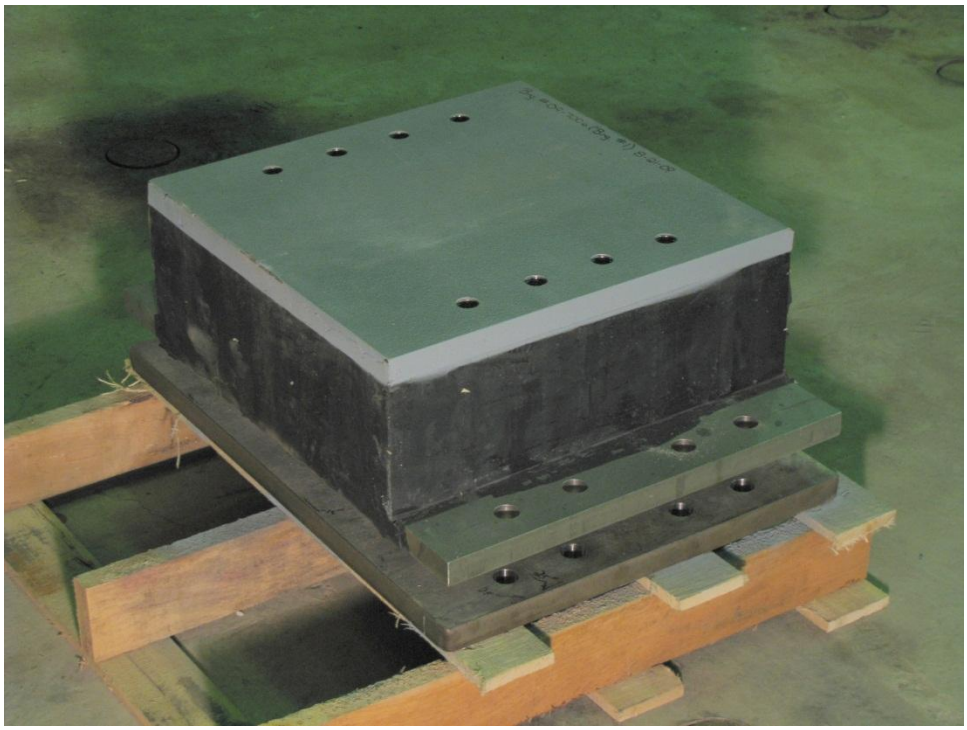

Figure 13-92: Load Cell Bearing Assembly upon Arrival

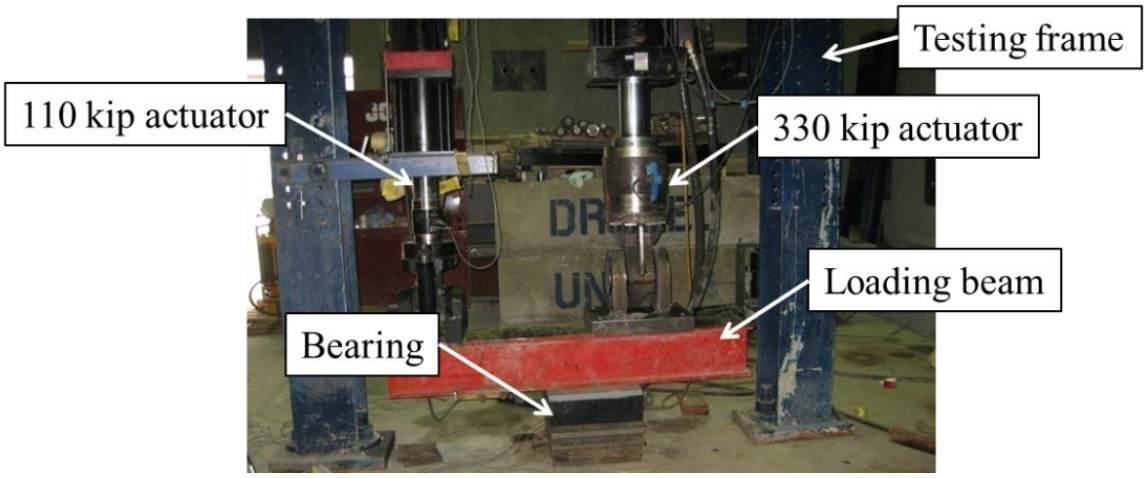

Figure 13-93: Loading Frame Configuration

There were three main types of tests performed on the bearing assembly, with multiple iterations of each test. The first test performed was a full capacity test of the bearing assembly. The bearing assembly shipped to Drexel University was the tower span bearing, requiring a design capacity of 392 kips. This bearing was selected since it would experience the highest stress and have the highest potential for overloading one of the load cells.

All five load cells within the bearing assembly and the two load cells from the actuators were all recorded with a Campbell Scientific CR5000 data logger with custom developed programming and user interface. Alarms were configured as each load cell neared its designed limit so that the test could be safely shut down in the event of an overload.

The first testing on the bearing required a force input of 400 kips. Extreme caution was taken during the course of this test considering the large forces and potential to brittle, sudden failure. At each increase in load, the research team inspected the bearing to ensure that it was being loaded vertically and that the bearing was not shifting or leaning in any direction. Also, the verticality of the actuators was established with a level to ensure that they were not rotating out of position. Only after all of these factors were established was the load increased to the next level. The time history of the full capacity loading is shown in Figure 13-94, and shows excellent correlation between the measured response and applied force, as shown in Figure 13-95. The high degree of correlation between the measured response and applied force is shown by the near perfect linearity between the two indices in Figure 13-95.

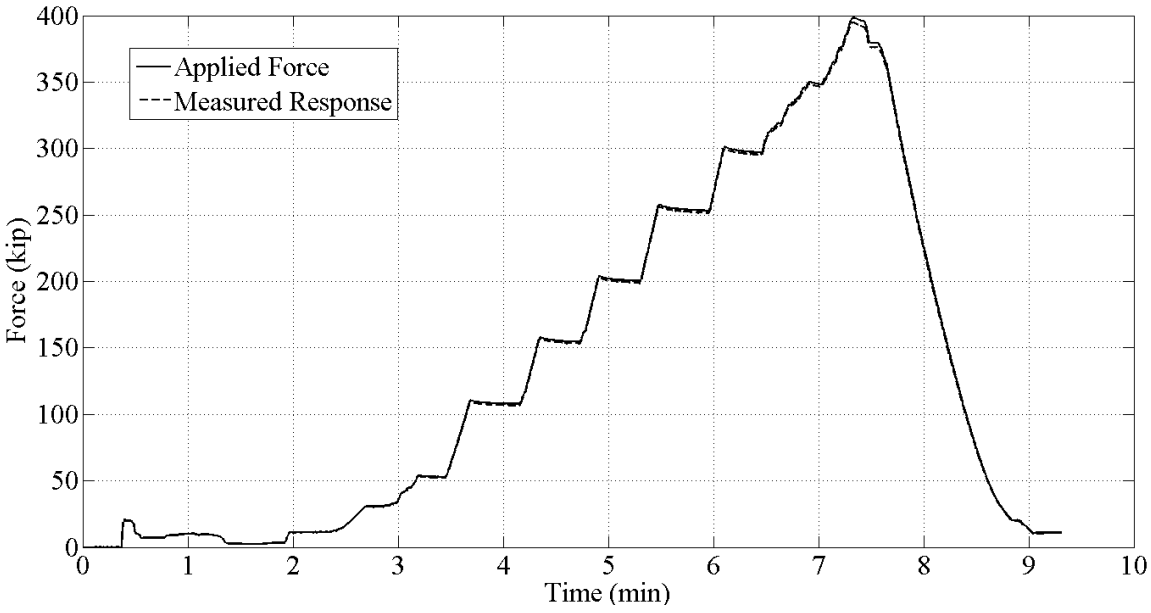

Figure 13-94: Time History of Measured Response and Applied Force during Full Scale Testing

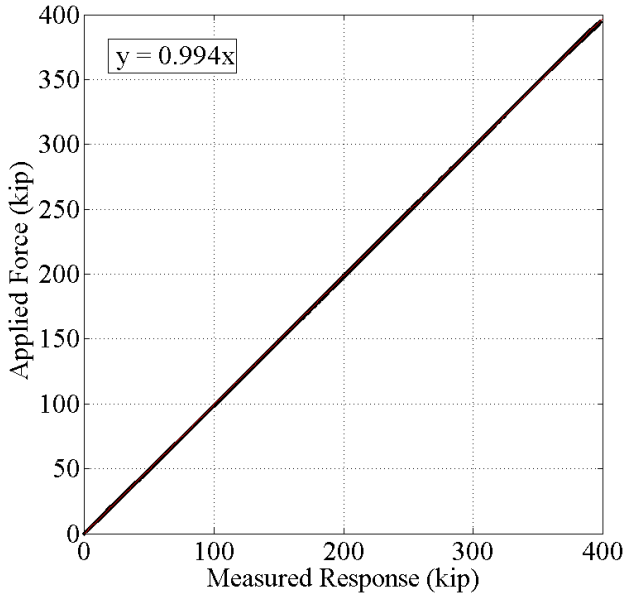

Figure 13-95: Scatterplot of Measured Response vs Applied Force with Equation for Line of Best Fit

The next test performed on the bearing assembly was the 100 to 300 kip cyclic loading. This test was performed to mimic repeated extreme changes in loading over a relatively short period of time. One of the goals of the test was to determine the effects of measurement hysteresis on the output of the sensors compared to the applied loads. The time history for this test is shown in Figure 13-96, while the scatter plot of the measured response and applied force is shown in Figure 13-97. Once again, a very high degree of linearity is shown between the two indices, which demonstrates a high level of precision.

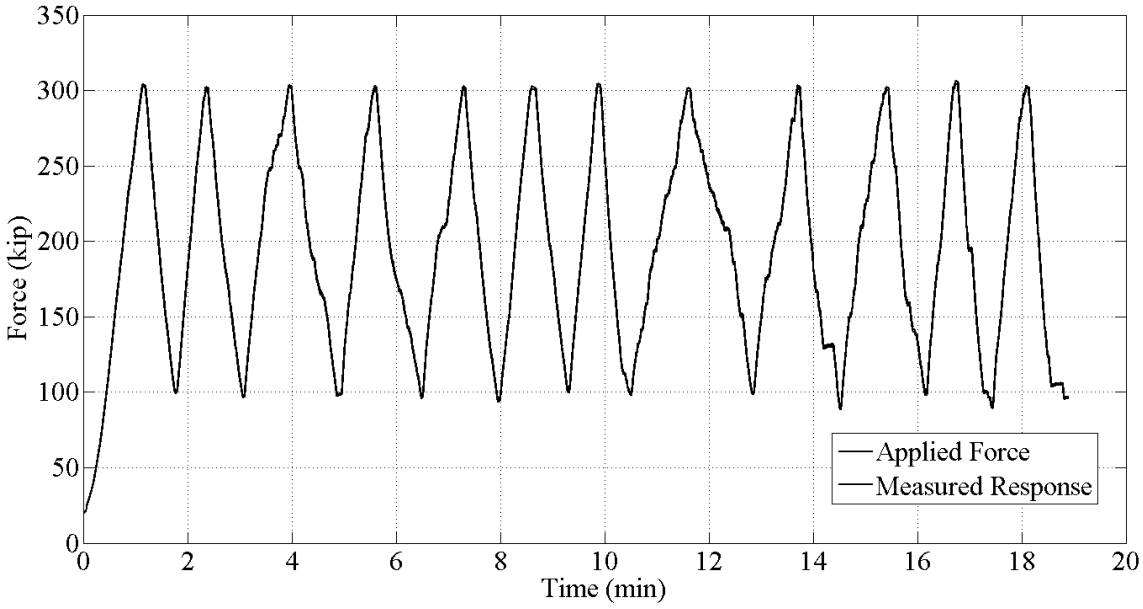

Figure 13-96: Time History of Measured Response and Applied Force during Cyclic Loading Testing

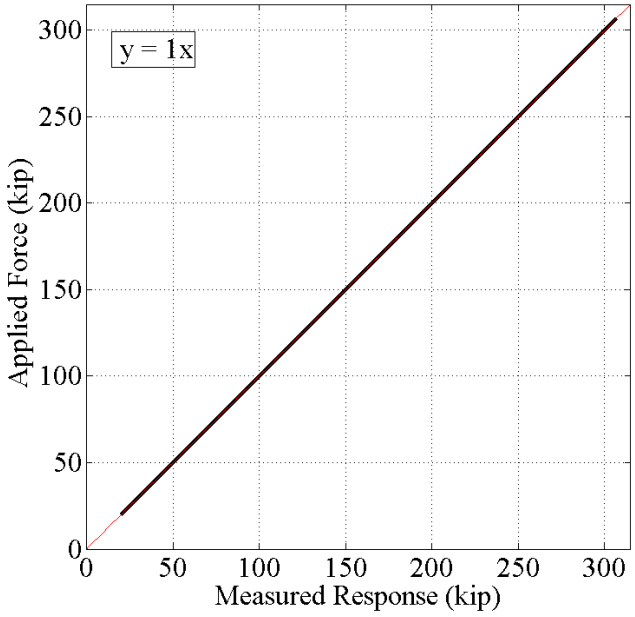

Figure 13-97: Scatterplot of Measured Response vs Applied Force with Equation for Line of Best Fit

Each of these tests was repeated for a minimum of five times, each of which showed similar levels of success in terms of correlation between measured response and applied force. After the detailed vertical loading of the bearing was complete and determined to produce satisfactory results in terms of measurement accuracy from the load cell bearings, a third test was performed to determine the effects of shear force applied to the bearing on the accuracy of measurement output. From preliminary testing on the load cells themselves, there was little effect of shear loading, however by testing the actual bearing assembly a more realistic scenario is explored.

To produce a significant shear force within the bearing assembly, a special loading plate was machined which tilted the bearing assembly by 10° from a horizontal plane (Figure 13-98). By loading the tilted bearing in a vertical direction, two components of force would be generated, one force normal to the bearing and one force in direct shear. The maximum shear force that the bearing would see in service was estimated to be 20 kips, based on heuristics. To achieve a 20 kip shear force, a normal force of approximately 113 kips would be required.

The total force then required to be provided by the actuator was approximately 115 kips. Since both actuators were not required for this force level, the 330 kip actuator was used to provide the total force. The rotatable head of the actuator made it possible to ensure solid contact between the loading head and the top of the bearing at the appropriate angle. The actuator was also able to be locked into position, thereby eliminating any chance that the actuator would simply slip out of place after the load was applied.

Figure 13-98: Loading Configuration for Shear Testing

The loading of the bearing assembly in a configuration which provides shear force was done for two reasons: (1) to ensure that the accuracy in measuring the normal force experienced by the bearing was not compromised and (2) that the load cells and pockets in the bottom bearing plate and masonry plate provided enough stability in the lateral directions to ensure a safe bearing assembly. Even though the final design of the bearing assembly allowed for fail safe mechanical devices to ensure that the bearing assembly

would never become dislodged, it was critical to ensure that the load cells could handle the shear forces themselves.

The time history of the applied and measured normal forces and applied shear force are shown in Figure 13-99, while the linearity of the measured and applied normal forces is verified in Figure 13-100. Additionally, Figure 13-101 shows the effect on the bearing assembly by loading the unit up to 20k in direct shear. The loading level of 20 kips was justified by visually seeing the degree of lateral deflection of the top bearing plate.

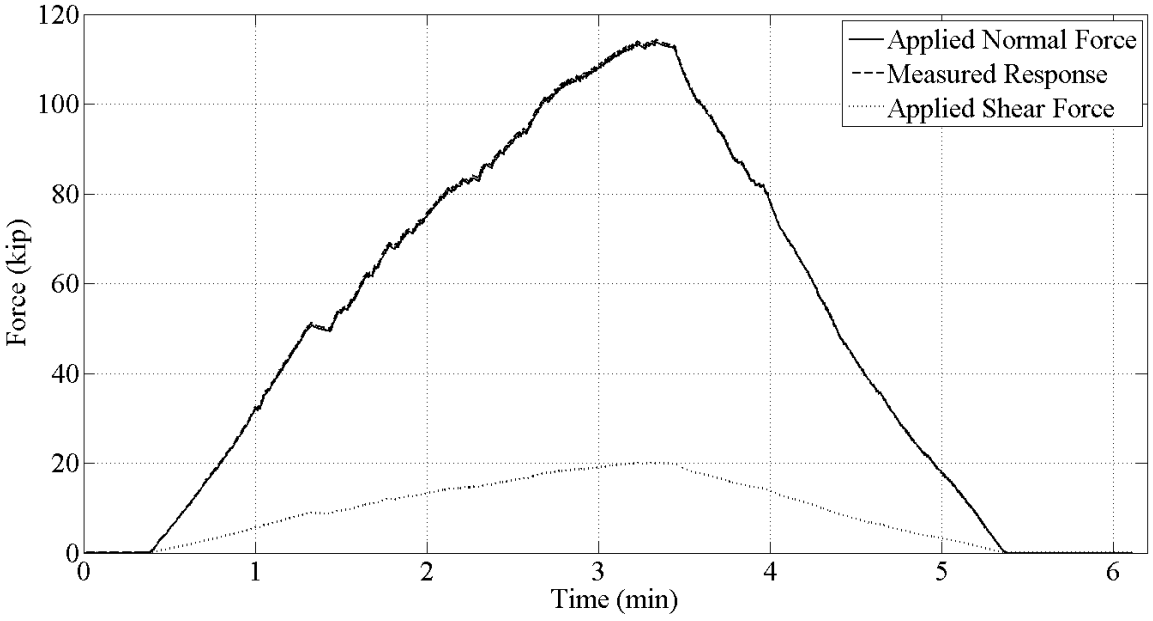

Figure 13-99: Time History of Measured Response, Applied Force and Applied Shear during Shear Test

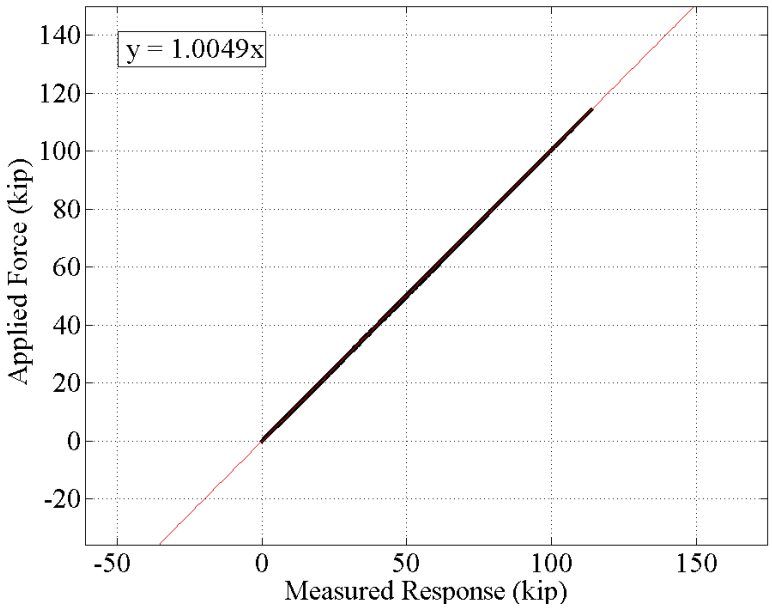

Figure 13-100: Scatterplot of Measured Response vs Applied Force with Equation for Line of Best Fit

Figure 13-101: Bearing Assembly under 20 kip of Shear Force

As seen in the results above, the accuracy of the load cell bearing assembly was not compromised by incorporating a significant shear force into the assembly. This was the final testing applied to the bearing assembly, and after all data was processed and analyzed, the contractor was given notice to proceed in manufacturing all bearings and acquiring all load cells to be installed on the BBB.

13.3.6. Installation

The bearings were installed on the BBB beginning in the spring of 2010. Temporary shims were used in place of the load cells until all of the bearings were fully installed on the spans. Due to the weather over the winter of 2010 into 2011 and separate construction activity on the bridge, the load cells were not able to be installed on the spans until the summer of 2011.

The load cells were installed by first jacking the bridge up from the piers just enough to remove the temporary supports. After the supports were removed, the load cells were slid into place in between the masonry plate and the bottom bearing plate. After their position was verified, each load cell was connected to the same CR5000 data logger used in the Drexel University laboratories for the assembly verification. The jacks supporting the structure were then released, and the bridge was allowed to fully bear on the load cell bearing assembly. In the event of a misplaced load cell, or an uneven distribution of loads to the five load cells, the operator of the CR5000 was able to immediately alert the contractors to stop the lowering of the bridge and to jack the structure up to release the load from the load cells. Shims were then used to adjust the position of the load cells, if

needed, to mitigate such a problem. When the bridge was fully seated on the bearing assembly, traffic was monitored for a few minutes to ensure that the assembly was behaving properly.

The time history for the seating of one bearing from the NJ tower span is shown in Figure 13-102, while the time history for the seating of one bearing from the NJ truss span is shown in Figure 13-103. The final installed bearing assembly is shown in Figure 13-104.

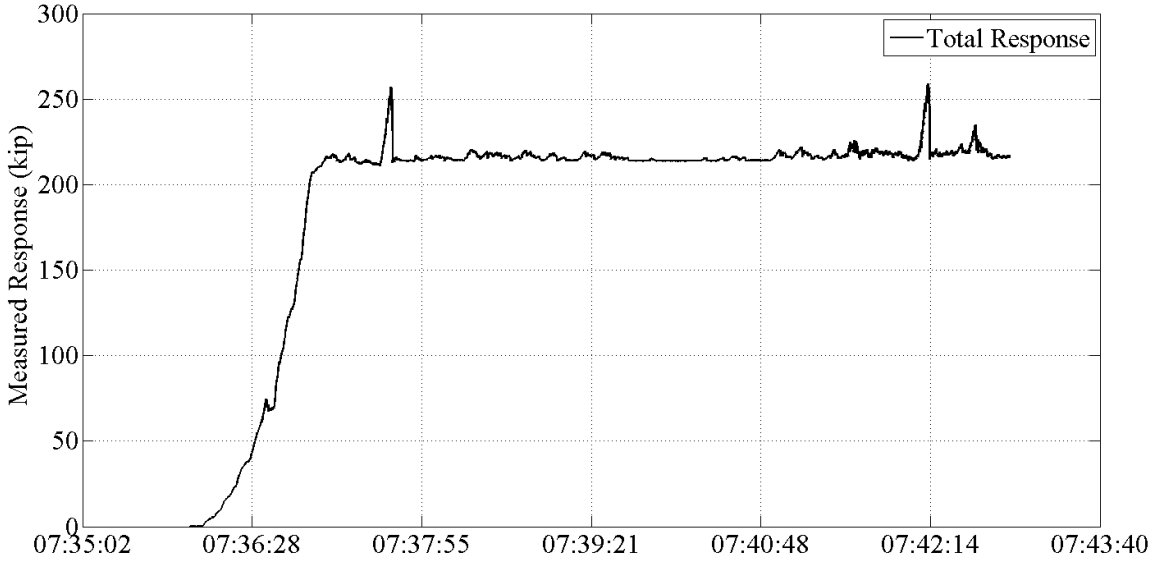

Figure 13-102: Measured Load Cell Bearing Response from Seating of NJ Tower Span West Bearing and Measurement of Traffic Effects

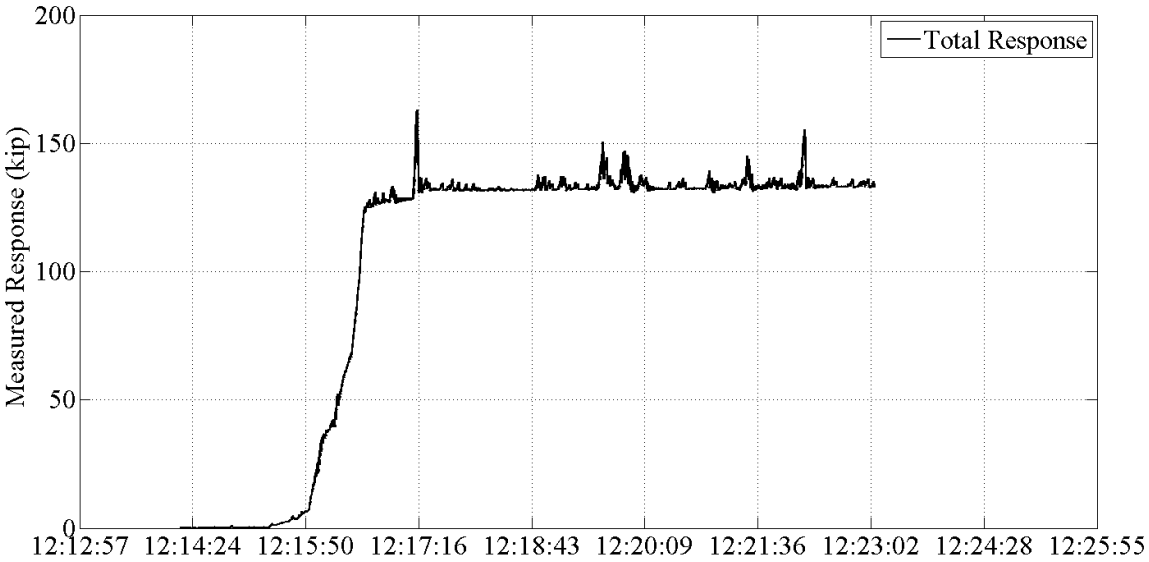

Figure 13-103: Measured Load Cell Bearing Response from Seating of NJ Truss Span

Figure 13-104: Installed Load Cell Bearing Assembly

The full instrumentation network for the load cell assembly network was not installed at the time of publication of this thesis. However, the anticipated results from this monitoring system will be able to be leveraged immediately into more refined estimates of load rating for the spans as well as to learn how the dead load distribution of such spans change over the course of days or months.

13.4. Full Ambient Vibration Monitoring of the BBB

The full ambient vibration monitoring program for the BBB was developed at the completion of the preliminary vibration monitoring survey. However, due to the time of the year after the completion of all data processing and instrumentation design for the full ambient vibration test, it was decided to delay the field work until the summer of 2009. The goals of the vibration monitoring project were to characterize the natural frequencies and modeshapes for the major spans for model correlation, investigate the difference in vibration characteristics between the NJ and PA tower spans and identify any anomalies within the boundary conditions. The full ambient vibration monitoring required a great amount of planning and coordination between research staff, engineers and BCBC maintenance staff to ensure a successful project. To carry out the vibration monitoring, the following tasks needed to be completed and will be discussed in subsections: (1) instrumentation design, (2) data acquisition design, (3) field work, (4) data processing and (5) presentation of results.

13.4.1. Instrumentation Design

The success of any experimental program hinges primarily on the development of an appropriate instrumentation plan. For the vibration monitoring of the BBB, it was decided to monitor each of the five main spans individually. This would allow the Drexel University research staff to focus the entire set of instruments on one span at a time. This was critical because spans such as the tower spans required measurements in all three coordinate axes both along the length of the span as well as along the height of the tower. The maximum number of accelerometers able to be used by Drexel University research staff included thirty PCB 393C accelerometers and fifteen PCB 3701 capacitive accelerometers.

13.4.1.1. NJ Truss Span

The instrumentation plan for the NJ truss span was developed in a manner so that the vertical, torsional and lateral modeshapes could be characterized with a high degree of confidence. It was envisioned at this point that the PA truss spans would not be instrumented as heavily as the NJ truss span, so it was important to characterize this span so that the spans of the PA trusses could be identified with the assistance of the NJ truss vibration results. The instrumentation plan (Figure 13-105 through Figure 13-107) includes four longitudinal accelerometers, sixteen vertical accelerometers and thirteen lateral accelerometers for a total of thirty-three required accelerometers.

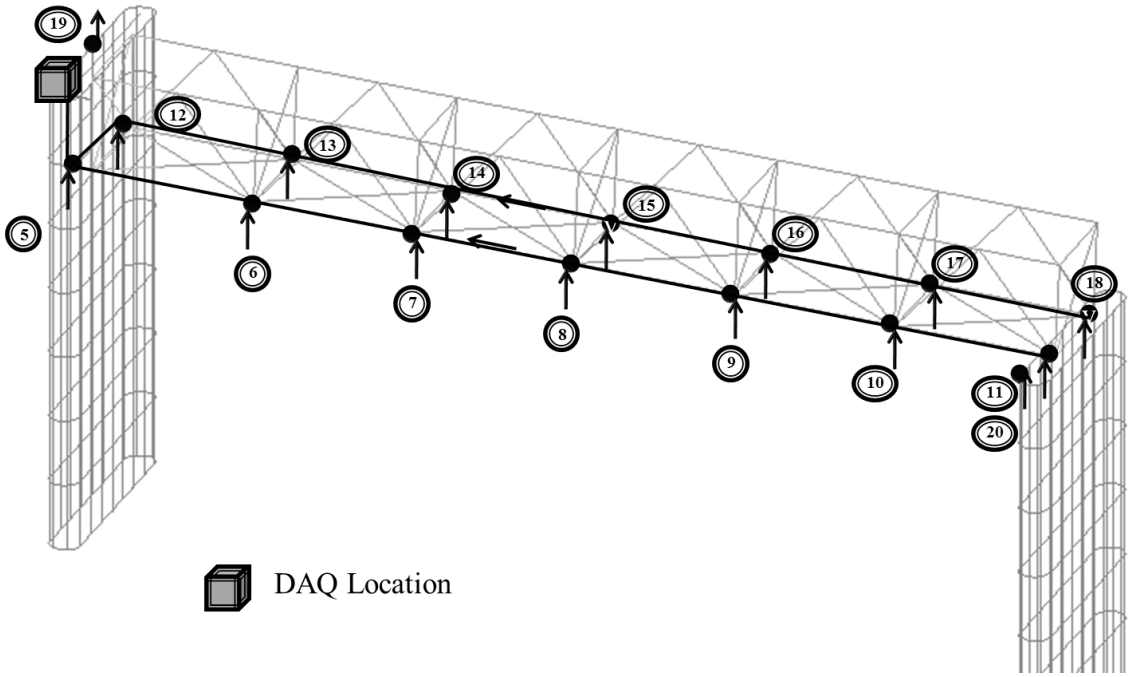

Figure 13-105: NJ Truss Span Vertical Instrumentation Plan

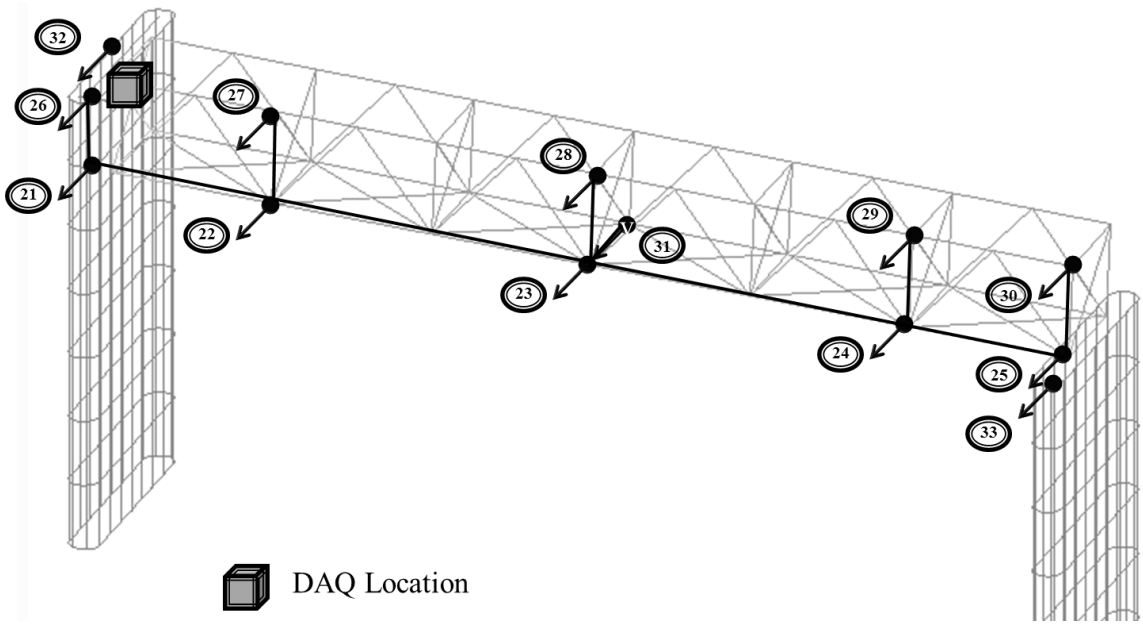

Figure 13-106: NJ Truss Span Lateral Instrumentation Plan

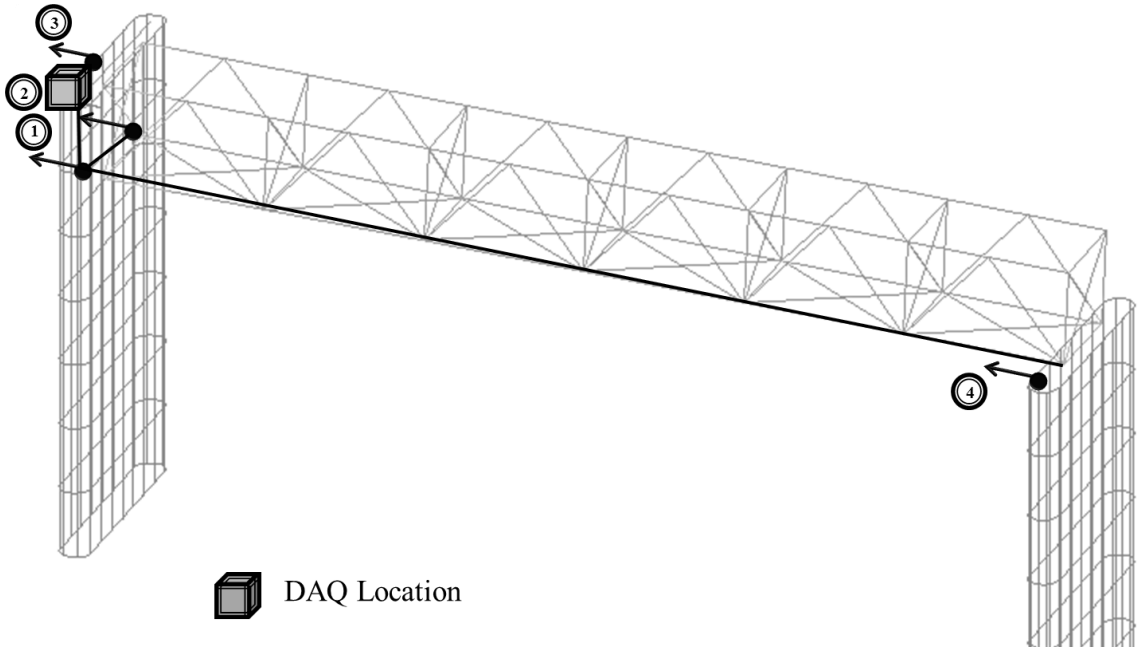

Figure 13-107: NJ Truss Span Longitudinal Instrumentation Plan

The truss span was instrumented with vertical accelerometers at every panel point along the bottom chord of both trusses and lateral accelerometers on both the top and bottom chords at five of the seven panel points along a single truss. Each pier was planned to have an acceleration measurement in each direction. The truss span was also instrumented with two longitudinal accelerometers at its expansion bearings.

13.4.1.2. NJ & PA Tower Spans

The tower spans required the most accelerometers to fully capture the mode shapes. Since the discrepancy between the NJ and PA tower spans were of interest to the Drexel University research team as well as the BCBC staff, it was important to capture any

difference between the two spans. For this reason, a dense array of vertical, lateral and longitudinal sensors was planned (Figure 13-108 through Figure 13-110) for the roadway truss and tower structure to capture the global characteristics.

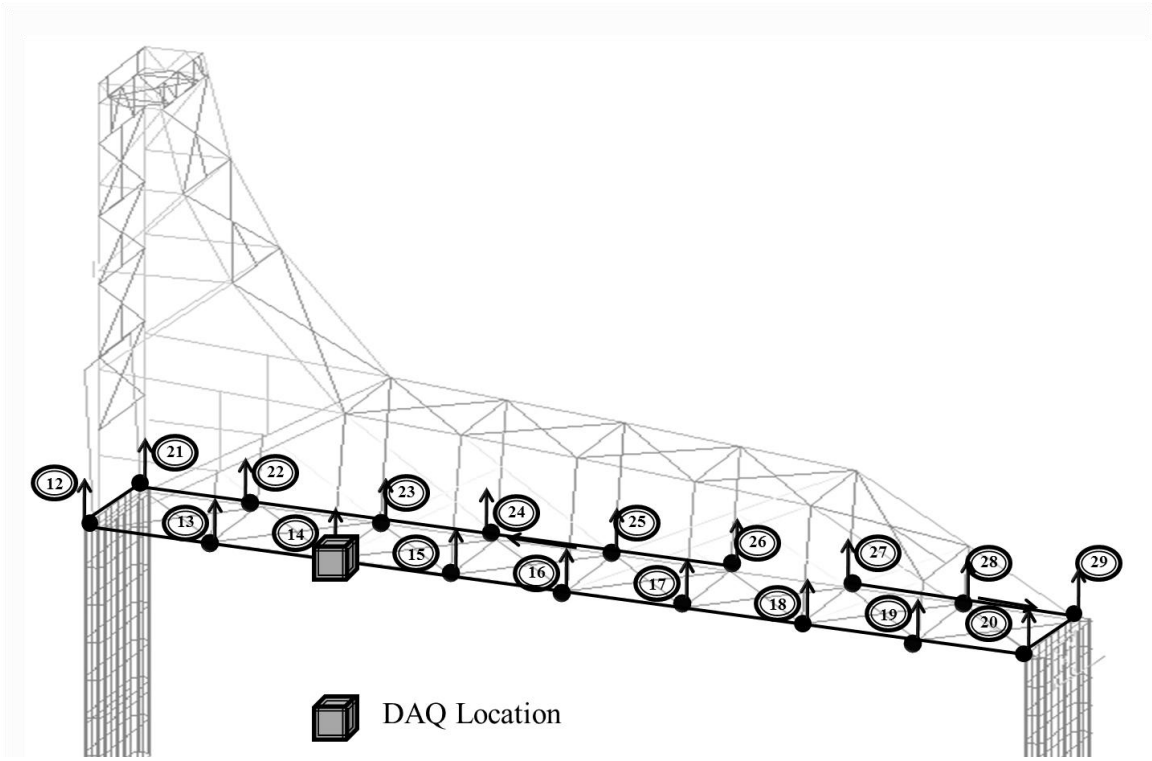

Figure 13-108: Tower Span Vertical Instrumentation Plan

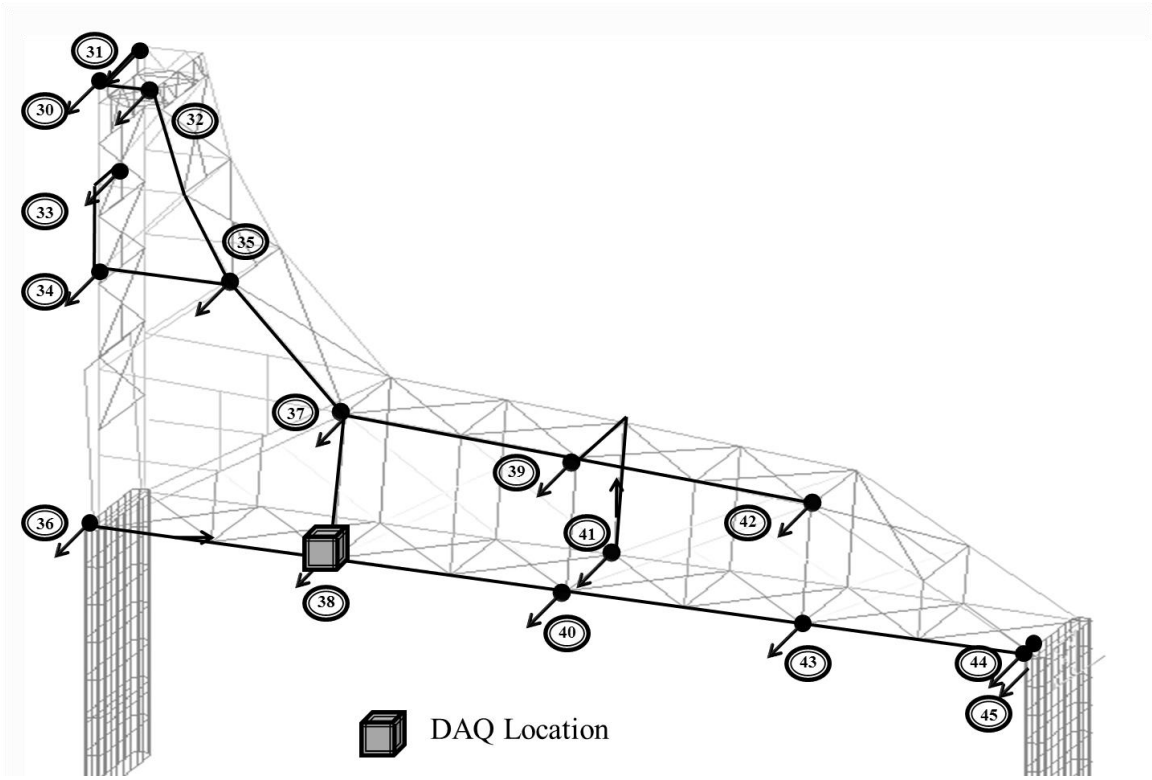

Figure 13-109: Tower Span Lateral Instrumentation Plan

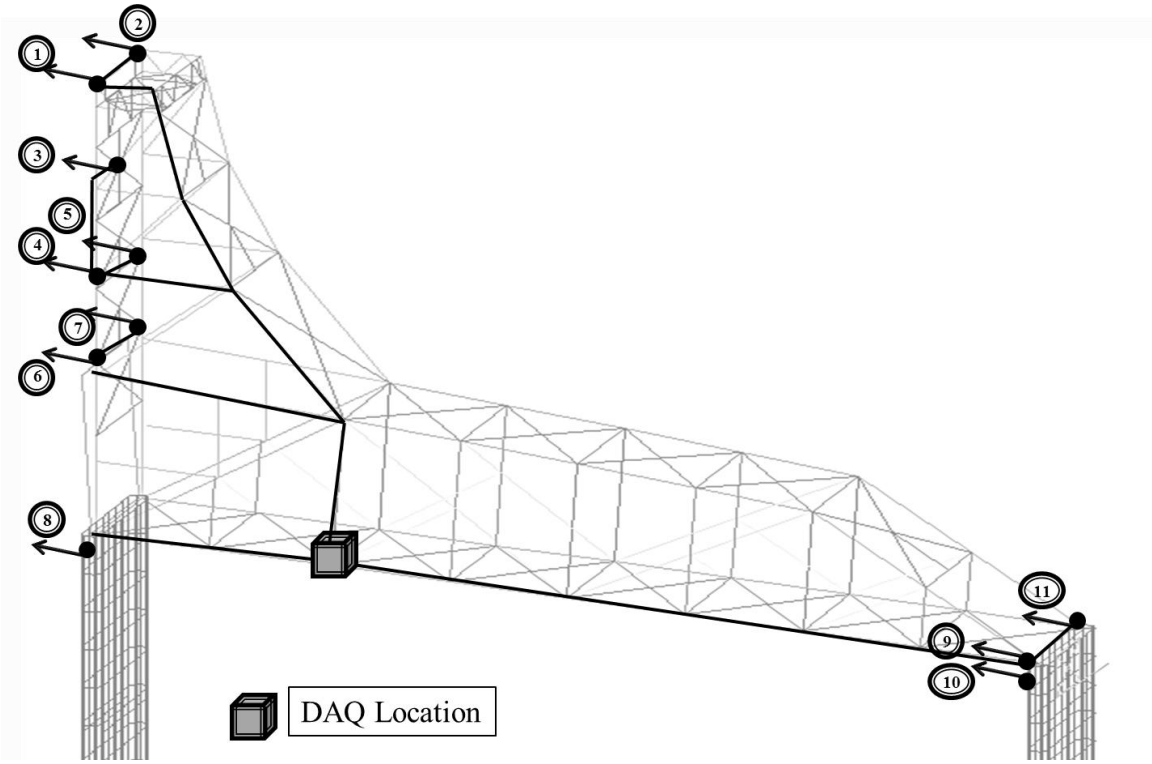

Figure 13-110: Tower Span Longitudinal Instrumentation Plan

The sensors located at 3 and 33, as indicated above, were planned to be installed on the counterweights of the tower span. This was aimed at capturing the degree of coupling between the counterweight and the tower span, as a direct measure to inform some of the uncertainties identified as model building blocks in Chapter 12.

13.4.1.3. Lift Span

The instrumentation design for the lift span required a more thorough analysis of the structure to determine the most efficient locations for sensor installation. The size of the structure prohibited a thorough instrumentation plan as utilized for the NJ truss and tower spans. To produce an efficient instrumentation plan for vibration monitoring, it is important to analyze a priori models for modeshape nodal points. The nodal points of a mode shape serve as poor monitoring locations since the magnitude of vibration will be very little. Therefore, a modal analysis was carried out using the SAP2000 a priori model to determine the nodal locations of the fundamental modeshapes associated with the lift span. The nodal points were plotted on a CAD drawing of the lift span for vertical modes (Figure 13-111) and lateral modes (Figure 13-112) associated with the first three modes after the first mode in each direction, which has no nodal points. While the supports are essentially nodal points for every mode, they are typically measured to capture any support movement.

The measurement points, also plotted on the nodal point diagrams, were selected based on their ability to intersect as few nodal points as possible. In some cases, it is not

possible to completely avoid nodal points however it is important to make sure that all sensors are not located at nodal points of certain modeshapes.

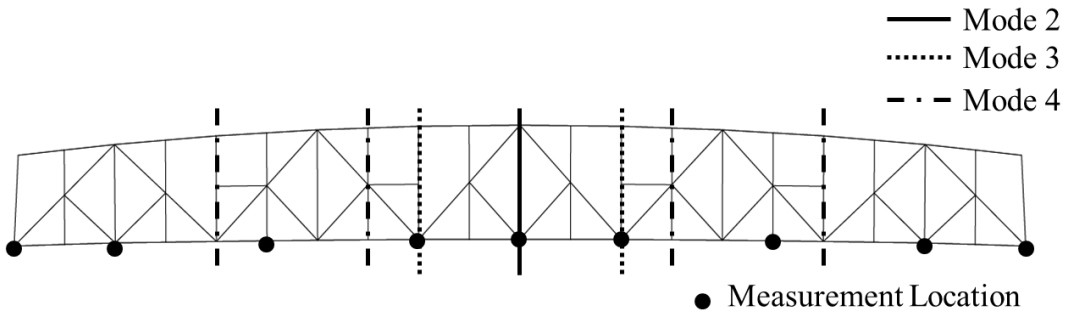

Figure 13-111: Elevation View of Lift Span Highlighting Nodal Locations Associated with Vertical Modes 2 through 4

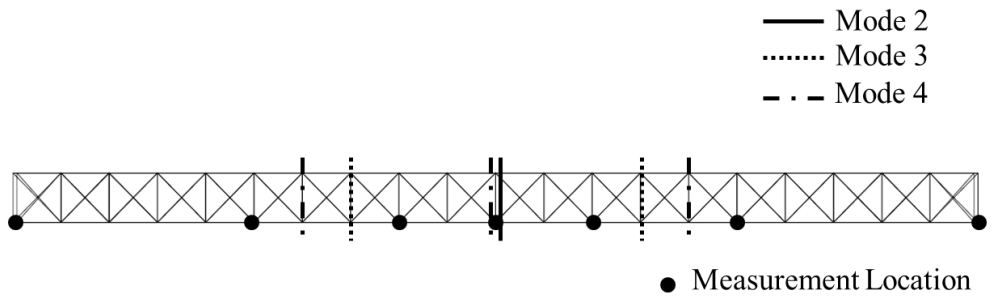

Figure 13-112: Plan View of Lift Span Highlighting Nodal Locations Associated with Lateral Modes 2 through 4

After the nodal points were explored for the lift span, the instrumentation plan could be fully conceptualized for the vertical (Figure 13-113), lateral (Figure 13-114), and longitudinal (Figure 13-115) measurements. The total number of sensors used on the lift span includes six longitudinal, twenty vertical and sixteen lateral accelerometers for a total of forty-two sensors.

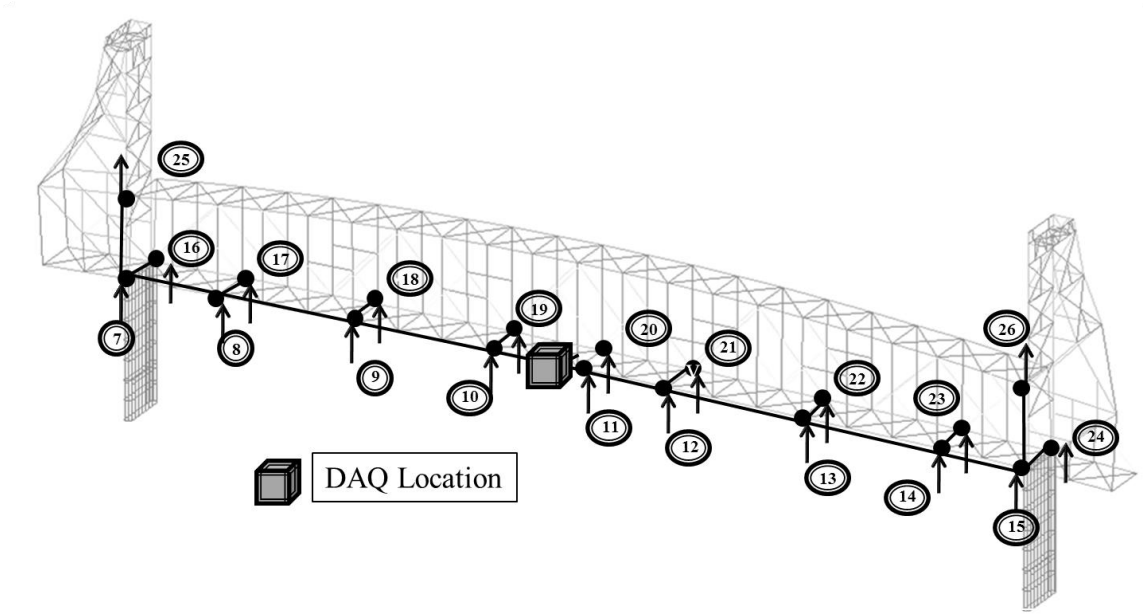

Figure 13-113: Lift Span Vertical Instrumentation Plan

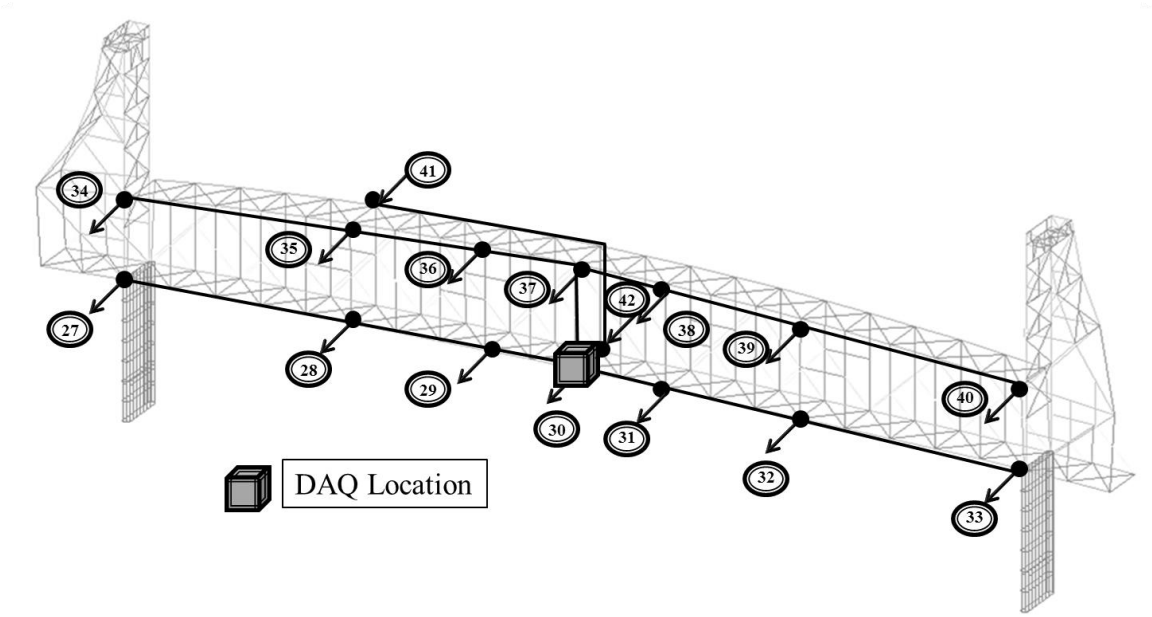

Figure 13-114: Lift Span Lateral Instrumentation Plan

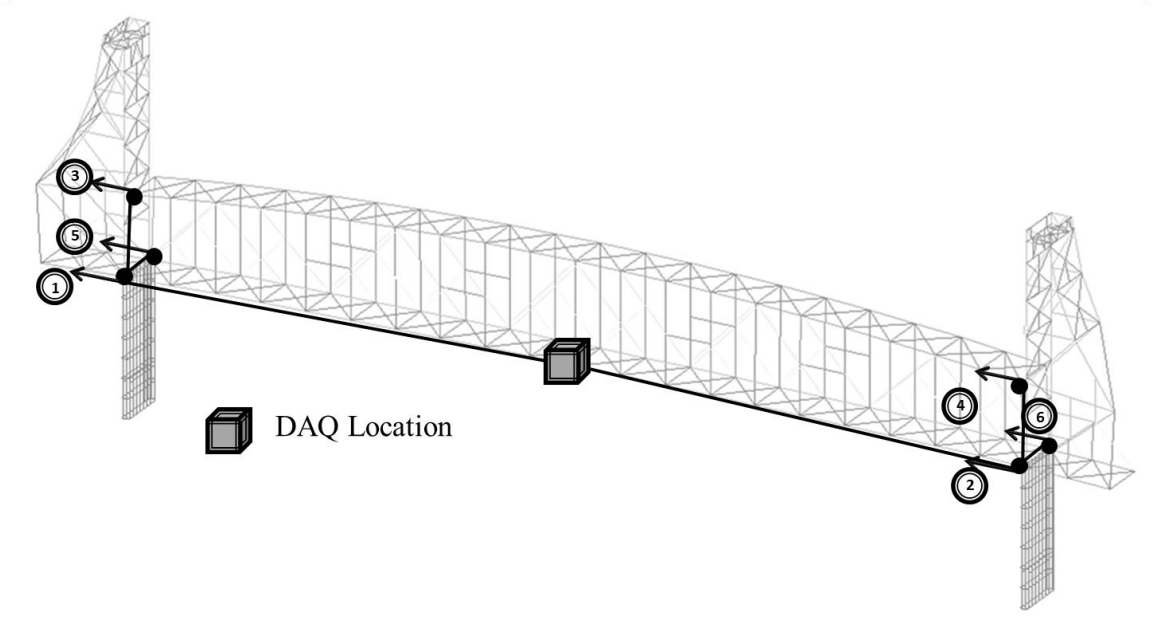

Figure 13-115: Lift Span Longitudinal Instrumentation Plan

13.4.1.4. PA Truss Spans

The instrumentation plan for the PA truss spans was developed with the knowledge that the NJ truss span was going to be densely instrumented. With this in mind, the PA truss spans were instrumented with a less dense instrumentation plan initially, with an option to deploy a more dense instrumentation if needed. The results from the PA truss spans could be compared to the NJ truss spans to identify frequencies which occur at similar magnitudes and the available modeshape information could be correlated to help identify the PA truss span modes.

The instrumentation plans for the vertical (Figure 13-116), lateral (Figure 13-117), and longitudinal (Figure 13-118) are shown below. The instrumentation required the use of twenty-four accelerometers in the vertical direction, thirteen accelerometers in the lateral direction and seven accelerometers in the longitudinal directions for a total of forty-four sensors.

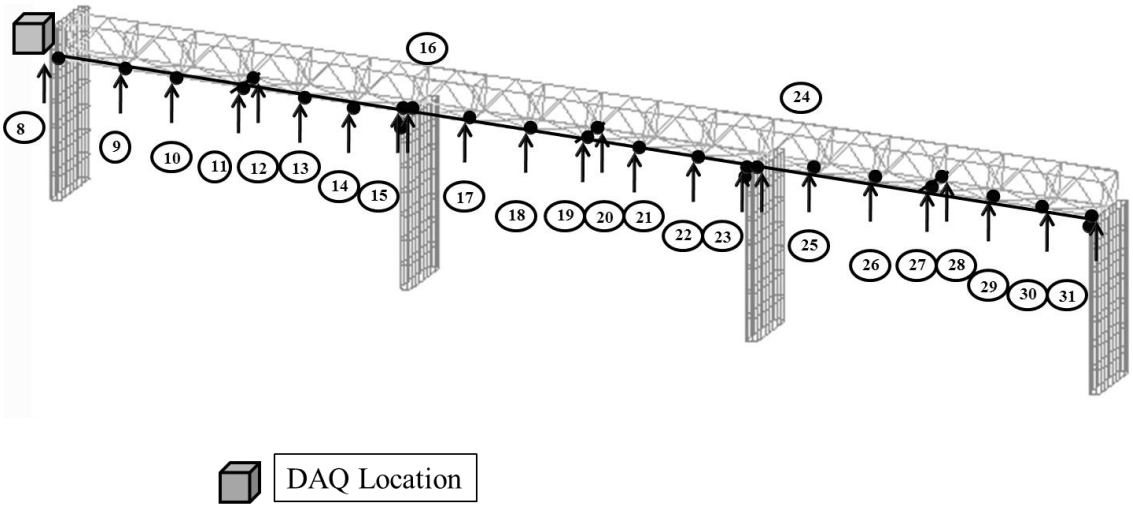

Figure 13-116: PA Truss Vertical Instrumentation Plan

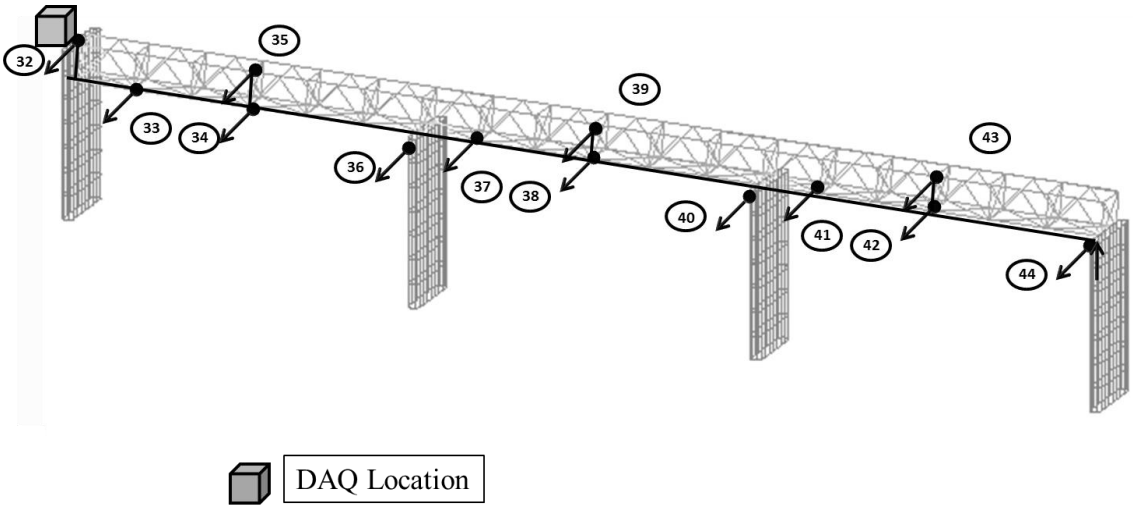

Figure 13-117: PA Truss Lateral Instrumentation Plan

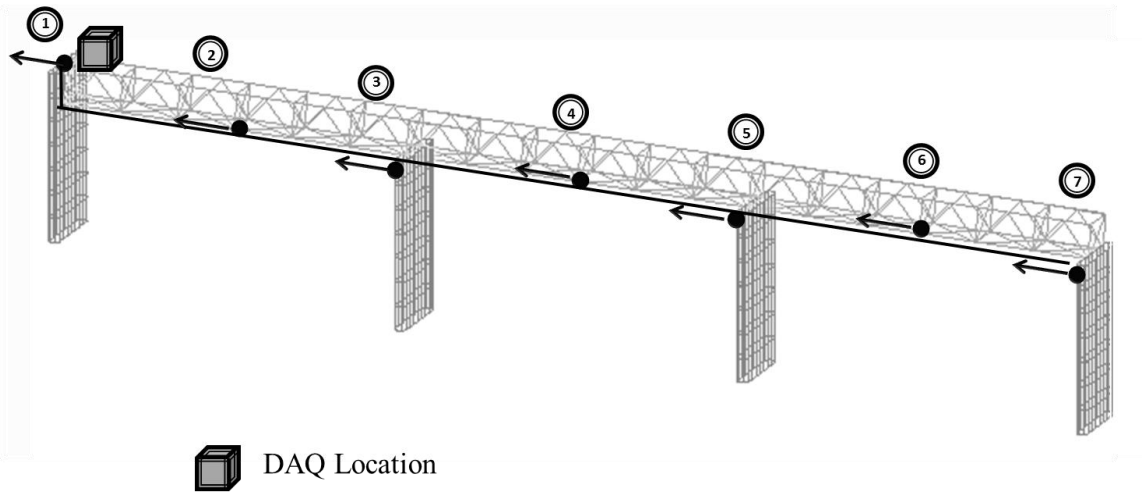

Figure 13-118: PA Truss Longitudinal Instrumentation Plan

Due to limitations in the number of available sensors and DAQ channels, the instrumentation spans shown above could not be carried out simultaneously. To implement the above instrumentation plans, a series of five set-ups were defined: (1) NJ Truss Span, (2) NJ Tower Span, (3) Lift Span, (4), PA Tower Span and (5) PA Truss Span.

13.4.2. Design of Data Acquisition

The data acquisition for the BBB ambient vibration monitoring effort was designed based on the results of the preliminary ambient vibration monitoring study. While the frequency bands of the structure fell far below the Nyquist frequency for the sampling rate used at the time, there was significant acceleration clipping which could compromise an acceleration magnitude study. For this reason, it was decided to increase the sampling rate of the full ambient vibration monitoring study to 200 Hz.

The data acquisition used was the same HBM MGCplus data acquisition system used for the preliminary study, this time with an increased number of cards giving a total capacity of forty-eight sensors. The sensors comprised 30 PCB 393C piezoelectric accelerometers and 15 PCB 3701 capacitive accelerometers. The PCB 393C accelerometers have a measurement range of +/- 2.5g and a frequency range of 0.025 – 800Hz. The PCB 3701 accelerometers have a +/- 3g measurement range and a frequency range of 0 – 100Hz.

To fully capture the peak rush hour traffic excitation for the BBB, which was identified as the period of time between 5:30AM and 10:30AM during weekdays by the top chord strain monitoring system, the data acquisition system was set to record for a period of at least twenty-four hours for each of the five set ups. To minimize the size of the data files, the DAQ system was configured to automatically write a new data file after a period of one hour. This also allowed for easy retrieval of the data during periods of the day when traffic is the heaviest.

The DAQ locations were defined in the instrumentation plans so that cable lengths could be computed ahead of time. Drexel University research staff then compiled a set of

standard cable lengths, and defined which combination of cable lengths were required to go from each sensor to the data acquisition location.

13.4.3. Field Work

On July 12, 2009 a kick-off meeting was held to discuss the anticipated schedule for the five instrumentation set ups, best practice approaches to installing sensors and running cables, safety guidelines specific to the BBB environment and to ensure all team members had met each other. The engineer of record for the BCBC provided team members for assistance due to the anticipated workload.

On July 13, 2009 the Drexel University research team travelled to the bridge and began the first phase of instrumentation on the NJ truss span. The installation of sensors and running of cables for each of the five set ups followed the same guidelines. Due to the entire superstructure being of steel construction, it was possible to utilize the magnetic bases for the sensors. For sensors which were installed on truss members, the magnetic bases were used to simply mount them to a cleaned steel surface (Figure 13-119).

Figure 13-119: A PCB 393C Accelerometer Installed with a Magnetic Base to the Top of the NJ Tower Span

The measurements which were planned on occurring at the tops of Piers 2, 3, 4, 5, 6, 7 and 8 were mounted by magnetically attaching the sensors to the masonry plates mounted directly to the tops of the piers (Figure 13-120). In cases where the longitudinal movement of the expansion bearing was to be measured, the sensor was installed on the gusset plate connection above the bearing. This way, the accelerometers did not need to be modified to mount to the concrete, which would have increased the time needed for installation and tear down of the sensors.

Figure 13-120: A PCB 393C Accelerometer (R) and a PCB 3701 Accelerometer (L) Mounted to the Masonry Plate of a Bearing to Measure the Response of the Pier Cap

The cables were run in a manner which was organized and out of the way of maintenance staff or Drexel University personnel. Additionally, the cables were mounted and supported as often as possible to reduce the effects of wind or the cables being pulled taught by excessive span lengths (Figure 13-121). The bundled cables were fastened to the structures with spring-loaded hand clamps and wire ties.

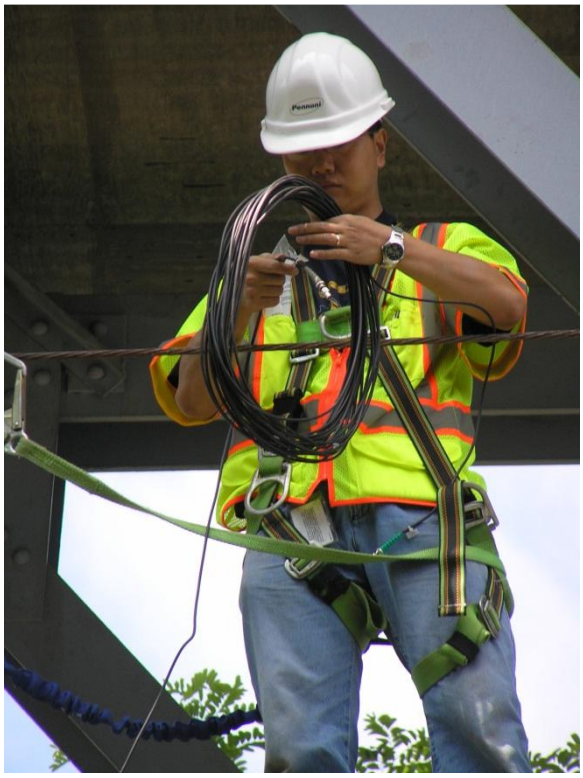

Figure 13-121: Drexel University Research Staff Installing Cables

After all cables were installed and sensors were mounted for a given set up, the sensors were attached to the coaxial cables with a small microdot connection (Figure 13-122). This connection required extra fastening so that the wind did not interfere with the connectors. Typically, the hard connectors were wire-tied to the structure so that the wires were not accidentally cut.

Figure 13-122: Microdot Cable Fastened to a Gusset Plate Connection with a Hand Clamp

The DAQ station was set up on the sidewalk for each of the five sensor configurations. Considering the sidewalk for the entire BBB structure is fairly narrow, it was important to maintain a DAQ station which was safe to the traffic as well as to the DAQ operator. For this reason, the DAQ was placed inside a steel cabinet (Figure 13-123) and positioned in a manner so that the operator was always facing traffic and was protected from flying debris by the cabinet. Additionally, any time the cabinet was in use it was required that Drexel research staff have a flagger on hand to watch for traffic which might strike the operator and alert them to move out of the way. In this manner, Drexel

staff was able to maintain a safe work zone and prevent any unnecessary injuries from occurring.

Figure 13-123: Data Acquisition Cabinet with Equipment Inside

Figure 13-124: DAQ System under Interrogation by Research Staff on Bridge

13.4.4. Data Processing

The vibration data from each setup was preliminarily processed after each period of recording was complete and before the sensors and cables were moved. The data was processed in the same manner as the preliminary vibration survey to evaluate the quality of the measurements. A power spectral density (PSD) was generated for each of the sensors, grouped by their orientation. The final data processing was performed using commercial software, LMS Operational Modal Analysis, to perform the signal processing and frequency and modeshape extraction. The vibration signals were processed using the Stochastic Subspace Index (SSI) algorithm for identifying frequencies and modeshapes by a Drexel University research associate.

An independent review of the LMS data processing was performed by another Drexel University research team member using a manual CMIF based approach to analyze the vertical and torsional modeshapes. The results of the PSD studies are presented below and a listing of the final presentation of results is discussed in the next subsection.

13.4.4.1. NJ Truss Span Time History and PSD Analysis

The time histories for the NJ Truss span (Figure 13-125, Figure 13-127 and Figure 13-129) are plotted from a recording of traffic events over the period of 5:45AM to 6:45AM on July 17, 2009. A plot showing a few specific events is also shown underneath a plot of the entire time history for each of the respective acceleration directions (Figure 13-126, Figure 13-128 and Figure 13-130).

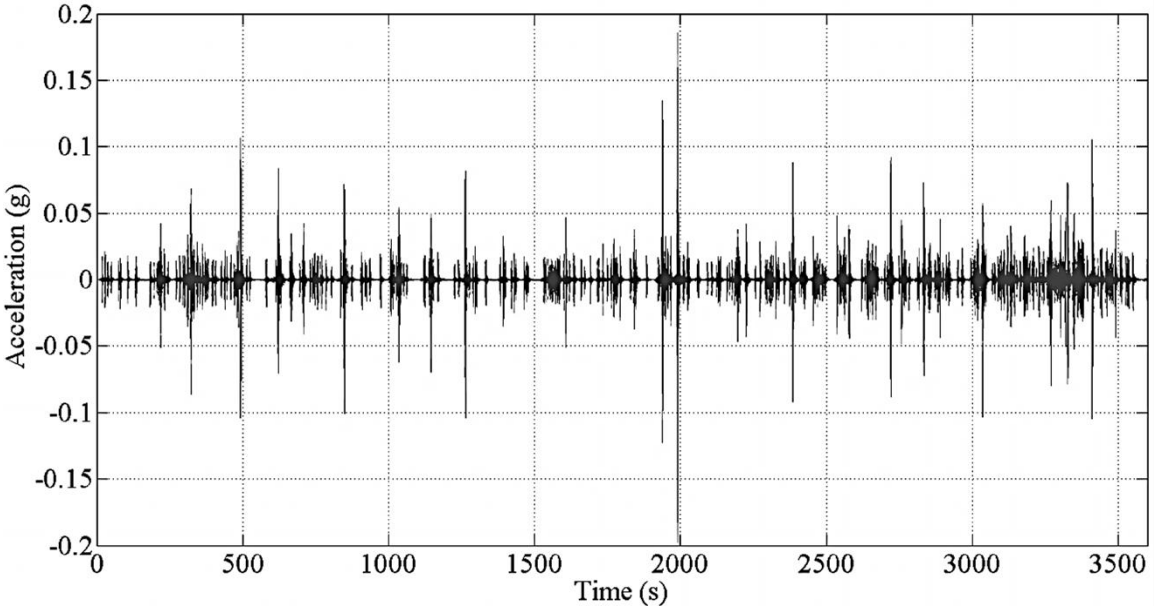

Figure 13-125: NJ Truss Span Vertical Acceleration Time History (Channel 8)

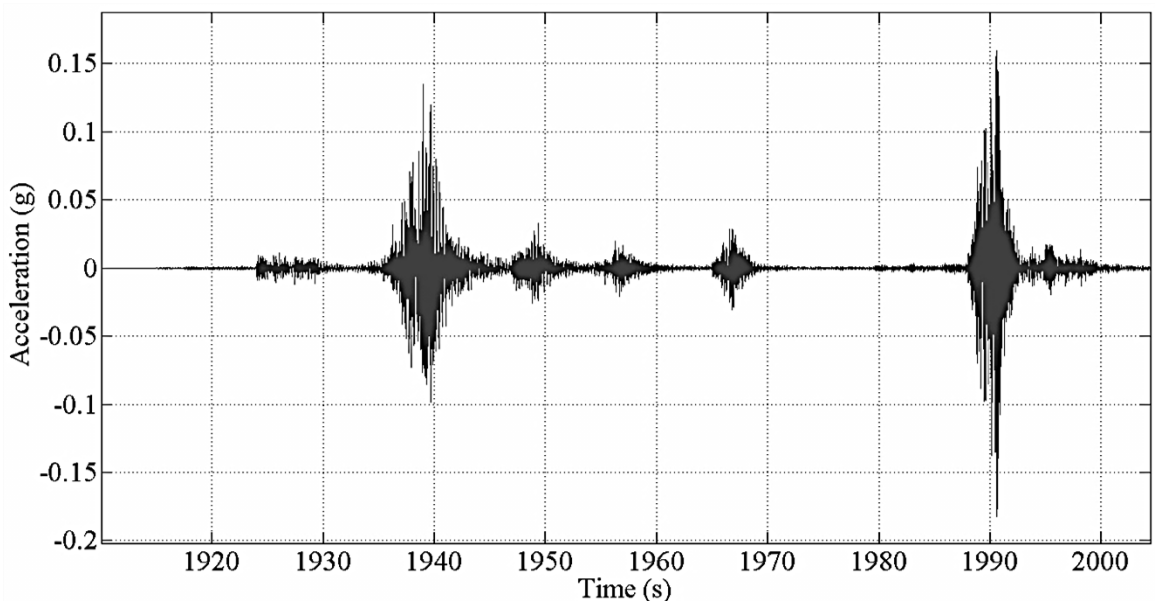

Figure 13-126: NJ Truss Span Vertical Acceleration Time History of a Traffic Event (Channel 8)

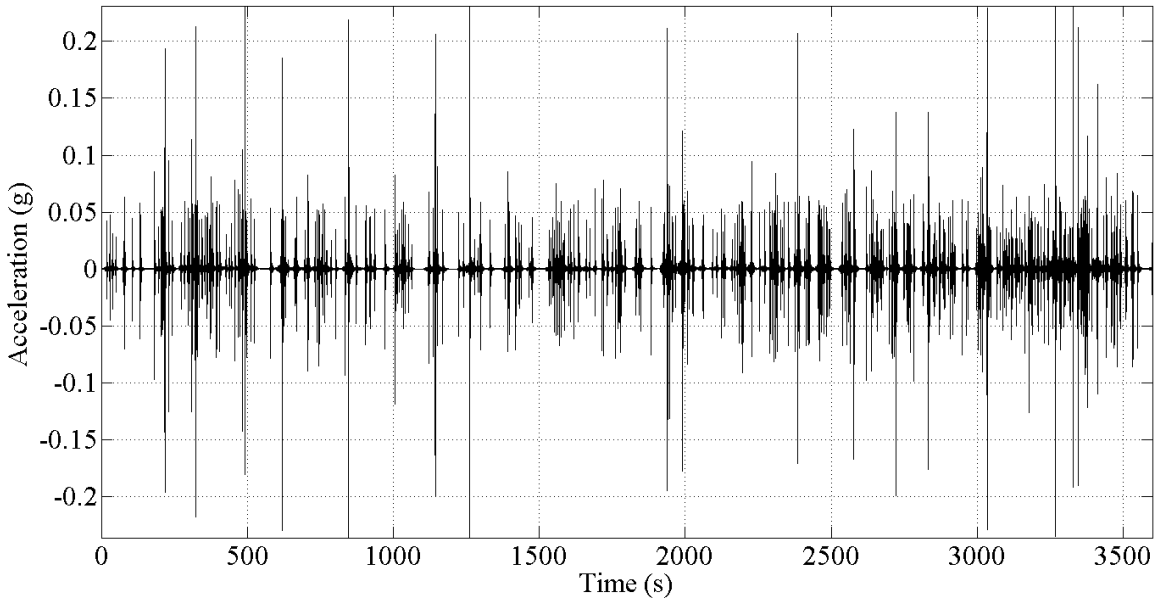

Figure 13-127: NJ Truss Span Lateral Acceleration Time History (Channel 29)

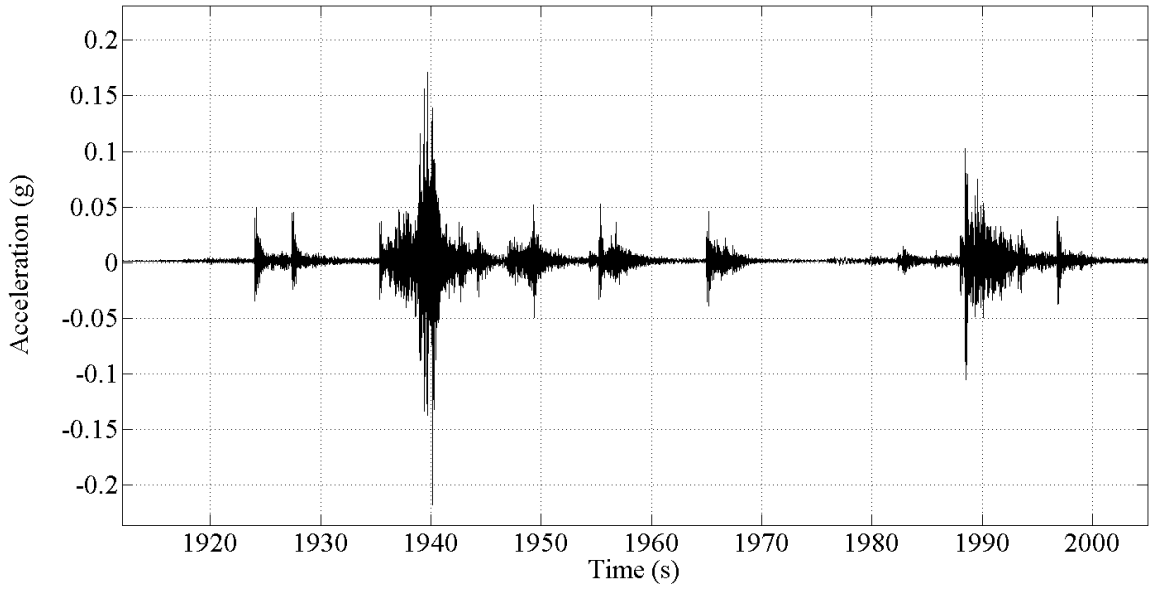

Figure 13-128: NJ Truss Span Lateral Acceleration Time History of a Traffic Event (Channel 29)

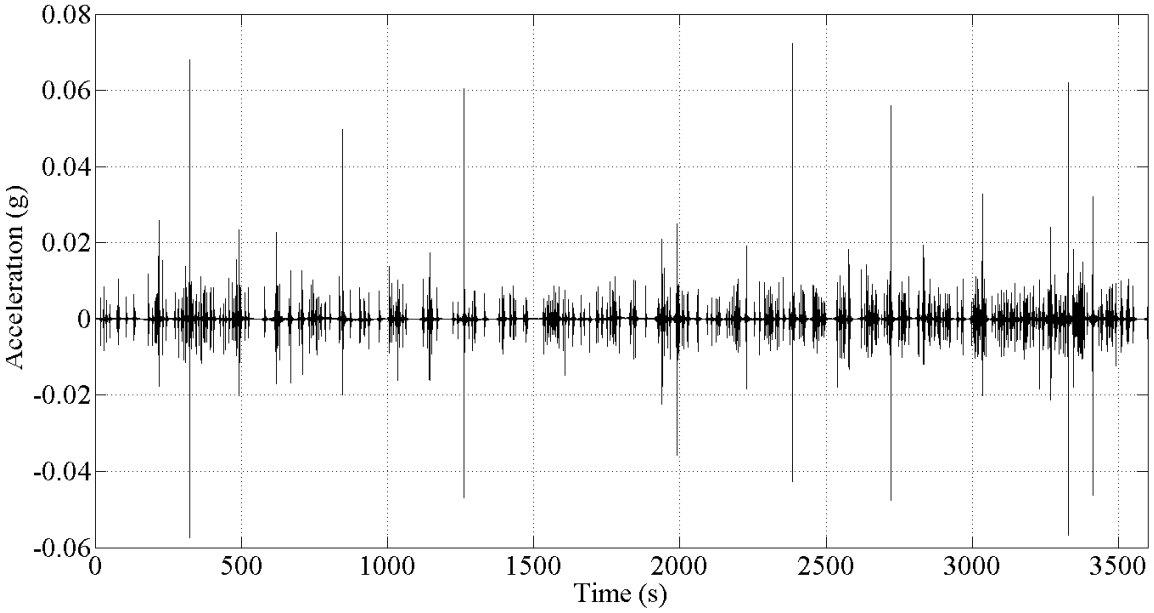

Figure 13-129: NJ Truss Span Longitudinal Acceleration Time History (Channel 1)

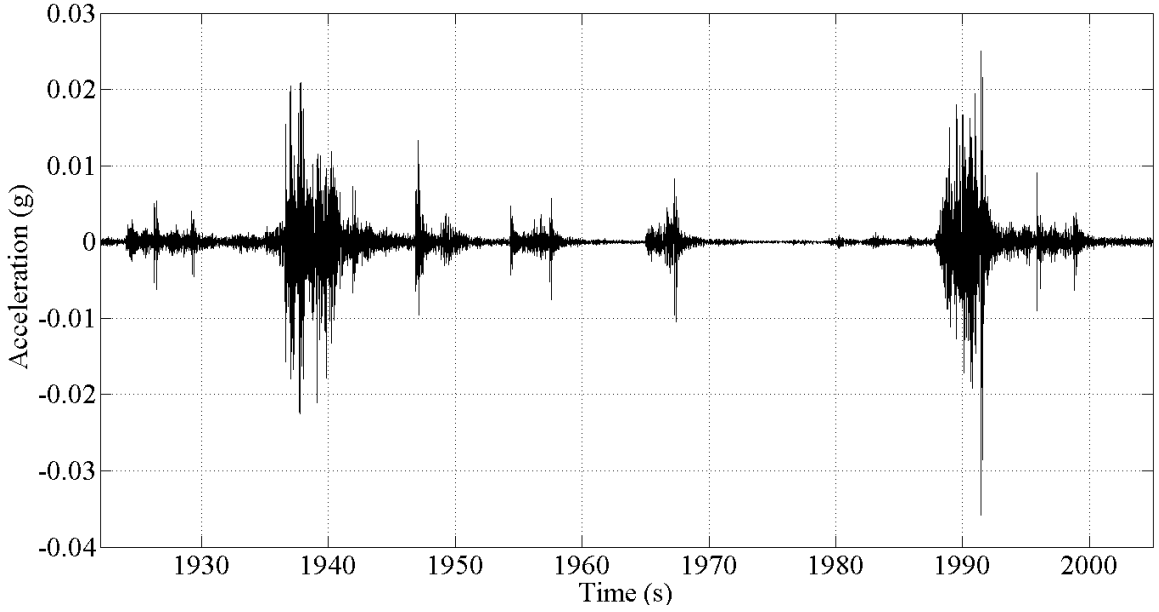

Figure 13-130: NJ Truss Span Longitudinal Acceleration Time History of a Traffic Event (Channel 1)

The time histories show that the magnitude of the lateral acceleration is the highest over this period of time for the NJ Truss span, with maximum response just above 0.2g. The vertical acceleration showed the next highest response with a magnitude of around 0.1g. The longitudinal acceleration saw limited events giving maximum magnitude response of about 0.06g, however more consistently fell within the +/- 0.02g range. To explore the frequency content of these signals, the PSD's for each of the time histories was computed and shown in Figure 13-131, Figure 13-132 and Figure 13-134. In Figure 13-133 a close-up plot of the 0 – 10Hz range is shown since the magnitude of the pole at approximately 13.5Hz exhibits much greater power and dominates the plot.

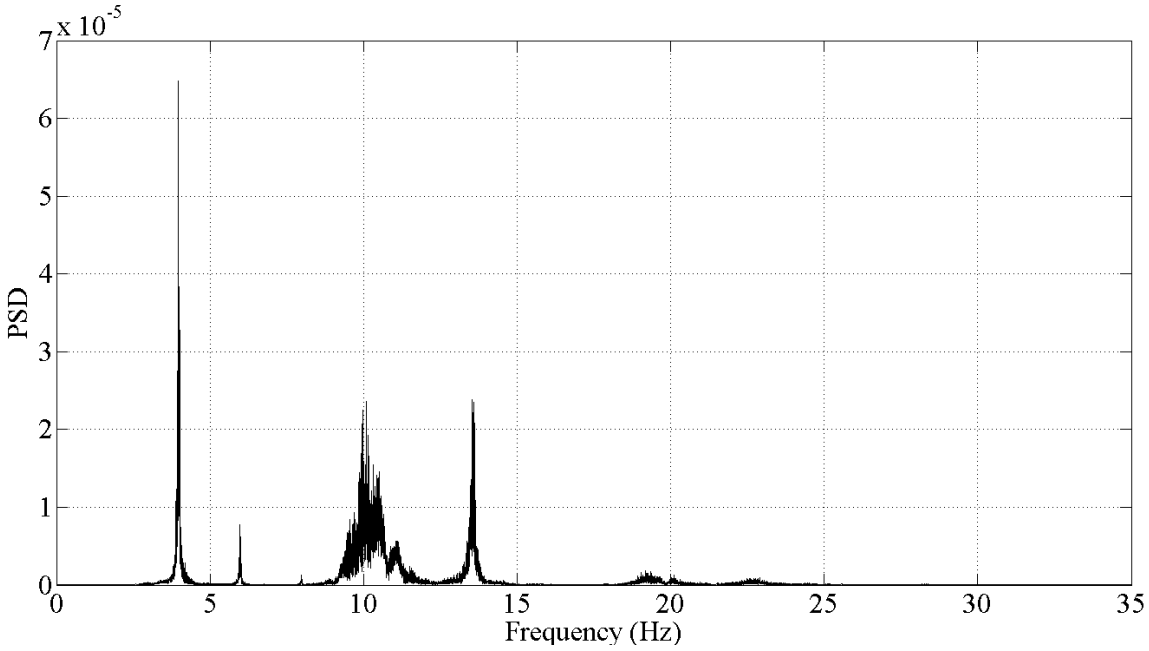

Figure 13-131: PSD of Vertical Truss Response

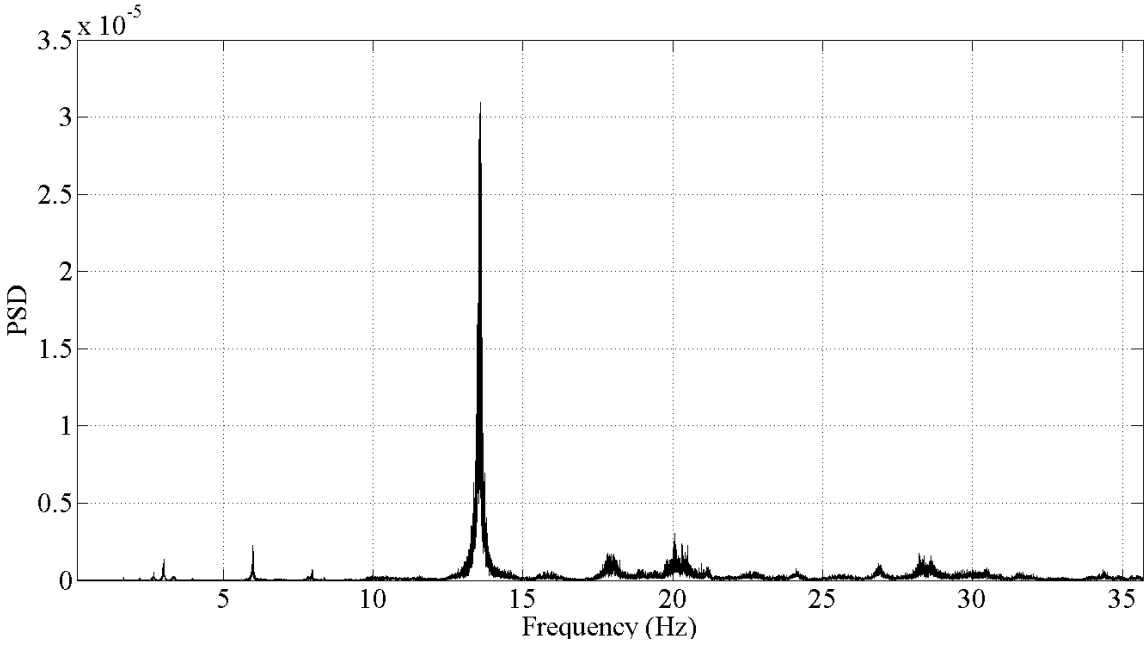

Figure 13-132: PSD of Lateral Truss Response

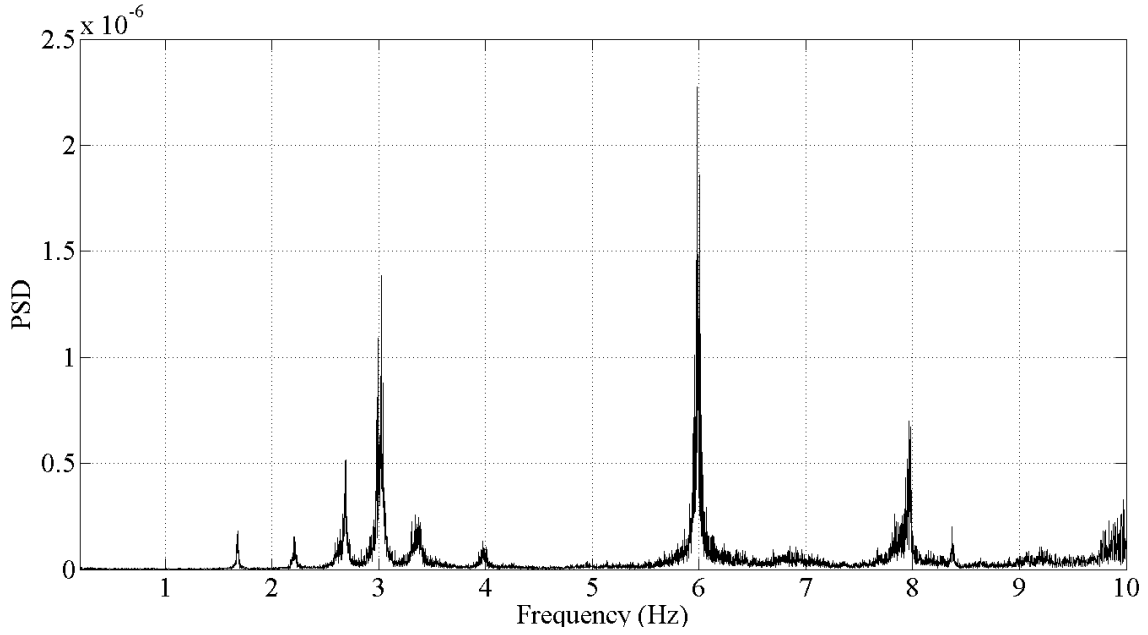

Figure 13-133: PSD of Lateral Truss Response - 0 - 10Hz Range

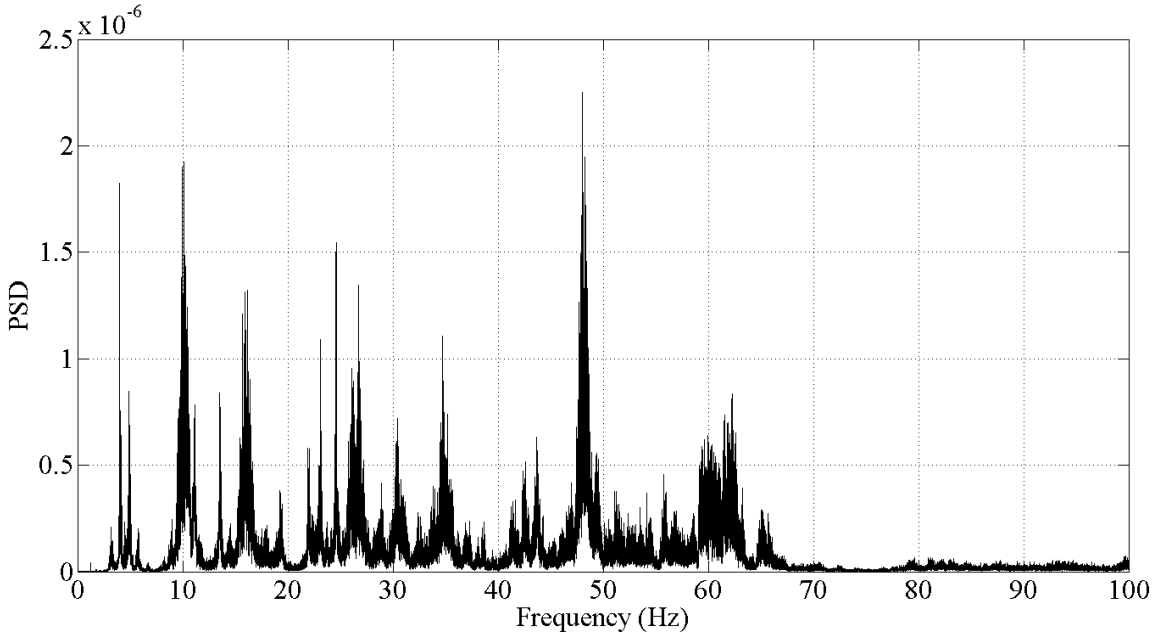

Figure 13-134: PSD of Longitudinal Truss Response

The acceleration time histories and respective PSD analyses indicated good data quality and the setup could be removed from the structure and moved to the next span. Clear poles existed in the vertical and lateral directions, while the longitudinal responses indicated low power levels of response and were most likely correlated with vertical and lateral modeshapes.

13.4.4.2. NJ Tower Span Time History and PSD Analysis

The time histories from the period of 6:44AM to 7:44AM are plotted in **Figure 13-135**, **Figure 13-137** and **Figure 13-139**. A zoomed in plot around a specific event is shown in

under each respective full time history plot for each measurement direction in Figure 13-136, Figure 13-138 and Figure 13-140.

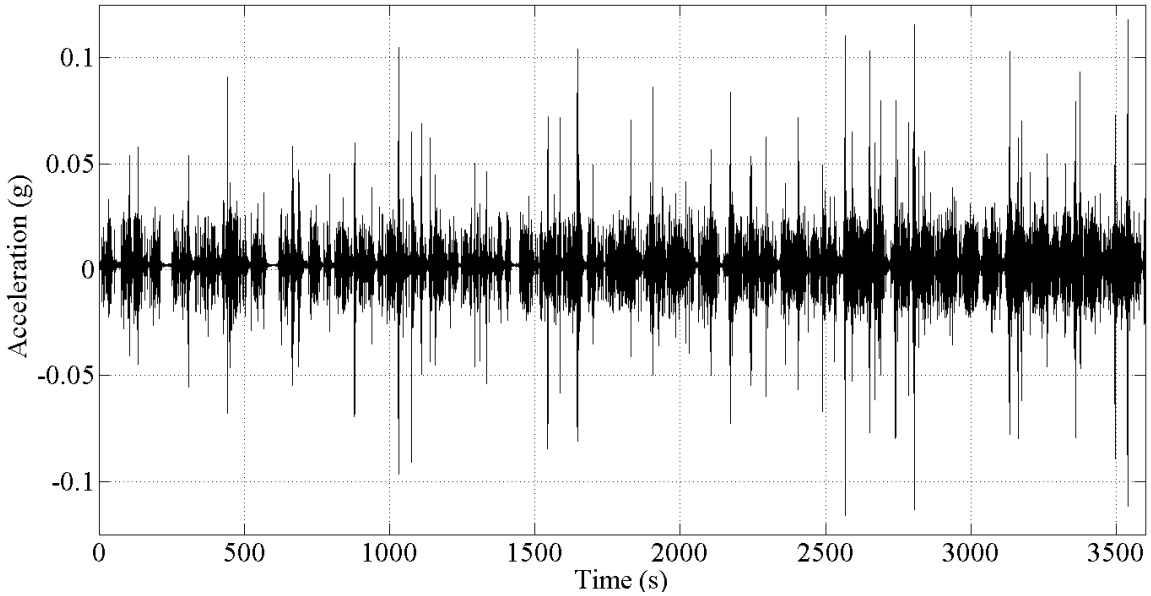

Figure 13-135: NJ Tower Span Vertical Acceleration Time History (Channel 27)

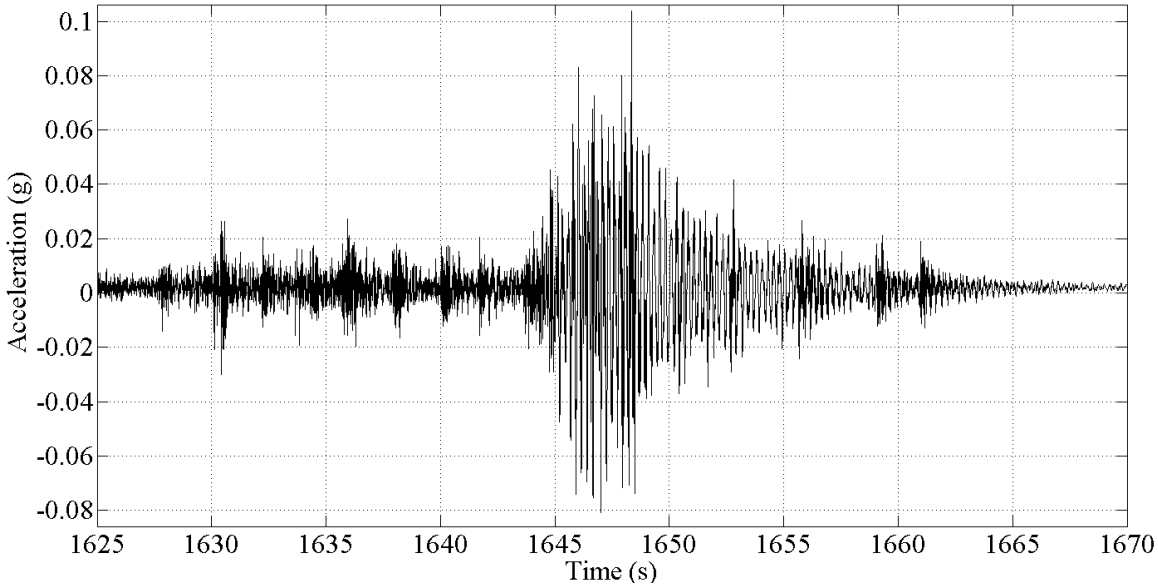

Figure 13-136: NJ Tower Span Vertical Acceleration Time History of a Traffic Event (Channel 27)

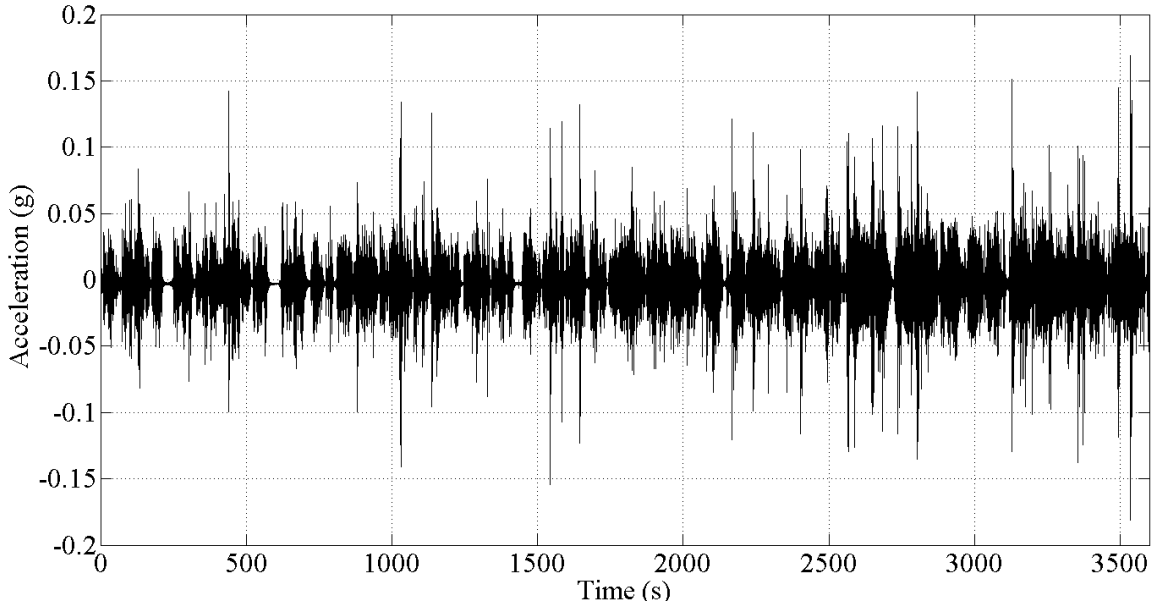

Figure 13-137: NJ Tower Span Lateral Acceleration Time History (Channel 38)

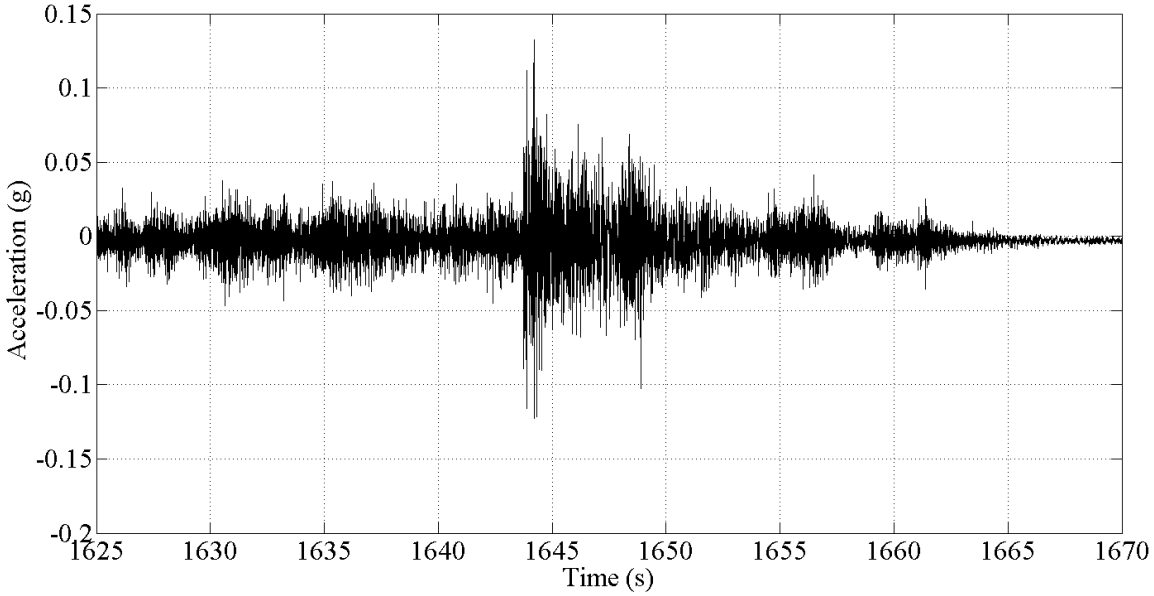

Figure 13-138: NJ Tower Span Lateral Acceleration Time History of a Traffic Event (Channel 38)

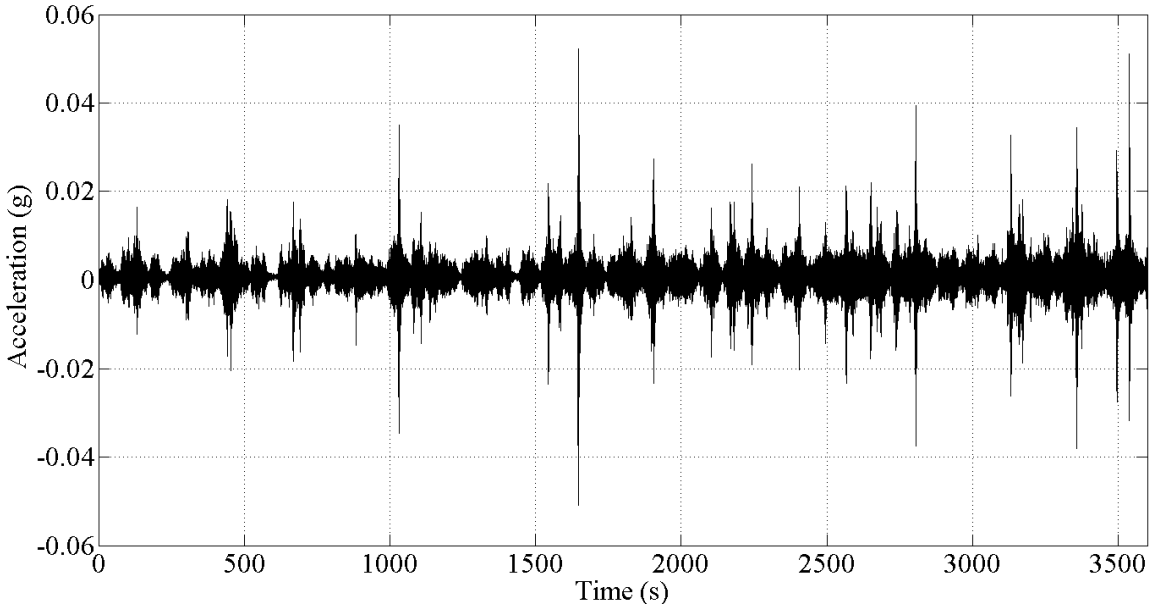

Figure 13-139: NJ Tower Span Longitudinal Acceleration Time History (Channel 1)

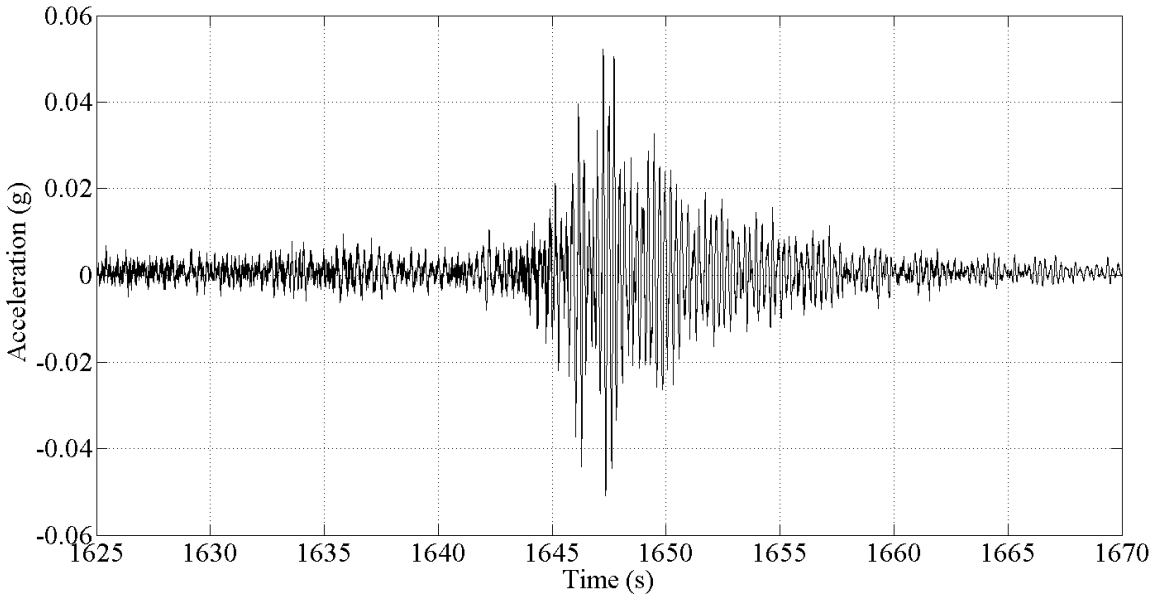

Figure 13-140: NJ Tower Span Longitudinal Acceleration Time History of a Traffic Event (Channel 1)

For the NJ Tower span, the lateral acceleration response of the truss once again showed slightly higher magnitudes than the vertical response. The longitudinal varied depending on the location of the sensors. At the top of the tower, Channel 1, the response was the smallest. However, at Channels 4/5 and 6/7 the acceleration magnitudes were incrementally larger. This phenomenon is most likely due to the fact that the top of the tower spans is restrained by the counterweight cables stretching over the sheaves located at the top of the tower. The PSD for each signal was computed to check for frequency content before the setup was torn down and is shown in Figure 13-141, Figure 13-142 and Figure 13-143.

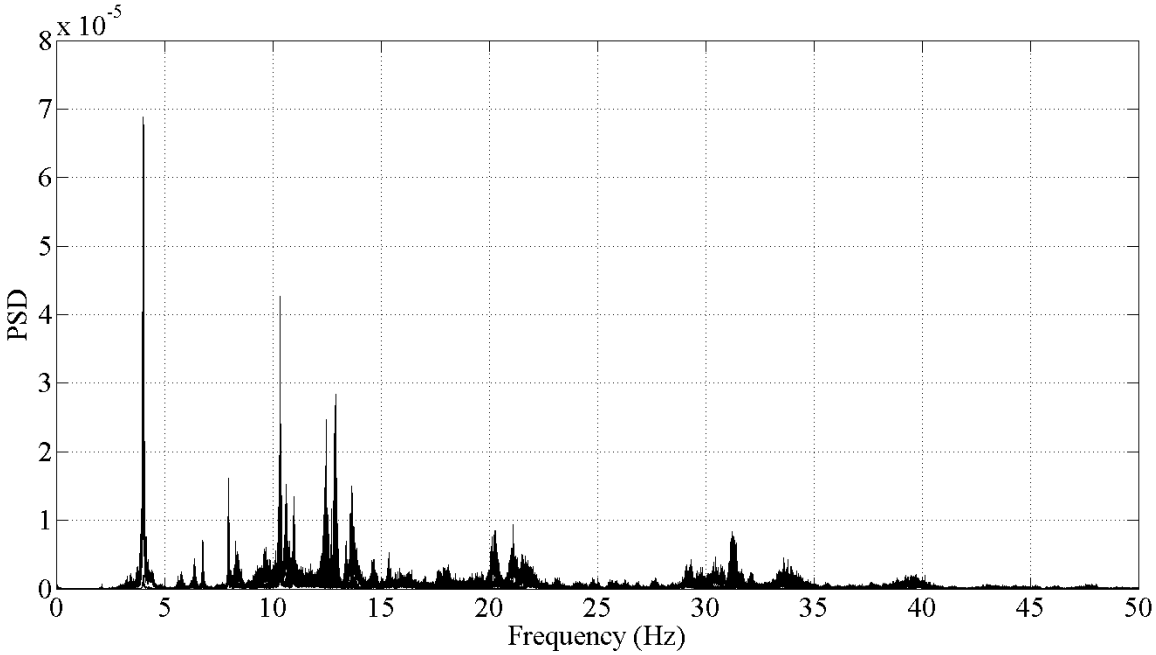

Figure 13-141: PSD of NJ Tower Span Vertical Response

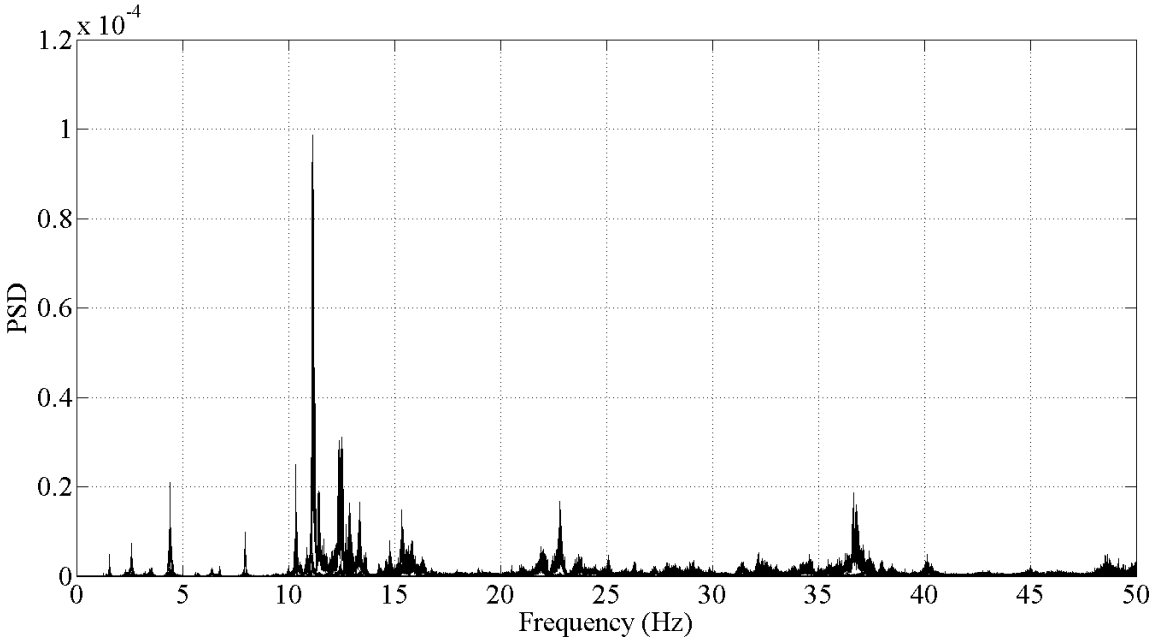

Figure 13-142: PSD of NJ Tower Span Lateral Response

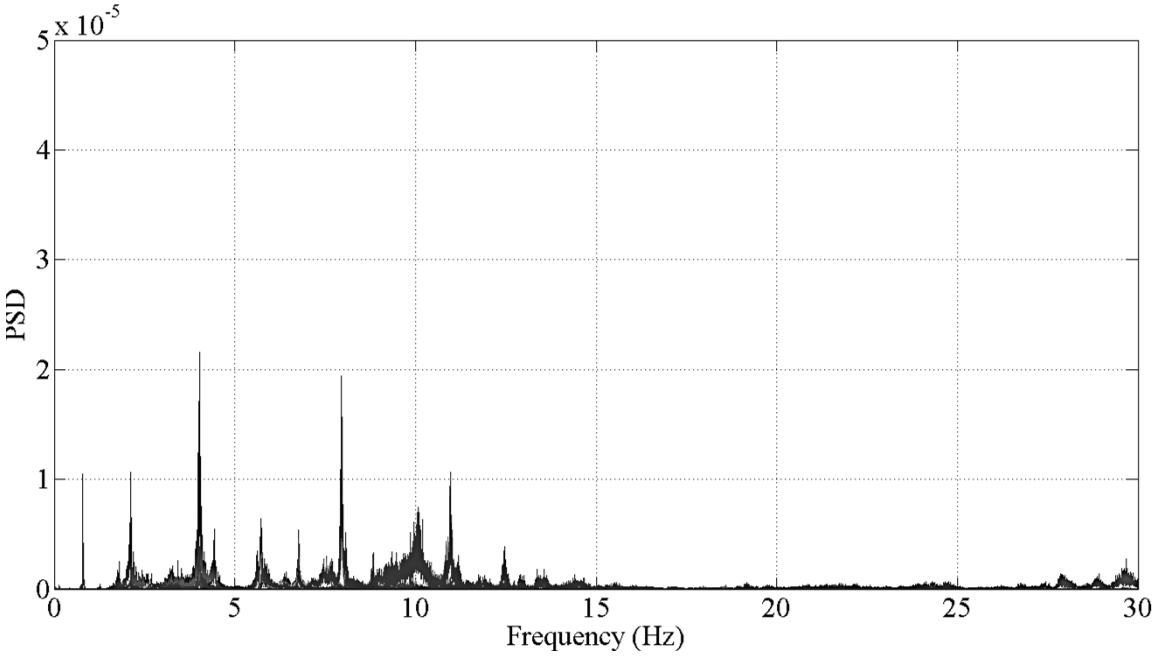

Figure 13-143: PSD of NJ Tower Span Longitudinal Response

Once again, the time history and PSD analysis showed that the vibration response collected for the NJ Tower span was of sufficient quality to proceed with the ambient vibration monitoring project and move to the lift span. Once again, the lateral vibration response of the NJ tower span was slightly higher than its vertical acceleration response due to the traffic input. The longitudinal response was more significant for the NJ tower span due to the coupling between longitudinal movement of the tower and vertical movement of the roadway truss.

13.4.4.3. Lift Span Time History and PSD Analysis

The time histories from the period of 6:38AM to 7:38AM are plotted in Figure 13-144, Figure 13-146 and Figure 13-148. A zoomed in plot around a specific event is shown in under each respective full time history plot for each measurement direction in Figure 13-145, Figure 13-147 and Figure 13-149.

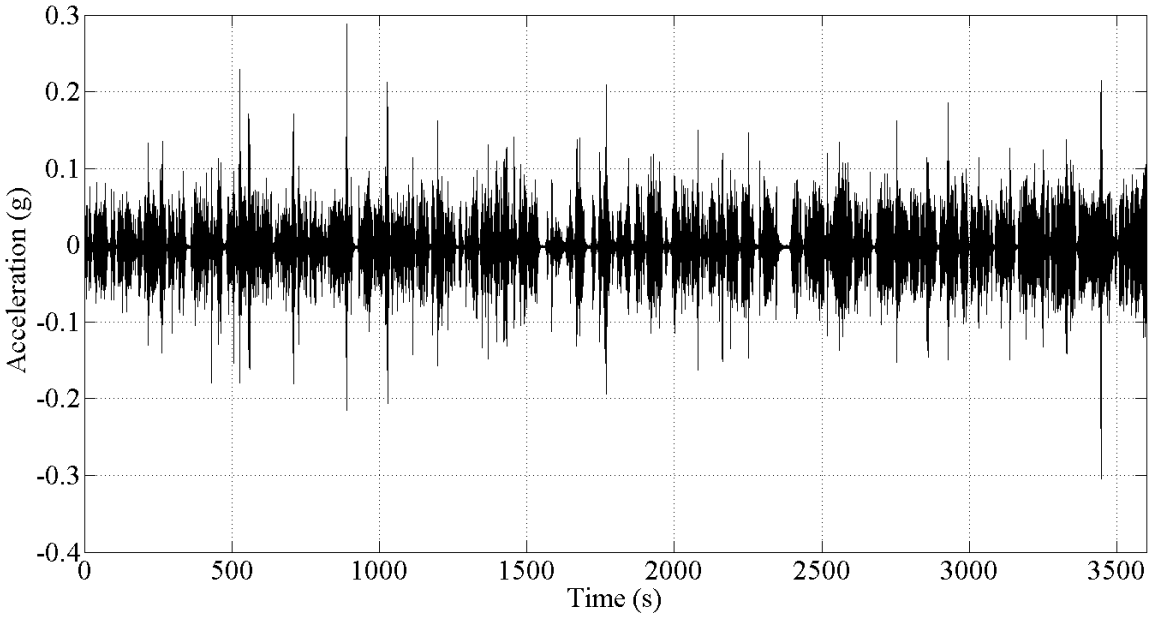

Figure 13-144: Lift Span Vertical Acceleration Time History (Channel 9)

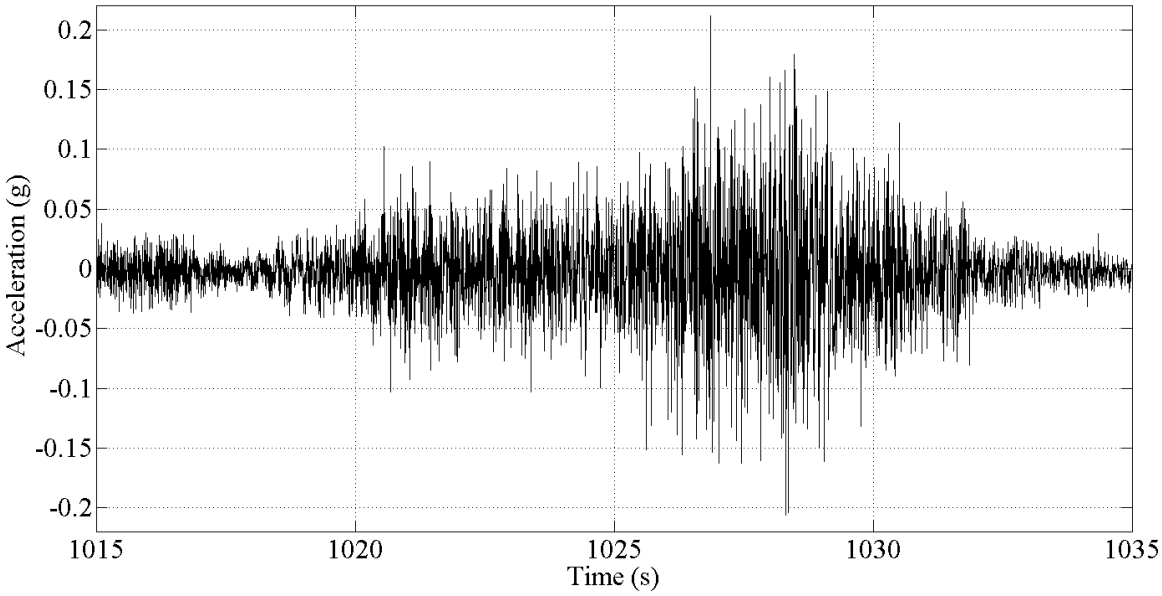

Figure 13-145: Lift Span Vertical Acceleration Time History of Traffic Event (Channel 9)

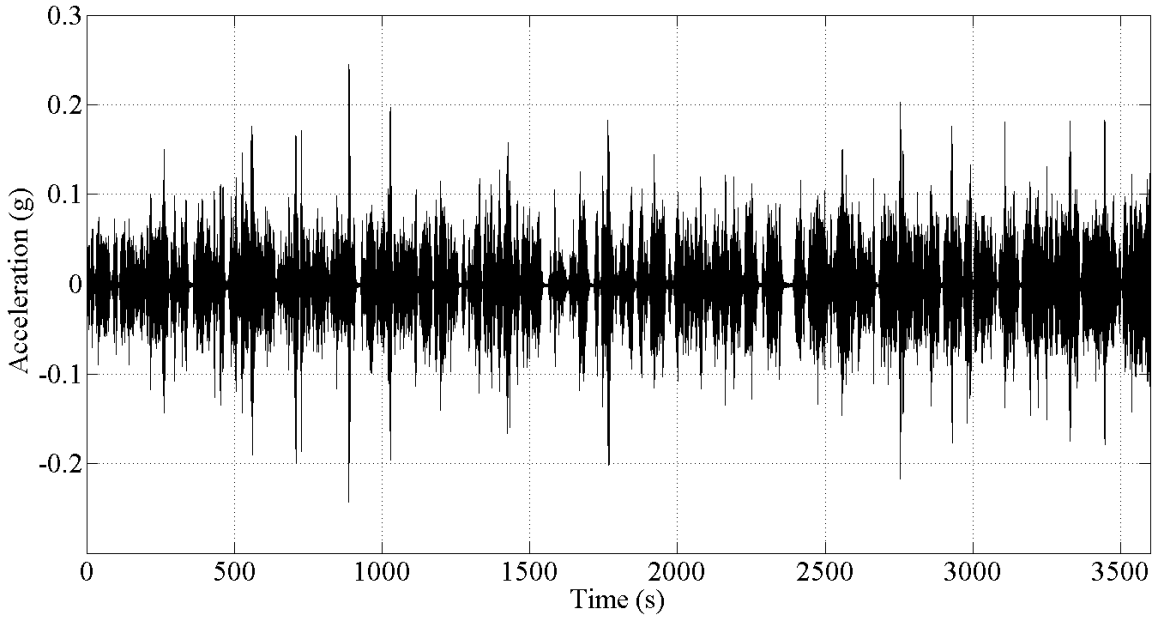

Figure 13-146: Lift Span Lateral Acceleration Time History (Channel 41)

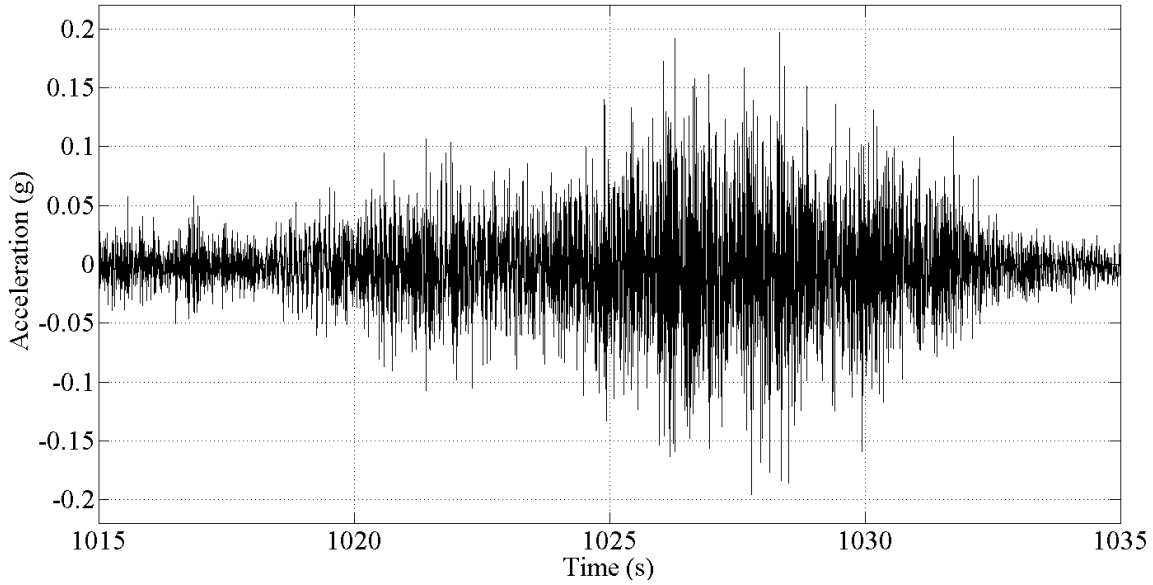

Figure 13-147: Lift Span Lateral Acceleration Time History of Traffic Event (Channel 41)

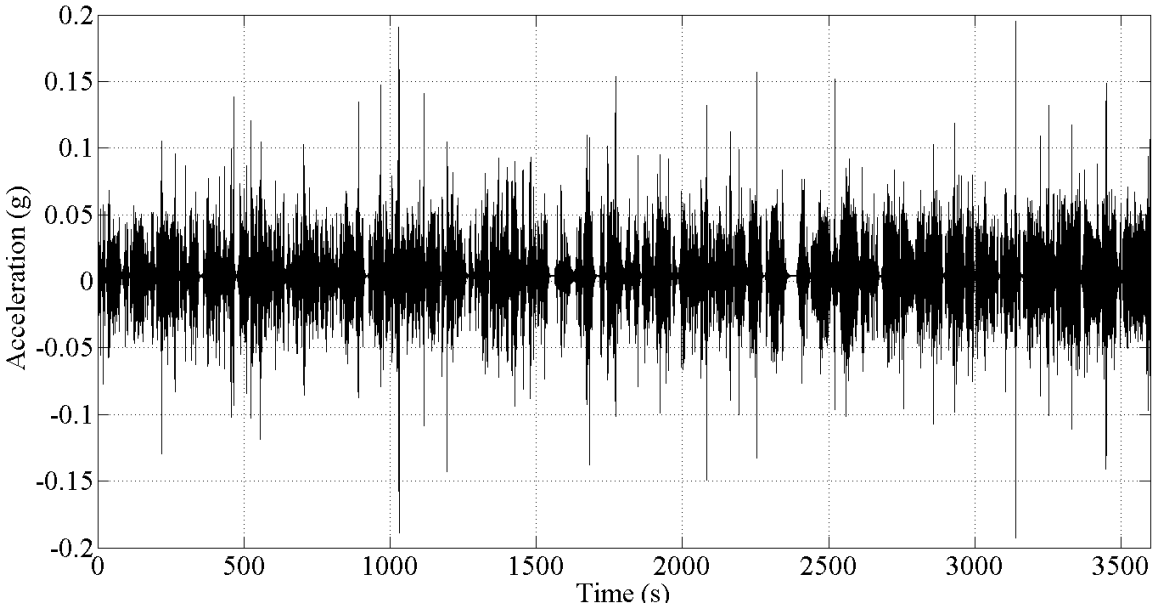

Figure 13-148: Lift Span Longitudinal Acceleration Time History (Channel 5)

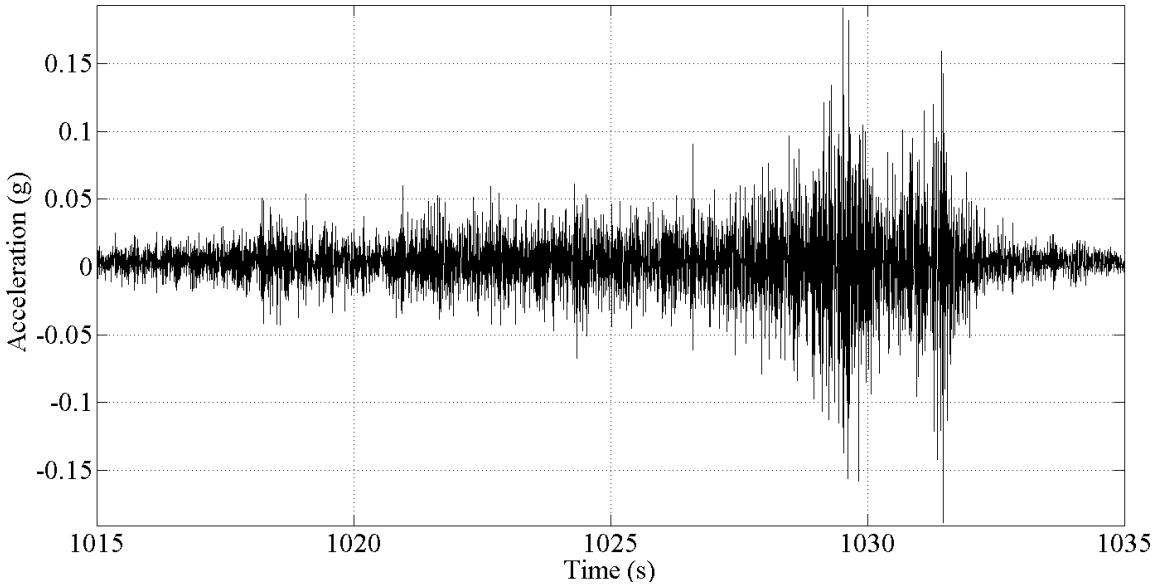

Figure 13-149: Lift Span Longitudinal Acceleration Time History of Traffic Event (Channel 5)

The lift span vertical and lateral acceleration response showed very similar levels of response for the lift span. This is reasonable given the fact that the lift span is a long span and the roadway is not symmetric with respect to the main trusses. The PSD's shown below in Figure 13-150, Figure 13-151 and Figure 13-152 show that the lift span has much lower frequency content than any of the other spans analyzed thus far. This is also reasonable given the length of the lift span.

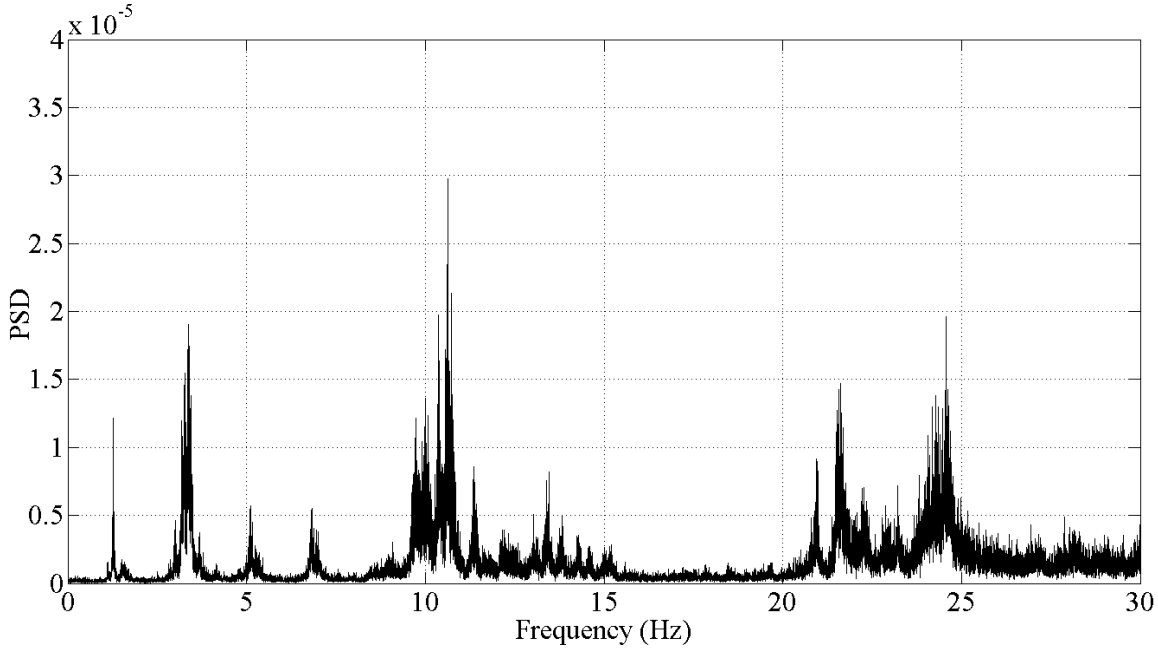

Figure 13-150: PSD of Lift Span Vertical Response

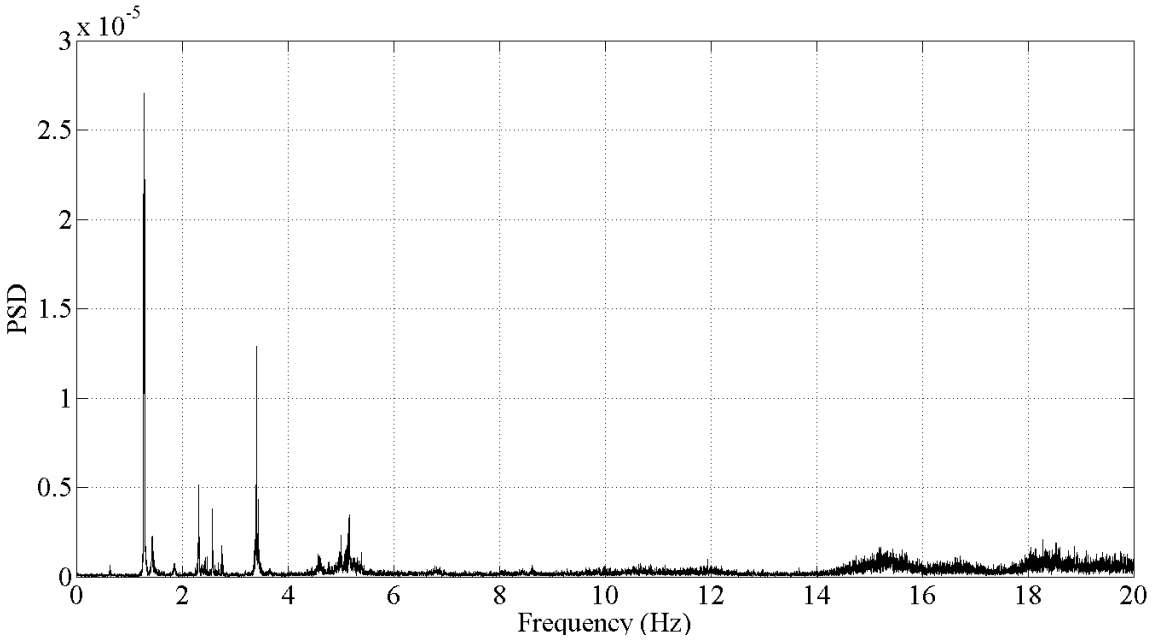

Figure 13-151: PSD of Lift Span Lateral Response

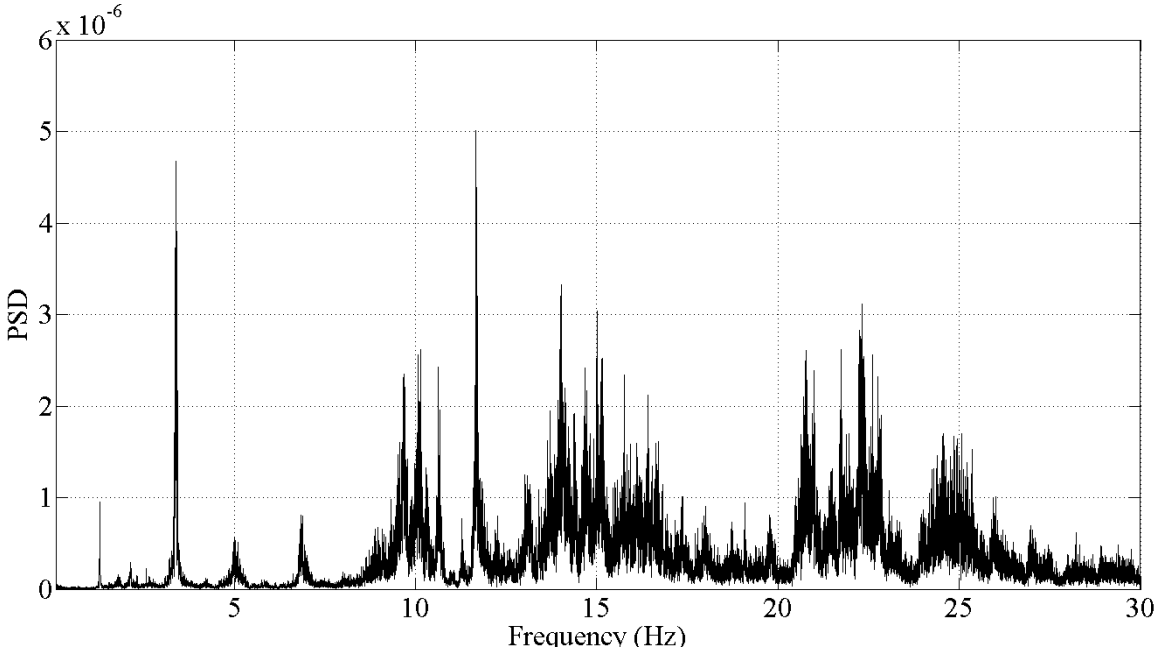

Figure 13-152: PSD of Lift Span Longitudinal Response

13.4.4.4. PA Tower Span Time History and PSD Analysis

The time histories from the PA tower span during the period of 7:42AM to 8:42AM are plotted in Figure 13-153, Figure 13-155 and Figure 13-157. A zoomed in plot around a specific event is shown in under each respective full time history plot for each measurement direction in Figure 13-154, Figure 13-156 and Figure 13-158 .

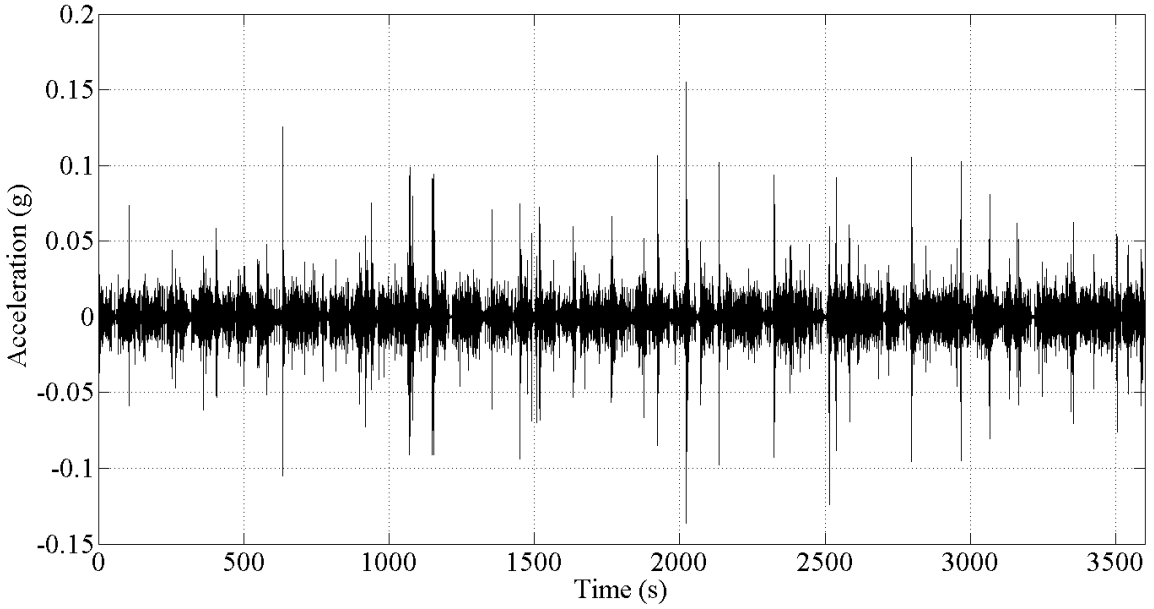

Figure 13-153: PA Tower Span Vertical Acceleration Time History (Channel 27)

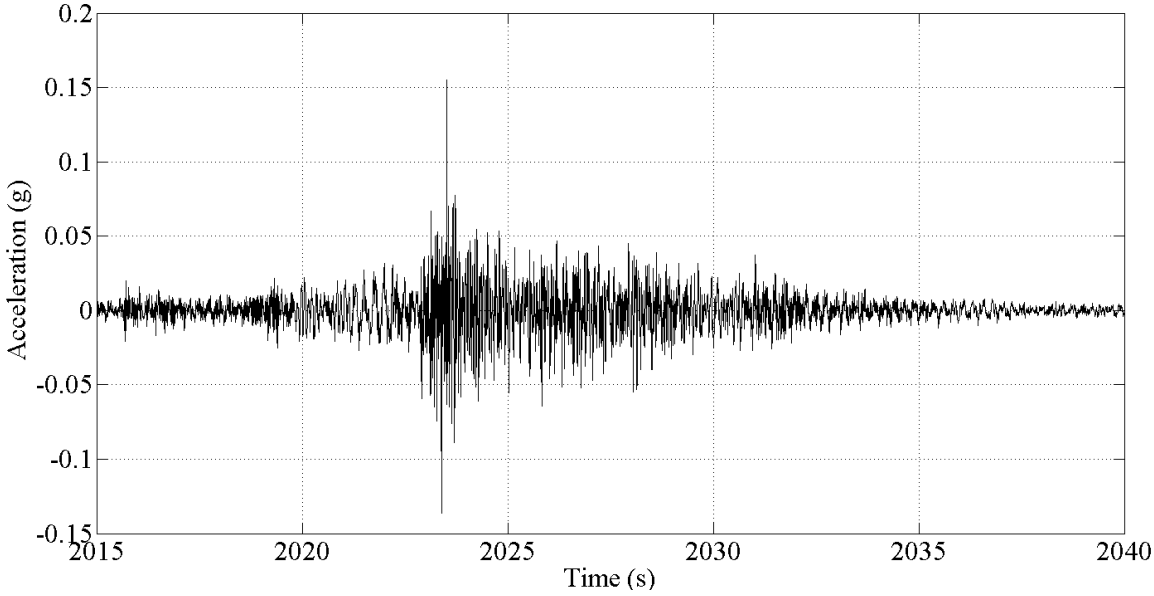

Figure 13-154: PA Tower Span Vertical Acceleration Time History for Traffic Event (Channel 27)

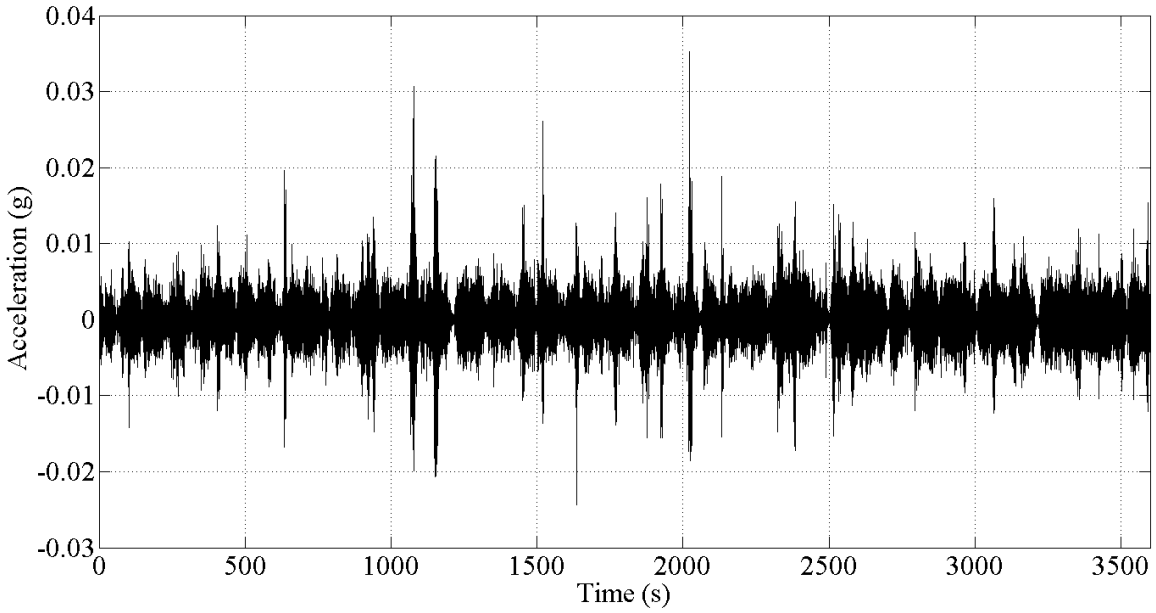

Figure 13-155: PA Tower Span Lateral Acceleration Time History (Channel 38)

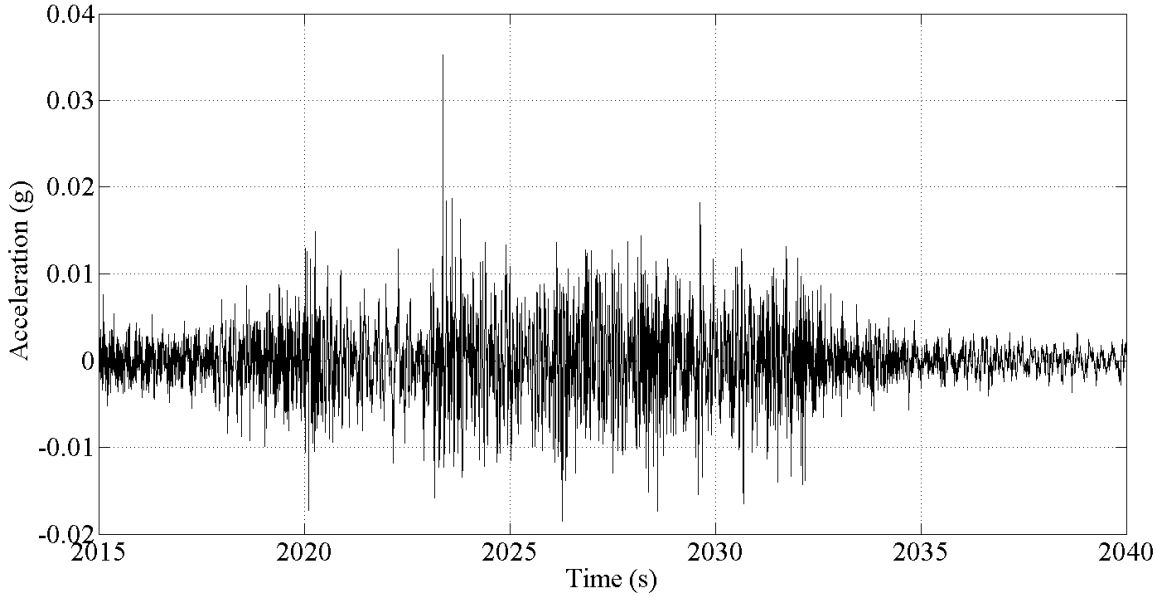

Figure 13-156: PA Tower Span Lateral Acceleration Time History for Traffic Event (Channel 38)

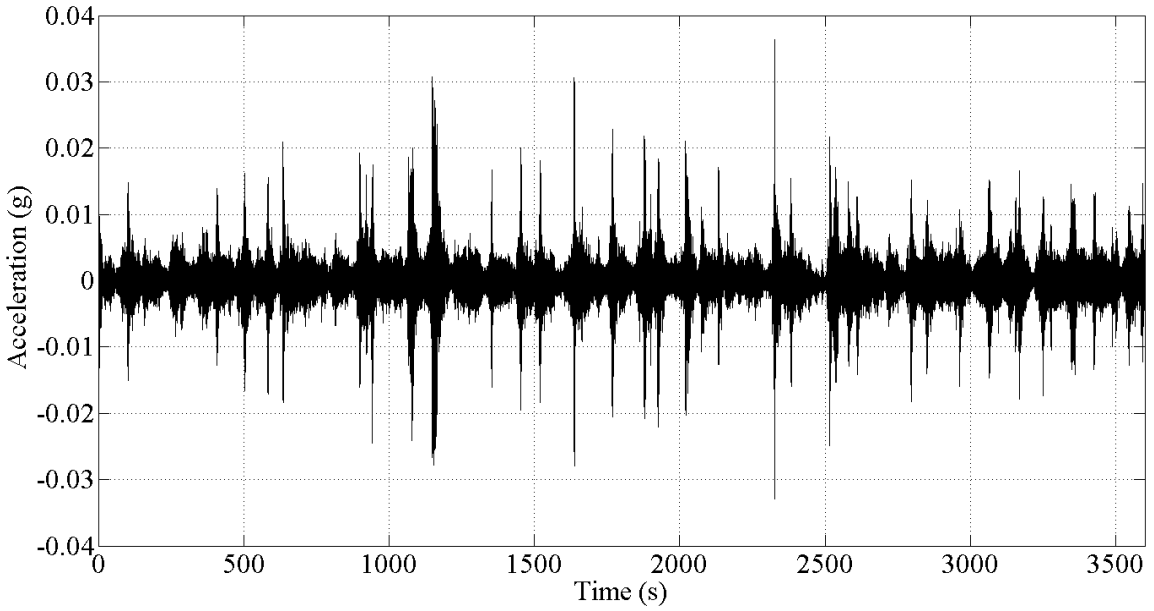

Figure 13-157: PA Tower Span Longitudinal Acceleration Time History (Channel 1)

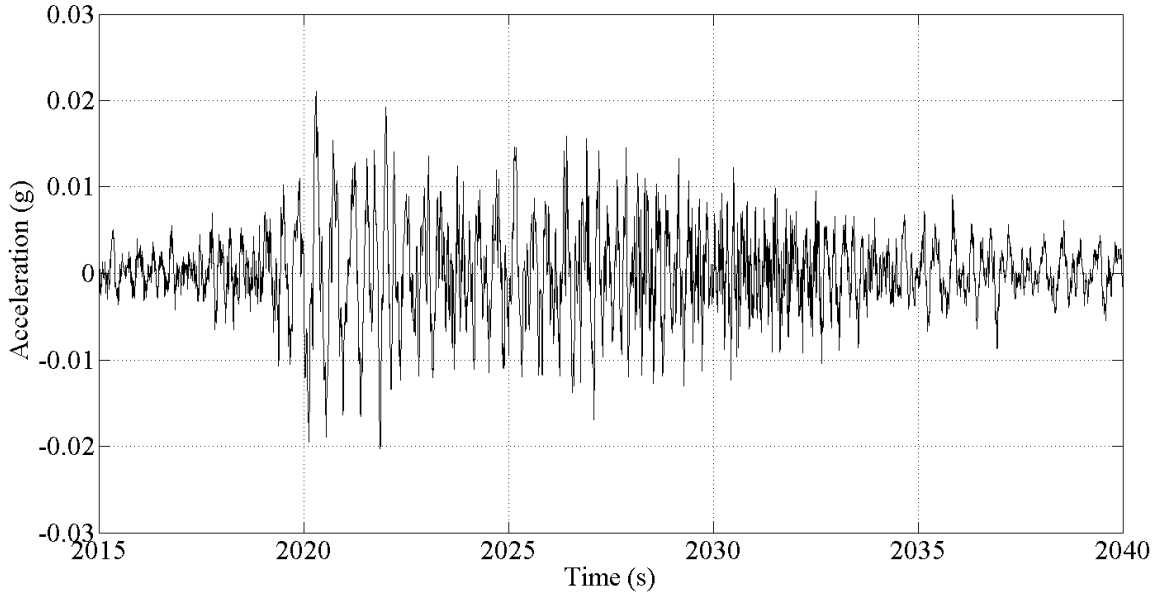

Figure 13-158: PA Tower Span Longitudinal Acceleration Time History for Traffic Event (Channel 1)

The time histories show that the magnitude of the vertical acceleration is the highest over this period of time for the PA tower span, with maximum response just above 0.1g. The lateral acceleration time history of Channel 38 for the PA tower span showed a typical peak acceleration response of 0.04g, much less than its NJ counterpart, for similar levels of vertical acceleration response. This vibration difference was noted for further exploration as potential proof that the NJ tower span does indeed vibrate more than the PA tower span. To explore the frequency content of these signals, the PSD's for each of the time histories was computed and shown in Figure 13-159, Figure 13-160 and Figure 13-161.

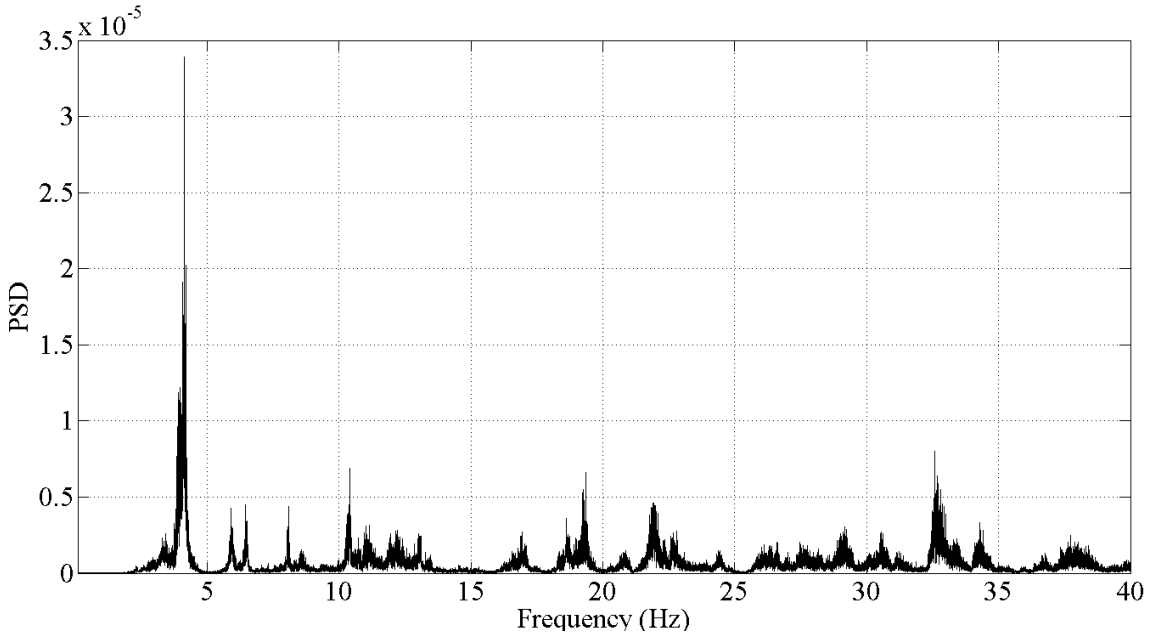

Figure 13-159: PSD of PA Tower Vertical Response

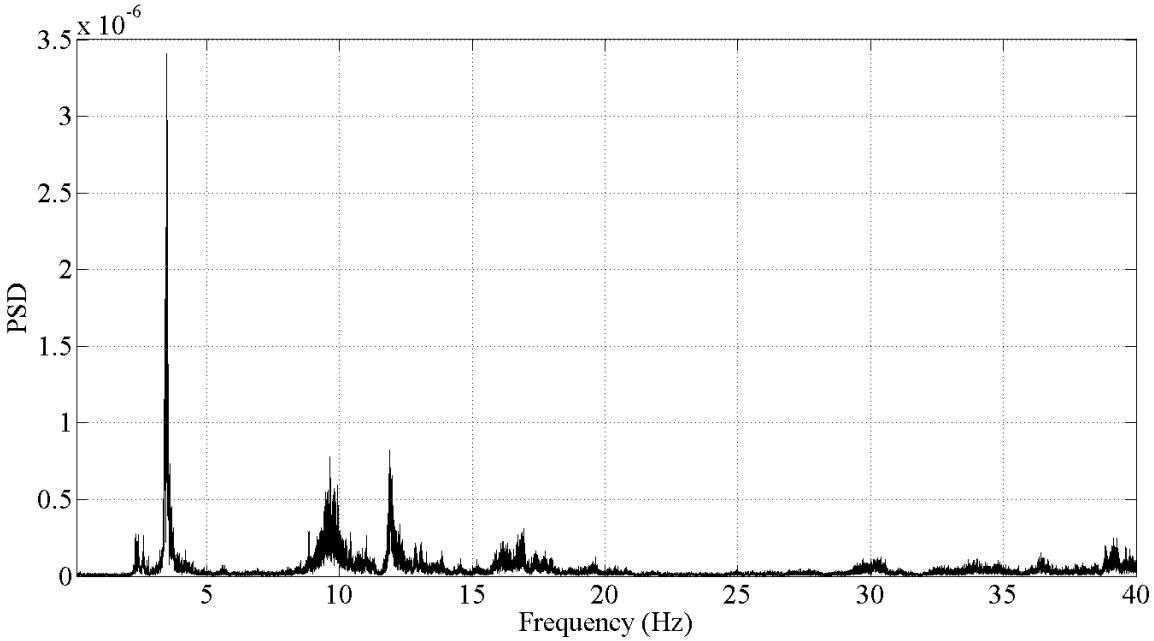

Figure 13-160: PSD of PA Tower Lateral Response

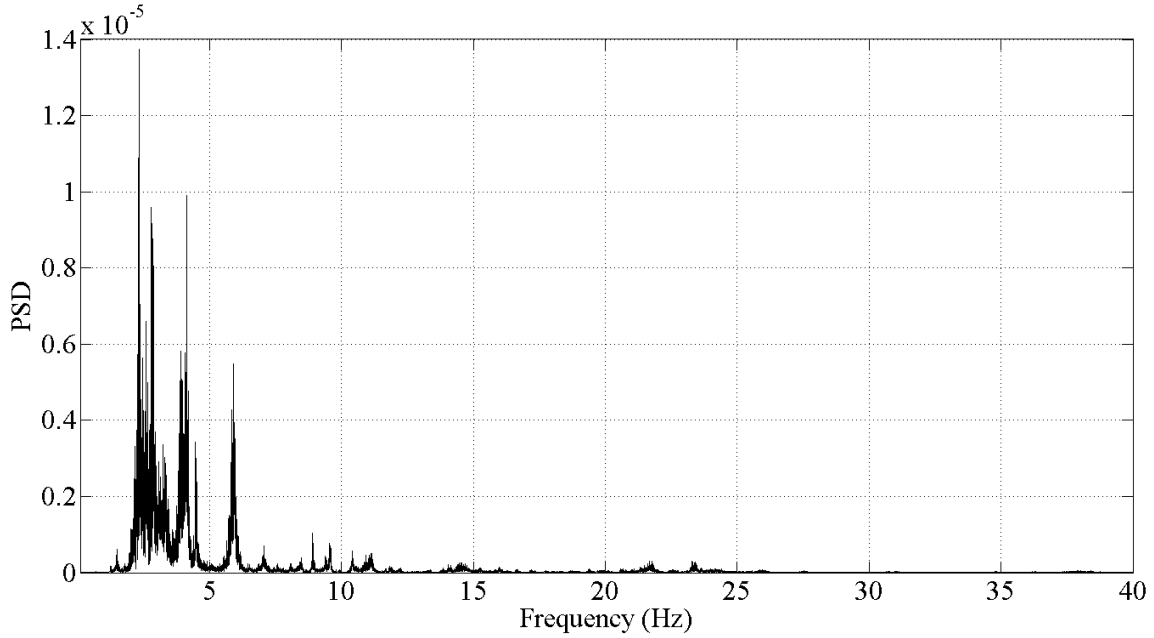

Figure 13-161: PSD of PA Tower Longitudinal Response

After the quality of the data from the PA Tower span was verified with the time history and PSD analysis, the setup was torn down and moved to the final setup: the PA Truss spans.

13.4.4.5. PA Truss Span Time History and PSD Analysis

The time histories for the PA Truss spans (Figure 13-162, Figure 13-164 and Figure 13-166) are plotted from a recording of traffic events over the period of 6:24AM to 7:24AM. A plot showing a few specific events is also shown underneath a plot of the entire time history for each of the respective acceleration directions (Figure 13-163, Figure 13-165 and Figure 13-167).

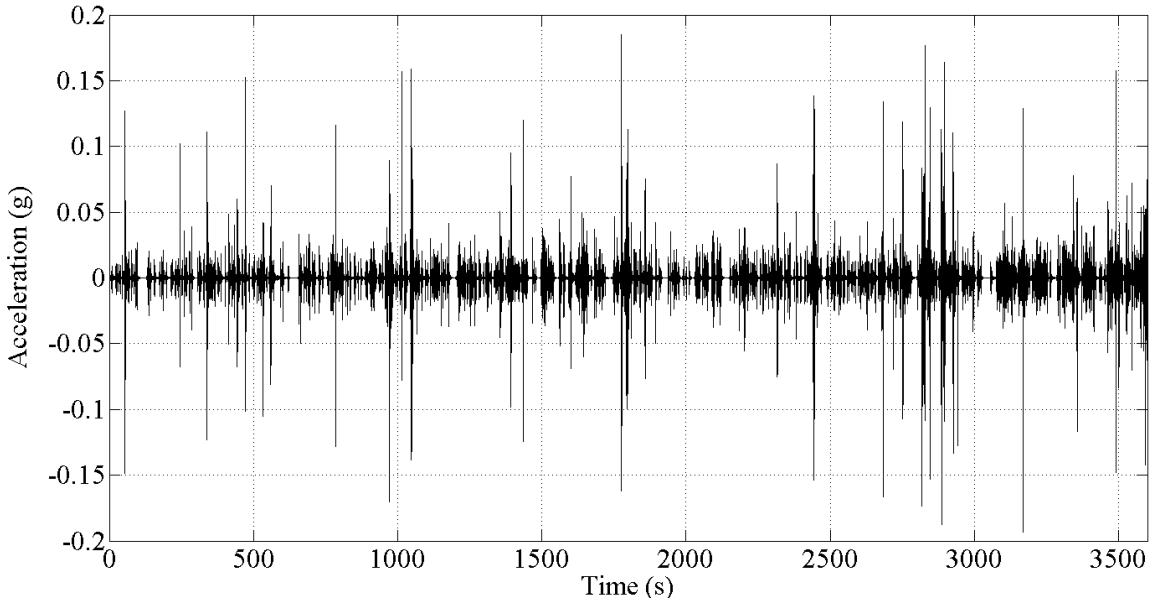

Figure 13-162: PA Truss Span Vertical Acceleration Time (Channel 30)

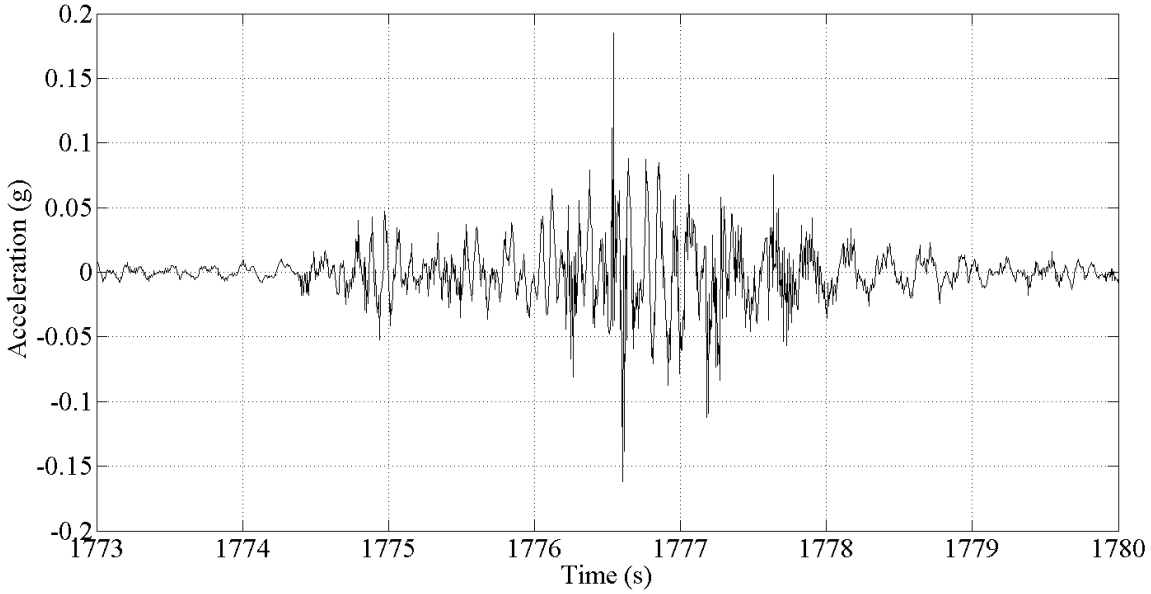

Figure 13-163: PA Truss Span Vertical Acceleration Time History of Traffic Event (Channel 30)

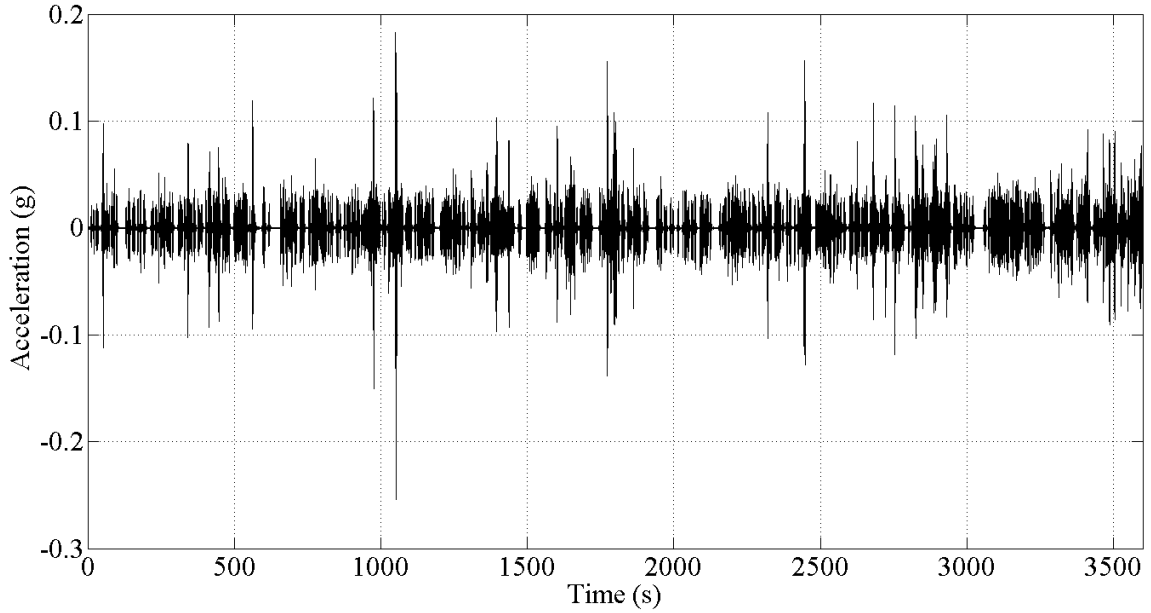

Figure 13-164: PA Truss Span Lateral Acceleration Time History (Channel 39)

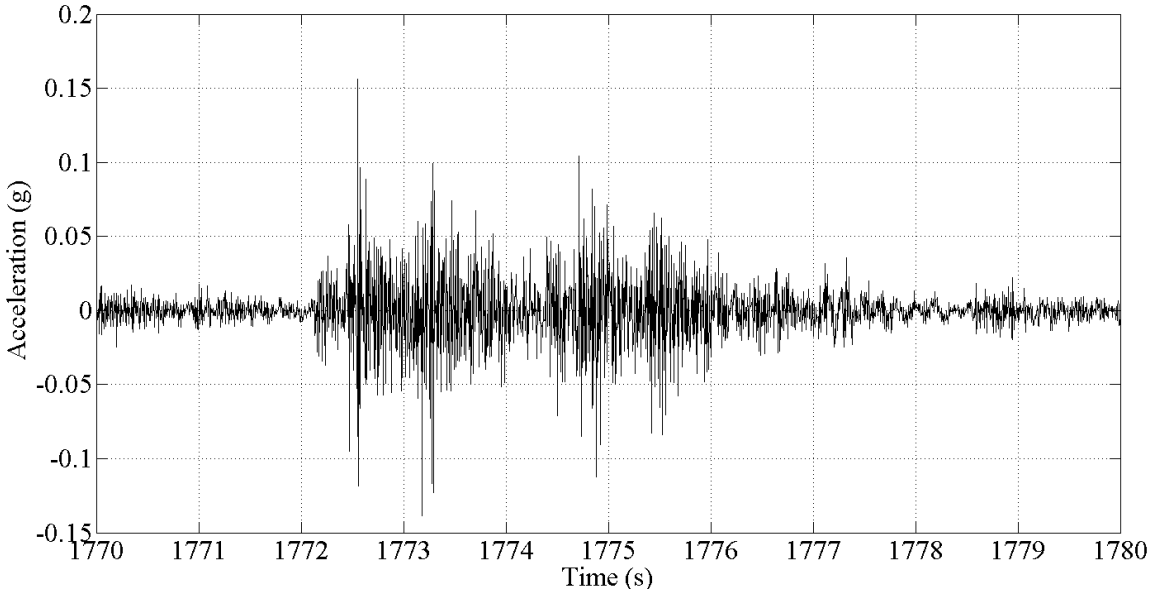

Figure 13-165: PA Truss Span Lateral Acceleration Time History of Traffic Event (Channel 39)

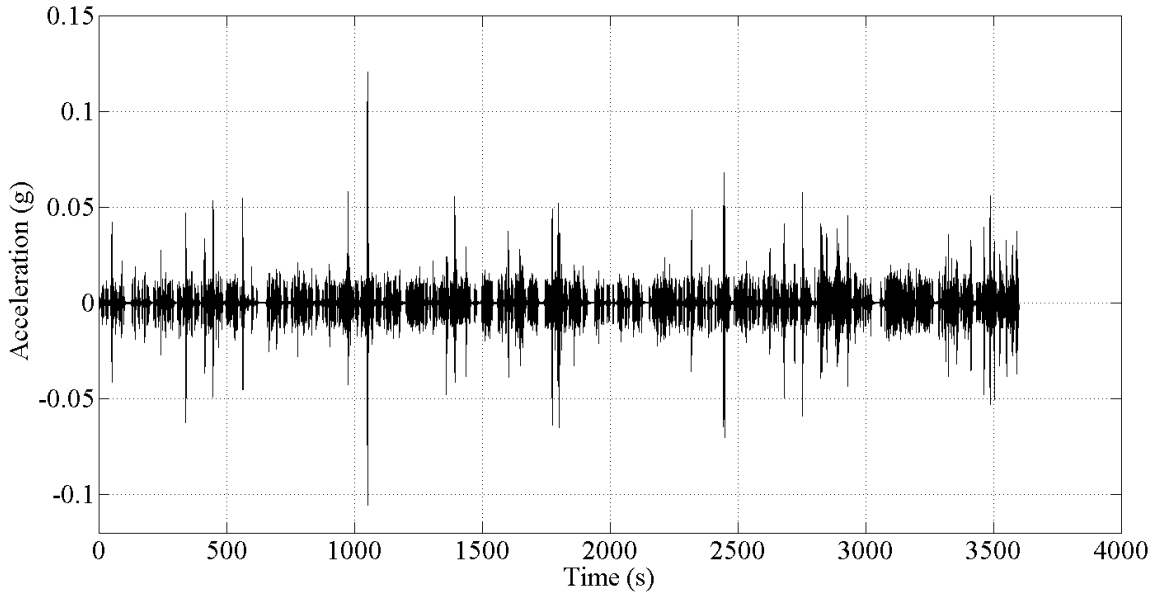

Figure 13-166: PA Truss Span Longitudinal Acceleration Time (Channel 5)

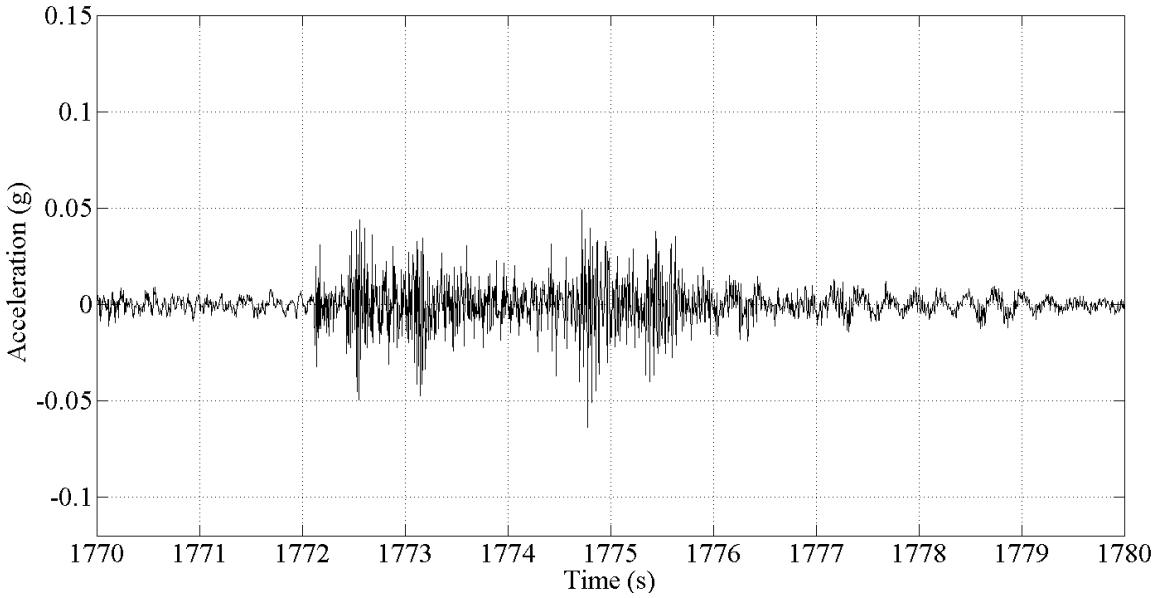

Figure 13-167: PA Truss Span Longitudinal Acceleration Time History of Traffic Event (Channel 5)

The vibration amplitudes of the PA truss spans were fairly consistent with the NJ truss span, except with respect to the lateral vibration peak magnitudes. The PA truss span had peak vertical and lateral vibration amplitudes of roughly 0.15g, while the NJ truss span had peak lateral vibration amplitudes of 0.2g. This is another finding that was used towards explaining the difference in vibration of the two tower spans. The PSD analysis was performed on the PA truss span time histories to determine whether the frequency content of the spans had been sufficiently captured for processing and are shown in Figure 13-168, Figure 13-169 and Figure 13-170.

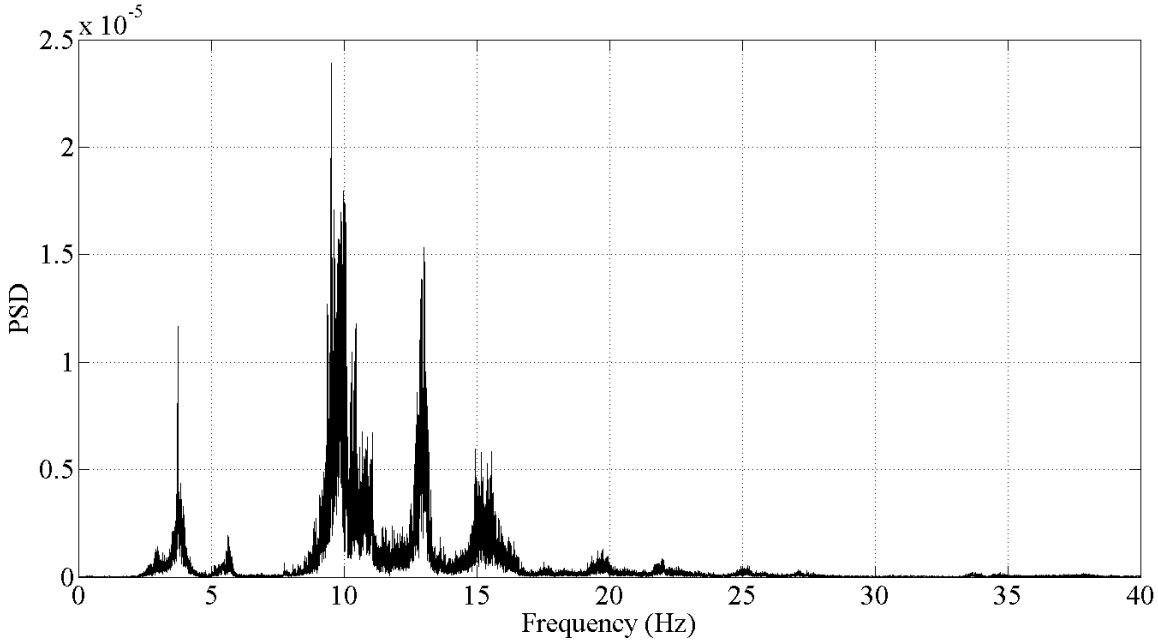

Figure 13-168: PSD of PA Truss Span Vertical Response

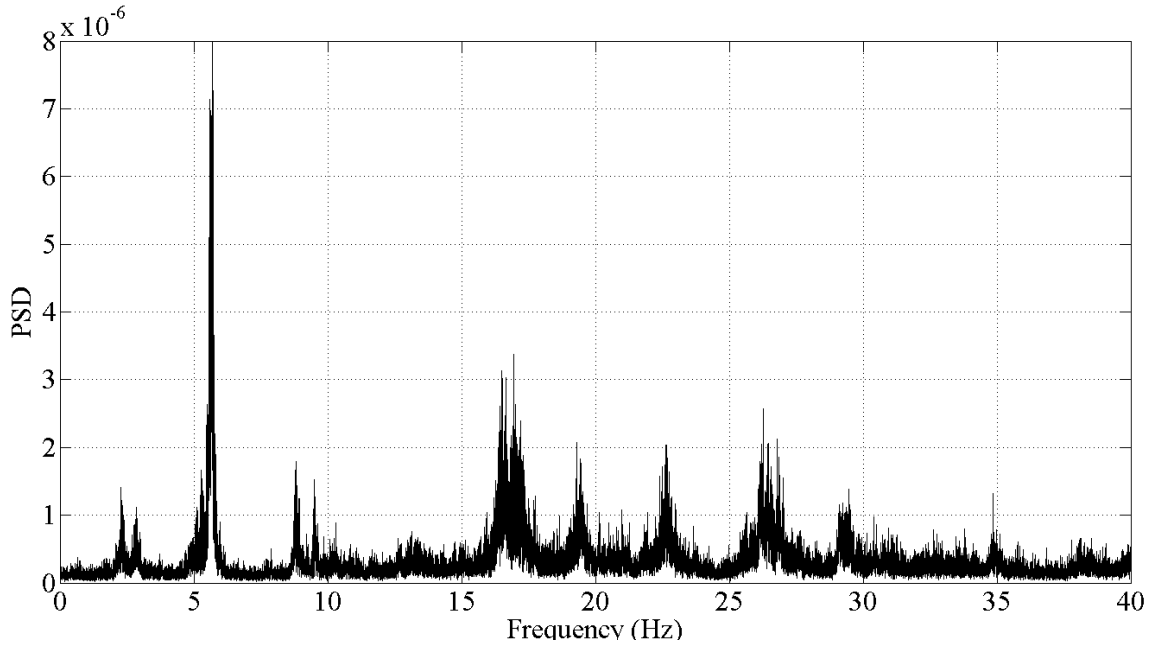

Figure 13-169: PSD of PA Truss Span Lateral Response

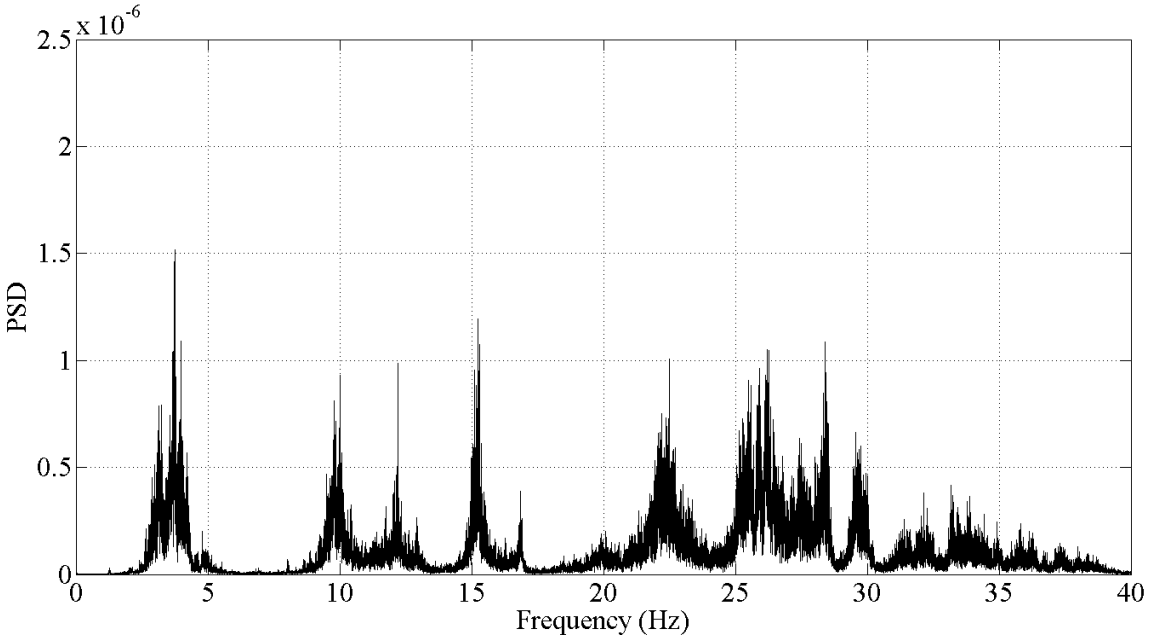

Figure 13-170: PSD of PA Truss Span Longitudinal Response

The PSD analysis of the PA truss spans showed that the signals measured in the field were sufficient for further data processing and the ambient vibration monitoring equipment could be completely removed from the span. The PSD analysis also highlighted a difference in the lateral vibration response of the NJ truss span and the PA truss spans. In the NJ truss span PSD, there was a large pole at approximately 13.5Hz, which did not exist in the PA truss span PSD. This further highlights some lack of symmetry between the responses of the PA structures and NJ structures.

13.4.5. Presentation of Results

The results from the SSI and CMIF data processing methods were generated by others but are presented below for completeness. The modeshapes are presented in two dimensional format based on the measurement direction being shown.

13.4.5.1. NJ Truss Span

The vertical and torsional frequencies and modeshapes for the NJ Truss span are listed in Table 13-10 and shown in Figure 13-171 through Figure 13-177.

Table 13-10: NJ Truss Span Vertical and Torsional Frequencies

NJ Truss - Vertical / Torsional Modeshapes		
Description	SSI (Hz)	CMIF (Hz)
1st Vertical	4.003	3.996
2nd Vertical	10.112	9.961
3rd Vertical	14.035	14.021
4th Vertical	20.076	20.043
1st Torsion	5.982	5.911
2nd Torsion	13.548	13.503
3rd Torsion	17.79	-

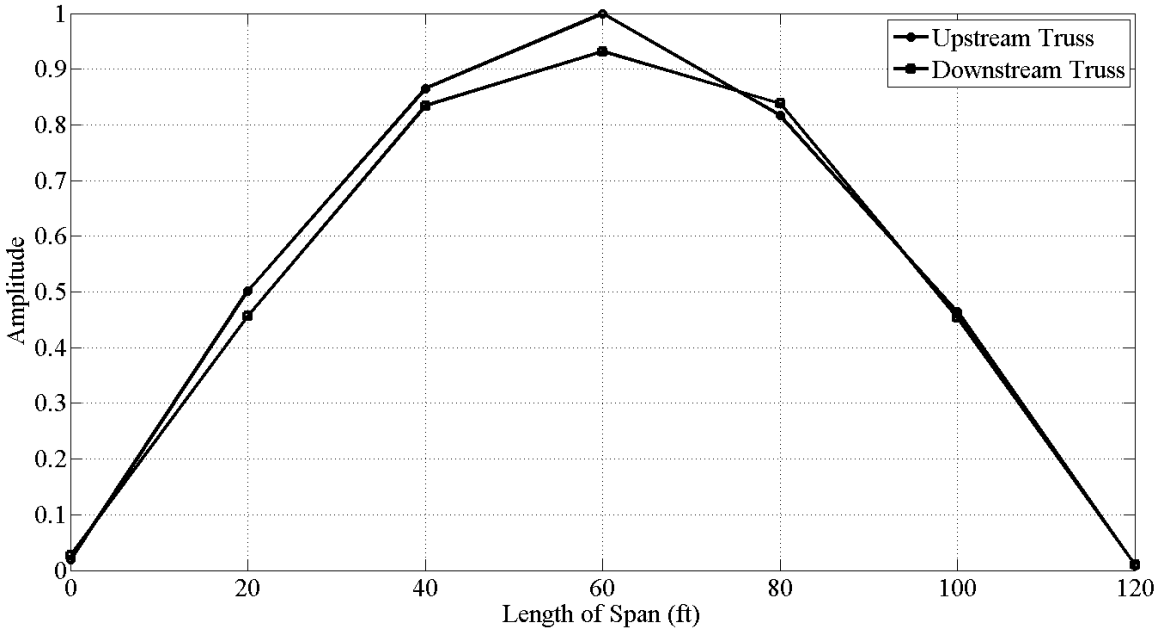

Figure 13-171: NJ Truss Span 1st Vertical Mode

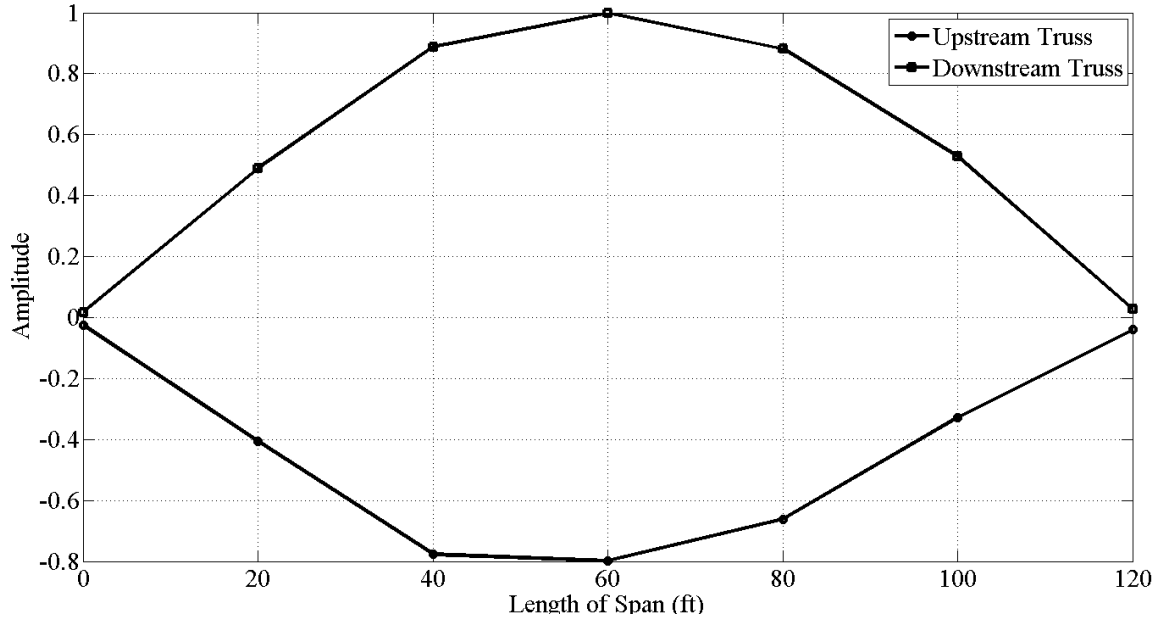

Figure 13-172: NJ Truss Span 2nd Vertical Mode

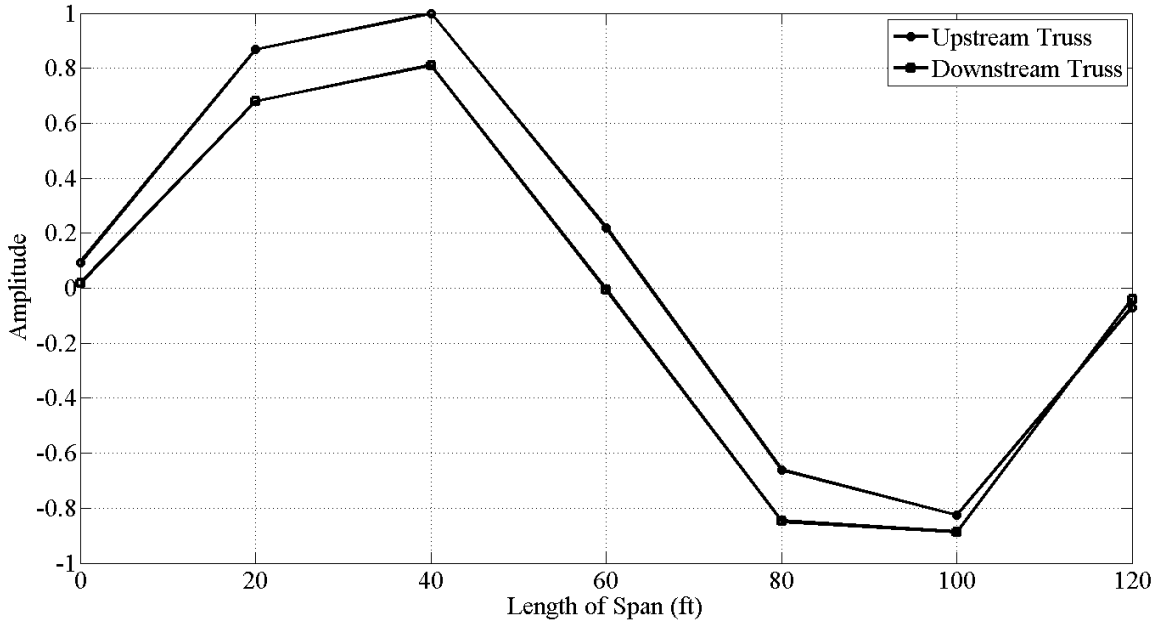

Figure 13-173: NJ Truss Span 3rd Vertical Mode

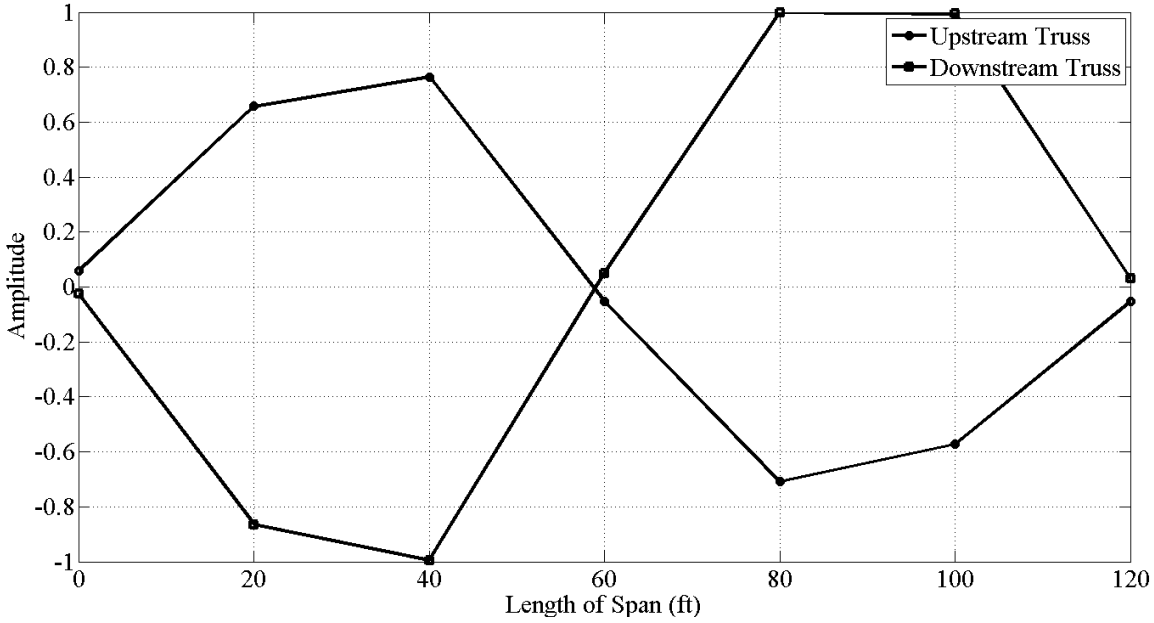

Figure 13-174: NJ Truss Span 4th Vertical Mode

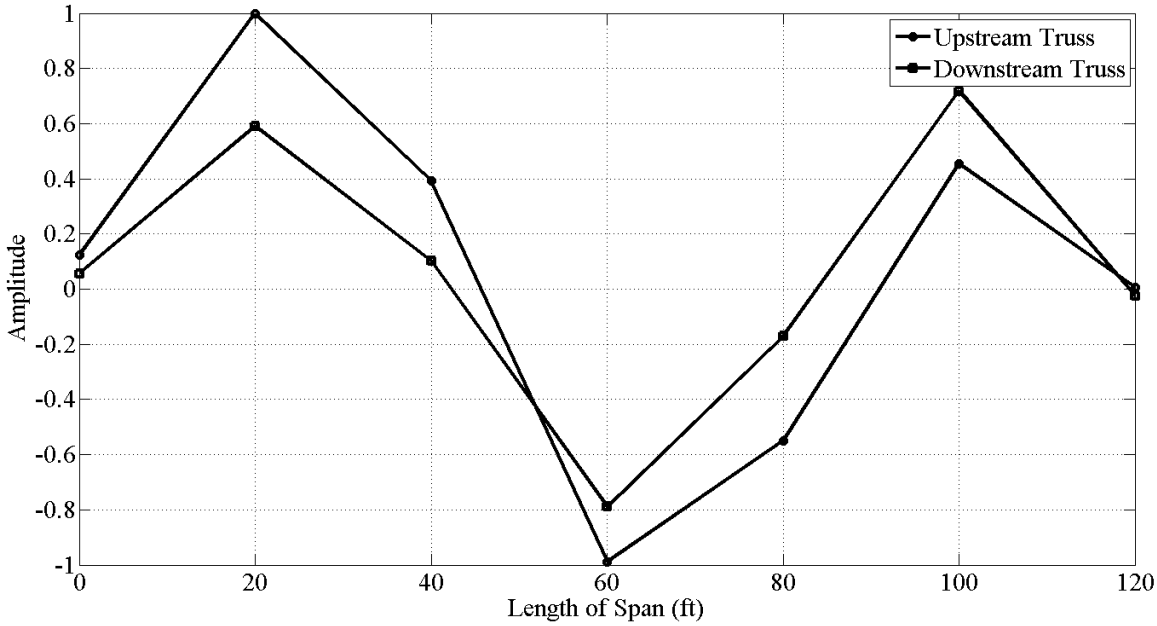

Figure 13-175: NJ Truss Span 5th Vertical Mode

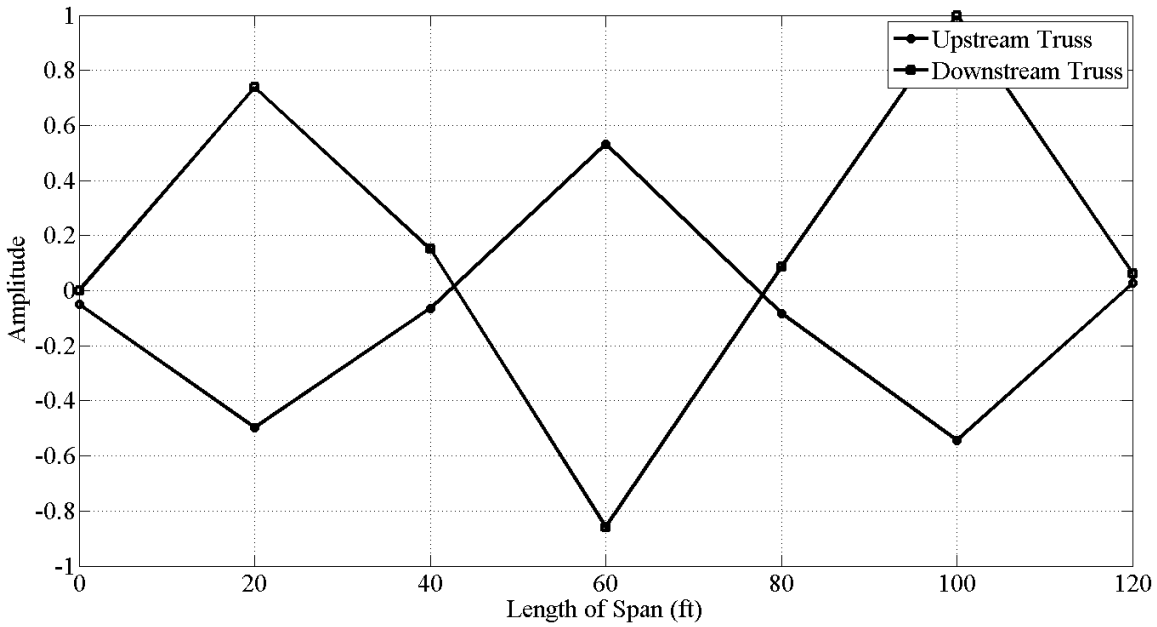

Figure 13-176: NJ Truss Span 6th Vertical Mode

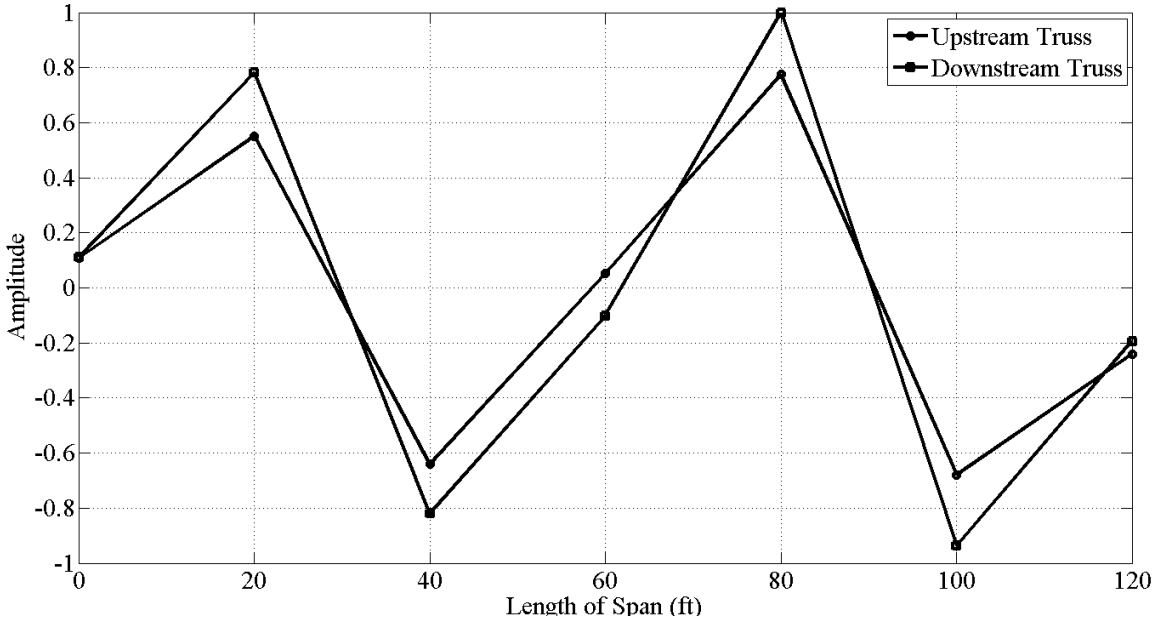

Figure 13-177: NJ Truss Span 7th Vertical Mode

The vertical and torsional frequencies and modeshapes for the NJ Truss span are listed in Table 13-11 and shown in Figure 13-178 through Figure 13-183.

Table 13-11: NJ Truss Span Lateral Frequencies

NJ Truss - Lateral Modeshapes	
Description	SSI (Hz)
1st Lateral	2.99
2nd Lateral	4.536
3rd Lateral	5.36
4th Lateral	13.525
5th Lateral	15.953
6th Lateral	17.555

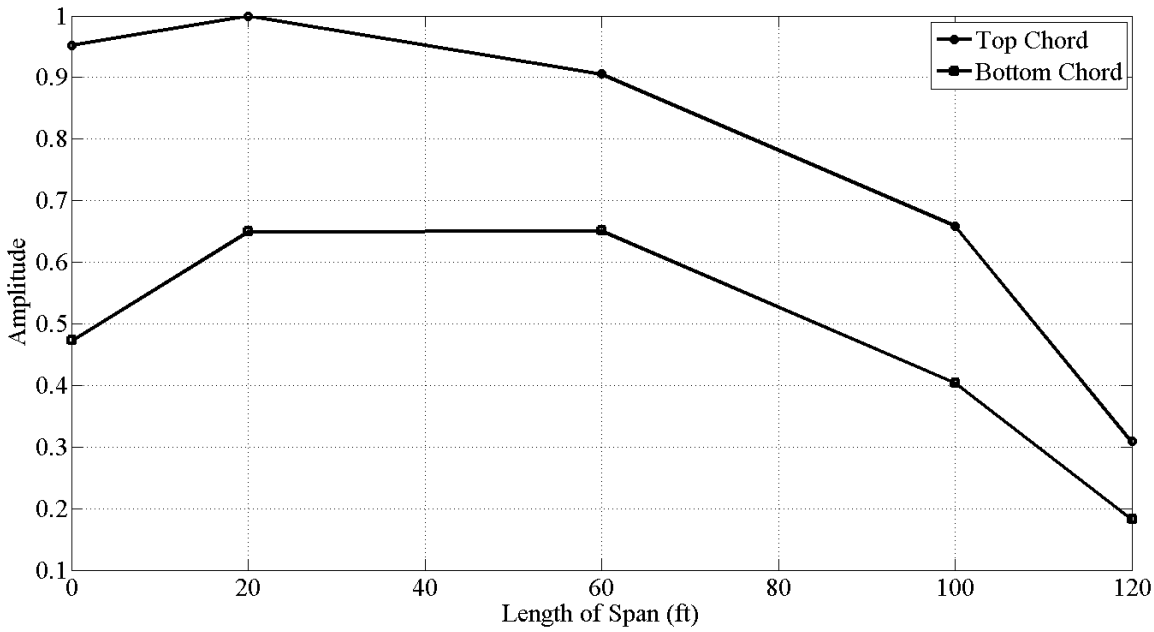

Figure 13-178: NJ Truss Span 1st Lateral Mode

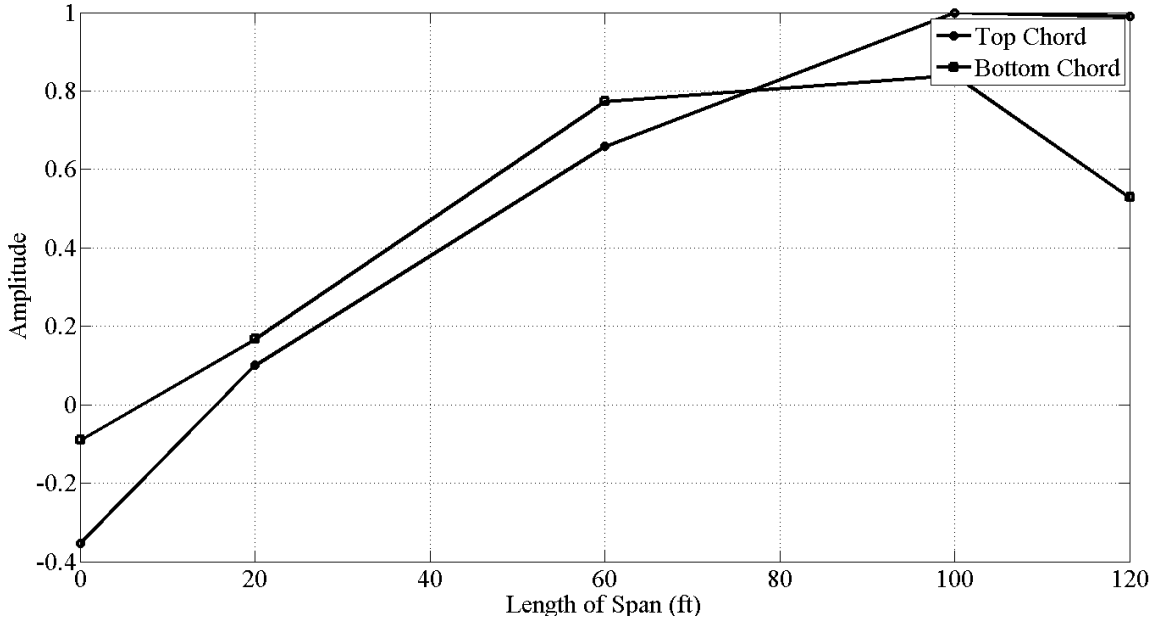

Figure 13-179: NJ Truss Span 2nd Lateral Mode

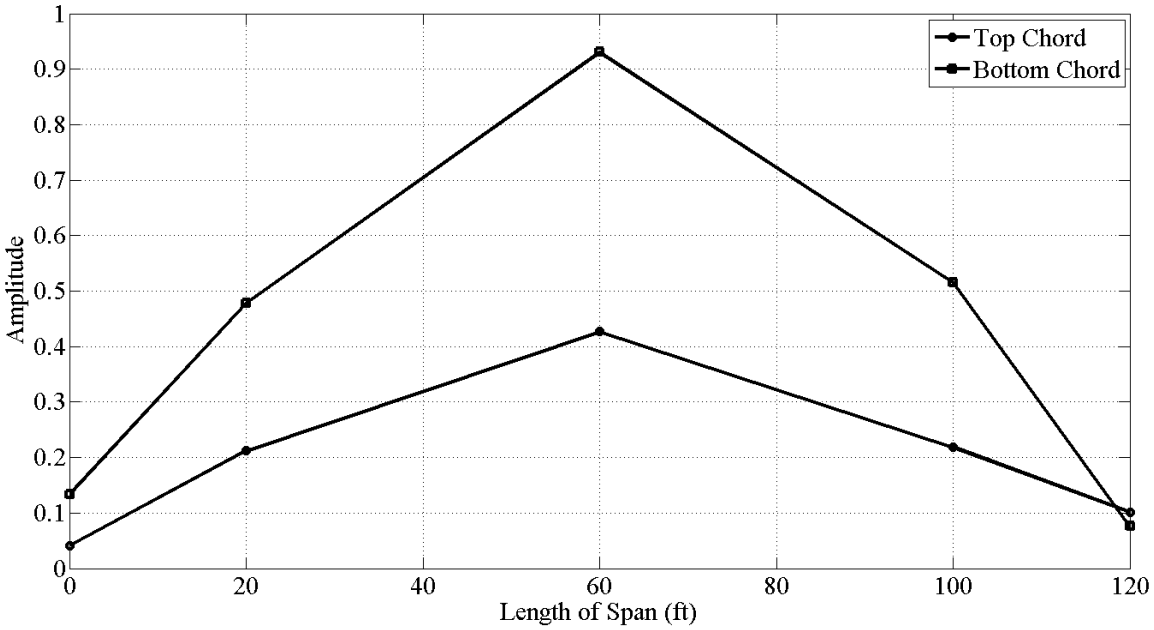

Figure 13-180: NJ Truss Span 3rd Lateral Mode

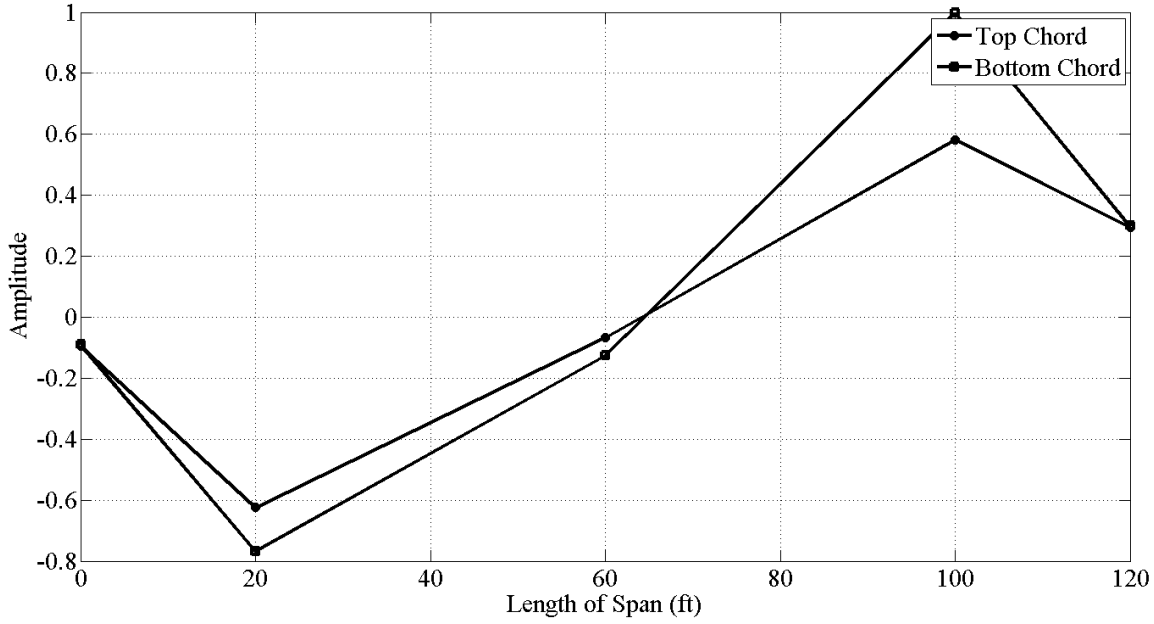

Figure 13-181: NJ Truss Span 4th Lateral Mode

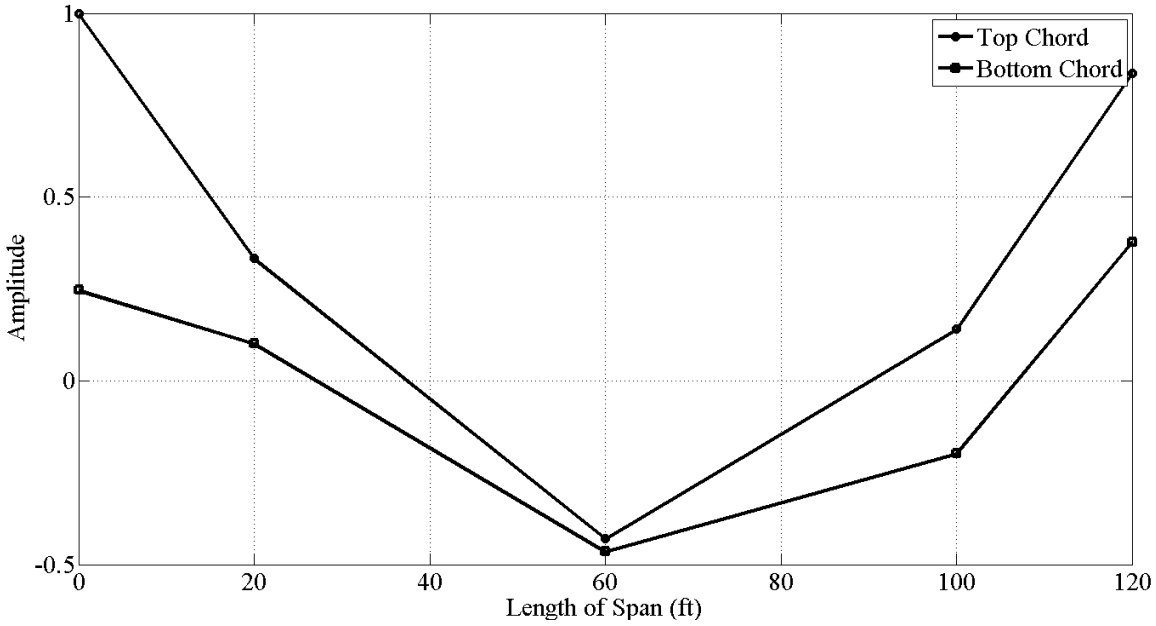

Figure 13-182: NJ Truss Span 4th Lateral Mode

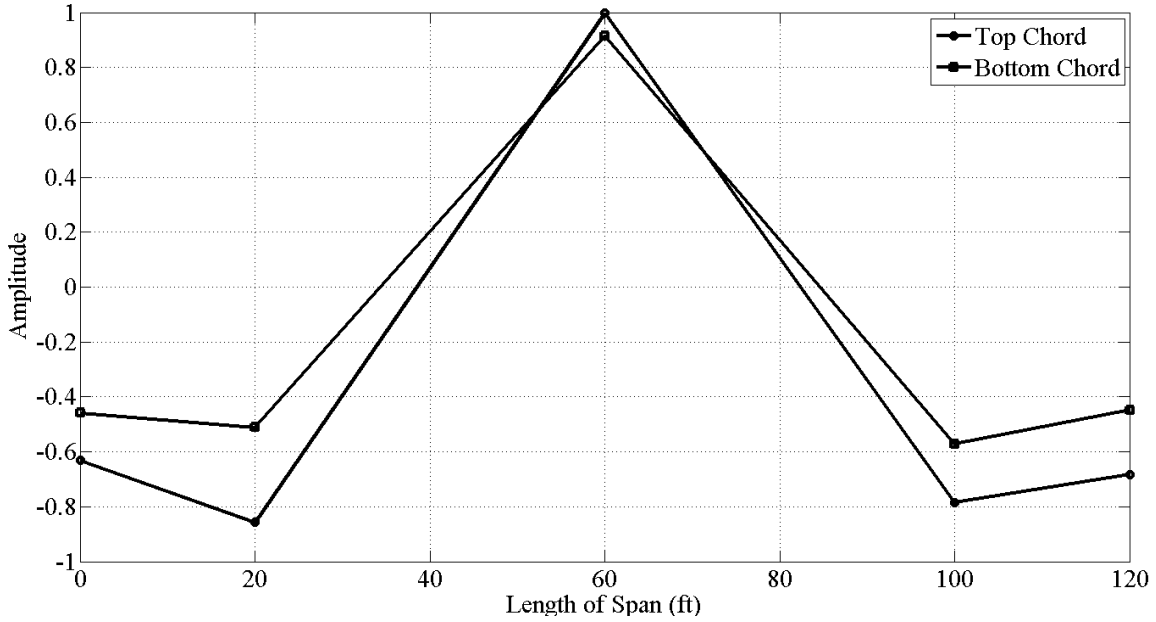

Figure 13-183: NJ Truss Span 6th Lateral Mode

13.4.5.2. NJ Tower Span

The vertical and torsional frequencies for the NJ tower span are listed in Table 13-12 and shown in Figure 13-184 through Figure 13-189. Note that the figures are drawn in elevation view, showing the longitudinal movement of the towers and vertical movement of the roadway.

Table 13-12: NJ Tower - Vertical / Torsional Frequencies

NJ Tower - Vertical / Torsional Modeshapes		
Description	SSI (Hz)	CMIF (Hz)
1st Vertical	2.070	2.084
2nd Vertical	4.050	4.033
3rd Vertical	5.775	5.653
4th Vertical	8.278	8.028
1st Torsion	6.461	6.341
2nd Torsion	10.395	10.036

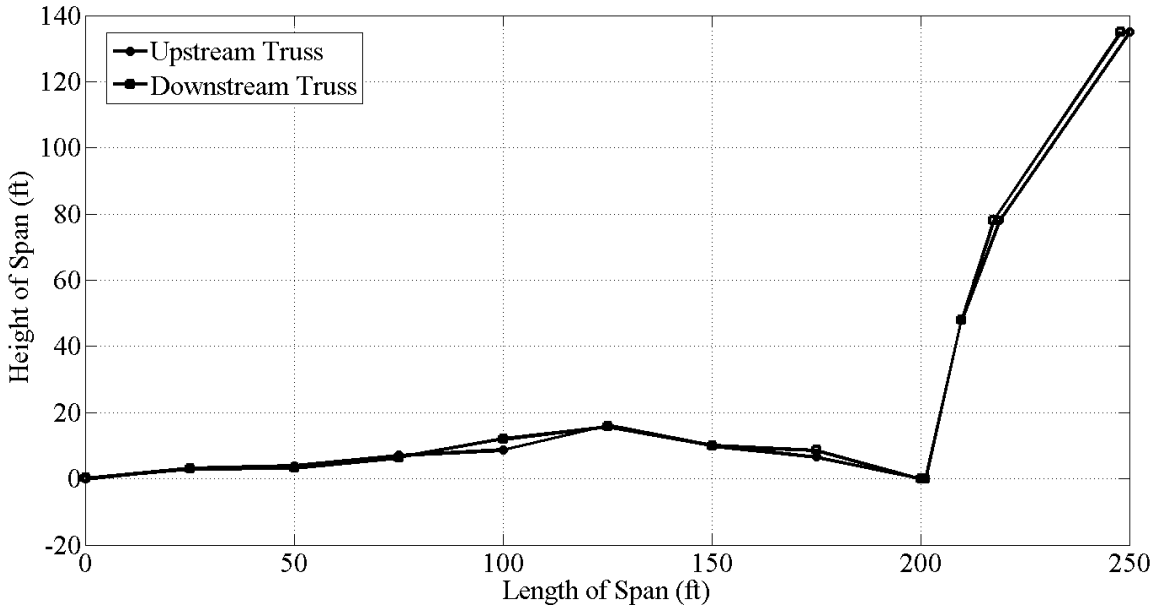

Figure 13-184: NJ Tower Span 1st Vertical Mode

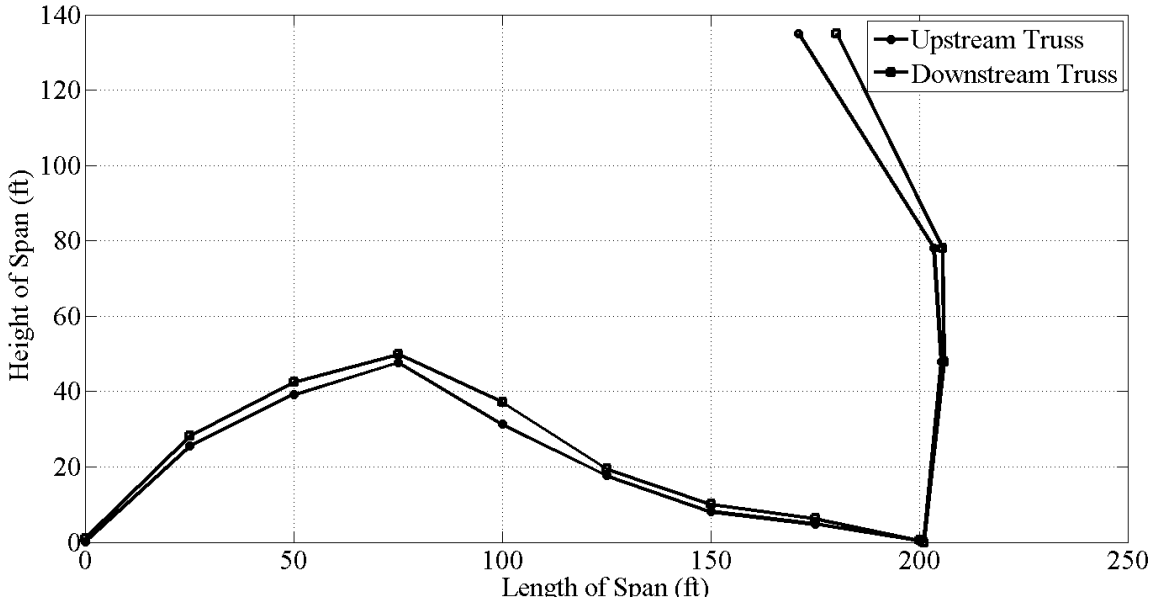

Figure 13-185: NJ Tower Span 2nd Vertical Mode

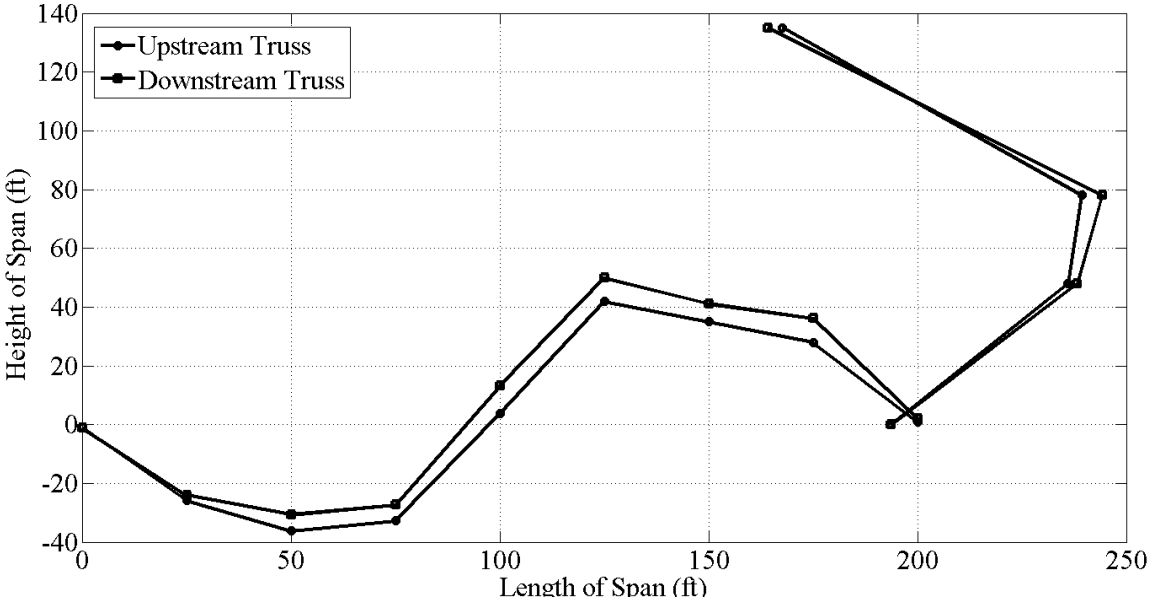

Figure 13-186: NJ Tower Span 3rd Vertical Mode

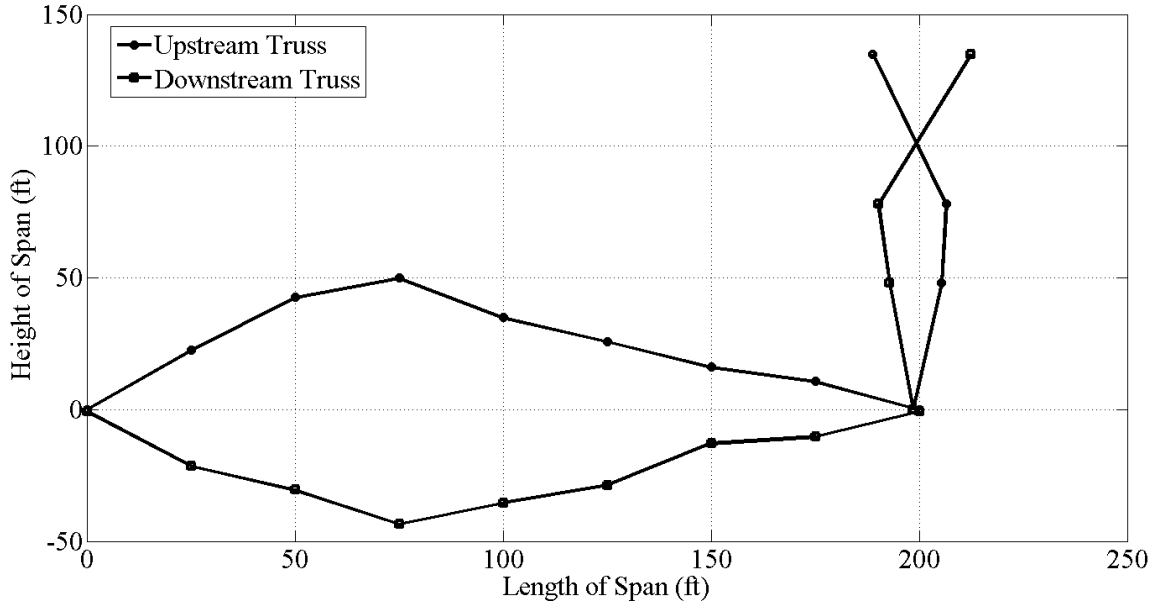

Figure 13-187: NJ Tower Span 4th Vertical Mode

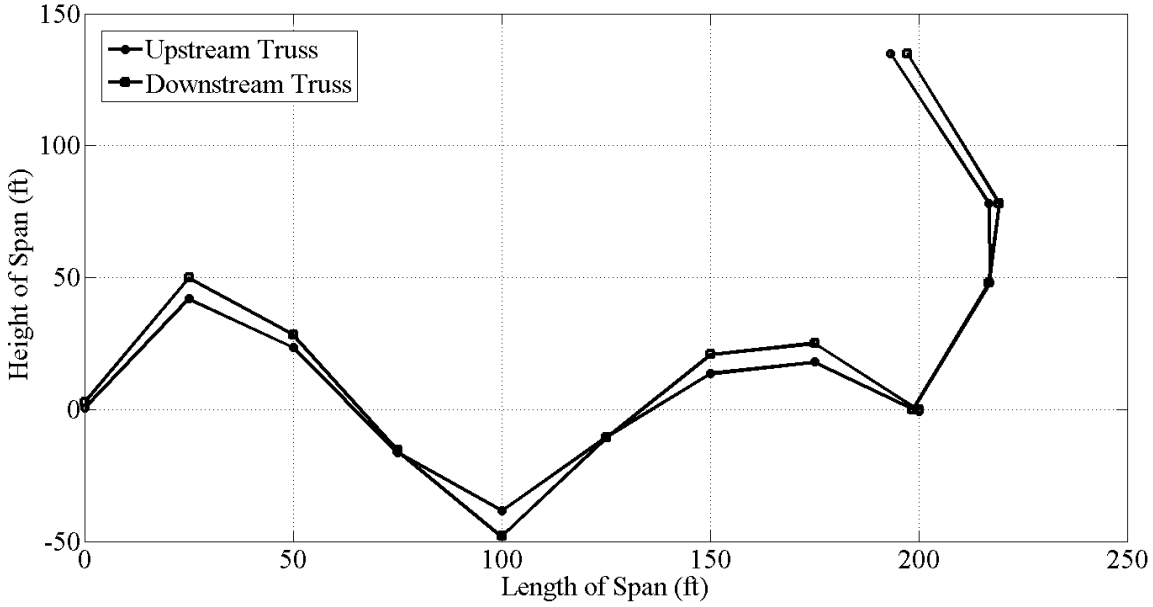

Figure 13-188: NJ Tower Span 5th Vertical Mode

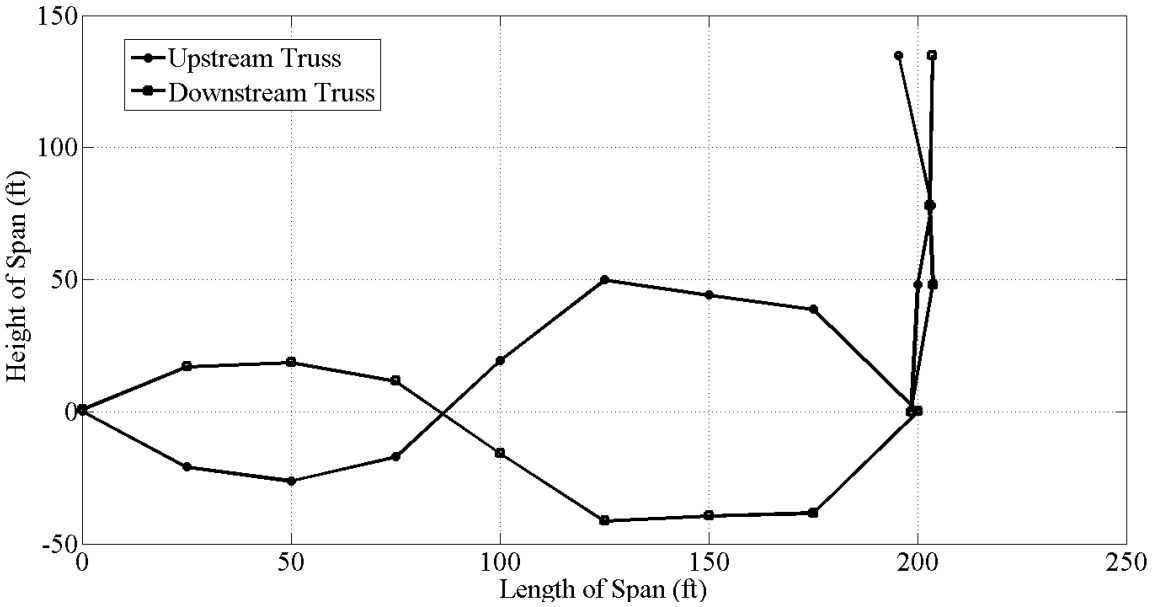

Figure 13-189: NJ Tower Span 6th Vertical Mode

The lateral frequencies for the NJ tower span are listed in Table 13-13 and shown in Figure 13-190 through Figure 13-193. Note that the lateral modeshapes are drawn in plan view and show the lateral movement of the top of the tower, top chord of the truss and bottom chord of the truss.

Table 13-13: NJ Tower Span Lateral Frequencies

NJ Tower - Lateral Modeshapes	
Description	SSI (Hz)
1st Lateral	1.568
2nd Lateral	2.565
3rd Lateral	3.527
4th Lateral	4.378

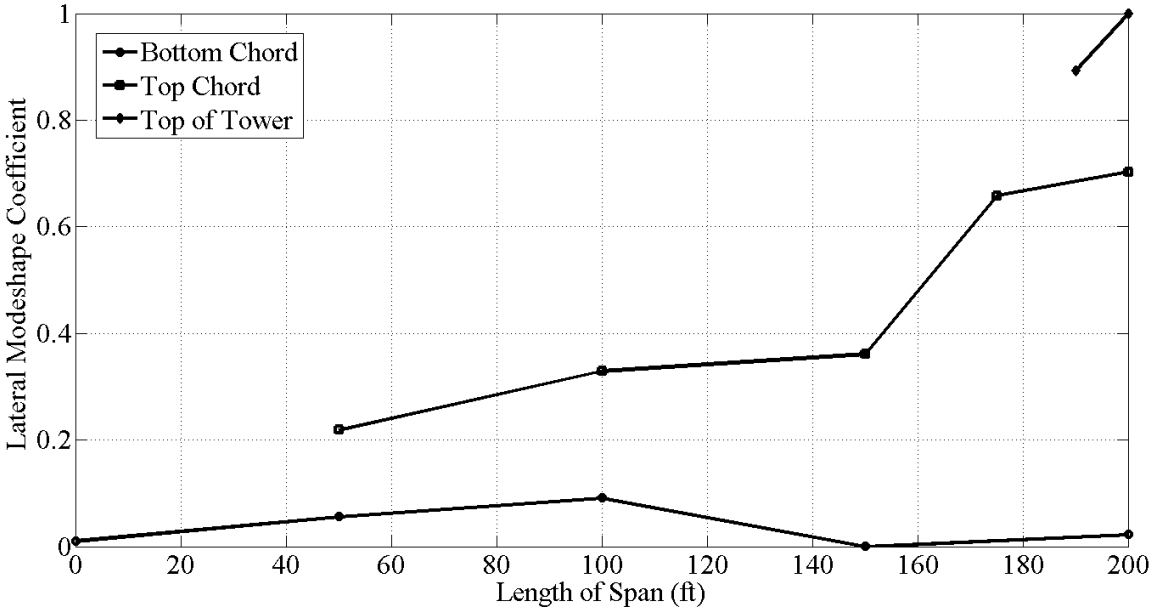

Figure 13-190: NJ Tower Span 1st Lateral Mode

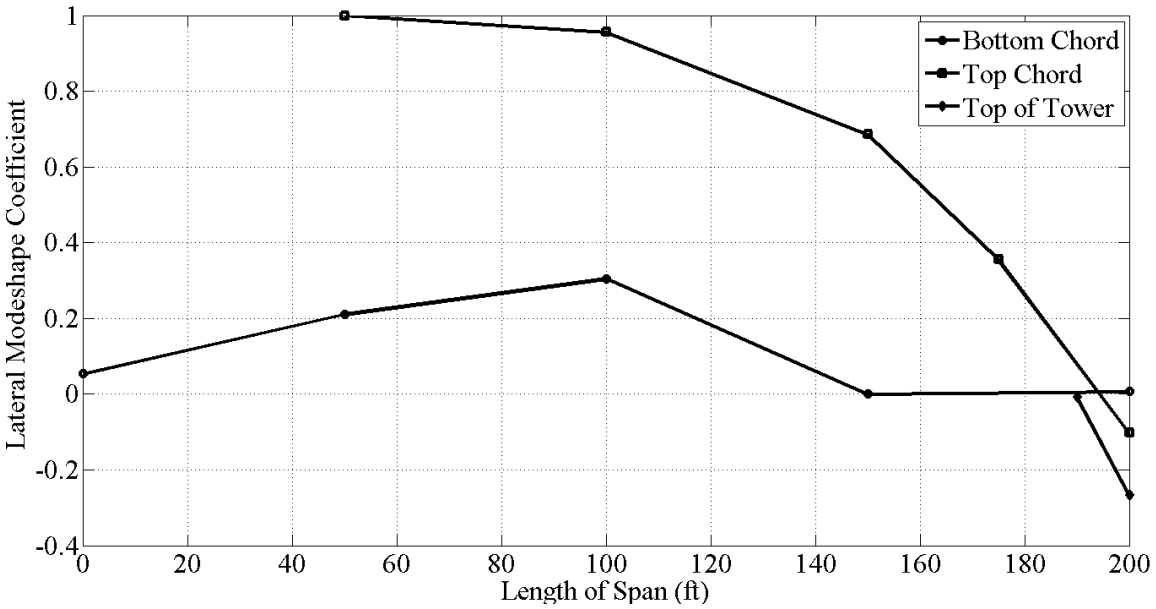

Figure 13-191: NJ Tower Span 2nd Lateral Mode

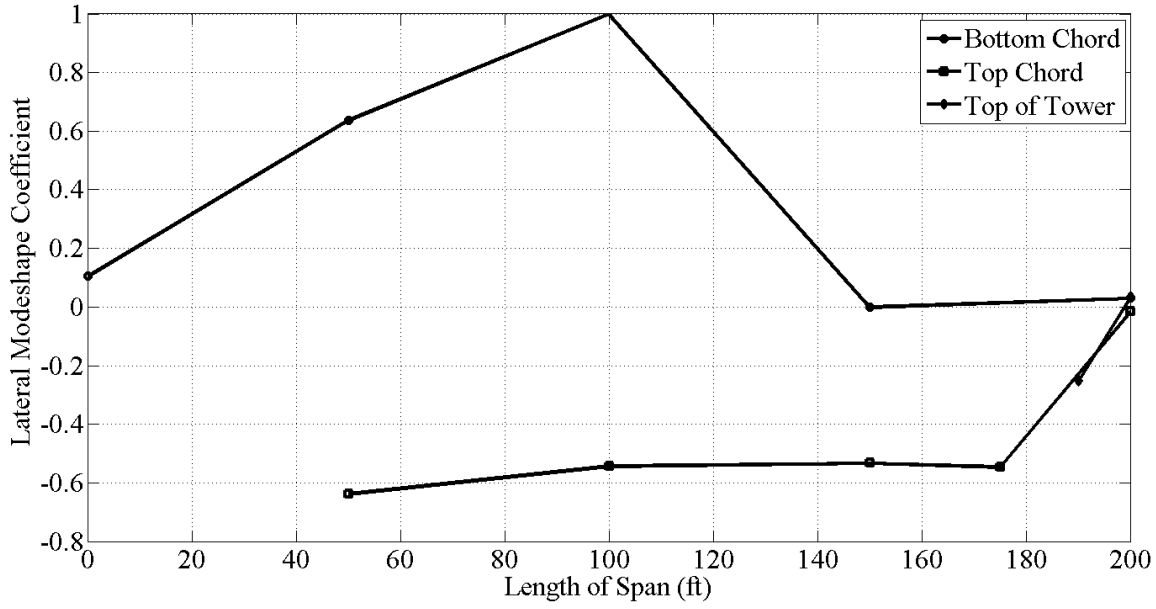

Figure 13-192: NJ Tower Mode 3rd Lateral Mode

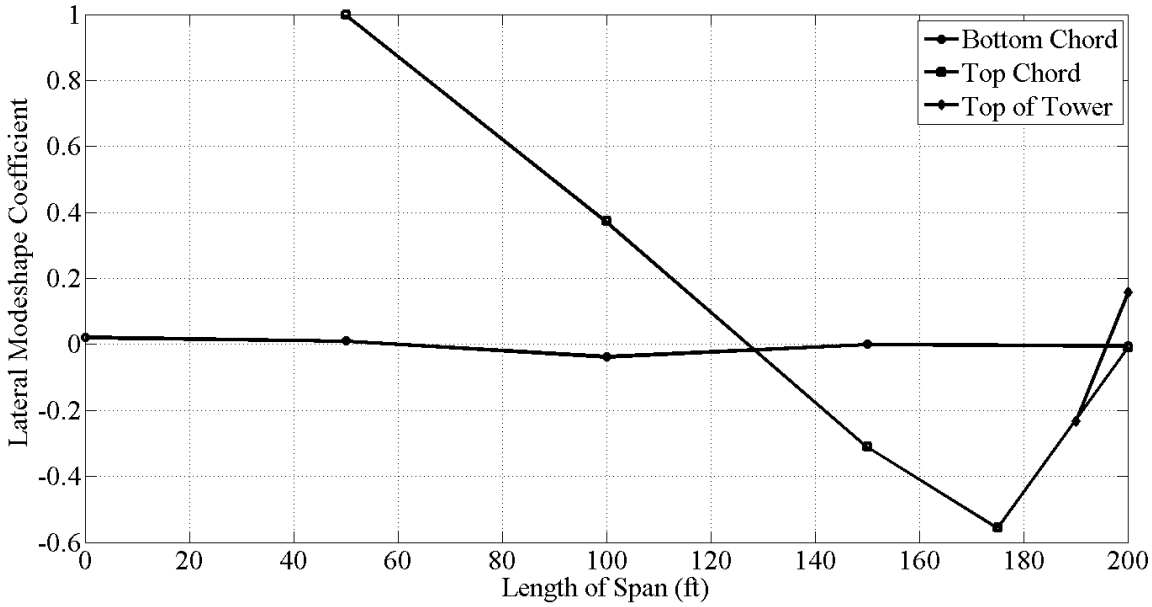

Figure 13-193: NJ Tower Span 4th Lateral Mode

13.4.5.3. Lift Span

The vertical and torsional modeshapes for the lift span are listed in Table 13-14 and shown in Figure 13-194 through Figure 13-199. Note that the modeshapes are drawn in elevation view.

Table 13-14: Lift Span Vertical / Torsional Frequencies

Lift - Vertical / Torsional Modeshapes		
Description	SSI (Hz)	CMIF (Hz)
1st Vertical	1.257	1.264
2nd Vertical	3.283	3.234
3rd Vertical	4.732	5.027
4th Vertical	6.889	-
5th Vertical	9.139	-
1st Torsion	1.113	1.127
2nd Torsion	4.667	4.607

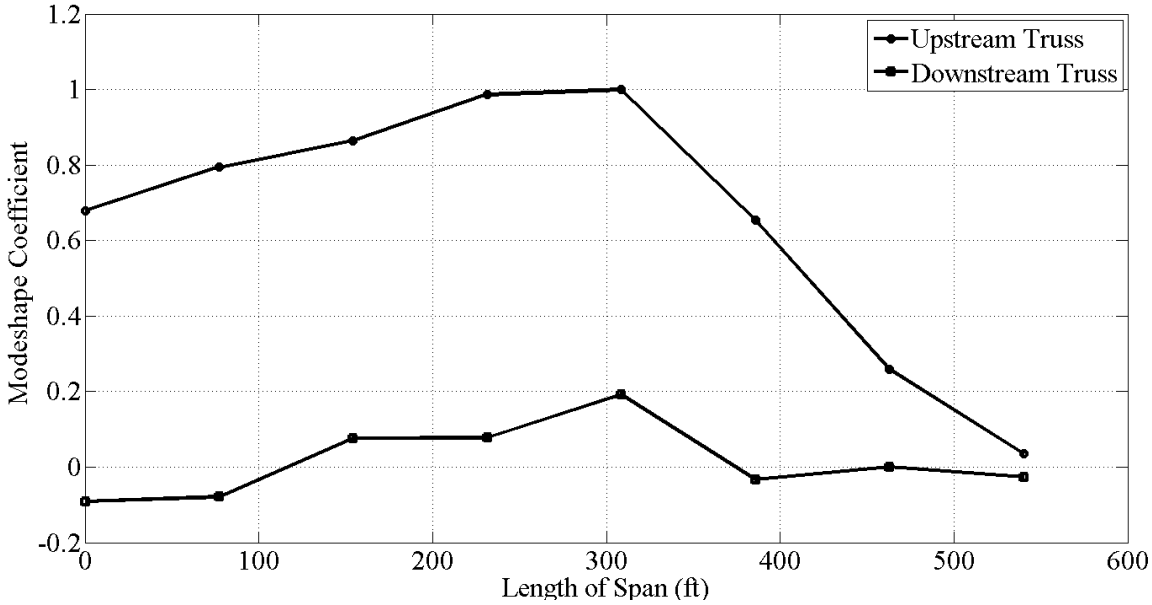

Figure 13-194: Lift Span 1st Torsion Mode

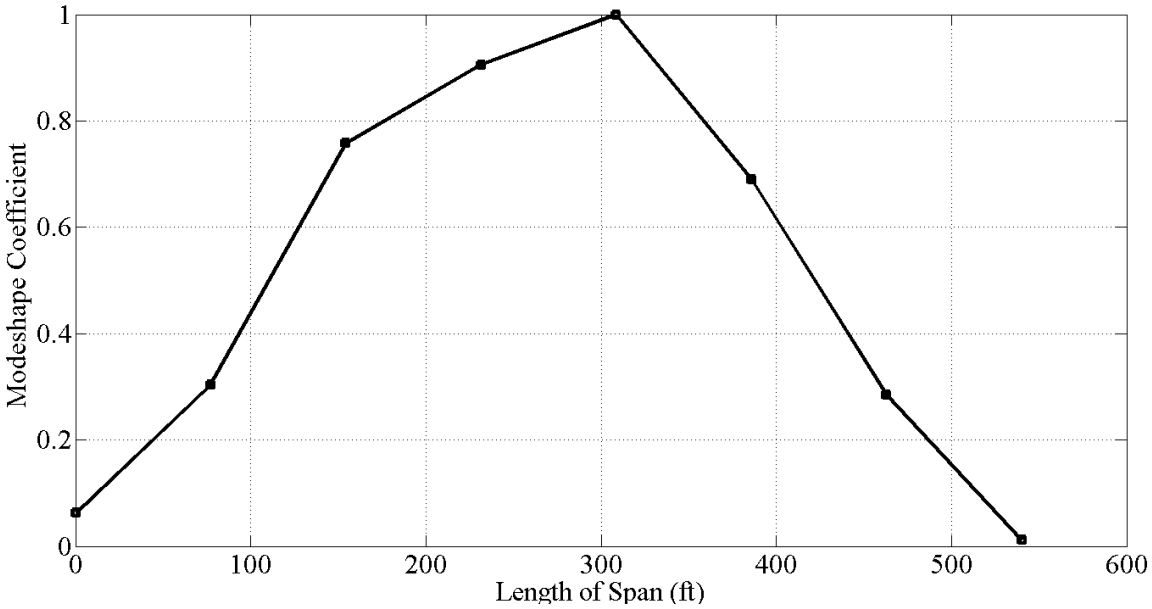

Figure 13-195: Lift Span 1st Vertical Mode

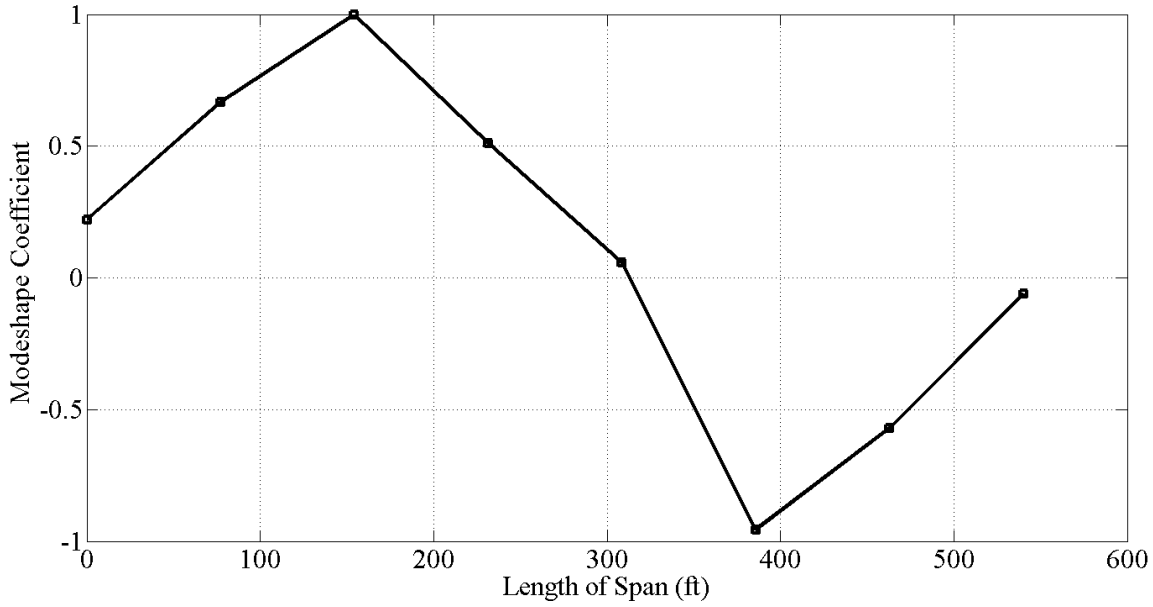

Figure 13-196: Lift Span 2nd Vertical Mode

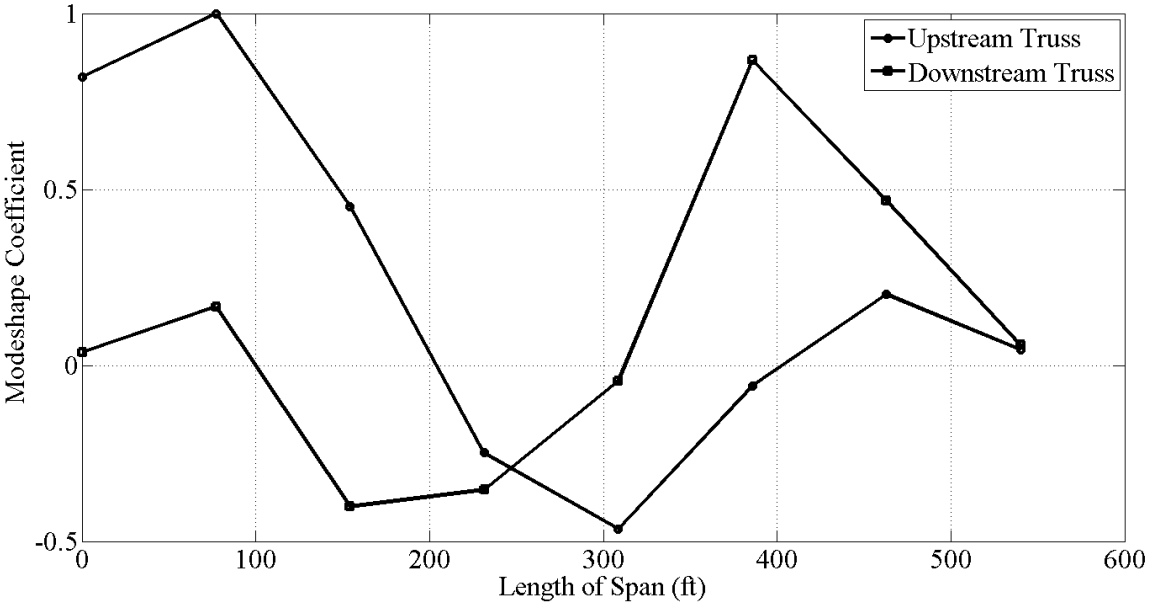

Figure 13-197: Lift Span 2nd Torsion Mode

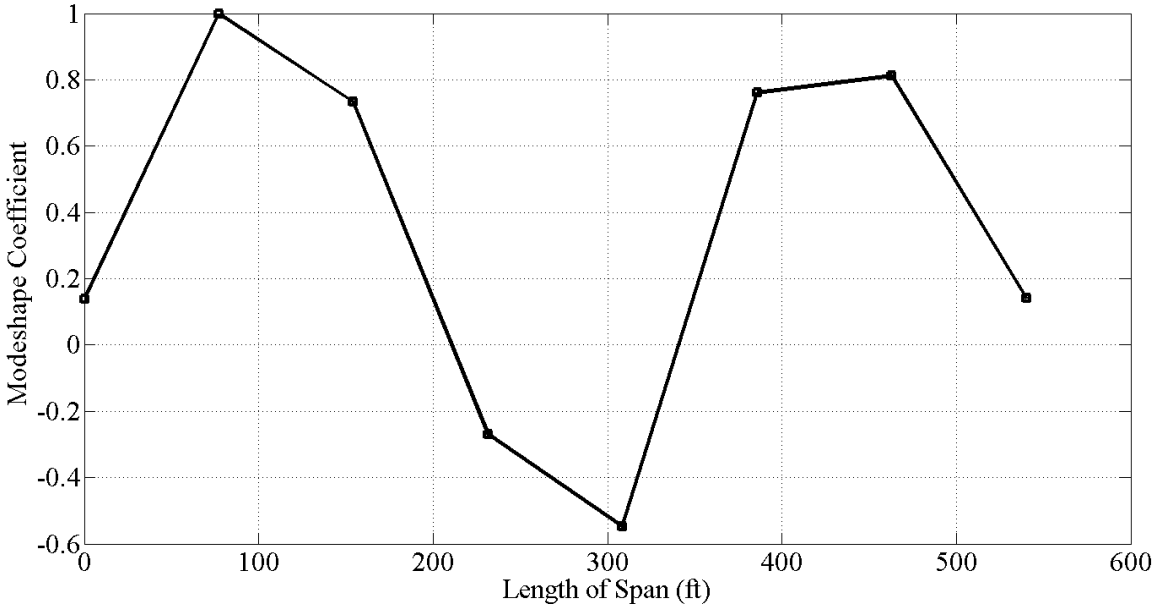

Figure 13-198: Lift Span 3rd Vertical Mode

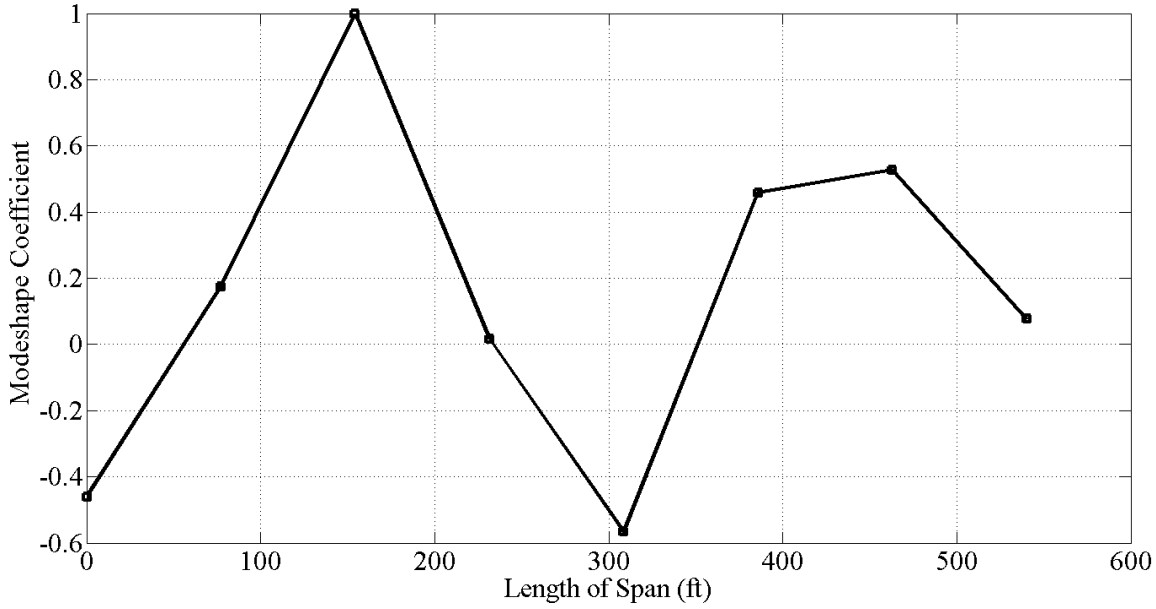

Figure 13-199: Lift Span 4th Vertical Mode

The lateral frequency identified for the lift span is listed in Table 13-15 and shown in Figure 13-200.

Table 13-15: Lift Span Lateral Frequency

Lift - Lateral Modeshapes	
Description	SSI (Hz)
1st Lateral	0.549

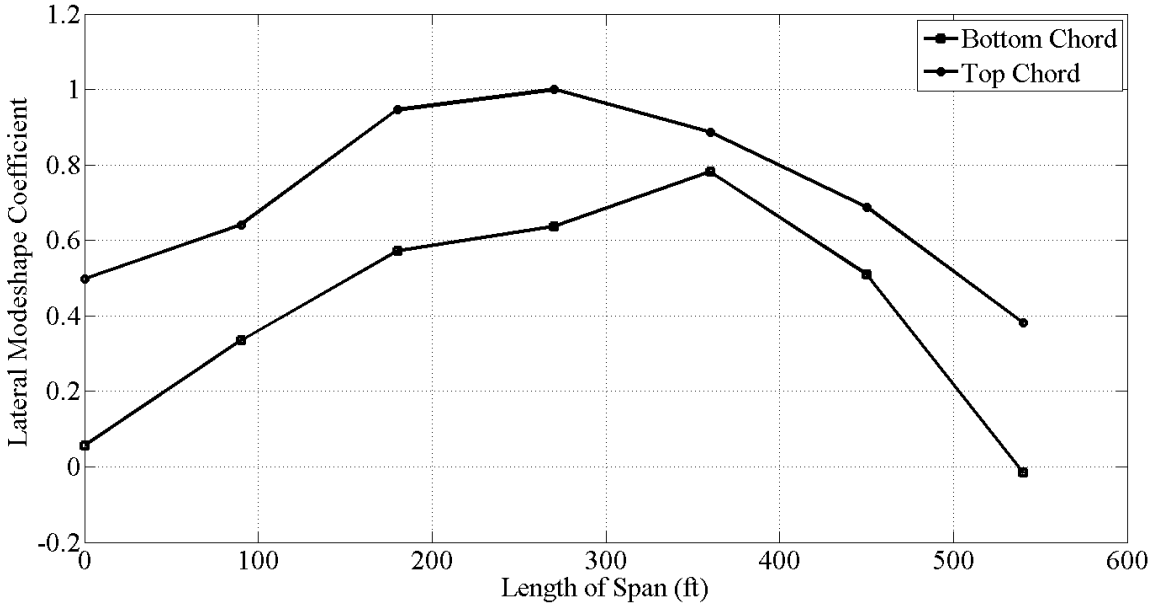

Figure 13-200: Lift Span 1st Lateral Mode

13.4.5.4. PA Tower Span

The vertical and torsional frequencies for the PA tower span are listed in Table 13-16 and shown in Figure 13-201 through Figure 13-206. Note that the modeshapes are drawn in elevation view.

Table 13-16: PA Tower Span Vertical / Torsional Frequencies

PA Tower - Vertical / Torsional Modeshapes		
Description	SSI (Hz)	CMIF (Hz)
1st Vertical	2.420	2.435
2nd Vertical	4.065	4.18
3rd Vertical	5.936	5.982
4th Vertical	8.540	8.178
1st Torsion	6.484	6.498
2nd Torsion	10.439	10.276

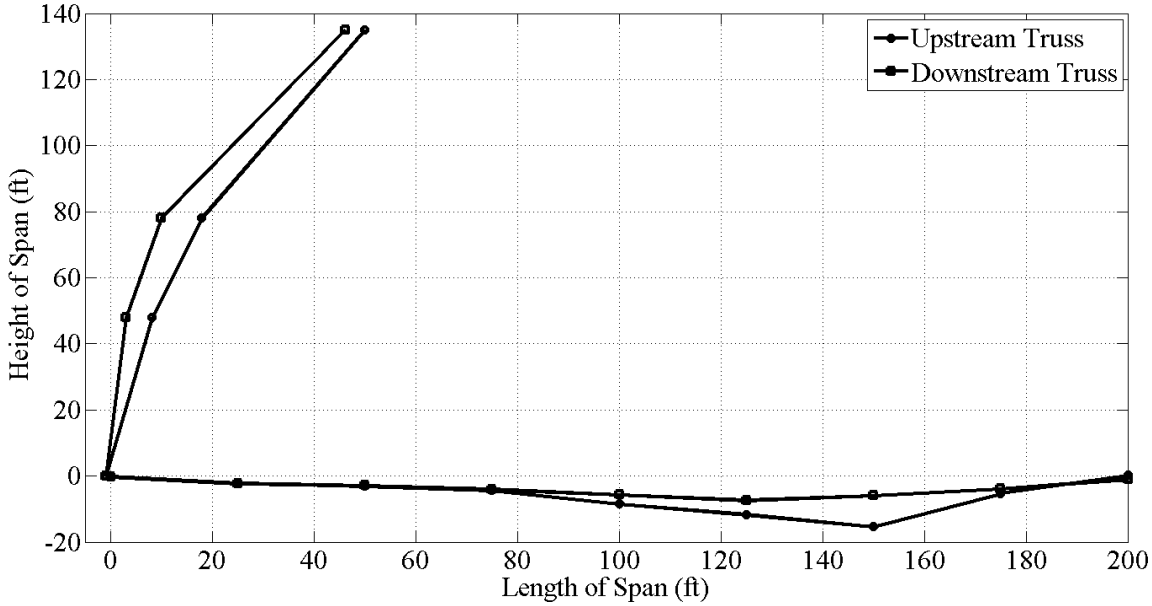

Figure 13-201: PA Tower Span 1st Vertical Mode

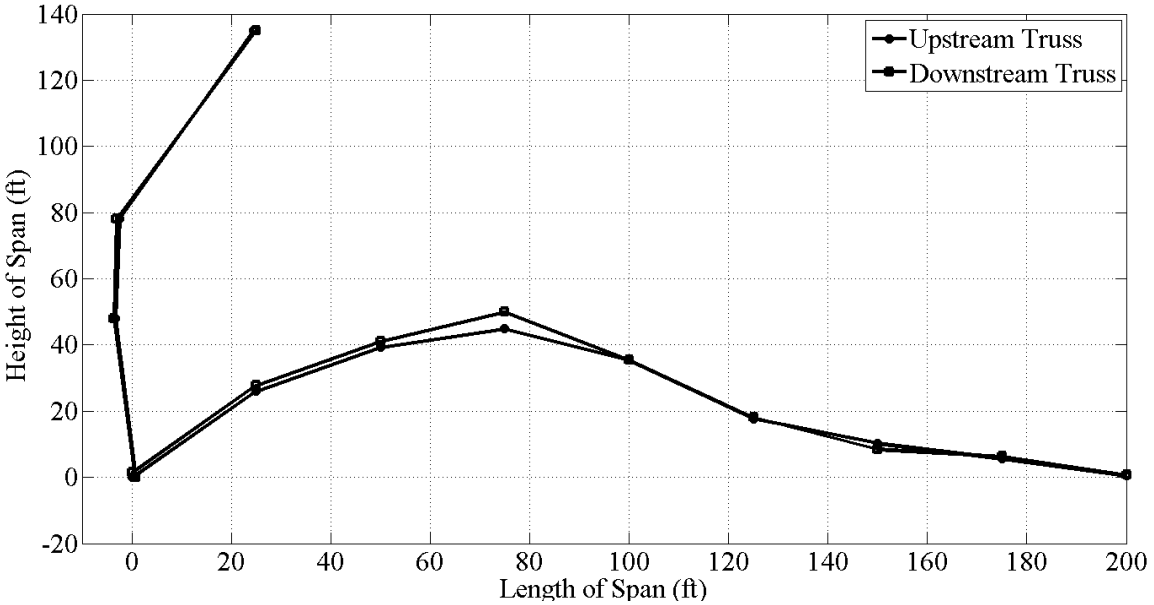

Figure 13-202: PA Tower Span 2nd Vertical Mode

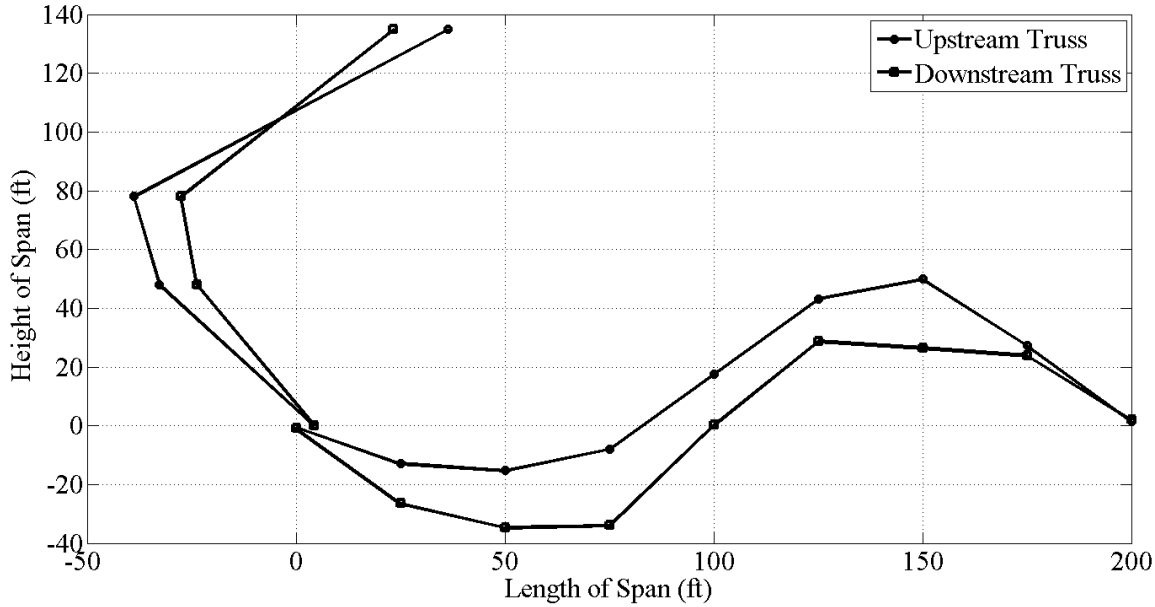

Figure 13-203: PA Tower Span 3rd Vertical Mode

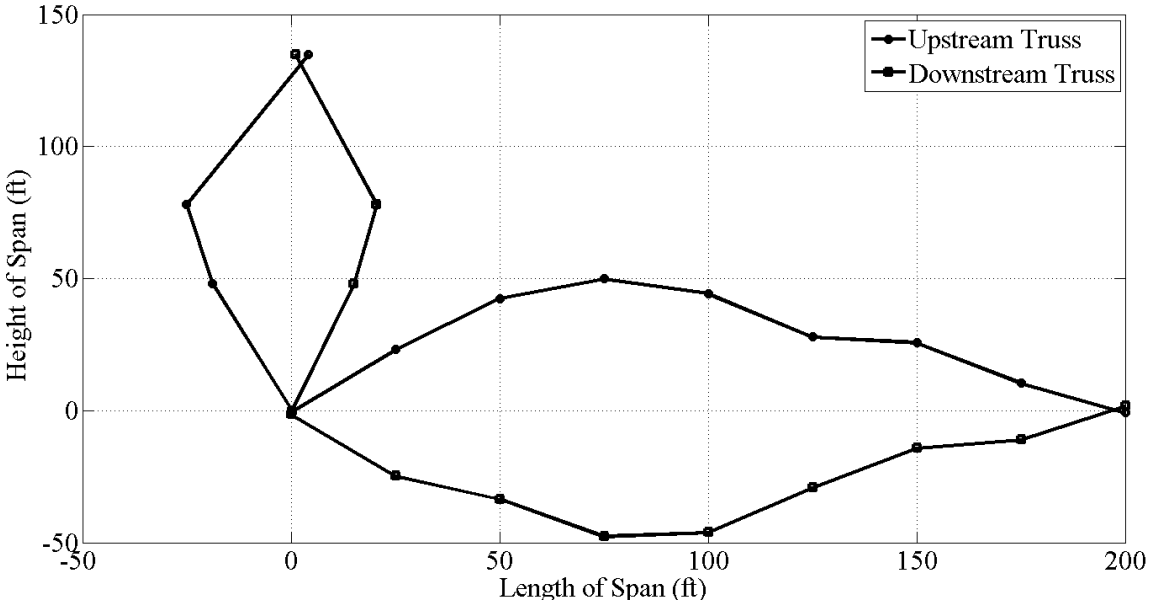

Figure 13-204: PA Tower Span 1st Torsion Mode

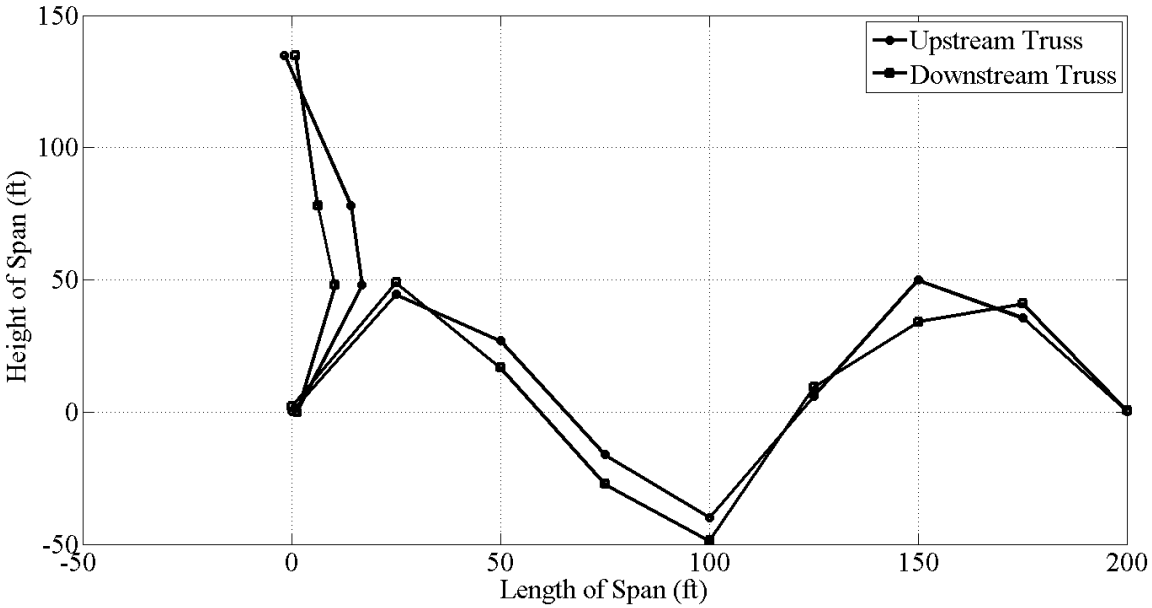

Figure 13-205: PA Tower Span 4th Vertical Mode

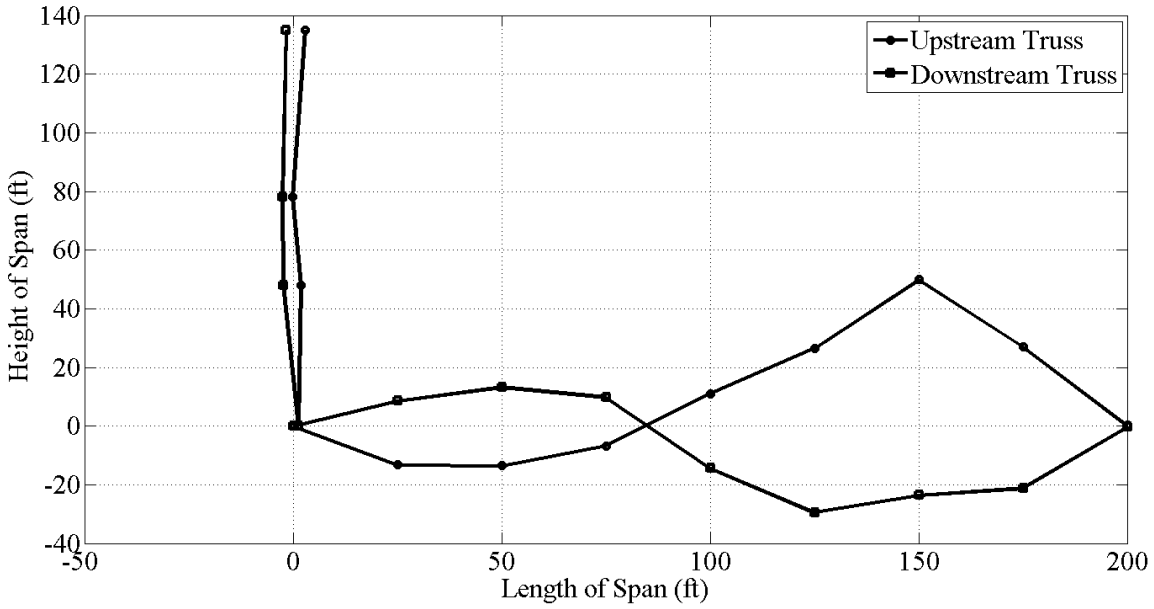

Figure 13-206: PA Tower Span 2nd Torsion Mode

The lateral frequencies for the PA tower span are listed in Table 13-17 and shown in Figure 13-207 through Figure 13-210. Note that the modeshapes are drawn in plan view and show the lateral modeshape coefficient for the top of the tower, top chord of the truss and bottom chord of the truss.

Table 13-17: PA Tower Span Lateral Frequencies

PA Tower - Lateral Modeshapes	
Description	SSI (Hz)
1st Lateral	2.394
2nd Lateral	3.160
3rd Lateral	3.504
4th Lateral	4.408

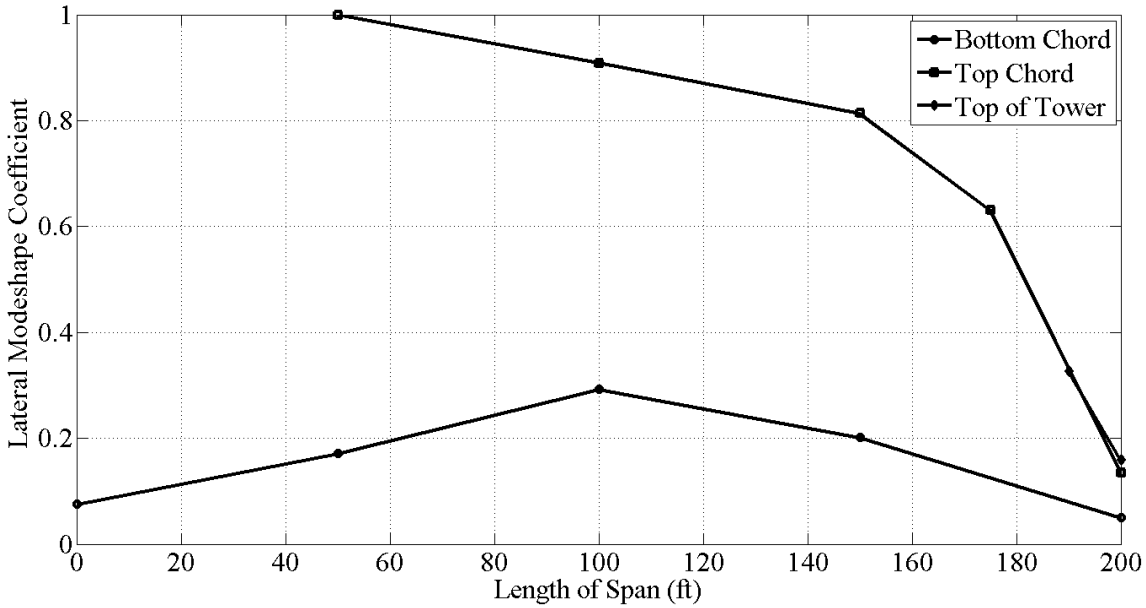

Figure 13-207: PA Tower Span 1st Lateral Mode

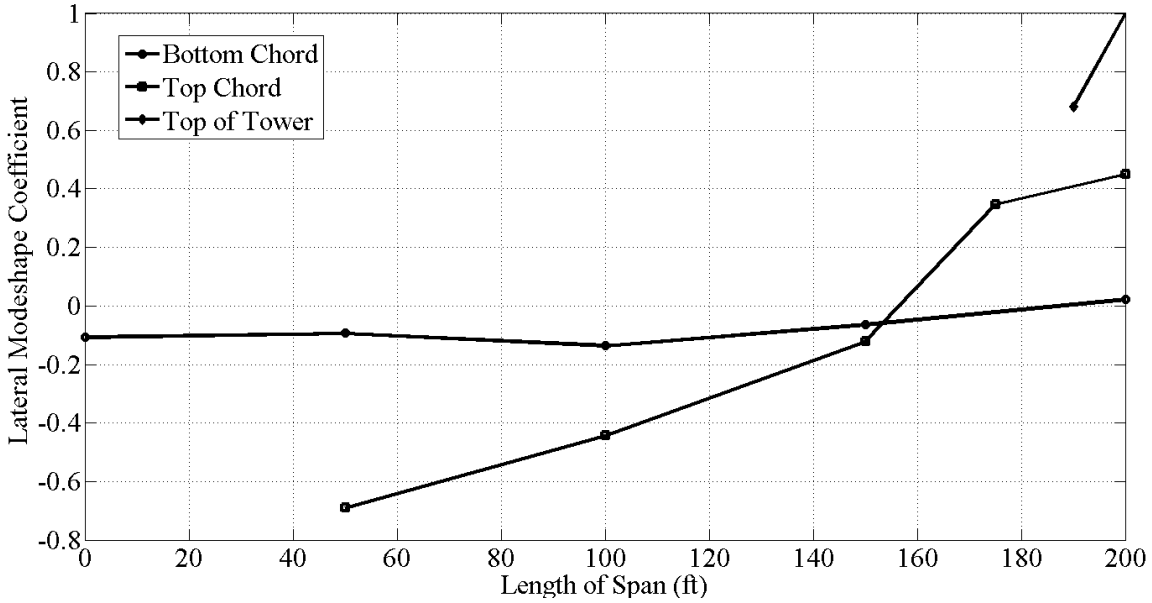

Figure 13-208: PA Tower Span 2nd Lateral Mode

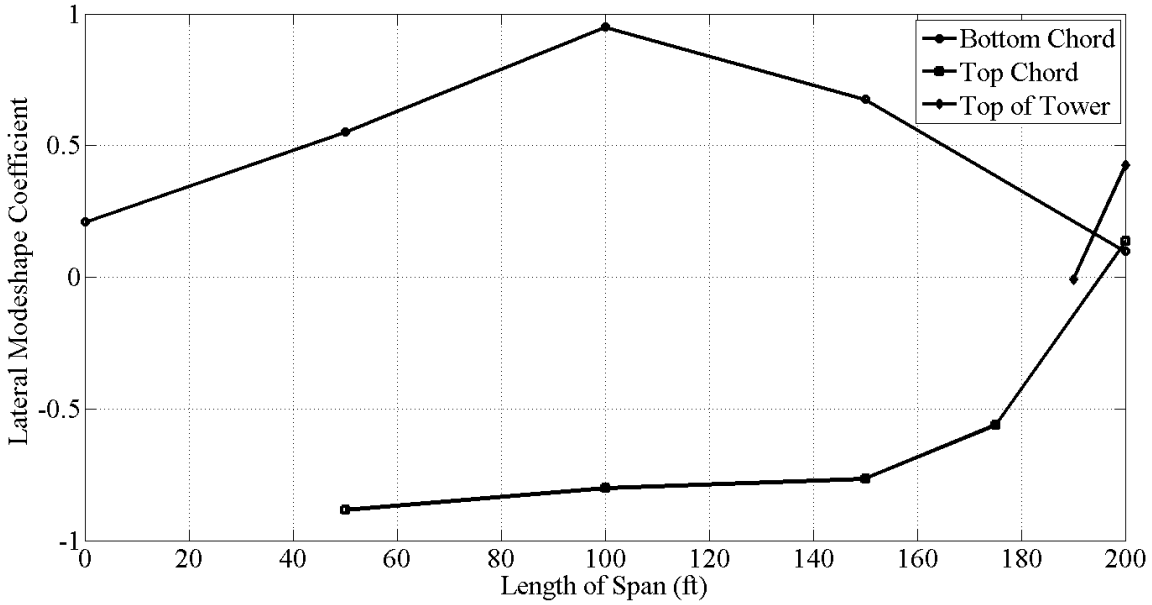

Figure 13-209: PA Tower Span 3rd Lateral Mode

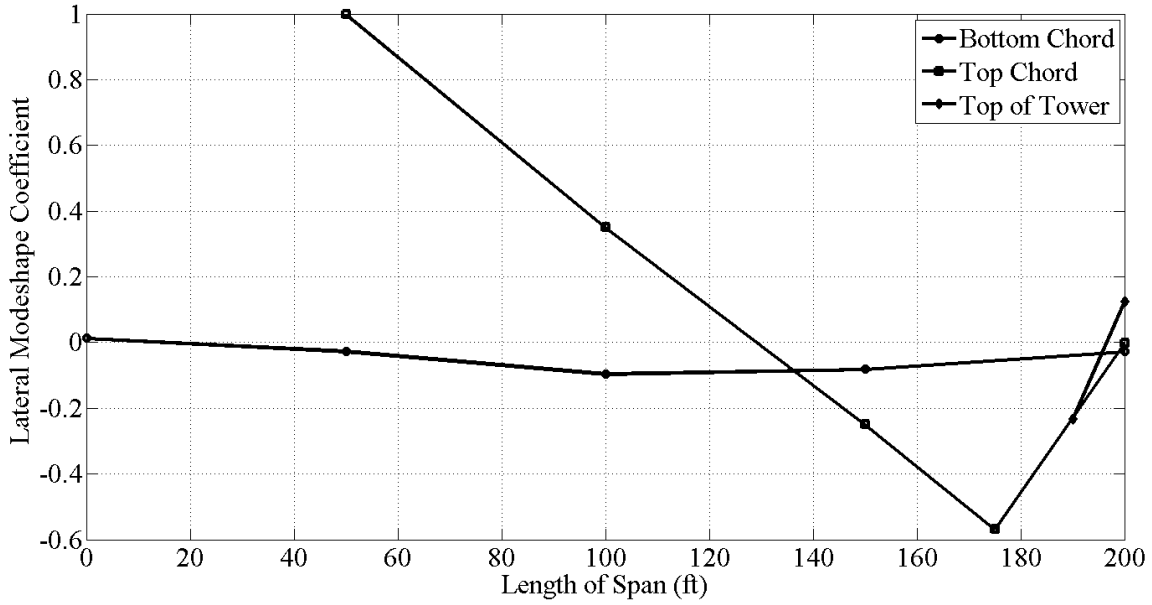

Figure 13-210: PA Tower Span 4th Lateral Mode

13.4.5.5. PA Truss Spans

The vertical and torsional modeshapes for the three spans of the PA truss spans (Span 1, Span 2 and Span 3 from PA towards NJ respectively) are listed in Table 13-18 and shown in Figure 13-211 through Figure 13-225. Note that the modeshapes are drawn in elevation view. The reference sensor on the downstream chords of the trusses is plotted as a single point. While this measurement was able to distinguish between the first vertical and first torsional modeshapes by indicating the phase of the downstream truss, the second vertical and second torsional modes were distinguished by correlating the frequencies with the NJ truss span, which are all very close for the vertical and torsional shapes.

Table 13-18: PA Truss Span Vertical / Torsional Frequencies

PA Truss - Vertical / Torsional Modeshapes			
Description	Span 1	Span 2	Span 3
1st Vertical	3.735	3.784	3.809
2nd Vertical	9.79	9.79	10.03
3rd Vertical	15.11	15.26	15.06
1st Torsion	5.664	5.615	5.566
2nd Torsion	13.04	12.92	12.72

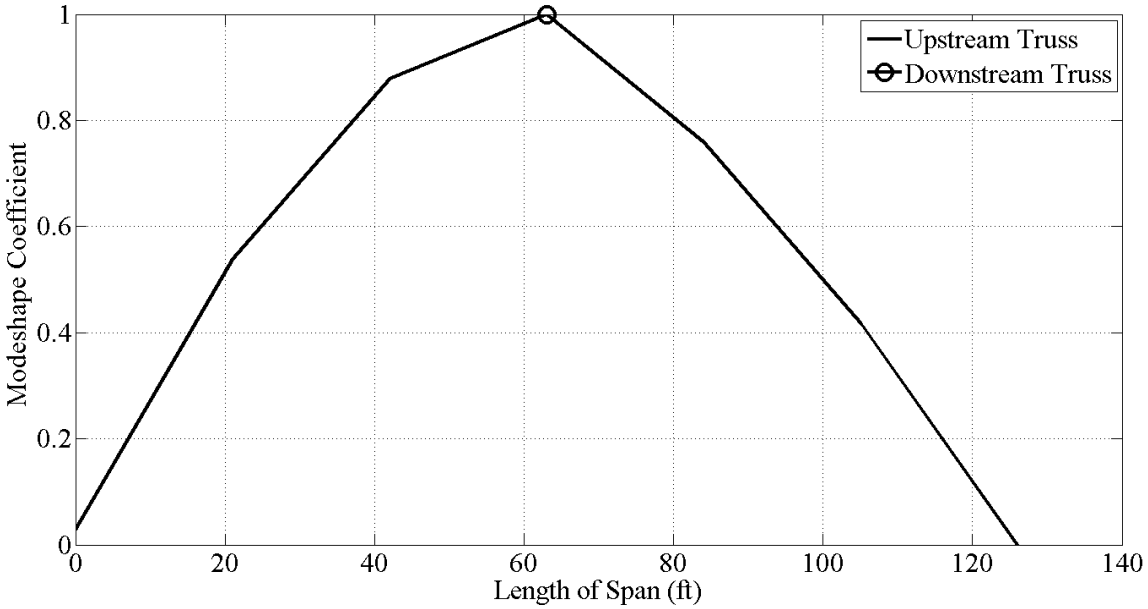

Figure 13-211: PA Truss Span 1 1st Vertical Mode

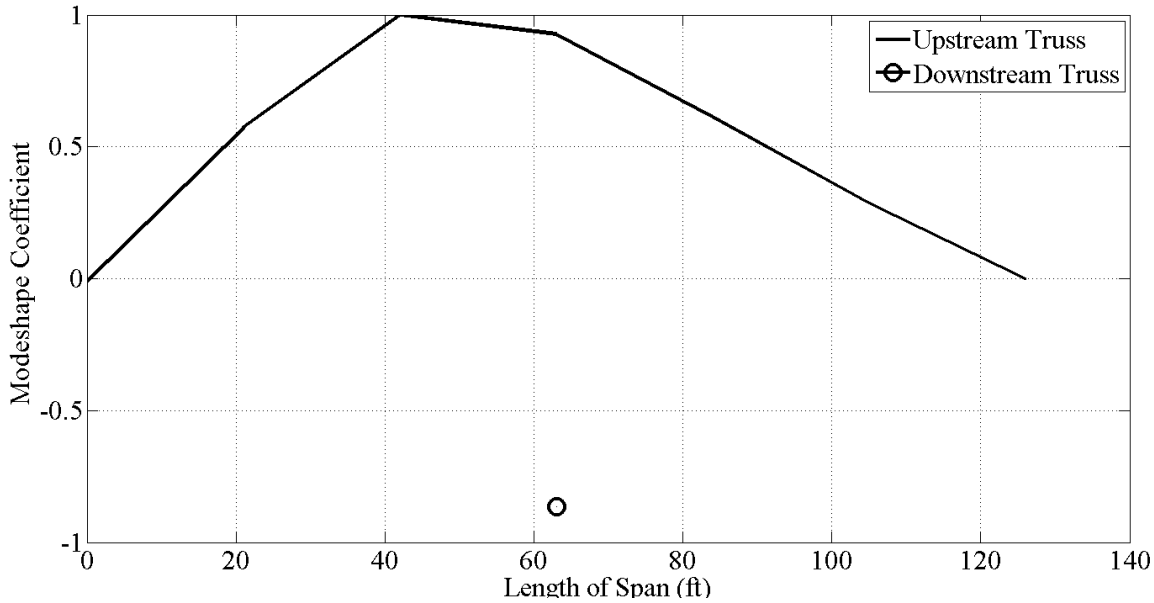

Figure 13-212: PA Truss Span 1 1st Torsion Mode

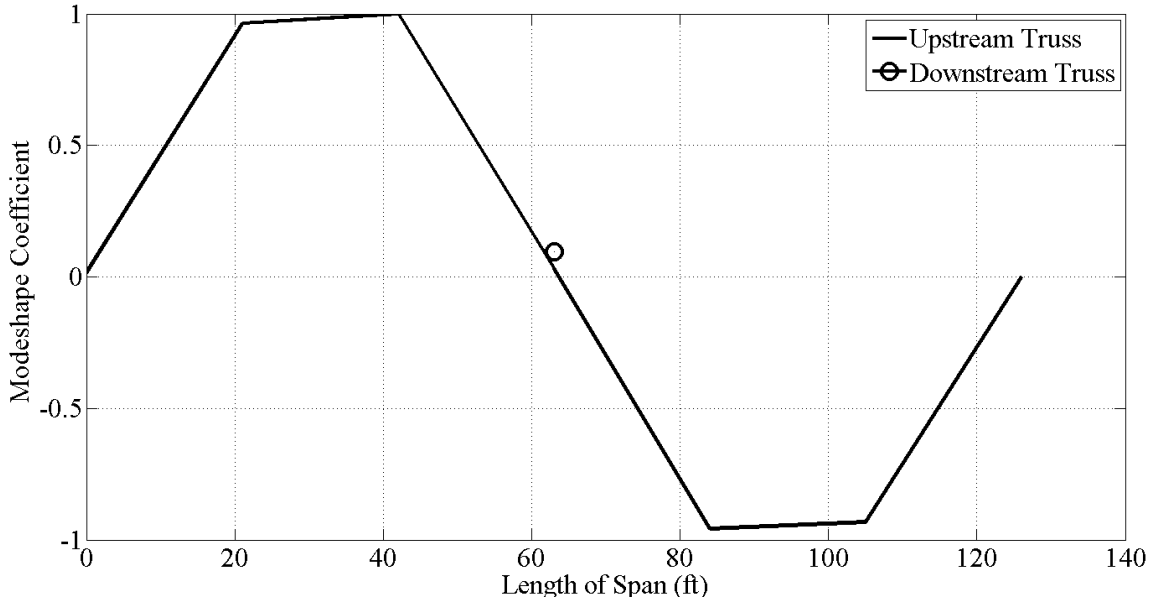

Figure 13-213: PA Truss Span 1 2nd Vertical Mode

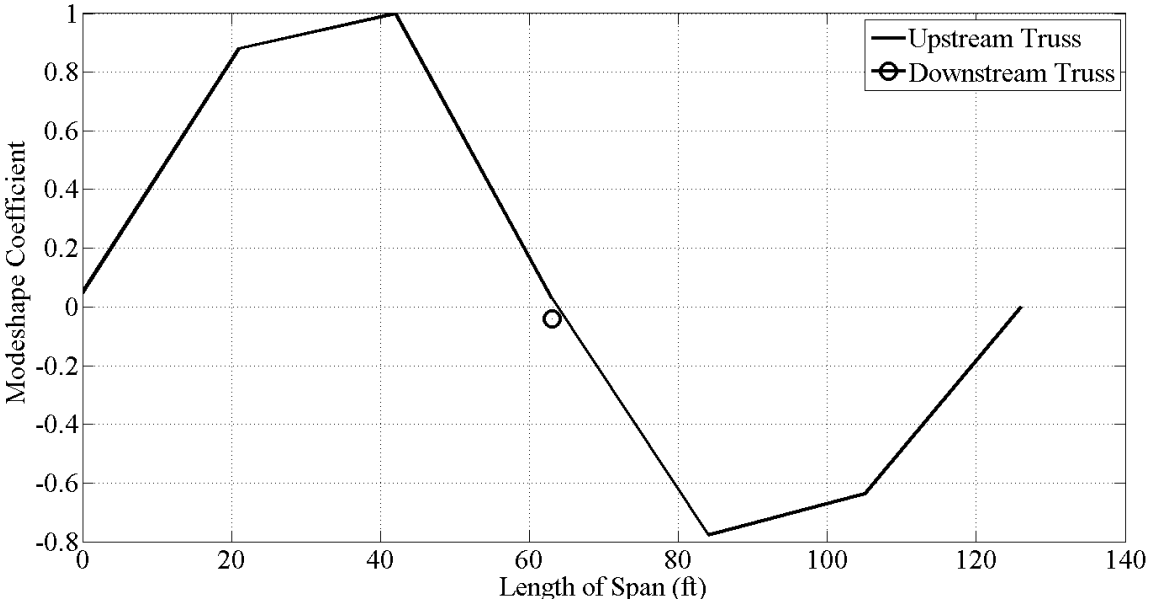

Figure 13-214: PA Truss Span 1 2nd Torsion Mode

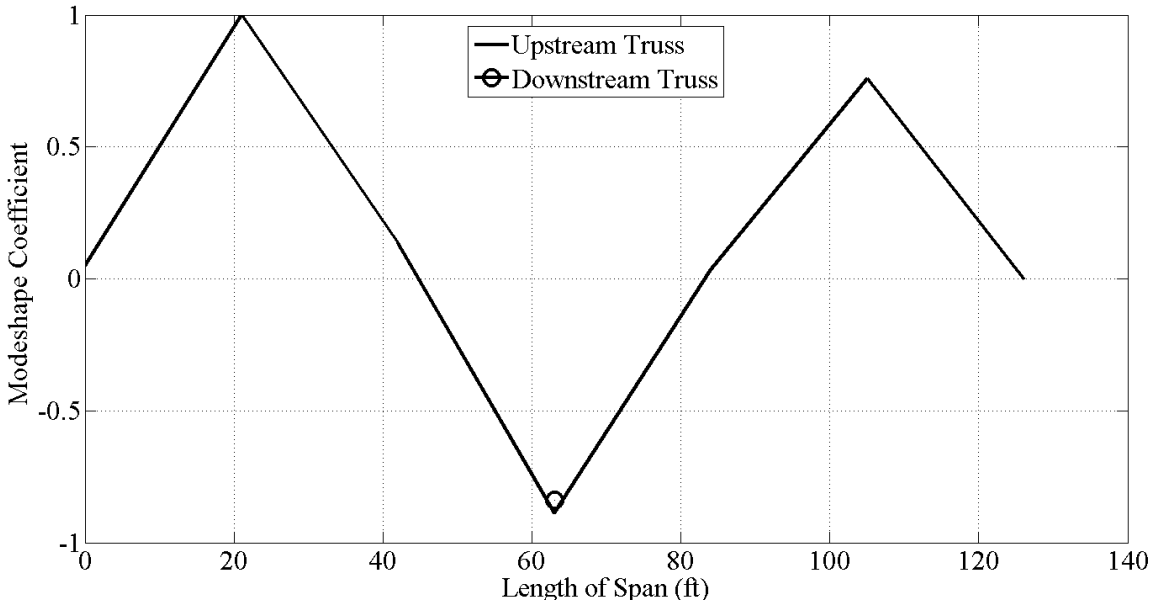

Figure 13-215: PA Truss Span 1 3rd Vertical Mode

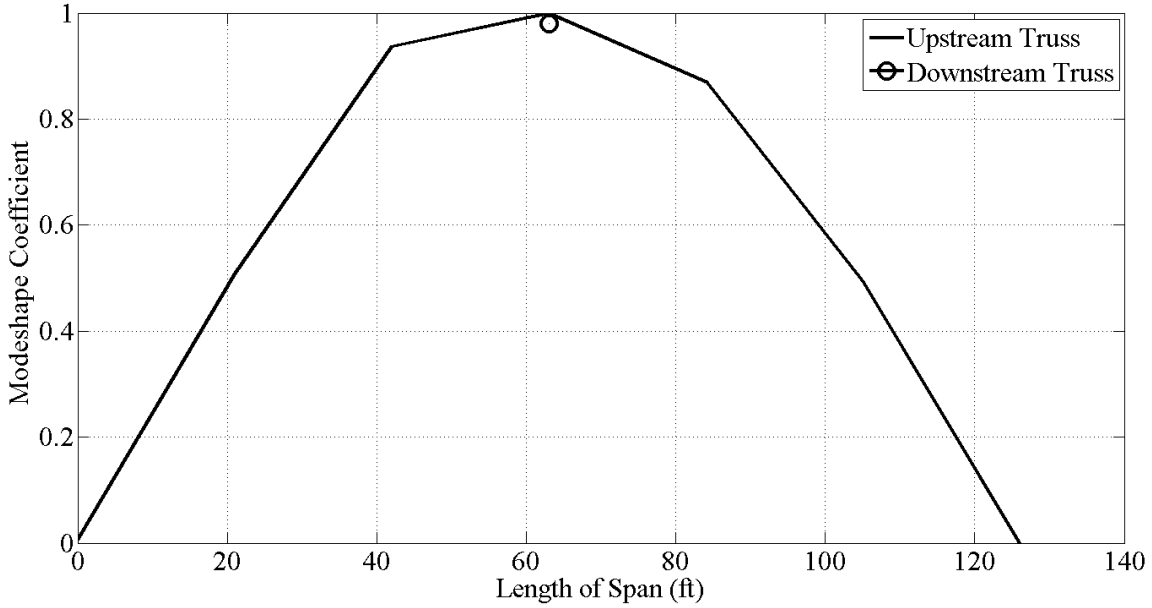

Figure 13-216: PA Truss Span 2 1st Vertical Mode

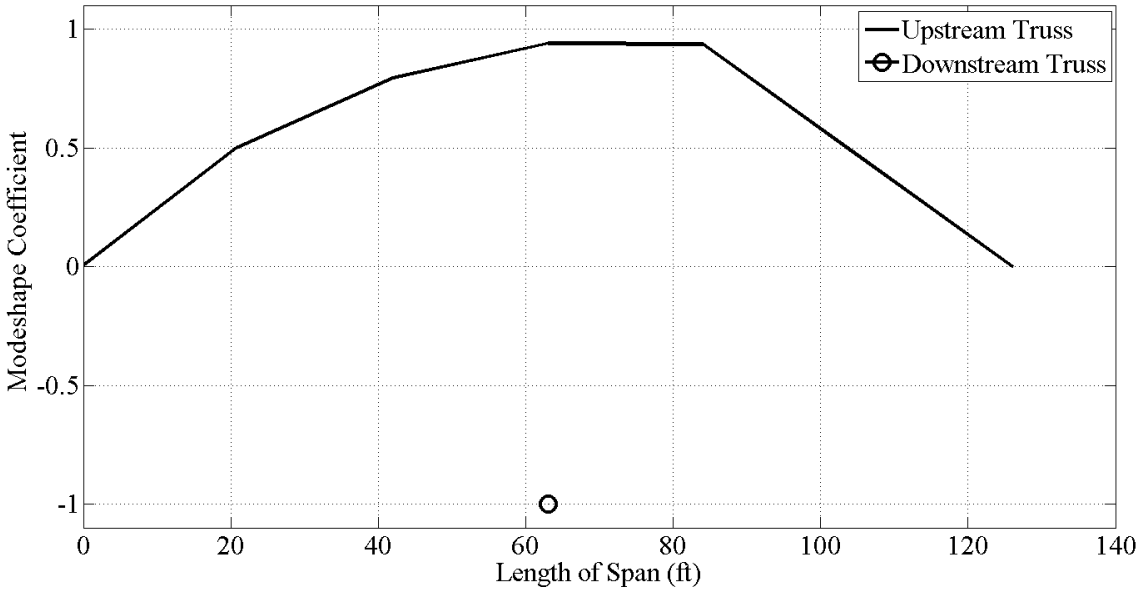

Figure 13-217: PA Truss Span 2 1st Torsion Mode

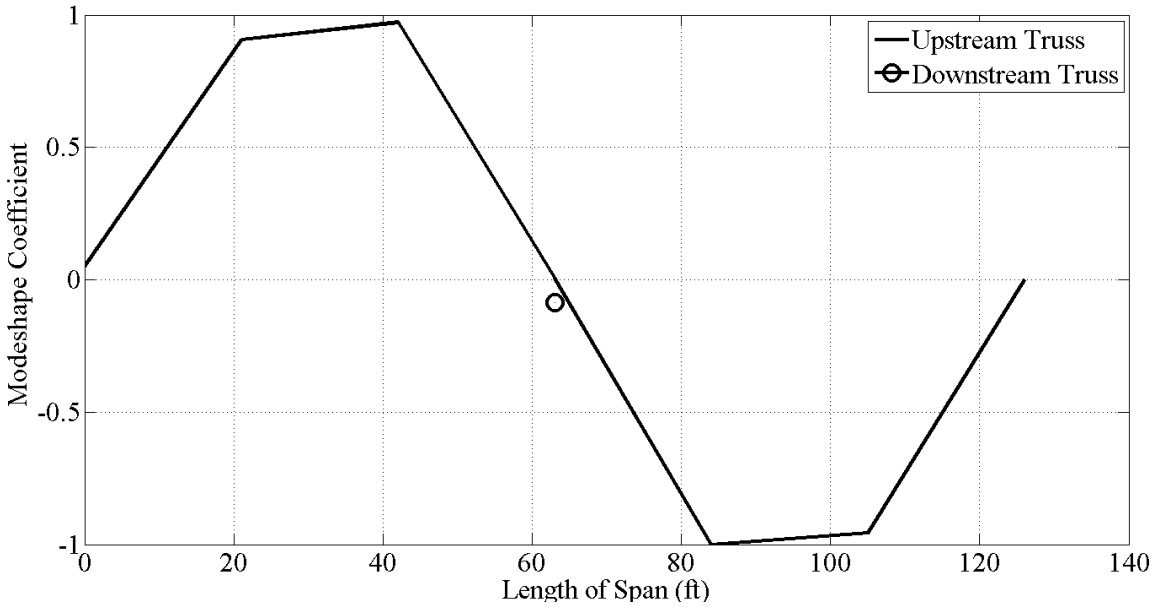

Figure 13-218: PA Truss Span 2 2nd Vertical Mode

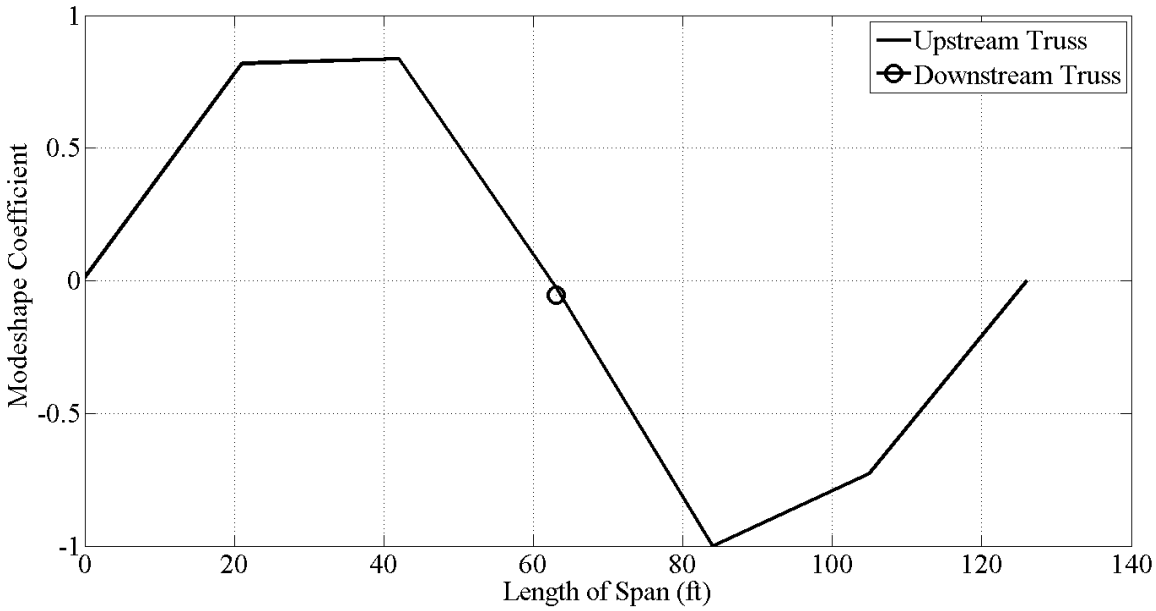

Figure 13-219: PA Truss Span 2 2nd Torsion Mode

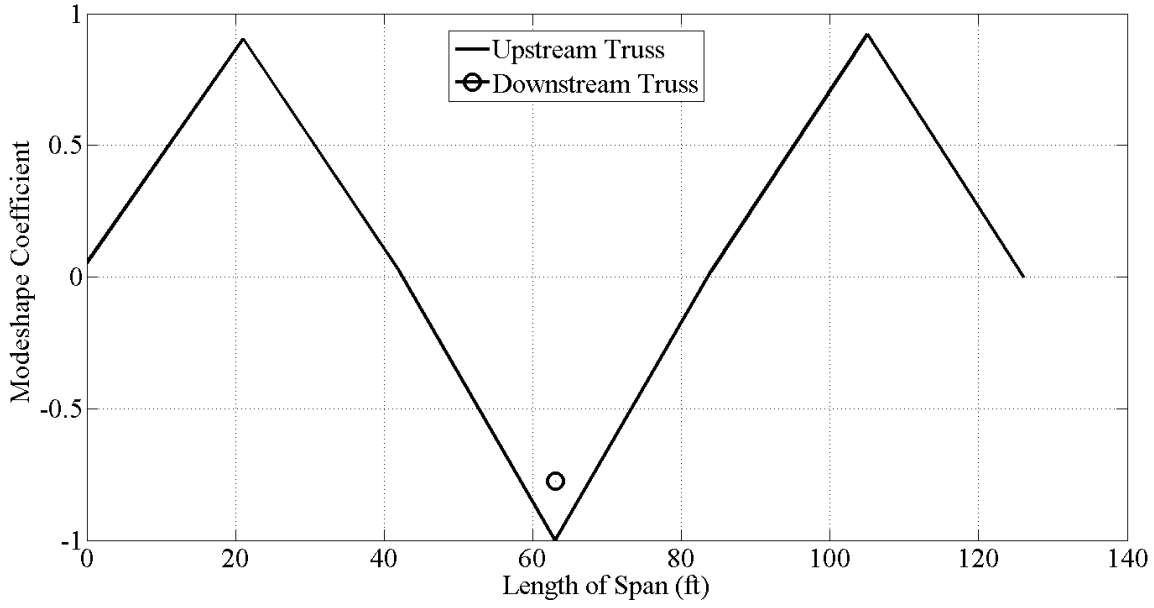

Figure 13-220: PA Truss Span 2 3rd Vertical Mode

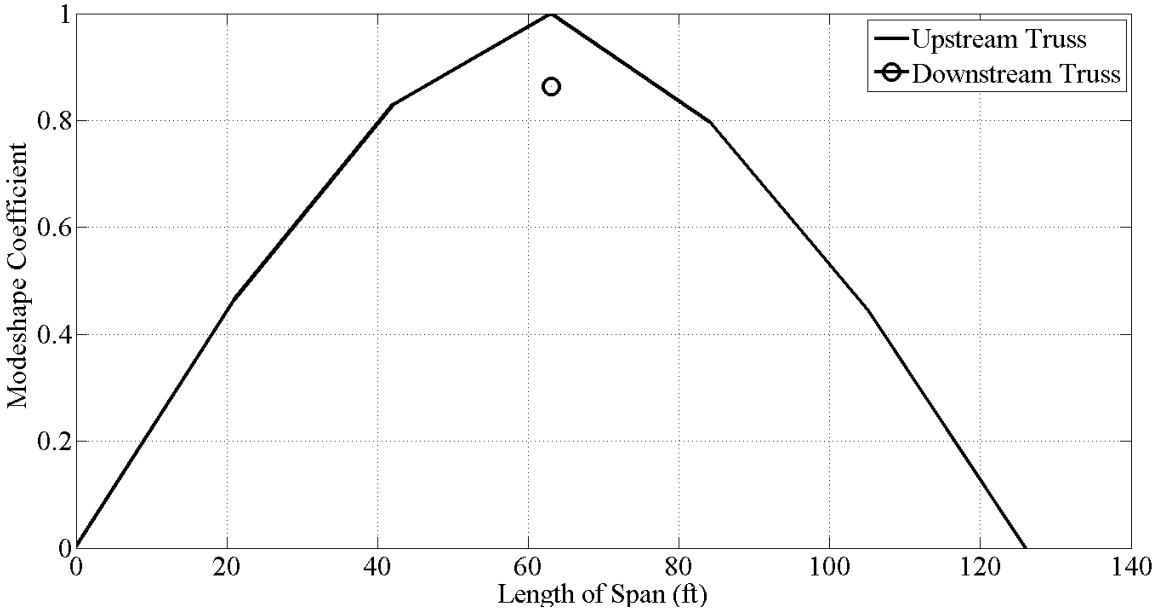

Figure 13-221: PA Truss Span 3 1st Vertical Mode

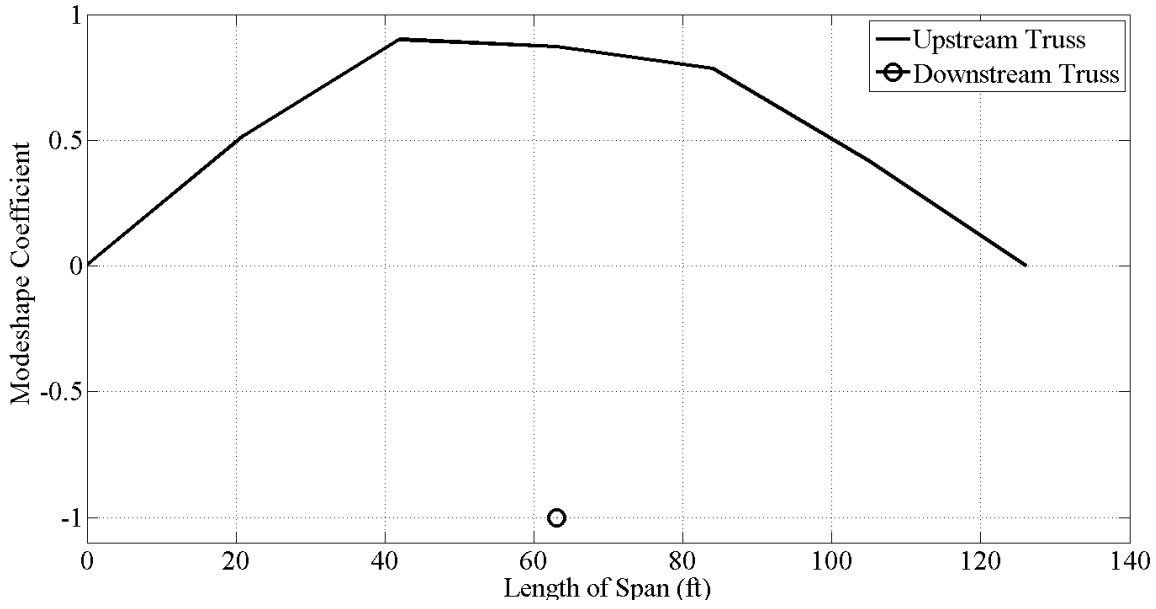

Figure 13-222: PA Truss Span 3 1st Torsion Mode

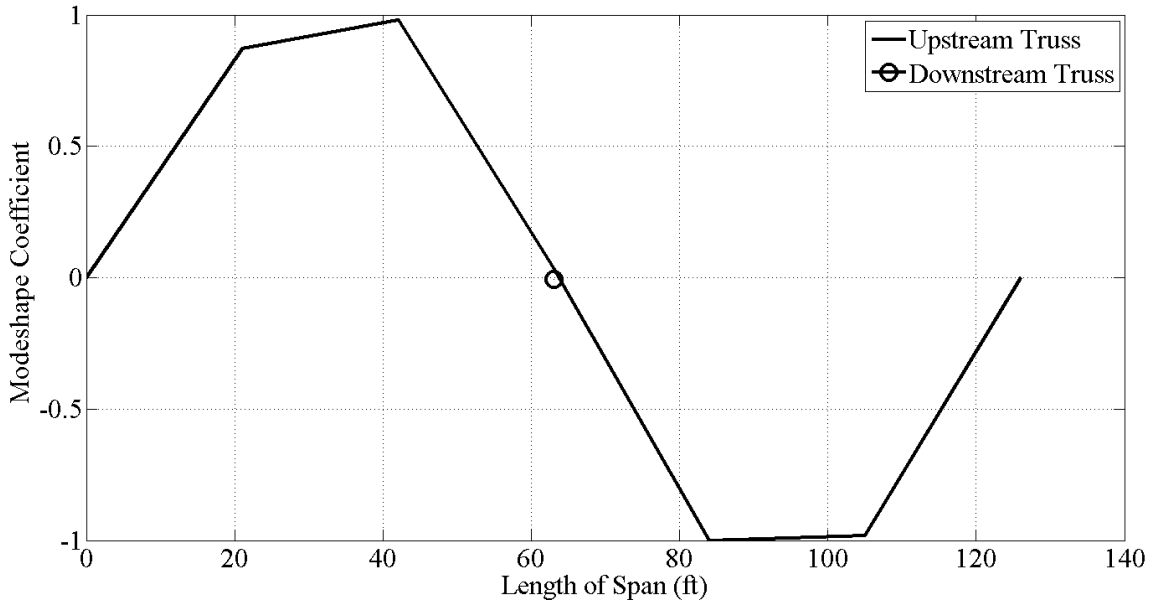

Figure 13-223: PA Truss Span 3 2nd Vertical Mode

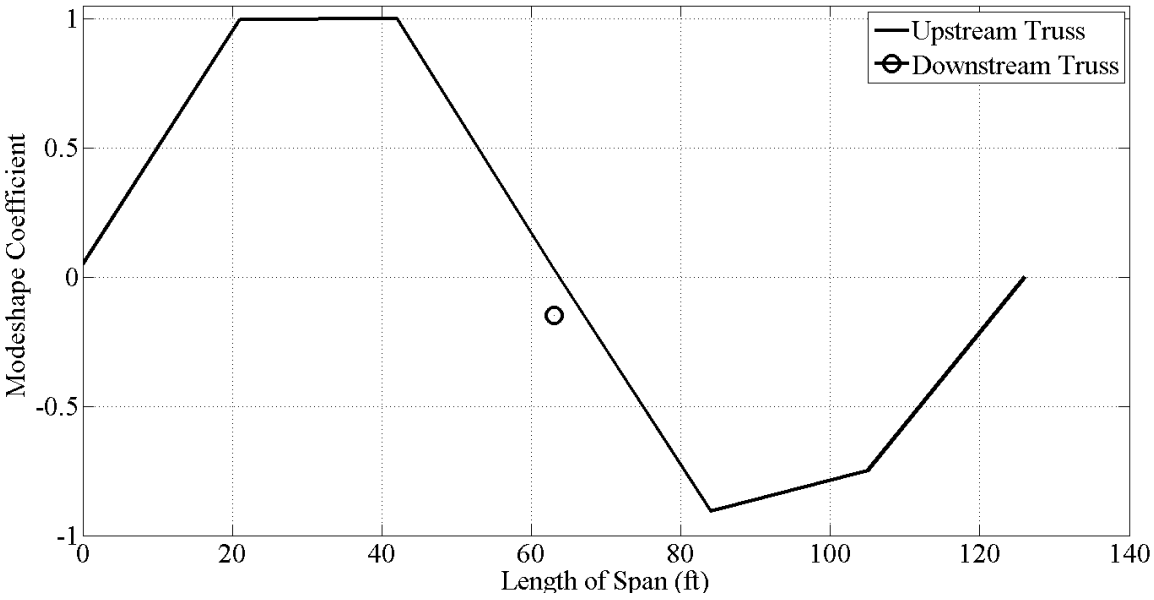

Figure 13-224: PA Truss Span 3 2nd Torsion Mode

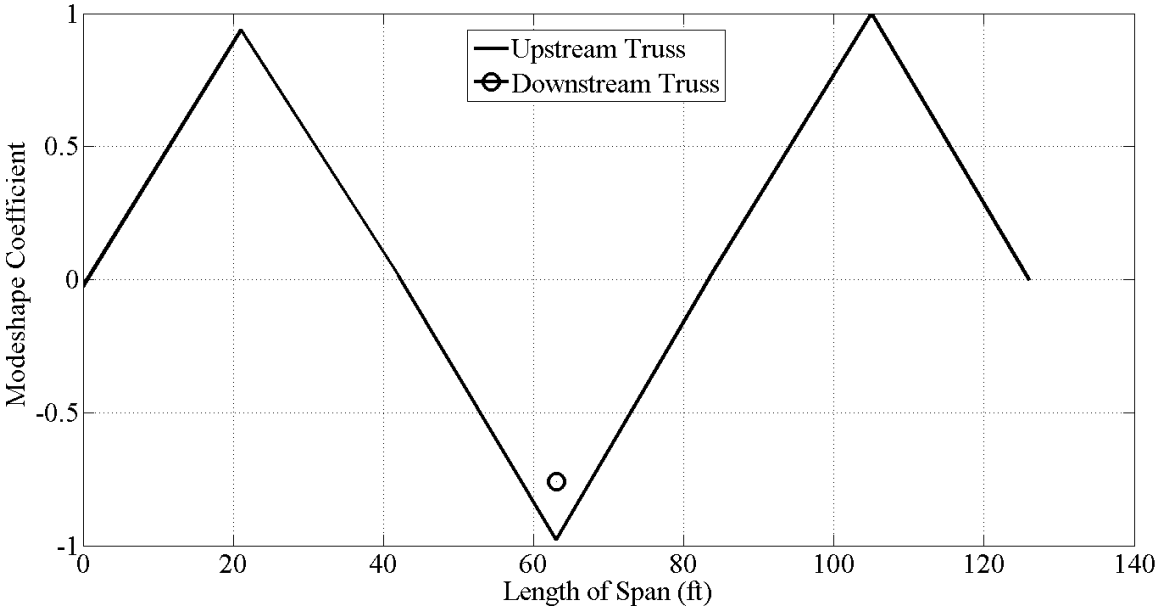

Figure 13-225: PA Truss Span 3 3rd Vertical Mode

The lateral mode for the three PA truss spans is listed in Table 13-19 and shown in Figure 13-226. Only two lateral modes were found for the three spans combined together. There were additional lateral responses, however they were coupled with torsional modes and were not shown.

Table 13-19: PA Truss Span Lateral Modeshape

PA Truss - Lateral Modeshape	
Description	SSI (Hz)
1st Lateral	2.881

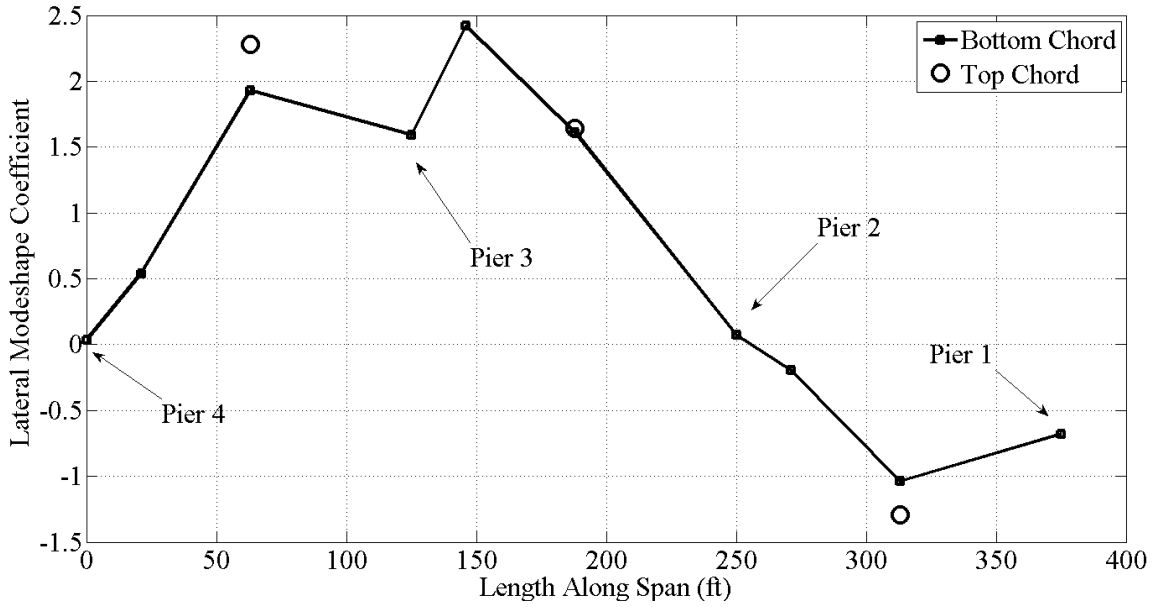

Figure 13-226: PA Truss Span 1st Lateral Modeshape

13.5. Design and Implementation of a Laser Height Monitoring System

The BCBC maintenance staff and operators rely on a system of pulleys and cables to raise the lift span from its seated position to allow for ship passage. Over time, the operating ropes, which transmit the movement applied by the motors in the machine house at mid-span of the lift span to the counterweights, become stretched out from the constant use. The machine house is also equipped with an original mechanical system indicating the current height of the lift span as it is raised and lowered. However, this mechanical system is dependent upon the movement of the operating ropes, and as they become slack, the height indicator loses accuracy for the last few feet of the lift spans descent. This resulted in the operators relying heavily upon the breaks as they slowly

seated the span so that they would not jar the span by dropping it too fast. This lack of knowledge about where the lift span was over the last few feet while lowering the span in addition to the benefits of more accurately knowing the height of the span as ships pass by, prompted BCBC staff to request from Drexel University a monitoring system that was capable of digitally and accurately displaying and recording the height of the lift span during an opening sequence.

To address this request by the BCBC, Drexel University research staff investigated the potential for electronic sensors to be incorporated into such a system and automatically display the pertinent information to the operators with minimal interaction by the operators. The first challenge was to identify the most appropriate sensor to accomplish this task, and then verify in the laboratory whether or not the sensor would be applicable. Finally, the system would need to be installed and tested with openings of the lift span against known means of measuring the height of the span.

13.5.1. Selection of Sensors

The lift span travels seventy-five vertically in the air as it is raised from its seated position to a fully open position. This large distance requires specialized sensing equipment capable of reliably capturing the height of the span with minimal maintenance and long term stability. Given the range required, the selection of sensors came down to two main types: (1) string pot based displacement transducer and (2) laser based, time-of-flight sensor.

After investigating the two sensor types applicable to this specific task, it was found that the string pot based potentiometers were both expensive and would require maintenance if exposed to conditions where dirt and debris were to collect on the cable. Given the nature of the BBB lift span, the open grate allows a variety of dirt and debris to fall through the roadway deck to the piers supporting it. It was feared that for the great cost of these sensors, they might easily become damaged or unreliable given the conditions of the BBB structure.

After investigating multiple types of laser-based distance sensors, a specific sensor with a full range of 90 feet without a target and roughly 500 feet with an approved reflective target was identified as a promising candidate for the BBB. Further investigation in the sensor found that it was not operational over the full temperature conditions of the bridge, however this could be mitigated by constructing a temperature controlled box to house the sensor.

The AR1000 laser sensor (Figure 13-227), produced by Acuity Laser Measurement was selected as the sensor to use. The laser sensor has an accuracy of +/- 2.5mm over the full range and can be sampled at speeds up to 6Hz. The sensor uses a phase-shift comparison measurement principle to compute the distance between the sensor and its target. The relatively low sampling speed of the sensor is not a problem for this application, given that the operator would not be able to discern information at much more than a 1 or 2Hz as they are operating the structure.

Figure 13-227: Acuity AR1000 Laser Distance Sensor

13.5.2. Construction of Laser Box and Laboratory Verification

Once the laser sensors were acquired, a temperature controlled box needed to be designed to house the sensors throughout all conditions the bridge might face. Once installed in the box, the system must be verified in the laboratory for accuracy before being installed in the field.

The boxes were constructed by ordering basic plastic enclosures for electronic equipment. The enclosures were then modified by drilling a hole in the bottom of the box to allow the laser light to shine out of the box and the camera to detect the reflected laser light. To seal the hole, a plastic window encasement was constructed that held an angled piece of glass in place over the hole. The glass needed to be angled (Figure 13-228) so that any laser light reflecting off of the glass was not directed back into the laser, thus leading to a false measurement, but was directed to a corner of the box where it would do no harm.

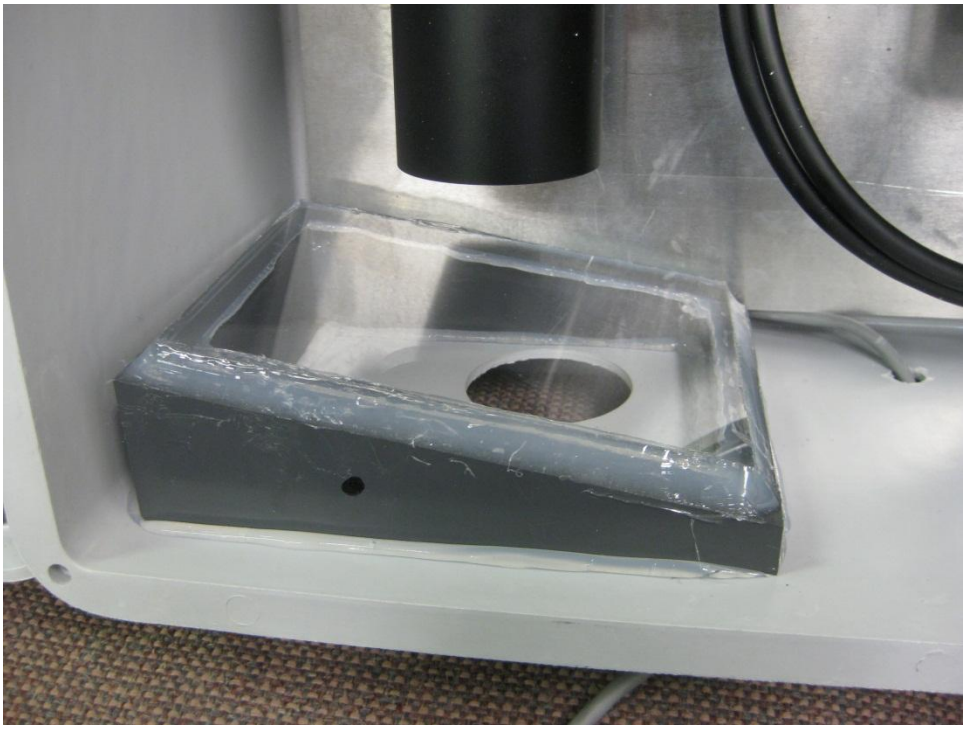

Figure 13-228: Custom Developed Enclosure Window to Allow for Laser Measurements

The box also required the installation of a thermostat controlled freeze-protection strip heater. The strip heater is programmed to turn on at 40°F until an internal temperature of 60° is reached at which point it is turned off. The minimum operating temperature of the AR1000 was specified as 14°F, which easily could be exceeded in the climate of the BBB. The upper temperature limit of the sensor was not however an issue given the climate of the BBB. The enclosure was also equipped with a fuse protected power strip, so that in the event of a short circuit the laser box would not affect the power circuit of

the BBB. Additionally, a 10V DC power converter and serial adapter was provided by the sensor manufacturer. The final laser box enclosure is shown in Figure 13-229.

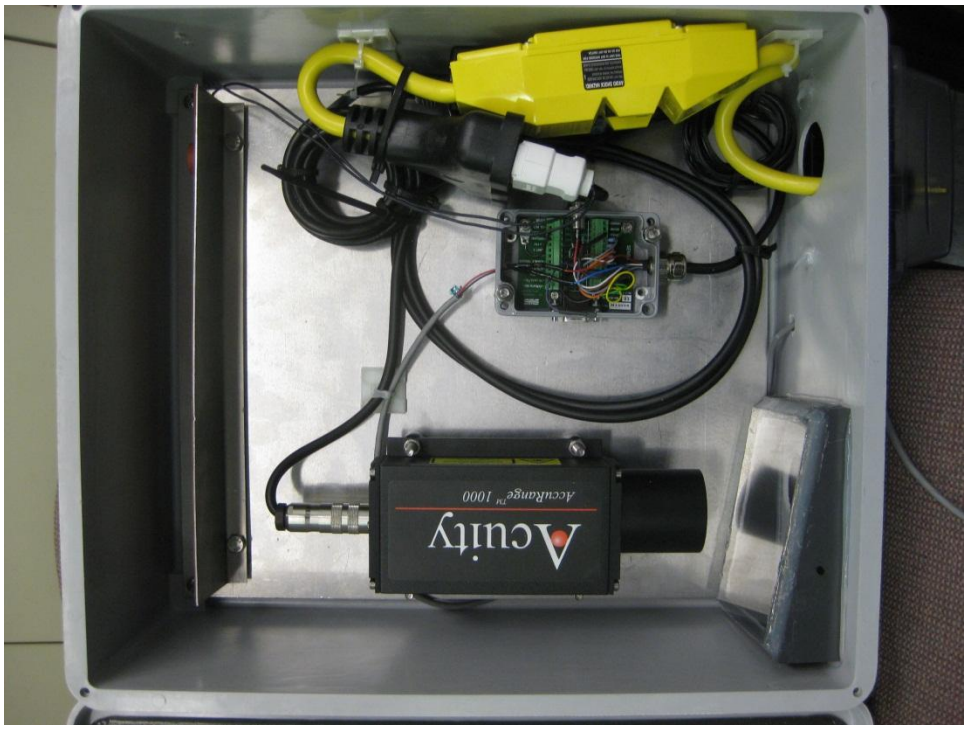

Figure 13-229: The Final Laser Enclosure

After the design of the laser enclosure was finalized, the system was verified in the laboratory by mounting the laser enclosure on a movable stand. The stand was then set up in a long straight hallway next to a surveyor's tape measure. The tape measure was stretched out along the floor from one wall to a distance 100' away. The laser box was

then measured with a Campbell Scientific CR1000 data logger with a 4-20mA terminal input module to allow for the conversion from the proportional current supplied by the laser to a differential voltage able to be measured by the data logger. No other equipment was needed to measure the laser sensor.

The read-out from the laser sensor was then verified against the tape measure as the stand was rolled down the length of the hallway. This procedure was repeated several times to ensure that the laser sensor was configured correctly and was reading accurately.

13.5.3. Installation of Laser Box

The laser boxes were installed in two locations: the southeast and northwest corners of the lift span bottom chord. The sensors were mounted to the lift span itself so that the instrumentation cables connecting the sensor to the data logger, which was housed in the machine house, did not need to span the joint between the lift span and the tower span. The boxes were bolted directly to a frame constructed by BCBC staff and then mounted to the bottom chord of the lift span (Figure 13-230).

Figure 13-230: The Laser Enclosure Mounted to the BBB Lift Span

The target for the laser sensor was found through trial and error of various materials and installation practices. The first target attempted was a piece of stainless steel mounted parallel with the top of the piers, directly underneath the laser enclosure. However, the surface proved to be too reflective and was causing errors within the laser sensor. A concrete block was then laid on top of the steel plate, which proved to be a much better target type than the steel plate. However, after a period of two weeks, the measurements were noted to have been very noisy during periods of inclement weather, specifically rain. It was then discovered that water was forming puddles on the surface of the concrete block and was scattering the laser light, leading to poor measurements. Finally, the

concrete block was tilted a few degrees to allow water to run off of its surface in the event of rain. This configuration and material proved to be the best target for the laser system and has been in place ever since its installation.

The lasers were instrumented with two-pair instrumentation cable which was housed in hard conduit from the ends of the lift span to the machine house located at mid-span. The data logger was then housed in the machine house and connected to a laptop which automatically records each opening and displays the height in an effective manner for the operators (Figure 13-231). A time history of a series of openings is shown in Figure 13-232, and a single opening is shown in Figure 13-233.

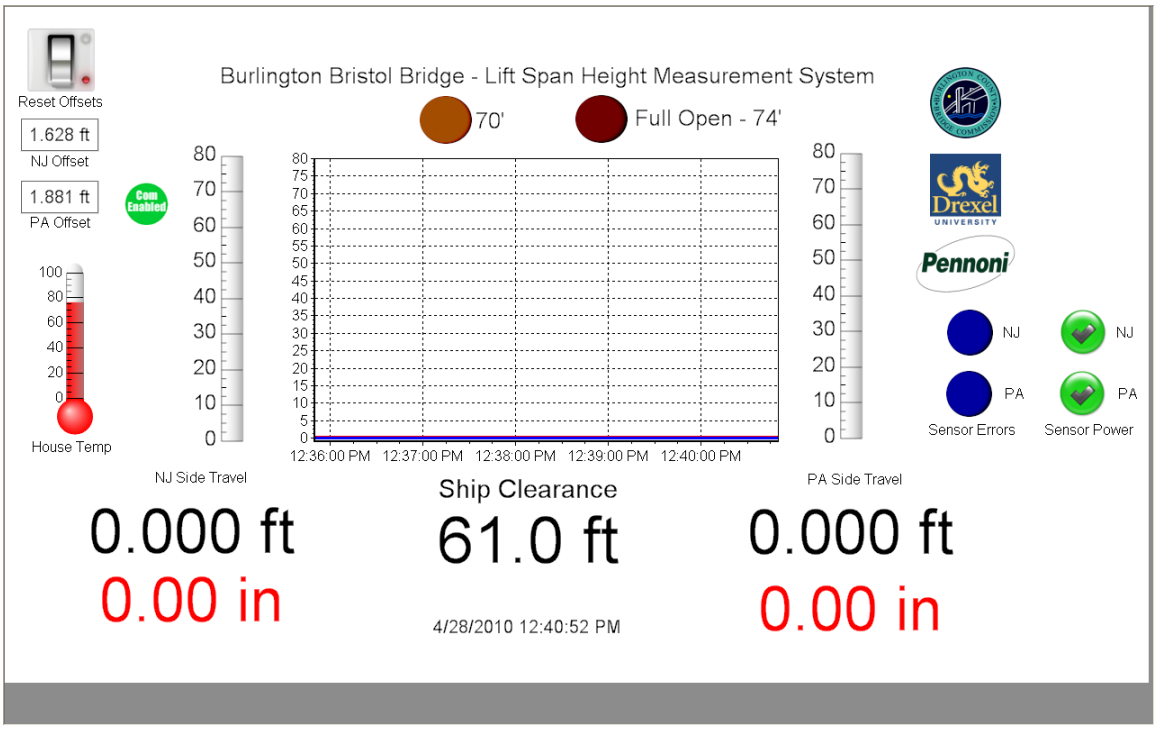

Figure 13-231: Screenshot of Operator's Portal to Viewing Lift Span Heights and Ship Clearance

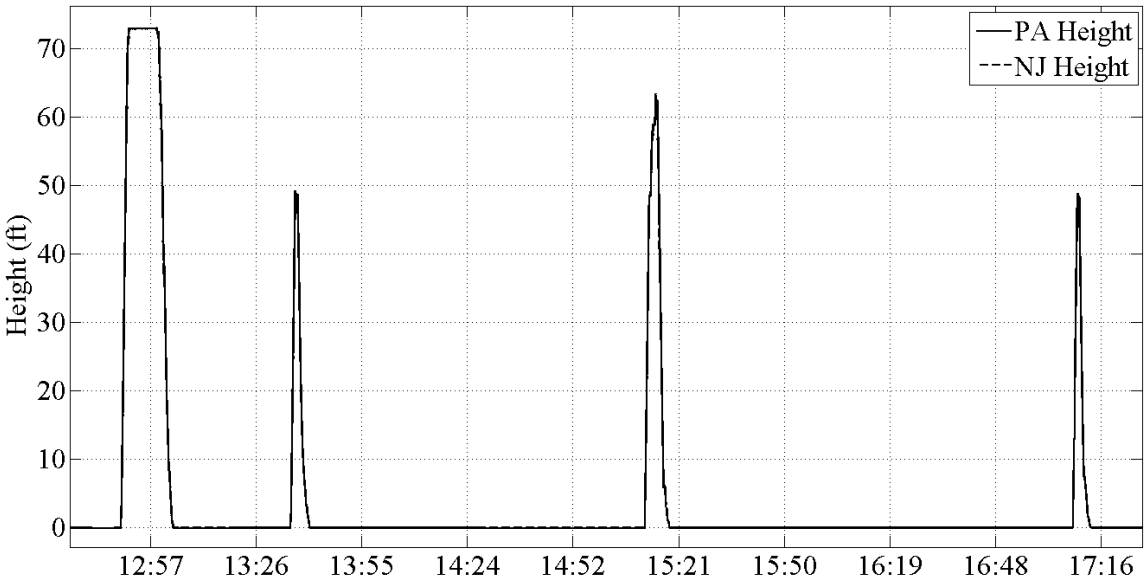

Figure 13-232: A Series of Lift Span Openings

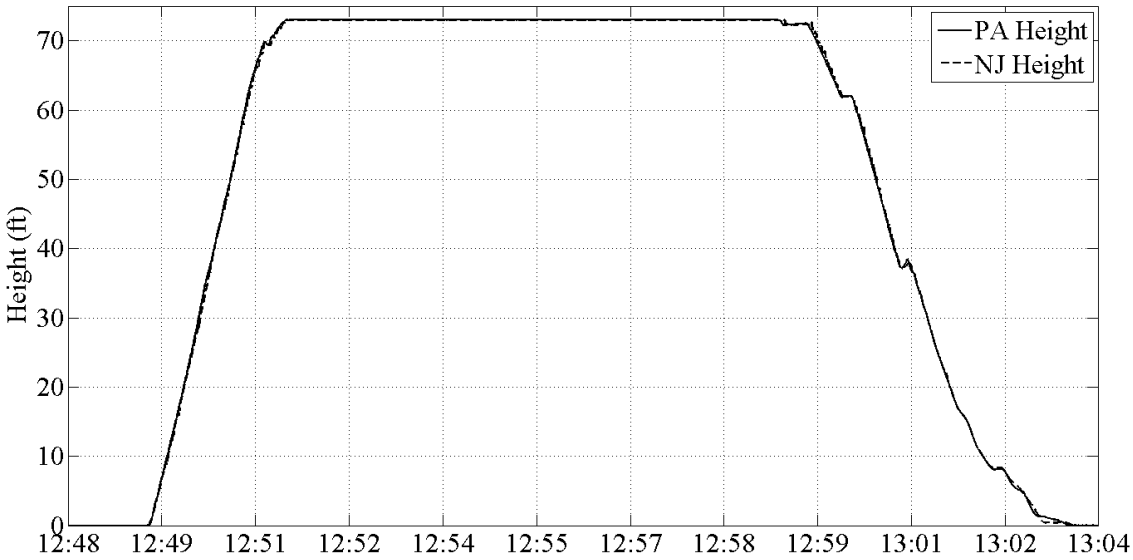

Figure 13-233: A Zoomed-in Plot of a Single Lift Span Opening

The data acquisition was custom developed to automatically trigger recorded data when the NJ laser sensor measures a distance of more than 5'. A buffer then makes it possible to record the previous 2 minutes of data. The data is continuously recorded until the height drops below 5' once again from which another 2 minutes of data is stored. During the debugging phase of the project, the recorded time histories from the data acquisition were compared against manually updated operator's logs (Figure 13-234). These logs indicate the height to which the span was raised as well as what time the span was raised and for how long it was open. Having access to these logs led to the successful development of a data collection regime which was most beneficial to the BCBC staff.

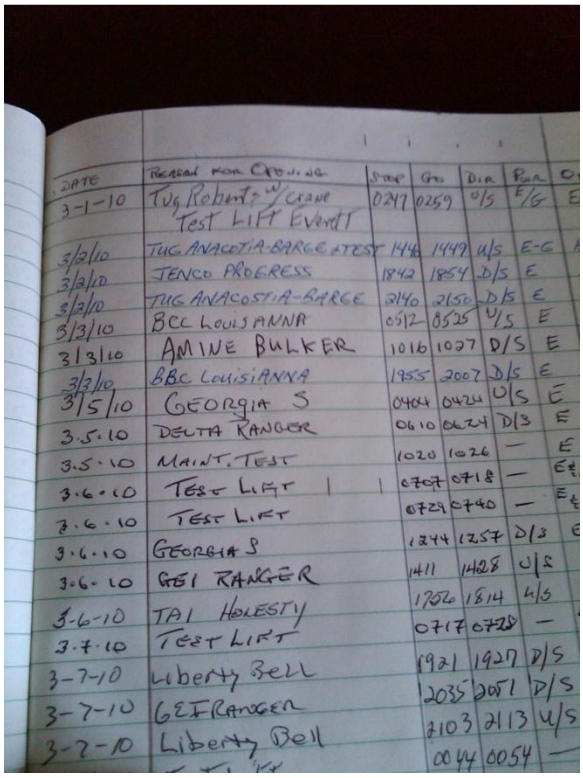

Figure 13-234: Operator Logs used for Correlation and Verification of Data Acquisition Automatic Triggering

The laser height monitoring system will not only by useful for the purpose of real time viewing of heights by the BCBC operators, however it can be used as a direct means of investigating the risk of the lift span becoming jammed during the opening sequence due to differential lifting. The monitoring system also directly serves as a means of mitigating any risk associated with differential lifting, as appropriate alarms can be set so that the operators can stop the span before a problem occurs.

CHAPTER 14: TRADITIONAL AND MULTIPLE MODEL STRUCTURAL IDENTIFICATION OF THE BURLINGTON BRISTOL BRIDGE

The Structural Identification of the Burlington Bristol Bridge was driven by a diverse set of objectives. First and foremost, the BCBC and their engineer of record requested a more accurate assessment of the structural load rating of critical members as a recent conventional load rating analysis indicated that the bridge may require a posting. In addition, given the indefinite preservation goal of the BCBC, it was desirable to identify a more complete set of hazards (in addition to live load) and assess their respective risk levels through the MM St-Id process. In addition to these owner-driven requests, the application of the MM St-Id process to the BBB allowed the feasibility of this approach for a large-scale complex structure with a commensurate element-level FE model to be assessed. Finally, an explanation to the cause of the perceived vibration difference between the PA and NJ tower spans was requested by all parties involved with the bridge. The difference in vibration was measured and documented in Chapter 13, but the cause needed to be verified with advanced modeling and traditional St-Id.

The MM St-Id process discussed in relation to the grid structure was followed exactly in developing the MM St-Id for the BBB. The first step, identifying relevant hazards and vulnerabilities, was discussed in Chapter 11. The required structural responses/attributes that must be estimated by the MM St-Id approach to better inform the identified risks are repeated here for convenience:

1. Dead load member responses
2. Live load member responses according to AASHTO configurations

3. Live load member responses according to loading of calibration truck described in Chapter 13.
4. Live load member responses to a lateral load condition

Following the establishment of this clear of set outcomes, a set of model building blocks was generated within the framework of an a priori model and was analyzed for sensitivity to the anticipated experimental observation. The goal of this step was to identify which building blocks (which represented the most uncertain aspects of the model) exerted the most significant influence over the desired predictions. This process was discussed in Chapter 12 and the key building blocks and there assumed distributions are repeated in Table 14-1 for convenience.

Table 14-1: Set of Defined Model Building Blocks

Building Block	Description
1	Elastic Modulus Steel
2	Elastic Modulus Concrete Deck
3	Lift Span - Tower Span Lateral Continuity
4	Lift Span - Tower Span Longitudinal Continuity at NJ BC
5	NJ CTWT Connectivity
6	PA CTWT Connectivity
7	PA Tower Span Expansion Bearings
8	NJ Tower Span Expansion Bearings
9	Lift Span Diagonal Member Connection Stiffness
10	NJ Tower Span Diagonal Member Connection Stiffness
11	PA Tower Span Diagonal Member Connection Stiffness

To drive the sampling and weighing process, a set of experimental observations in the form of modal frequencies and mode shapes obtained from a comprehensive ambient vibration test of the BBB were employed. The experimental program and a discussion of the results were presented in Chapter 13.

Driven by these three key ingredients (namely, the desired predictions, the identified set of building blocks and their distributions, and the experimental observations) the following sections detail the MM St-Id application to the BBB.

14.1. Generation of Candidate Models

The final set of model building blocks were sampled over the bounds shown in Table 14-2. The final model building block set includes the elastic moduli of steel and concrete, continuity conditions between the lift span and tower span in the lateral direction, lift span and tower span in the longitudinal direction at the NJ side, and finally the continuity conditions between the counterweights and tower spans for the PA and NJ sides. Additionally, the expansion bearings of the PA and NJ tower spans were modified by altering the stiffness of the associated rotational and translational springs by a percent rigidity factor. Finally, all major connection stiffness modification factors were sampled between a pinned and fixed condition. The first sample was randomly drawn from the prior probability distributions shown in Table 14-3 and the subsequent samples followed the MCMC procedure discussed in Chapter 7.

Table 14-2: Model Building Block Bounds

Building Block	Description	Lower Bound	Upper Bound
1	Elastic Modulus Steel (*E_0)	0	2
2	Elastic Modulus Concrete Deck (*E_0)	0	2
3	Lift Span - Tower Span Lateral Continuity	1 kip/in	$1x10^6$ kip/in
4	Lift Span - Tower Span Longitudinal Continuity at NJ BC	1 kip/in	$1x10^6$ kip/in
5	NJ CTWT Connectivity	1 kip/in	$1x10^6$ kip/in
6	PA CTWT Connectivity	1 kip/in	$1x10^6$ kip/in
7	PA Tower Span Expansion Bearings	0%	100%
8	NJ Tower Span Expansion Bearings	0%	100%
9	Lift Span Diagonal Member Connection Stiffness	0%	100%
10	NJ Tower Span Diagonal Member Connection Stiffness	0%	100%
11	PA Tower Span Diagonal Member Connection Stiffness	0%	100%

Table 14-3: Prior Probability Distributions for the Building Blocks

Building Block	Prior Probability Distribution
1	Normal (0,0.06)
2	Uniform
3	Uniform
4	Uniform
5	Uniform
6	Uniform
7	Uniform
8	Uniform
9	Uniform
10	Uniform
11	Uniform

The MCMC analysis was run until the convergence criteria defined for the grid study was sufficiently met, requiring a total of 36,000 models to be analyzed for the Burlington Bristol Bridge model. The analysis time for this study totaled 762 hours, or just over 29 days. While the analysis time seems to be extremely long for this case, it is worth noting that the method will only be enhanced by improvements in computing power. By examining the time histories of the building block sampling, the burn-in period was determined to consist of 5,000 models. The convergence plots for the building blocks defined within the process, showing the expected value and variance of the posterior distribution of each building block, are shown in Figure 14-1 through Figure 14-11 and stabilize after approximately 31,000 models. As discussed in Chapter 7, convergence was considered established when the expected value and variance remained reasonably within a ±5% bounds of its current value. While the plots seen below seem quite jagged in nature, it is important to recall that the expected value and variance are only computed in periodic increments to conserve computation, thus leading to a more discrete representation.

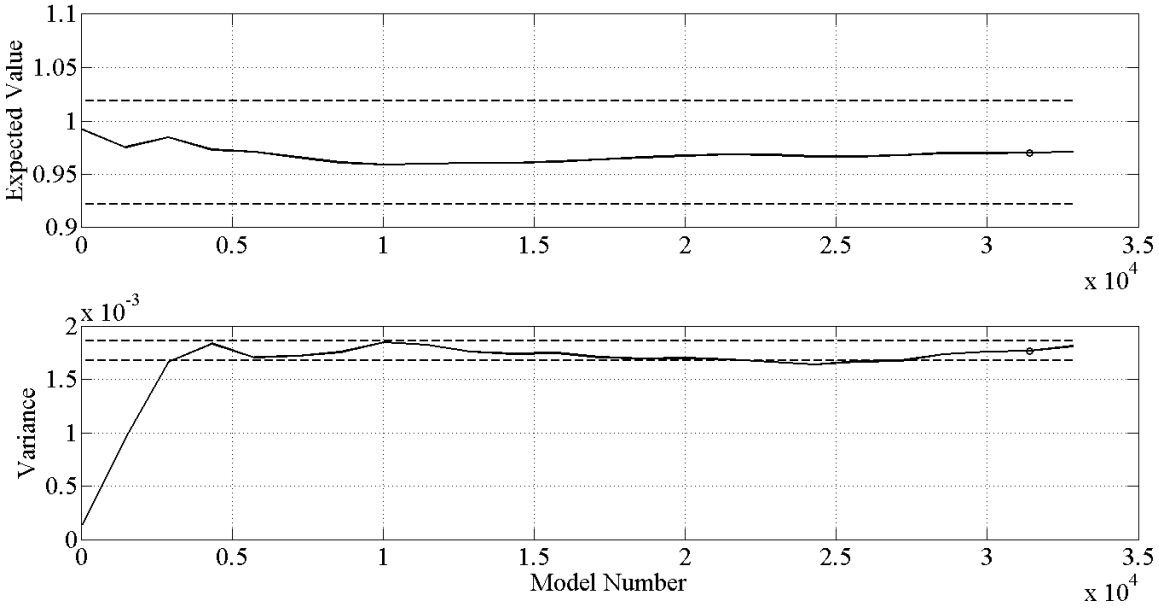

Figure 14-1: Convergence Diagrams for the Normalized Elastic Modulus of Steel

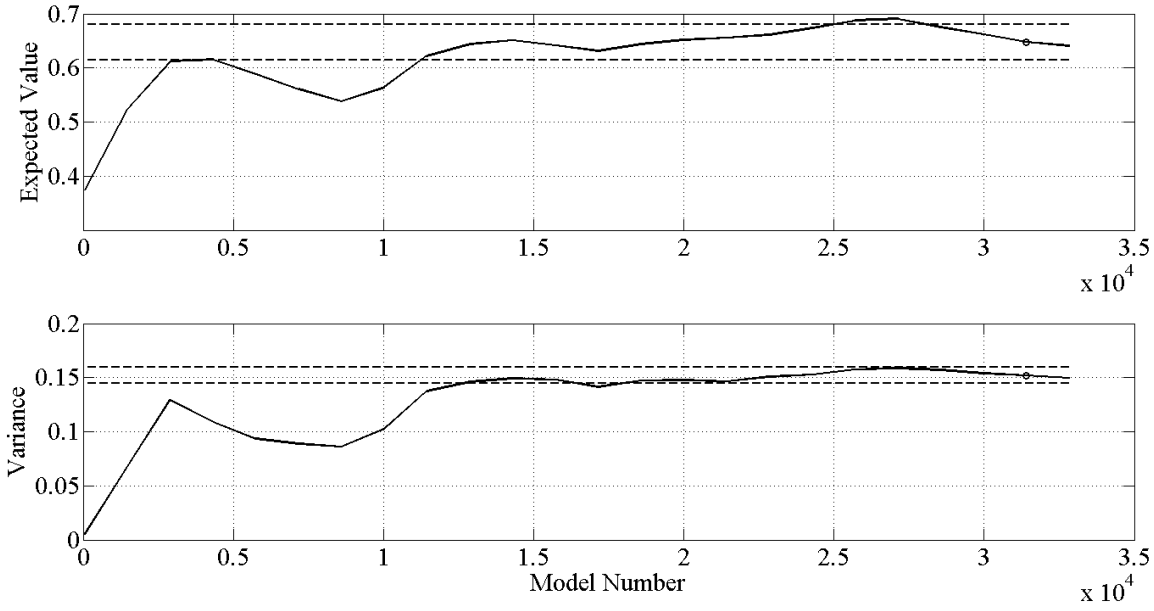

Figure 14-2: Convergence Diagram for the Normalized Elastic Modulus of Concrete

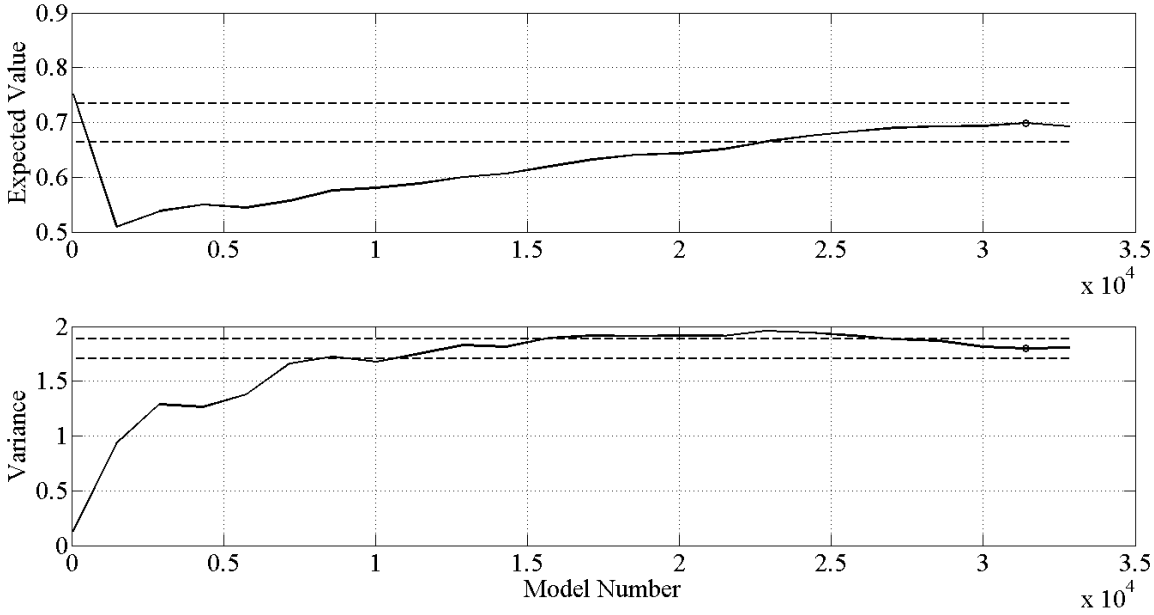

Figure 14-3: Convergence Diagrams for Lift Span - Tower Span Lateral Continuity

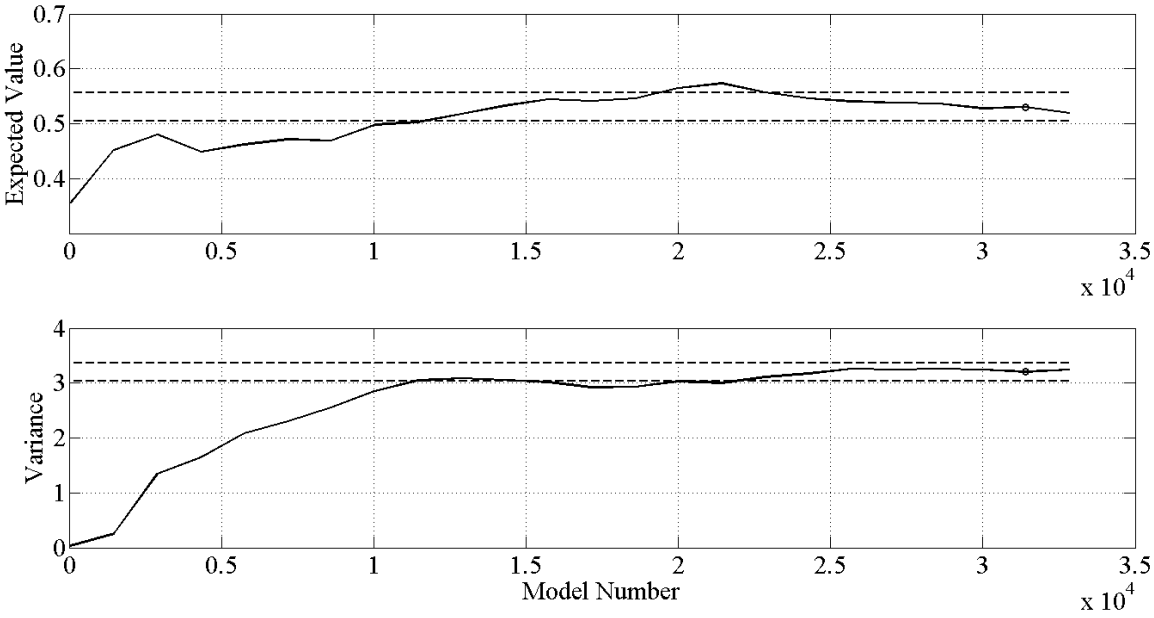

Figure 14-4: Convergence Diagrams for the Lift Span - Tower Span NJ Longitudinal Continuity

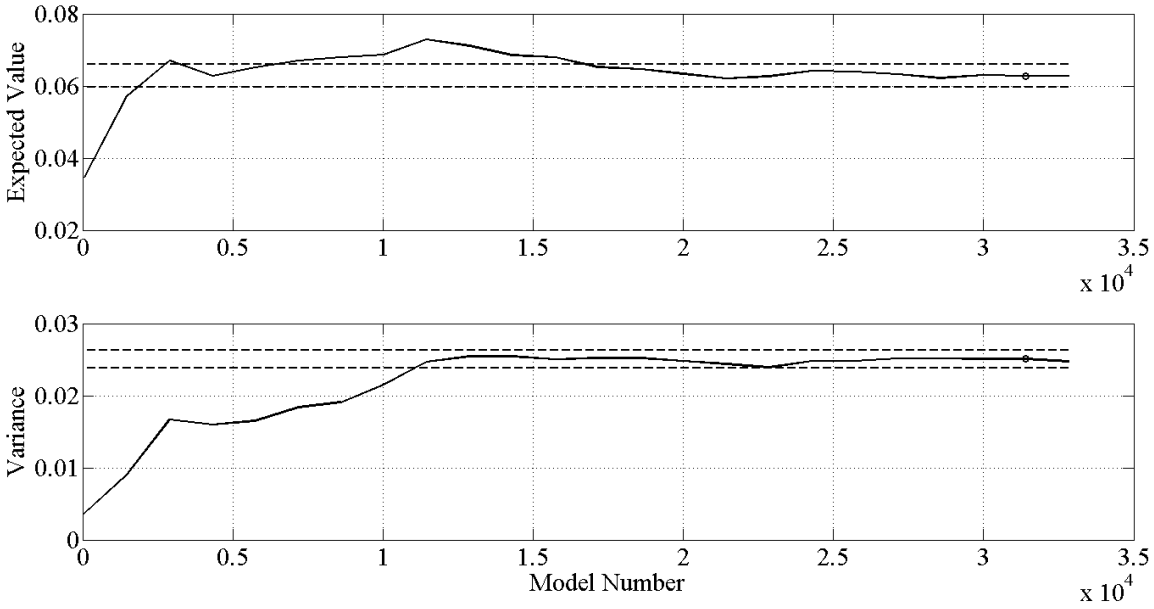

Figure 14-5: Convergence Diagrams for the NJ Counterweight Continuity

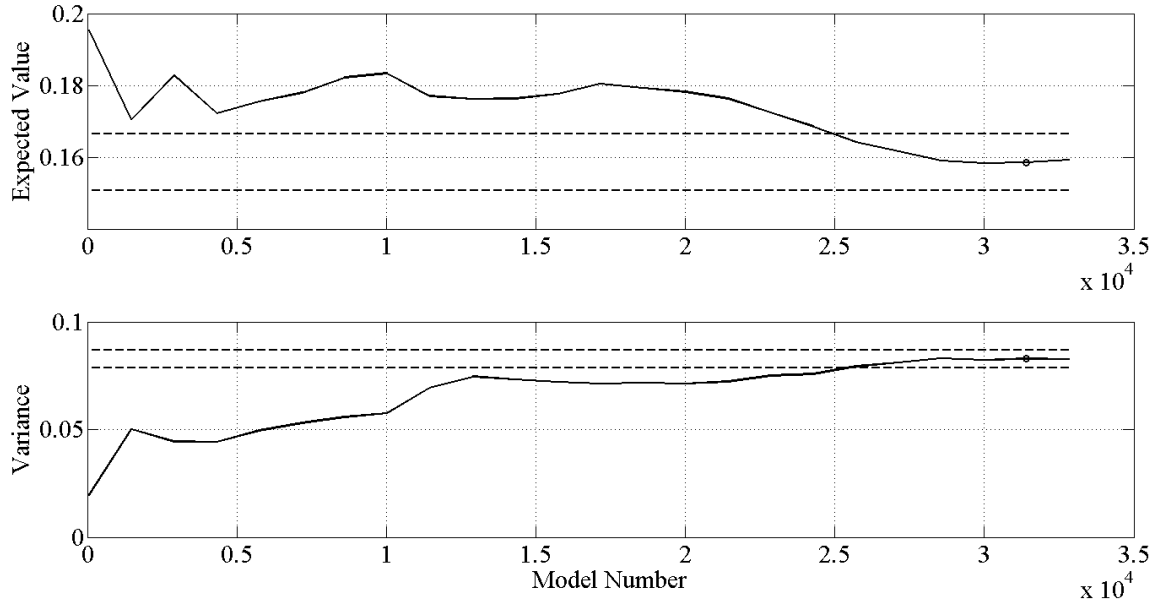

Figure 14-6: Convergence Diagrams for the PA Counterweight Continuity

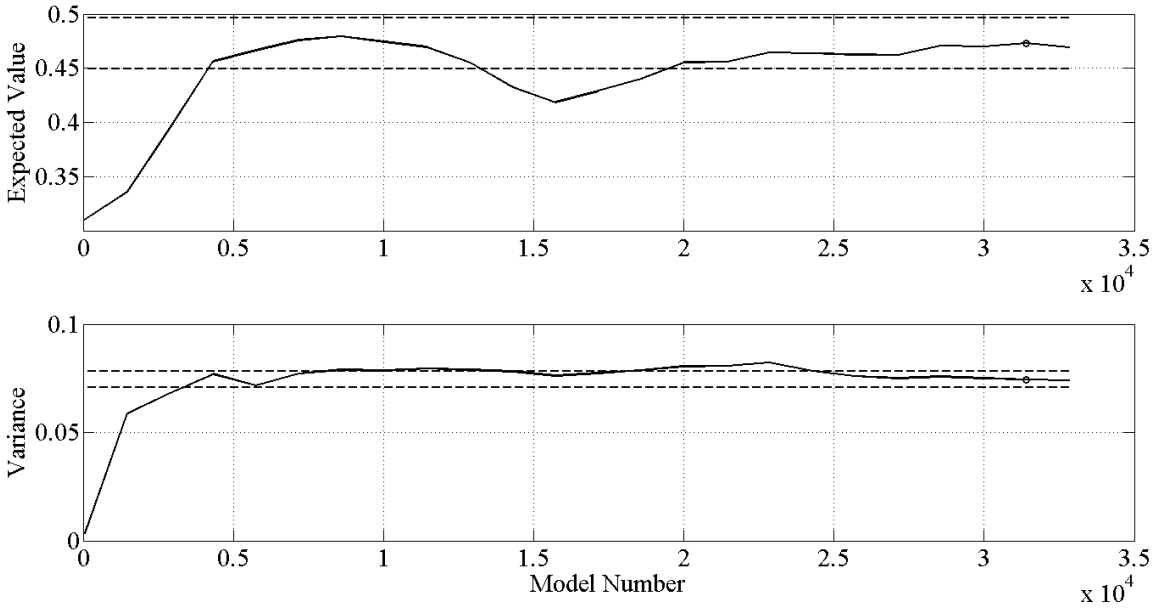

Figure 14-7: Convergence Diagrams for the PA Tower Span Expansion Bearings

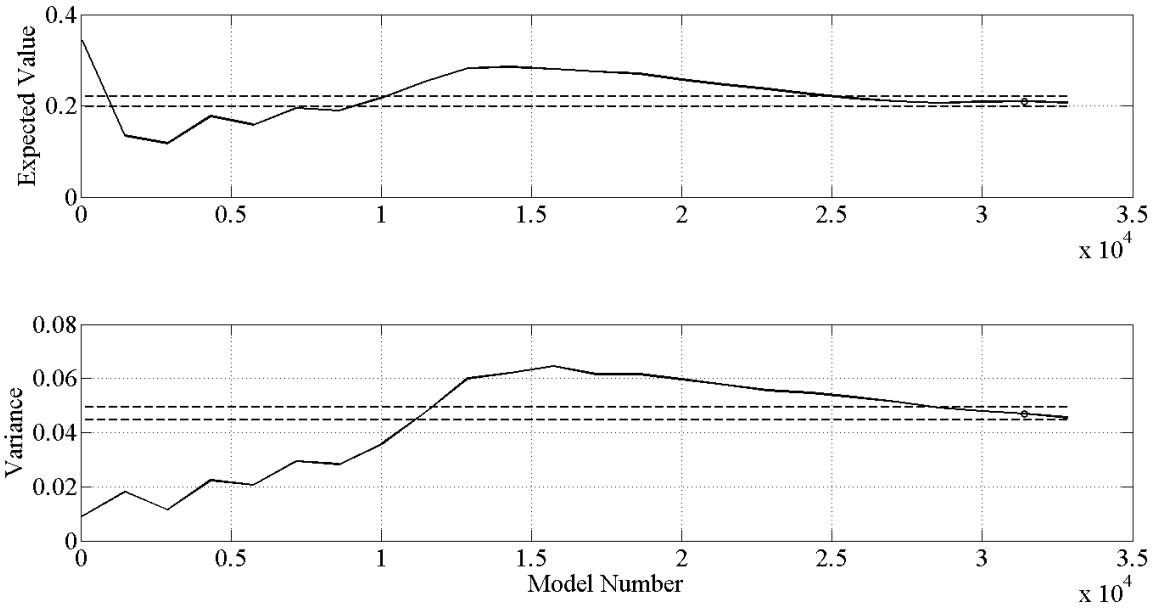

Figure 14-8: Convergence Diagrams for the NJ Tower Span Expansion Bearings

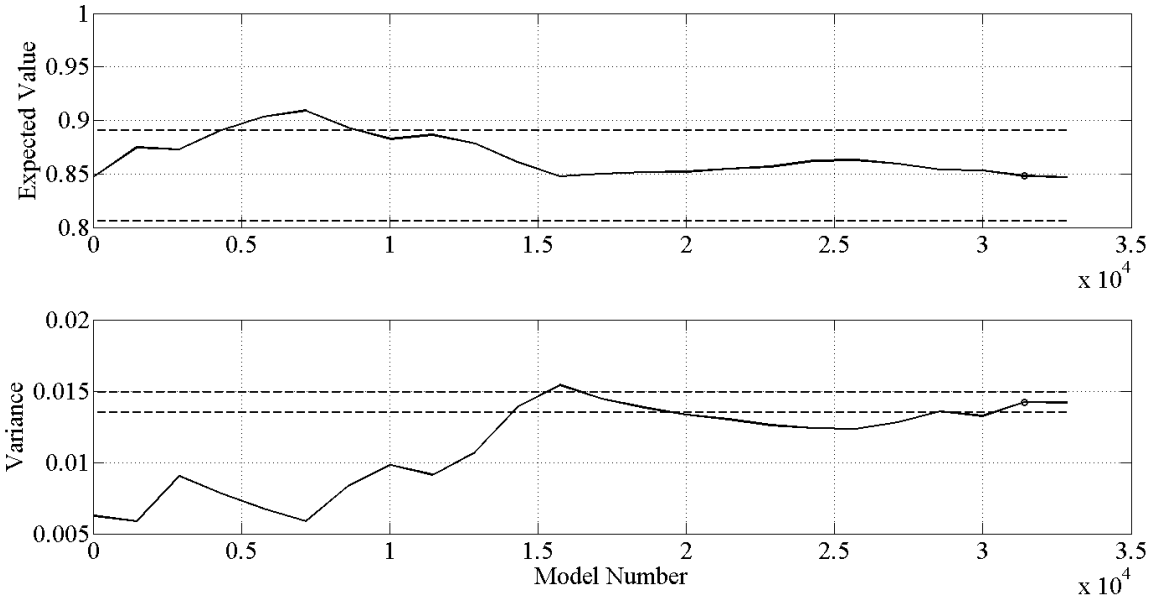

Figure 14-9: Convergence Diagrams for the Lift Span Diagonal Member Connection Stiffness

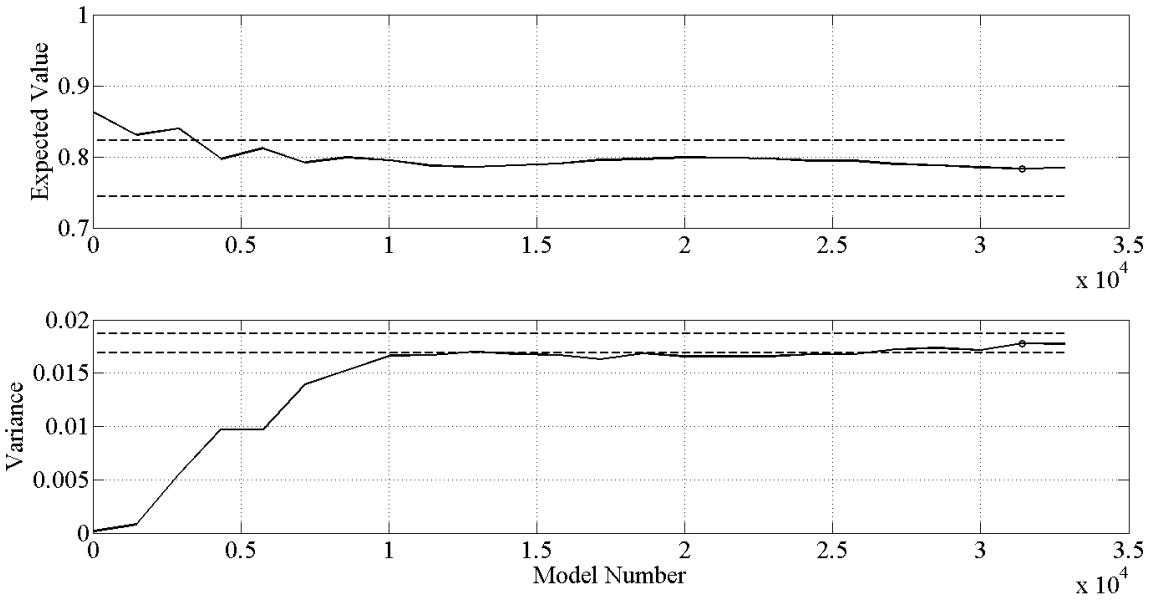

Figure 14-10: Convergence Diagrams for the NJ Tower Span Diagonal Member Connection Stiffness

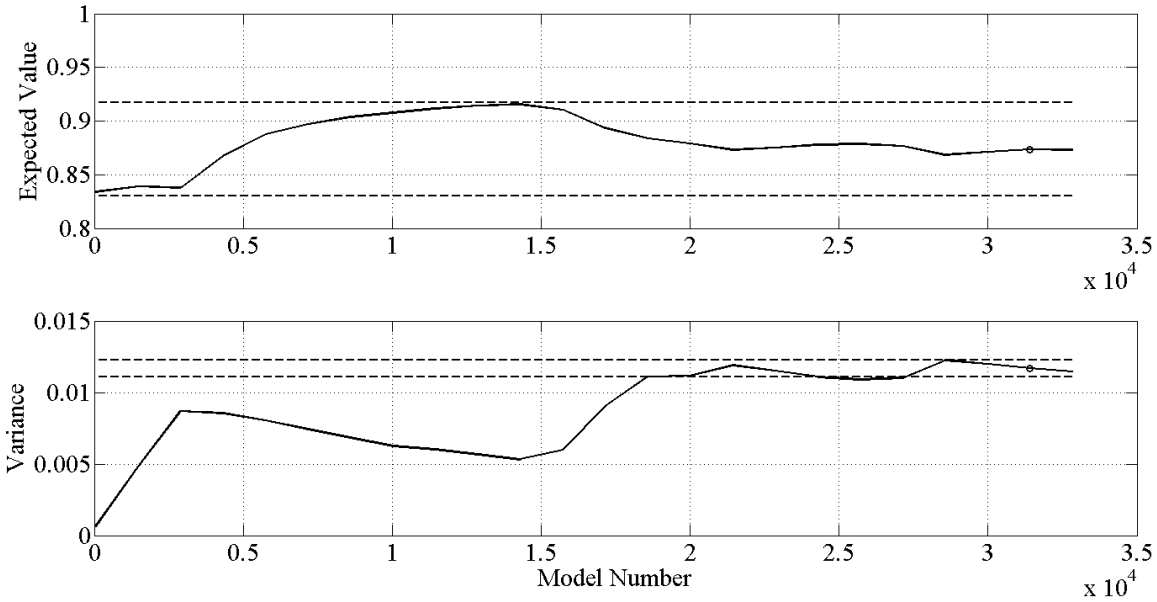

Figure 14-11: Convergence Diagram for the PA Tower Span Diagonal Member Connection Stiffness

After the convergence of the MCMC analysis was confirmed, the updated model building block distributions were examined. Each of the CDF functions for the updated model building blocks was plotted against each respective prior probability CDF. This analysis allows for the direct comparison between weighed and un-weighed models to determine what effects the process had on each of the building blocks (Figure 14-12 - Figure 14-14). It is also important to determine whether the process has distorted any deterministic building blocks incorporated within the process. For the sake of brevity, each of the model building blocks was labeled 1 through 11, with respect to Table 14-2. The building

blocks representing continuity stiffness conditions were normalized based on the upper bound assigned.

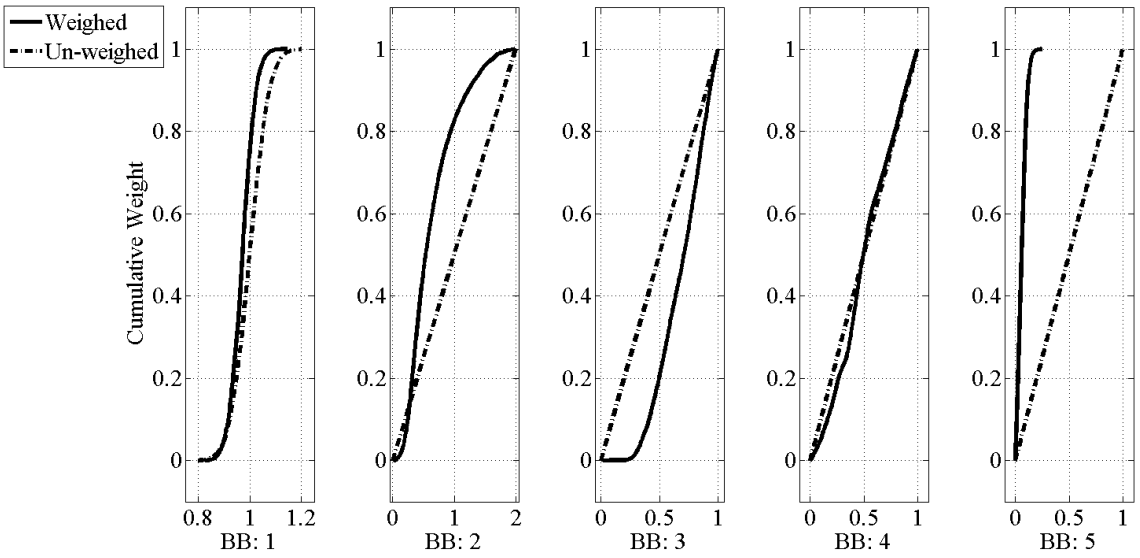

Figure 14-12: Effect of Weighing Models on Building Blocks 1 - 5

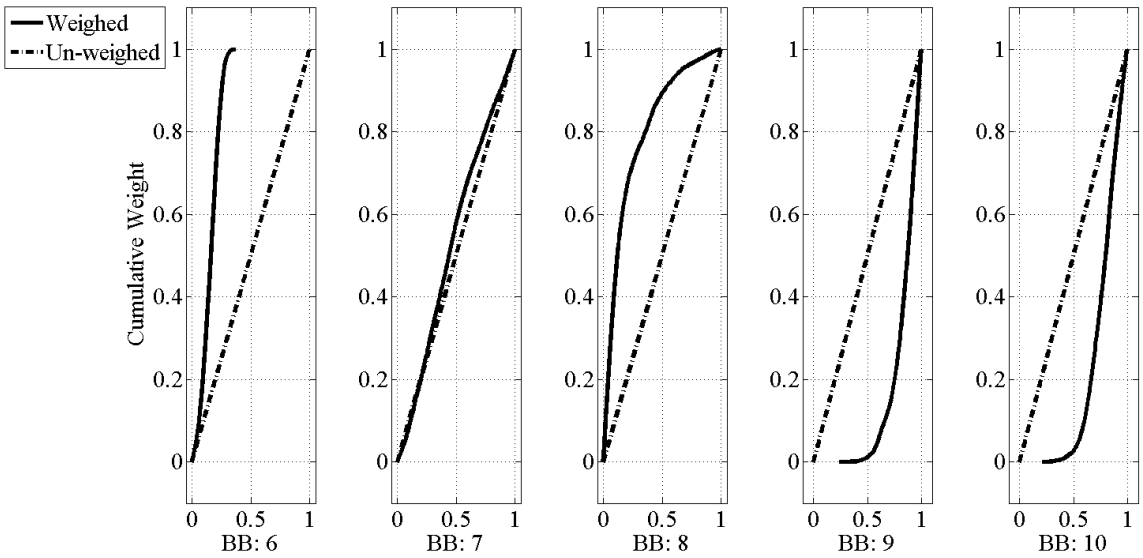

Figure 14-13: Effect of Weighing Models on Building Blocks 6 – 10

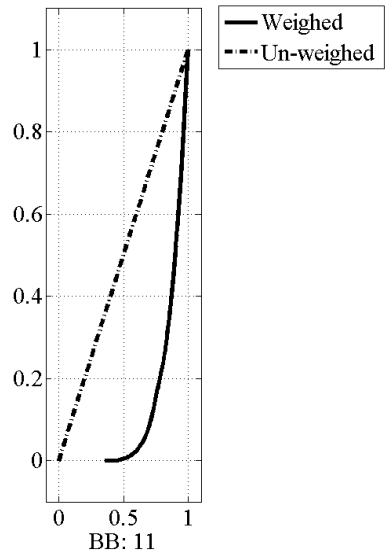

Figure 14-14: Effect of Weighing Models on Building Block 11

As seen in the updated building block distributions above, specific conclusions can be drawn regarding the physical meaning of the updated building block distributions. The following sections provide discussions of these distributions with specific references to the structure's physical details and modeling assumptions employed.

14.1.1. Distribution of Elastic Modulus of Steel

First and foremost, the first building block representing the elastic modulus of steel was not distorted and the updated distribution from the models indicated a tighter distribution than what was used in the prior case. While the effect was somewhat minor, the steel elastic modulus had a mean value below the deterministic value of 29,000 ksi by around 3%. While such a same distortion may be due to several sources, one possible

explanation is that the built up sections (especially those with lattice work) may not have been 100% fully composite and so the slight softening of the elastic modulus was essentially compensating for this fact.

14.1.2. Distribution of Elastic Modulus of Concrete

Building block 2, the elastic modulus of concrete, had an updated building block distribution which indicated that the stiffness of the material is less than the nominal value assigned within the model. Due to the complicated nature of the actual deck represented by this building block, a concrete filled steel grid, this is not surprising. More specifically, although this model building block consisted of a material property, in reality this was used a surrogate to also correct the modeling assumption that the concrete-filled grid could be simulated with thin shell elements with smeared properties. Given this modeling approach, the low value of this material property is not surprising as it also reflects the model form simplification included. A manufacturer photo (Figure 14-15) shows the nature of the concrete filled grid deck system, including the concrete overlay which is utilized on the BBB.

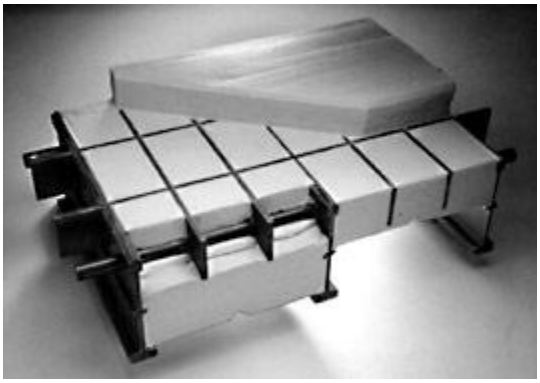

Figure 14-15: Cut-away View of a Concrete Filled Steel Grid Deck (www.idsi.org)

14.1.3. Lift / Tower Span Lateral Continuity

The distribution representing the third building block, lateral continuity between the lift and tower spans, was updated to indicate that the models accepted within the process tended to have high, but finite, stiffness values representing this uncertainty. Once again, this is reasonable given the fact that the physical detail providing the lateral constraint between the two spans is not necessarily in contact at all points in time and also has some degree of flexibility due to the fact that the lateral restraint is provided by a steel member extending from the lift span around the column of the tower span, as shown in (Figure 14-16).

Figure 14-16: Tower / Lift Span Lateral Restraint

14.1.4. Lift / Tower Span NJ Longitudinal Continuity

The fourth building block, longitudinal continuity at the New Jersey joint between the lift span and tower spans (Figure 14-17), had an updated building block distribution which did not appreciably differ from its assumed distribution. This is most likely do to the fact that the models generated with respect to the measured observations could not provide enough information to inform this building block. To mitigate this issue, it would be necessary to provide a measurement which was highly dependent upon this particular continuity condition and thus could inform the uncertainty directly. An example of such a measurement would be the longitudinal acceleration at this location or the longitudinal

displacement under heavier vehicles, since ambient levels of vibration may not be enough to overcome the static friction of the detail.

Figure 14-17: Lift / Tower Span Lateral and Longitudinal Restraint at NJ End

14.1.5. Counterweight / Tower Span Continuity Conditions

The fifth and sixth building blocks, representing the continuity between the counterweights and the tower span structure (Figure 14-18), were sampled in a manner which indicates that models with low levels of continuity at this connection were

accepted more often. This is reasonable given the fact that the counterweights sit within a system of guides which control the global movement of the counterweights during operation of the lift span. However, small levels of stiffness associated with this connection are feasible due to the fact that the counterweight may be engaging the tower span guides and participating in a low degree, instead of freely hanging from the top of the tower span.

Figure 14-18: Tower Span Column Guide and Counterweight Restraint

14.1.6. Tower Span Expansion Bearing Stiffness

The seventh and eighth building blocks, representing the tower span expansion bearings (Figure 14-19) degree of fixity were sampled in a manner that shows the accepted models tended to have higher bearing restraint at the PA span than in the NJ span, which is apparently able to expand and rotate to a greater degree than its PA counterpart. One potential explanation for this is the difference in exposure for the two bearing locations. The PA Tower span expansion bearing is located roughly 400 feet from the nearest shore of the Delaware River, while the NJ Tower span expansion bearing is located on the banks of the river. Thus, it is possible that the PA Tower span bearing is more exposed to the elements (and thus corrosion) while the NJ Tower span is lightly surrounded by trees and not exposed to the air currents traveling along the river. However, it is possible that other causes are in fact the reason why the PA Tower span bearing may be more frozen than its NJ counterpart.

Figure 14-19: PA Tower Span Expansion Bearing

14.1.7. Diagonal Member Connection Stiffness

All of the building blocks representing the rotational connection stiffness of the diagonal members were sampled in a manner which suggests that the connections all have near rigid rotational connections, in a smeared sense across each of the main spans. This conclusion is justified in examining the detail of rotational restraint provided by the connection details for theses members (Figure 14-20). By examining the amount of fixity at the end of these diagonal elements, the finding of the MM St-Id process can be confirmed.

Figure 14-20: Gusset Plate Connection at the Diagonal Member Connection Location

The analysis of how the model building blocks were sampled to generate the population of models for prediction purposes showed that the models were reasonable in terms of whether they made physical sense and whether they were reasonable given the information that was present in an a priori sense. The next step within the process was to analyze the accepted models for the desired prediction cases.

14.2. Model Predictions

Following the MM St-Id analysis of the BBB model, a suite of scenarios was identified for analysis of unobservable response indices of interest. In this case, one of the largest uncertainties within the structure is the available linear elastic capacity of critical members throughout the structure. The dead load demand for long span structures consumes a large portion of the available capacity of structural members, and yet is an index which cannot be directly measured in a reliable and cost-effective manner (although some technologies are currently being developed and are available to spot measurements). For this reason, the total dead load demand on the structure was selected as one of the load cases to analyze.

An additional load case included the forces induced by a unit lateral point load at mid-span for an analysis of member redundancy in lateral loading scenarios. This case once again represents the opportunities made available with the MM St-Id analysis, in that potential hazards of the structure can be analyzed for their effects on the structure, given the measured observations. Finally, two load cases were selected where a static load configuration was applied identical to the loaded truck configuration from the top chord strain monitoring calibration efforts described in Chapter 13. This truck was loaded to approximately 37 tons and induced strain levels up to twenty-six microstrain within the top chord members. Two positions of this loaded truck were selected for incorporation into the analysis, one located in the upstream lane and one located in the downstream lane. The final listing of load cases included in the analysis incorporated seven linear static analysis cases.

Table 14-4: Hazards Studied with the MM St-Id Approach for the BBB and Relevant Desired Responses

Hazard	Desired Response
Live Load	Strain Under Vertical Load / Member Action
Dead Load	Member Action
Ship Impact	Strain Under Lateral Load

Table 14-4 shows the final set of identified hazards to be studied with the MM St-Id approach for the BBB as well as the corresponding desired response indices. Critical members strain was identified as the immeasurable response index for the live load hazard for a verification case of the method. Additionally, typical member action due to AASHTO loading was also selected as a live load hazard for the analysis of member redundancy in load path as well as for load rating purposes. Member action due to a dead load hazard was selected again to compute load ratings, which in turn are indicative of the elastic capacity of the structure. Finally, the hazard of a ship impact was analyzed by also studying member action and redundancy in how the load path varies within the structural system.

Due to the size of the final finite element model representing the Burlington Bristol Bridge, a total of 3,874 beam elements, it was very computationally expensive to export the reaction and displacement data for each member and for each load case of the accepted model set. To mitigate this, a subset of members was identified in which the element responses were exported and saved for analysis. The members selected include

the two top chord members currently instrumented with the top chord strain monitoring system (NJ U9-U10) in addition to twelve members, all listed in Table 14-5.

Table 14-5: Description of Members Included in Analysis Scenarios

Member	Span	NJ / PA	US / DS	End 1	End 2
1	Lift	NJ	US	L8	M7
2	Lift	NJ	US	M7	U6
3	Lift	NJ	DS	L8	M7
4	Lift	NJ	DS	M7	U6
5	Lift	NJ	US	L8	L9
6	Lift	NJ	DS	L8	L9
7	Lift	NJ	US	L9	M9
8	Lift	NJ	DS	L9	M9
9	Lift	NJ	DS	U7	INT
10	Lift	NJ	DS	U8	INT
11	Lift	NJ	US	U8	INT
12	Lift	NJ	US	U7	INT
13	Lift	NJ	US	U9	U10
14	Lift	NJ	DS	U9	U10

* INT Represents an interior node connecting the four lateral bracing elements between the two trusses

Once again, the notation in Table 14-5 describing the included members is as follows: U stands for upper chord node, L stands for lower chord node, M stands for mid-truss height node and the numbers denote which panel point the node is located at. The major truss elements were selected for load rating purposes and the lateral bracing elements (9 through 12) were selected for analysis due to the lateral load cases applied (wind and ship). The examples demonstrated by using the MM St-Id process on these elements will

highlight the benefits of the method and show its potential for the application of the method to a variety of analysis cases and specific members.

14.2.1. Prediction of Live Load Strain within Instrumented Members to Known Truck Input

While the benefits of the MM St-Id method will be fully realized by evaluating responses indices which cannot be physically measured, it was decided to include a measured output within the model predictions to serve as an analysis of the accuracy of the method. By applying the loading configuration of the calibration truck used for the top chord strain monitoring system and extracting the model's prediction of strain in the instrumented members a direct evaluation can be made on the method's reliability for a model of this size and complexity. Two load cases were used for this purpose: 1) calibration truck in the upstream lane and 2) calibration truck in the downstream lane. The model output was obtained for both the upstream and downstream chord members for the two analysis cases, and the prediction results are shown in Figure 14-21 through Figure 14-24.

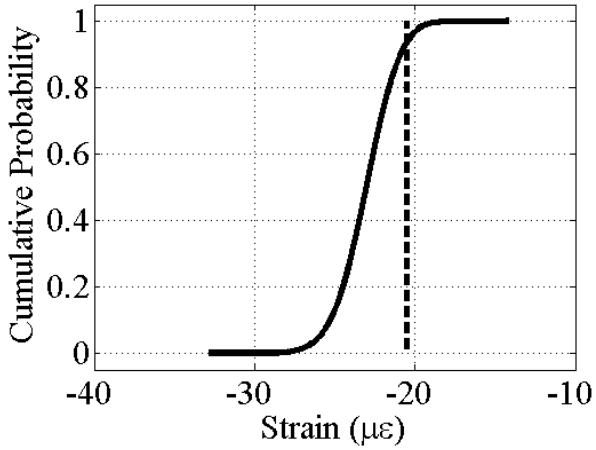

Figure 14-21: Response Prediction for DS Top Chord Member due to Calibration Truck in DS Lane

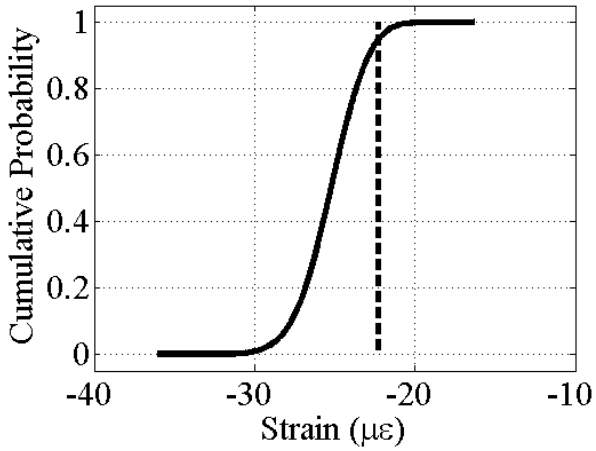

Figure 14-22: Response Prediction for US Top Chord Member due to Calibration Truck in DS Lane

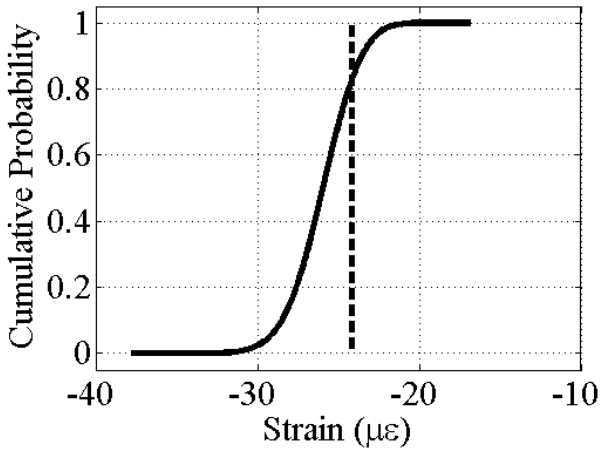

Figure 14-23: Response Prediction for US Top Chord Member due to Calibration Truck in US Lane

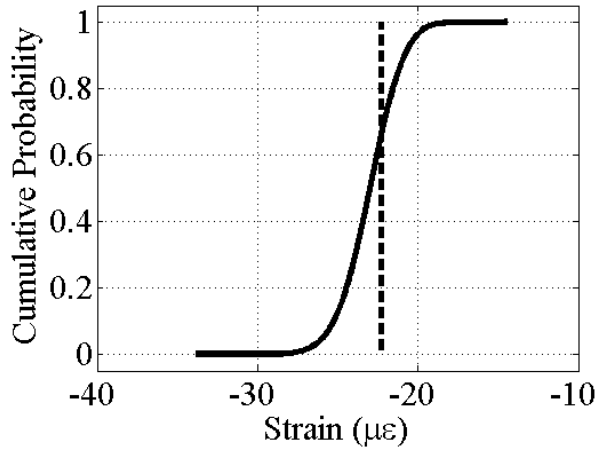

Figure 14-24: Response Prediction for DS Top Chord Member due to Calibration Truck in US Lane

While it may appear that the measurements for both of the cases where the truck was in the downstream lane appear to be on the edge of the prediction distributions (20-45% from the mean), it is also important to remember that the position of the trucks as it moved across the span was being called out by visual identification and then radioed to the DAQ operator. Similarly, the lateral location of the truck was assumed to be centered within the lane, however this may have not have been the case during the test. Additional error sources could lie within temperature variation, which could have altered load paths of the structure in carrying the load of the calibration truck.

In analyzing the above figures, it is also important to recall that the ability of global dynamic observations to predict local static strain response was not as successful as it was to predict global displacement predictions. This similarity between the BBB response predictions and the grid response predictions further validates the claim regarding the ability of dynamic measurements in predicting local strain responses.

The MM St-Id method provided response distributions which contained the actual observed response. While the accuracy of the response prediction distribution may not have been perfect, the distribution contained the measurement nonetheless. It is expected that if one were to identify displacement of the span as a critical response prediction, that it would be much more accurate with comparison to an actual observed value.

14.2.2. LRFD Load Rating of Critical Truss Elements and Lateral Bracing of the Lift Span

The true benefit of the MM St-Id methodology is seen in producing response predictions where the indices of interest cannot be measured or observed. To this point, physical measurements of the "desired" response were made (live load strain response to a known truck input) so that the reliability of the method could be verified before producing response predictions of unobservable attributes. The first unobservable structural attribute investigated for the BBB is the load rating of several critical elements per current AASHTO standards. The members selected include upstream and downstream truss members from the top chord, main truss diagonals, and bottom chord in addition to lateral bracing of the trusses between the upstream and downstream trusses.

To produce the load ratings, the specified loading scenarios within the AASHTO 2011 Manual for Bridge Condition Evaluation (Section 6) and AASHTO 1997 Manual for Bridge Condition Evaluation (Section 6) were implemented into the Strand7 model for the structure. The Load and Resistance Factor Rating (LRFR) defined in the 2011 Manual for Bridge Condition Evaluation consists of a rating equation which applies factors to reduce the available capacity of a member and factors up the live and dead loads placed on a member by specified factors. The Load Factor Rating (LFR) and Allowable Stress Rating (ASR) are both specified in the older 1997 manual, and were subsequently replaced by the LRFR methodology. However, according to NBIS standards, for structures where the code used for design is unknown then the analyst must report all three ratings.

The load case used within the LRFR analysis consisted of the enveloped demands from a single HS20 truck with a 0.64 kpf lane load for the length of the span in each individual lane and in both lanes. The HS20 design vehicle has a total weight of 36 tons, distributed over three axles as follows: 8 kip front axle, 32 kip fixed distance axle and a 32 kip variable distance axle and has a dynamic impact factor of 1.33 applied to the static loads to represent amplifications corresponding to vehicle damping systems and structural vibration resonance. For this analysis, the minimum axle spacing was used to produce a concentrated and maximum loading effect on the lift span. The load case used within both the LFR and ASR analyses consisted of the enveloped demands from a single HS20 truck with no lane loads.

The load rating cases were then analyzed for the set of accepted models and the results for the twelve members identified for this scenario analysis were evaluated using the specified load rating equations in each of the manuals and are presented below.

The equations for the three load rating equations are presented in Table 14-6. The equations are all functions of DC, the dead load demand, LL, the live load demand with impact factor IM, and the capacity, C. For the LRFR method, the nominal capacity R_n is factored with condition ratings of the member φ_c, and system factors which describe the redundancy of the member φ_s, and finally an overall resistance factor φ. The LFR method does not factor the capacity of the member, only the demands while the ASR method only factors the capacity, and not the demands. Each of the equations listed below has inventory and operating levels of rating equations. Inventory ratings represent the capacity rating for the vehicle used in the analysis for indefinite use on the structure,

the factors for which are presented in Table 14-7. Operating ratings represent the capacity rating for occasional use of the rating vehicle used. Typically, operating ratings are used to develop ratings for permit loads.

For all three rating methods, the allowable capacity to be used within the rating equations varies based upon the methodology used. For instance, the LRFR method applies factors based upon the condition of the member, the level of redundancy of the member within the structural system, and the function of the member (compression member, tension member, flexural, etc.). The ASR method reduces the allowable capacity heavily as a function of structural nature of the member (compression member, etc.). For example, a compression member has its overall elastic capacity reduced by 45% and tension members are reduced by 25%.

Table 14-6: Rating Factor Equations for the Three Methodologies Applied

Rating Methodology	Rating Equation
LRFR	$RF = \frac{C - (\gamma_{DC})(DC)}{(\gamma_{LL})(LL + IM)}$
LFR	$RF = \frac{C - (A_1)(DC)}{(A_2)(LL + IM)}$
ASR	$RF = \frac{C - (DC)}{(LL + IM)}$

Table 14-7: LRFR and LFR Rating Factors

	Inventory Level				Inventory Level			
Rating Methodology	γ_{DC}	γ_{LL}	A_1	A_2	γ_{DC}	γ_{LL}	A_1	A_2
LRFR	1.25	1.75	-	-	1.25	1.35	-	-
LFR	-	-	1.3	2.17	-	-	1.3	1.3

Based on the form of the equations listed above, it is apparent that a rating of 1.0 is physically interpreted as the structure's available capacity is equal to the demand of the legal truck loading. Therefore, a rating below 1.0 would indicate that the structure does not provide sufficient capacity for the defined demand. A rating below 1.0 does not mean that collapse is imminent, however due to the safety factors placed on the various components of the rating equation and the ability for the structure to redistribute loads due to inelastic actions. However, a rating below 1.0 ensures further detailed analysis and posting of the structure to a truck class which rates above 1.0.

Each of the three rating methodologies were implemented on the identified members within this study and the results are presented below. The CDF of the load ratings for each of the members and rating methodologies were explored not only for what the rating factors represented in terms of the factored capacity of the structure, but the variability within the ratings based on the building blocks used and the observations used to weigh the models (Figure 14-25 through Figure 14-42).

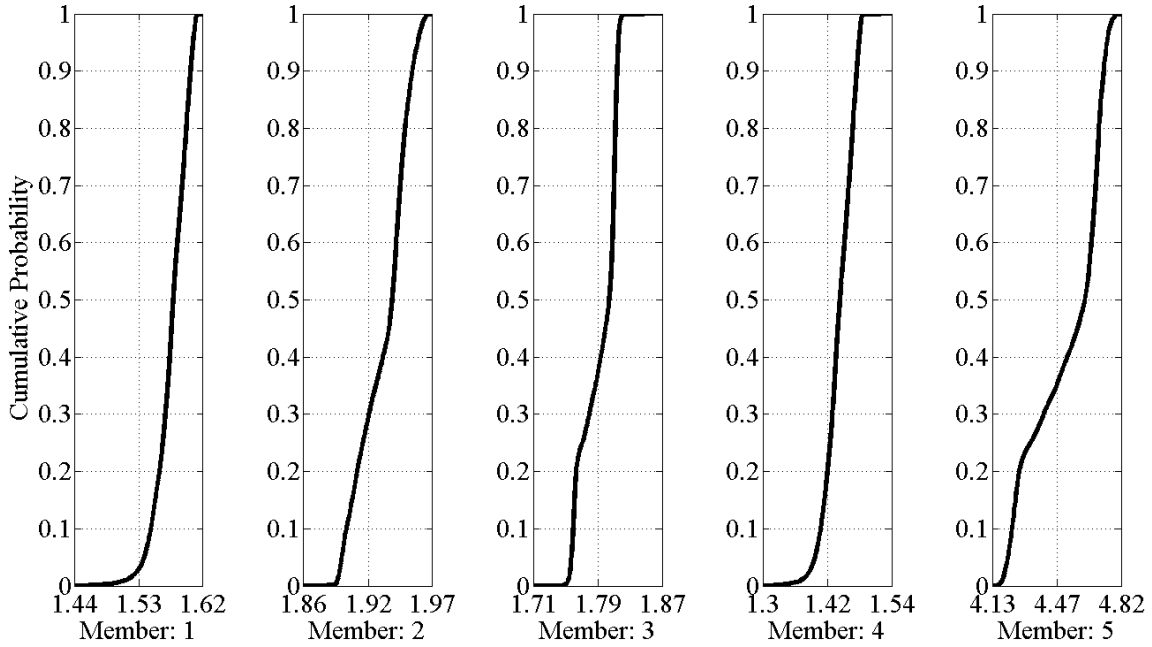

Figure 14-25: LRFR Inventory Ratings for Members 1 through 5

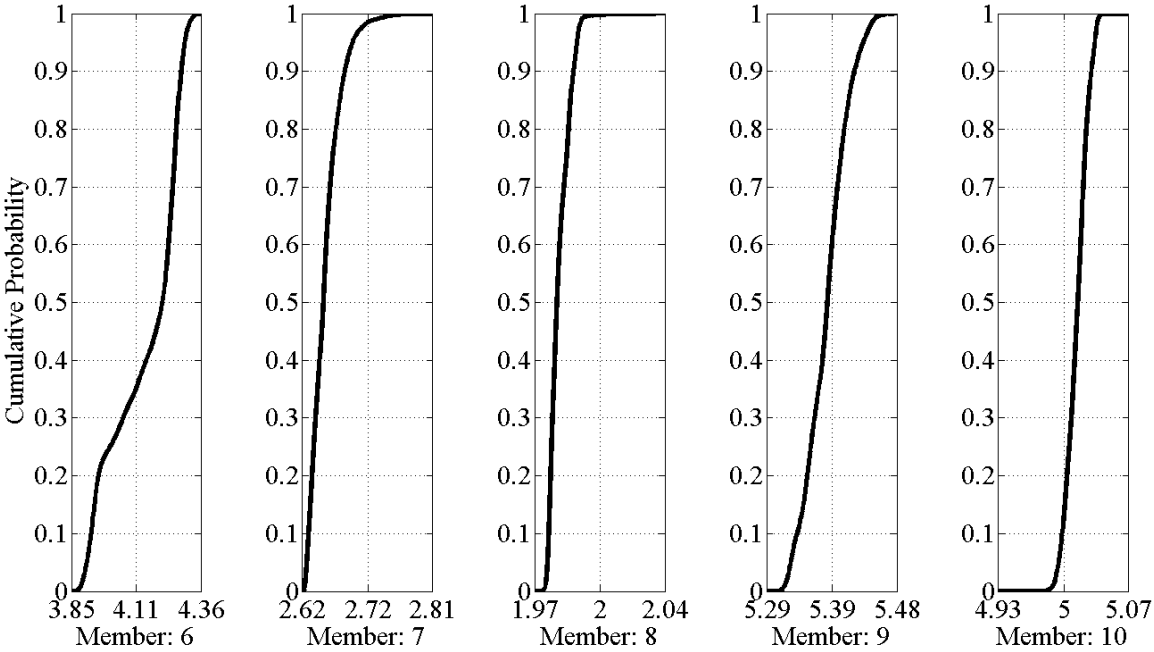

Figure 14-26: LRFR Inventory Ratings for Members 6 through 10

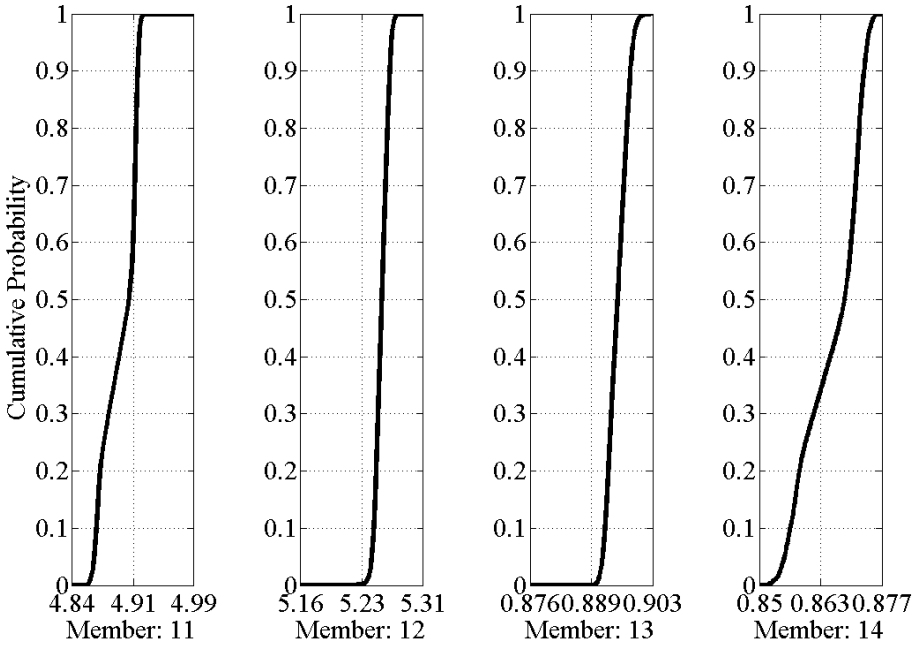

Figure 14-27: LRFR Inventory Ratings for Members 11 through 14

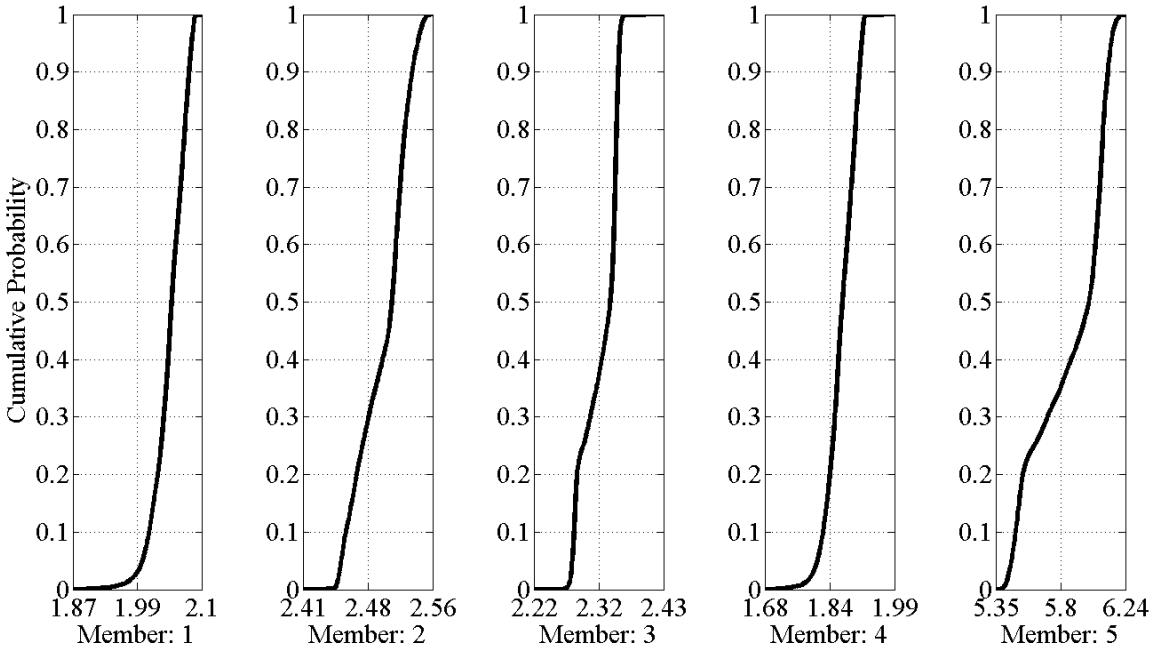

Figure 14-28: LRFR Operating Ratings for Members 1 through 5

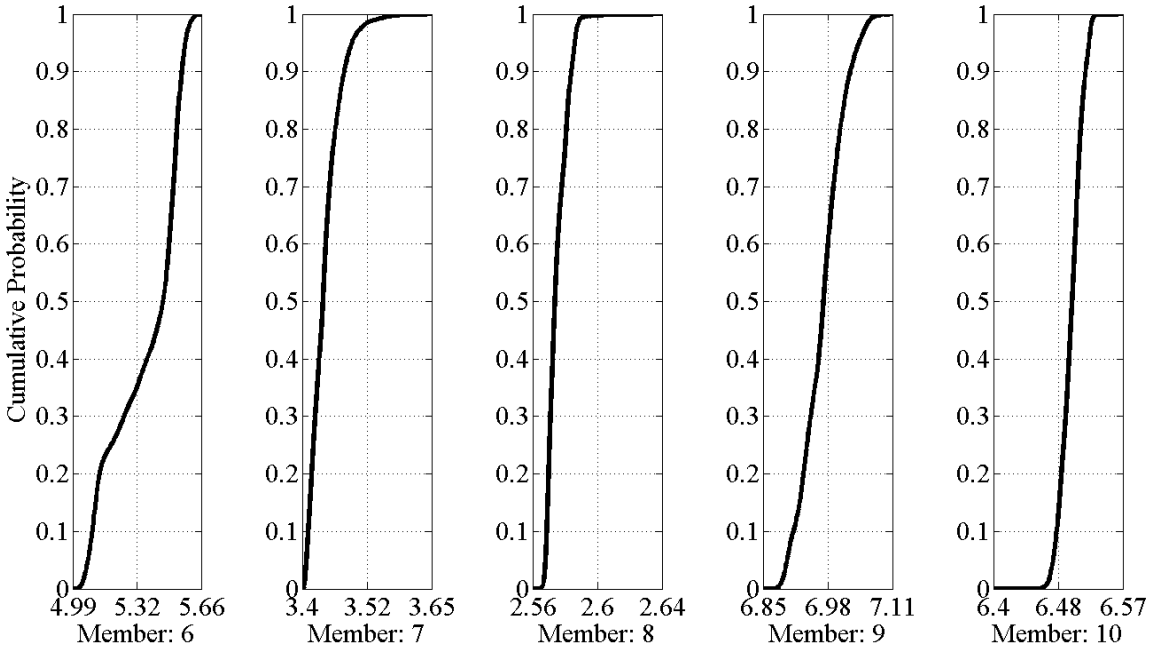

Figure 14-29: LRFR Operating Ratings for Members 6 through 10

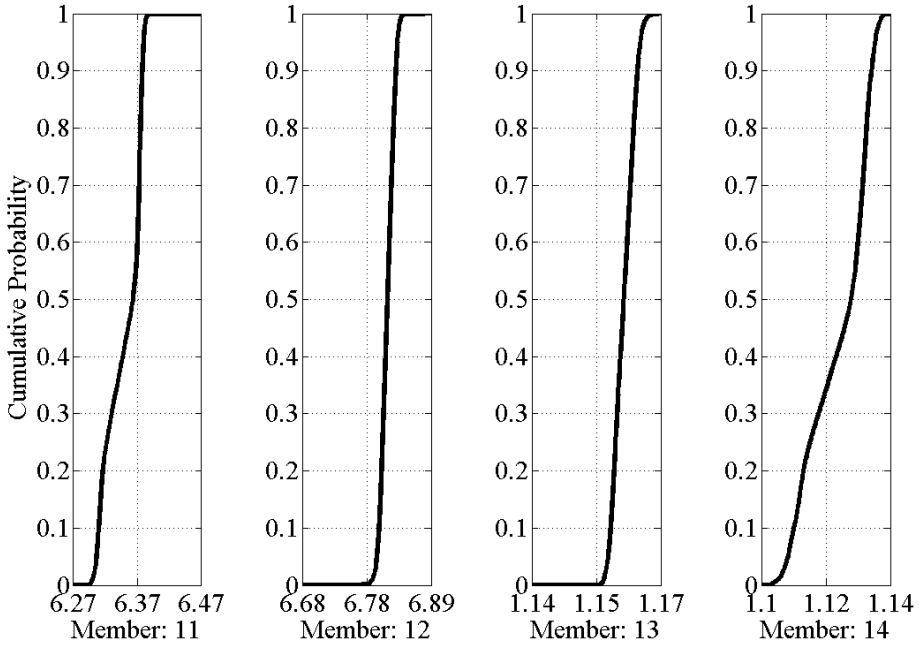

Figure 14-30: LRFR Operating Ratings for Members 11 through 14

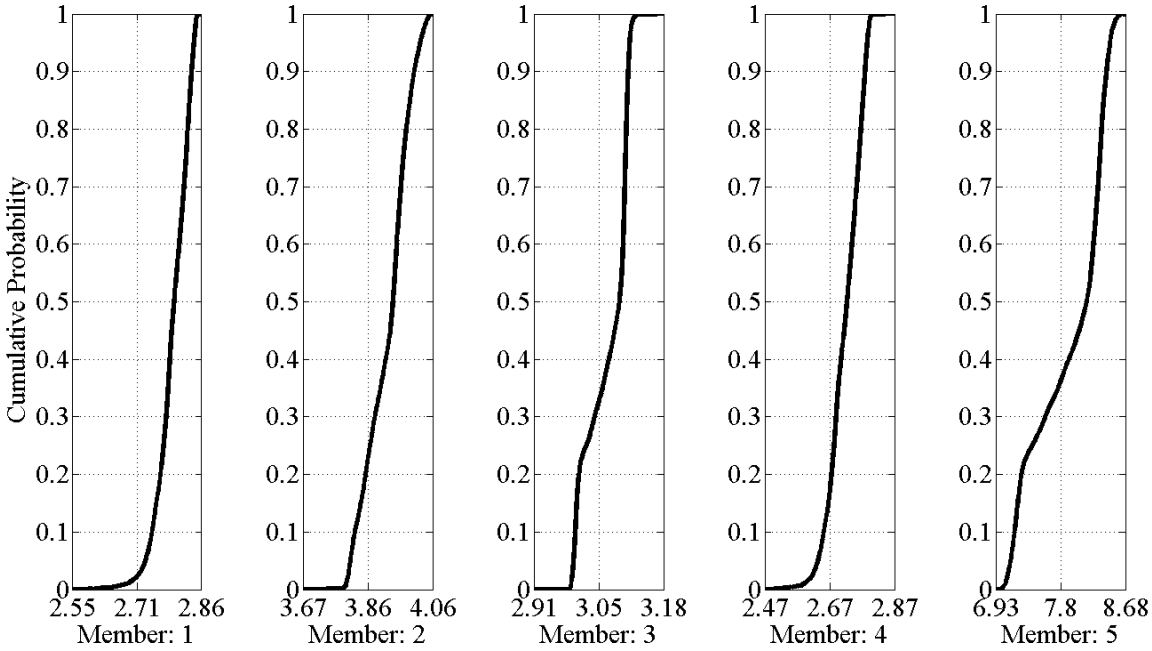

Figure 14-31: LFR Inventory Ratings for Members 1 through 5

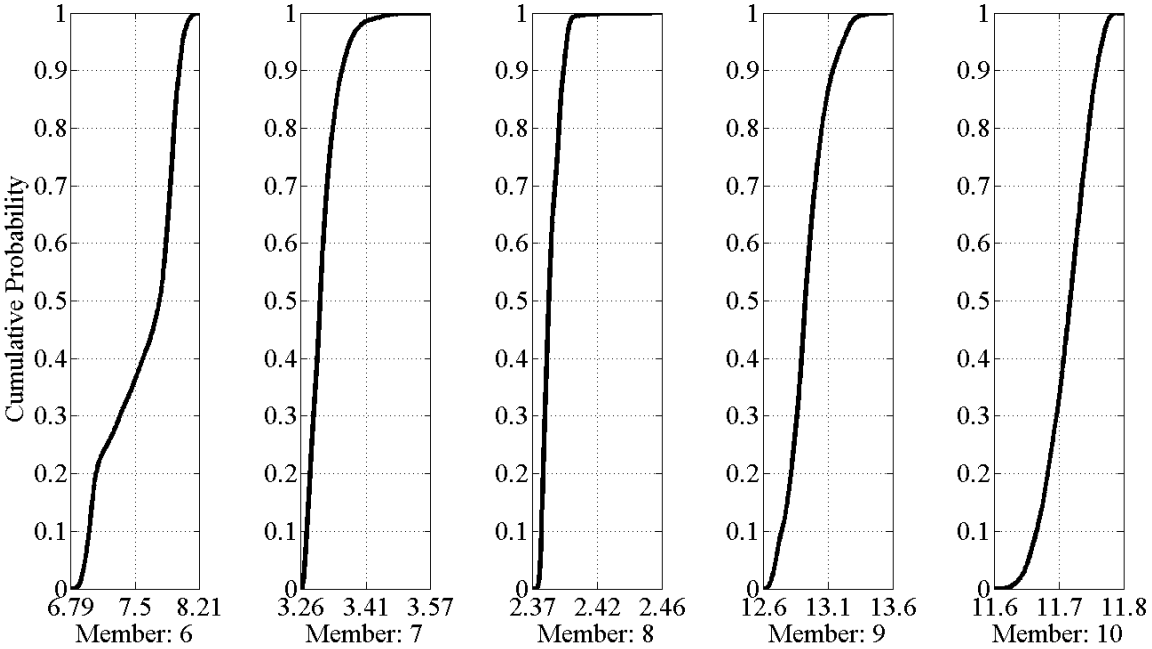

Figure 14-32: LFR Inventory Ratings for Members 6 through 10

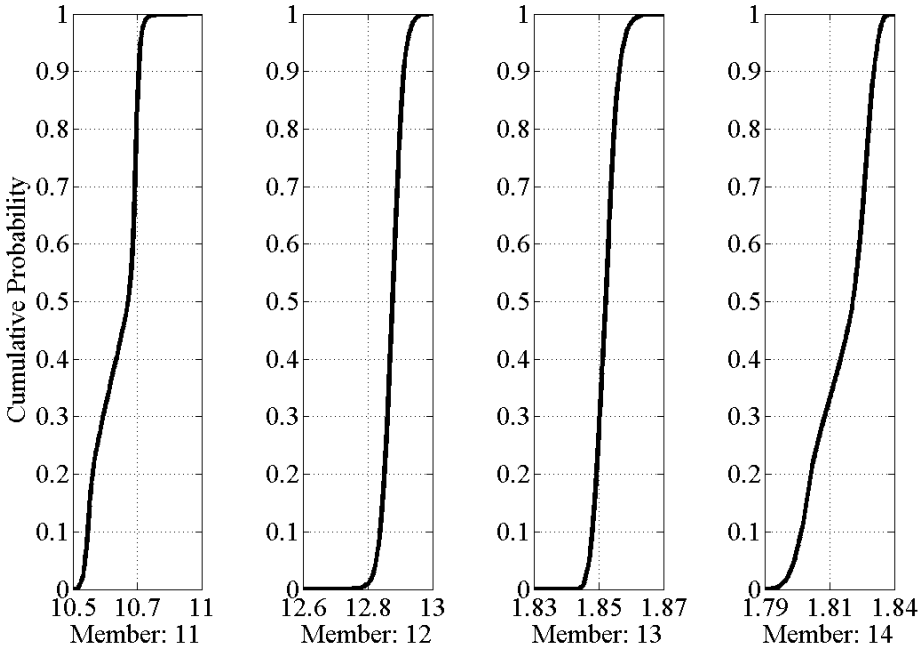

Figure 14-33: LFR Inventory Ratings for Members 11 through 14

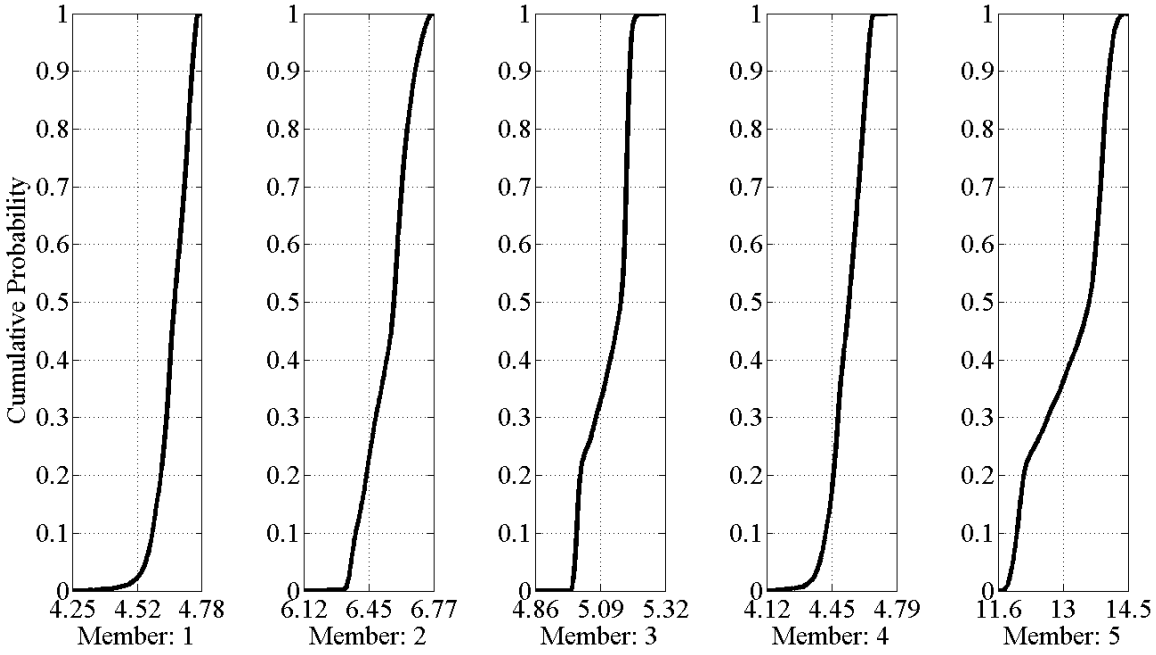

Figure 14-34: LFR Operating Ratings for Members 1 through 5

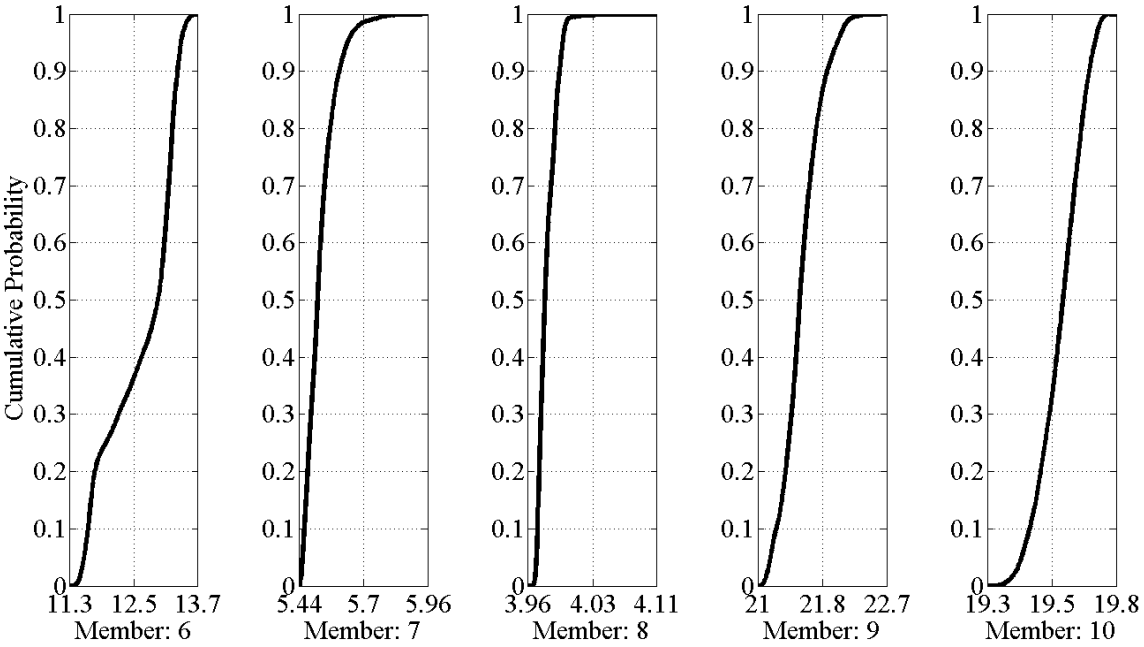

Figure 14-35: LFR Operating Ratings for Members 1 through 5

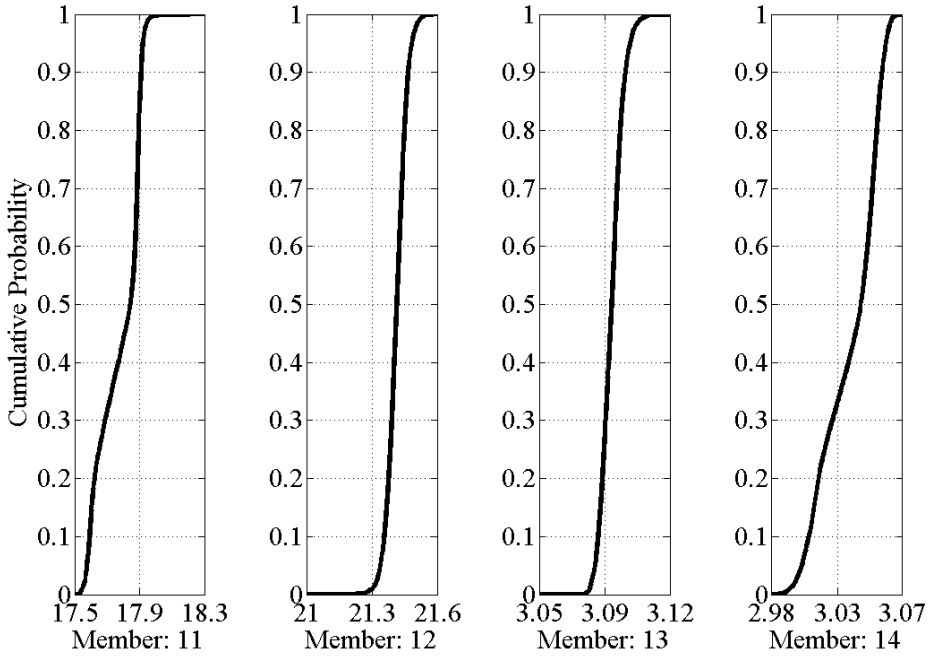

Figure 14-36: LFR Operating Ratings for Members 11 through 14

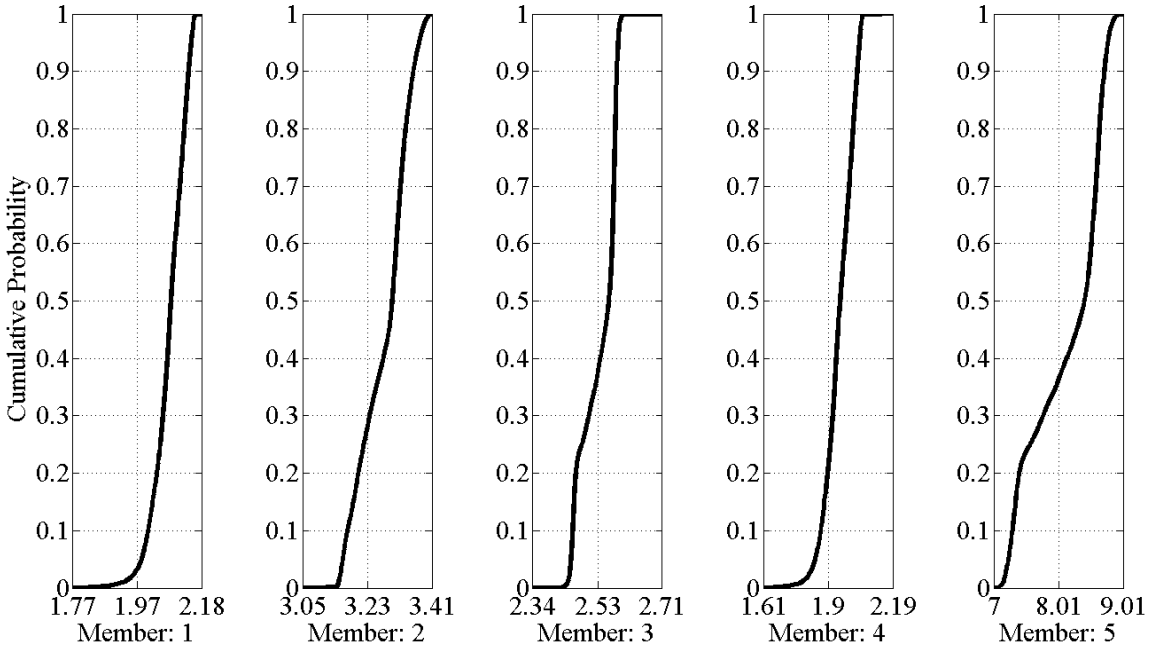

Figure 14-37: ASR Inventory Ratings for Members 1 through 5

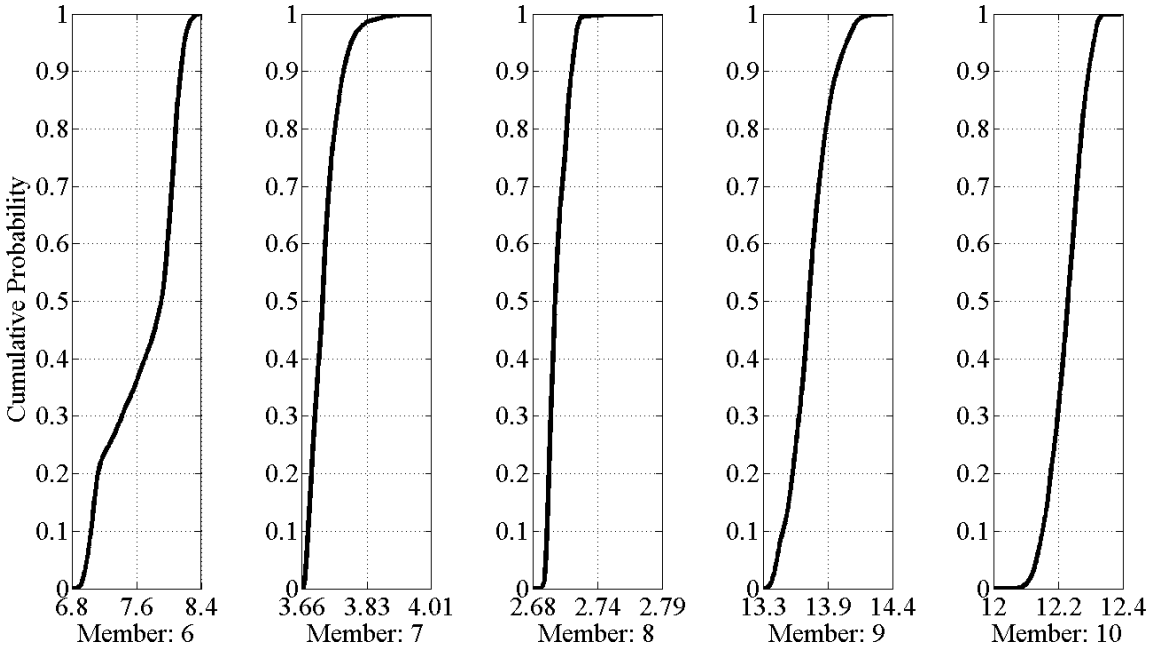

Figure 14-38: ASR Inventory Ratings for Members 6 through 10

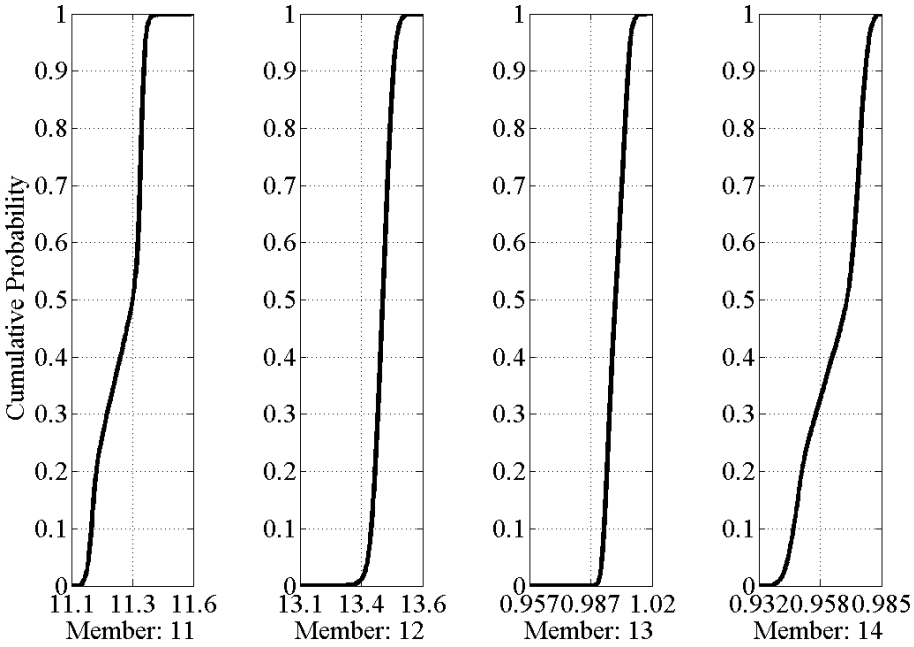

Figure 14-39: ASR Inventory Ratings for Members 11 through 14

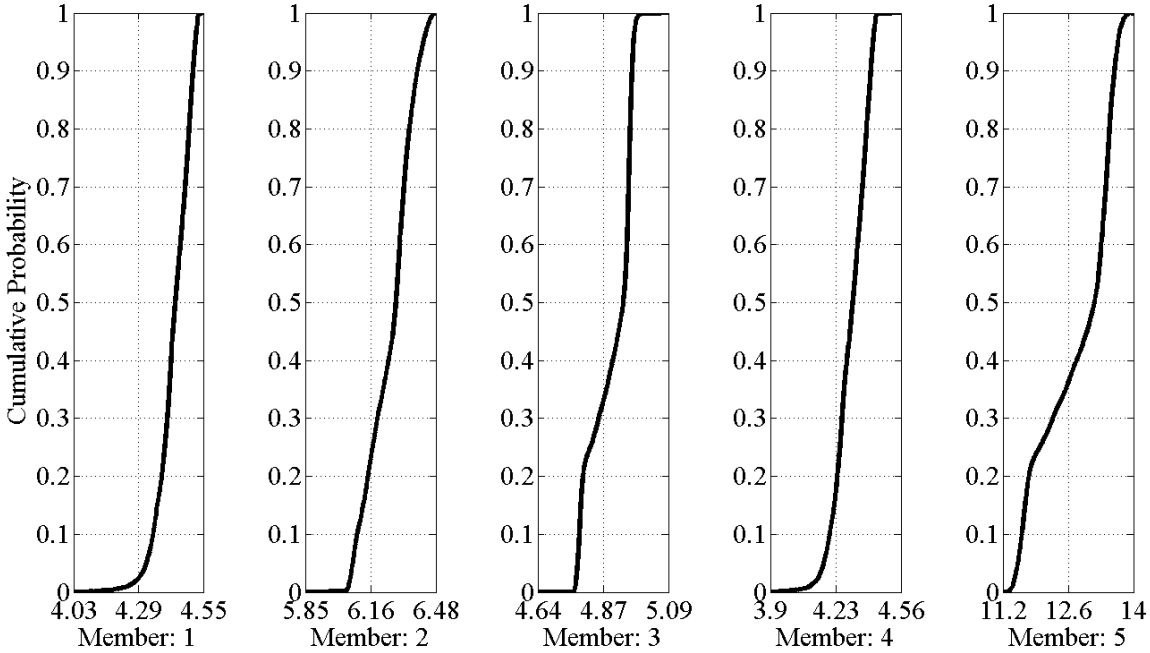

Figure 14-40: ASR Operating Ratings for Members 1 through 5

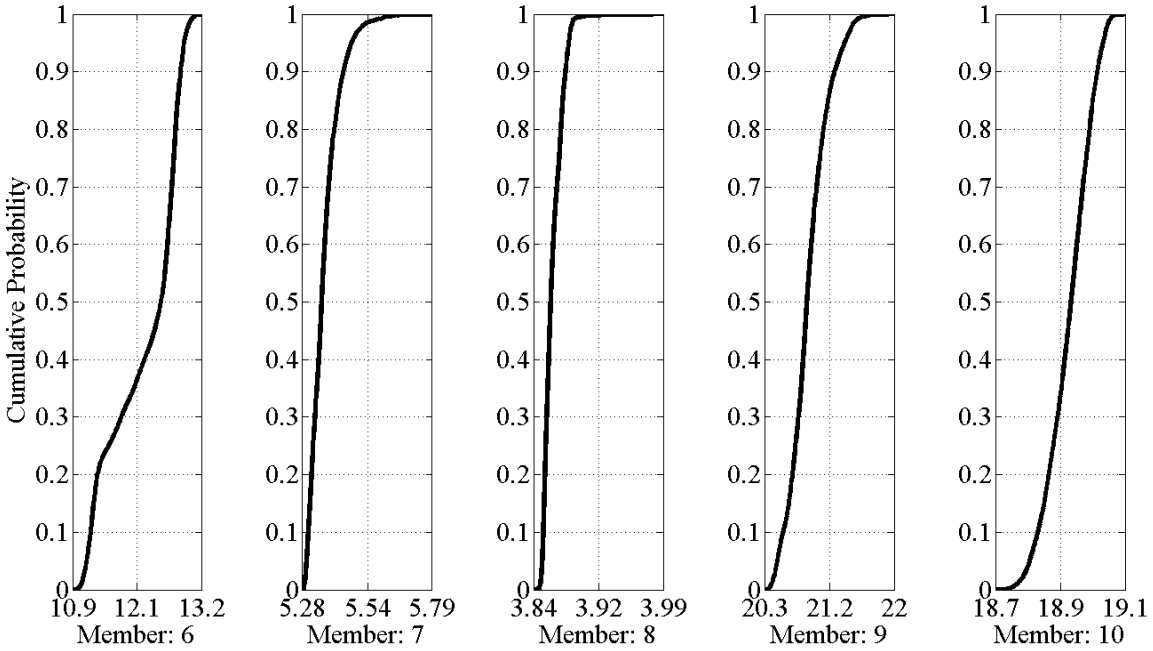

Figure 14-41: ASR Operating Ratings for Members 6 through 10

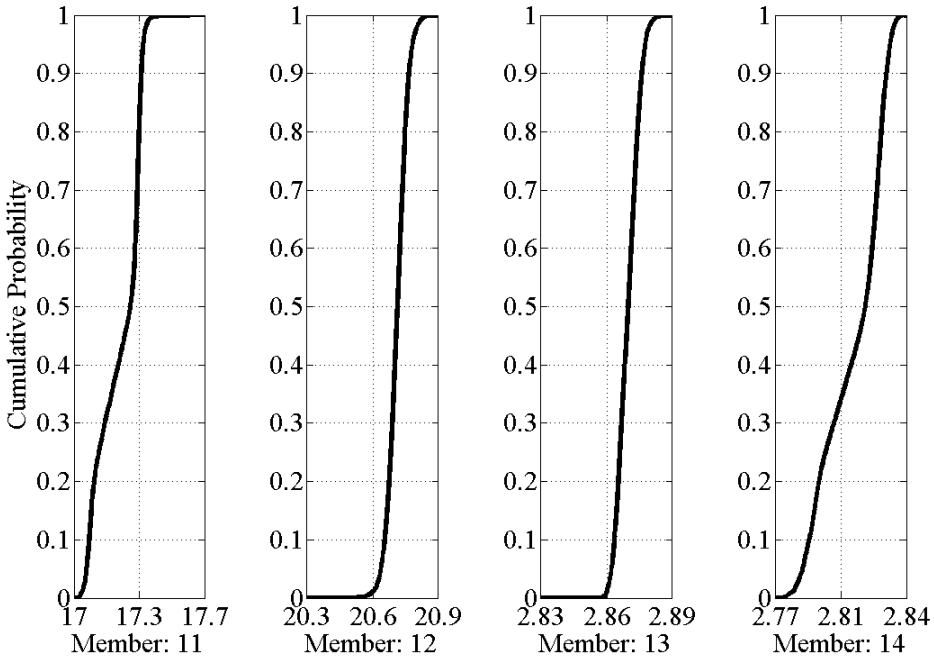

Figure 14-42: ASR Operating Ratings for Members 11 through 14

In analyzing the above plots, it is apparent that there are different types of distributions seen for the various members. In some cases, the ratings for the members shown above do not have significant variance, while other members do. Additionally, and most important to the structure, all members meet the rating requirements for the various codes used to generate them. While the ratings are below 1.0 for the LRFD Inventory case for members 13 and 14, the top chord members of the upstream and downstream trusses at mid-span, they are above 1.0 for the Operating case, which according to the AASHTO LRFD Load Rating Flowchart is sufficient and does not require the structure to be posted for a lower truck weight class.

In analyzing the variance of the rating factors for the various members, the first metric which was developed was the overall range for the distribution, and then the standard deviation for the distributions were also computed as an additional metric to quantify the spread of the prediction distributions in the event that outliers would provide false interpretations in the analysis of distribution range. Finally, the coefficient of variation was analyzed so that a normalized measure of dispersion could be generated. This way, a member which rates at 1 but has a standard deviation of 1 (which would be redundant) is compared appropriately against a member with a rating of 100 and a standard deviation of 1. The range, standard deviation and coefficient of variation metrics were computed for each member and rating equation and are shown below in Table 14-8 through Table 14-10, respectively.

Table 14-8: Analysis of Distribution Range for Each Member and Load Rating Methodology for Legal Vehicular Loading

	Distribution Range													
Rating Methodology	1	2	3	4	5	6	7	8	9	10	11	12	13	14
LRFR - Inventory	**0.20**	**0.15**	**0.22**	**0.25**	**0.69**	**0.53**	**0.24**	**0.09**	**0.24**	**0.14**	**0.17**	**0.16**	**0.03**	**0.03**
LRFR - Operating	**0.26**	**0.19**	**0.29**	**0.33**	**0.90**	**0.68**	**0.31**	**0.12**	**0.31**	**0.18**	**0.23**	**0.20**	**0.04**	**0.04**
LFR - Inventory	**0.34**	**0.49**	**0.41**	**0.42**	**1.77**	**1.46**	**0.39**	**0.13**	**1.29**	**0.30**	**0.79**	**0.40**	**0.05**	**0.06**
LFR - Operating	**0.57**	**0.82**	**0.69**	**0.70**	**2.95**	**2.44**	**0.65**	**0.22**	**2.15**	**0.50**	**1.32**	**0.67**	**0.09**	**0.10**
ASR - Inventory	**0.45**	**0.45**	**0.50**	**0.61**	**2.02**	**1.65**	**0.44**	**0.16**	**1.36**	**0.41**	**0.84**	**0.49**	**0.06**	**0.05**
ASR - Operating	**0.56**	**0.79**	**0.67**	**0.69**	**2.87**	**2.37**	**0.63**	**0.22**	**2.08**	**0.49**	**1.27**	**0.65**	**0.07**	**0.07**

Table 14-9: Analysis of Distribution Standard Deviation for Each Member and Load Rating Methodology for Legal Vehicular Loading

	Distribution Standard Deviation													
Rating Methodology	1	2	3	4	5	6	7	8	9	10	11	12	13	14
LRFR - Inventory	**0.03**	**0.02**	**0.02**	**0.04**	**0.20**	**0.15**	**0.03**	**0.01**	**0.03**	**0.01**	**0.02**	**0.01**	**0.00**	**0.01**
LRFR - Operating	**0.04**	**0.03**	**0.03**	**0.05**	**0.26**	**0.19**	**0.04**	**0.01**	**0.04**	**0.01**	**0.03**	**0.01**	**0.00**	**0.01**
LFR - Inventory	**0.06**	**0.07**	**0.05**	**0.07**	**0.51**	**0.41**	**0.05**	**0.01**	**0.17**	**0.05**	**0.08**	**0.04**	**0.00**	**0.01**
LFR - Operating	**0.10**	**0.12**	**0.08**	**0.11**	**0.86**	**0.68**	**0.09**	**0.02**	**0.28**	**0.09**	**0.13**	**0.06**	**0.01**	**0.02**
ASR - Inventory	**0.07**	**0.07**	**0.06**	**0.09**	**0.59**	**0.46**	**0.06**	**0.01**	**0.18**	**0.06**	**0.09**	**0.04**	**0.00**	**0.01**
ASR - Operating	**0.09**	**0.11**	**0.08**	**0.11**	**0.84**	**0.66**	**0.09**	**0.02**	**0.27**	**0.08**	**0.13**	**0.06**	**0.01**	**0.02**

Table 14-10: Analysis of Coefficient of Variation for Each Member and Load Rating Methodology for Legal Vehicular Loading

	Distribution Coefficient of Variation													
Rating Methodology	1	2	3	4	5	6	7	8	9	10	11	12	13	14
LRFR - Inventory	**0.02**	**0.01**	**0.01**	**0.03**	**0.05**	**0.04**	**0.01**	**0.00**	**0.01**	**0.00**	**0.00**	**0.00**	**0.00**	**0.01**
LRFR - Operating	**0.02**	**0.01**	**0.01**	**0.03**	**0.05**	**0.04**	**0.01**	**0.00**	**0.01**	**0.00**	**0.00**	**0.00**	**0.00**	**0.01**
LFR - Inventory	**0.02**	**0.02**	**0.02**	**0.03**	**0.07**	**0.05**	**0.02**	**0.00**	**0.01**	**0.00**	**0.01**	**0.00**	**0.00**	**0.01**
LFR - Operating	**0.02**	**0.02**	**0.02**	**0.03**	**0.07**	**0.05**	**0.02**	**0.00**	**0.01**	**0.00**	**0.01**	**0.00**	**0.00**	**0.01**
ASR - Inventory	**0.04**	**0.02**	**0.02**	**0.05**	**0.07**	**0.06**	**0.02**	**0.00**	**0.01**	**0.00**	**0.01**	**0.00**	**0.00**	**0.01**
ASR - Operating	**0.02**	**0.02**	**0.02**	**0.03**	**0.07**	**0.06**	**0.02**	**0.00**	**0.01**	**0.00**	**0.01**	**0.00**	**0.00**	**0.01**

Note that in the tables above, the cells are defined with a rule which shades the cell based on its value, from high to low. This presentation format makes it very obvious as to which members exhibit low measures of dispersion (highlighted in dark gray) and which members exhibit high levels of dispersion (highlighted in white). First and foremost, it is obvious from the comparison between the two tables that outliers do not affect the analysis of range, since the standard deviations of the members provide the same conclusions.

By analyzing the variance of the response prediction distributions, it is possible to obtain a sense of relative redundancy of the members considered for analysis. This is possible due to the fact that member predictions which have very little dispersion, exhibit little to no change in variation of load path (i.e., they are critical in the sense that no other member can assume the load if the member in question were to fail). Conversely, if members have high variation in their predictions, it can be concluded that alternate load paths are available for the member under consideration.

However, to state that the method presented can be indicative of the redundancy within the structural system, it is important to state the assumptions and limitations with respect to the model and analysis type. Since a linear elastic analysis was carried out, it is important to recognize that while in the model loads might be able to transfer from one structural component to another (due to redundancy) it may in actuality be overstressing a connection, which would not be realized with the model.

Based upon the analysis of the two tables, it is obvious that members 13 and 14 have very little dispersion. These members, the top chord members for both trusses, are completely

non-redundant, in that if the integrity of these members were compromised, the stability of the truss as a structure would also be compromised. By studying the load distribution mechanisms of the lift span truss, it is noted that the top chord of the truss acts in a manner similar to an arch, tied at its ends by the lower chord. The top chord carries significant loads, regardless of how the model was varied throughout the MM St-Id process, which is made evident by its lack of variability in the process.

To that end, one would also think that the lower chord would be largely non-redundant since it is tying the ends of the top chord system. However in studying the above tables, members 5 and 6 (lower chord member, upstream and downstream truss respectively) consistently have the highest degree of dispersion throughout the rating methodologies, as made evident by their cells being colored white. If level of redundancy where able to be estimated by the variance of the predicted load distribution of the truss system, then the analysis would suggest that the lower chord is the most redundant of the members analyzed. This makes sense physically when looking closely at the structural system of the lift span truss. If a lower chord member were removed from service, the force it was carrying would be able to travel through the floor system of the truss, which consists of three longitudinal stringers along the entire span and floor beams at every panel point. The floor beams must deform consistently in a global sense with the panel points of the truss, thus engaging the longitudinal stringers in axial tension. This level of redundancy, while not immediately obvious when analyzing a truss, was highlighted with the MM St-Id method and immediately gave insight into the load carrying mechanisms which the lift span truss can support.

The next most obvious observation to be made from the tables above is that member 8 has a relatively low variance. The analysis of this member, the downstream vertical sub-hanger located between the lower chord at location L9 and the mid-height of truss intersection with a main diagonal at location M9, would suggest that it is a relatively non-redundant member. The interesting point of this conclusion is that its upstream truss symmetric counterpart, member 7, has a much more variable distribution describing its load carrying capacity. While at first this may seem counterintuitive, since these symmetric members should have similar load carrying mechanisms which was demonstrated by the top and lower chord members discussed above. However, upon closer inspection it is realized that the centerline of the roadway passing through the lift span truss is not coincident with the centerline of the truss, and is in fact closer to the downstream truss than the upstream truss. Additionally, there is a four foot sidewalk between the edge of the roadway and the upstream truss. This asymmetric alignment of the roadway within the truss places higher demand on some downstream truss components than their upstream counterparts. More specifically, the downstream vertical hanger is much more critical within the load carrying mechanisms of the lift span than the upstream vertical hanger at the same location.

The ability of the MM St-Id method to highlight relative levels of redundancy within a structural system is a very important contribution to the understanding of how a given structural system behaves, and more importantly it provides the analyst with invaluable information in light of real decision making requirements. For example, if a vehicle were to careen out of control and impact the structure in such a way that it buckled the member, engineers would need to be able to immediately assess the redundancy of the

member and what actions need to be taken (shut down the structure, limit vehicle loads, emergency repair, etc). By having a list of relative member redundancies, engineers would be able to quickly assess the criticality of the member and make a well informed decision, which would have significant consequences in terms of safety and cost.

Similarly, the ability to identify critical members to monitor with Structural Health Monitoring applications is possible by identifying those members with little variation in rating predictions (i.e., non-redundant) and which are below a rating of 1.0. If a member were to have a large variance, with some values below 1.0, this should not be of utmost concern due to the fact that alternate load paths exist. Those members which have little variance and ratings completely below 1.0 make prime candidates for monitoring applications since the load has no other path to follow.

Section 14.2.3: Load Rating Analysis of the Top Chord Truss Members using Observed Demand Quantities

Due to the low load ratings seen in the top chord member of the lift span and the comprehensive experimental characterization of live load described in Chapter 13, a load rating analysis using observed demand quantities was carried out to provide realistic computations of load ratings for these two members. In order to develop ratings based on experimental characterization of live load demand, it is critical that long term monitoring is carried out to obtain sufficient characterization of low occurrence events. Since the top chord strain monitoring system was installed in 2008, there is sufficient data to characterize the typical daily loading events on the structure.

The high speed strain data files were processed with an algorithm which searched the recorded events for locations of the peaks and stored characteristics about each event, including: time, maximum overall measured strain, maximum filtered strain and impact factor. The algorithm was used to analyze a series of time history data over the course of an entire year of high speed truck data, consisting of 19,951 events in total. The strains were filtered by applying a low pass filter with a band stop below the fundamental frequency of the lift span. This subsequently removed the effects from the dynamic interaction of the span and the vehicle and provided a smoothed strain response equivalent to the static strain response of the vehicle crawling along the span. The impact factor was then determined by dividing the unfiltered maximum response by the filtered maximum response. The impact factors were plotted against the nominal strain for each event to study the relationship between truck weight and impact factor (Figure 14-43). This is an important relationship since AASHTO codes apply the same impact factor regardless of truck size.

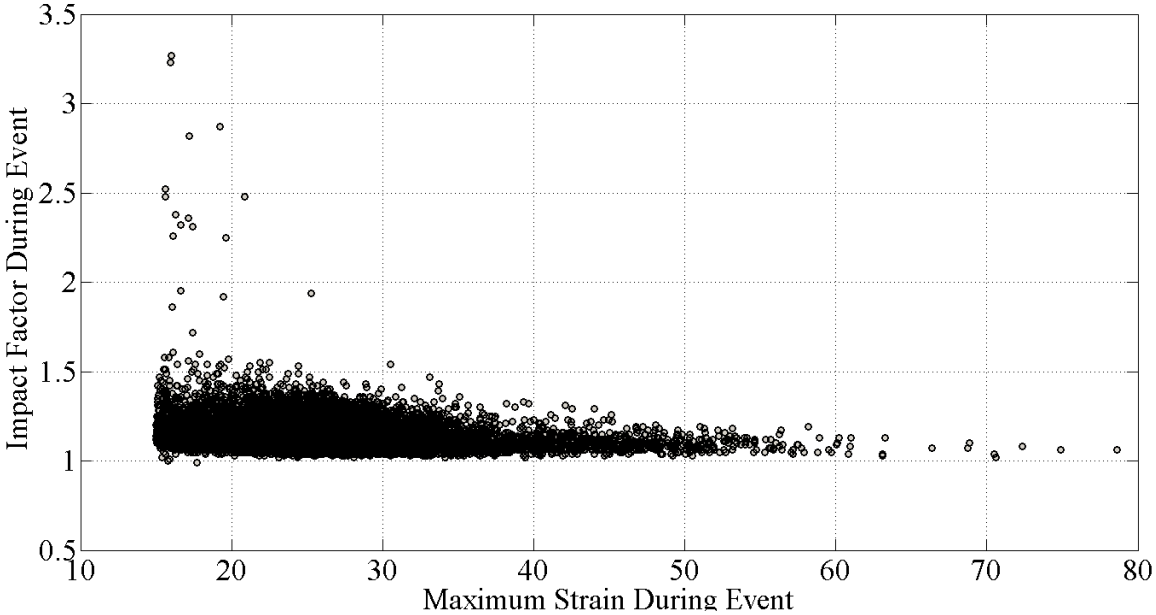

Figure 14-43: Observed Truck Impact Factors

In inspecting the plot of impact factors, a very clear trend is observed between the weight of the truck and its respective impact factor. Trucks with relatively lower weights have a very broad range of observed impact factors, while those with very high weights have almost negligible impact factors. However, this isn't to say that the trucks at legal load equivalents have negligible impact factors. When observing the impact factors around the legal load equivalent response (-26με), a range of impact factors from 1 to 1.4 is established. In order to utilize the observed data with minimally applied factors representing uncertainty in the live load demands, the cumulative density function of the maximum strain response during each event (with impact factor inherently included) was produced (Figure 14-44). To represent inventory and operating levels of loading, the maximum overall response seen was incorporated as the live load demand. Inventory

rating represents the loading condition allowed for the bridge to serve its purpose indefinitely, thus requiring the safe carrying capacity of all events seen during its service.

The operating rating load level was chosen as the 75th percentile of the observed CDF of live load events. This is percentile was chosen because it is the ratio between the rating factors between inventory and operating rating levels within the LRFR approach (1.75 compared to 1.35 for live load demand factors). The two levels of loading used for the ratings are shown in (Figure 14-44). The ratings produced using the LRFD factored capacity, factored dead load demand from the MM St-Id method and live load levels extracted from observations are shown below (Figure 14-45 and Figure 14-46).

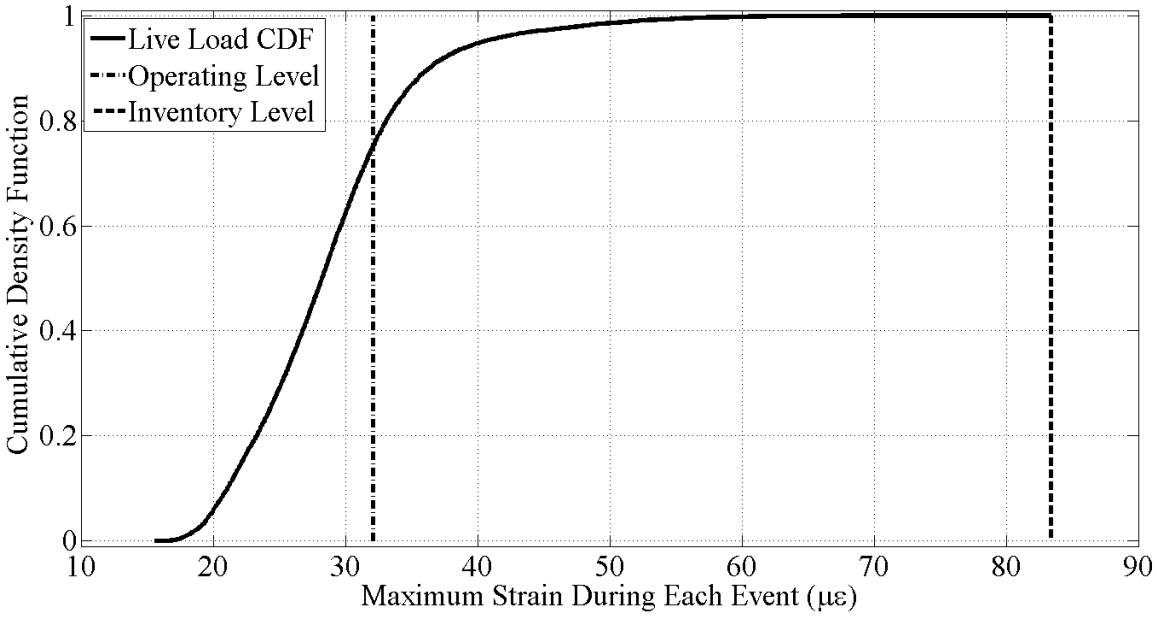

Figure 14-44: Live Load Demand CDF for the BBB with Inventory and Operating Loads Indicated

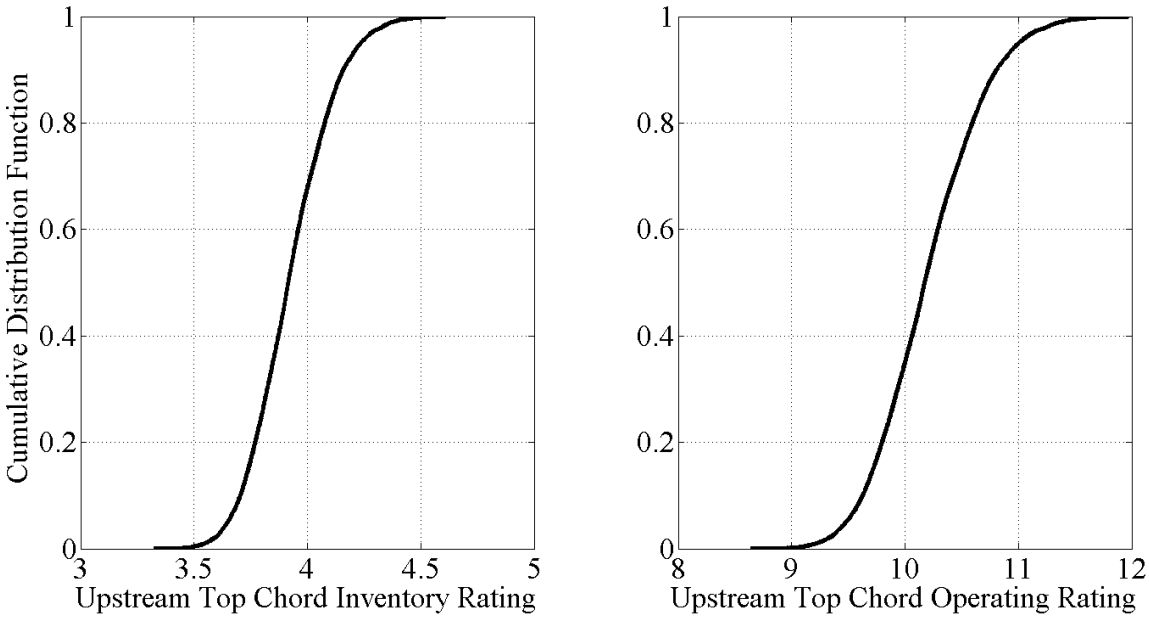

Figure 14-45: Upstream Top Chord Inventory and Operating Rating Factors

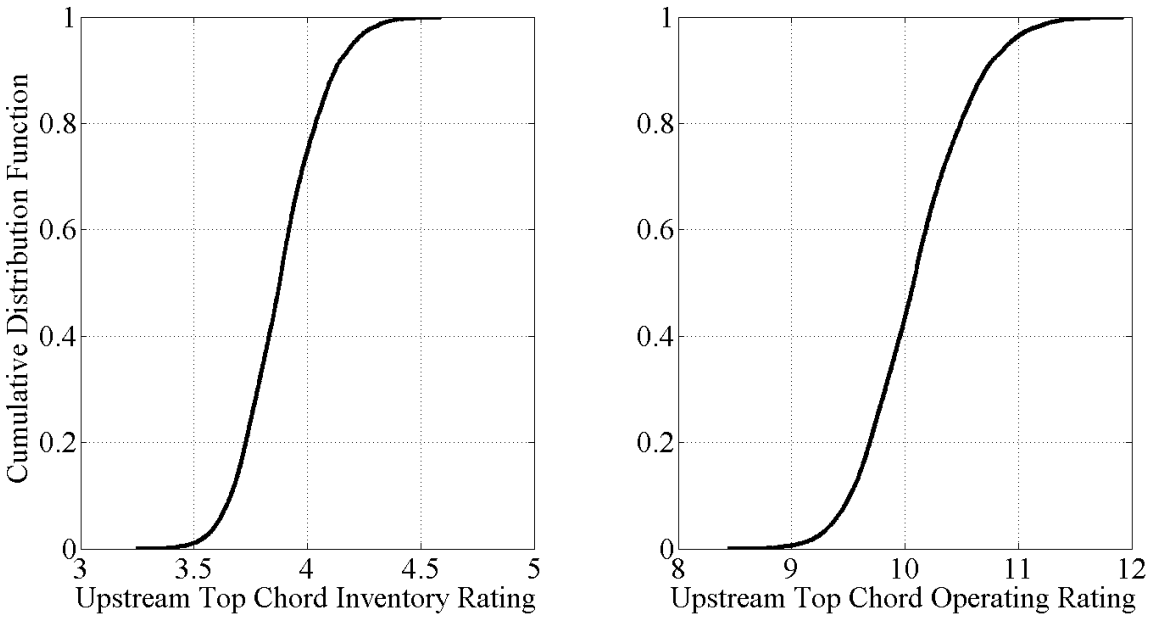

Figure 14-46: Downstream Top Chord Inventory and Operating Rating Factors

In inspecting the distributions of load ratings generated above, the first observation made is that the distributions have much more variance built into them as opposed to the CDF's presented in the previous section for these members. This is due to the necessary conversion of observed live load strains to stresses for each of the accepted models. This conversion of strain to stress requires the multiplication of the elastic modulus of steel and the observed strains. Each model has a unique elastic modulus of steel and subsequently a unique equivalent live load stress to be used within the rating equation. This process incorporated the variance of the elastic modulus of steel into the rating equation, one which is physically realistic considering the inability to directly observe stress.

An important conclusion to make from the computed load ratings based on observed live load demand due to traffic is that there is sufficient capacity within these critical members for both extreme events (seen only once within a one year period) and typical daily events. This investigation clearly demonstrates the conservatism placed within the LRFD method of rating structural components in estimating live load demand and factors. However, it is also important to note that this estimate of live load demand does not take into account the induced forces from thermal effects, wind loads and other limit states. The implementation of temperature based responses within the capacity rating of members is still an ongoing research project carried out by others, who are going to implement the vast amounts of temperature based strains into the rating analysis. This study has substantiated the costs required in putting such a strain monitoring system together and developing the appropriate analysis techniques in extracting the live load information.

14.2.3. Lateral Load Demand Analysis of Redundancy within the Lift Span

To further implement the MM St-Id analysis method in scenario analysis for the BBB structure, a load case was applied to the model which consisted of a single transverse unit load applied to the lower chord of the lift span truss. This load could then be scaled accordingly depending on the level of load to analyze with the linear analysis. A potential use for such an analysis is the investigation into the scenario where a passing ship would impact the lift span in a transverse direction. Currently, AASHTO requirements use energy formulations to develop the energy of a ship collision in terms of its weight and velocity. However, the code then transforms this into a static equivalent load so that the analyst can compute the reactions in a linear static analysis. While at this stage, it is not practical to run a nonlinear analysis within the MM St-Id framework due to computational demand, it is practical to study the relative redundancy within the structure due to such an impact. Such an analysis is important, because it provides the analyst with critical load paths due to an atypical loading scenario.

As mentioned, a unit lateral load was applied at the middle of the bottom chord of the lift span. After all of the models were analyzed for this load case, the responses within the fourteen members were scaled until the ratings for the members began approaching 1.0 in an LRFR rating methodology. This scaling was carried out so that the range and standard deviations of the response prediction distributions were not physically meaningless (i.e., rating factors of 0.001 or $1x10^4$). It was determined that a scaling factor of 200, or the equivalent of a 200 kip lateral point load, brought the ratings close enough to 1.0 where numerical issues would not compromise the direct interpretation of the statistical analysis of the response predictions.

The measures of dispersion for the LRFR ratings of all 14 members are shown in Table 14-11 and Table 14-12. Once again, the cells corresponding to each member and rating level was highlighted based on its relative magnitude with respect to the other 13 members. This approach makes it visually obvious which members are highly non-redundant (dark shades) and which members are highly redundant (light shades).

Table 14-11: Analysis of Distribution Range for Each Member and Load Rating Methodology for a Unit Lateral Load

	Distribution Range													
Rating Methodology	1	2	3	4	5	6	7	8	9	10	11	12	13	14
LRFR - Inventory	**5.65**	**8.40**	**9.31**	**5.80**	**1.18**	**1.21**	**2.41**	**2.60**	**13.23**	**12.84**	**10.52**	**13.49**	**0.93**	**0.97**
LRFR - Operating	**7.33**	**10.89**	**12.07**	**7.52**	**1.53**	**1.56**	**3.12**	**3.37**	**17.16**	**16.65**	**13.63**	**17.48**	**1.20**	**1.26**

Table 14-12: Analysis of Distribution Standard Deviation for Each Member and Load Rating Methodology for a Unit Lateral Load

	Distribution Standard Deviation													
Rating Methodology	1	2	3	4	5	6	7	8	9	10	11	12	13	14
LRFR - Inventory	**1.40**	**1.41**	**1.51**	**1.45**	**0.44**	**0.39**	**0.36**	**0.42**	**1.56**	**2.00**	**1.29**	**1.45**	**0.30**	**0.32**
LRFR - Operating	**1.82**	**1.82**	**1.95**	**1.88**	**0.57**	**0.50**	**0.47**	**0.55**	**2.02**	**2.59**	**1.68**	**1.87**	**0.40**	**0.41**

Table 14-13: Analysis of Distribution Coefficient of Variation for Each Member and Load Rating Methodology for a Unit Lateral Load

	Coefficient of Variation													
Rating Methodology	1	2	3	4	5	6	7	8	9	10	11	12	13	14
LRFR - Inventory	**0.18**	**0.15**	**0.15**	**0.19**	**0.11**	**0.11**	**0.06**	**0.06**	**0.18**	**0.22**	**0.16**	**0.18**	**0.12**	**0.13**
LRFR - Operating	**0.18**	**0.15**	**0.15**	**0.19**	**0.11**	**0.11**	**0.06**	**0.06**	**0.18**	**0.22**	**0.16**	**0.18**	**0.12**	**0.13**

In interpreting the tables above, it is visually obvious that the members with the least levels of dispersion throughout the analysis are lower chord members L8-L9 for upstream and downstream trusses (members 5 and 6) and sub-hanger members L9-M9 for both upstream and downstream trusses (members 7 and 8). However, it is important to notice that the coefficient of variation (COV) suggests a different conclusion than the other two means of analysis. According to the COV, members 13 and 14, top chord members U9-U10, are not as redundant as they would have appeared from the standard deviation and range analysis. This is due to the fact that the measure of dispersion was not normalized, something which is necessary when comparing distributions like this. It is clear that the top chord members are more redundant than the bottom chord and vertical hanger members. The diagonal truss members (members 1 through 4) and lateral bracing (members 9 through 12) appear to be the most variable in the response prediction distributions.

In interpreting these findings, it is important to justify their physical meaning before making conclusions. The fact that the upper chord was more redundant than the lower chord with a lateral loading input is reasonable, given that as the truss deforms laterally, because each truss acts as a global flange with one truss entering into primarily tension

while the second enters into primarily compression. However, more force is attracted to the lower chord because it is stiffened by the floor system. In this analysis case, it was assumed that the lateral impact could be applied in either direction, thus explaining why upstream and downstream members have similar rating levels when in reality some members would be exhibiting relieving of compression and thus increased capacity for a unidirectional load. Since each truss is acting as a flange, the top and bottom chords are going to attract a vast majority of the load due to their relatively large stiffness. Thus, even though the bottom chord was the most redundant member in the vehicular load rating analysis, it is one of the least redundant when considering lateral loading of the truss.

14.2.4. Discussion of Redundancy

In light of the discussion above regarding the ability of the method to establish relative redundancy within the BBB, it is important to establish the criteria for which redundancy was considered. In this case, there are four main criteria that must be met to define a plausible load path for a given member: (1) equilibrium and compatibility of the model must be maintained, (2) the model building blocks must all be within their predefined bounds, (3) no members are overstressed (thus remaining in an elastic analysis), and (4) the model agrees with measured global properties. If these four criteria are met, then the load path present within that model is considered plausible. This being said, if multiple load paths are present for a given member, all of which meet the criteria above, then it is possible to state that the member has a higher level of redundancy than one with fewer variation in its available load paths.

14.3. Traditional St-Id of the Burlington Bristol Bridge and Investigation into Vibration Differences

To address the challenge of identifying the cause of the perceived and observed vibration difference between the NJ and PA tower spans, an advanced modeling analysis was required. Due to the complexity of the analysis, a linear transient dynamic analysis, the MM St-Id method highlighted above could not be applied for computation time requirements of the analysis. In order to ensure that the FE model used was reasonable with respect to the observed natural frequencies and modeshapes, the FE model was roughly correlated by utilizing manual methods of perturbing the identified model building blocks until sufficient correlation was achieved.

Another cause for the inability of applying the MM St-Id method to the model was that a more detailed and comprehensive model was required for this analysis and included all major truss spans and stringer approach spans. By correlating the model to the observed dynamic data, the author was confident that the model was representative of the physical structure with respect to the interaction of the major spans and the transmission of vibration throughout the structure. This section will describe the FE model utilized, detailed analyses run, and comparison of simulated responses with observed values. Finally, a cause for the lack of symmetric vibration between these spans is offered.

14.3.1. Finite Element Model Description for the Vibration Analysis

The FE model utilized for this study consisted of 30,929 nodes, 7,203 beam elements, 1,910 shell elements, 90,018 solid elements and 4,020 link elements. The model was

representative of the structure from abutment to abutment and was inclusive of all major piers and other substructure elements in addition to all superstructure systems. The separate, reduced models utilized for the MM St-Id study above could not be used because this analysis required the determination of how vibrations were transmitted throughout the structure. Screenshots of the model are seen below in Figure 14-47 and Figure 14-48. This model served as the basis for the FE model utilized in the MM St-Id study, so the error-screening, model construction and validation and correlation processes will not be explained here since they have been done so already in Chapter 12, Chapter 13 and this chapter.

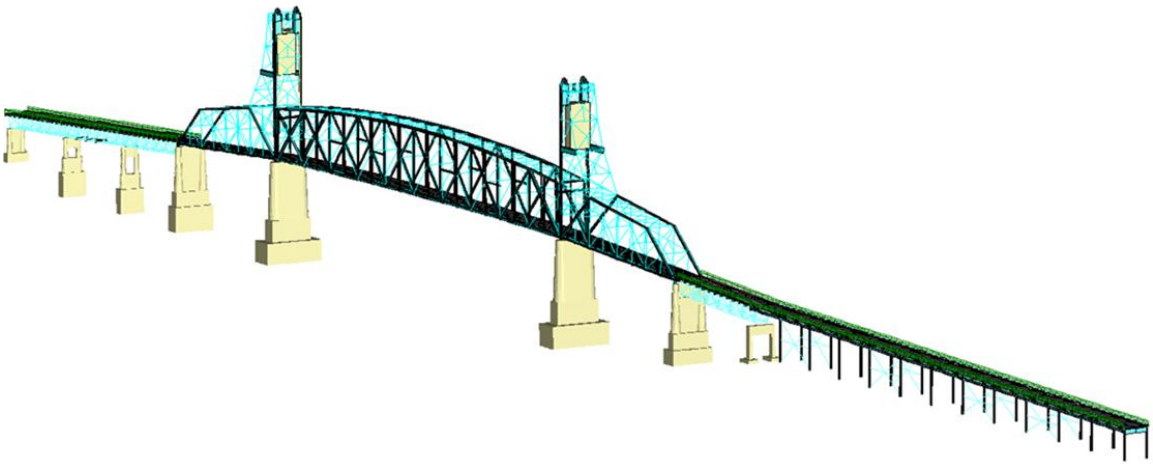

Figure 14-47: The Full BBB FE Model

Figure 14-48: The Full BBB FE Model, as Seen from a Different View

14.3.2. Linear Transient Dynamic Analysis

In order to investigate the correlated model for potential causes of the asymmetric vibration response of the tower spans, a series of linear transient dynamic analyses were carried out. This analysis type is beneficial because it allows for the computation of a series of response variable outputs over time due to a pre-defined forcing function and set of initial conditions. In this case, it was desired to simulate the effects of traffic along the bridge in such a manner that comparison to physically measured vibration responses was possible. In order to prepare the analysis, a forcing function needed to be defined within the model. For this analysis, two cases were created which simulated traffic on the NJ and PA truss spans (Case I), and a separate case which simulated traffic on the NJ and PA

tower spans. In this case, traffic was modeled as a single HS20 AASHTO truck configuration, totaling 36 tons (as seen in Figure 14-49). The trucks were positioned in the downstream lane of the structures' mid-span location so as to excite both vertical and torsional fundamental modes adequately (Figure 14-49).

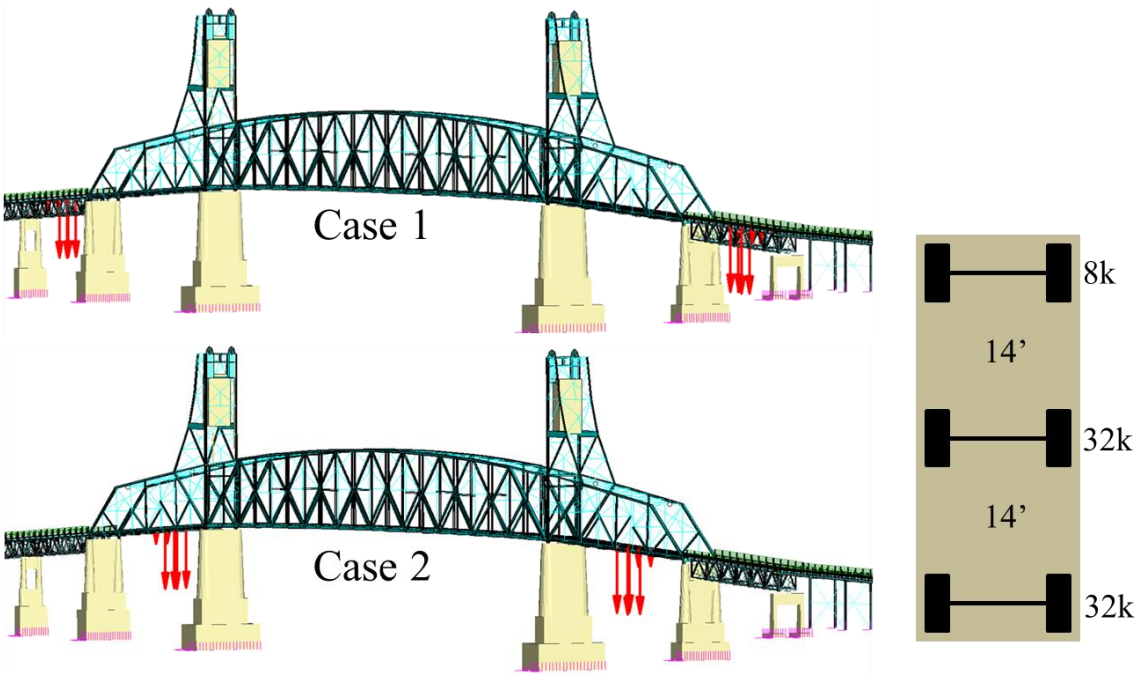

Figure 14-49: Forcing Function Loads for the Linear Transient Dynamic Solver

With the forcing function loads defined, the remaining piece of information to be defined within the solver was the time history to which the forces are applied. In order to simulate traffic traversing the structure, the forces defined above were applied with a banded random input over the range of 6 to 14Hz, a common vibration input range for heavy

trucks on bridge structures. The random input was generated using MATLAB's random number generator functions, and was banded specifically to the range identified above by applying a banded Butterworth filter. This filter applied a low-pass 14Hz filter in combination with a high-pass 6Hz filter. The characteristics of the signal were verified by computing the PSD of the signal to ensure that it had non-zero power between the desired frequency ranges (Figure 14-50 and Figure 14-51).

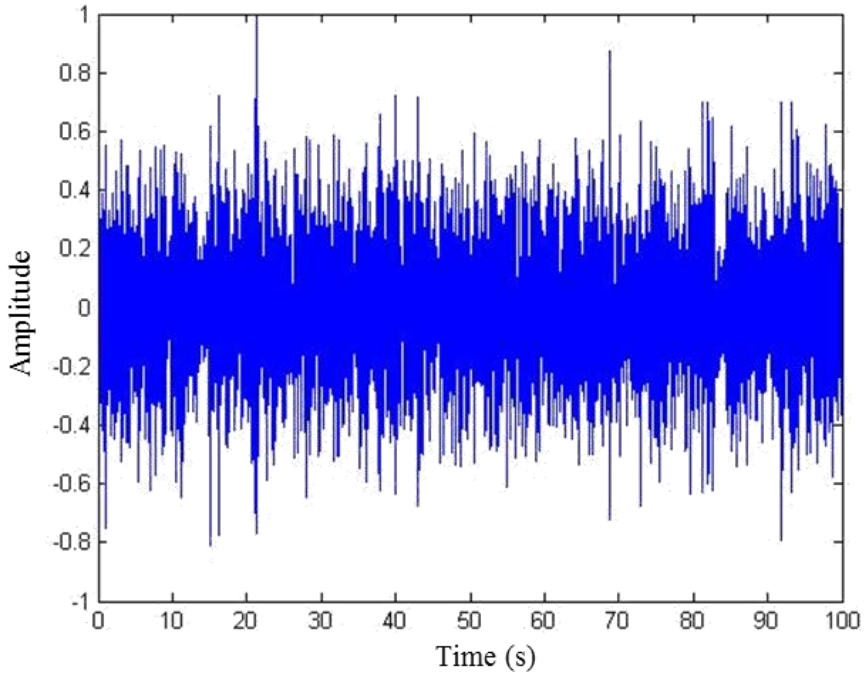

Figure 14-50: Forcing Function Time History

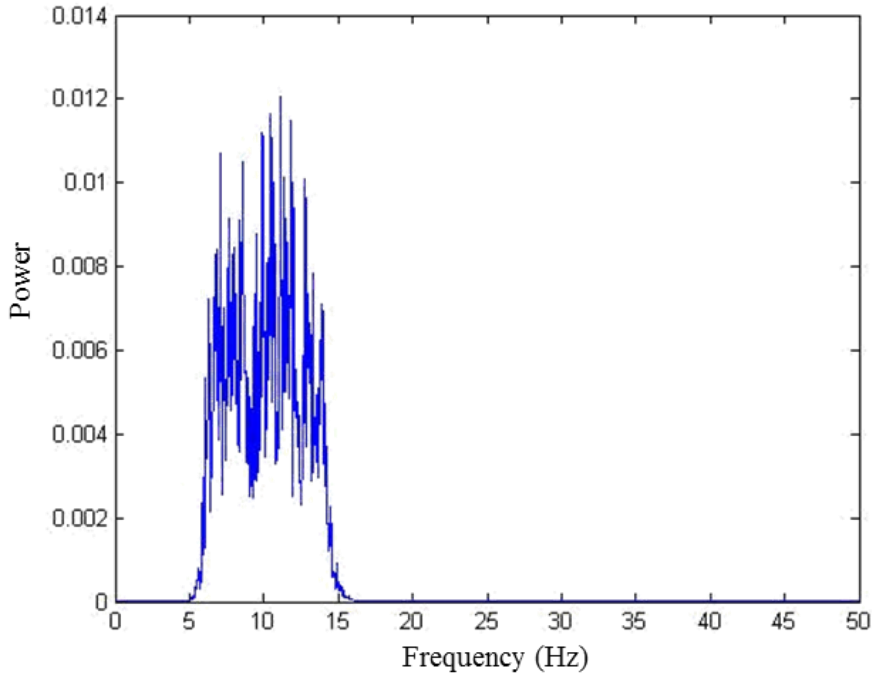

Figure 14-51: PSD of Forcing Function Time History

With the forces and force time history defined within Strand7, the final information required for the analysis included the time steps and number of steps required for the analysis. The selection of time step magnitude and quantity directly affect the analysis time, however for this case it was determined that a very fine time step over a long duration was to be computed so that the vibration response computed from the model could be characterized sufficiently. To this end, a time step of 0.01 seconds was selected (analogous to a 100Hz sampling speed) over a total time of 100 seconds (requiring 10,001 time step analyses). A set of response variables were then defined on the tower spans in both vertical and lateral directions so that the acceleration output could be written to a file and saved upon completion of the analysis. Due to the high number of

time steps and the overall complexity of the model, the total analysis time approached ten hours. Upon completion of the analysis, the computed vibration responses due to the defined forcing functions described above were compared against the observed values.

14.3.3. Comparison of Simulated Vibration Response with Observed Data

Before the comparisons between the observed and simulated responses, the observed responses are shown again in Figure 14-52 and Figure 14-53 for clarity. It is seen in these figures that the top chord lateral response of the PA and NJ tower spans have roughly four times the difference in observed peak acceleration magnitude recorded. Meanwhile, the bottom chord lateral response and both upstream and downstream vertical acceleration responses were nearly identical with respect to acceleration magnitude.

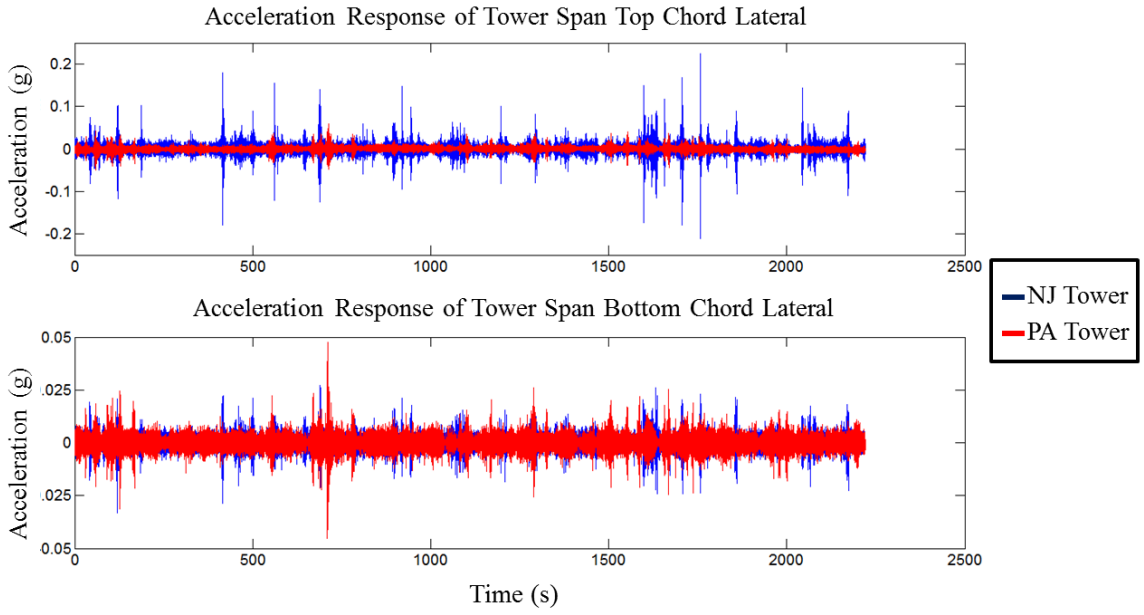

Figure 14-52: Comparison of Measured Lateral Responses for PA and NJ Tower Spans

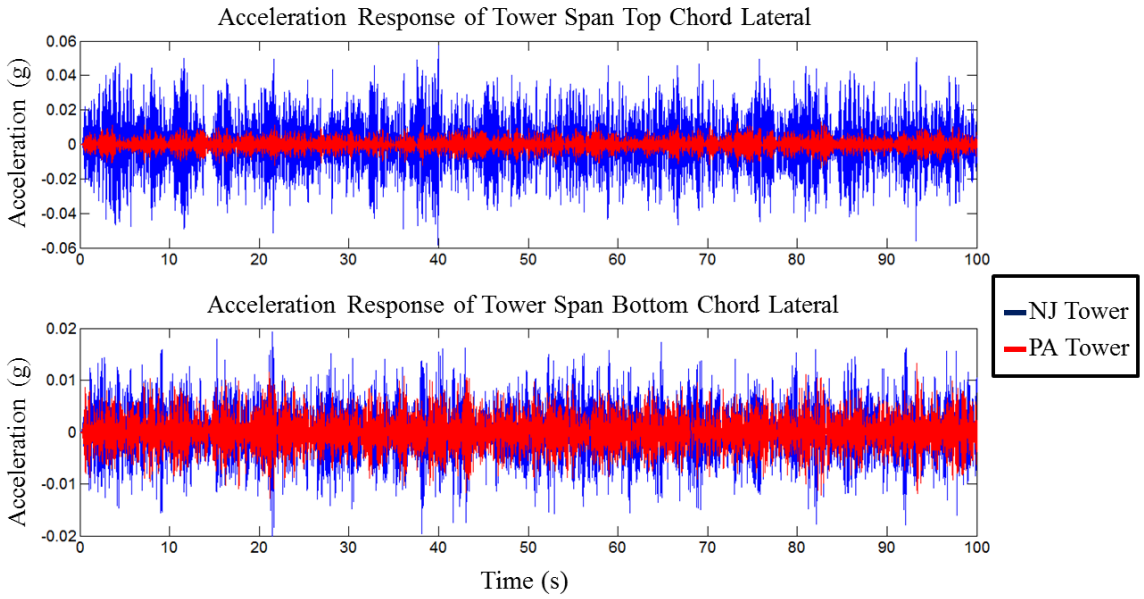

Figure 14-53: Comparison of Measured Vertical Responses for PA and NJ Tower Spans

When the results from the linear transient dynamic solver were compiled and plotted in a manner similar to those shown above, the model simulated responses were shown to nearly match those observed on the physical structure for the Case II loading scenario. It was found that with the Case I loading scenario, all simulated vibration responses were identical for the PA and NJ tower spans. However, as seen in Figure 14-54, the magnitudes of the top chord lateral response of the tower spans have four times the difference in order of magnitude, while the bottom chord lateral are nearly identical when loaded in the Case II configuration. The tower span vertical responses were also nearly identical in terms of magnitude, but are not shown here. In order to physically justify the reason why the FE model was able to simulate the asymmetric vibration response

measured and perceived, the structure was investigated for major sources of asymmetry which may influence how trucks traveling along the approach spans transmit vibrations throughout the structure.

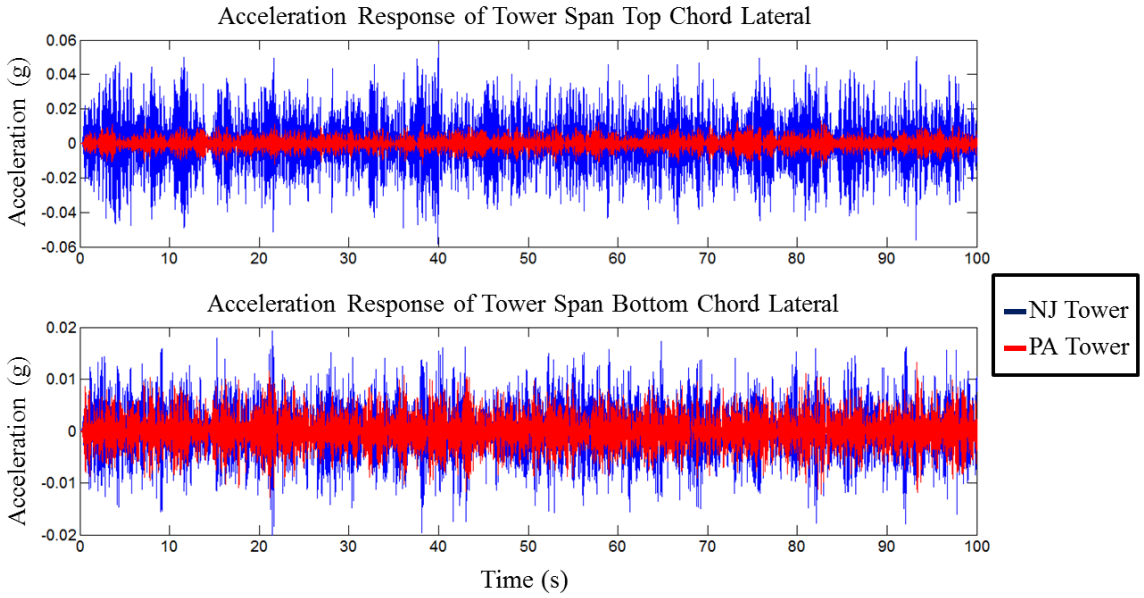

Figure 14-54: Comparison of Simulated Lateral Responses for PA and NJ Tower Spans

14.3.4. Conclusion of Vibration Amplitude Study

In justifying the results of the linear transient dynamic analysis, the structure was conceptualized from a global perspective. The major difference in simulated vibration responses was a result of the adjacent truss spans being loaded with the forcing function. When viewing the substructure of the BBB, it became fairly obvious that a major lack of symmetry was present in the lateral stiffness of the approach spans. Specifically, in

comparing piers 1 through 4 to Pier 7 and Pier 8 and supports S1 through S12 (as seen in Figure 14-55). The PA approach substructures (Piers 1 through 4) consist of reinforced concrete piers founded on driven timber piles. The NJ approach superstructure Pier 7 is also of reinforced concrete construction and founded on driven timber piles, however Pier 8 is founded on a spread concrete foundation and steel columns S1 through S12 are all founded on shallow concrete pads. The observed asymmetric vibrations seen between the tower spans of the BBB were therefore attributed to the natural behavior of the system, in that the mass, stiffness and geometry of the structure directly lead to the asymmetric vibration response, as validated with the correlated FE model. The lateral stiffness of the NJ approaches is far less than that of the PA approaches, and therefore induce a higher amount of mass participation in the NJ structural system when compared to its PA counterparts.

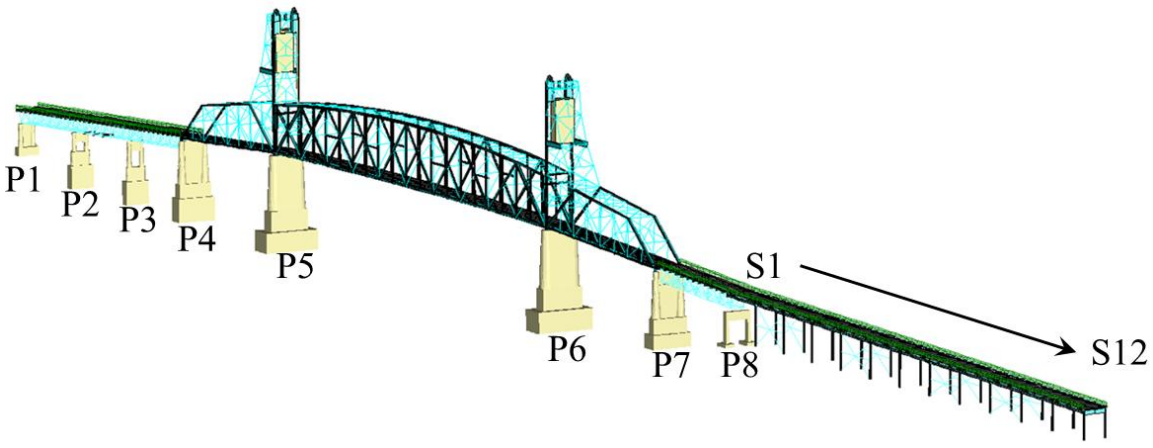

Figure 14-55: Substructure of BBB

The finding that the difference in vibrations was due to the natural behavior of the structure, and not due to any significant damages or structural inadequacies with the NJ tower span greatly highlight the benefits of utilizing traditional St-ID methods for complex analysis. This type of analysis, as previously mentioned, would not be possible within an MM St-Id realm due to the vast length of analysis for one model and the overall complexity of the FE model itself. That being said, the FE model was able to be correlated with observed data by hand and analyzed for an investigation into the behavior of the entire superstructure and substructure systems and more importantly, the transmissibility between the various systems.

This type of analysis brought to light a few important findings. The first is that the common practice of isolating piers and other substructure elements as well as adjacent spans from an FE model of a bridge can introduce a great deal of errors and uncertainty. In the MM St-Id application on the BBB, these systems were not removed ad hoc, but were condensed from the model using properties of the structure. Finally, it is highly recommended, based upon the findings of this study, that a time history correlation should be carried out in conjunction with modal property correlation of models since much more information can be contained within the observed acceleration response other than what is seen in a fast Fourier transformation.

With this finding, the engineer of record and the BCBC were notified that the vibration difference was due to the natural properties of the structure, and that with the replacement of the original expansion bearings with new elastomeric bearing pads, this transmitted vibration between the spans would most likely be greatly reduced. A second vibration

analysis of the BBB has been planned to determine whether these key response indices are now symmetric, but not yet executed.

14.4. Conclusions

This chapter has presented a significant amount of results and information obtained from the MM St-Id analysis which would not have been possible using classical St-Id. Conversely, the chapter has also shown the great deal of value which still exists by utilizing traditional St-Id applications on complicated models and analyses. The first analysis explored was a test-bed case, where the actual observations were previously made via experimental measurements of the top chord strain due to a known input. The method was able to successfully produce a set of accepted models which characterized the top chord strain response to this input when comparing to the measured value.

The elastic capacity of the structure was then analyzed using current professional approaches including three methodologies for load rating, where ratios are developed describing the relationship of the available factored capacity to factored live load demands. In developing this study, it was noted that a relationship existed between the level of dispersion within the predicted force distribution for a given member and the level of redundancy that the member has. The conclusion was validated by exploring the load paths which may or may not have provided redundant load paths for a specific member. For example, the MM St-Id method was able to identify the top chord of the lift span as the most non-redundant member with respect to the members studied and the loading applied. Additionally, the lower chord member was identified as the most

redundant with respect to the members studied and loading applied, validated by realizing that the floor system of the lift span provides alternate load paths for the global tension carried by the lower chord. Further redundancy analysis was carried out by studying which members were critical in resisting a unit lateral load at mid-span of the structure and the results were discussed.

Finally, a unique load rating analysis was carried out where the well characterized live load traffic demand of the structure was used in place of the factored live load demands as stated within LRFR rating methodologies. This study was carried out in response to ratings of the lift span top chord members being close to 1.0, and showed that when measured live load distributions were used in place of the code defined levels, the members rated well above 1.0.

The MM St-Id method was able to provide a wealth of knowledge about the BBB structure which may not have been as readily available given traditional St-Id methods. While St-Id will always have its place in good engineering practices, the tools provided by MM St-Id have warranted the computational efforts placed in carrying out such an analysis.

CHAPTER 15: CONCLUSIONS

15.1. Summary

Structural Identification aims to develop reliable estimates of structural vulnerability and performance through the correlation of analytical models with experimental observations. In this manner, St-Id can be viewed as a tool to translate observable responses, such as accelerations, strains and displacements, into estimates of unobservable attributes, such as safety factors, seismic vulnerability, etc. From this perspective, the well-documented non-uniqueness of the model-experiment correlation processes is not always problematic. That is, the fact that multiple models (or parameter groups) may equally match the experimental observations is not, in and of itself, a challenge to St-Id. Rather non-uniqueness (from a practical standpoint) only becomes problematic when the various models provide disparate estimates of the desired predictions.

The aim of this thesis was to develop, implement, and assess the ability and value of a multiple model (MM) St-Id approach to quantify the degree of non-uniqueness (related to model predictions) that results from the model-experiment correlation process. The MM St-Id approach developed generates large population of models to map out the model space and examine to what extent such information is useful and distinct from conventional single model St-Id approaches for the estimation of desired attributes. To achieve this overarching goal, three primary objectives were adopted:

4. Investigate and validate shortcomings in model correlation to experiment including identifying primary challenges and their relevance to common applications

5. Establish and validate an approach for quantifying non-uniqueness and quantifying vulnerabilities within Structural Identification using multiple models
6. Demonstrate with a case study, the application of the developed method to an actual constructed system, and compare with conventional single model approaches.

To satisfy these objectives, the research was organized into two phases: (1) Method Development and Validation, and (2) Application. The first phase included three primary activities. First, the MM St-Id method was formally developed and then compared to competing approaches that employed deterministic, threshold and probabilistic sampling and weighing methods. This not only placed the developed method in context, it also permitted the investigation and identification of appropriate convergence criteria to define when a sufficient number of models were sampled. The second activity of Phase 1 focused on the development and validation of the use of heuristic-based and mechanistic-based weighing approaches that explicitly considered the desired predictions.

The last thrust of Phase 1 focused on the development of an additional analysis technique that employed multiple a prior model forms to highlight the ability of not only incorporating uncertainties associated with specific model parameters, but also the uncertainty associated with parameter discretization, element type, geometric representation, etc. The RJMCMC approach was demonstrated with an analysis employing various levels of parameter discretization for the grid structure. The prediction

distributions were then shown with the specific contributions from each model form highlighted.

Phase 2 of this research focused on the application of the developed and validated MM St-Id approach to examine the performance and vulnerability of the Burlington-Bristol Bridge. The Burlington Bristol Bridge is a long-span, moveable through truss bridge that spans the Delaware River near Philadelphia, PA. The structural conceptualization, identification of model building blocks, development of finite element models, experimental program and application of the MM St-Id algorithm to generate samples and subsequent model predictions were all carried out and presented in this thesis.

15.2. Conclusions

To organize their presentation, the conclusions have been structured into three groups: (1) Overarching conclusions, (2) Conclusions associated with the method development and validation (Phase 1), and (3) Conclusions associated with the application (Phase 2) to a long-span bridge.

15.2.1. Overarching Conclusions

- The MM St-Id approach does not replace the need for sound engineering judgment in terms of element selection and the perturbation of uncertain model building blocks. However, it was shown to serve as a tool to explicitly account for the inherent non-uniqueness of the model-experiment correlation process and thus

provides important insight into the nature and reliability of the desired predictions.

- The correlation of the structural observations and the desired responses/attributes were shown to have significant influence over the accuracy of the predictions. While this is true for all St-Id approaches, only multiple model approaches explicitly reflect the strength of this correlation (which is often complex and not identifiable in an a priori sense) within the predictions.
- The MM St-Id approach was shown to be capable of identifying relative member redundancies within complex structural systems. Specifically, the variability of the predicted member forces is a direct indication of the presence of multiple load paths and thus a direct measure of member redundancy. Through an application to a long-span bridge, it was shown that member redundancy can vary significantly throughout a structure and also for different loading scenarios even for a single member.

15.2.2. Selection of Sampling and Weighing Techniques within MM St-Id

15.2.2.1. Deterministic Methods

- The deterministic sampling method is not effective for applications of response prediction computation when little a priori information is known about the model space due to the sparse nature of the user-defined sampling scheme. It is, however, sufficient for use in experimental design where no information is known

about the structure and the model space can be covered in a systematic grid in order to explore variation of desired responses in light of model uncertainty.

- The deterministic weighing function which summed the inverse of model-experiment discrepancies does not sufficiently distinguish the weighed model set from the un-weighed model set to make informed decisions.
- The deterministic weighing function, which multiplied the inverse of model-experiment discrepancies proved to be too strict and only identified a single model as being well correlated with experimental observations.

15.2.2.2. Error Threshold Methods

- The error threshold method eliminates an entire class of sampling approaches by weighing models against a strict accept/reject threshold, and thus was shown to be inefficient in producing response prediction distributions representative of the weighed model space.
- The error threshold method relies too heavily on computation of precise estimates of uncertainty for measurement yet utilizes a single large uncertainty for representing errors within the finite element method. This rather arbitrary approach to assigning uncertainties should not be used with the strict weighing approach employed within threshold methods.

15.2.2.3. Probabilistic

- The completeness and the stationarity of parameter and prediction distributions obtained through probabilistic approaches provided clear convergence criteria, allowing for minimum necessary models to characterize the weighed model space.
- The probabilistic approach lends itself to direct quantification of the non-uniqueness associated with the model space by displaying the variability in desired response predictions given the uncertainty of the model experiment correlation process (defined at the outset with respect to a particular experimental observation).
- Bayesian methods of computing estimates of response prediction distributions were shown to become more accurate and less varied with additional experimental observations when the desired response prediction was well correlated with the observations, while the estimates of prediction distributions do not benefit from increased information when the desired response prediction was not well-correlated with the experimental observations.
- The probabilistic approach was shown to provide accurate response prediction distributions, with increased variability than seen with the Structure 1 application, in light of the more complex and limited experimental observations associated with the Structure 3 grid configuration.
- The inherent standard deviation included within the updating process has significant influence over the results and is difficult to identify in an a priori sense. This study found that a 4% variance consistently provided prediction

distributions that enveloped the measured value. It is recognized that this parameter is dependent on numerous factors and so it should be identified on a case by case basis.

15.2.2.3.1. Sampling

- In cases where the posterior probability is associated with a small portion of the prior probability distribution, the Monte Carlo method of sampling the model space requires too many samples to sufficiently characterize high probability regions.
- MCMC methods are far more efficient for cases where the prior probability distribution is broad compared with the posterior distributions. The precise efficiency depends on the proper selection of a proposal function for each parameter.
- The Delayed Rejection Adaptive Metropolis algorithm was found to robustly increase the efficiency of the sampling even where appropriate proposal functions were not initially known. For example, when compared with a traditional MCMC approach which produced an acceptance rate of 0.1, this adaptive approach was able to maintain an acceptance rate of 0.5.

15.2.3. Correlation of Measured and Predicted Responses

- It was shown that using global measures of structural response provided accurate and low variable response predictions for both global and local structural response

indices (nominal local member actions). Conversely, local measures of structural response (nominal local member actions) provided inaccurate and variable response prediction distributions for global structural response indices. This finding points to a superiority of global measures during experimental studies (of course, this also depends on the desired predictions).

- Any predictions made when weighing the models with static strain observations that are not functions of the same physical characteristics as strains (which were modified in the MM St-Id process (EI)) will have prediction distributions with large variances.
- When using static displacement response observations to predict dynamic properties it is critical to use multiple load patterns, preferably ones which do not produce displacement surfaces similar to structural modeshapes (as these would be orthogonal to others and thus offer little information related to their parameters), to meaningfully estimate multiple frequencies.

15.2.4. Weighing of Experimental Observations

- It was shown that certain mechanistic or heuristic-based weighing approaches can increase the accuracy of predictions by accentuating the well-correlated responses and suppressing the poorly correlated responses. For example, it was shown that by weighing the observed natural frequencies and modeshapes by their respective modal mass and stiffness (mechanistic values), a more accurate and less variable estimate of global structural response was achieved.

15.2.4. Application of Multi-dimensional Techniques to MM St-Id

- The RJMCMC method was shown to provide similar levels of accurate response predictions in light of exploring multiple implementations of building block spatial resolutions. For the specific structure examined with this method the more complex spatial variations of the parameters were not needed to properly simulate the structure, but their inclusion within the method did not skew the results.

15.2.5. Application of MM St-Id to Complex Models of Constructed Systems

15.2.5.1. Computation of Demands

- The MM St-Id method was shown to provide meaningful estimates of load carrying capacity of the Burlington Bristol Bridge with respect to current design methodologies, of which all critical members analyzed passed current code requirements.

15.2.5.2. Redundancy

- The MM St-Id method was able to provide an estimate of member redundancy given a certain load case by evaluating the likelihood of additional available load paths, given the selection of model building blocks and available experimental observations.
- The MM St-Id method identified the top chord members as non-redundant with respect to vertical (gravity) loads and redundant with respect to lateral loads (ship impact or wind). In contrast, the MM St-Id method identified the bottom chord

members as redundant with respect to gravity loads and non-redundant due to lateral loads.

- The traditional St-Id carried out on the BBB identified the difference of lateral stiffness in the approach spans as the prime cause for asymmetric vibrations in the tower spans.

15.3. Recommendations

- The probabilistic methods, specifically the MCMC algorithm, should be utilized for MM St-Id analysis given the efficiency of the approach and the well characterized response prediction distributions.
- It is recommended that the user investigate the effect of selecting an inherent standard deviation on the desired response predictions. It is not anticipated that a value of 4% will be appropriate for all implementations.
- An experienced user is required for the construction of any FE models to be included with any St-Id application. The flowchart for model construction and error screening presented is demonstrated as a way to ensure common errors are avoided.
- An experienced user is to develop the MCMC framework and select key parameters such as proposal functions, starting values, adaptive properties, burn-in, and convergence.
- When using RJMCMC methods, care is to be taken in developing the jump equations that satisfy the defined requirements.

15.4. Future Work

The work presented in this thesis served as the groundwork for a probability based MM St-Id. There is a great degree of future work required to further refine the methodology presented within to address a set of remaining issues:

- The ability to detect when a critical building block is missing from the analysis
- Refining the RJMCMC approach to more efficiently sample models in the regions of high likelihood, such as incorporating an adaptive algorithm.
- Evolving the RJMCMC approach to include a priori models with various levels of discretization and element types.
- Evolving the RJMCMC approach to account for uncertainties associated with construction staging.
- Development of more weighing schemes for specific applications, such as weighing methods for observations which are not modal in nature.
- The development and refinement of steps 3 and 4 within the MM St-Id process, mainly designing and implementing experiments which most effectively inform the process.

List of References

Aktan, A. E., F. N. Catbas, et al. (1998). "Structural Identification: Analytical Aspects." Journal of Structural Engineering 124(7): 817-829.

Aktan, A. E., D. Farhey, et al. (1996). "Condition Assessment for Bridge Management." Journal of Infrastructures Systems 2(3): 108-117.

Aktan, A. E., D. Farhey, et al. (1997). "Structural Identification for Condition Assessment: Experimental Arts." Journal of Structural Engineering 123(12): 1674-1684.

Allemang, R. (2003). "The Modal Assurance Criterion - Twenty Years of Use and Abuse." Journal of Sound and Vibration: 14-21.

Allemang, R. J. (1999). Vibrations: Experimental Modal Analysis. Cincinnati, OH, University of Cincinnati: SDRL.

Anderson, H. L. (1986). "Metropolis, Monte Carlo and the MANIAC." Los Alamos Science(Fall 1986).

Barroso, M. F. S., R. H. C. Takahashi, et al. (2007). "Multi-objective parameter estimation via minimal correlation criterion." Journal of Process Control 17(4): 321-332.

Beck, J. and S. K. Au (2002). "Bayesian Updating of Structural Models and Reliability using Markov Chain Monte Carlo Simulation." Journal of Engineering Mechanics 128(4): 380-391.

Beck, J. L. and L. S. Katafygiotis (1998). "Updating Models and Their Uncertainties. I: Bayesian Statistical Framework." Journal of Engineering Mechanics 124(4): 455-461.

Beck, J. L. and K.-V. Yuen (2004). "Model Selection Using Response Measurements: Bayesian Probabilistic Approach." Journal of Engineering Mechanics 130(2): 192-203.

Brownjohn, J. M. W., P. Moyo, et al. (2003). "Assessment of Highway Bridge Upgrading by Dynamic Testing and Finite-Element Model Updating." Journal of Bridge Engineering 8(3): 162-172.

Brownjohn, J. M. W., P.-Q. Xia, et al. (2001). "Civil Structure Condition Assessment by FE Model Updating: Methodology and Case Studies." Finite Elements in Analysis and Design 37: 761-775.

Brun, R., M. Kuhni, et al. (2002). "Practical Identifiability of ASM2d Parameters - Systematic Selection and Tuning of Parameter Subsets." Water Research 36: 4113-4127.

Brun, R. and P. Reichert (2001). "Practical Identifiability Analysis of Large Environmental Simulation Models." Water Resources Research 37(4): 1015-1030.

Catbas, F. N. and A. E. Aktan (2000). Modal Analysis as a Bridge Health Monitoring Tool. Structures Congress 2000, Philadelphia, Pennsylvania, USA, ASCE.

Catbas, F. N., D. L. Brown, et al. (2004). "Parameter Estimation for Multiple-Input Multiple-Output Modal Analysis of Large Structures." Journal of Engineering Mechanics 130(8): 921-930.

Catbas, F. N., S. K. Ciloglu, et al. (2007). "Limitations in Structural Identification of Large Constructed Structures." Journal of Structural Engineering 133(8): 1051-1066.

Catbas, F. N., F. L. Moon, et al. (2008). Structural Identification of Constructed Systems: An Integrated Approach by the ASCE Committee. Crossing Borders, Vancouver, BC, Canada, ASCE.

Chen, M.-H., Q.-M. Shao, et al. (2000). Monte Carlo Methods in Bayesian Computation. New York, USA, Springer-Verlag.

Cheng, F. Y. and D. Li (1997). "Multiobjective Optimization Design with Pareto Genetic Algorithm." Journal of Structural Engineering 123(9): 1252-1261.

Cheung, S. H. and J. L. Beck (2009). "Bayesian Model Updating Using Hybrid Monte Carlo Simulation with Application to Structural Dynamic Models with Many Uncertain Parameters." Journal of Engineering Mechanics 135(4): 243-255.

Ching, J. and J. L. Beck (2004). "Bayesian Analysis of the Phase II IASC--ASCE Structural Health Monitoring Experimental Benchmark Data." Journal of Engineering Mechanics 130(10): 1233-1244.

Ching, J. and Y.-C. Chen (2007). "Transitional Markov Chain Monte Carlo Method for Bayesian Model Updating, Model Class Selection, and Model Averaging." Journal of Engineering Mechanics 133(7): 816-832.

Christodoulou, K., E. Ntotsios, et al. (2008). "Structural model updating and prediction variability using Pareto optimal models." Computer Methods in Applied Mechanics and Engineering 198(1): 138-149.

Deblauwe, F., R. J. Allemang, et al. (1987). The Polyreference Time Domain. International Modal Analysis Conference.

Diemer, K. (2007). "Williamsburg Bridge Rehabilitation." Metals in Construction Spring: 36-41.

Doebling, S. W., C. R. Farrar, et al. (1996). "Damage Identification and Health Monitoring of Structural and Mechanical Systems from Changes in Their Vibration Characteristics: A Literature Review." Los Alamos National Laboratory: 1-136.

Dynamic-Design-Solutions (2009). FEMTools. Leuven, Belgium, Dynamic Design Solutions.

Franco, G., R. Betti, et al. (2004). "Identification of Structural Systems Using an Evolutionary Strategy." Journal of Engineering Mechanics 130(10): 1125-1139.

Friswell, M. I., D. J. Inman, et al. (1998). "The Direct Updating of Damping and Stiffness Matrices." AIAA 36(3): 491-493.

Friswell, M. I., J. E. Mottershead, et al. (2000). "Finite-element model updating using experimental test data: parametrization and regularization." Phil. Trans. R. Soc. Lond.(359): 169-186.

Galambos, T. V. and T. V. Ravindra (1978). "Properties of Steel for Use in LRFD." Journal of the Structural Division, ASCE 104(ST9).

Gelman, A., J. B. Carlin, et al. (1995). Bayesian Data Analysis. London, UK, Chapman & Hall.

Geyer, C. (1992). "Practical Markov Chain Monte Carlo." Statistical Science 7(4): 473-483.

Glaser, R., C. Lee, et al. (2007). "Markov Chain Monte Carlo-Based Method for Flaw Detection in Beams." Journal of Engineering Mechanics 133(12): 1258-1267.

Goulet, J., P. Kripakaran, et al. (2010). "Multimodel Structural Performance Monitoring." Journal of Structural Engineering 136(10): 1309-1318.

Green, P. J. (1995). "Reversible jump Markov chain Monte Carlo computation and Bayesian model determination." Biometrika 82(4): 711-732.

Green, P. J. (2002). Trans-dimensional Markov chain Monte Carlo. SAMSI Stochastic Computation.

Green, P. J., N. L. Hjort, et al. (2003). Trans-dimensional Markov Chain Monte Carlo. Highly Structured Stochastic Systems, Oxford University Press: 179-206.

Gul, M. and F. N. Catbas (2008). "Ambient Vibration Data Analysis for Structural Identification and Global Condition Assessment." Journal of Engineering Mechanics 134(8): 650-662.

Gurian, P., F. Castro, et al. (2004). A Bayesian Monte Carlo Approach to Model Calibration for Queuing Systems. 84th Annual Meeting of hte Transportation Research Board. Washington, D.C.

Haario, H., M. Laine, et al. (2006). "DRAM: Efficient adaptive MCMC." Statistics and Computing 16: 339-354.

Jaishi, B. and W.-X. Ren (2005). "Structural Finite Element Model Updating Using Ambient Vibration Test Results." Journal of Structural Engineering 131(4): 617-628.

Katafygiotis, L. S. and J. L. Beck (1998). "Updating Models and Their Uncertainties. II: Model Identifiability." Journal of Engineering Mechanics 124(4): 463-467.

Kim, S. and A. S. Nowak (1997). "Load Distribution and Impact Factors for I-Girder Bridges." Journal of Bridge Engineering 2(3): 97-104.

Kirkpatrick, S., C. D. Gelatt, et al. (1983). "Optimization by Simulated Annealing." Science 220(4598): 671-680.

Koh, C. G., B. Hong, et al. (2000). "Parameter Identification of Large Structural Systems in Time Domain." Journal of Structural Engineering 126(8): 957-963.

Levin, R. I. and N. A. J. Lieven (1998). "DYNAMIC FINITE ELEMENT MODEL UPDATING USING SIMULATED ANNEALING AND GENETIC ALGORITHMS." Mechanical Systems and Signal Processing 12(1): 91-120.

Liu, S. C. and J. T. P. Yao (1978). "Structural Identification Concept." J. Struct. Div. 104(12): 1845-1858.

Lounis, Z. and M. Z. Cohn (1993). "Multiobjective Optimization of Prestressed Concrete Structures." Journal of Structural Engineering 119(3): 794-808.

Mathworks (2008). Matlab. Natick, MA.

Metropolis, N. (1987). "The Beginning of the Monte Carlo Method." Los Alamos Science Special Issue.

Modak, S. V., T. K. Kundra, et al. (2002). "Comparative Study of Model Updating Methods Using Simulated Experimental Data." Computers and Structures 80: 437-447.

Moller, P. W. and O. Friberg (1998). "Updating Large Finite Element Models in Structural Dynamics." AIAA 36(10): 8.

Moon, F. (2008). CAREER: Structural Identification to Support Infrastructure Decision-Making. Washington, D.C., National Science Foundation.

Moon, F. and A. E. Aktan (2006). "Impacts of Epistemic Uncertainty on Structural Identification of Constructed Systems." The Shock and Vibration Digest 38(5): 399-420.

Mosegaard, K. (1995). "Monte Carlo Sampling of Solutions to Inverse Problems." Journal of Geophysical Research 100(B7): 12,431-412,447.

Mottershead, J. E. and C. Foster (1991). "On the Treatment of Ill-Conditioning in Spatial Parameter Estimation From Measured Vibration Data" Mechanical Systems and Signal Processing 3(2): 139-154.

Mottershead, J. E. and C. D. Foster (1991). "On the treatment of ill-conditioning in spatial parameter estimation from measured vibration data." Mechanical Systems and Signal Processing 5(2): 139-154.

Mottershead, J. E. and M. I. Friswell (1993). "Model Updating in Structural Dynamics: A Survey." Journal of Sound and Vibration 167(2): 347-375.

Pan, Q. (2007). System Identification of Constructed Civil Engineering Structures and Uncertainty. Civil, Architectural and Environmental Engineering. Philadelphia, Drexel University. Ph.D. : 243.

Richardson, W. R. S. and D. J. Spiegelhalter (1996). Markov Chain Monte Carlo in Practice. London, Chapman & Hall.

Robert-Nicoud, Y., B. Raphael, et al. (2005). "Model Identification of Bridges Using Measurement Data." Computer-Aided Civil and Infrastructure Engineering 20: 118-131.

Sanayei, M., E. S. Bell, et al. (2006). "Damage Localization and Finite-Element Model Updating Using Multiresponse NDT Data." Journal of Bridge Engineering 11(6): 688-698.

Sanayei, M., J. A. S. McClain, et al. (1999). "Parameter Estimation Incorporating Modal Data and Boundary Conditions." Journal of Structural Engineering 125(9): 1048-1055.

SAP2000 (2009). CSI Analysis Reference Manual, Computers and Structures, Inc.

Smith, I. (2010). "Structural Identification with Correlated Uncertainties." Engineering Structures.

Smith, I. and S. Saitta (2006). Multiple-Model Updating to Improve Knowledge of Structural System Behavior. 17 Analysis and Computation Specialty Conference.

Smith, I. and S. Saitta (2008). "Improving Knowledge of Structural System Behavior through Multiple Models." Journal of Structural Engineering 134(4): 553-561.

Sohn, H. and K. Law (1997). "A Bayesian Probabilistic Approach for Structural Damage Detection." Earthquake Engineering and Structural Dynamics 26: 1259-1281.

Strand7 (2010). Strand7 Finite Element Analysis Software.

Suykens, J., J. Vandewalle, et al. (2001). "Intelligence and Cooperative Seaerch by Coupled Local Minimizers." International Journal of Bifurcation and Chaos 11(8): 2133-2144.

Teughels, A. (2003). INVERSE MODELLING OF CIVIL ENGINEERING STRUCTURES BASED ON OPERATIONAL MODAL DATA. Civil Engineering. Leuven, Katholieke Universiteit. Ph.D.: 298.

Teughels, A., J. Maeck, et al. (2002). "Damage Assessment by FE Model Updating Using Damage Functions." Computers and Structures 80: 1869-1879.

Teughels, A. and G. D. Roeck (2004). "Structural Damage Identification of the Highway Bridge Z24 by FE Model Updating." Journal of Sound and Vibration 248: 589-610.

Teughels, A. and G. D. Roeck (2005). "Damage Detection and Parameter Identification by Finite Element Model Updating." Archives of Computational Methods in Engineering 12(2): 123-164.

UC-SDRL (2004). X-Modal. Cincinnati, OH.

Vanik, M. W., J. L. Beck, et al. (2000). "Bayesian Probabilistic Approach to Structural Health Monitoring." Journal of Engineering Mechanics 126(7): 738-745.

W.G. Halvorsen, A. C., David L. Brown (1977). "Impulse Technique for Structural Frequency Response Testing." Sound and Vibration 11: 8-21.

Wasserman, L. (2000). "Bayesian Model Selection and Model Averaging." Journal of Mathematical Psychology 44(1): 92-107.

Wei, L. and Y. Yuying (2008). "Multi-objective optimization of sheet metal forming process using Pareto-based genetic algorithm." Journal of Materials Processing Technology 208(1-3): 499-506.

Yang, Y. B. and Y. J. Chen (2009). "A new direct method for updating structural models based on measured modal data." Engineering Structures 31(1): 32-42.

Yun, C.-B., H.-J. Lee, et al. (1997). "Sequential Prediction-Error Method for Structural Identification." Journal of Engineering Mechanics 123(2): 115-122.

Zhang, R. and S. Mahadevan (2000). "Model Uncertainty and Bayesian Updating in Reliability-Based Inspection." Structural Safety 22: 145-160.

Zhao, J. and J. DeWolf (1999). "Sensitivity Study for Vibrational Parameters Used in Damage Detection." Journal of Structural Engineering 125(4): 410-416.

Živanović, S., A. Pavic, et al. (2007). "Finite element modelling and updating of a lively footbridge: The complete process." Journal of Sound and Vibration 301(1-2): 126-145.

Vita

Nathaniel Charles Dubbs graduated from Bethlehem Catholic High School, Bethlehem, PA in 2003. He then enrolled in the dual degree B.S. / M.S. program in civil engineering at Drexel University in Philadelphia, PA during the fall of 2003. For his last co-op position, Nathaniel accepted a research position under the advisement of Dr. Franklin Moon focusing on the evaluation of bridges using experimental techniques. Part of the research presented within his doctoral thesis utilized experimental analyses carried out at that time. Upon receiving his B.S. and M.S. diplomas, Nathaniel continued working under Dr. Moon and enrolled in the Ph.D. program at Drexel University with a concentration in Structural Engineering. While finalizing his thesis, Nathaniel began employment at Pennoni Associates in Philadelphia, PA within the Intelligent Infrastructure Systems Division, where he continues to pursue his passion of advanced finite element modeling and experimental evaluation of bridges.

This manuscript was typed by the author.